PALEOMAGNETISM AND THERMOCHRONOLOGY IN TERTIARY SYNTECTONIC SEDIMENTS OF THE SOUTH-CENTRAL PYRENEES:

CHRONOSTRATIGRAPHY, KINEMATIC AND EXHUMATION CONSTRAINTS

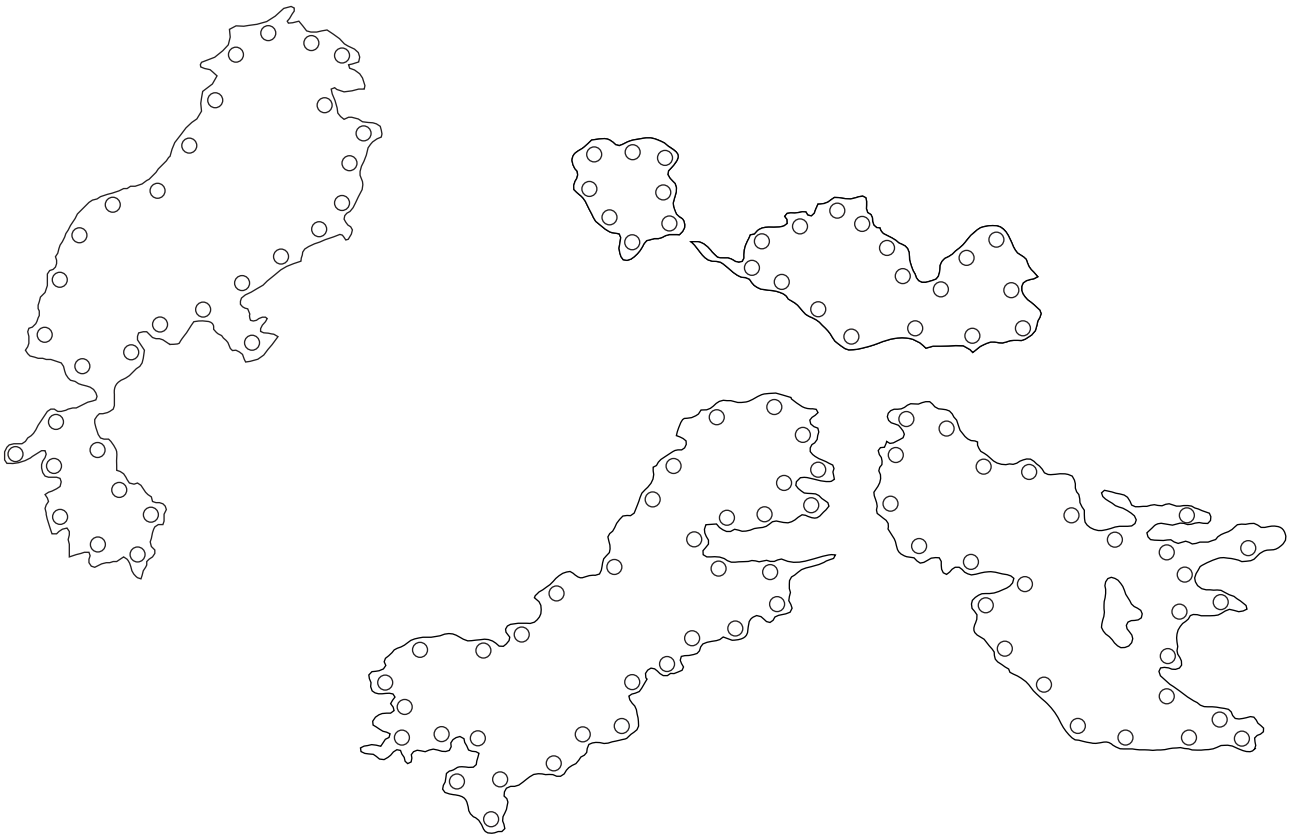

Departament de Geodinàmica i Geofísica
Grup de Recerca Consolidat de Geodinàmica i Anàlisi de Conques
Institut de Recerca Geomodels
Universitat de Barcelona

Elisabet Beamud Amorós
Memòria de Tesi Doctoral
setembre 2013

Departament de Geodinàmica i Geofísica

Universitat de Barcelona

Grup de Recerca de Geodinàmica i Anàlisi de Conques

Institut de Recerca Geomodels

PALEOMAGNETISM AND THERMOCHRONOLOGY IN TERTIARY SYNTECTONIC SEDIMENTS OF THE SOUTH-CENTRAL PYRENEES: CHRONOSTRATIGRAPHY, KINEMATIC AND EXHUMATION CONSTRAINTS

Memòria de Tesi Doctoral presentada per **Elisabet Beamud Amorós** per optar al grau de Doctora en Ciències Geològiques per la Universitat de Barcelona. Aquesta memòria ha estat realitzada dins el Programa de Doctorat "Ciències de la Terra" RD 778/1998 sota la direcció del **Dr. Josep Anton Muñoz de la Fuente** i el **Dr. Miguel Garcés Crespo**

Elisabet Beamud Amorós

Barcelona, setembre de 2013

Dr. Josep Anton Muñoz

Dr. Miguel Garcés

This PhD Thesis has been carried out in the *Departament de Geodinàmica i Geofísica*, the *Grup de Recerca de Geodinàmica i Anàlisi de Conques* (sponsored by the *Comissió d'Universitats i Recerca* 2009SGR-1198) and the *Institut de Recerca Geomodels*. Financial Support was provided by a grant of the *Programa Nacional de Formación de Personal Investigador* (*Subprograma de Promoción General del Conocimiento* linked to the Project PB97-0882-C03-03) of the *Secretaría de Estado de Universidades, Investigación y Desarrollo* (*Ministerio de Educación y Cultura*). Paleomagnetic measurements were made in the Paleomagnetic Laboratory of Barcelona (CCiTUB-ITCJA CSIC)

Sete & Deli,

GRACIES

AGRAÏMENTS/AGRADECIMIENTOS/ACKNOWLEDGEMENTS

Oooooleeeee…. ja ha arribat el dia!!!

En tots aquests anys (uns quants... no ens enganyem) han estat moltes les persones que m'han ajudat per arribar fins aquí. No voldria deixar-me ningú, però espero comprensió si em despisto, tants anys comencen a passar factura a les meves neurones!

En primer lloc voldria agrair als meus directors, Josep Anton Muñoz i Miguel Garcés. Lluny queda aquell dia en que vaig anar a dir-li a l'Anton que m'havien concedit la beca FPI i em va dir "no sé si felicitar-te o donar-te el condol", segurament si hagués sabut que em portaria tants anys i li donaria a ell tants mals de cap m'hagués donat el condol directament. Gràcies per ensenyar-me tantes coses del Pirineu, per deixar-me l'espai i temps necessaris quan els vaig necessitar, per motivar-me en els moments en què les forces minvaven i pels "va... vinga... acaba Bet!" acompanyats d'un copet a l'esquena tan necessaris a la recta final. Al Miguel Garcés, gràcies per tantes coses que no sé ni per començar. Per introduir-me en el món paleomagnètic, ensenyar-me les entranyes del laboratori, per compartir tantes estones de camp a La Pobla i Sis i en tantes altres zones de mostratge, per inculcar-me el "yo por menos de 1000 metros de serie no me pongo" i "la independència en la correlació" les maneres de fer que defineixen la forma de treballar al laboratori i, per estar sempre disposat a donar un cop de mà en matèria científica i personal, inclús ajudant-me a transportar la nevera en una mudança.

Al Lluis Cabrera, el meu tercer director durant una bona pila d'anys. Gràcies per confiar en mi i oferir-me el tema de tesi en un inici, per estar sempre disponible per resoldre qualsevol dubte i per preocupar-te tant del progrés de la tesi com de la persona que la feia durant tots aquests anys.

Thanks to Dr. Robert Scholger, from the Paleomagnetic Laboratory of the Montanuniversität of Leoben (Austria) for allowing me to visit and stay for two months in the Laboratory to measure part of the samples. Thanks also to Dr. Hugh Sinclair from the Geology and Geophysics Department of the University of Edinburgh for his hospitality and assistance while I was there. Thanks to the PhD students I met during these stages: Wolfgang Thöny and Christine Latal in Gams; Mark Naylor, Matthew Gibson, Gwylim Lynn, Fabio at Edinburgh. Thanks also to my housemates in Edinburgh: Simon, Ross and Naginah (I still listen to Eva Cassidy's cd).

Thanks to all the coauthors and reviewers of the papers and to the editors of the different journals. Special thanks to Paul Fitzgerald for the thermochronology of *the silly conglomerates*. Gràcies Oscar per proposar-me anar a Ainsa a perforar unes quantes estacions "per veure si li donem una empenteta" i haver pogut gaudir de la geologia de la zona i dels menjars fantàstics de la Fonda Carrera i els seus *entreteneos*.

Gràcies a l'Eduard Roca per la seva ironia, bromes i preses de pèl contínues. Però alhora per burxar i empènyer per a que acabés i per estar sempre disposat a donar una visió crítica de la feina feta i aportar comentaris i suggeriments per millorar.

Gràcies a l'Ana Gómez per mesurar una bona pila de mostres i al personal de les diferents secretaries per portar tota la paperassa endavant. Especials gràcies a la Carmen Rebellón i al Carles Martín Closas per tenir tanta paciència i per l'ajuda en tots els dubtes sobre la burocràcia del doctorat.

Gràcies a la Dolors Barsó, amb qui vam començar juntes aquesta aventura. Compartir el camp a La Pobla i el pis de Senterada van ser una bona experiència i en guardo molts bons records. Gràcies a tota la gent que vaig aconseguir enredar per a que m'ajudessin a mostrejar, començant per la mateixa Dolors, Oscar Gratacós, Oriol Font, Anna Cierco, Jesús Carner, Francisco Giner, Marta Rejas, Javi Pérez-Rivarés, Ylènia Almar. I a la Duna per fer alguns dels mostrejos a la Pobla més entretinguts amb un anar i tornar de pinyes i pedretes. A la Núria Carrera, gràcies per les hores de camp compartides mirant "els conglos" i per no guardar-me rancúnia després d'un passeig entre punxes per posar la brúixola sobre "els potatos", espero poder mirar molts més conglomerats amb tu. I al Jesus Garcia-Senz per ensenyar-me el Cretaci de La Pobla, les calcàries són molt més agradables de mirar si abans te les ha explicat el Jesu!

Magnetonenes: GRÀCIES PER TOT, compartir la feina i l'oci amb vosaltres és un veritable plaer i, sí, si no existíssiu us haurien d'inventar. Elisenda, gràcies per totes les coses compartides, tantes i tan bones que destacar-ne una en concret no faria justícia. Ylènia, ets l'autèntic *duende* del laboratori, sense la teva ajuda no hagués pogut acabar mai aquesta tesi. I gràcies Arnau per ser tan agut i haver-nos batejat així. A la gent que està o ha estat pel laboratori, Míriam, Juan Cruz, Lluis Valero, Eloi Carola, tots vosaltres aporteu llum i alegria a la foscor del soterrani de l'Almera.

Gracias al *clan magnetomaño*, Ruth Soto, Belén Oliva (el mejor equipo de perforación en blandos). Gracias Emilio por ser un gran compañero de piso en Graz, por el viaje a Sicilia y por abrirme tu casa de Zaragoza en multitud de ocasiones. Y muchas gracias a todos los compañeros *Magiberos*, tenemos un nombre poco serio, cierto, pero he aprendido un montón de cosas en todas las reuniones.

A tots els companys del departament i sobre tot de la 226. Hi ha passat molta gent per aquest despatx i inclús el seu aspecte ha canviat moltíssim en aquest temps. Segur que em descuidaré d'algú, així que GRÀCIES a tots els que en algun moment l'han ocupada i en especial, a la Marta Puig per ensenyar-me a fer servir el Corel i compartir un munt de bones estones a la sala i fora d'ella. Al Pau per saber tanta geologia, tant de microstation i tantes i tantes coses i ser sempre generós per compartir-les i gràcies per les estades a Fuencalderas, pels cinemes dels divendres, concerts, cervesetes... per ser un molt bon amic, en definitiva. A Marco por las cenas, cines y por dar siempre un golpecito en la espalda camino a tu sitio mientras yo miraba "bolitas" de MS-DOS en la pantalla. A Pablo, gracias por saber escuchar y dar un toque cuando es necesario, por las clases de yoga, las fabadas... y por estar siempre ahí. Gràcies Oscar per estar al cas de l'Ainsa, plotter, llicències i coses vàries. I gràcies Roger per ser un magnífic company darrera les pantalles de l'ordinador i a l'altre cantó del skype.

A tota la gent que m'ha apartat en algun moment de la tesi durant aquests anys, també gràcies perquè amb això també han contribuït a formar-me. En especial, al Jaume Vergés per les campanyes als Zagros i al Carles Soriano per les boniques campanyes perforant dics volcànics al costat del mar a Tenerife. A Manolo Montes, Paco Nozal y Sergio Santillana, gracias por ser unos excelentes compañeros antárticos en "Barrambio".

Gràcies al grup dels esmorzars i "els pulpos": Aida, Jordi, Maria José, Maite i Teresa, començar el dia fent un cafè amb vosaltres dóna gust!

Moltes gràcies a tots els amics *extramuros* per les bones estones, els ànims, les sortides, les paraules d'alè... sempre he dit que el meu principal patrimoni són els meus amics i, sí, em considero molt rica! Gràcies Núria per les birrilles, les escapades, els vespres filosofant davant d'una ampolla de "licorcillo chocolatero-cerecil" (viva Aida!), cines, sopars, expos, els teus espectacles de trapezi i per les infinites menjades de tarro que t'he arribat a fer! A *les nenes* de la facultat (Montse, Glòria, Anna i Ester) sou fantàstiques i *els vostres associats* també. A la Natàlia i la Mar abans a l'ICTJA i ara a l'IDAEA gràcies per tot el que hem compartit i per tots els soparets fets i els que farem. Alle ragazze d'italià (Àngela i Carmen) per Umbria, Vilassar, els cappuccinos i els jazzsis dels diumenges. A l'Oriol i la Maria, la Montse i el Pedro, Ana e Iván, Silvia i Froy, Ana "la pamplonita", perquè hi heu estat i encara hi sou, malgrat aquest darrer any he estat més que desapareguda. And Lisa, thanks for being my mental balm during the English lessons this year, I can't remember how many times I've been complaining about my thesis...

Als puskos, gràcies per ser els millors amics puskils del món. Gracias Berta por ser mi otra hermana desde los 5 años y por estar siempre allí, a pesar de haber tenido varias veces a todo un oceáno entre medio poniéndonoslo difícil. I Oscar, ja t'he donat les gràcies abans per liar-me per anar a Ainsa, però gràcies també per... TOT, per ser tu tal i com ets, també haurien d'inventar-te si no existissis. Gràcies per volar des de Londres i fer-me una abraçada en un moment en que, literalment, no tenia forces ni per respirar. I gràcies als vostres pusko-consortes i els micropuskos per aportar tanta qualitat humana a la família puskil.

Juanjo, gracias por compartir tantas cosas conmigo. Por tu apoyo y tus continuas palabras de ánimo. Y gracias por esas magníficas vistas de Montserrat cuando apartaba los ojos de la pantalla del ordenador mientras trabajaba en la tesis los fines de semana.

I, finalment, gràcies a la meva família. Als meus pares, gràcies per *la marca Beamud*. Gràcies per ser-hi sempre, a la distància suficient per a que haguem aprés a fer les coses per nosaltres mateixes, però exercint de xarxa de seguretat si era necessari. Teresaaa... Ieia, gràcies per ser la millor germana que es pot tenir i fer-me una estirada d'orelles de tant en tant per a que espavilés amb la tesi i la posés per davant d'altres coses... sovint cal una mirada externa que et faci veure que t'estàs equivocant. I gràcies per ser *tan flamenca* i pel càtering, segur que el pica-pica te l'agrairé jo i la resta del departament, artista! Jordi... Ronxiet, gràcies per ser més que un cunyat, un germà de totes totes. I gràcies Maria Dolors, la Yoyes, per donar sempre ànims per continuar endavant.

I si m'he deixat algú... aquí va un GRÀCIES A TOTS! Sobre tot per la paciència... que ha estat llarg això!!!

INDEX

FIGURES and TABLES INDEX

Page 57 – Figure 1.7 – Schematic representation of types of orogenic curvatures based on timing relationships between thrusting and vertical axis rotations (VAR). Dr: reference direction, D1: direction recorded in time 1. No VAR are detected in primary arcs, whereas in secondary and progressive arcs VARs are observed.

Page 61 – Figure 1.8 - Schematic representation of the erosion of a mountain range. The source is progressively unroofed and the sedimentary detritus is deposited in the adjacent basin. Time slices 1 to 4 correspond to 4 progressive and continuous intervals of erosion and deposition. Samples from basin deposits 1-4 record integrated exhumation rates between cooling through tc (closure temperature) and te (time of erosion). Samples buried deeply in the basin may be partially or completely annealed. Modified from *Garver et al.* (1999).

Page 66 – Figure 1.9 - Subdivision of the European continental Paleogene based on mammals as proposed by the Symposium in Mainz, February 1987. Modified from *Schmidt-Kittler* (1987).

CHAPTER 2: RESULTS

CHAPTER 2.1 - A new Middle to Late Eocene chronostratigraphy for NE Spain

Page 78 – Figure 1. Geological map of the South-Central Pyrenees and stratigraphy of the Ainsa, Graus-Tremp and La Pobla de Segur basins with indication of the vertebrate localities and the Charophyte assemblage. The faunistical list for each locality is provided in [20]. The Capella mine fossil locality is characterised by *Pseudoloris (Pivetonia) isabenae* and *Lophiodon rhinocerodes* among other taxa [13, 20]. Sossis, Claverol and Roc de Santa fossil mammal assemblages include *Therydomis euzetensis* and *Palaeotherium medium euzetensis* among a extense list of taxa [14, 20]. *Therydomis euzetensis* also occurs in Can Gramuntill fossil site [15].

Page 82 – Figure 2. Demagnetization diagrams of representative samples and mean directions from the La Pobla de Segur Basin and the Sierra de Sis sections. **(a)** demagnetization diagrams of samples of Paleozoic derived sediments in La Pobla de Segur basin, displaying normal and reversed polarities. **(b)** demagnetization diagram of a sample with a Cretaceous source area, showing a erratic behaviour at high temperature. The diagram below shows the demagnetisation circles [27] used to obtain the site mean direction. **(c)** demagnetization diagram of samples from the Cornudella and Sis Fms. in the Sierra de Sis section, yielding normal and reversed polarities. **(d)** demagnetization diagrams of a lacustrine limestone from the Ermita allogroup in La Pobla de Segur basin, after alternating field demagnetization (specimen 1A) and thermal treatment (specimen 1B) displaying a reverse polarity. **(e)** mean directions of the La Pobla de Segur basin and the Sierra de Sis sections. No significant vertical axis rotations are observed.

Page 83 – Figure 3. Local litho- and magnetostratigraphic sections from the Sierra de Sis (Cajigar section) and the La Pobla de Segur basin (Claverol, Can Gramuntill and Rocs de Queralt-Montsor sections) with indication of the Charophyte and the vertebrate localities.

Page 85 – Figure 4.(a) Correlation of the local magnetostratigraphic sections to the GPTS [29] with indication of the Charophyte association and the vertebrate localities with their corresponding MP reference levels. The Mediano area log is a composite section from the Mediano and Eripol magnetostratigraphic sections [32]. **(b)** sedimentation rates derived from the proposed correlation for the Mediano area log and the La Pobla de Segur basin section. An important decrease is recorded in both sectors around 40 My.

Page 86 – Figure 5. Chronostratigraphy of the continental sediments of the Ainsa, Graus-Tremp and La Pobla de Segur basins. The fossil localities are indicated as follows CP: Capella; LA: Laguarres; SO: Sossís, CL: Claverol, CG: Can Gramuntill and RS: Roc de Santa.

Page 87 – Figure 6. Correlation of the Middle Eocene MP reference levels to the international reference geochronological scales. Geomagnetic chronology from [29]. Calcareous nannoplankton zonation from *Martini* (1971) [48] in *Berggren et al.* (1995) [49]

CHAPTER 2.2 - Magnetostratigraphy and detrital apatite fission track thermochronology in syntectonic conglomerates: constraints on the exhumation of the South- Central Pyrenees.

Page 95 – Figure 1.- A) Geological sketch of the South Central Pyrenees highlighting the outcrops of the Upper Paleogene continental conglomerates and the granitic massifs of the Axial Zone. The map area corresponding to the Axial Zone modified from *Zwart* (1979). The position of the magnetostratigraphic logs "La Pobleta - LP" and "Montcortés - MC" within the Senterada basin is shown. Position of the cross-section A-A' in figure 2 is also indicated. AFT ages (Ma) of the granitic massifs after (*) *Morris et al*. (1998), (**) *Fitzgerald et al*. (1999), (***) *Sinclair et al.* (2005) and (****) *Gibson et al.* (2007). **B)** Simplified stratigraphic logs of the syntectonic conglomerates of Sis, Gurp and La Pobla de Segur-Senterada with indication of the position of the detrital AFT samples. **C)** Cross-section for the ECORS seismic profile modified after *Muñoz* (2002). The square indicates the position of the cross-section of figure 2.

Page 97 – Figure 2.- A) Detailed geological map of the La Pobla de Segur and Senterada basins. The position of the cross-section A-A' and the magnetostratigraphic sections La Pobleta (LP) and Montcortes (MC) within the Senterada basin are shown. The magnetostratigraphic sections of *Beamud et al*. (2003) (Claverol: CL, Carretera Sort: CS, Can Gramutill: CG, Rocs Queralt: RQ and Montsor: MS) within the La Pobla de Segur basin are also located. **B)** Cross-section A-A' across the La Pobla and Senterada basins showing the main structural features of the syntectonic conglomerates. b-b' corresponds to an enlargement of the central area of cross-section A-A'.

Page 99 – Figure 3.- A) Demagnetization diagrams of representative samples of La Pobleta and Montcortes magnetostratigraphic logs showing normal and reversed polarities. Black and white dots, respectively, indicate horizontal and vertical projection of the vector end points. Diagrams are in tectonic corrected coordinates. **B)** Mean direction of the Senterada materials from the La Pobleta and Montcortes sections. No vertical axis rotations are observed.

Page 100 – Figure 4.- Paleolatitude of the VGP and local magnetoestratigraphy for the Senterada basin.

Page 100 – Figure 5.- Correlation of the local magnetostratigraphy to the GPTS (*Gradstein et al.*, 2004) and integration with the previously published data of La Pobla and Sis conglomerates (*Beamud et al.*, 2003). The stratigraphic position of the AFT samples along the magnetostratigraphic sections is shown.

Page 104 – Figure 6.- Lag-time plot (e.g., *Garver et al.* 1999) for the Sis, La Pobla and Senterada samples.

Page 106 – Figure 7.- Samples plotted against stratigraphic position. Temperature-time models of AFT thermochronology data, including stratigraphic constraints for these granitic clasts, were undertaken using HeFTy (*Ketcham*, 2005). Samples are also grouped (1 – 5 shown

in colored circles) according to similar AFT and stratigraphic ages, also shown on the lag-time plot (Figure 6). For the inverse thermal models, the magenta envelope is a "good fit" (i.e., the T-t path is supported by the data) and the green envelope an "acceptable fit" (i.e., the T-t path is not ruled out by the data). Model inputs are multiple T-t boxes with loose constraints designed to offer the opportunity for the model to explore pre-depositional rapid cooling events and post-depositional burial as well as a small T-t box for the stratigraphic (depositional) age of the sample constrained at 10-20°C to reflect a representative mean paleo-land surface temperature. Note that the T-t path for each sample must go through the small T-t box for the stratigraphic (depositional) age of the sample. 10,000 paths were run in each model. Modelled track length distributions (dashed line) are compared to measured track length distribution (grey histograms) with measured mean length, standard deviation and number of tracks measured (e.g., 13.1 µm, 1.5 µm, 75 for sample CJ-5) shown for easy reference.

Page 107 – Figure 8.- Evolution of the exhumation rates through time deduced from the AFT of the cobbles in the conglomerates and from the AFT ages from plutons in the hinterland from previous studies (*Fitzgerald et al.*, 1999; *Metcalf et al.*, 2009). The evolution of the sedimentation rates obtained from the magnetostratigraphy of the syntectonic conglomerates is also plotted (*Beamud et al.*, 2003; this study). Timing of thrust sheet movement and re-excavation is represented on the right side of the figure.

Page 108 – Figure 9.- Evolution of the Paleogene piggy-back basins of conglomerates in the Central Pyrenees and their relationships with the structural evolution of the southern Pyrenees as deduced from the magnetostratigraphic and AFT ages. Only the main structures and source areas active during the deposition of the syntectonic conglomerates are represented. For each time interval a simplified cross-sectional view and a map representation have been sketched. Sections are based on the ECORS cross-section across the Pallaresa valley (Figure 2) and on the partially restored cross-sections along the ECORS transect (*Muñoz*, 2002). Paleocurrent directions in the map sketches are compiled from *Mellere* (1992, 1993), *Vincent* (2001) and *Barsó* (2007). Sketches not to scale.

Page 102 – Table 1.- AFT analytical results. Stratigraphic ages of the samples, as discussed in the text, are largely based on the magnetostratigraphy of these conglomerates (Beamud et al., 2003; this study).

Page 103 – Table 2.- Binomial peak-age fitting for samples containing multiple age populations. N, number of grains counted; P1 and P2 are fitted binomial peak ages (rounded) quoted at $\pm 1\sigma$ (68% confidence interval). Numbers in the square brackets represent percentage of grains in a given peak.

CHAPTER 2.3 - The Ainsa Fold and Thrust Oblique Zone of the Central Pyrenees: Kinematics of a curved contractional system from paleomagnetic and structural data.

Page 121 – Figure 1. Location of the study area. Structural sketch showing the main structural units of the central Pyrenees and the major anticlines of the Ainsa Oblique Zone at the western boundary of the major thrust salient in the central Pyrenees. Crustal cross-sections at both sides of the Ainsa Oblique Zone illustrate changes of the structural style along strike. ECORS section from *Muñoz* [1992] and the Arzacq section modified from *Teixell* [1998]. AOZ: Ainsa Oblique Zone, A: Añisclo Anticline, B: Boltaña Anticline, M: Mediano Anticline, C: Cotiella, PM: Peña Montañesa, SCU: South Pyrenean Central Unit, Bx: Bóixols, SM: Serres Marginals.

Page 123 – Figure 2. Structural map of the Ainsa Oblique Zone and surrounding areas. Location of the paleomagnetic sites with mean values of rotation from previous studies (B: *Bentham* [1992]; BE: *Beamud et al.* [2003]; D: *Dinarès-Turell* [1992]; H: *Hogan* [1993]; MO: *Mochales et al.* [2012b]; OU: *Oliva-Urcia and Pueyo* [2007]; P: *Pueyo et al.* [2003a]; RP: *Rodríguez-Pintó et al.* [2013]). Cones represent α95 values of the paleomagnetic directions. Red sites correspond to remagnetized sites from *Oliva-Urcia* [2004]. See location in Figure 1 and data in Table S1 of supplementary material. Red square indicates the position of the study area represented in Figure 3.

Page 124 – Figure 3. Paleomagnetic sites and vertical-axis rotations within the study area. See location in Figure 2. Cones represent the declination error obtained from α95/cosI. The map legend is the same as in Figure 2. Red lines indicate the location of the cross-sections presented in Figures 5 and 6. f: fault, f&t: fold and thrust system, ant: anticline, s: sincline

Page 126 – Figure 4. Chronostratigraphic diagram showing the main stratigraphic units of the Gavarnie thrust sheet and surroundings. Lithostratigraphic units: Es, Escanilla; Bu, Buil; So, Sobrarbe; Gu, Guara; Gr, Grustán; Pa, Pano; Cp, Capella; Pr, Perarrúa; Cm, Campanué; Cst, Castissent; SM, Santa Marina, Cg, Castigaleu; Ro, Roda; Yb, Yeba; Ri, Riguala, Me, Metils; Mi, Millaris; Al, Alveolina limestone. SV1-2: San Vicente Formation. Turbidite systems: gu, Guaso; og, O Grao; ga, Gabardilla; c, Coscojuela; fo, Formigales; s, Sieste; m, Morillo; a, Ainsa; gb, Gerbe-Banastón; ar, Arro; f, Fosado. Horizons: O, Olsón; EL, Escanilla limestone; SB, Santa Bárbara; SP, San Pedro; SL, San Lino; M, Morillo limestone; A, Ascaso; LP, La Puebla. Thrust sheets: C, Cotiella; M, Montsec; PM, Peña Montañesa; B & G, Bielsa and Guarga; LF, La Fueba thrust system.Unconformities: AT, L'Atiart; CL, Charo-Lascorz. Litho- and chronostratigraphic information compiled from: *Bentham et al.* [1992], *Bentham and Burbank* [1996], *Barnolas and Gil-Peña* [2001], *López-Blanco et al.* [2003], *Mochales et al.* [2012a], *Rodríguez-Pintó et al.* [2012], *Serra-Kiel et al.* [1994]. Eocene time scale from *Gradstein et al.* [2004]. SBZ biozones calibration to the time scale integrates data from *Costa et al.* [2013] and *Rodriguez-Pintó et al.* [2012].

Page 128 – Figure 5. A. Cross-section of the northern part of the Ainsa Oblique Zone, across the Boltaña and Añisclo anticlines in the Gavarnie thrust sheet and the Peña Montañesa and Cotiella thrust sheets. Lithostratigraphic units like in figure 4. **B.** Photograph of the Añisclo anticline. **C.** Photograph and structural sketch of the Peña Montañesa and Cotiella thrust sheets.

Page 129 – Figure 6. A. Cross-section of the southern part of the Ainsa Oblique Zone. Lithostratigraphic units like in figure 4. **B.** Enlargement of the Mediano anticline and location of the paleomagnetic sites with respect to the syn-folding growth sequence. W1, W2, E1 and E2 correspond to four stratigraphic columns constructed across the growth sequence, two of them in the west limb and two of them in the east limb of the anticline.

Page 130 – Figure 7. Detailed map of the Boltaña anticline and paleomagnetic data in this area from this and previous studies (see Table S1 in supplementary material). White square indicates the position of the 3D block diagram **(B)** which shows in detail the unconformity between the pre-folding platform and slope sediments and the growth strata. Pp: paleocurrent directions of the pre-folding slope; Pg: paleocurrent directions of the growth strata. The stereogram represents the poles of bedding of the pre-folding platform and the pre-folding slope sediments, and the poles of bedding of the growth strata. The intersection lineations between the slope and the platform bedding and between the growth strata and the pre-folding platform are also included.

Page 132 – Figure 8. Detailed map and kinematic data of the main thrusts in the La Fueba fold and thrust system.

Page 136 – Figure 9. A) Zijderveld demagnetization diagrams of representative samples. Open (solid) symbols represent projection onto the vertical (horizontal) planes. All diagrams are represented after bedding correction (abc). AF: alternating field demagnetization, units are mT, TH: thermal demagnetization, units are ºC. Grey lines in sample 23-4A represent the characteristic components calculated: an intermediate temperature component between 280-390 ºC of reversed polarity and a high temperature component of normal polarity, defined between 390 and 430 ºC. **B)** Stereographic projection of the mean directions and obtained $\alpha 95$ at site level before (BBC) and after (ABC) bedding correction. Projections are on upper (grey color, dashed lines) and lower hemisphere (black color, solid lines).

Page 138 – Figure 10. Results of the fold tests [*McFadden*, 1990] and the direction-correction tilt tests [*Enkin*, 2003] performed in the study area. Tests have been done in the Boltaña (sites 16 to 22), Añisclo (sites 30-31 and 34-35) and Mediano (sites 3 to 5 and 7 to 10) anticlines and in site 15, an outcrop scale anticline in the hangingwall of the Almuzaras thrust south of El Pueyo de Araguás. Open (solid) symbols represent projection on the upper (lower) hemisphere.

Page 141 – Figure 11. Simplified map and sketch of the vertical-axis rotations within the study area. Vertical-axis rotations are grouped in three categories according to the age of the sampled sediments. Remagnetized sites are distinguished as black arrows. f: fault, a:anticline, t.s.: thrust sheeet

Page 142 – Figure 12. Rotation vs. time plots for the Mediano (a) and the Boltaña anticlines (b to d). **(a)** Data for the Mediano anticline from this study and from *Bentham* [1992] as cited in *Mochales et al.* [2012b]. Blue line within the amount of rotation represents the mean rotational angle for the data before the growth of the structure at 47.5 Ma. After 47.5 Ma the data follow a decreasing exponential function. **(b)** Data from this and previous studies along the Ara River transect (sites located in Figure 7). Blue line within the amount of rotation represents the mean rotational angle for the data before the growth of the structure at 42.5 Ma, the light blue band represents a +/- 10º envelope. **(c)** Data from this work and from previous studies fit by linear regressions before and after 42.5 Ma. Sites marked as outliers in (d) have been removed in this plot, as well as site CAS5 from *Mochales et al.* [2012b]. **(d)** Data from *Mochales et al.* [2012b] with logarithmic and linear regression adjustments. Red line represents the logarithmic adjustment published in *Mochales et al.* [2012b]. Blue line represents a new linear regression for data before the growth of the anticline at 42.5 Ma. Green line represents the linear regression for data within the growth strata. Sites marked as outliers in the figure have not been included to calculate the regression lines.

Page 144 – Figure 13. Schematic diagram showing the different stages of the evolution of the main fault-related folds of the Ainsa Oblique Zone and their longitudinal propagation during the CW vertical-axis rotation. The box in stage 1 of the regional evolution marks the area enlarged and shown in the local evolution section (growth of the Boltaña anticline). Note the differences on the amount of vertical-axis rotation along-strike in the fold termination despite the constant strike of the fold. Regional and local transport directions are distinguished. Grey arrows on local evolution section represent paleomagnetic directions.

Page 145 – Figure 14. (A) Simplified structural map with location of the paleomagnetic sites used for the strike-test of the study area. Only sites from pre-tectonic units with $\alpha 95$ less than

15º have been considered (see supplementary material Table S2 for details). Red dots represent sites from the Boltaña anticline and the grey ones represent sites suspicious of being remagnetized. **(B)** Strike-test for the Ainsa Oblique Zone. Regression lines and t-test parameters for the significance of the slope of the obtained regression are indicated. Black line represents the regression taking into account only the sites represented in black (without the Boltaña sites and the ones suspicious of being remagnetized). Grey line represents the regression taking into account black and grey sites (without the Boltaña sites). Finally, all the sites (black, grey and red) have been considered to obtain the red regression line.

Pages 149-150 – Figure 15. Map reconstructions of the Ainsa Oblique Zone for the Middle to Late Eocene time span. **(A)** Late Bartonian to early Priabonian (~37 Ma), **(B)** Middle Lutetian (42 Ma) and **(C)** Early Lutetian (48 Ma). Colors represent facies and sedimentary systems. Red lines represent the active structures in every stage. Same legend for B and C.

Page 152 – Figure 16. Synthesis of the evolution of the study area during the different stages (48 Ma, 42 Ma, 37 Ma and present day). Structures and arrows depicting CW vertical-axis rotation have been colored for each stage. The Montsec thrust has been depicted as a passive marker as a reference for the rotation of pre-Gavarnie structures during the differential displacement on the Gavarnie thrust (that led to the CW vertical-axis rotation and the formation of the Ainsa Oblique Zone structures).

Page 140 – Table 1 – Geographic, stratigraphic, structural and paleomagnetic information of the studied sites. (1) UTM coordinates, (2) Stratigraphic age, (3) Structure: anticline or syncline name and fold axis trend and plunge (if determined), (4) bedding attitudes for the different sites in dip direction/dip, (5) N: number of samples considered per site, (6) tectonic corrections applied – cyl: cylindrical fold geometry considered, bc: bedding correction, con: conical fold geometry considered, corr3 represents the correction taken into account in this study, (7) Fold Test scale, O: outcrop, S: structure. Declination error calculated as $\alpha 95/\cos I$. The net rotation (β) has been obtained after comparison of the mean directions at the site level with the Eocene reference direction for stable Iberia from *Taberner et al.* [1999] relocated to the study area coordinates according to the via pole conversion method. Confidence values for the calculated rotations obtained after *Demarest* [1983].

Supplementary material of chapter 2.3

Page 159 to 164 – TABLE S1 - Data from previous authors, represented in Figure 2 and, partly, in Figure 14. This table includes: A heading with the name of the author and year of publication. Columns: label: name in the present manuscript; site: author's original site name; polarity: if the site has normal (N) or reversed (R) polarity; chron: if know, the assigned chron; unit: rock unit sampled; age: attributed age to the sampled site; UTM coordinates or latitude/longitude coordinates depending on the available information; bedding dd/dip: bedding attitude in dip direction and dip at the sampling site; Columns BBC: Paleomagnetic directions before tectonic correction, including: Dg: declination in geographic coordinates, Ig: inclination in geographic coordinates, $\alpha 95$ and k); Columns ABC: Paleomagnetic direction after tectonic correction, including: Ds: declination in stratigraphic coordinates, Is: inclination in stratigraphic coordinates, $\alpha 95$ and k; Column beta (β): mean rotation obtained from the comparison of the Ds with the reference direction for stable Iberia.

Page 165 – TABLE S2 - Data used for the strike test represented in Figure 14. This table includes: label: the name used in this work; site: the author's site name; author: the source for the data; structure: name of the main structure where the site is located; UTM coordinates:

x and y coordinates for zone 31; Ds: mean direction after tectonic correction ; Dr: reference direction referred to the Ainsa coordinates; Ds-Dr: difference between the site mean direction and the reference direction; S: strike of the structure at the sampling site; source: origin of the obtained strike at the sampling site; Sr: undeformed reference strike; S-Sr: difference between the strike at the sample site and the reference strike

CHAPTER 3: SYNTHESIS and DISCUSSION

3.1 – CHRONOSTRATIGRAPHY OF THE TERTIARY SYNTECTONIC MATERIALS

Page 170 – Figure 3.1- Eocene Chronostratigraphy of the South-Central Pyrenees, from the Ainsa basin to the La Pobla de Segur. Lithostratigraphic units: Mr, Merli reef; Is/Be: Iscles-Berganuy reefs; Bu, Buil; So, Sobrarbe; Cp, Capella; Pr, Perarrúa; Cst, Castissent; Al, Alveolina limestone. SV1-2: diferent units making the San Vicente Formation. Turbidite systems: gu, Guaso; og, O Grao; ga, Gabardilla; c, Coscojuela; fo, Formigales; s, Sieste; m, Morillo; a, Ainsa; gb, Gerbe-Banastón; ar, Arro; f, Fosado. Horizons: O, Olsón; EL, Escanilla limestone; SB, Santa Bárbara; SP, San Pedro; SL, San Lino; M, Morillo limestone; A, Ascaso; LP, La Puebla; Lu, Santa Llucia. Thrust sheets: C, Cotiella; Bo, Bóixols; M, Montsec; PM, Peña Montañesa; B & G, Bielsa and Guarga; LF, La Fueba thrust system. Litho and chronostratigraphic information compiled from: *Barnolas & Gil-Peña* (2001), *Bentham et al.* (1992), *Bentham & Burbank* (1996), *López-Blanco et al.* (2003), *Mochales et al.* (2012), *Rodríguez-Pintó et al.* (2012), *Serra-Kiel et al.* (1994). Time scale from *Gradstein et al.* (2004). SBZ biozones calibration to the GPTS integrates data from *Costa et al.* (2013) and *Rodríguez-Pintó et al.* (2012)

3.2 – BIOCHRONOLOGICAL IMPLICATIONS

Page 173 – Figure 3.2.- Correlation of the south Pyrenean and Ebro Basin Eocene fossil sites and their assigned MP reference levels to the GPTS (*Gradstein et al.*, 2004) and comparison with previous calibrations. So-CG: Sossís-Can Gramuntill, Lg: Laguarres, Po: Pontils and Cp: Capella fossil sites.

3.3 – KINEMATICS, EXHUMATION and TECTONOSEDIMENTARY EVOLUTION OF THE SOUTH-CENTRAL PYRENEES

Page 175 – Figure 3.3- Geological map and main structural units of the South-Central Pyrenees, with indication of the vertical axis rotations derived from this (red arrows) and previous works (grey arrows). See Table S3.3 in this section for details on the compilation from previous authors and Table 1 in chapter 2.3 for details of the sites from this work.

Page 178 – Figure 3.4- Chronostratigraphy of the South-Central Pyrenees, from the Ainsa basin to the La Pobla de Segur with indication of vertical axis rotations from this and previous studies (*Bentham*, 1992; *Dinarès-Turell*, 1992; *Pueyo*, 2000; *Mochales et al*., 2012a; *Pascual et al.*, 1993). On the right, the evolution of exhumation rates with time on the Axial Zone derived from vertical profiles (*Fitzgerald et al.*, 1999) and from this work (section 2.3: *Beamud et al.*, 2011) are indicated. See figure caption of Figure 3.1 for description of the lithostratigraphic units.

Page 179 – Figure 3.5- Tectonosedimentary evolution of the South-Central Pyrenees for Middle Lutetian times. Red lines indicate active structures. Sedimentation rates in the Ainsa basin from *Mochales et al.* (2012b).

Page 180 – Figure 3.6- Tectonosedimentary evolution of the South-Central Pyrenees for Late Bartonian to early Priabonian times. Same legend as in Figure 3.5. Sedimentation rates in the Jaca basin from *Hogan & Burbank* (1996) reinterpreted by *Costa et al.* (2010) and, in the Ainsa basin from *Bentham* (1992) and *Mochales et al.* (2012b).

Page 181 – Figure 3.7- Tectonosedimentary evolution of the South-Central Pyrenees for Late Priabonian times. Same legend as in Figure 3.5. Sedimentation rates in the Jaca basin from *Hogan & Burbank* (1996) reinterpreted by *Costa et al.* (2010) and, in the Ainsa basin from *Bentham* (1992). Data from the Oliana anticline from *Sussman et al.*, (2004), *Vergés* (1993), *Burbank et al.* (1992) and *Burbank & Vergés* (1994).

Page 182 – Figure 3.8 - Tectonosedimentary evolution of the South-Central Pyrenees for Oligocene times. Same legend as in Figure 3.5. Data from the Oliana-Comiols area from *Vergés* (1993) and *Burbank et al.* (1992). Alluvial systems in the western sector, from *Luzón et al.* (2005). Sedimentation rates for the Jaca basin from *Hogan & Burbank* (1996) reinterpreted by *Costa et al.* (2010)

Pages 185 to 191 – Table S3.3- Detailed information for sites in Figure 3.3

SUPPLEMENTARY MATERIAL 1 – MAGNETOSTRATIGRAPHIC SECTIONS

Page 205 – Figure S1.1- A) Simplified geological map of the South-Central Pyrenees. Modified from *Beamud et al.*(2003). La Pobla de Segur, Senterada and Sis conglomeratic bodies are highlighted in red. **B)** Stratigraphy of the La Pobla de Segur and Senterada basins and location of the magnetostratigraphic sections. (Modified from *Mellere*, 1992)

Page 206 – Figure S1.2- Location of the magnetostratigraphic section CJ in Sis. (Modified from *Vincent*, 1993)

Page 207 to 210 – Table BM: Boumort magnetostratigraphic section (BM), coordinates, sample, stratigraphic level (m), Dg: declination in geographic coordinates, Ig: inclination in geographic coordinates, Ds: declination in stratigraphic coordinates; Is: inclination in stratigraphic coordinates; latp: paleolatitude of the virtual geomagnetic pole, int: intensity; error, quality, Trange: temperature of the characteristic component, comments: temperature interval used to calculate the characteristic component.

Page 211 to 213 – Table CL: Claverol magnetostratigraphic section (CL), coordinates, sample, Gcmean N: number of demagnetization circles used to calculate the characteristic component, stratigraphic level (m), Dg: declination in geographic coordinates, Ig: inclination in geographic coordinates, Ds: declination in stratigraphic coordinates; Is: inclination in stratigraphic coordinates; latp: paleolatitude of the virtual geomagnetic pole, int: intensity; error, quality, Trange: temperature of the characteristic component, comments: temperature interval used to calculate the characteristic component.

Page 214 to 217 – Table CS: Carretera de Sort magnetostratigraphic section (CS), coordinates, sample, N: number of demagnetization circles used to calculate the characteristic component, stratigraphic level (m), Dg: declination in geographic coordinates, Ig: inclination in geographic coordinates, Ds: declination in stratigraphic coordinates; Is: inclination in stratigraphic coordinates; latp: paleolatitude of the virtual geomagnetic pole, int: intensity; error, quality, Trange: temperature of the characteristic component, comments: temperature interval used to calculate the characteristic component.

Page 218 to 219 – Table CG: Can Gramuntill magnetostratigraphic section (CG), coordinates, sample, N: number of demagnetization circles used to calculate the characteristic component, stratigraphic level (m), Dg: declination in geographic coordinates, Ig: inclination in geographic coordinates, Ds: declination in stratigraphic coordinates; Is: inclination in stratigraphic coordinates; latp: paleolatitude of the virtual geomagnetic pole, int: intensity; error, quality, Trange: temperature of the characteristic component, comments: temperature interval used to calculate the characteristic component.

Page 220 to 222 – Table RQ: Rocs de Queralt magnetostratigraphic section (RQ), coordinates, sample, N: number of demagnetization circles used to calculate the characteristic component, stratigraphic level (m), Dg: declination in geographic coordinates, Ig: inclination in geographic coordinates, Ds: declination in stratigraphic coordinates; Is: inclination in stratigraphic coordinates; latp: paleolatitude of the virtual geomagnetic pole, int: intensity; error, quality, Trange: temperature of the characteristic component, comments: temperature interval used to calculate the characteristic component.

Page 223 to 224 – Table MS: Montsor magnetostratigraphic section (MS), coordinates, sample, stratigraphic level (m), Dg: declination in geographic coordinates, Ig: inclination in geographic coordinates, Ds: declination in stratigraphic coordinates; Is: inclination in stratigraphic coordinates; latp: paleolatitude of the virtual geomagnetic pole, int: intensity; error, quality, Trange: temperature of the characteristic component, comments: temperature interval used to calculate the characteristic component.

Page 225 to 228 – Table LP: La Pobleta magnetostratigraphic section (LP), coordinates, sample, stratigraphic level, Dg: declination in geographic coordinates, Ig: inclination in geographic coordinates, Ds: declination in stratigraphic coordinates; Is: inclination in stratigraphic coordinates; latp: paleolatitude of the virtual geomagnetic pole, int: intensity; error, quality, Trange: temperature of the characteristic component, comments: temperature interval used to calculate the characteristic component.

Page 229 to 231 – Table MC: Montcortés magnetostratigraphic section (MC), coordinates, sample, stratigraphic level, Dg: declination in geographic coordinates, Ig: inclination in geographic coordinates, Ds: declination in stratigraphic coordinates; Is: inclination in stratigraphic coordinates; int: intensity; latp: paleolatitude of the virtual geomagnetic pole, error, quality, Trange: temperature of the characteristic component, comments: temperature interval used to calculate the characteristic component.

Page 232 to 239 – Table CJ: Cajigar magnetostratigraphic section (CJ), coordinates, sample, stratigraphic level (m), composite stratigraphic level (m), Dg: declination in geographic coordinates, Ig: inclination in geographic coordinates, Ds: declination in stratigraphic coordinates; Is: inclination in stratigraphic coordinates; int: intensity; latp: paleolatitude of the virtual geomagnetic pole, error, quality.

SUPPLEMENTARY MATERIAL 2 – MAGNETOSTRATIGRAPHY of the PONTILS SECTION

Page 244 – FIGURE 1. Geological map of the eastern Ebro Basin. The position of the cross section A-A* and the lithostratigraphic sketch (Figure 2) are shown. M indicates the Montserrat area, CCR: Catalan Coastal Ranges. Cross section A-A* redrawn from *Anadón et al.* (1987)

Page 245 – FIGURE 2. Lithostratigraphic sketch of the Central Sector of the SE margin of the Ebro Basin. The position of the magnetostratigraphic sections is shown. PO indicates the Pontils fossil locality in the Bosc d'en Borràs Fm, (BdB in this figure), RQ indicates the Rocafort de Queralt fossil locality, LP indicates La Portella Fm, Md indicates the Mediona Fm, C indicates the Cairat Fm and LS indicates the La Salut Fm. Redrawn from *Anadón et al.* (1979) and *Costa et al.* (in press).

Page 246 – FIGURE 3. Stratigraphic section and demagnetization diagrams of selected samples for the different formations.

Page 247 – Figure S2.1- A) Geological map of the central sector of the SE margin of the Ebro Basin (Modified from the ICC 1:250000 map). Red lines represent magnetostratigraphic sections; LT: La Tossa, MM: Santa Maria de Miralles (*Costa et al.*, in press); RQ: Rocafort-Vinaixa (*Barberà et al.*, 2001) and PT: Pontils. B-B*) Cross-section through the study area (modified from *Anadón et al.*, 1987). Location of mammal fossil sites PT (Pontils, MP15) and RQ (Rocafort de Queralt, MP19-20) is indicated.

Page 248 – Figure S2.2- Location of the paleomagnetic sites, in white, and the mammal fossil sites Pontils (PT) and Rocafort de Queralt (RQ), in yellow. Bedding dips are also represented in yellow.

Page 249 – Figure S2.3- Stratigraphic log for the Pontils section and demagnetization diagrams of selected samples from the different formations. Black (white) dots represent projection of the demagnetization vector end-point into the horizontal (vertical) plane. Thermal demagnetization in all cases, temperatures are shown in the diagrams. ABC: after bedding correction

Page 250– Figure S2.4- Local magnetostratigraphy of the Pontils section and correlation to the GPTS (*Gradstein et al.*, 2004). The RQ site was previously dated by magnetostratigraphy as Priabonian (*Barberà et al.*, 2001). With the proposed correlation, the Pontils fossil site correlates to chron 19n (Upper Lutetian).

Abstract

Resum Extens en Català

ABSTRACT

This PhD Thesis presents the Tertiary kinematic evolution of the South-Central Pyrenees from the integration of magnetostratigraphic, magnetotectonic and thermochronological analyses on its synorogenic sedimentary record. The integration of these datasets permits unravelling the interplay between thrust emplacement, deposition in the adjacent basins and exhumation and denudation in the interior of the orogen.

One of the main contributions of this PhD thesis is the continuous absolute dating of the syntectonic conglomerates of La Pobla de Segur, Senterada and Sis. Magnetostratigraphy of these synorogenic materials establishes their deposition during Middle Eocene-Late Oligocene times (from chron 19r up to chron 9n). Integration of these results with previous magnetostratigraphic works within the Ainsa Basin has allowed the establishment of a new chronostratigraphy for the Eocene-Oligocene materials of the South-Central Pyrenees.

The obtained chronostratigraphy has biochronological implications as it substantially changes the traditionally accepted ages of the European reference levels MP14 to MP17. The South Pyrenean and Ebro basin fossil localities attributed to MP14 to MP17 reference levels would be significantly older than previously considered. MP14 and MP15 reference levels are proposed to correlate to Lutetian whereas MP16 and MP17 would be Bartonian in age. These results challenge the currently accepted Eocene marine-continental correlations in Europe but are not in conflict with the available biostratigraphic data of other western European reference basins. These results also reveal that the correlation between the continental and marine Paleogene record needs further refinement and therefore, that the chronostratigraphic age attributions based on MP reference levels should be taken with caution.

The magnetostratigraphic ages have been combined with detrital thermochronology on 13 granitic cobbles contained within the syntectonic conglomerates. The detrital apatite fission track ages obtained vary from 63 to 27 Ma. When these ages are combined with the stratigraphic ages, samples define 5 groups with thermochronological ages generally increasing down-section except in the most deeply buried ones due to post-depositional partial annealing. Thermal models reveal three periods of rapid-cooling within the Axial Zone: two well-defined periods around 50-40 Ma (exhumation rates around 0.2-0-3 km/My), and 30-25 Ma (exhumation rates higher than 1 km/My); and a poorly defined period around 70-60 Ma with exhumation rates around 0.2 km/My. These results, together with the available information of in-situ thermochronological data of the source region, reveal that these materials represent the stratigraphic record of the most intense period of exhumation in the

interior of the orogen due to movement on large-thrust sheets. The dramatic increase in exhumation rate occurred during the latest Eocene-Early Oligocene would be related to the onset of movement in the Rialp thrust sheet and the increase in structural relief of the Axial Zone by underthrusting. The magnetostratigraphic and thermochronological ages obtained permit the link between the sedimentation rates in the surrounding basins and the exhumation rates in the hinterland, and reveal that accommodation space exerted the main control on sedimentation rates within the piggy-back basins. Post-depositional annealing of the stratigraphically lowest samples suggests about 2 km of burial by the younger synorogenic materials during progressive burial of the South Pyrenean fold and thrust belt. Thermal models also suggest a rapid exhumation event during the Late Neogene, linked to re-excavation caused by the base level drop during the Ebro River capture to the Mediterranean Sea.

Sedimentation of the studied synorogenic materials during Middle Eocene-Oligocene times occurred coeval to the development of thrust salients in the southern Pyrenees. Among them the most significant one is defined by the N-S trending structures of the Ainsa Oblique Zone. The magnetotectonic study of 36 sites carried out in the Ainsa Oblique Zone reveal clockwise vertical-axis rotations varying from ~80° in the lower Lutetian materials of the Mediano anticline to ~20° in middle Ilerdian materials cropping out at the northern edge of the Añisclo anticline. Sites in the central part of the Montsec and Bóixols thrust sheets don't record any significant rotation as neither do the syntectonic materials of La Pobla, Sis and Senterada. An axial surface of rotation can be traced coinciding with the eastern edge of the circular bend connecting the N-S trending structures of the Ainsa Oblique Zone and the western edge of the Montsec thrust sheet with the E-W to WNW-ESE structural trend further east. The amount of CW vertical-axis rotation depends also on the age of the sampled sediments. The highest values of rotation have been recorded by the Lower Eocene sediments and these values generally decrease with age. The age of the main rotation event within the Gavarnie thrust sheet is constrained to Lutetitan to Bartonian times, when all the structures of the Ainsa Oblique Zone were active. This vertical-axis rotation stage obeys to a difference of about 50 km in the amount of displacement on the Gavarnie thrust sheet controlled by the NE-SW pinch out of the Triassic salts at its basal detachment. A second rotation event of at least 10° took place since Priabonian times, as a result of the differential displacement of about 22 km of the Serres Marginals thrust sheet, respect the Gavarnie one, on top of the upper Eocene-Oligocene evaporites. The synchronicity between thrusting and vertical-axis rotations suggests that the curved fold and thrust belt formed by progressive curvature with divergent thrust transport.

The results exposed in this Thesis reveal a strong relationship between the stratigraphic record of the synorogenic materials, thrusting and exhumation in the Axial Zone and the structural evolution of the South Pyrenean thrust system. Tectonic forces controlled the observed patterns of exhumation, the evolution of the synorogenic topography of the piggy-back and foreland basins and the depositional features of the synorogenic sediments.

RESUM EXTENS EN CATALÀ

R1. MOTIVACIÓ i OBJECTIUS

L'estudi dels materials sinorogènics proporciona informació molt valuosa sobre els processos que tenen lloc durant el creixement orogènic, ja que permeten relacionar l'exhumació i denudació de les parts internes de l'orogen amb la sedimentació a les conques adjacents. Les relacions geomètriques entre les estructures tectòniques i els materials sinorogènics proporcionen una cronologia relativa dels esdeveniments que van tenir lloc durant la seva sedimentació. No obstant, la cronologia i taxes precises d'aquests processos només es poden aconseguir quan es disposa d'edats absolutes. La magnetostratigrafia és una eina molt útil per datar successions continentals de manera contínua. Sèries magnetostratigràfiques suficientment llargues i mostrejades amb prou densitat proporcionen un patró d'inversions prou característic com per correlacionar-lo amb l'escala de temps de polaritat geomagnètica (ETPG) de manera inequívoca i independent d'altra informació cronològica. Una vegada aconseguida una datació absoluta contínua dels materials sintectònics, l'edat i quantificació dels processos tectònics ocorreguts durant la seva sedimentació es pot obtenir ràpidament. De manera semblant, les edats proporcionades per la termocronologia detrítica afegeixen informació a l' exhumació i història tectònica de l'àrea font així com els canvis en la procedència dels sediments i en l'evolució del relleu. A més, les edats relatives entre els encavalcaments i les rotacions d'eix vertical contribueixen a la construcció de models cinemàtics pels cinturons de plecs i encavalcaments. Models cinemàtics que compleixin les evidències geològiques d'una àrea són necessaris per a la correcta restitució de les estructures geològiques, especialment quan les estructures que s'han de restituir són obliqües a la direcció estructural de l'orogen, ja que el material es transporta fora del pla de transport regional.

Els materials sinorogènics rarament es preserven a l'interior dels orogens, bé sigui perquè no s'hi acumulen o perquè son erosionats. Generalment es dipositen en les conques d'avant-país no deformades i, eventualment, en conques *piggy-back* de les làmines encavalcants frontals. Els Pirineus són una serralada muntanyosa ben coneguda entre la comunitat geològica per l'excepcional estat de conservació dels sediments sinorogènics a la vessant sud. Les altes taxes de subsidència associades a les conques intramontanyoses dels Pirineus sud-centrals i el caràcter endorreic de la conca d'avantpaís de l'Eocè superior fins al

Miocè mig (*Coney et al.,* 1996; *Costa et al.*, 2010) van afavorir la inusual i excel·lent conservació dels materials sinorogènics.

L'objecte d'estudi de la present Tesi Doctoral son els materials terciaris sintectònics de la Zona Central Sudpirinenca: conglomerats de la Pobla de Segur/Senterada (*Rosell & Riba*, 1966; *Mellere*, 1992) i Serra de Sis (*Vincent*, 1993) i els materials eocens de la conca d'Ainsa (*Barnolas & Gil-Peña*, 2001).

Els motius per estudiar aquests materials són diversos. Estudis previs en els materials sintectònics dels Pirineus Centre-meridionals van permetre deduir les relacions tectònica-sedimentació i establir una cronologia relativa de la seqüència de deformació i de l'evolució de les zones internes de l'orogen durant la seva sedimentació (*Mellere & Marzo*, 1992; *Mellere*, 1993).No obstant, els conglomerats de La Pobla de Segur/Senterada i de la serra de Sis disposaven d'una cronologia poc precisa que assignava a la part mitjana de la successió estratigràfica una edat eocena superior, per correlació de dades biostratigràfiques puntuals amb el nivell de referència MP17 de l'escala biocronològica de mamífers continentals (atribuïda al Priabonià) (*Casanovas*, 1975; *López-Martínez*, 1998). Restaven, per tant, moltes incerteses sobre l'edat de bona part de la successió sedimentària. En conseqüència, la majoria dels conglomerats que recobrien discordantment les estructures que afecten els sediments mesozoics i eocens es van considerar oligocens (*Rosell & Riba*, 1966; *Robles*, 1984; *mapa geològic de Catalunya 1:250000*, 1989, 2002). D'altra banda, la biocronologia de mamífers europeus està basada majoritàriament en sèries continentals curtes no correlacionables amb sèries marines amb major control biocronològic o bé, en rebliments càrstics que presenten seriosos problemes de correlació. Per tant, la correlació dels diferents nivells de referència amb l'escala de temps pot requerir en molts casos una revisió.

Els materials sinorogènics objecte d'estudi enregistren tant els darrers estadis de transport de les làmines encavalcants de les unitats sudpirinenques com l'inici de la ràpida exhumació de la Zona Axial de l'orogen (*Fitzgerald et al.*, 1999). En els darrers anys s'han dut a terme nombrosos estudis termocronològics en les zones internes dels Pirineus centrals que han aportat informació sobre la exhumació associada a l'activitat dels diferents encavalcaments de la Zona Axial i han revelat una exhumació major i més recent en el vessant sud de l'orogen (*Morris et al.*, 1998; *Fitzgerald et al.*, 1999; *Sinclair et al.*, 2005; *Gibson et al.*, 2007; *Metcalf et al.*, 2009). Els models realitzats a partir d'aquesta extensa base de dades termocronològica (*Fillon & van der Beek*, 2012) precisen la història de l'exhumació dels

Pirineus meridionals ocorreguda a partir dels 40 Ma i revelen que els canvis al nivell de base de la conca d'avantpaís de l'Ebre van controlar la seva evolució postorogènica. Aquests estudis, no obstant, se centren en la termocronologia obtinguda en els massissos granítics de les zones internes, pel que el registre és incomplet per l'erosió dels materials a mida que es van exhumar. La termocronologia detrítica pot completar la història de l'exhumació i reconstruir l'evolució de les xarxes de drenatge, ja que aporta informació de les parts erosionades a les zones internes i preservades a les conques adjacents (*Whitchurch et al.*, 2011). La termocronologia detrítica aplicada a gresos de dues conques *piggy-back* dels Pirineus Sud-Centrals (*Fillon et al.*, 2013) xifra la potència i extensió dels sediments de l'Eocè superior-Oligocè que van cobrir el cinturó de plecs i encavalcaments en 0.7-1.6 km i la seva posterior re-excavació durant el Miocè. Aplicant termocronologia detrítica en els clastes de granit continguts en els conglomerats sinorogènics objecte d'estudi podem obtenir informació de la part erosionada dels massissos granítics que constituïen la seva àrea font, estenent per tant el registre de l'evolució de la Zona Axial pirinenca.

La sedimentació durant l'Eocè mig-Oligocè dels materials sinorogènics estudiats coincideix amb un gradient en el desplaçament dels encavalcaments a les làmines encavalcants responsables de les estructures oblíqües i *thrust salients* de la zona central sudpirinenca. Entre ells, el més important es localitza a la part oest dels Pirineus centrals, a la zona d'Ainsa, o a on abunden estructures que mostren una orientació molt obliqua respecte la direcció de les estructures principals pirinenques. Així els anticlinals de Boltaña, Añisclo o Mediano presenten una orientació N-S, que contrasta amb la traça E-W de la resta d'estructures. Aquesta zona ha estat objecte de nombrosos estudis, sobre tot paleomagnètics, per tal d'entendre l'origen d'aquesta obliqüitat, identificant i quantificant les rotacions d'eix vertical que han tingut lloc a la zona (*Dinarès-Turell*, 1992; *Pueyo*, 2000; *Mochales et al.*, 2012). No obstant, la seva cronologia i cinemàtica encara no s'havien establert amb precisió.

Per tant, els principals objectius d'aquesta Tesi Doctoral són:

I) Establir una cronologia absoluta contínua pels conglomerats de la Pobla de Segur, Senterada i Serra de Sis mitjançant datació magnetostratigràfica.

II) Establir una cronostratigrafia integrada pels materials eocens de la zona central Sudpirinenca correlacionant els resultats obtinguts al sector de La Pobla de Segur-

Senterada i Sis amb altres sèries magnetostratigràfiques existents a la zona d'Ainsa (*Bentham*, 1992; *Mochales et al*., 2012; *Rodríguez-Pintó et al.*, 2012).

III) Revisar la calibració de l'escala biocronològica de mamífers continentals del Paleogen (nivells de referencia MP) a partir de les sèries magnetostratigràfiques realitzades a la zona central Sudpirinenca i d'altres sèries a la conca de l'Ebre.

IV) Establir la termocronologia dels conglomerats sintectònics a partir de l'estudi de les traces de fisió en apatits dels blocs de granit derivats de la Zona Axial continguts en els conglomerats.

V) Relacionar el patró de deformació de les zones internes de l'orogen amb la sedimentació a les conques adjacents mitjançant la integració de dades magnetostratigràfiques i termocronològiques. Obtenir i relacionar taxes d'exhumació i de sedimentació.

VI) Precisar l'origen de les estructures oblíqües de la zona d'Ainsa a partir de l'estudi de les rotacions d'eix vertical i la seva integració amb altres dades paleomagnètiques disponibles i establir un model cinemàtic per a la zona Central Sudpirinenca.

R2. ESTRUCTURA de la MEMÒRIA de TESI

Aquesta Tesi Doctoral, organitzada en 4 capítols, es presenta sota la modalitat de compilació d'articles de recerca publicats i/o enviats a revistes pertanyents al *Journal Citation Report* de *l'Institute for Scientific Information*. Les tres publicacions presentades resumeixen gran part del treball científic dut a terme durant la realització d'aquesta tesi doctoral.

El **capítol 1** és un capítol introductori en el que es descriu el context geològic de la zona d'estudi, el seu marc estratigràfic i les metodologies utilitzades per aconseguir els objectius d'aquesta tesi (Paleomagnetisme i Termocronologia detrítica de traces de fisió) i la Biocronologia de mamífers continentals paleogens.

El **capítol 2** constitueix el cos principal de la tesi i està format per dos articles publicats i un tercer article recentment acceptat per publicació.

El **capítol 2.1** l'integra l'article ***Beamud, E., Garcés, M., Cabrera, L., Muñoz, J.A., Almar, Y. (2003) A new Middle to Late Eocene chronostratigraphy for NE Spain. Earth and***

Planetary Science Letters **216, 501-514.** En aquest article es presenta una nova cronostratigrafia per les unitats eocenes continentals dels Pirineus Sud-Centrals. Aquesta cronostratigrafia es basa en la integració de la datació magnetostratigràfica dels conglomerats de la Pobla de Segur i de la Serra de Sis amb la cronologia establerta prèviament pels materials continentals de la zona d'Ainsa (Fm. Escanilla). L'edat dels conglomerats de La Pobla de Segur s'havia atribuït en base als jaciments de mamífers presents a les sèries i la seva assignació al nivell de referència MP17 de l'escala biocronològica de mamífers Paleògens (nivells MP), atribuït al Priabonià. Els resultats de la correlació de les sèries magnetostratigràfiques amb l'escala de temps de polaritat geomagnètica, basada en el patró d'inversions obtingut, assigna a aquests materials una edat considerablement més antiga. Conseqüentment, l'edat dels jaciments i la del nivell de referència al que s'associen també es veu modificada per aquests resultats. En aquest article, per tant, es presenta una nova cronostratigrafia pels conglomerats sintectònics de La Pobla de Segur i la serra de Sis i la seva integració amb la cronologia prèviament establerta pels conglomerats de la zona d'Ainsa, així com una proposta de calibració de les MP's 14 a 17 derivada de la nova cronologia.

El **capítol 2.2** està format per l'article ***Beamud, E., Muñoz, J.A., Fitzgerald, P.G., Baldwin, S.L., Garcés, M., Cabrera, L., Metcalf, J.R. (2011) Magnetostratigraphy and detrital apatite fission track thermochronology in syntectonic conglomerates: constraints on the exhumation of the South-Central Pyrenees.*** ***Basin Research*** **23, 309-331.** En aquest article es combina la datació magnetostratigràfica dels conglomerats sintectònics continentals amb dades de termocronologia de traces de fisió en apatits procedents de clastes d'aquests mateixos materials. La datació magnetostratigràfica presentada al capítol 2.1 es completa en aquest treball amb la datació magnetostratigràfica dels conglomerats de la subconca de Senterada. Les noves dades estenen el registre de la sedimentació en conques situades a les parts internes de la serralada dins de l'Oligocè, disposant doncs d'una cronologia contínua pels conglomerats del Lutecià al Rupelià. D'altra banda, la distribució de les edats de les traces de fisió i les seves longituds al llarg de les sèries estudiades junt amb les seves edats deposicionals han aportat informació sobre el moment i taxes dels episodis d'exhumació de l'orogen i la resposta sedimentària associada a les conques adjacents.

El **capítol 2.3** conté l'article ***Muñoz, J.A., Beamud, E., Fernández, O., Arbués, P., Dinarès-Turell, J., Poblet, J. The Ainsa Fold and Thrust Oblique Zone of the Central Pyrenees: kinematics of a curved contractional system from paleomagnetic and structural data.***

***Tectonics* (en premsa)**. En aquest article es presenta un model cinemàtic per les estructures N-S de la Zona Obliqua d'Ainsa i l'origen de la curvatura dels Pirineus centrals. Tot i que nombrosos estudis previs havien identificat rotacions d'eix vertical en sentit horari en els materials eocens de la conca d'Ainsa, no es disposava d'un model cinemàtic consistent entre els diferents estudis degut, principalment, a la manca d'integració amb dades estructurals i sedimentològiques. El nou model presentat en aquest treball integra les dades paleomagnètiques (noves i preexistents) amb dades estructurals i sedimentològiques obtenint un model coherent amb tota la informació disponible.

El **capítol 3** inclou una síntesi i discussió dels resultats obtinguts, articulada en tres apartats:

3.1 - Cronostratigrafia dels materials sintectònics Terciaris de la zona Central Sudpirinenca

3.2 – Implicacions biocronològiques

3.3 – Implicacions cinemàtiques i tectonosedimentàries

Finalment, el **capítol 4** recull les principals conclusions derivades d'aquesta Tesi Doctoral.

R3. PALEOMAGNETISME als PIRINEUS CENTRE-MERIDIONALS

En aquesta tesi doctoral s'ha aplicat el Paleomagnetisme amb dos objectius diferents, la datació magnetostratigràfica per una banda i la magnetotectònica (identificació de rotacions d'eix vertical), per l'altra. A continuació es resumeixen els principals resultats obtinguts.

R3.1. MAGNETOSTRATIGRAFIA dels MATERIALS SINTECTÒNICS

Per a la datació magnetostratigràfica s'han realitzat 3 sèries magnetostratigràfiques compostes: La Pobla, Senterada i Sis (integrades pels perfils CL, CS, CG, RQ i MS a la conca de la Pobla, CJ a Sis i LP i MC a Senterada; veure Annex 1). Aquests perfils comprenen la part alta de l'al·logrup Pessonada i els al·logrups Ermita, Pallaresa i Senterada (*Mellere*, 1992) a la conca de la Pobla/Senterada i les formacions Cajigar, Cornudella i Sis (fins a la base del membre Sis 2) (*Vincent*, 1993) a la zona de Sis. En total, s'han mostrejat més de 700 estacions en aproximadament 2000 m de successió estratigràfica, el que dóna una resolució de 2-3 m entre estacions. La correlació de les diferents sèries amb l'escala de temps de polaritat

geomagnètica (ETPG) (*Cande & Kent*, 1995; *Gradstein et al.*, 2004) (Figura 4 del capítol 2.1; Figura 5, del capítol 2.2) s'ha basat fonamentalment en el patró d'inversions obtingut en les magnetostratigrafies locals i en les relacions estratigràfiques dels diferents materials mostrejats. A partir d'aquesta correlació, l'edat dels conglomerats de La Pobla de Segur s'estableix en Lutecià-Priabonià (cron 19r a cron 13r), els conglomerats de Senterada s'haurien dipositat íntegrament durant l'Oligocè (cron 12r a cron 9n) i els conglomerats de Sis mostrejats tindrien una edat Lutecià-Bartonià (cron 19r a cron 18n).

R3.2. MAGNETOTECTÒNICA

L'anàlisi de les rotacions d'eix vertical procedeix de dues aproximacions diferents, el mostreig d'estacions paleomagnètiques discretes a la zona oblíqua d'Ainsa i el càlcul de les direccions mitjanes de les mostres de bona qualitat dels perfils magnetostratigràfics de La Pobla, Senterada i Sis (Figures 2 i 3 del capítol 2.3; Figura 3.3 i taula S3.3 del capítol 3.3).

Les direccions mitjanes obtingudes dels perfils magnetostratigràfics no són significativament diferents de les direccions de referència per l'Eocè i l'Oligocè, del que es dedueix que en aquestes zones no es van produir rotacions d'eix vertical del Lutecià a l'Oligocè. A la zona de La Pobla de Segur i Senterada, aquests resultats concorden amb estudis previs que tampoc identificaven rotacions d'eix vertical en els materials mesozoics (*Dinarès-Turell*, 1992) i eocens inferiors de la zona (*Pascual et al.*, 1992) i no resulten sorprenents donada la seva posició en la Zona Central Sudpirinenca, sense cap estructura obliqua que les afecti. En canvi, a la zona de Sis, l'absència de rotació significativa en els conglomerats lutecians-bartonians contrasta amb els prop de 30° de rotació horària que enregistren els materials infrajacents (*Dinarès-Turell*, 1992). La manca de rotació en els conglomerats de Sis, permet acotar l'edat de la rotació en aquest sector entre el Cuisià i el Lutecià.

A la zona oblíqua d'Ainsa, en canvi, s'han mostrejat 36 estacions paleomagnètiques discretes, amb unes 12 mostres per estació; estacions que se sumen a l' abundant base de dades paleomagnètica existent en aquest sector. L'objectiu d'aquestes estacions és explicar l'origen de l'obliqüitat de les estructures de la zona d'Ainsa (anticlinals d'orientació N-S de Boltaña, Añisclo o Mediano). Els resultats per aquest sector revelen rotacions d'eix vertical en sentit horari que varien dels ~80° als materials del Lutecià inferior de l'anticlinal de Mediano als ~20°dels materials de l'Ilerdià mig que afloren al límit nord de l'anticlinal d'Añisclo. El marc

cronostratigràfic per aquest sector (*Bentham*, 1992; *Mochales et al.*, 2012; *Rodríguez-Pintó et al.*, 2012) permet conèixer amb precisió quan van tenir lloc aquestes rotacions, amb rotacions d'entre 45 i 60° entre el Lutecià inferior i el Bartonià superior. Aquesta rotació obeeix a una diferència de 50 km en el desplaçament de la làmina encavalcant de Gavarnie, causada per la distribució de les sals triàsiques al seu desenganxament basal. La sincronia entre els encavalcaments i les rotacions d'eix vertical suggereixen un model d'arc progressiu degut a l'emplaçament divergent dels encavalcaments per explicar l'origen de la curvatura de la Zona Obliqua d'Ainsa. Els problemes d'espai que ocasionà aquesta rotació es van resoldre mitjançant la formació de falles extensives transversals i diapirs en els arcs externs. La translació de la lamina encavalcant de Serres Marginals al damunt de l'avantpaís a partir del Priabonià va afegir una rotació secundària d'uns 10° al sector occidental.

R4. TERMOCRONOLOGIA DETRITICA

Els resultats de la datació magnetostratigràfica dels conglomerats sintectònics estudiats que s'acaben de presentar (Lutecià superior-Oligocè superior) indiquen que aquests materials es van dipositar durant un període d'intensa activitat tectònica a l'orogen i no durant els darrers estadis de l'estructuració pirinenca, com s'havia considerat clàssicament. Per tant, el seu estudi termocronològic pot aportar informació molt important sobre els processos que tenien lloc a l'interior de l'orogen durant la seva sedimentació.

Els estudis termocronològics de perfils verticals en els massissos rocosos proporcionen una informació de l'evolució de l'orogen que pot resultar parcial, ja que una bona part de la història termotectònica de la roca ha estat eliminada per la pròpia erosió del massís durant la seva exhumació. Si el producte d'aquesta erosió queda preservat en les conques sedimentàries adjacents, és possible aplicar termocronologia detrítica al llarg de la successió sedimentària per tal d'estendre el registre i completar la història termotectònica de l'àrea font. Aquest és el cas de les conques intramontanyoses sudpirinenques, a on hi ha preservats productes de l'erosió de les zones internes de la serralada. Durant el desenvolupament d'aquesta tesi doctoral s'han estudiat les traces de fisió en apatits procedents de blocs de granits erosionats de la Zona Axial pirinenca i incorporats com a clastes en els conglomerats sintectònics estudiats. En total s'han estudiat 13 mostres de blocs de granit a Sis i La Pobla de Segur/Senterada (Figures 1 i 5 i taula 1 capítol 2.2). Les edats de traces de fisió obtingudes varien de 63 a 27 Ma (Taula 1, capítol 2.2). Algunes de les edats termocronològiques

obtingudes són considerablement més antigues que les edats termocronològiques publicades pels massissos granítics que afloren actualment a la Zona Axial, indicant l'erosió des de nivells de l'escorça més alts que els que afloren actualment o bé des de massissos completament erosionats. La majoria de les mostres de granit estudiades procedeixen de les sèries mostrejades per magnetostratigrafia, pel que es disposa d'un bon control de la seva edat deposicional. Combinant les edats termocronològiques i deposicionals, les mostres formen 5 grups (Figura 6, capítol 2.2) que reflecteixen variacions en la taxa d'exhumació al llarg del temps amb valors que augmenten de < 0.15 km/My a 0.3 km/My i taxes superiors al km/My en les mostres estratigràficament més altes. Els models tèrmics revelen dos períodes ben definits de refredament a la Zona Axial a ~ 50-40 Ma i ~ 30-25 Ma, amb un altre període pitjor definit al voltant de 70-60 Ma. Aquests models suggereixen també que les mostres inferiors de la serra de Sis van experimentar *annealing* parcial postenterrament i un event de refredament postorogènic durant el Miocè.

R5. CRONOSTRATIGRAFIA dels MATERIALS SINTECTÒNICS dels PIRINEUS CENTRALS

Una de les principals contribucions d'aquesta tesi doctoral és la datació absoluta i contínua dels materials sintectònics de La Pobla de Segur/Senterada i Sis (capítols 2.1 i 2.2). La integració de la nova cronologia obtinguda en el marc cronostratigràfic previ de la zona central sudpirinenca (*Barnolas & Gil-Peña*, 2001; *Bentham*, 1992; *Mochales et al.*, 2012; *Rodríguez-Pintó et al.*, 2012), ha permès l'establiment d'una nova cronostratigrafia pels materials eocens i oligocens dels Pirineus Centre-meridionals (Figura 3.1 del capítol 3). En el nou marc cronostratigràfic, els materials més antics de la conca de la Pobla de Segur (al·logrup Pessonada), dipositats durant el Lutecià, serien equivalents laterals dels conglomerats de la Fm. Gurp i parcialment equivalents als materials de la Fm. Cajigar i de les Fm. Capella i Sobrarbe. Per damunt, els materials bartonians dominantment lacustres de l'al·logrup Ermita es correlacionen amb els materials, també predominantment lacustres, de la Fm. Cornudella i, parcialment amb els materials deltaics de la Fm. Sobrarbe i els nivells basals de la Fm. Escanilla a la zona d'Ainsa. Els conglomerats de l'al·logrup Pallaresa tenen els seus equivalents laterals en els conglomerats de les Fms. Sis i Escanilla i s'haurien acumulat entre el Bartonià i el Priabonià. Els conglomerats dels al·logrup Senterada i Antist, dipositats durant l'Oligocè, es correlacionen amb la Fm. Collegats de la serra de Sis i els conglomerats de Graus. L'edat i rang de la discordança per sota dels conglomerats oligocens varia d'est a oest. A la zona de La Pobla la discordança abraça els crons C13r i C12r, representant 2 milions d'anys sense registre

aproximadament, mentre que a la zona d'Ainsa, la manca de registre començaria a sostre del C15n (darrers nivells datats per Bentham, 1992) i finalitzaria a l'inici de l'Oligocè, tot i que la datació en aquesta zona no és massa precisa.

R6. IMPLICACIONS BIOCRONOLÒGIQUES

La nova cronostatigrafia presentada per als materials eocens de la Zona Sudpirinenca Central té implicacions en la calibració de l'escala de nivells de referència de mamífers paleogens per Europa occidental (nivells MP). Com s'ha mencionat anteriorment, la sèrie de La Pobla contè jaciments fòssils de mamífers continentals que contenen fauna comparable a la del jaciment Fons 4, que correspon al nivell de referència MP17a, correlacionat classicament amb el Priabonià (*López-Martínez*, 1998). No obstant, la correlació magnetostratigràfica dels perfils de La Pobla, basada en el patró d'inversions, assigna a aquests jaciments una edat Bartoniana (dintre del cron C18r) (Figura 4 del capítol 2.1). A partir d'aquests resultats, s'ha dut a terme una revisió d'altres jaciments de la Zona Sudpirinenca central i de la conca de l'Ebre, amb l'objectiu de precisar la calibració dels nivells de referència als que s'assignen: jaciments de Capella (MP14), Pontils (MP15) i Laguarres (MP16). La proposta de calibració d'aquests nivells de referència amb l'ETPG (*Cande & Kent*, 1995) està recollida a la figura 6 del capítol 2.1. Durant l'elaboració d'aquesta memòria , s'ha actualitzat aquesta figura per l'ETPG del 2004 (*Gradstein et al.*, 2004) i s' hi ha incorporat la informació procedent de la sèrie magnetostratigràfica de Pontils (*Beamud et al.*, 2012; Annex 2) per a la calibració de la MP15, obtenint-se la figura 3.2 del capítol 3 d'aquesta memòria. En la nova proposta de correlació els nivells de referència MP14 i MP15, queden correlacionats amb el Lutecià superior. La localitat de Pontils (MP15) queda, a més, acotada dins del cron C19n (Annex2). El nivell de referència MP17a correspondria al Bartonià inferior, quedant per tant, poc marge de temps per al nivell de referència MP16. Aquests resultats canvien substancialment les correlacions marí-continental d'Europa però no estan en conflicte amb les dades biostratigràfiques disponibles per altres conques de referència europees. Aquests resultats també revelen que la correlació entre els registres marí i continental paleògens necessita més precisió i que les atribucions cronostratigràfiques basades en els nivells de referència MP s'han de prendre amb precaució i revisar-les amb tota la informació lito-, bio- i magnetostratigràfica disponible.

R7. IMPLICACIONS CINEMÀTIQUES I TECTONOSEDIMENTÀRIES

A partir de la integració dels resultats obtinguts mitjançant el paleomagnetisme, tant resultats magnetostratigràfics com magnetotectònics, i la termocronologia de traces de fisió, s'ha pogut deduir l'evolució tectonosedimentària per la zona central sudpirinenca i la Zona Axial de l'orogen. Aquesta evolució s'ha sintetitzat en 4 estadis entre el Lutecià i l'Oligocè, representats a les figures 3.5 a 3.8. A continuació es detallen els principals esdeveniments a la zona d'estudi:

A inicis del Lutecià (~ 48 Ma) la deformació progressa de la làmina de Peña Montañesa-Montsec cap a l'avantpaís per formar la làmina encavalcant de Gavarnie-Serres Marginals. Això causa la transformació de la conca d'Ainsa de *foredeep* a conca *piggy-back*. La sedimentació tenia lloc simultàniament a la deformació del substrat de la conca pel sistema de plecs del Sobrarbe (Figura 3.1). Les taxes de sedimentació durant aquest període són baixes, al voltant de 0.03 km/My per les calcàries de Guara (*Rodríguez-Pintó et al.*, 2012) i 0.07 km/My durant la sedimentació de les turbidites de la Fm. San Vicente (*Mochales et al.*, 2012). Comencen a formar-se en aquest moment els anticlinals de Mediano, Olson i Añisclo amb una orientació ENE-WSW. En aquest moment el sistema d'encavalcaments emergent frontal de la làmina de Gavarnie es localitzava al cinturó de plecs i encavalcaments de Monte Perdido, que connectava amb el sistema d'encavalcaments de La Fueba mitjançant una rampa obliqua que dibuixava un arc primari. (Figura 15c, capítol 2.3). Cap a l'est, la zona de La Pobla de Segur era una zona aixecada en la que no hi havia sedimentació (Figura 3.1). Al nord, la Zona Axial s'estava aixecant a una taxa de ~ 0.3 km/ka amb erosió localitzada a la làmina de Nogueres causada per l'*underthrusting* de la làmina d'Orri.

Durant el Lutecìa mig, al voltant dels 42 Ma, s'inicia el creixement de l'anticlinal de Boltaña com una estructura obliqua a l'encavalcament frontal de la làmina de Gavarnie, amb una traça paral·lela al de Mediano, que ja havia experimentat uns 15° de rotació horària degut a la propagació de la deformació a la làmina de Gavarnie. Les taxes de sedimentació a la conca turbidítica d'Ainsa augmenten fins a valors propers a 0.3 km/My (*Mochales et al.*, 2012). A la zona de La Pobla de Segur i Gurp la generació d'espai d'acomodació davant de l'apilament antiformal de la Zona Axial permet la sedimentació de les formacions Espills i Gurp i dels conglomerats de Pessonada. L'encavalcament de Bóixols es reactiva sincrònicament a l'activitat dels encavalcaments a la zona frontal. Al seu bloc superior es desenvolupen encavalcaments fora-seqüència durant la sedimentació de l'al·logrup Pessonada, tal i com demostra la generació de discordances progressives (*Mellere*, 1992). Al nord, la Zona Axial

continua exhumant-se a una taxa de 0.3 km/My amb erosió localitzada a Nogueres causada per l'*underthrusting* del mantell d'Orri, tot i que l'àrea font principal dels ventalls al·luvials de La Pobla se situa en materials mesozoics de zones properes (*Mellere*, 1992; *Barsó*, 2007)

Entre el Bartonià i el Priabonià (~ 37 Ma) totes les estructures de la zona oblíqua d'Ainsa eren actives amb rotacions horàries de fins a 45° sincròniques al moviment dels encavalcaments i el creixement de les estructures. Aquesta sincronia indica que la curvatura de la zona obliqua d'Ainsa respon a un model d'arc progressiu degut a l'emplaçament d'encavalcaments amb trajectòries divergents. Aquest model requereix una extensió longitudinal que en aquesta zona es resol mitjançant un conjunt de falles normals, d'orientació obliqua a perpendicular, i la formació de diapirs a on el gruix de les sals triàsiques era significativa. En contrast amb la rotació general de la Zona Obliqua d'Ainsa, els materials de Sis i La Pobla de Segur no enregistren rotacions d'eix vertical en aquesta etapa. Per tant pot establir-se una línia llindar de no-rotació que coincideix amb el límit oriental de la traça circular que connecta les estructures N-S de la Zona Obliqua d'Ainsa amb el límit oest de l'encavalcament del Montsec amb una traça E-W cap a l'est (Figura 11, capítol 2.3). Una dràstica i generalitzada reducció de les taxes de sedimentació té lloc a les conques sudpirinenques en aquests moments. Valors tan baixos com 0.05 km/My i 0.16 km/My s'enregistren a la zona de La Pobla i Ainsa, respectivament *(Beamud et al.*, 2003, 2011; *Mochales et al.*, 2012; *Bentham*, 1992). Cap a l'oest, a la conca de Jaca, la taxa de sedimentació se situa al voltant de 0.25 km/My (*Hogan & Burbank*, 1996 reinterprtetat per *Costa et al.*, 2010). Aquests valors revelen un gradient en les taxes de sedimentació d'est a oest. Aquest gradient seria causat per la reducció en l'espai d'acomodació a mida que la deformació progressava cap al SW.

La desconnexió de l'Atlàntic als 36 Ma (*Costa et al.*, 2010) controlà la sedimentació a les conques sudpirinenques durant el Priabonià, creant un solc sedimentari en el que quedava preservat tot el material mentre es frenava el *by-pass* de sediment cap a l'oest. Aquesta nova configuració va provocar un increment generalitzat de les taxes de sedimentació. A la zona de la conca de Jaca, la sedimentació augmenta de 0.25 km/My a 0.63 km/My (*Hogan & Burbank*, 1996 reinterpretat per *Costa et al.*, 2010) i a la zona de La Pobla, les taxes augmenten fins als 0.1 km/My, amb un canvi general de la direcció de les paleocorrents, de predominantment E-W a direccions N-S. El tancament de la conca i el rebliment associat també provoca una migració de la deformació cap a zones internes de l'orogen, manifestada amb l'activitat al

retroencavalcament de Morreres i amb un increment notable de la taxa d'exhumació de la zona Axial, a valors superiors a 1 km/My, degut a l'inici de l'activitat a la làmina de Rialp. En aquest moment no s'enregistren rotacions d'eix vertical a la zona de La Pobla Cap a l'est, té lloc una rotació antihorària de 20° a l'anticlinal d'Oliana associada a la reactivació de la làmina del Montsec i el moviment al llarg de la làmina de Serres Marginals sobre l'avantpaís (*Sussman et al.*, 2004). La translació de la làmina encavalcant de Serres Marginals sobre les sals eocenes superiors durant aquest període afegí una rotació horària d'uns 10° al thrust salient format prèviament a la Zona Obliqua d'Ainsa.

L'Oligocè (~ 31-27 Ma) es caracteritzà per una sedimentació al·luvial generalitzada a les conques sudpirinenques, amb taxes de sedimentació similars a les de l'estadi anterior.. A la zona de La Pobla, l'àrea deposicional principal es traslladà al nord, a la subconca de Senterada, creada al bloc inferior del retroencavalcament de Morreres, sobre la làmina de Nogueres. L'àrea font es localitzava immediatament al nord, a la Zona Axial amb l'erosió de la làmina d'Orri causada per *l'underthrusting* de la de Rialp. Les taxes d'exhumació de la Zona Axial continuaven elevades, superiors a 1 km/My, i causaven l'erosió del massís granític de la Maladeta. Els materials de Senterada no enregistraren rotacions d'eix vertical durant aquesta etapa. La sedimentació al·luvial generalitzada durant l'Oligocè va fossilitzar les estructures tectòniques i va cobrir el front de deformació amb gruixos d'uns 2 km, tal i com es dedueix de l'annealing parcial que van experimentar les mostres estratigràficament més baixes de la zona de Sis (secció 2.2). Models termocronològics recents (*Fillon et al.*, 2013) confirmen el rebliment de la conca de l'Ebre durant l'Oligocè-Miocè, amb l'agradació de fins a 1.6 km de sediments al seu límit nord. Les dades de *Fillon et al.*, (2013) també suggereixen que la conca d'Àger, localitzada sobre el bloc inferior de l'encavalcament del Montsec (Figura 3.8) va estar cobert per uns 2.6 km de conglomerats, bé per l'extensió del sistema d'Osca cap a l'est o pel d'Oliana cap a l'oest (Figura 3.8)

Els models tèrmics presentats a la secció 2.3 indiquen refredament postorogènic durant el Miocè superior. El mecanisme que explicaria aquest esdeveniment d'exhumació seria l'erosió i re-excavació dels materials que enterraven el cinturó de plecs i encavalcaments dels Pirineus meridionals causada per la captura del riu Ebre cap al Mediterrani a partir dels darrers 10 Ma. Els models de *Fillon & van der Beek* (2012) prediuen un descens de l'elevació màxima dels conglomerats i la incisió de les valls dels Pirineus meridionals dels 9 Ma a l'actualitat. Per tant, aquests autors proposen que l'apertura de la conca de l'Ebre va tenir lloc durant el

Tortonià, molt abans del Messinià, com es suggeria prèviament i que el canvi climàtic del Neogen superior/Quaternari va tenir poc efecte en la història erosional postorogènica dels Pirineus meridionals.

Els resultats exposats en aquesta Tesi revelen una forta relació entre el registre estratigràfic dels materials sinorogènics, l'activitat dels encavalcaments i l'exhumació de la Zona Axial i l'evolució estructural del sistema de plecs i encavalcaments dels Pirineus centre-meridionals. Les forces tectòniques van controlar tant els patrons d'exhumació observats com l'evolució de la topografia sinorogènica de les conques *piggy-back* i d'avantpaís i les característiques deposicionals dels sediments sintectònics.

R8. BIBLIOGRAFIA

Barnolas, A. & Gil-Peña, I. (2001). Ejemplos de relleno sedimentario multiepisódico en una cuenca de antepaís fragmentada: La Cuenca Surpirenaica. *Boletín Geológico y Minero*, *112*(3), 17–38.

Barsó, D. (2007). *Análisis de la procedencia de los conglomerados sinorogénicos de La Pobla de Segur (Lérida) y su relación con la evolución tectónica de los Pirineos centro-meridionales durante el Eoceno medio-Oligoceno*. PhD Thesis. Universitat de Barcelona. 209 pp.

Beamud, E., Garcés, M., Cabrera, L., Muñoz, J.A., Almar, Y. (2003). A new Middle to Late Eocene chronostratigraphy for NE Spain. *Earth and Planetary Science Letters*_216, 501-514.

Beamud, E., Muñoz, J.A., Fitzgerald, P.G., Baldwin, S.L., Garcés, M., Cabrera, L., Metcalf, J.R. (2011). Magnetostratigraphy and detrital apatite fission track thermochronology in syntectonic conglomerates: constraints on the exhumation of the South-Central Pyrenees. *Basin Research* 23, 309-331.

Beamud, E., Costa, E., Garcés, M., Marín, M. A., Cabrera, L., Roca, E., & Gómez-Paccard, M. (2012). An integrated Eocene chronostratigraphy for the central sector of the SE margin of the Ebro Basin. *VIII Congreso Geológico de España - Geotemas 13* (p. 350). Oviedo.

Bentham, P. (1992). *The tectono-stratigraphic development of the western oblique ramp of the South-Central Pyrenean thrust system, Northern Spain*. PhD Thesis. University of Southern California. 253 pp.

Cande, S. C., & Kent, D. V. (1995). Revised calibration of the geomagnetic polarity timescale for the Late Cretaceous and Cenozoic. *Journal of Geophysical Research B Solid Earth Planets*, *100*, 6093–6095.

Casanovas-Cladellas, M. L. (1975). Estratigrafía y paleontología del yacimiento ludiense de Roc de Santa (Area del Noguera Pallaresa). *Paleontologia i Evolució*, *10*, 1–158.

Coney, P. J., Muñoz, J. A., Mcclay, K. R. & Evenchick, C. A. (1996). Syntectonic burial and post-tectonic exhumation of the southern Pyrenees foreland fold-thrust belt. *Journal of the Geological Society*, *153*(1), 9–16.

Costa, E., Garcés, M., López-Blanco, M., Beamud, E., Gómez-Paccard, M. & Larrasoaña, J. C. (2010). Closing and continentalization of the South Pyrenean foreland basin (NE Spain): magnetochronological constraints. *Basin Research*, *22*(6), 904-917

Dinarès-Turell, J. (1992), *Paleomagnetisme a les unitats sudpirinenques superiors. Implicacions estructurals*. PhD thesis, Universitat de Barcelona. 462 pp.

Fillon, C., & van der Beek, P. (2012). Post-orogenic evolution of the southern Pyrenees: constraints from inverse thermo-kinematic modelling of low-temperature thermochronology data. *Basin Research*, 24, 418-436.

Fillon, C., Gautheron, C. & van der Beek, P. (2013). Oligocene-Miocene burial and exhumation of the Southern Pyrenean foreland quantified by low-temperature thermochronology. *Journal of the Geological Society, London*, 170, 67-77.

Fitzgerald, P. G., Muñoz, J. A., Coney, P. J. & Baldwin, S. L. (1999). Asymmetric exhumation accross the Pyrenean orogen: implications for the tectonic evolution of a collisional orogen. *Earth and Planetary Science Letters*, *173*(3), 157–170.

Gibson, M., Sinclair, H. D., Lynn, G. & Stuart, F. M. (2007). Late- to post-orogenic exhumation of the Central Pyrenees revealed through combined thermochronological data and modelling. *Basin Research*, *19*(3), 323–334.

Gradstein, F. M., Ogg, J. G., & Smith, A. A. (2004). *A Geologic Time Scale 2004* (p. 589). Cambridge: Cambridge University Press.

Hogan, P. J., & Burbank, D. W. (1996). Evolution of the Jaca piggy-back basin and emergence of the External Sierras, southern Pyrenees. In P. F. Friend & C. J. Dabrio (Eds.), *Tertiary basins of Spain* (pp. 153–160). Cambridge University Press.

López-Martínez, N. (1998). Los yacimientos de mamíferos del Eoceno de la Pobla de Segur. In N. López-Martínez, J. Civis, M. L. Casanovas & R. Daams (Eds.), *Geología y Paleontología del Eoceno de La Pobla de Segur (Lleida)* (pp. 9–17). Universitat de Lleida.

Mapa geològic de Catalunya 1:250000. (1989). Ed. Servei Geològic de Catalunya (SGC) i Institut Geològic de Catalunya (IGC)

Mapa geològic de Catalunya 1:250000, 2ª edició. (2002). Ed. Servei Geològic de Catalunya (SGC) i Institut Geològic de Catalunya (IGC)

Mellere, D. (1992). *I conglomerati di Pobla de Segur: Stratigrafia fisica e relazioni tettonica-sedimentazione*. PhD Thesis. Universita degli studi di Padova. 203 pp.

Mellere, D., & Marzo, M. (1992). Los depósitos aluviales sintectónicos de la Pobla de Segur: alogrupos y su significado tectonoestratigráfico. *Acta Geológica Hispánica*, *27*(1-2), 145–149.

Mellere, D. (1993). Thrust generated back-fill stacking of alluvial fan sequences, south-central Pyrenees, Spain (La Pobla de Segur conglomerates). *Special Publication of the Internal Association of Sedimentology*, *20*, 259–276.

Metcalf, J. R., Fitzgerald, P. G., Baldwin, S. L. & Muñoz, J. A. (2009). Thermochronology of a convergent orogen: constraints on the timing of thrust faulting and subsequent exhumation of the Maladeta Pluton in the Central Pyrenean Axial Zone. *Earth and Planetary Science Letters*, *287*(3-4), 488–503.

Mochales, T., Barnolas, A., Pueyo, E. L., Casas, A. M., Serra-Kiel, J., Samsó, J. M. & Ramajo, J. (2012). Chronostratigraphy of

the Boltaña anticline and the Ainsa Basin (Southern Pyrenees). *Geological Society of American Bulletin*, *124*(7-8), 1229–1250.

Morris, R., Sinclair, H., Yelland, A., Hovius, N. & Leeder, M. (1998). Exhumation of the Pyrenean orogen; implications for sediment discharge. *Basin Research*, *10*(1), 69–85.

Muñoz, J.A., Beamud, E., Fernández, O., Arbués, P., Dinarès-Turell, J., Poblet, J. The Ainsa Fold and Thrust Oblique Zone of the Central Pyrenees: kinematics of a curved contractional system from paleomagnetic and structural data. *Tectonics* (in press).

Pascual, J. O., Parés, J. M., Langereis, C. G., & Zijderveld, J. D. A. (1992). Magnetostratigraphy and rock magnetism of the Ilerdian stratotype at Tremp, Spain. *Physics of the Earth and Planetary Interiors*, *74*, 139–157.

Pueyo, E. (2000), *Rotaciones paleomagnéticas en sistemas de pliegues y cabalgamientos. Tipos, causas, significado y aplicaciones. (Ejemplos de las Sierras Exteriores y Cuenca de Jaca, Pirineo Aragonés).* PhD thesis, Universidad de Zaragoza. 296pp.

Robles, S. (1984). El complejo sedimentario aluvial y lacustre de edad paleógena de la Pobla de Segur entre los ríos Noguera Pallaresa y Flamisell (Prepirineo de Lérida). *Ilerda*, 24, 110-144.

Rodríguez-Pintó, A., E.L. Pueyo, J. Serra-Kiel, J.M. Samsó, A. Barnolas, and A. Pocoví (2012), Lutetian magnetostratigraphic calibration of larger foraminifera zonation (SBZ) in the Southern Pyrenees: The Isuela section, *Palaeogeography, Palaeoclimatology, Palaeoecology, 333-334*, 107-120.

Rosell, J. & Riba, O. (1966). Nota sobre la disposicion sedimentaria de los conglomerados de Pobla de Segur (Provincia de Lerida). *Pirineos*, *22*(81-82), 61–74.

Sinclair, H. D., Gibson, M., Naylor, M. & Morris, R. G. (2005). Asymmetric growth of the Pyrenees revealed through measurement and modeling of orogenic fluxes. *American Journal of Science*, *305*(5), 369–406.

Sussman, A. J., Butler, R. F., Dinarès-Turell, J., & Vergés, J. (2004). Vertical-axis rotation of a foreland fold and implications for orogenic curvature: an example from the Southern Pyrenees, Spain. *Earth and Planetary Science Letters*, *218*(3-4), 435–449.

Vincent, S. (1993). *Fluvial Paleovalleys in Mountain Belts: An Example from the South Central Pyrenees*. PhD Thesis. University of Liverpool. 407 pp.

Whitchurch, A., Carter, A., Sinclair, H., Duller, R.A., Whittacker, A.C. & Allen, P.A. (2011). Sediment routing system evolution within a dyachronously uplifting orogeny: insights from detrital zircon thermochronological analyses from the south-central Pyrenees. *American Journal of Science*, 311, 442-482

MOTIVATION, OBJECTIVES and STRUCTURE of the THESIS

MOTIVATION and OBJECTIVES

The study of synorogenic materials provides important information about the events occurred during mountain building, as they permit the link between exhumation and denudation in the interior of the orogen and sedimentation in the surrounding basins (Figure I).

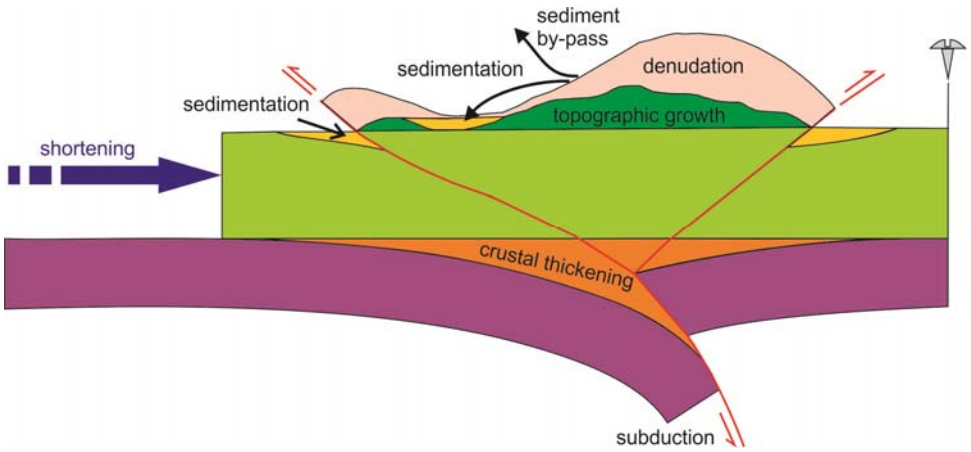

Figure I.- Diagram illustrating the processes involved during mountain building. (Modified from *Beaumont et al.*, 2000)

Geometric relationships between tectonic structures and synorogenic materials provide a relative chronology of the tectonic events occurred during their deposition. However, the precise timing and rates of these processes can only be attained when absolute ages are obtained. Magnetostratigraphy has revealed as a powerful tool to date continental successions in a continuous way. Long and densely sampled magnetostratigraphic sections provide a distinctive reversal pattern that can be unambiguously correlated to the GPTS deprived of any other temporal constraints. Once a continuous and absolute dating of the syntectonic materials is achieved, the timing and quantification of the tectonic processes occurred during their deposition can be readily determined. Similarly, the ages provided by detrital thermochronology add constraints to the exhumation and tectonic history of the source region as well as to changes in sediment provenance and landscape evolution. Additionally, the relative timing between thrusting and rotations contributes to the construction of kinematic models for fold and thrust belts. Kinematic models fitting the geological evidences of an area are necessary to correctly restore geological structures, especially when the structures to be restored are oblique to the regional structural trend of the orogen, as material is transported out of the regional transport plane.

Synorogenic sediments in fold and thrust belts are rarely preserved in the inner part of the orogenic systems, as they have either been removed by erosion or not been deposited. They are usually stored in the adjacent undeformed foreland basins and eventually in piggy-back basins in the frontal thrust sheets (Figure I). The Pyrenees is a mountain range well known among the geological community by the exceptional preservation of synorogenic sediments in its southern flank. The high subsidence rates associated to the South-Central Pyrenees intramontane basins and the fact that the South Pyrenean foreland basin became endorheic from Late Eocene until Middle Miocene times (*Coney et al.,* 1996, *Costa et al.*, 2010) favored the unusual and excellent preservation of the synorogenic deposits.

In this PhD the Tertiary syntectonic sediments of the South-Central Pyrenees have been studied: Pobla de Segur/Senterada conglomerates (*Rosell & Riba*, 1966; *Mellere*, 1992), Sis conglomerates (*Vincent*, 1993) and the Eocene succession of the Ainsa Basin (*Barnolas & Gil-Peña*, 2001).

There are several reasons that justify the study of these materials. Previous studies in the syntectonic materials of the South-Central Pyrenees established a relative chronology of the deformation sequence and the tectonic evolution of the inner parts of the orogen during their deposition (*Mellere & Marzo*, 1992; *Mellere*, 1993). However, the age of the syntectonic conglomerates of La Pobla de Segur/Senterada and Sis was not precisely established. It was based on scarce mammal fossil sites located in the middle part of the succession which suggested an MP17 age of the European continental mammal biochronological scale (correlated to the Upper Eocene) (*Casanovas*, 1975; *López-Martínez*, 1998). Hence, many meters of the sedimentary succession remained unconstrained. As a result, most of the conglomeratic successions unconformably overlying the structures affecting the Mesozoic to Eocene sediments were considered as Oligocene (*Rosell & Riba*, 1966; *Robles*, 1984; *mapa geològic de Catalunya 1:250000*, 1989, 2002). Moreover, the European mammal biochronology is based either on short sections disconnected from marine successions with better biochronological constraints or on karstic infillings with serious correlation difficulties. Therefore a review of the calibration of the reference levels with the time scale can be necessary in some cases.

The studied syntectonic materials record both the last stages of transport of the South Pyrenean thrust sheets and the onset of fast exhumation rates within the Axial Zone of the orogen (*Fitzgerald et al.*, 1999). Many thermochronological studies in the inner parts of the central Pyrenees have been conducted in the last years providing information about the timing

of the activity of the different thrusts of the Axial Zone and revealing greater and younger exhumation in the southern side of the orogen (*Morris et al.*, 1998; *Fitzgerald et al.*, 1999; *Sinclair et al.*, 2005; *Gibson et al.*, 2007; *Metcalf et al.*, 2009). The modelling of this extensive thermochronological database (*Fillon & van der Beek*, 2012) constrains the history of exhumation in the southern Pyrenees since 40 Ma and reveals that changes in base level within the Ebro foreland Basin exerted a major control on its post-orogenic evolution. The aforementioned studies are focused on the thermochronological information derived from granitic massifs within the Axial Zone. However, the earlier thermal history of rocks from the inner parts of the orogen may be absent due to denudation. Detrital thermochronology can complete the exhumation history and reconstruct the sediment routing of an orogen as it yields thermal information of the eroded parts preserved in the surrounding sedimentary basins (*Whitchurch et al.*, 2011). Detrital thermochronology applied to sandstones from two piggy-back basins of the southern Pyrenees, (*Fillon et al.*, 2013) quantifies thickness and extent of the Upper Eocene-Oligocene sediments covering the fold-and-thrust belt in about 0.7-1.6 km, before their re-excavation during Miocene times. As the synorogenic materials studied in this PhD were deposited during fast exhumation within the Axial Zone, the detrital thermochronology of Axial Zone derived granite clasts enclosed within the syntectonic conglomerates will contribute to extend the earlier exhumation history of the interior of the chain.

Sedimentation of the studied synorogenic materials during Middle Eocene-Oligocene times occurred coeval to the development of thrust salients in the southern Pyrenees. Among them the most significant one is located in the western part of the central Pyrenees in the Ainsa area where many structures with an oblique orientation to the main Pyrenean structures occur (Ainsa Oblique Zone). The N-S trend of the Boltaña, Añisclo and Mediano anticlines contrasts with the mostly E-W trend of the Pyrenean structures. This area has been exhaustively studied, especially from a paleomagnetic point of view, with the aim of unravelling the origin of such obliquity, identifying and quantifying the vertical axis rotations occurred in the area (*Dinarès-Turell*, 1992; *Pueyo*, 2000; *Mochales et al.*, 2012a). Nevertheless, their kinematics and chronology were not precisely established yet.

Therefore, the main objectives of this PhD Thesis are:

I) The establishment of a continuous chronology for the La Pobla, Senterada and Sis syntectonic conglomerates by means of magnetostratrigraphic dating.

II) The establishment of an integrated chronostratigraphy for the Eocene materials of the Pyrenean South-Central Unit, by correlation of the obtained results with the magnetostratigraphic logs developed in the Ainsa Basin (*Bentham*, 1992*; Mochales et a.l*, 2012b; *Rodríguez-Pintó et al*., 2012).

III) The calibration of the Paleogene continental mammal biochronological scale (MP reference levels) from the magnetostratigraphic sections done within the South-Central Pyrenees and other areas of the Ebro Basin.

IV) The establishment of the thermochronology of the syntectonic conglomerates from the study of the apatite fission tracks in granite clasts derived from the Axial Zone and contained within the conglomerates.

V) To relate the deformation pattern of the internal parts of the orogeny with the sedimentation within the adjoining basins by integrating magnetostratigraphic and thermochronological data and to obtain exhumation and sedimentation rates.

VI) To establish the origin of the oblique structures of the Ainsa basin from the study of the vertical axis rotations and their integration with other available paleomagnetic data in the study area and to establish a kinematic model for the Southern Pyrenees.

STRUCTURE

This PhD Thesis has been prepared as a research papers compilation. These research papers have been published and/or submitted to journals belonging to the *Journal Citation Report* of the *Institute for Scientific Information*.

The thesis is organized in 4 chapters:

Chapter 1 is an introductory chapter that describes the geological setting of the study area, the stratigraphic framework, the methodologies used to accomplish the objectives of this thesis (Paleomagnetism and detrital fission track thermochronology) and the European Paleogene continental mammal biochronology.

Chapter 2 represents the core of the thesis and includes the main results of the study. It is formed by two published papers and a third one already accepted for publication:

Chapter 2.1 is composed by the paper: ***Beamud, E., Garcés, M., Cabrera, L., Muñoz, J.A., Almar, Y. (2003) A new Middle to Late Eocene chronostratigraphy for NE Spain. Earth and Planetary Science Letters* 216, 501-514**. In this paper a new chronostratigraphy for the Eocene continental units of the South-Central Pyrenees is presented. It is based on the integration of the magnetostratigraphic dating of the La Pobla de Segur and Sis conglomerates to the previously established chronology of the continental units within the Ainsa Basin (Escanilla Fm.). The age of La Pobla de Segur conglomerates was losely constrained based on fossil localities within the succession that were assigned to the MP17 reference level of the European Paleogene mammal reference levels, suggesting a Priabonian age for the middle part of the succession. The magnetostratigraphic results of this work challenge the previous dating of these materials and implications for the calibration of the European Paleogene mammal reference levels (MP bichronology) are also derived from the new chronology.

Paper ***Beamud, E., Muñoz, J.A., Fitzgerald, P.G., Baldwin, S.L., Garcés, M., Cabrera, L., Metcalf, J.R. (2011) Magnetostratigraphy and detrital apatite fission track thermochronology in syntectonic conglomerates: constraints on the exhumation of the South-Central Pyrenees. Basin Research* 23, 309-331** forms Chapter 2.2. In this paper the magnetostratigraphic dating of the continental syntectonic conglomerates is combined with detrital apatite fission track thermochronology applied on granite clasts within these syntectonic materials. The magnetostratigraphy already introduced in chapter 2.1 is extended up with the magnetostratigraphic dating of the Senterada sub-basin conglomerates. The distribution of the fission-track ages and lengths through the studied sections combined with their depositional ages has yield information about the time and amount of exhumation in the Pyrenean orogen.

Chapter 2.3. is formed by the paper ***Muñoz, J.A., Beamud, E., Fernández, O., Arbués, P., Dinarès-Turell, J., Poblet, J. The Ainsa Fold and Thrust Oblique Zone of the Central Pyrenees: kinematics of a curved contractional system from paleomagnetic and structural data. Tectonics* (accepted)**. In this paper a new kinematic model for the N-S trending structures of the Ainsa Oblique Zone and the origin of the curved shape of the South-Central Pyrenees are presented. Although many previous studies had already identified clockwise vertical axis rotations within the Eocene materials of the Ainsa Basin, a consistent kinematic model for the Ainsa Oblique Zone was still not available. The new model presented in this paper integrates new and previous paleomagnetic data with structural and sedimentological data yielding a coherent model with all the available information.

Chapter 3 includes a synthesis and discussion of the obtained results, presented as three sub-sections:

3.1. Chronostratigraphy of the Tertiary syntectonic materials of the South-Central Pyrenees.

3.2. Biochronological implications

3.3. Kinematic and exhumation model for the South-Central Pyrenees.

Finally, **chapter 4** summarizes the main conclusions derived from this PhD Thesis.

REFERENCES

Barnolas, A., & Gil-Peña, I. (2001). Ejemplos de relleno sedimentario multiepisódico en una cuenca de antepaís fragmentada: La Cuenca Surpirenaica. *Boletín Geológico y Minero*, *112*(3), 17–38.

Beamud, E., Garcés, M., Cabrera, L., Muñoz, J.A., & Almar, Y. (2003). A new middle to late Eocene continental chronostratigraphy from NE Spain. *Earth and Planetary Science Letters*, *216* (4), 501–514.

Beamud, E., Muñoz, J. A., Fitzgerald, P. G., Baldwin, S. L., Garcés, M., Cabrera, L., & Metcalf, J. R. (2011). Magnetostratigraphy and detrital apatite fission track thermochronology in syntectonic conglomerates: constraints on the exhumation of the South-Central Pyrenees. *Basin Research*, *23* (3), 309–331.

Beaumont, C., Muñoz, J.A., Hamilton, J. & Fullsack, P. (2000). Factors controlling the Alpine evolution of the central Pyrenees inferred from a comparison of observations and geodynamical models. *Journal of Geophysical Research*, 105, B4, 8121-8145.

Bentham, P. (1992). *The tectono-stratigraphic development of the western oblique ramp of the South-Central Pyrenean thrust system, Northern Spain*. PhD Thesis. University of Southern California. 253 pp.

Casanovas-Cladellas, M. L. (1975). Estratigrafía y paleontología del yacimiento ludiense de Roc de Santa (Area del Noguera Pallaresa). *Paleontologia i Evolució*, *10*, 1–158.

Coney, P. J., Muñoz, J. A., Mcclay, K. R. & Evenchick, C. A. (1996). Syntectonic burial and post-tectonic exhumation of the southern Pyrenees foreland fold-thrust belt. *Journal of the Geological Society*, *153*(1), 9–16.

Costa, E., Garcés, M., López-Blanco, M., Beamud, E., Gómez-Paccard, M. & Larrasoaña, J. C. (2010). Closing and continentalization of the South Pyrenean foreland basin (NE Spain): magnetochronological constraints. *Basin Research*, *22*(6), 904-917

Dinarès-Turell, J. (1992). *Paleomagnetisme a les unitats sudpirinenques superiors. implicacions estructurals*. PhD Thesis. Universitat de Barcelona. 462 pp.

Fitzgerald, P. G., Muñoz, J. A., Coney, P. J., & Baldwin, S. L. (1999). Asymmetric exhumation accross the Pyrenean orogen: implications for the tectonic evolution of a collisional orogen. *Earth and Planetary Science Letters*, *173* (3), 157–170.

Fillon, C., & van der Beek, P. (2012). Post-orogenic evolution of the southern Pyrenees: constraints from inverse thermo-kinematic modelling of low-temperature thermochronology data. *Basin Research*, 24, 418-436.

Fillon, C., Gautheron, C. & van der Beek, P. (2013). Oligocene-Miocene burial and exhumation of the Southern Pyrenean foreland quantified by low-temperature thermochronology. *Journal of the Geological Society, London*, 170, 67-77.

Gibson, M., Sinclair, H. D., Lynn, G. ., & Stuart, F. M. (2007). Late- to post-orogenic exhumation of the Central Pyrenees revealed through combined thermochronological data and modelling. *Basin Research*, *19* (3), 323–334.

López-Martínez, N. (1998). Los yacimientos de mamíferos del Eoceno de la Pobla de Segur. In N. López-Martínez, J. Civís, L. Casanovas, & R. Daams (Eds.), *Geología y Paleontología del Eoceno de la Pobla de Segur (Lleida)* (p. 267). Universitat de Lleida.

Mapa geològic de Catalunya 1:250000. (1989). Ed. Servei Geològic de Catalunya (SGC) i Institut Geològic de Catalunya (IGC)

Mapa geològic de Catalunya 1:250000, 2ª edició. (2002). Ed. Servei Geològic de Catalunya (SGC) i Institut Geològic de Catalunya (IGC)

Mellere, D. (1992). *I conglomerati di Pobla de Segur: Stratigrafia fisica e relazioni tettonica-sedimentazione*. PhD Thesis. Universita degli studi di Padova. 203 pp.

Mellere, D. (1993). Thrust generated back-fill stacking of alluvial fan sequences, south-central Pyrenees, Spain (La Pobla de Segur conglomerates). *Special Publication of the Internal Association of Sedimentology*, *20*, 259–276.

Mellere, D., & Marzo, M. (1992). Los depósitos aluviales sintectónicos de la Pobla de Segur: alogrupos y su significado tectonoestratigráfico. *Acta Geológica Hispánica*, *27* (1-2), 145–149.

Metcalf, J. R., Fitzgerald, P. G., Baldwin, S. L., & Muñoz, J. A. (2009). Thermochronology of a convergent orogen: constraints on the timing of thrust faulting and subsequent exhumation of the Maladeta Pluton in the Central Pyrenean Axial Zone. *Earth and Planetary Science Letters*, *287* (3-4), 488–503.

Mochales, T., Casas, A. M., Pueyo, E. L., & Barnolas, A. (2012a). Rotational velocity for oblique structures (Boltaña anticline, Southern Pyrenees). *Journal of Structural Geology*, *35*, 2–16. doi:10.1016/j.jsg.2011.11.009

Mochales, T., Barnolas, A., Pueyo, E. L., Casas, A. M., Serra-Kiel, J., Samsó, J. M., & Ramajo, J. (2012b). Chronostratigraphy of the Boltaña anticline and the Ainsa Basin (Southern Pyrenees). *Geological Society of American Bulletin*, *124* (7-8), 1229–1250.

Morris, R., Sinclair, H., Yelland, A., Hovius, N., & Leeder, M. (1998). Exhumation of the Pyrenean orogen; implications for sediment discharge. *Basin Research*, *10* (1), 69–85.

Muñoz, J.A., Beamud, E., Fernández, O., Arbués, P., Dinarès-Turell, J., Poblet, J. (accepted).The Ainsa Fold and Thrust Oblique Zone of the Central Pyrenees: kinematics of a curved contractional system from paleomagnetic and structural data. Tectonics.

Pueyo, E. (2000). *Rotaciones paleomagnéticas en sistemas de pliegues y cabalgamientos. Tipos, causas, significado y aplicaciones. (Ejemplos de las Sierras Exteriores y Cuenca de Jaca, Pirineo Aragonés)*. PhD Thesis. Universidad de Zaragoza. 296 pp.

Robles, S. (1984). El complejo sedimentario aluvial y lacustre de edad paleógena de la Pobla de Segur entre los ríos Noguera

Pallaresa y Flamisell (Prepirineo de Lérida). *Ilerda*, 24, 110-144.

Rodríguez-Pintó, A., Pueyo, E. L., Serra-Kiel, J., Samsó, J. M., Barnolas, A., & Pocoví, A. (2012). Lutetian magnetostratigraphic calibration of larger foraminifera zonation (SBZ) in the Southern Pyrenees: The Isuela section. *Palaeogeography, Palaeoclimatology, Palaeoecology*, *333-334*, 107–120.

Rosell, J., Riba, & O. (1966). Nota sobre la disposicion sedimentaria de los conglomerados de Pobla de Segur (Provincia de Lerida). *Pirineos*, *22* (81-82), 61–74.

Sinclair, H. D., Gibson, M., Naylor, M., & Morris, R. G. (2005). Asymmetric growth of the Pyrenees revealed through measurement and modeling of orogenic fluxes. *American Journal of Science*, *305* (5), 369–406.

Vincent, S. (1993). *Fluvial Paleovalleys in Mountain Belts: An Example from the South Central Pyrenees*. PhD Thesis. University of Liverpool. 407 pp.

Whitchurch, A., Carter, A., Sinclair, H., Duller, R.A., Whittacker, A.C. & Allen, P.A. (2011). Sediment routing system evolution within a dyachronously uplifting orogeny: insights from detrital zircon thermochronological analyses from the south-central Pyrenees. *American Journal of Science*, 311, 442-482

CHAPTER 1- INTRODUCTION

1.1.- Geological Setting

1.2.- Stratigraphic framework

1.3.- Methods:
1.3.1.- Paleomagnetism
1.3.2.- Fission track thermochronology

1.4.- Paleogene mammal biochronology

1.1.- GEOLOGICAL SETTING

The Pyrenees formed as the result of the collision between the European and Iberian plates from late Cretaceous to Miocene times (*Roest & Srivastava*, 1991, *Rosenbaum et al.*, 2002, *Muñoz*, 2002). The Pyrenean orogen is strongly asymmetric, with a much wider wedge and foreland basin in its southern side than in the northern one. The Central Pyrenees include a duplex structure of south-directed Hercynian basement thrust sheets, the Axial Zone, which is flanked north and south by oppositely vergent fold and thrust belts and the associated Ebro and Aquitaine foreland basins (Figure 1.1). The amount of shortening in the central Pyrenees is around 150 km (147 km according to *Muñoz*, 1992; 165 km according to *Beaumont et al.*, 2000) with a transport direction to the south (*Vergés*, 1993; *Rosenbaum et al.*, 2002).

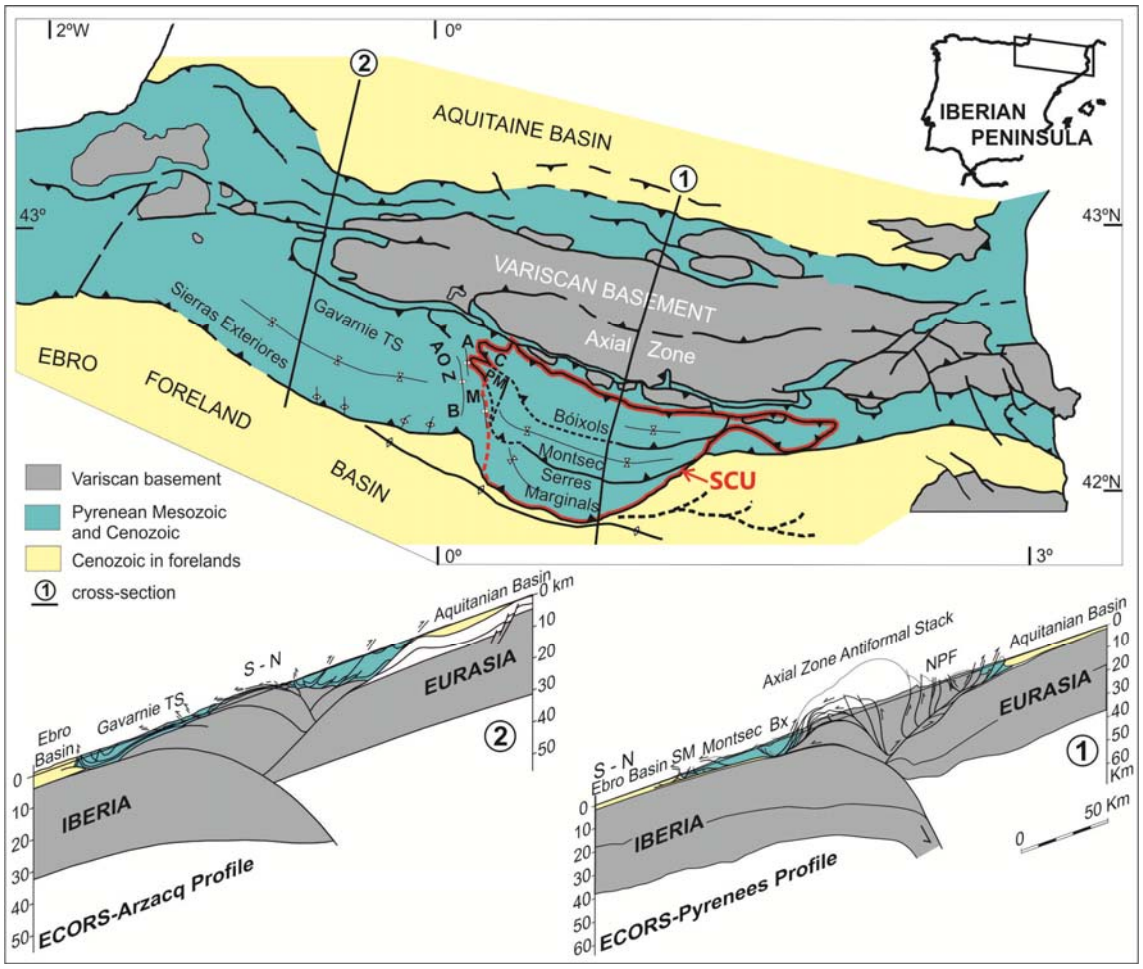

Figure 1.1- Structural sketch showing the main structural units of the Central Pyrenees. Crustal cross-sections 1 and 2 illustrate changes of the structural style along strike. Ecors section from *Muñoz* (1992) and the Arzacq section modified from *Teixell* (1998). SCU: South Pyrenean Central Unit, AOZ: Ainsa Oblique Zone, A: Añisclo Anticline, B: Boltaña Anticline, M: Mediano Anticline, C: Cotiella, PM: Peña Montañesa, Bx: Bóixols, SM: Serres Marginals, NPF: North Pyrenean Fault.

In the central Pyrenees the Axial Zone culminates in an antiformal stack of three upper crustal thrust sheets emplaced between the Late Cretaceous and the Oligocene. From top to bottom they are named: Nogueres, Orri and Rialp (*Muñoz*, 1992). To the north, the Axial Zone antiformal stack is bounded by the North Pyrenean Fault Zone (Figure 1.1), where metamorphic Jurassic to Lower Cretaceous carbonates and breccias crops out together with lower crustal and mantle rocks. This fault was considered as a Cretaceous major strike slip fault system between the European and the Iberian plates (*Choukroune*, 1976; *Fischer*, 1984). However, the observed geological features along this zone have been recently interpreted as the result of the evolution of the Cretaceous hyperextended rift margin and the related exhumation of deep crustal and mantle rocks by low-angle extensional faults (Jammes et al., 2009; Lagabrielle et al., 2010). The Axial Zone encloses numerous Hercynian granitoids from which an extensive thermochronological database is now available (*Morris et al.*, 1998; *Fitzgerald et al.*, 1999; *Sinclair et al.*, 2005; *Gibson et al.*, 2007; *Metcalf et al.*, 2009). These studies have revealed an asymmetric pattern of exhumation related to the thrusting, uplift and erosion of the stacked thrust sheets, with greater and progressively younger exhumation in the southern side of the orogen.

Thrusting in the southern fold and thrust belt occurred coeval to the formation of the Axial Zone from Late Cretaceous onwards *(Beaumont et al.*, 2000; *Sinclair et al.*, 2005). The southern fold and thrust belt is formed by three imbricated major thrust sheets developed in a piggy-back sequence on top of the autochthonous rocks of the Ebro foreland basin (*Séguret*, 1972; *Garrido-Megías*, 1973; *Cámara and Klimowitz*, 1985; *Muñoz*, 1992). These thrust sheets involve Mesozoic and Tertiary materials and from north to south and in order of emplacement they are: the **Cotiella-Bóixols thrust sheet**, emplaced during the Late Cretaceous as a consequence of the inversion of Lower Cretaceous extensional basins (*Garrido-Megías*, 1973; *García-Senz*, 2002), the **Peña Montañesa-Montsec thrust sheet**, active from the Paleocene to the late Ypresian (*Soler & Garrido-Megías*, 1970; *Garrido-Megías & Ríos Aragüés*, 1972; *Farrell et al.*, 1987; *Teixell & Muñoz*, 2000) and the **Gavarnie-Serres Marginals-Sierras Exteriores** thrust sheet developed during Lutetian- Late Oligocene times (*Garrido-Megías*, 1972; *Teixell*, 1996; *Teixell & Muñoz*, 2000) (Figure 1.1 and Figure 1.2).

Syntectonic sediments accumulated both in the foreland basin and within piggy-back basins preserved on top of the three major thrust sheets (Figure 1.2). As deformation migrated southwards so did the depocenters of the southern foreland basin. In a first stage (Late Santonian to Maastrichtian), the Pyrenean foreland basin developed and was partially

incorporated into the thrust sheets of the Bóixols-Cotiella unit. Next stage (Maastrichtian to Early Eocene) was characterized by a widespread continental and shallow marine sedimentation during a period of relative quiescence. Afterwards, the reactivation of the southern Pyrenean thrusts caused the foreland depocenter to migrate southwards to the Graus-Tremp Basin, in the hangingwall of the Montsec thrust (Figure 1.2) and further south in the foreland ahead of the emergent frontal thrust system. The Graus-Tremp Basin opened to the west into the foreland Eocene Ainsa Basin, which in turn fed the Jaca Basin (Figure 1.2). The emplacement of the Serres Marginals-Sierras Exteriores thrust sheet during Middle Eocene to Late Oligocene times confined the Ainsa-Jaca system to a piggy- back setting and enhanced sediment transfer towards the Ebro basin. The Ebro basin was initially marine while it was opened towards the Bay of Biscay, followed by a continental stage once it became a closed basin (Late Eocene-Middle Miocene) (*Costa et al*, 2010). This continental stage resulted from the cut-off from the Atlantic Ocean by the uplift of the western Pyrenees (*Riba et al.*, 1983). Sediment aggradation in the endorheic Ebro basin raised the base level resulting in the progressive burying of the south Pyrenean fold and thrust belt by continental conglomerates (*Coney et al.*, 1996; *Muñoz et al.*, 1997). Such burial of the thrust wedge enhanced internal deformation resulting in a migration of the tectonic activity hindwards. As burial by syntectonic conglomerates progressed hindwards, a break-back thrust sequence developed, both by reactivation of previously developed thrusts and by formation of new ones (*Vergés & Muñoz*, 1990; *Muñoz et al.*, 1997; *Muñoz*, 2002). In spite of the hindward migration of the thrust activity during the syntectonic burial, the thrust front remained active and overthrust onto the Ebro foreland.

A major structural change occurs between the central and the west-central southern Pyrenees. As already mentioned in the central Pyrenees the basement thrust sheets form the Axial Zone antiformal stack with a significant structural relief (cross-section 1 in Figure 1.1.) (*Muñoz*, 1992). Uplift and exhumation was mainly located in this central part of the chain and sediment supply during the late continental foreland basin stage was mostly derived from the basement units. The pile of basement units flexed down the Iberian lithosphere and synorogenic conglomerates buried the south-Pyrenean cover thrust sheets south of the basement antiformal stack and even overlapped their eroded frontal basement units (*Coney et al.* 1996). Southward, the Mesozoic cover sequence is detached from the Triassic evaporites to form the Bóixols, Montsec and Serres Marginals thrust sheets (Figure 1.1). Conversely, in the west-central Pyrenees basement thrust sheets are mostly imbricated, instead of piled one on

top of the other, and constitute an imbricate hinterland dipping duplex (cross-section 2 in Figure 1.1) (*Cámara and Klimowitz*, 1985; *Teixell*, 1996, 1998). As a result, uplift was distributed in a wider area during its late tectonic evolution instead of being concentrated in the centre of the chain. Consequently, the basement thrust sheets along the Axial Zone highest Pyrenees plunge westward as the structural relief decreases in the same direction (Figure 1.1). Southward, the cover thrust sheets are widely exhumed in the west, as basement thrust sheets are located further south than in the central Pyrenees, and the lower Gavarnie-Sierras Exteriores thrust sheet occupies a wide area (Figure 1.1). The Mesozoic and Paleogene cover of the northern part of this thrust sheet is coupled to the basement at surface, as no Triassic evaporites exist between the Upper Cretaceous limestones and the Paleozoic rocks. The described change in structural relief and the presence of a Triassic detachment, from the central to the western Pyrenees, is not sharp and occurs across a wide area with N-S trending structures within the Ainsa Oblique Zone (AOZ in Figure 1.1, left red box in Figure 1.2).

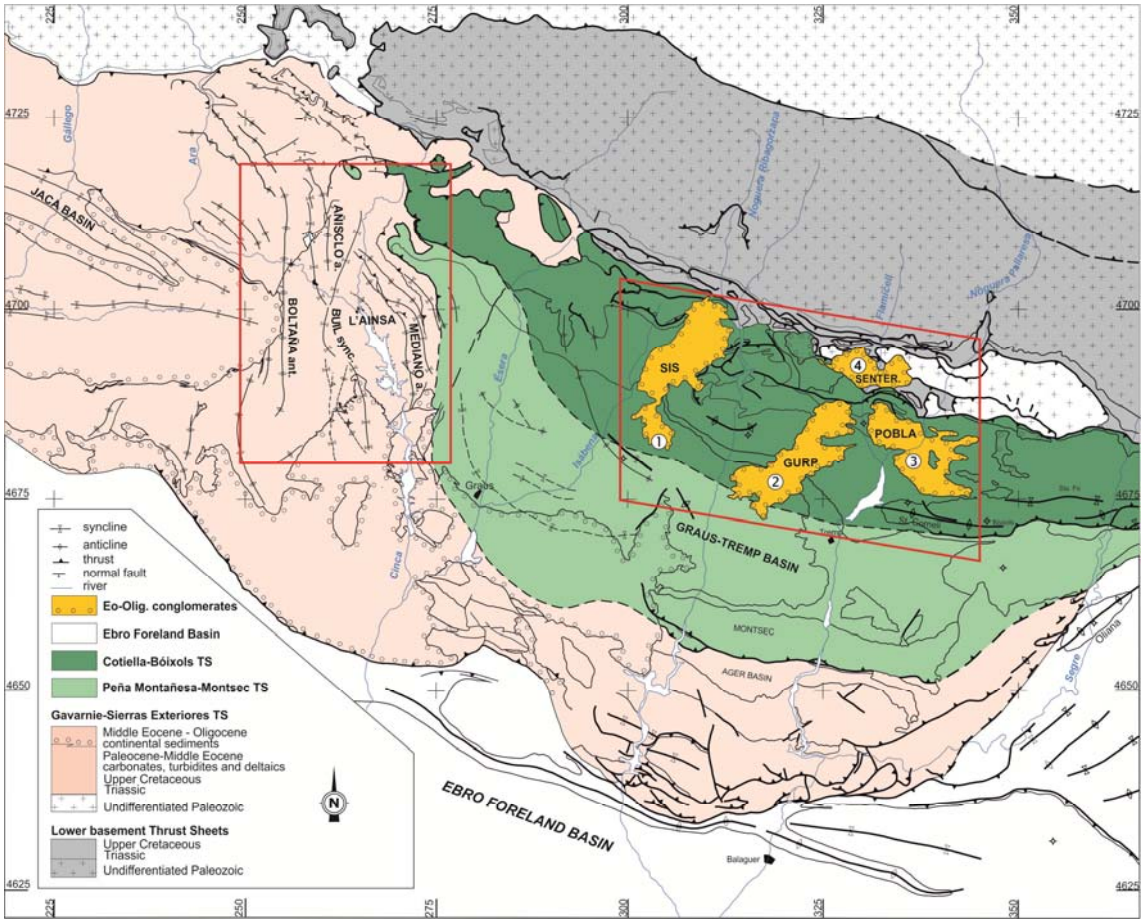

Figure 1.2- Geological map and main structural units of the South-Central Pyrenees. Red boxes indicate the location of the study areas: La Pobla-Senterada, Gurp and Sis in the central sector and the Ainsa Oblique Zone at the western boundary of the major thrust salient in the central Pyrenees. Numbers in circles refer to the stratigraphic sections shown in Figure 1.4.

1.2.- STRATIGRAPHIC FRAMEWORK

The South-Central Pyrenean basins formed during the Eocene as a system of elongated and connected troughs with a marine connection towards the west. They were efficiently fed with siliciclastic material derived from the uplifting Central and Eastern Pyreenes, which caused a rapid basin infill with a westward gradation from terrestrial to shallow-water and slope marine facies. As a result, the vertical transition from marine to continental sediments becomes younger westward. This transition varies from a conformity or paraconformity in the Ainsa area, to a marked erosional unconformity along the Isábena river area (Figure 1.2, Figure 1.3). The time gap under this unconformity increases towards the east, to the point that in the La Pobla de Segur area, the marine Paleogene record is no longer preserved, and the Eocene continental conglomerates unconformably overlie Mesozoic rocks (Figure 1.3).

The Eocene stratigraphic framework will be described from west to east, from the Ainsa basin to the La Pobla de Segur area:

Figure 1.3- Lithostratigraphy of the South-Central Pyrenees, from the Ainsa basin to the La Pobla de Segur. Lithostratigraphic units: Mr, Merli reef; Is/Be: Iscles-Berganuy reefs; Bu, Buil; So, Sobrarbe; Cp, Capella; Pr, Perarrúa; Cst, Castissent; Al, Alveolina limestone. SV1-2: diferent units making the San Vicente Formation. Turbidite systems: gu, Guaso; og, O Grao; ga, Gabardilla; c, Coscojuela; fo, Formigales; s, Sieste; m, Morillo; a, Ainsa; gb, Gerbe-Banastón; ar, Arro; f, Fosado. Horizons: O, Olsón; EL, Escanilla limestone; SB, Santa Bárbara; SP, San Pedro; SL, San Lino; M, Morillo limestone; A, Ascaso; LP, La Puebla; Lu, Santa Llucia. Thrust sheets: C, Cotiella; M, Montsec; PM, Peña Montañesa; B & G, Bielsa and Guarga; LF, La Fueba thrust system

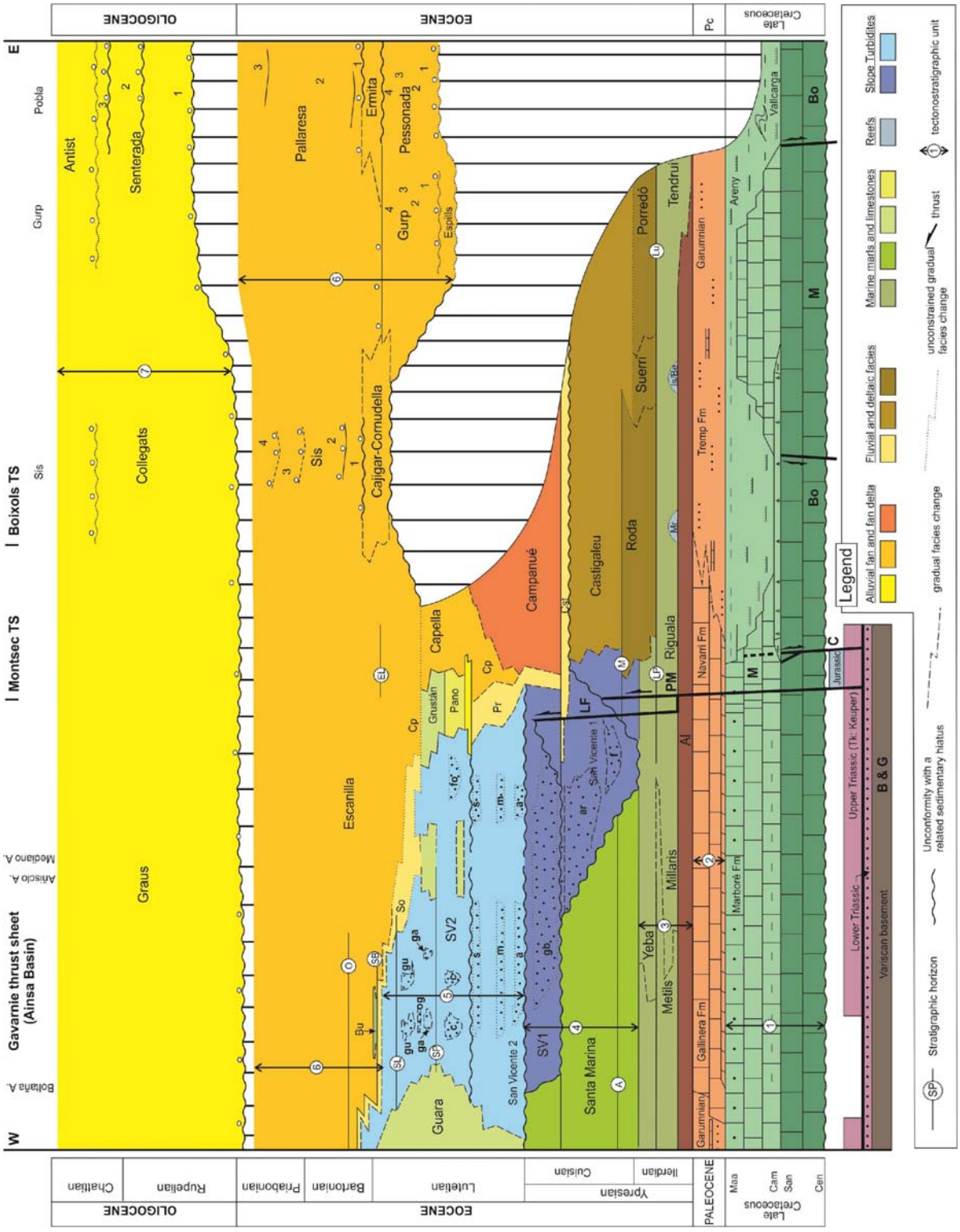
W
E
Gavarnie thrust sheet (Ainsa Basin)
Montsec TS
Boixols TS
Bolaña A.
Ainsclo A.
Medlano A.
Gurp
Pobla
Sis
OLIGOCENE
EOCENE
Pc
Late Cretaceous
Chattian
Rupelian
Priabonian
Bartonian
Lutetian
Ypresian
Cuisian
Ilerdian
PALEOCENE
Maa
Cam
San
Cen
Graus
Antist
Senterada
Collegats
Escanilla
Guara
San Vicente 2
Gallinera Fm
Garumnian
Pallaresa
Ermita
Pessonada
Esplús
Gurp
Sis
Cajigar-Comudella
Capella
Grusián
Pano
Cp
Pr
SV2
SV1
Santa Marina
Campanué
Castigaleu
Roda
Riguala
Millaris
Yeba
Metis
Al
LF
PM
Navarri Fm
Marboré Fm
Tremp Fm
Garumnian
Suerri
Porredó
Tendruí
Areny
Vallcarga
Bo
M
B & G
Variscan basement
Lower Triassic
Upper Triassic (Tk: Keuper)
Jurassic
Legend
Alluvial fan and fan delta
Fluvial and deltaic facies
Marine marls and limestones
Reefs
Slope Turbidites
Stratigraphic horizon
Unconformity with a related sedimentary hiatus
gradual facies change
unconstrained gradual facies change
thrust
tectonostratigraphic unit

In the **Ainsa basin**, the lower Ilerdian is represented by the *Alveolina* Limestones Fm. (*Mey et al.,* 1968) (Figure 1.2, Figure 1.3). Above, the marls and limestones of the Millaris, Metils and Yeba Fms complete the lower Eocene series (*Van Lunsen,* 1970; *Barnolas and Gil-Peña,* 2001). On top, the Ainsa slope complex is as much as a 4 km thick succession of primarily mudstones with several encased turbidite systems, each one being a few hundreds of meters thick (*Arbués et al.,* 2007). These sediments, described as the San Vicente Formation (*Van Lunsen,* 1970) are the main infill of the Ainsa basin and represent the proximal slope facies of the Hecho Group deeper water siliciclastic complexes of the Jaca basin to the west (*Mutti et al.,* 1972). The slope sediments were primarily fed from a fluviodeltaic complex located in the east, on top of the Montsec thrust sheet (the Montañana Group of the Graus-Tremp piggy-back basin) (*Nijman and Nio,* 1975). Southward, the turbiditic trough of the Ainsa basin was bounded by the Santa Marina Fm. carbonate platform (*Barnolas et al.,* 1991). At Middle Eocene times, the Ainsa basin changed from a foredeep to a piggy-back basin and its infill developed a shallowing-upward sequence. The upper part of the slope sediments of the San Vicente Fm. have the deltaic sandstones of the Sobrarbe Fm. as its lateral equivalents (*de Federico*, 1981; *Dreyer et al.*, 1999) which in turn represent the lateral gradation of the Escanilla Fm. fluvial red beds (Garrido-Megías, 1968). The youngest marine sediments in this area correspond to the latestmost Lutetian Buil Nummulitic banks directy underlying the Escanilla Fm. (*Mateu-Vicens et al.,* 2012). The fluvial sediments of the Escanilla Fm. are Bartonian to Priabonian in age (*Bentham*, 1992; *Bentham et al.,* 1992; *Mochales et al.*, 2012). They represent the culmination of a rapid basin infill and are characterised by a marked westward progradation onto deltaic and marine deposits of both the Graus-Tremp and the Ainsa basins. The middle to upper part of the Escanilla Fm. is equivalent to the Campodarbe Group, which lies unconformably on top of the Middle Eocene limestones in the western limb of the Boltaña anticline.

East of the Mediano anticline (Figure 1.2 and 1.3), **between the Esera and the Noguera Ribagorçana rivers**, the Lower Eocene marine sediments are represented by the Ager and Fígols sequence (*Mutti et al.*, 1985; *Puigdefàbregas & Souquet*, 1986; *Barnolas & Gil-Peña*, 2001), composed by the Alveolina limestone, the Riguala marls, the La Puebla limestone (*Cuevas-Gozalo et al*., 1985) and the Roda sandstones Fm. (*Tosquella*, 1988). On the structural highs, the Merli and Iscles/Berganuy reefs grew on top of the Alveolina limestone during Ilerdian times (*Fonnesu*, 1984; *Eichenseer*, 1988). Between the Isábena and the Noguera Ribagorçana rivers, the Roda sandstone interfingers and partly overlies the detrital Suerri Fm.,

which is formed either by deltaic progradation or infilling of interdistributary channels. Overlying the Roda sandstone, the Cuisian Castigaleu Gp. is composed by the transgressive Morillo limestone (*Cuevas-Gozalo et al*., 1985) also known as "miliolid bed" (*Nijman & Nio*, 1975), the deltaic San Esteban Fm. (*Nio*, 1976) and the fluvial Montllobat Fm. (*Nijman & Nio*, 1975). Unconformably on top, the Cuisian Castissent Fm. (N*ijman & Nio,* 1975) is composed by fluvial arkosic sandstones. It is covered by the Cuisian to Lutetian Upper Montanyana Gp., composed by the fan-delta conglomerates of the Lower Campanué Fm. (*Garrido-Megías*, 1968) and the near-shore sandstones and shelf mudstones of the Perarrúa Fm. (*Nijman & Nio*, 1975), which is overlaid and partially interfingers with the tidally influenced Capella Fm. (*Garrido-Megías*, 1968; *Cuevas-Gozalo*, 1989). East and south of the Isábena valley, the upper boundary of the Capella Fm. is formed by the laterally extensive lacustrine Escanilla limestone (*Cuevas-Gozalo*, 1989) placed at the base of the Escanilla Fm. (*Garrido-Megías*, 1968). On top of the Escanilla Fm., the Graus conglomerates are considered to have been deposited during the Oligocene (*Reynolds*, 1987). Between the Isabena and the Noguera Ribagorçana rivers, the syntectonic conglomerates of Sis crop out unconformably on top of the Capella Fm. The stratigraphy of the Paleogene syntectonic conglomerates will be described in more detail in the following subsection.

Between the Noguera Ribargoçana and the Noguera Pallaresa rivers (Figure 1.2), the Fígols Gp. is represented by the marls of the Tendrui Fm. which are partly a lateral equivalent of the *Alveolina* limestone and the Riguala marls (*Serra-Kiel et al*., 1994) (Figure 1.3). On top, the Santa Llúcia limestone (*Fonnesu*, 1984) represents the lateral equivalent of the La Puebla limestone. The final stage of marine sedimentation in this area is represented by the deposition of the upper Ilerdian Porredó deltaic marls and arkosic sandstones (*Fonnesu*, 1984). Overlying them, the Castigaleu Gp. is represented in this area by the arkosic fluvial materials of the Montllobat Fm. (*Nijman & Nio*, 1975). Unconformably on top, the Gurp syntectonic conglomerates crop out. They will also be described in the next section.

Finally, in the La Pobla de Segur area, the lower-middle Eocene marine record is no longer preserved and, as explained above, the syntectonic conglomerates of La Pobla de Segur unconformably overlie Upper or even Lower Cretaceous and Triassic rocks.

1.2.1. Stratigraphy of the syntectonic conglomerates

The South Central Pyrenees Paleogene syntectonic conglomerates crop out as three main conglomeratic remnants between the Isábena and the Noguera Pallaresa rivers (Figure

1.2) in what it is referred to as the Sis, Gurp and La Pobla de Segur/Senterada massifs (Vincent, 1993; Vincent, 2001; Mellere, 1993). The presently disconnected outcrops of these sediments are located along ridges at high altitude between the present rivers and thus were most likely connected forming a single basin before the Neogene exhumation and excavation of the present fluvial network (Coney et al., 1996, Fitzgerald et al., 1999). They are mainly composed by alluvial conglomerates with some lacustrine and fluvial deposits. These sediments were previously considered post-tectonic based on the spectacular unconformity between the less deformed Paleogene conglomerates above and the folded Mesozoic and Early Paleogene sediments below (Mey et al., 1968). However, their deposition occurred synchronously to the main tectonic events in the region and they are often folded and thrusted (Rosell & Riba, 1966; Robles, 1982; Mellere, 1992; Vincent 1993). Moreover, these materials back-step toward the mountain belt, with progressively younger materials located northwards.

The Sis conglomerate body (Figure 1.2 and Figure 1.4) is divided into 4 stratigraphic units defined by distinct bounding surfaces which delimit significant provenance and facies changes (*Vincent*, 2001). From base to top, the ~ 1500 m thick succession is internally organized into the Cajigar, Cornudella, Sis and Collegats Fms. (*Koops & Rossem*, 1985; *Vincent,* 1993; 2001) (Figure S1.2 in Supplementary material). Sediments of the Cajigar Fm. are characterized by red silts and conglomerates with very low proportion of Axial Zone derived clasts and a lack of granitic components (*Vincent*, 2001). The overlying Cornudella Fm. represents a decrease in reddening, an increase in paleosol profiles and the influx of clasts derived from inner areas. It is composed of interbedded fluvial and lacustrine sediments. Clast compositions are dominated by Mesozoic limestones with a significant component of granitic and other Axial Zone derived clasts. On top, the Sis Fm. (*Vincent*, 1993) is organized into 4 members (Sis 1 to 4). A marked increase in channel stacking and dimensions mark its lower boundary with the Cornudella Fm. Deposits are characterized by reddish stacked coarse grained conglomerates. Interbedded within the Cornudella Fm. and the lowermost units of Sis 1, coal levels and lacustrine limestones occur. These levels have provided *Raskyella peckii* (Figure 1.4), a charophyte specie that pointed to an early Bartonian age for this part of the section. Granite clasts are regularly encountered from Sis 1 up to Sis 3, lacking in Sis 4 member (*Vincent*, 2001). Overlying an unconformity on top of the succession, the Collegats Fm. as defined by Vincent (2001) records a marked change in clast provenance with reintroduction of granitic material and an increase in Paleozoic and Triassic clasts derived from the Axial Zone. The Collegats Fm. correlates with the Graus Fm. (*Reynolds*, 1987; *Vincent*, 1993). The Graus

Fm. basal unconformity was dated as younger than late Priabonian based on magnetostratigraphy (*Bentham & Burbank*, 1996).

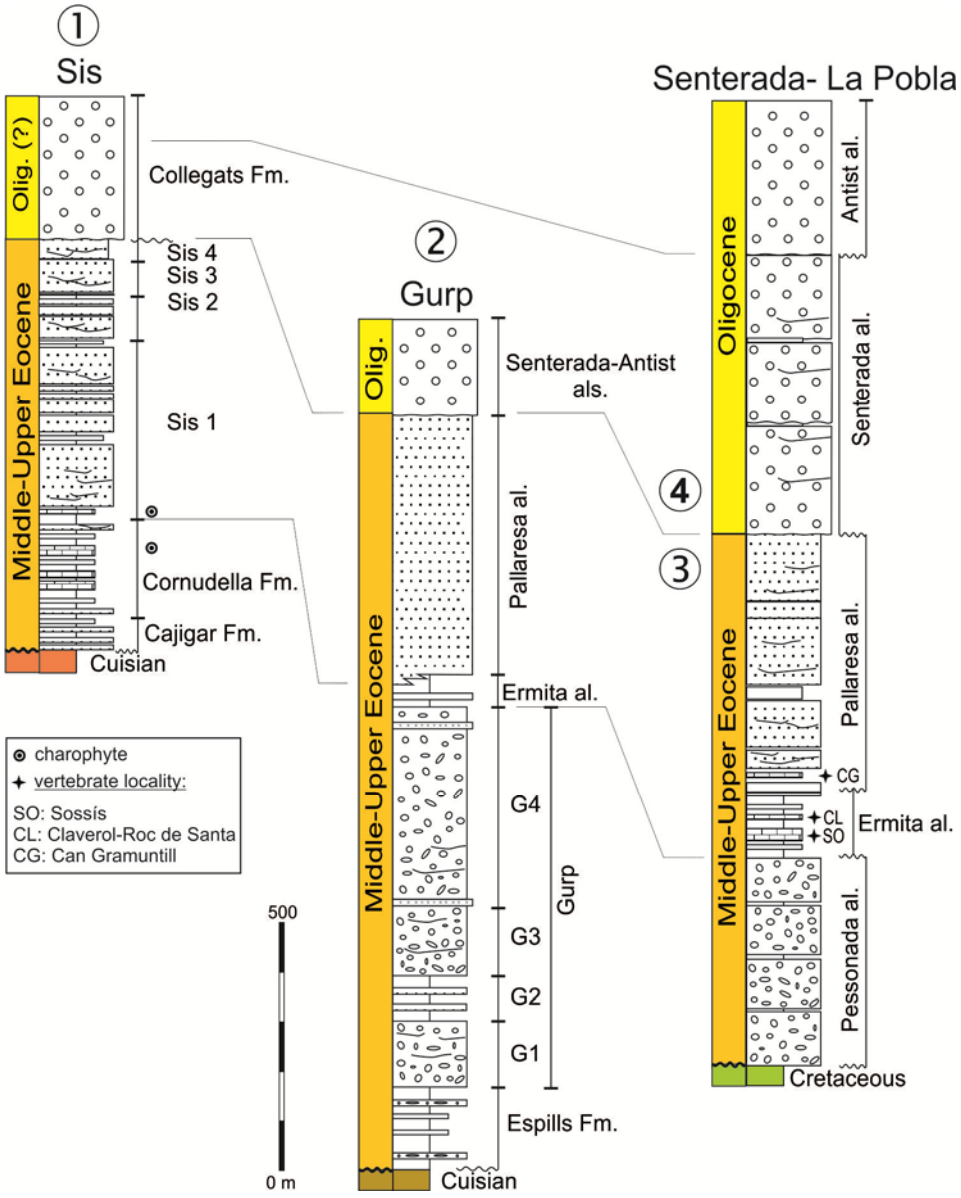

Figure 1.4- Simplified stratigraphic logs of the syntectonic conglomerates of Sis, Gurp and La Pobla de Segur/Senterada. Encircled numbers refer to location in Figure 1.2.

To the east, around the Noguera Pallaresa River, the La Pobla de Segur conglomerates (*Rosell & Riba*, 1966; *Mellere*, 1993) onlap a previously deformed substratum of Mesozoic rocks. They were studied in the 80's by Robles (*Robles*, 1982; *Robles*, 1984) and by *Robles & Ardévol* (1984). An exhaustive study of their stratigraphy and tectonosedimentary relationships was conducted by Mellere (1992). Later, a clasts and heavy minerals provenance study was carried out by Barsó (2007). The La Pobla de Segur conglomerates are organized in 5

allogroups, from base to top: the Pessonada, Ermita, Pallaresa, Senterada and Antist allogroups (*Mellere*, 1993). The basal units, the Pessonada and Ermita allogroups, are characterized by monomict conglomerates of local provenance mainly composed by pebbles and cobbles of Mesozoic rocks (Cretaceous and Jurassic clasts) (*Mellere*, 1993; *Barsó & Ramos*, 2007). The Pessonada allogroup is arranged in 4 sequences bounded by progressive unconformities related to the emplacement of a system of out-of-sequence thrusts (*Mellere*, 1992). The Ermita allogroup represents an alluvial fan and fan delta system which includes lacustrine limestones with interbedded coal layers. Within these lacustrine levels, the classical fossil sites of Sossís, Claverol and Roc de Santa were found (*Casanovas*, 1975) (Figure 1.4), which yield fauna assigned to the MP17 reference level, suggesting a Priabonian age. First occurrence of Axial Zone clasts takes place within the Pallaresa allogroup and extends up to the Senterada and Antist allogroups. The Pallaresa allogroup represents the major alluvial fan complex of the basin. It is composed by converging alluvial fan systems: the Montsor, Collegats, Roca del Peso, Roc de Santa, Roca Llania and La Creu systems (Figure S1.1 in Supplementary material (*Mellere*, 1993). The Montsor system is the biggest alluvial fan of the basin, composed by stacked red polimict conglomerates with a source area localized within the Axial Zone as evidenced by the high proportion of Paleozoic and Triassic clasts. The Collegats and Roca del Pesó systems are monomict conglomerates composed mostly by Mesozoic clasts deposited by alluvial fans and fan deltas with a source area located nearby and within the Axial Zone Nogueres unit (*Mellere*, 1993; *Barsó*, 2007). These interfingering alluvial systems grade laterally into lacustrine levels. The Casa Gramuntill mammal fossil site is located in one of those lacustrine levels (Figure 1.4) and yields a fossil association that suggests an MP17 age, the same age as the Sossis and Claverol fossil sites (*López-Martínez*, 1998). The Senterada allogroup unconformably overlies both the Pallaresa allogroup in the La Pobla basin and a Paleozoic and Mesozoic substratum above the Nogueres unit in the Senterada basin (Figure 2). It is composed of polymict conglomerates organized in 3 sequences (S1 to S3) with a source area located to the N-NE within the Nogueres unit (*Mellere*, 1993). Unconformably overlying the Senterada allogroup, both in the La Pobla and the Senterada basins, the Antist allogroup is characterised by massive very coarse alluvial fan conglomerates composed mainly of Paleozoic clasts from the Axial Zone, with a minor contribution of Triassic clasts (*Mellere*, 1993, *Barsó and Ramos*, 2007).

Cropping out between the Sis and La Pobla de Segur conglomerates, the basal units of the Gurp conglomeratic body consist of the Espills and Gurp formations (*Picart et al*., 2009).

Paleozoic clasts are present both in the Espills and Gurp Formations (*Picart et al*., 2009). The upper sequences of the Gurp Formation (Gurp 3 and 4) are characterized by massive alluvial fan conglomerates with a higher proportion of Paleozoic clasts than the lower units (*Picart et al*., 2009), which contrast with the facies and composition of their equivalents in the La Pobla de Segur conglomerates (the Pesonada allogroup) composed of Mesozoic clasts (Figure 1.4). On top of the Gurp Fm. the sequence of units is equivalent to the Ermita, Pallaresa (Montsor system) and Senterada allogroups of La Pobla area.

REFERENCES

Arbués, P., Mellere, D., Falivene, O., Fernández-Bellón, O., Muñoz, J. A., Marzo, M. & De Gibert, J. M. (2007). Context and architecture of the Ainsa-1-quarry channel complex, Spain. In T. H. Nilsen, R. D. Shew, G. S. Steffens, & J. R. J. Studlick (Eds.), *Atlas of deep-water outcrops* (p. 20). AAPG Studies in Geology 56, cd-rom.

Barnolas, A. & Gil-Peña, I. (2001). Ejemplos de relleno sedimentario multiepisódico en una cuenca de antepaís fragmentada: La Cuenca Surpirenaica. *Boletín Geológico y Minero*, *112*(3), 17–38.

Barnolas, A., Samsó, J. M., Teixell, A., Tosquella, J. & Zamorano, M. (1991). *Evolución sedimentaria entre la Cuenca de Graus-Tremp y la Cuenca de Jaca-Pamplona* (p. 123). Vic: I Congreso del Grupo Español del Terciario, Guide Book 1.

Barsó, D. (2007). *Análisis de la procedencia de los conglomerados sinorogénicos de La Pobla de Segur (Lérida) y su relación con la evolución tectónica de los Pirineos centro-meridionales durante el Eoceno medio-Oligoceno*. Universitat de Barcelona.

Barsó, D. & Ramos, E. (2007). Procedencia de los conglomerados sinorogénicos de La Pobla de. *Geogaceta*, *41*, 19–22.

Bentham, P. (1992). *The tectono-stratigraphic development of the western oblique ramp of the South-Central Pyrenean thrust system, Northern Spain*. PhD Thesis. University of Southern California. 253 pp.

Bentham, P. A. & Burbank, D. W. (1996). Chronology of Eocene foreland basin evolution along the western oblique margin of the South-Central Pyrenees. In P. F. Friend & C. J. Dabrio (Eds.), *Tertiary basins of Spain* (pp. 144–152). Cambridge University Press.

Bentham, P. A., Burbank, D. W. & Puigdefàbregas, C. (1992). Temporal and spatial controls on the alluvial architecture of an axial drainage system: late Eocene Escanilla Formation, southern Pyrenean foreland basin, Spain. *Basin Research*, *4*, 335–352.

Beaumont, C., Muñoz, J. A., Hamilton, J. & Fullsack, P. (2000). Factors controlling the Alpine evolution of the central Pyrenees inferred from a comparison of observations and geodynamical models. *Journal of Geophysical Research*, *105*(B4), 8121–8145.

Cámara, P. & Klimowitz, J. (1985). Interpretación geodinámica de la vertiente centro-occidental surpirenaica

(Cuencas de Jaca-Tremp). *Estudios Geológicos*, *41*, 391–404.

Casanovas-Cladellas, M. L. (1975). Estratigrafía y paleontología del yacimiento ludiense de Roc de Santa (Area del Noguera Pallaresa). *Paleontologia i Evolució*, *10*, 1–158.

Choukroune, P. (1976). Structure et évolution tectonique de la zone Nord-Pyrénéenne. Analyse de la déformation dans une portion de chaîne à schistosité subverticale. *Mémoire de la Societè Géologique de France*, *127*, 1–116.

Coney, P. J., Munoz, J. A., Mcclay, K. R. & Evenchick, C. A. (1996). Syntectonic burial and post-tectonic exhumation of the southern Pyrenees foreland fold-thrust belt. *Journal of the Geological Society*, *153*(1), 9–16.

Costa, E., Garcés, M., López-Blanco, M., Beamud, E., Gómez-Paccard, M. & Larrasoaña, J. C. (2010). Closing and continentalization of the South Pyrenean foreland basin (NE Spain): magnetochronological constraints. *Basin Research*, *22*(6), 904-917

Cuevas-Gozalo, M. (1989). *Sedimentary facies and sequential architecture of tide-influenced alluvial deposits. An example from the Middle Eocene Capella Fm; South-Central Pyrenees; Spain*. *Geologica Ultraiectina* (Vol. 61, p. 152).

Cuevas-Gozalo, M., Donselaar, M. E. & Nio, S. D. (1985). Eocene clastic tidal deposits in the Tremp-Graus Basin (Provs. of Lérida and Huesca). *6th European Regional Meeting IAS Guidebook Excursion n^{o} 6* (pp. 215–266).

De Federico, A. (1981). La sedimentación de talud en el sector occidental de la cuenca paleógena de Ainsa. *Publicaciones de Geología* (Vol. 13, p. 271). Universitat de Barcelona.

Dreyer, T., Corregidor, J., Arbués, P. & Puigdefàbregas, C. (1999). Architecture of the tectonically influenced Sobrarbe deltaic complex in the Ainsa Basin, northern Spain. *Sedimentary geology*, *127*, 127–169.

Eichenseer, H. (1988). *Facies geology of Late Maastrichtian to Early Eocene coastal and shallow marine sediments, Tremp-Graus basin, northeastern Spain*. PhD Thesis. University of Tübingen. 237 pp.

Farrell, S. G., Williams, G. D. & Atkinson, C. D. (1987). Constraints on the age of movement of the Montsech and Cotiella thrusts, south central Pyrenees, Spain. *Journal of the Geological Society of London*, *144*, 907–914.

Fischer, M. W. (1984). Thrust tectonics in the North Pyrenees. *Journal of Structural Geology*, *6*(6), 721–726.

Fitzgerald, P. G., Muñoz, J. A., Coney, P. J. & Baldwin, S. L. (1999). Asymmetric exhumation accross the Pyrenean orogen: implications for the tectonic evolution of a collisional orogen. *Earth and Planetary Science Letters*, *173*(3), 157–170.

Fonnesu, F. (1984). *Estratigrafía física y análisis de facies de la secuencia de Fígols, entre el río Noguera Pallaresa e Iscles (prov. de Lérida y Huesca)*. PhD Thesis. Universitat Autònoma de Barcelona. 317 pp.

García-Senz, J. (2002). *Cuencas extensivas del Cretácico inferior en los Pirineos centrales, formación y subsecuente inversión*. PhD Thesis. Universitat de Barcelona. 310 pp.

Garrido-Megías, A. (1968). Sobre la estratigrafía de los conglomerados de Campanué (Santa Liestra) y formaciones superiores del Eoceno (extremo

occidental de la cuenca Tremp-Graus, Pirineo central, provincia de Huesca). *Acta Geológica Hispánica*, *3*, 39–43.

Garrido-Megías, A. (1972). Precisiones sobre la "mise en place" del manto de Gavarnie en el borde norte del valle del Ebro (Región de Barbastro, provincia de Huesca). *Acta Geológica Hispánica*, *VII*(2), 50–52.

Garrido-Megías, A. (1973). *Estudio geológico y relación entre tectónica y sedimentación del Secundario y Terciario de la vertiente meridional pirenaica en su zona central (provincias de Huesca y Lérida).* PhD Thesis. Universidad de Granada. 395 pp.

Garrido-Megías, A. & Ríos, L. M. (1972). Síntesis geológica del Secundario y Terciario entre los ríos Cinca y Segre (Pirineo Central de la vertiente surpirenaica, provincias de Huesca y Lérida). *Boletín Geológico y Minero*, *LXXXIII*, 1–47.

Gibson, M., Sinclair, H. D., Lynn, G. & Stuart, F. M. (2007). Late- to post-orogenic exhumation of the Central Pyrenees revealed through combined thermochronological data and modelling. *Basin Research*, *19*(3), 323–334.

Jammes, S., Manatschal, G., Lavier, L., & Masini, E. (2009). Tectonosedimentary evolution related to extreme crustal thinning ahead of a propagating ocean: Example of the western Pyrenees. *Tectonics*, *28*(4).

Koops, M. & Van Rossem, S. (1985). Cajigar and Cornudella Formations. In M. E. Donselaar & C. R. Geel (Eds.), *Guide to the Sedimentology of the Tremp-Graus Basin* (pp. 111–121). Utrecht: State University of Utrecht.

Lagabrielle, Y., Labaume, P., & De Saint Blanquat, M. (2010). Mantle exhumation, crustal denudation, and gravity tectonics during Cretaceous rifting in the Pyrenean realm (SW Europe): Insights from the geological setting of the lherzolite bodies. *Tectonics*, *29*(4).

López-Martínez, N. (1998). Los yacimientos de mamíferos del Eoceno de la Pobla de Segur. In N. López-Martínez, J. Civis, M. L. Casanovas & R. Daams (Eds.), *Geología y Paleontología del Eoceno de La Pobla de Segur (Lleida)* (pp. 9–17). Universitat de Lleida.

Mateu-Vicens, G., Pomar, L. & Ferrández, C. (2012). Nummulitic banks in the upper Lutetian "Buil level", Ainsa Basin, South Central Pyrenean Zone: the impact of internal waves. *Sedimentology*, *59*(2), 527–552.

Mey, P. H. W., Nagtegaal, P. J. C., Roberti, K. J. & Hartevelt, J. J. A. (1968). Lithostratigraphic subdivision of post-hercynian deposits in the south-central Pyrenees, Spain. *Leidse Geol. Meded.*, *41*, 221–228.

Mellere, D. (1992). *I conglomerati di Pobla de Segur: Stratigrafia fisica e relazioni tettonica-sedimentazione*. PhD Thesis. Universita degli studi di Padova. 203 pp.

Mellere, D. (1993). Thrust generated back-fill stacking of alluvial fan sequences, south-central Pyrenees, Spain (La Pobla de Segur conglomerates). *Special Publication of the Internal Association of Sedimentology*, *20*, 259–276.

Metcalf, J. R., Fitzgerald, P. G., Baldwin, S. L. & Muñoz, J. A. (2009). Thermochronology of a convergent orogen: constraints on the timing of thrust faulting and subsequent exhumation of the Maladeta Pluton in the Central Pyrenean Axial Zone. *Earth and Planetary Science Letters*, *287*(3-4), 488–503.

Mochales, T., Barnolas, A., Pueyo, E. L., Casas, A. M., Serra-Kiel, J., Samsó, J. M. & Ramajo, J. (2012). Chronostratigraphy of the Boltaña anticline and the Ainsa Basin (Southern Pyrenees). *Geological Society of American Bulletin*, *124*(7-8), 1229–1250.

Morris, R., Sinclair, H., Yelland, A., Hovius, N. & Leeder, M. (1998). Exhumation of the Pyrenean orogen; implications for sediment discharge. *Basin Research*, *10*(1), 69–85.

Muñoz, J.A., Coney, P. McClay, K. R. & Evenchick, C. A. (1997). Discussion on syntectonic burial and post-tectonic exhumation of the southern Pyrenees foreland fold-thrust belt - Reply. *Journal of the Geological Society*, *154*, 361–365.

Muñoz, J.A. (1992). Evolution of a continental collision belt: ECORS-Pyrenees crustal balanced cross-section. In K. McClay (Ed.), *Thrust Tectonics* (pp. 235–246). Chapman & Hall.

Muñoz, J.A. (2002). The Pyrenees Alpine tectonics; I, The Alpine system north of the Betic Cordillera. *The Geology of Spain* (p. 649). The Geological Society, London.

Muñoz, J.A. & Vergés, J. (1990). Thrust sequences in the Southern Central Pyrenees. *Bulletin de la Societè Geologique de France*, *6*(2), 265–271.

Mutti, E., Luterbacher, H. P., Ferrer, J. & Rosell, J. (1972). Schema estratigrafico e lineamenti di facies del Paleogeno marino della zona centrale sudpirenaica tra Tremp (Catalogna) e Pamplona (Navarra). *Mem. Soc. Geologica Italia*, *11*, 391–416.

Mutti, E., Remacha, E., Sgavetti, M., Rosell, J., Valloni, R. & Zamorano, M. (1985). Stratigraphy and facies characteristics of the Eocene Hecho Group turbidite systems, South-Central Pyrenees. *6th European Regional Meeting IAS Guidebook Excursion n^{o}12* (pp. 519–576).

Nijman, W. & Nio, S. D. (1975). The Eocene Motañana delta. In J. Rosell & C. Puigdefàbregas (Eds.), *Sedimentary evolution of the Paleogene South Pyrenean Basin* (p. 56). IAS 9th International Congress, Nice.

Nio, S. D. (1976). Marine transgressions as a factor in the formation of sand waves complexes. *Geol. en Mijnbouw*, *55*, 18–40.

Pérez-Rivarés, F. J., Garcés, M., Arenas, C. & Pardo, G. (2004). Magnetostratigraphy of the Miocene continental deposits of the Montes de Castejón (central Ebro basin, Spain): geochronological and paleoenvironmental implications. *Geologica Acta*, *2*(3), 221–234.

Picart, J., Carrera, N., Solé, J., Montaner, J., Rivas, G., Muñoz, J. A., Serra, L., Beamud, E., Arbués, P., Mencos, J. & Perea, H. (2009). Tremp 252-1-2 (65-22) [document cartogràfic]. 1:25000. Sèrie Mapa Geològic de Catalunya 1:25000, Geotreball 1. Institut Cartogràfic de Catalunya (ICC) Servei Geològic de Catalunya (IGC).

Puigdefàbregas, C. & Souquet, P. (1986). Tecto-sedimentary cycles and depositional sequences of the Mesozoic and Tertiary of the Pyrenees. *Tectonophysics*, *129*, 173–203.

Pujalte, V., Baceta, J.I., Schmitz, B., Orue-Etxebarria, X., Payros, A. & Bernaola, G. (2009). Redefinition of the Ilerdian Stage (early Eocene). *Geologica Acta*, 7(1-2), 177-194

Reynolds, A. (1987). *Tectonically controlled fluvial sedimentation in the South-Pyrenean Foreland Basin,*. University of Liverpool.

Riba, O., Reguant, S. & Villena, J. (1983). Ensayo de síntesis estratigráfica y evolutiva de la cuenca terciaria del Ebro. In J. M. Ríos (Ed.), *Geología de España. Libro Jubilar* (pp. 131–159). Instituto Geológico y Minero de España (IGME).

Robles, S. (1982). Estudio comparativo del sistema aluvial del borde suroccidental de los Catalánides, en la transversal de Prat de Compte (Tarragona) y los abanicos aluviales de La Pobla de Segur (Prepirineo de Lérida). *Acta Geológica Hispánica*, *17*(4), 255–269.

Robles, S. (1984). El complejo sedimentario aluvial y lacustre de edad paleógena de la Pobla de Segur entre los ríos Noguera Pallaresa y Flamisell (Prepirineo de Lérida). *Ilerda*, *24*, 110–144.

Robles, S. & Ardévol, L. (1984). Evolución paleogeográfica y sedimentológica de la cuenca lacustre de Sossís (Eoceno superior, Prepirineo de Lérida): ejemplo de influencia de la actividad de abanicos aluviales en el desarrollo de una cuenca lacustre asociada. *Publicaciones de Geología*, *20*(Homenaje a Luis Sánchez de la Torre), 233–268.

Roest, W. R. & Srivastava, S. P. (1991). Kinematics of the plate boundaries between Eurasia, Iberia, and Africa in the North-Atlantic from the Late Cretaceous to the present. *Geology*, *19*(6), 613–616.

Rosell, J. & Riba, O. (1966). Nota sobre la disposicion sedimentaria de los conglomerados de Pobla de Segur (Provincia de Lerida). *Pirineos*, *22*(81-82), 61–74.

Rosenbaum, G., Lister, G. S. & Duboz, C. (2002). Relative motions of Africa, Iberia and Europe during Alpine orogeny. *Tectonophysics*, *359*(1-2), 117–129.

Schaub, H. (1981). Nummulites et Assilines de la Tethys Paléogène. Taxonomie, phylogénése et biostratigraphie. *Mémoires Suisses Paléont*, *104-106*, 1–236.

Séguret, M. (1972). Étude tectonique des nappes et séries décollées de la partie centrale du versant sud des Pyrénées – Charactère synsedimentaire, role de la comprension et de la gravité. *Publications USTELA, Montpellier, Série géologie structurale*, *2*, 155.

Serra-Kiel, J., Canudo, J. I., Dinares, J., Molina, E., Ortiz, N., Pascual, J. O., Samsó, J. M. & Tosquella, J. (1994). Cronoestratigrafía de los sedimentos marinos del Terciario inferior de la Cuenca de Graus-Tremp (Zona Central Surpirenaica). *Revista de la Sociedad Geológica de España*, *7*(3-4), 273–297.

Sinclair, H. D., Gibson, M., Naylor, M. & Morris, R. G. (2005). Asymmetric growth of the Pyrenees revealed through measurement and modeling of orogenic fluxes. *American Journal of Science*, *305*(5), 369–406.

Soler, M. & Garrido-Megías, A. (1970). La terminación occidental del manto de Cotiella. *Pirineos*, *98*, 5–12.

Teixell, A. (1996). The Anso transect of the southern Pyrenees: basement and cover thrust geometries. *Journal of the Geological Society*, *153*(2), 301–310.

Teixell, A. (1998). Crustal structure and orogenic material budget in the west central Pyrenees. *Tectonics*, *17*(3), 395–406.

Teixell, A. & Muñoz, J. A. (2000). Evolución tectono-sedimentaria del Pirineo meridional durante el Terciario: una síntesis basada en la transversal del río Noguera Ribagorçana. *Revista de la*

Sociedad Geológica de España, *15*(2), 251–264.

Tosquella, J. (1988). *Estudi sedimentològic i biostratigràfic de la Formació Gresos de Roda (Eocè, conca de Tremp-Graus)*. Tesi de llicenciatura. Universitat de Barcelona. 540 pp.

Van Eden, J. G. (1970). A reconaissance of deltaic environment in the middle Eocene of the south-central Pyrenees, Spain. *Geol. en Mijnbouw*, *49*(2), 145–157.

Van Lunsen, H. (1970). Geology of the Ara-Cinca region, Spanish Pyrenees. *Bull. Soc. Géol. France*, *VI*(2), 265–271.

Vergés, J. (1993). *Estudi tectònic del vessant sud del Pirineu oriental i central. Evolució cinemàtica 3D*. PhD Thesis. Universitat de Barcelona. 203 pp.

Vergés, J., & Muñoz, J. A. (1990). Thrust sequence in the south-central Pyrenees. *Bull. Soc. Géol. France*, *6*(2), 265–271.

Vincent, S. (1993). *Fluvial Paleovalleys in Mountain Belts: An Example from the South Central Pyrenees*. PhD Thesis. University of Liverpool. 407 pp.

Vincent, S. J. (2001). The Sis palaeovalley: a record of proximal fluvial sedimentation and drainage basin development in response to Pyrenean mountain building. *Sedimentology*, *48*, 1235–1276.

1.3.- METHODS

1.3.1.- PALEOMAGNETISM

Paleomagnetism is the study of the Earth's magnetic field recorded by rocks. The Earth's magnetic field is originated by the convection of the iron rich material of the Earth's outer core. At the Earth's surface the geomagnetic field is approximately that of a geocentric axial dipole (GAD) (*Hospers*, 1954). This means that it is a two opposite sign field centered at the center of the Earth and aligned with the spin axis of the Earth. However, this dipolar field is not static and it is currently tilted 10.7° from the rotation axis. Nevertheless, when the paleomagnetic field is averaged over a sufficient time interval (tens to hundreds of thousand years), it conforms to the field expected from a geocentric axial dipole and validates the GAD hypothesis. Only the 90% of the magnetic field can be explained by the geocentric axial dipole model (*Langereis et al.*, 2010), the remainder of the field is referred to as the non-dipole field and it is the sum of non geocentric dipolar fields, fields of non-dipolar origin and of external origin. The magnetic field at any point of the Earth surface is defined by two angles (Figure 1.5): declination (Dec), defined as the angle between the geographic north and the horizontal component of the magnetic field and which ranges from 0 to 360°; and inclination (Inc), defined as the angle between the magnetic field and the horizontal plane, ranging from -90 to 90° and being positive downwards.

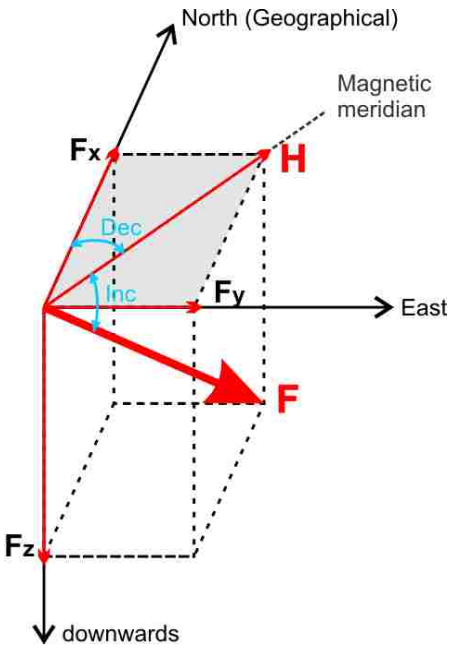

Figure 1.5 – Description of the direction of the magnetic field (F). Inclination (Inc) is the vertical angle (= dip) between the horizontal and F; declination (Dec), is the azimuthal angle between the horizontal component of F (H) and the geographic north. Modified from *Opdyke & Channel* (1996)

The bases of Paleomagnetism are that the Earth's magnetic field changes its intensity and direction both in time and space and that the rocks contain minerals that can lock in and

preserve a record of the ambient magnetic field. The magnetization naturally present in a rock is termed Natural Remanent Magnetization (NRM). Common minerals contributing to the NRM are usually iron oxides such as magnetite, hematite, and maghemite, iron hydroxides (goethite), and iron sulphides including pyrrhotite and greigite. There are mainly three different mechanisms in nature by which these minerals are magnetized:

- Thermoremanent Magnetization (TRM): is the magnetization produced by cooling across the Curie temperature of the magnetic minerals, which lock their magnetic domains parallel to the ambient magnetic field. This is the form of acquisition for most igneous rocks. Most common carriers of TRM belong to the titanomagnetite solid solution series.

- Chemical Remanent Magnetization (CRM): acquired due to precipitation of magnetic minerals below their blocking temperatures in presence of a magnetic field. The magnetic moment is blocked when the crystal grows through a critical size. Chemical reactions leading to precipitation of ferromagnetic minerals include the alteration of a preexisting mineral or precipitacion of a ferromagnetic mineral from solution. Processes leading to a CRM acquisition can occur in an early postdepositional stage, but also in later stage during burial or the exhumation history of the rocks. It is commonly found in sedimentary rocks acquired during early burial and diagenetic processes. Typical CRM carriers in continental sediments are hematite and goethite cements.

- Detrital Remanent Magnetization (DRM): acquired after deposition of detrital magnetic grains and lithification of sedimentary rocks. If the magnetic grains are sufficiently small, they act as a compass needle producing a statistical particle alignment with the ambient field as they settle. Magnetization is blocked as early compaction of the sediment reduces porosity and prevents further mechanical rotation of magnetic particles. Postdepositional reworking processes such as bioturbation can affect magnetization in different ways causing either randomization or re-alignment of magnetic grains. Common carriers of a DRM are magnetite and hematite, because they resist erosion and transport along the sediment transfer system.

Therefore, NRM may contain several remanences, resulting from the addition of a number of components of different age, each carried by a characteristic population of

magnetic particles. The primary magnetization is the component of the NRM that was acquired when the rock formed. After formation the primary magnetization may decay either partly or completely and additional components (secondary magnetizations) may overprint it by several processes. One of the main tasks in all paleomagnetic investigations is to identify and separate the magnetic components in the NRM, using a range of demagnetization procedures, being stepwise thermal and/or alternating field (AF) demagnetization the most common ones (*As & Zijderveld*, 1958; *Zijderveld*, 1967; *Butler*, 1992; *Opdyke & Channell*, 1996; *Tauxe*, 1998). During demagnetization experiments, samples are subjected to stepwise increasing values of temperature or AF in a zero field environment. The remaining magnetisation is measured after each demagnetization step and the resulting changes in direction and intensity are displayed and analyzed. Measurements are made of components of magnetic moment of the specimen (Mx, My and Mz, in sample coordinates) and then converted to geographic and stratigraphic coordinates. Although projections on a sphere are commonly used, the most common representation of results of progressive demagnetization are vector end point or orthogonal projection diagrams, also known as Zijderveld diagrams (*Zijderveld*, 1967). The power of this display is the ability to display directional and intensity information on a single diagram by projecting the vector onto two orthogonal planes. Significant scatter exists in the expected linear trajectories of vector component diagrams. Therefore a rigorous, quantitative technique is needed to determine the direction of the best-fit line through the scattered points. Principal component analysis and least-square analysis is used for this purpose (*Kirschvink*, 1980)

The most stable and consistent component that can be isolated is referred to as the characteristic remanent magnetization (ChRM). This ChRM is further investigated to establish the timing of the remanence acquistition relative to the age of the rock and the age of deformation. To achieve this several stability tests exist:

- Fold test: it consists in comparing the magnetic directions from opposing flanks of a folded rock unit before and after rotating them about the bedding strike. If tilt correction causes clustering of directions from both flanks, the test is positive meaning that the remanence was acquired before deformation. Conversely if directions cluster in present-day coordinates and disperse upon tilt correction, the test is negative, meaning that magnetization occurred after the deformation event. Strictly speaking, a positive fold test only proves that the remanence predates folding, but not necessarily its primary origin.

- Consistency test: a ChRM is considered primary in origin when it defines a sequence of polarity reversals laterally traceable by independent means (e.g. lithostratigraphy) between distant sections from different parts of a basin.

- Reversal test: the observation of ChRM directions with different polarity and, in particular, the occurrence of antiparallel (within statistical error) directions is usually taken as a strong indication for the primary origin of that ChRM. However, it only informs about the effectiveness in isolating the paleomagnetic components which may actually be primary or secondary.

Changes with time in magnitude and direction of the geomagnetic field range from milliseconds, hours, or days (pulsations or short-term fluctuations, daily magnetic variations, or magnetic storms) to centuries, thousands of years, or million of years (secular variations, magnetic excursions, and polarity reversals). Changes with periods between 1 year and 10^5 years constitute which is known as Geomagnetic Secular Variation. Among the longer term variations of the geomagnetic field, the polarity reversals, with durations ranging from 10^4 to 10^6 years, are the switch of north and south magnetic poles. The present configuration of the dipole field with the north magnetic pole close to the north geographic pole is considered a normal polarity interval, while opposite configuration is considered a reversed polarity interval (Figure1.6).

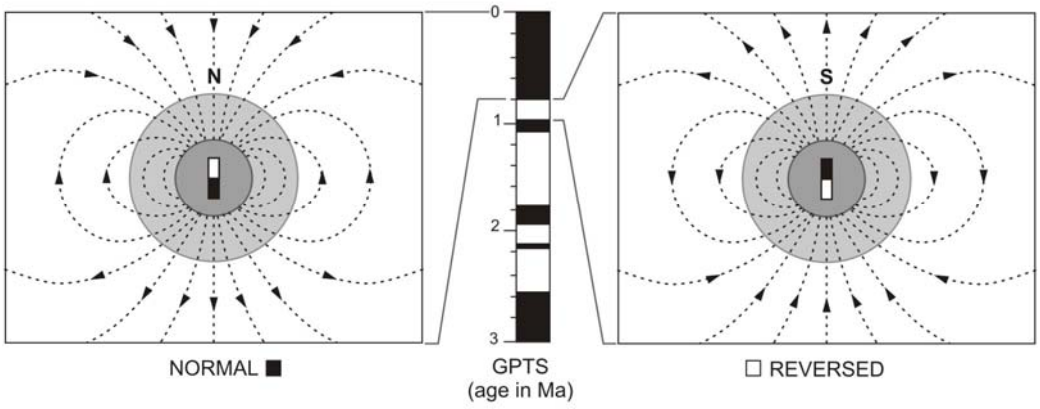

Figure 1.6 – Schematic representation of the magnetic field created by a geocentric axial dipole. During normal polarity intervals the average magnetic north is at the geographic north pole and inclination is positive in the northern hemisphere (downward directed). Conversely, during reverse polarity intervals, inclination is negative in the northern hemisphere and positive in the southern one. In the Geomagnetic Polarity Time Scale (GPTS, in the centre of the figure) normal polarity periods are represented as black intervals and reversed polarity periods as white ones. Modified from *Langereis et al.,* (2010).

Intervals of geological time having a constant geomagnetic field polarity are defined as polarity chrons. The magnetic reversals are not periodic but instead appear to occur randomly in time, so that a sequence of reversals defines polarity chrons and subchrons of very variable lengths (Figure 1.6). The duration of a polarity transition is imperfectly known but it is probably in the order of 10^3 to 10^4 years, fast enough to be considered globally synchronous on geologic time scales. Hence, each polarity reversal is a global feature, which is very useful for magnetic stratigraphy because a short sequence of 10-20 reversals forms a distinctive pattern which can be used for geological correlations on a worldwide basis. The association of radiometric ages with key biostratigraphic stage boundaries, which have been correlated by magnetostratigraphy to the seafloor magnetic anomaly record, yields a dated geomagnetic polarity timescale (GPTS) (*LaBreque et al.*, 1977; *Cande & Kent*, 1992) (Figure 1.6). Magnetostratigraphy refers to the application of the well-known principles of stratigraphy to the pattern of polarity reversals registered in a rock succession by means of NRM acquisition processes. The dated GPTS is used to date magnetostratigraphic sections by correlation to the GPTS of the local reversal patterns. The sample and data processing in magnetostratigraphic studies are the same as in other paleomagnetic studies and strict criteria have been proposed to define the quality of magnetostratigraphy (*Opdyke & Channell*, 1996).

The ability of rocks to record the direction of the ancient magnetic field also provides the key quantitative information for unravelling tectonic deformation in orogenic belts. The application of paleomagnetism to tectonics at subcontinental scale is referred to as Magnetotectonics (*McClelland et al.*, 1985). Rocks in an orogenic environment are more likely to have their primary magnetism partially or completely overprinted by magnetizations linked to the deformation, but at the same time the deformed nature of the rocks means that the paleomagnetic fold test is more readily applied to constrain the geological ages of the magnetizations than in less deformed settings. Paleomagnetic analysis assumes that the mean direction of magnetization recovered from the rock-unit is a record of the time averaged dipole field source at the time of magnetization. The cumulative deformation can then be resolved by comparing this direction with the predicted direction at the study location at the time of magnetization. Usually, the difference is the resultant of more than one episode of deformation and in favourable circumstances it can be decomposed using geological evidence or from studying the paleomagnetism of rocks of different ages. The angular deformation is usually considered in terms of differences of declination and inclination with respect to the reference direction from the stable plate. The difference between the observed and expected

directions is described in terms of rotation and flattening. A difference in declination implies rotation about a quasi-vertical axis. When applied to curved orogens, vertical axis rotations (VARs) can help unraveling if the orogenic curvature is primary, secondary or progressive (*Weil & Sussman*, 2004; *Weil et al.*, 2010) (Figure 1.7).

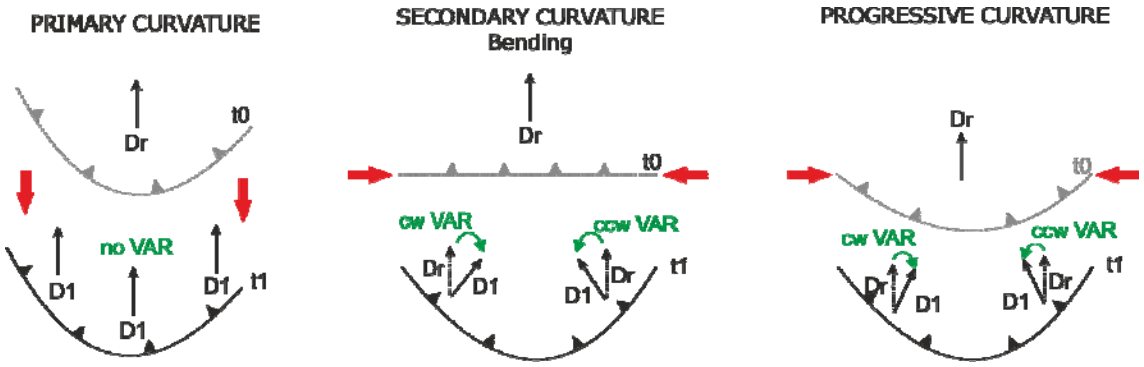

Figure 1.7 – Schematic representation of types of orogenic curvatures based on timing relationships between thrusting and vertical axis rotations (VAR). Dr: reference direction, D1: direction recorded in time 1. No VAR are detected in primary arcs, whereas in secondary and progressive arcs VARs are observed.

REFERENCES

As, J. A. & Zijderveld, J. D. A. (1958). Magnetic cleaning of rocks in palaeomagnetic research. *Geophysical Journal of Royal Astronomical Society*, *1*, 308–319.

Butler, R. F. (1992). *Paleomagnetism: Magnetic domains to geologic terranes* (p. 319). Boston: Blackwell Scientific Publications.

Cande, S. C., & Kent, D. V. (1992). A new geomagnetic polarity time scale for the late Cretaceous and Cenozoic. *Journal of Geophysical Research*, *97*(B10), 13917–13951.

Hospers, J. (1954). Rock magnetism and polar wandering. *Nature*, 173, 1183.

Kirschvink, J. L. (1980). The least-squares line and plane and the analysis of paleomagnetic data. *Geophysical Journal of the Royal Astronomical Society*, *62*, 699–718.

LaBreque, J. L., Kent, D. V. & Cande, S. C. (1977). Revised magnetic polarity time scale for Late Cretaceous and Cenozoic. *Geology*, *5*, 330–335.

Langereis, C. G., Krijgsman, W., Muttoni, G. & Menning, M. (2010). Magnetostratigraphy - concepts, definitions, and applications. *Newsletter on Stratigraphy*, *43*, 207–233.

Mcclelland, E., Courtillot, V. & Tapponier, P. (1985). Introduction. In E. Mcclelland, V. Courtillot, & P. Tapponier (Eds.), *Magnetotectonics* (pp. 709–711). Tectonics 5 (5).

Merrill, R. T., McElhinny, M. W., & McFadden, P. L. (1996). *The Magnetic Field of the Earth: Paleomagnetism, the Core, and the Deep Mantle* (p. 531). San Diego: International Geophysical Series 63, Academic Press.

Merrill, R. T. & McFadden, P. L. (2007). Paleomagnetism. In D. Gubbins & E. Herrero-Berbera (Eds.), *Encyclopedia of Geomagnetism and Paleomagnetism* (pp. 776–781). Springer.

Opdyke, N. D. & Channell, J. E. (1996). *Magnetic Stratigraphy* (p. 346). San Diego: International Geophysical Series 64, Academic Press.

Sussman, A. J., Butler, R. F., Dinarès-Turell, J., & Vergés, J. (2004). Vertical-axis rotation of a foreland fold and implications for orogenic curvature: an example from the Southern Pyrenees, Spain. *Earth and Planetary Science Letters*, *218*(3-4), 435–449.

Tauxe, L. (1998). *Paleomagnetic principles and practice* (p. 299). Dordrecht: Kluwer Academic Publisher.

Weil, A. B. & Sussman, A. J. (2004). Classification of curved orogens based on the timing relationships between structural development and vertical-axis rotations. In A. J. Sussman & A. B. Weil (Eds.), *Orogenic curvature: Integrating paleomagnetic and structural analyses* (pp. 1–17). Geological Society of America Special Paper 383.

Weil, A. B., Yonkee, A. & Sussman, A. J. (2010). Reconstructing the kinematic evolution of curved mountain belts: A paleomagnetic study of Triassic red beds from the Wyoming salient, Sevier thrust belt, USA. *GSA Bulletin*, *122*(1/2), 3–23

Zijderveld, J. D. A. (1967). A.C. demagnetization of rocks: analysis of results. In D. W. Collinson, K. M. Creer, & S. K. Runcorn (Eds.), *Methods in Paleomagnetism* (pp. 254–286). Amsterdam: Elsevier.

1.3.2.- FISSION TRACK THERMOCHRONOLOGY

Thermochronology measures the timing and rates at which rocks cool and approach the Earth surface as a result of exhumation. It can constrain erosion rates and their spatial-temporal variations on timescales of 10^5–10^7 years. Three interrelated processes are commonly used to describe the tectonic geomorphology of orogens: rock uplift, surface uplift, and erosion. As clarified by *England & Molnar* (1990), rock and surface uplift describe the vertical motion of rock or a portion of Earth's surface, respectively, relative to a datum that is suitably fixed (like sea level). Erosion is the surficial removal of mass at a point in the landscape by both mechanical and chemical processes. Therefore, the difference between rock uplift and surface uplift is erosion. According to *Ring et al.* (1999) exhumation refers to the unroofing history of a rock, defined as the vertical distance traversed relative to the Earth's surface, and it can be either erosional or tectonic. Denudation, taken in the broad sense of *Ring et al.* (1999) relates to the removal of material at a particular point or under the Earth's surface by tectonic processes and/or erosion and is more correctly viewed as a measure of material flux.

Mountain belts are typically characterized by rapid uplift and denudation, which prevents many stratigraphic and structural records of tectonic evolution being preserved over the long-term at the surface. Thermal histories of rocks provide important constraints on exhumation histories and tectonic evolution of mountain belts. The thermochronological ages of metamorphic and plutonic rocks exposed by erosion and tectonic denudation are directly related to cooling caused by the exhumation experienced (e.g. *Clark & Jäger*, 1969; *Kamp et al.*, 1989). These isotopic ages provide important information about the evolution of denuded regions and they have been widely used to explain orogenic development and dynamics (*Clark & Jäger*, 1969; *Zeitler et al.*, 1982; *Copeland et al.*, 1987; *Morris et al*., 1998; *Fitzgerald et al.*, 1999; *Sinclair et al.*, 2005).

Fission track thermochronology is based on the spontaneous fission decay of ^{238}U in uranium-bearing minerals, mainly apatites and zircons, which creates a linear damage zone, known as fission track, within the crystal lattice. These tracks accumulate in the crystal lattice of a host mineral over time and may be revealed by chemical etching and then counted under a microscope. As with other forms of radioactivity, ^{238}U spontaneous fission decay is exponential, with a fission half-life around 9×10^{15} years (*Hurford and Carter*, 1991). The numerical density of spontaneous tracks counted on a polished and etched internal surface of a mineral is a function of the rate of spontaneous fission decay, the time during which the

tracks have been accumulating and of the uranium content of the crystal. The products of radioactive decay within a crystal are generally highly mobile and they are only quantitatively retained if a sample is cold enough that they lack the energy to diffuse through the crystal lattice (*Dodson*, 1973). The thermal dependence of this diffusive loss is commonly simplified through the concept of closure temperature, representing the temperature of transition from effectively open system loss of a radiogenic daughter product to its complete retention on geological time scales (*Dodson*, 1973). For apatite, tracks begin to be retained at temperatures below ca. 150-120 °C, depending on the cooling rate and the kinetic characteristics of the crystal (e.g. *Green et al.*, 1985; *Ketcham et al.*, 1999). Determining the density of spontaneous fission tracks and the concentration of ^{238}U yields a single-grain fission-track age (*Naeser*, 1976). As already mentioned, rocks can move closer to the Earth's surface due to either tectonism or erosion. In response to persistent erosion, deeply buried rocks move upward along the local geotherm toward the surface. During this cooling various minerals within the rocks will pass through the closure temperatures for the different radiometric dating systems. When cooling rates accelerate toward the present day, they are often interpreted to result from enhanced rates of denudation. If there is no local geological evidence for recent normal faulting which could have accelerated cooling, the rapid cooling is usually explained by enhanced erosion by surface processes.

Fission tracks are unstable features that shorten (anneal) by thermal and time-dependent re-crystallization processes. Initial tracks in apatites are about 15 μm long and they are progressively annealed over geological timescales if the temperature is sufficiently high during long enough time. *Gleadow & Fitzgerald* (1987) introduced the term partial annealing zone (PAZ), which defines the zone in the crust where fission tracks are partially retained owing to thermally activated diffusion or annealing. Track shortening in apatites occurs between 60 and 110 °C (*Laslett and Galbraith*, 1996). At sufficiently low temperatures, both old and new tracks are fully retained in the crystal, whereas at increasing temperatures within the PAZ, newly formed long tracks coexist with older tracks that are progressively shortened. Therefore a distribution of track lengths reflects the balance among the ongoing creation of new 15 μm tracks and the shortening of older tracks by annealing and it is a measure of the time spent within and below the PAZ that can be used to qualitatively asses the rate of cooling through this zone (*Gleadow et al.,* 1986). Interpretation of a fission-track data set requires an integrated analysis of fission-track age, track length distribution and kinetic characteristics of the apatite grains

FT thermochronology can be applied in orogenic systems in two different ways. One approach would be the analysis of samples from bedrock vertical profiles in order to quantify the exhumation history of the orogenic belt (*Yelland*, 1990; *Morris et al.*, 1998; *Fitzgerald et al.*, 1999; *Sinclair et al.*, 2005; *Metcalf et al.*, 2009). Studies using bedrock exposures are limited to only those rocks exposed at the surface and therefore provide limited information about the entire evolution of that orogenic system because the overlying rock, which could yield a record of the earlier thermotectonic events, has been removed and deposited in adjacent basins. However, it is possible to recover this record by applying detrital FT thermochronology. Detrital FT uses the distribution of grain ages from the sedimentary detritus deposited in the sedimentary basins surrounding the orogenic belt to constrain the exhumation history of the source region of the sediment (*Cerveny et al.*, 1988; *Ruiz et al.*, 2004; *Coutand et al.*, 2006; *Rahl et al.*, 2011; *Fillon et al.*, 2013). The goal in detrital FT thermochronology is to examine stratigraphic sequences to relate changes in FT grain ages to the thermal evolution of the source region, changes in sediment provenance and landscape evolution. However, converting a cooling age extracted from a detrital sample into an exhumation rate for the source area requires several major assumptions. *Garver et al.* (1999) describes in detail the procedure to derive the average exhumation rate of a hinterland source from a population of thermochronologic data collected through a reasonably well-dated sedimentary sequence (Figure 1.8).

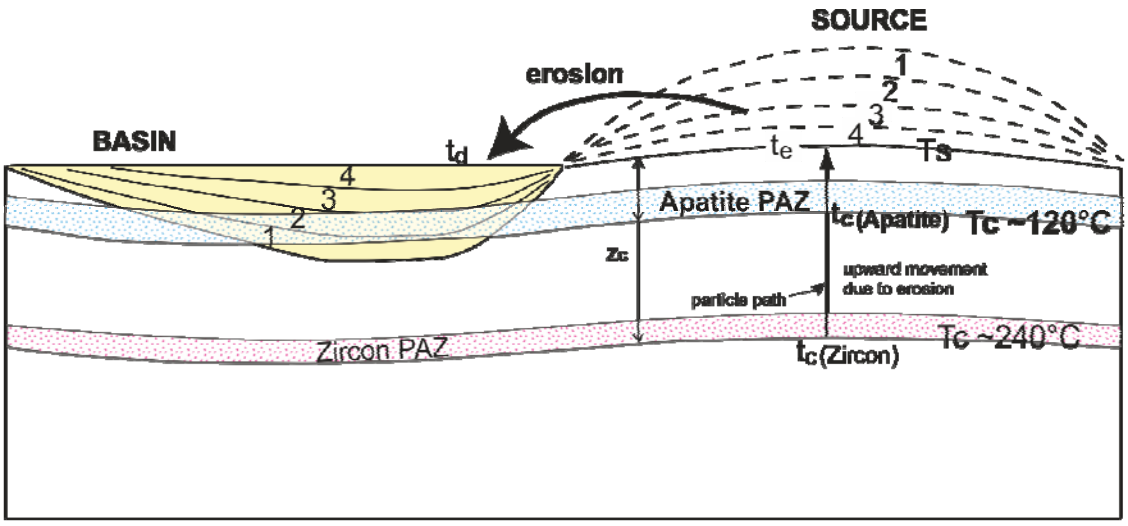

Figure 1.8 - Schematic representation of the erosion of a mountain range. The source is progressively unroofed and the sedimentary detritus is deposited in the adjacent basin. Time slices 1 to 4 correspond to 4 progressive and continuous intervals of erosion and deposition. Samples from basin deposits 1-4 record integrated exhumation rates between cooling through tc (closure temperature) and te (time of erosion). Samples buried deeply in the basin may be partially or completely annealed. Modified from *Garver et al.* (1999).

In summary, the average exhumation rate (dz/dt) is given by:

$dz/dt=((Tc-Ts)/(dT/dz))/Dt$, which is equivalent to: $dz/dt= Zc/Dt$

where Tc is the closure temperature of the thermochronometer, Ts is the surface temperature, dT/dz is the geothermal gradient, Dt is the lag time and Zc is the closure depth. The lag time is the time elapsed between the time of closure (tc in Figure 1.8) of a crystal of a given geochronological system in the source region and the time at which it is deposited in the sedimentary basin (td in Figure 1.8). Lag time can be obtained by substracting the stratigraphic age of the rock containing the detrital sample to the thermochronological age. The assumption is usually made that the time taken by the eroded detritus to be transported and deposited in the sedimentary basin is negligible compared to the time taken to reach the surface and be eroded from the closure depth (*Cerveny et al.*, 1988; Garver et al., 1999; *Ruiz et al.*, 2004). Thus, to be valid, the lag time concept implies that during their transit from the source to the basin, the detritus are not stored for time periods long enough to bias their stratigraphic age in the basin significantly (ca ≥ 1 Ma). In addition, subsequent to deposition, recycling of non-reset sediments does not significantly modify the initial stratigraphic age (*Ruiz et al.*, 2004). Short lag times reflect tectonic activity and rapid erosion in the source regions; whereas long lag times may suggest that the source regions underwent very slow exhumation as passing through the closure temperature. The latter may also include cannibalistic erosion of non-reset sediments, i.e. recycling, hence time between first deposition and redeposition may not be negligible, and as a consequence synorogenic exhumation rates cannot be constrained.

For hinterland regions other assumptions are usually made when interpreting FT data. It is necessary to assume a steady geothermal gradient at the time of closure of the geochronological system, although the geothermal gradient at that time is not trivial to derive (*Garver et al.*, 1999). Most commonly a “typical” continental geotherm of 20-30 °C/km is assumed and cooling rates are converted to erosion rates on this basis. Isotherms are assumed to remain horizontal and particle paths toward the surface, vertical. The exhumation rate is assumed to remain constant from the time of closure to the time of deposition of the crystal. Hence, this approach neglects isotherm distortion in the source region caused by topography and advection (*Stüwe et al*., 1994) as well as non vertical displacements of particles during exhumation (*Batt & Brandon,* 2002). Finally, the simplest model supposes that the exhuming topography is eroded principally from higher elevations and strictly in a vertical direction. In reality, the drainage basin may cover a large range of elevations in the source topography;

thus different peak ages identified in the detrital sediments will not necessarily be derived from distinct source terrains but rather could be derived from different elevations within a single catchment (*Garver et al.*, 1999). These restrictions imply that interpretation of detrital peak age provenance as well as long-term exhumation rates derived from them should always be treated with caution. Nevertheless, despite these simplifications and assumptions, detrital thermochronology remains a valuable tool for constraining the cooling and exhumation history of source terrains partially or totally eroded.

REFERENCES

Batt, G. E., & Brandon, M. T. (2002). Lateral thinking: 2-D interpretation of thermochronology in convergent orogenic settings. *Tectonophysics*, *349*(1-4), 185–201.

Burbank, D. W., & Anderson, R. S. (2001). *Tectonic Geomorphology* (p. 274). BLACKWELL SCIENCE LTD.

Cerveny, P. F., Naeser, N. D., Zeitler, P. K., Naeser, C. W., & Johnson, N. M. (1988). History of uplift and relief of the Himalaya during the past 18 million years: evidence from fission-track ages of detrital zircons from sandstones from the Siwalik Group. In K. L. Kleinspehn & C. Paola (Eds.), *New Perspectives in Basin Analysis* (pp. 43–61). New-York: Springer-Verlag.

Clark, S. P., & Jäger, E. (1969). Denudation rates in the Alps fro geochronologic and heat flow data. *American Journal of Science*, *267*, 1143–1160.

Copeland, P., Harrison, T. M., Kidd, W. S. F., Ronghua, X., & Yuquan, Z. (1987). Rapid early Miocene acceleration of uplift in the Gangdese Belt, Xizang (southern Tibet), and its bearing on accommodation mechamisms of the India-Asia collision. *Earth and Planetary Science Letters*, *86*, 240–252.

Coutand, I., Carrapa, B., Deeken, A., Schmitt, A. K., Sobel, E. R., & Strecker, M. R. (2006). Propagation of orographic barriers along an active reange front: insights from sandstone petrography and detrital apatite fission-track thermochronology in the intramontane Angastaco basin, NW Argentina. *Basin Research*, *18*, 1–26.

Dodson, M. H. (1973). Closure temperature in cooling geochronological and petrological systems. *Contributions to Mineralogy and Petrology*, *40*, 259–274.

England, P., & Molnar, P. (1990). Surface uplift, uplift of rocks, and exhumation of rocks. *Geology*, *18*, 1173–1177.

Fillon, C., Gautheron, C. & van der Beek, P. (2013). Oligocene-Miocene burial and exhumation of the Southern Pyrenean foreland quantified by low-temperature thermochronology. *Journal of the Geological Society, London*, 170, 67-77.

Fitzgerald, P. G., Muñoz, J. A., Coney, P. J., & Baldwin, S. L. (1999). Asymmetric exhumation accross the Pyrenean orogen: implications for the tectonic evolution of a collisional orogen. *Earth and Planetary Science Letters*, *173*(3), 157–170.

Fitzgerald, P. G., Sorkhabi, R. B., Redfield, T. F., & Stump, E. (1995). Uplift and denudation of the Central Alaska Range - a case-study in the use of apatite fission-track thermochronology to determine absolute uplift parameters. *Journal of*

Geophysical Research, Solid Earth, *100*(B10), 20175–20191.

Garver, J. I., Brandon, M. T., Roden-Tice, M., & Kamp, P. J. J. (1999). Exhumation history of orogenic highlands determined by detrital fission-track thermochronology. In U. Ring, M. T. Brandon, G. S. Lister, & S. D. Willett (Eds.), *Exhumation processes: normal faulting, ductile flow and erosion* (pp. 283–304). Geological Society London 154.

Gleadow, A. J., & Duddy, I. (1981). A natural long-term track annealing experiment for apatite. *Nuclear Tracks*, *5*, 169–174.

Gleadow, A. J. W., Duddy, I. R., Green, P. F., & Lovering, J. F. (1986). Confined fission track lengths in apatite: a diagnostic tool for thermal history analysis. *Contributions to Mineralogy and Petrology*, *94*, 405–415.

Gleadow, A. J. W., & Fitzgerald, P. G. (1987). Uplift history and structure of theTransantarctic Mountains: new evidence from fission track dating of basement apatites in the Dry Valley area, southern Victoria Land. *Earth and Planetary Science Letters*, *82*, 1–14.

Green, P. F., Duddy, I. R., Gleadow, A. J. W., & Tingate, P. R. (1985). Fission track annealing in apatite: track length measurements and the form of the Arrhenius plot. *Nucl. Tracks Radiat. Meas.*, *10*, 323–328.

Hurford, A. J., & Carter, A. (1991). The role of fission track dating in discrimination of provenance. In A. C. Morton, S. P. Todd, & P. D. W. Haughton (Eds.), *Developments in sedimentary provenance studies* (pp. 67–78). Geological Society Special Publication 57.

Kamp, P. J. J., Green, P. F., & White, S. H. (1989). Fission track analysis reveals character of collisional tectonics in New Zealand. *Tectonics*, *8*, 169–195.

Ketcham, R. A., Donelick, R. A., & Donelick, M. B. (1999). Variability of apatite fission-track annealing kinetics: III. Extrapolation to geological time scales. *Am. Mineral.*, *84*, 1235–1255.

Laslett, G. M., & Galbraith, R. F. (1996). Statistical modeling of thermal annealing of fission tracks in apatite. *Geochim. Cosmochim. Acta*, *60*, 5117–5131.

Morris, R., Sinclair, H., Yelland, A., Hovius, N., & Leeder, M. (1998). Exhumation of the Pyrenean orogen; implications for sediment discharge. *Basin Research*, *10*(1), 69–85.

Naeser, C. W. (1976). Fission track dating. *US Geological Survey*, 65.

Rahl, J. M., Haines, S. H., & Van der Pluijm, B. A. (2011). Links between orogenic wedge deformation and erosional exhumation: Evidence from illite age analysis of fault rock and detrital thermochronology of syn-tectonic conglomerates in the Spanish Pyrenees. *Earth and Planetary Science Letters*, *307*(1-2), 180–190.

Reiners, P. W., & Brandon, M. T. (2006). Using Thermochronology to understand orogenic erosion. *Annu. Rev. Earth Planet. Sci.*, *34*, 419–466.

Ring, U., Brandon, M. T., Willett, S. D., & Lister, G. S. (1999). Exhumation processes. In U. Ring, M. T. Brandon, G. S. Lister, & S. D. Willett (Eds.), *Exhumation processes: Normal faulting, ductile flow and erosion*. London: Geological Society London Special Publication 154.

Ruiz, G. M. H., Seward, D., & Winkler, W. (2004). Detrital thermochronology - a new perspective on hinterland tectonics, an example from the Andean Amazon

Basin, Ecuador. *Basin Research*, *16*(3), 413–430.

Sinclair, H. D., Gibson, M., Naylor, M., & Morris, R. G. (2005). Asymmetric growth of the Pyrenees revealed through measurement and modeling of orogenic fluxes. *American Journal of Science*, *305* (5), 369–406.

Stüwe, K., White, L., & Brown, R. (1994). The influence of eroding topography on steady-state isotherms. Application to fission track analysis. *Earth and Planetary Science Letters*, *124*(1-4), 63–74.

Yelland, A. J. (1990). Fission-track thermotectonics in the Pyrenean orogen. *Nucl. Tracks Radiat. Meas.*, *17*(3), 293–299.

Zeitler, P. K., Tahirkheli, R. A. K., Naeser, C. W., & Johnson, N. M. (1982). Unroofing history of a suture zone in the Himalaya of Pakistan by means of fission track annealing ages. *Earth and Planetary Science Letters*, *57*, 227–240.

1.4.- EUROPEAN PALEOGENE MAMMAL BIOCHRONOLOGY

The Western Europe Paleogene mammal biochronology is based on a succession of reference levels (MP levels, named from 1 to 30 in chronological order) chosen by their paleobiological representativeness and defined by the evolution stage of mammals. The MP system was adopted in the Mainz Symposium in 1987 (*Schmidt-Kittler*, 1987) (Figure 1.9) and later refined in the BiochroM'97 in Montpellier (*Aguilar et al.*, 1997). This subdivision of the Paleogene in reference levels was considered to be applicable to all parts of Europe despite regional differences in faunal composition.

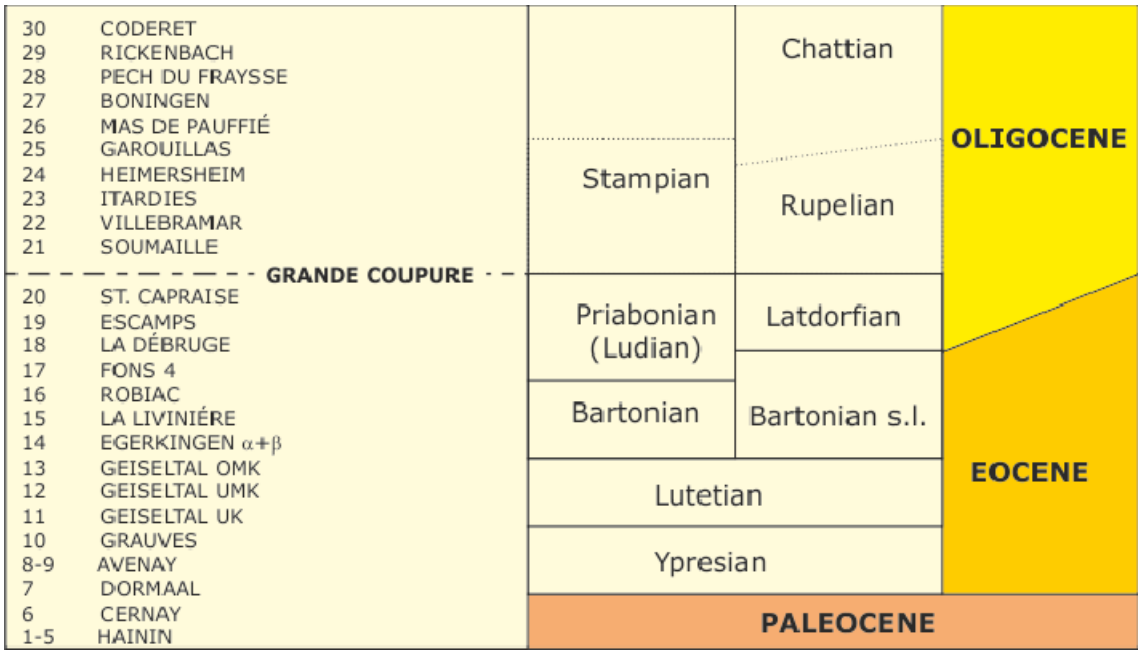

Figure 1.9- Subdivision of the European continental Paleogene based on mammals as proposed by the Symposium in Mainz, February 1987. Modified from *Schmidt-Kittler* (1987).

A reference level is justified by the presence of a determined taxon or group of taxa (association criteria in the charts of the Mainz Symposium), as well as the evolutionary and biometric stage of the different taxa when they are sufficiently well-known and described in the sites. Once defined, each reference level represents the unitary element of the biochronological scale. Conversely to other biochronological scales, a standard level does not represent an interval containing a mix of different local faunas supposed to be close in age, but a snapshot of a given single moment in the mammalian evolution in the area. Therefore, the faunas of the reference localities form points within the time axis, not intervals. No boundaries between the reference levels are defined and the faunal assemblages from other localities

have to be assigned to a particular level on the basis of their affinities as expressed by evolutionary stages and first or last evidence of species. As rates of evolution change and there is no method for measuring them, no reliable data exist to determine the duration of the time intervals laying between the reference levels.

Reference levels MP14 to MP16 are considered to represent the Bartonian (*Schmidt-Kittler*, 1987). The best defined reference locality corresponds to the Robiac site, representing MP16. It occurs in a stratified sequence and has diverse fauna well widespread in Europe. Also, it is well distinguished from later faunas by its last occurrences of many taxa. Fauna of La Livinière 2, the selected reference locality for MP15 is demonstrably older than Robiac. However, the fauna is rather small and not very widespread, although it is found in a stratified sequence. Reference locality for MP14 was typified from the karst infillings of Egerkingen α + β. This reference locality was difficult to select as stratified faunas for this age are scarce and of low diversity. Another problem arises as there are not common lineages in the faunas of La Livinière 2 and Egerkingen α + β, therefore it cannot be excluded that they may be contemporaneous, being the faunal differences due to ecological and sampling bias.

MP17 to 20 are considered to represent the Ludian (Priabonian) (*Schmidt-Kittler*, 1987). The chronological sequence of this period is mainly based on the evolution of *Palaeotherium* taxa. MP17 is represented by level Fons 4, which can be easily differentiated from the older Robiac locality. Fons 4 was preferred to other sites like Perrière or Euzet (*Hartenberger*, 1973; *Hooker*, 1987) as these sites yielded either too weak arguments or a narrower spectrum of faunas. However, since the Biochro'M congress (*Aguilar et al.*, 1997) the Perrière site was chosen to represent an intermediate reference level MP17b between MP17 and MP18 levels. Therefore, the Lower Priabonian is now represented by MP17a (Fons 4) and MP17b (Perrière) although the utility of MP17b is still under debate, especially concerning Spanish faunas (*Cuesta et al*., 2006). La Débruge, chosen to represent MP18, yielded numerous first appearances, mainly based on the *Palaeotherium* group. Although *Palaeotherium* species are not very well documented, the Escamps site was selected to represent MP19, as it contains a large number of small and large mammal species. Finally, the Saint-Capraise site was chosen to represent MP20 reference level (the last pre "Grande Coupure" level) (Figure 1.9).

1.4.1.- Regional significance and correlation of the MP Reference Levels to the Geological Time Scale

The MP system is considered to work well from regional to continental scale, although it is obvious that the spatial dispersion of the different taxa and their different evolutionary lineages are not instantaneous. Regional intermediate reference levels have been proposed to fill these gaps. Due to differences in quality of the faunal data from different parts of Europe and for different periods of the Paleogene, the degree of accuracy that can be attained by regional subdivisions varies largely. Therefore, a workable subdivision for whole Europe should be just as precise as to allow correlation of biochronological units between all parts of this bioprovince. Nevertheless, cross-correlations between different regional scales must be done inside and outside the continental area under study.

Middle and Late Eocene mammal faunistic provinces for Western Europe have been recognized by several authors (*Franzen*, 1968; *Schmidt-Kittler & Vianey-Liaud*, 1975; *Vianey-Liaud*, 1979; *Hooker*, 1986; *Peláez-Campomanes*, 1993). Provincialism phenomena in European Eocene faunas are a conspicuous feature, especially during the Late Eocene. The Eocene European paleogeography is pictured as a network of islands with varying extent and degrees of connectivity. This configuration favoured the taxonomical differentiation in Europe with endemism during insulation periods coexisting with times of faunal interchange due to migration bridges and connection between islands. Additionally, climatic changes also played a significant role on the faunal evolution during the Eocene (*Franzen*, 2003). Several works suggest the presence of an endemic Western Iberia Bio-province during the Eocene which would include most of the Iberian Peninsula and exclude the South Pyrenean area with typical European features (*Casanovas & Santafé*, 1987, 1989; *Cuesta*, 1999, 2003). This could be explained by a geographical barrier, like a sea gate, which would have isolated this area from the rest of Europe, coupled to more extreme ecological conditions than the rest of Europe. Similarly, *Checa* (1997) considers 2 paleogeographical areas in the Middle and Late Eocene of Catalonia, the pre-Pyrenean depression with fauna similar to the southern France one and the Catalan branch of the Iberian Range with exclusive forms. However, this endemism could partly represent an artifice due to the lack of both fossil remnants and paleontological works integrating European Eocene faunas with faunas from other unknown regions (*Cuesta et al.*, 2006). The North-eastern Iberian Peninsula would be excluded from the Iberian endemism area, as its faunas are coincident with those of the south of France. This is the case of the Sossís and Roc de Santa sites in La Pobla de Segur area (*Sudre*, 1978; *Casanovas*, 1975; *López-*

Martínez et al., 1998) which are similar to associations in the South of France (Euzet and Fons 4) and Switzerland. However, although they are pretty similar, the Spanish Pyrenean faunas show less evolved features than the French isochronous ones or, in other words, they would be slightly older (*Cuesta et al.*, 2006).

As already explained, many of the reference sites are placed in fissure-fillings and non-correlatable sections, therefore reliable stratigraphic relationships between successive MP levels are not existent. However, a correlation attempt of the MP scale has been built on the basis of the available correlations with marine units in the Paris and Hampshire basins (*Cavelier et al.*, 1983; Gély & Lorenz, 1991). Magnetostratigraphy has been rarely applied to this mammal Palaeogene chronology because of unsuitable stratigraphic sections in on the type mammal localities of Central and Western Europe. Previous attempts to calibrate the MP scale with the geomagnetic polarity time scale (GPTS) have not provided further constraints since they are based on very short sections that don't yield a distinctive pattern hindering an independent correlation to the GPTS (*Lévêque*, 1993; *Legendre & Lévêque*, 1997). Therefore, the reported ages of the MP scale are not sufficiently reliable and need further independent constraints from regions where the marine-continental correlations and magnetostratigraphy can be integrated and cross-checked. In contrast to other regions in Europe, the south Pyrenean basins offer a thick and continuous stratigraphic framework which is suitable for magnetostratigraphic dating. Recent magnetostratigraphic work in the Ebro Basin (*Barberà et al.*,2001) refined the chronology of several Ebro local biozones ranging from MP19-20 (Late Eocene) up to MN-1 (Early Miocene) by correlation of a ~ 1000 m thick composite magnetostratigraphic section to the GPTS. More recently, *Costa et al.* (2011) integrated magnetostratigraphic data from the Ebro basin (*Costa et al.*, 2011; *Barberà et al.*, 2001) and magnetostratigraphic and biochronological information from the Hampshire basin (*Gale et al.*, 2006; *Hooker*, 1992, 2010; *Hooker et al.*, 2004, 2007, 2009) establishing a precise age for the "Grande Coupure", the major mammal faunal turnover at the Eocene-Oligocene transition.

REFERENCES

Aguilar, J. P., Legendre, S., & Michaux, J. (1997). Synthéses et tableaux de corrélations. In J. P. Aguilar, S. Legendre, & J. Michaux (Eds.), *BiochroM'97: Biochronologie mammalienne du Cénozoïque ren Europe et domaines reliés. Actes du Congrès BiochroM'97.* (pp. 769–805). Montpellier: Inst. Montpellier Memoire Trav. E.P.H.E 21.

Barberà, X., Cabrera, L., Marzo, M., Parés, J. M., & Agustí, J. (2001). A complete

terrestrial Oligocene magnetostratigraphy from the Eastern Ebro Basin, Spain. *Earth and Planetary Science Letters*, *187*(1-2), 1–16.

Casanovas, M. L., & Santafé, J. V. (1987). Cantabrotherium truyolsi nov. gen. nov. sp. (Palaeotheriidae, Perissodactyla), un exemple d'endémisme dans le Paléogene ibérique. *Münch. Geowiss. Abh.*, *(A) 10*, 243–252.

Casanovas, M. L., & Santafé, J. V. (1989). Dos nuevos Paleotéridos (Perissodactyla, Mammalia) del yacimiento eocénico de Llamaquique (Oviedo). *Trabajos de Geología*, *18*, 337–352.

Casanovas-Cladellas, M. L. (1975). Estratigrafía y paleontología del yacimiento ludiense de Roc de Santa (Area del Noguera Pallaresa). *Paleontologia i Evolució*, *10*, 1–158.

Cavelier, C., & Pomerol, C. (1983). Échelle de corrélation stratigraphique du Paléogène, Stratotypes, étages standards, biozones, chimiozones et anomalies magnétiques. *Géol. Frances*, *3*, 261–262.

Checa, L. (1997). Los perisodáctilos (Mammalia, Ungulata) del Eoceno catalán. *Paleontologia i Evolució*, *30-31*, 149–234.

Checa Soler, L., & Casanovas-Cladellas, M. L. (1990). El Eoceno español: los yacimientos y sus faunas. *Paleontologia i Evolució*, *23*, 17–39.

Costa, E., Garcés, M., Sáez, A., Cabrera, L., & López-Blanco, M. (2011). The age of the "Grande Coupure" mammal turnover: New constraints from the Eocene–Oligocene record of the Eastern Ebro Basin (NE Spain). *Palaeogeography, Palaeoclimatology, Palaeoecology*, *301*(1-4), 97–107.

Cuesta, M. A. (1999). Las faunas de mamíferos del Eoceno de la Cuenca del Duero (Castilla y León, España). Síntesis bioestratigráfica y biogeográfica. *Revista Española de Paleontología*, *14*, 203–216.

Cuesta, M. A. (2003). Mamíferos del Paleógeno de la Cuenca del Duero. In E. Jiménez & J. Civis (Eds.), *Los vertebrados fósiles en la historia de la vida. Excavación, estudio y patrimonio* (pp. 197–236). Ediciones Universidad de Salamanca.

Cuesta Ruiz-Colmenares, M., Checa Soler, L., & Casanovas-Cladellas, M. L. (2006). Artiodáctilos del yacimiento de Sossís (Eoceno superior, Cuenca Prepirenaica, Península Ibérica). *Revista Española de Paleontología*, *21*(2), 123–144.

Franzen, J. L. (1968). *Revision der Gattung Palaeotherium Cuvier, 1804 (Palaetheriidae, Perissodactyla, Mammalia)*. Universität zu Freiburg.

Franzen, J. L. (2003). Mammalian faunal turnover in the Eocene of central Europe. *Geological Society of America, Special paper*, *369*, 455–461.

Gale, A. S., Huggett, J. M., Pälike, H., Laurie, E., Hailwood, E. A., & Hardenbol, J. (2006). Correlation of Eocene-Oligocene marine and continental records: orbital, ciclicity, magnetostratigraphy and sequence stratigraphy of the Solent Group, Isle of Wight, UK. *Journal of the Geological Society*, *163*, 401–415.

Gély, J. P., & Lorenz, C. (1991). Analyse séquentielle de L'Éocène et de L'Oligocène du Bassin Parisien (France). *Rev. Inst. Fr. Pét.*, *46*, 713–747.

Hooker, J. J. (1986). Mammals from the Bartonian (middle/late Eocene) of the Hampshire Basin, southern England. *Bulletin British Museum of Natural History*, *39*, 191–478.

Hooker, J. J. (1992). British mammalian paleocommunities across the Eocene-

Oligocene transition and their environmental implications. In D. R. Prothero & W. A. Berggren (Eds.), *Eocene/Oligocene Climatic and Biotic Evolution* (pp. 494–515). Princeton, NJ: Princeton University Press.

Hooker, J. J. (2010). The "Grande Coupure" in the Hampshire Basin, UK: taxonomy and stratigraphy of the mammals on either side of this major Paleogene faunal turnover. In J. E. Whittaker & M. B. Hart (Eds.), *Micropaleontology, Sedimentary environments and Stratigraphy: A Tribute to Dennis Curry (1912-2001)* (pp. 147–215). The Micropaleontological Society, Special Publications.

Hooker, J. J., Collinson, M. E., Grimes, S. T., Sille, N. P., & Mattey, D. P. (2007). Discussion on the Eocene-Oligocene boundary in the UK. *Journal of the Geological Society*, *163*, 401–415.

Hooker, J. J., Collinson, M. E., & Sille, N. P. (2004). Eocene-Oligocene mammalian faunal turnover in the Hampshire Basin, UK: calibration to the global time scale and the major cooling event. *Journal of the Geological Society*, *161*, 161–172.

Hooker, J. J., Grimes, S. T., Mattey, D. P., Collinson, M. E., & Sheldon, N. D. (2009). Refined correlation of the UK Late Eocene-Early Oligocene Solent Group and timing of its climate history. In C. Koeberl & A. Montanari (Eds.), *The Late Eocene Earth - Hothouse, Icehouse, and Impacts* (pp. 179–195). The Geological Society of America Special Paper 452.

López-Martínez, N. (1998). Los yacimientos de mamíferos del Eoceno de la Pobla de Segur. In N. López-Martínez, J. Civís, L. Casanovas, & R. Daams (Eds.), *Geología y Paleontología del Eoceno de la Pobla de Segur (Lleida)* (p. 267). Universitat de Lleida.

Peláez-Campomanes, P. (1998). Estudio sistemático del género Therydomis (Rodentia, Mammalia) del Eoceno Superior de la cuenca prepirenaica (prov. de Lleida). In N. López-Martínez, J. Civis, M. L. Casanovas-Cladellas, & R. Daams (Eds.), *Geología y Paleontología del Eoceno de La Pobla de Segur (Lleida)* (pp. 49–129). Universitat de Lleida.

Schmidt-Kittler, N. (1987). International Symposium on Mammalian Biostratigraphy and Paleoecology of the European Paleogene - Mainz February 18th-21st. *Münch. Geowiss. Abh. 10* (p. 312).

Schmidt-Kittler, N., & Vianey-Liaud, M. (1975). Les relations entre les faunes de rongeurs d'Allemagne du Sud et de France pendant l'Oligocène. *Comptes Rendus de l'Academie des Sciences*, *D*(281), 511–514.

Sigé, B., & Legendre, S. (1997). Un outil de la stratigraphie du Tertiaire continental: l'échelle de niveaux-repères de mammifères; spécificité; intérêt des faunes karstiques. In J. P. Aguilar, S. Legendre, & J. Michaux (Eds.), *BiochroM'97: Biochronologie mammalienne du Cénozoïque ren Europe et domaines reliés. Actes du Congrès BiochroM'97.* (pp. 47–54). Montpellier: Inst. Montpellier Memoire Trav. E.P.H.E 21.

Sudre, J. (1978). Les artyodactiles de l'Eocène moyen et supêrieur d'Europe occidentale: systématique et évolution. *Mémoires et Travaux de l'Institut de Montpellier (EPHE)*, *7*, 1–229.

Vianey-Liaud, M. (1979). Evolution des Rongeurs à l'Oligocène en Europe occidentale. *Palaentographica*, *166*, 136–236.

CHAPTER 2 - RESULTS

CHAPTER 2.1:

Beamud, E., Garcés, M., Cabrera, L., Muñoz, J.A., Almar, Y. (2003) A new Middle to Late Eocene chronostratigraphy for NE Spain. Earth and Planetary Science Letters 216, 501-514.

Available online at www.sciencedirect.com
SCIENCE DIRECT®
ELSEVIER
Earth and Planetary Science Letters 216 (2003) 501–514
EPSL
www.elsevier.com/locate/epsl

A new middle to late Eocene continental chronostratigraphy from NE Spain

Elisabet Beamud [a,*], Miguel Garcés [b], Lluís Cabrera [b], Josep Anton Muñoz [b], Ylènia Almar [b]

[a] *Grup de Geodinàmica i Anàlisi de Conques, Universitat de Barcelona, Laboratori de Paleomagnetisme (UB-CSIC), Institut de Ciències de la Terra 'Jaume Almera', Solé i Sabarís, s/n, 08028 Barcelona, Spain*
[b] *Grup de Geodinàmica i Anàlisi de Conques, Universitat de Barcelona, Zona Universitària de Pedralbes, 08028 Barcelona, Spain*

Received 1 April 2003; received in revised form 15 September 2003; accepted 19 September 2003

Abstract

The calibration of the European Paleogene mammal biochronology with the international reference geochronological scale is unconstrained due to the lack of direct marine–continental correlations and insufficient robust magnetostratigraphic data for mammal fossil-bearing sequences. The currently accepted European continental biochronology argues for a correlation of the Paleogene MP14 to MP16 mammal reference levels with the Bartonian stage, and of the MP17 to MP20 levels with the Priabonian. However, new magnetostratigraphic data of the continental sediments of the south-central Pyrenees substantially challenge this chronology. Our new results from the La Pobla de Segur Basin and Sierra de Sis have been integrated into the framework of previous marine–continental stratigraphic correlations and magnetostratigraphic data of the south-central Pyrenees. In this new chronology, MP14 and MP15 reference levels correspond to the Lutetian, whereas MP16 and early MP17 correlate with the early Bartonian. This calibration represents a significant revision of currently accepted marine–continental correlations in Europe, but is not in conflict with the available biostratigraphic data of the south Pyrenean Ebro foreland basin and other western European reference basins.

Keywords: Eocene; biostratigraphy; magnetostratigraphy; fossil mammals; Pyrenees; Ebro basin

1. Introduction

The development of a Paleogene continental chronostratigraphy in Europe has become an arduous task due to the scarcity of biostratigraphic information, and the lack of a robust stratigraphic context for many of the key reference fossil sites. The Paleogene mammal biochronological scale of western Europe [1,2] has been built on the basis of a series of reference fossil localities, called MP levels, numbered in chronological order. Each MP level corresponds to a local mammal fauna, chosen by its richness and representa-

* Corresponding author. Tel.: +34-93-409-54-10; Fax: +34-93-411-00-12.
E-mail addresses: betbeamud@ub.edu (E. Beamud), mgarces@ub.edu (M. Garcés), lluis@natura.geo.ub.es (L. Cabrera), josep@natura.geo.ub.es (J. Anton Muñoz), yalmar@natura.geo.ub.es (Y. Almar).

0012-821X/03/$ – see front matter © 2003 Elsevier B.V. All rights reserved.
doi:10.1016/S0012-821X(03)00539-9

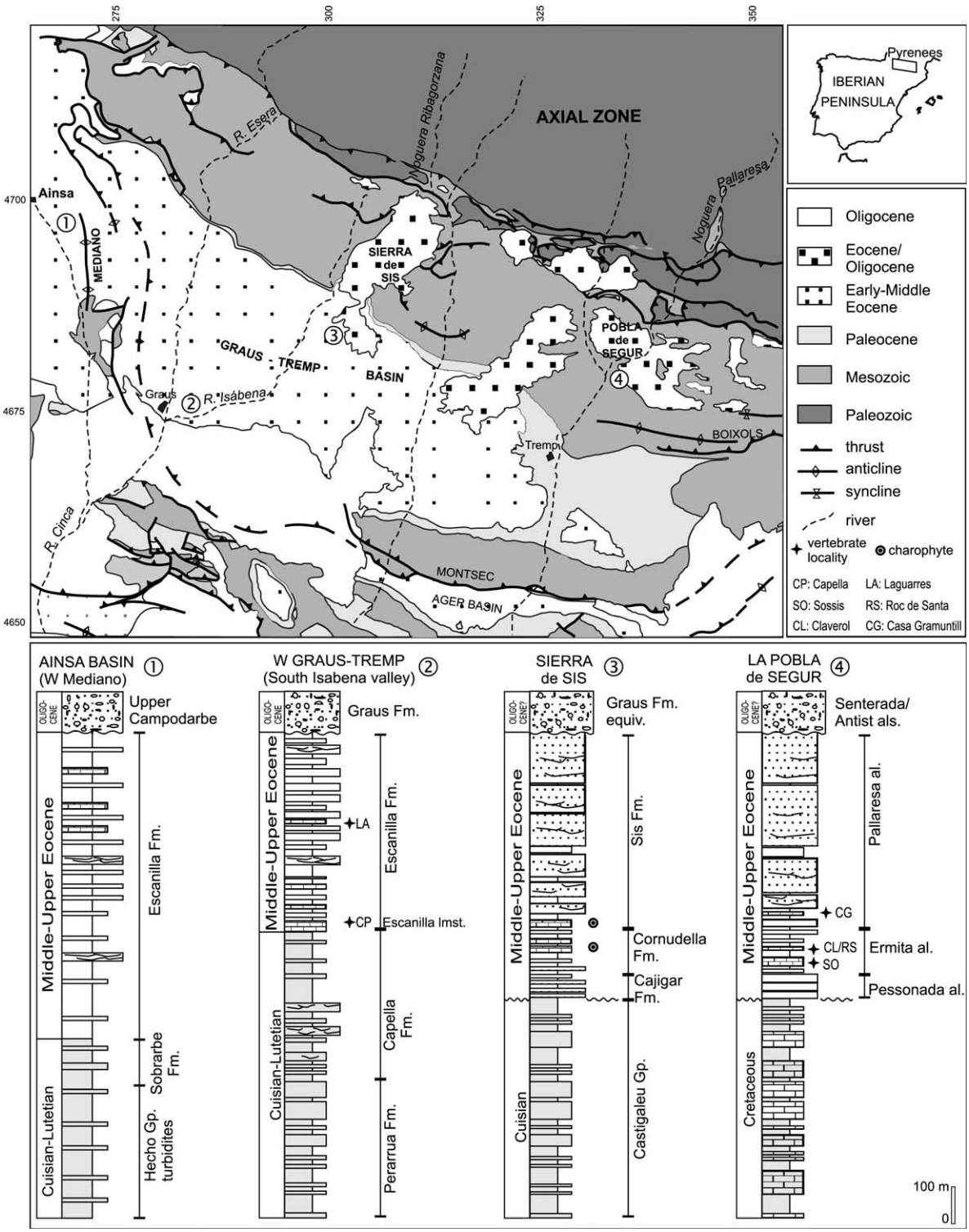
275
300
325
350
4700
4675
4650
Ainsa
MEDIANO
R. Esera
Noguera Ribagorzana
AXIAL ZONE
Noguera Pallaresa
SIERRA de SIS
GRAUS - TREMP BASIN
POBLA de SEGUR
Graus
R. Isábena
Tremp
BOIXOLS
R. Cinca
MONTSEC
AGER BASIN
Pyrenees
IBERIAN PENINSULA
Oligocene
Eocene/ Oligocene
Early-Middle Eocene
Paleocene
Mesozoic
Paleozoic
thrust
anticline
syncline
river
vertebrate locality
charophyte
CP: Capella
LA: Laguarres
SO: Sossis
RS: Roc de Santa
CL: Claverol
CG: Casa Gramuntill
AINSA BASIN (W Mediano)
W GRAUS-TREMP (South Isabena valley)
SIERRA de SIS
LA POBLA de SEGUR
OLIGO-CENE
OLIGO-CENE?
Middle-Upper Eocene
Cuisian-Lutetian
Cretaceous
Upper Campodarbe
Escanilla Fm.
Sobrarbe Fm.
Hecho Gp. turbidites
Graus Fm.
LA
CP
Escanilla lmst.
Capella Fm.
Perarrua Fm.
Graus Fm. equiv.
Sis Fm.
Cornudella Fm.
Cajigar Fm.
Castigaleu Gp.
Senterada/ Antist als.
Pallaresa al.
CG
CL/RS
SO
Ermita al.
Pessonada al.
100 m
0

tivity. The relative chronology between MP levels has been established on the basis of composition and evolutionary stage of the whole mammal assemblage [3]. Since many of the reference sites are placed in fissure fillings and non-correlatable sections, reliable stratigraphic relationships between successive MP levels are non-existent. However, a correlation attempt of the MP scale has been built on the basis of the available correlations with marine units in the Paris and Hampshire basins [4,5].

Magnetostratigraphy has been rarely applied to this mammal Paleogene chronology because of unsuitable stratigraphic sections on the type mammal localities of central and western Europe. Previous attempts to calibrate the MP scale with the geomagnetic polarity time scale (GPTS) [6,7] have not provided further constraints, since their results are based on extremely short sections, which do not yield an unambiguous magnetostratigraphic correlation. Therefore, the reported ages of the MP scale are not sufficiently reliable and need further independent constraints from regions where marine–continental correlations and magnetostratigraphy can be integrated and cross-checked. In contrast to other regions in Europe, the south Pyrenean basins (NE Spain) offer a thick and continuous stratigraphic framework which is suitable for magnetostratigraphic dating.

A precise bio-chronostratigraphy has been developed for the marine successions of the Jaca, Ainsa and Graus-Tremp basins [8–10]. Further magnetostratigraphic studies combined with marine–continental, well-exposed vertical and lateral stratigraphic relationships [11] yielded a robust chronostratigraphic frame for the continental units in the western sectors of the south-central Pyrenean domain.

In the eastern south-central Pyrenean basins, where neither marine–continental interfingering nor continuous vertical stratigraphic relationships are observed, the absolute age of the continental units has remained unconstrained. Dating of these successions is based on mammal fossil localities [12–15]. The new magnetostratigraphic data from the syntectonic continental sediments of La Pobla de Segur basin and the Sierra de Sis contribute to the chronostratigraphic frame of the south-central Pyrenees piggy-back basins. The results of this study challenge the currently accepted correlation of the Eocene mammal units with the standard marine stages and make evident that the correlation between the continental and marine Paleogene records still needs further refinement. Moreover, some aspects of the evolution in the south-central Pyrenees piggy-back basins have to be revised in the light of the new chronology.

2. Stratigraphic framework

The Eocene south-central Pyrenean basins are pictured as an elongated trough with a marine connection towards the west. At the eastern edge of these basins, a very efficient siliciclastic sediment supply was sourced from the uplifting central Pyrenees. This basin configuration led to a rapid basin infill with a northwestward gradation from terrestrial to shallow-water and slope marine facies. The vertical transition from marine to continental sediments varies from a conformity or paraconformity in the Mediano area, to a marked erosional unconformity along the Isábena river area. The time gap under this unconformity increases towards the east, to the point that in the La Pobla de Segur area, the marine Paleocene–Eocene record is no longer preserved, and the Eocene continental conglomerates unconformably overlie late Cretaceous rocks (Fig. 1).

West of the Mediano anticline, the Eocene marine sediments of the Ainsa basin are represented by the Cuisian to Lutetian turbidites of the Hecho Group [8,9,16], and the overlying shallow marine

←

Fig. 1. Geological map of the south-central Pyrenees and stratigraphy of the Ainsa, Graus-Tremp and La Pobla de Segur basins with indication of the vertebrate localities and the charophyte assemblage. The faunistic list for each locality is provided in [20]. The Capella mine fossil locality is characterized by *Pseudoloris (Pivetonia) isabenae* and *Lophiodon rhinocerodes* among other taxa [13,20]. Sossís, Claverol and Roc de Santa fossil mammal assemblages include *Therydomis euzetensis* and *Palaeotherium medium euzetensis* among an extensive list of taxa [14,20]. *Therydomis euzetensis* also occurs in the Can Gramuntill fossil site [15].

deltaic facies of the Sobrarbe Fm. [17]. The successive fluvial sediments of the Escanilla Fm. [18] represent the culmination of a rapid basin infill and are characterized by a marked westward progradation onto deltaic and marine deposits of both the Graus-Tremp and the Ainsa basins [11].

East of the Mediano anticline (Fig. 1), the Graus-Tremp basin records a middle Eocene thick succession of continental to shallow marine facies. The tidally influenced alluvial sediments of the Capella Fm. [13] overlie and partially interfinger with the Late Cuisian–Early Lutetian marine Perarrua Fm. [8,19]. Further east and south of the Isábena valley, the upper boundary of the Capella Fm. is formed by the laterally extensive lacustrine Escanilla limestone [13], placed at the base of the Escanilla Fm. [18]. Lignite intercalations within the Escanilla limestone have supplied the mammal fauna of the Capella mine fossil locality [12,13], which was assigned to the MP14 level [1]. In a higher stratigraphic position within the Escanilla Fm., the Laguarres mine fossil locality yielded a mammal assemblage of younger age, currently assigned to the MP16 level [20]. On top of the Escanilla Fm., the Graus conglomerates are considered to have been deposited during the Oligocene [21].

In the Sierra de Sis, the continental conglomerates are placed unconformably on top of the Cuisian deltaic facies of the Castigaleu Gp. [10]. The Sierra de Sis conglomerates are divided into the Cajigar, Cornudella and Sis formations [22,23]. Lacustrine limestones interbedded within the Cornudella Fm. and at the base of the Sis Fm. have yielded *Raskyella pecki*, a charophyte species which has an age range from Lutetian to Bartonian [24]. The top sediments in the Sierra de Sis have been interpreted as equivalents to the conglomerates of the Graus Fm. [23].

Further east, the Collegats Fm. of the La Pobla de Segur basin [25] is divided into five allogroups: Pessonada, Ermita, Pallaresa, Senterada and Antist [26]. Because of the absence of a straight correlation of the Collegats Fm. with marine levels, the age of the Collegats Fm. has exclusively relied on the mammal assemblages of the classical sites of Sossís, Claverol and Roc de Santa in the Ermita allogroup, and Casa Gramuntill in the Pallaresa allogroup [14,15]. All of the La Pobla de Segur fossil sites have been attributed to the MP17 (MP17a) level [2].

To date, the lack of an absolute temporal framework for the syntectonic continental materials of the eastern sector (Sierra de Sis and La Pobla de Segur) precludes a robust E–W correlation of the continental successions of the south-central Pyrenees piggy-back basins.

3. Magnetostratigraphy of the La Pobla de Segur and Sierra de Sis conglomerates

The magnetostratigraphic analysis of the syntectonic continental conglomerates of the La Pobla de Segur basin and Sierra de Sis is essential to constrain the relationships between sedimentation and tectonics. These sedimentary successions record both the late stages of thin-skinned transport of the south Pyrenean Central Units and the onset of the exhumation of the Pyrenean Axial zone.

Two parallel magnetostratigraphic successions have been studied in the adjacent areas of the La Pobla de Segur basin and the Sierra de Sis, now separated by the incision of the Ribagorçana river valley (Fig. 1).

3.1. The sampled sections

The magnetostratigraphic sections in La Pobla de Segur basin extend over the Ermita and the Pallaresa allogroups. Sediments of the Ermita allogroup mainly consist of alluvial red silts and conglomerates which laterally interfinger with a 70 m thick lacustrine unit in the Claverol section. The alluvial sediments are arranged in an overall aggradational stacking pattern, where fine-grained overbank deposits show a high degree of preservation. The dominance of Mesozoic carbonate clasts reflects a local source area. The lacustrine unit in the Ermita allogroup consists of meter-scale alternation of gray limestones and marls, with some occurrences of coal layers, where the Sossís mammal site occurs.

Unlike the Ermita allogroup, the coarser alluvial sediments of the overlying Pallaresa allogroup show a higher degree of amalgamation of con-

glomerate lenses and less preservation of fine-grained overbank mudstones. Vertical arrangement indicates an overall progradation of the converging Montsor and Collegats–Roca de Peso alluvial fan systems. The Montsor system is characterized by red, polymict conglomerates with a source area within the Axial Zone as evidenced by the high proportion of Triassic and Paleozoic clasts. The interfingering Collegats–Roca de Peso system is mainly formed by conglomerates with Cretaceous and Jurassic carbonate clasts.

The Sierra de Sis magnetostratigraphic section spans the Cajigar, Cornudella and lower Sis Fms. Sediments of the Cajigar Fm. are characterized by red silts and conglomerates with a very low proportion of Axial Zone-derived material. The overlying interbedded fluvial and lacustrine sediments of the Cornudella Fm. already record the input of granitic components from the Axial Zone. On top of the section, the Sis Fm. is mainly composed of stacked red conglomerates with a high proportion of Axial Zone-derived clasts. Lacustrine limestones are common in the first meters of the formation.

In the La Pobla de Segur basin 410 paleomagnetic sites were sampled spanning about 1000 m in a composite stratigraphic succession. In the Sierra de Sis area near the Cajigar locality, 170 sites were drilled along a 560 m thick stratigraphic succession. Sampling focused on the finer-grained overbank sediments interbedded with conglomerates and sandstone. Although unsuitable coarse sediments were frequent in the middle to upper parts of the stratigraphic record, an adequate sampling interval of 2–3 m was kept for most of the magnetostratigraphic section. In each site two to three oriented samples were obtained using a gasoline-powered drill and a magnetic compass with inclinometer for sample orientation.

3.2. Paleomagnetic analysis

The paleomagnetic laboratory analysis consisted in stepwise thermal demagnetization of the natural remanent magnetization (NRM) at intervals ranging between 30°C and 50°C. Alternating field demagnetization was only applied to limestones and marls in the lacustrine units in the Ermita allogroup and the Cornudella Fm. (Fig. 2). One to three samples were demagnetized to verify the paleomagnetic vector directions obtained at the site level. NRM was measured in superconducting rock magnetometers at the laboratories of the CSIC-University of Barcelona (Spain) and at the University of Leoben (Austria). Zijderveld plots show that the NRM consist of two magnetic components: a low temperature component which parallels the recent normal field and a high temperature characteristic component which yields both normal and reversed directions (Fig. 2).

Intensity of the NRM and stability of the paleomagnetic directions were found to be primarily controlled by the source rock composition. Sediments derived from Cretaceous carbonate rocks yielded low intensity of magnetization and, often, unstable demagnetization directions above 450°C. Then, great circles analysis [27] was used to obtain mean directions from a number of sites in the lower part of the La Pobla de Segur section (Fig. 2). Sediments derived from Triassic red beds and Paleozoic rocks, with a higher concentration of magnetic minerals, are more abundant towards the upper units. Samples from these sediments yielded a higher NRM intensity and more stable paleomagnetic directions, with unblocking temperatures up to 600–650°C, characteristic of hematite. This observation is significant because it stresses the importance of the detrital contribution to the remanence of these rocks.

Paleomagnetic directions were calculated by means of least squares analysis after visual inspection of the Zijderveld plots. A magnetic polarity stratigraphy was then produced after computing the latitude of the virtual geomagnetic pole.

The calculated directions passed a reversal test [28]. The reversal test was classified as C with γ_0: 9.5 and γ_c: 15.2 for La Pobla and γ_0: 8.3 and γ_c: 16.4 for the Cajigar directions. The primary character of the NRM could not be assessed by means of a fold test because of the near uniform bedding dip over the studied sections. However, the presence of a coherent sequence of normal and reversed polarity magnetozones suggests that the obtained paleomagnetic directions repre-

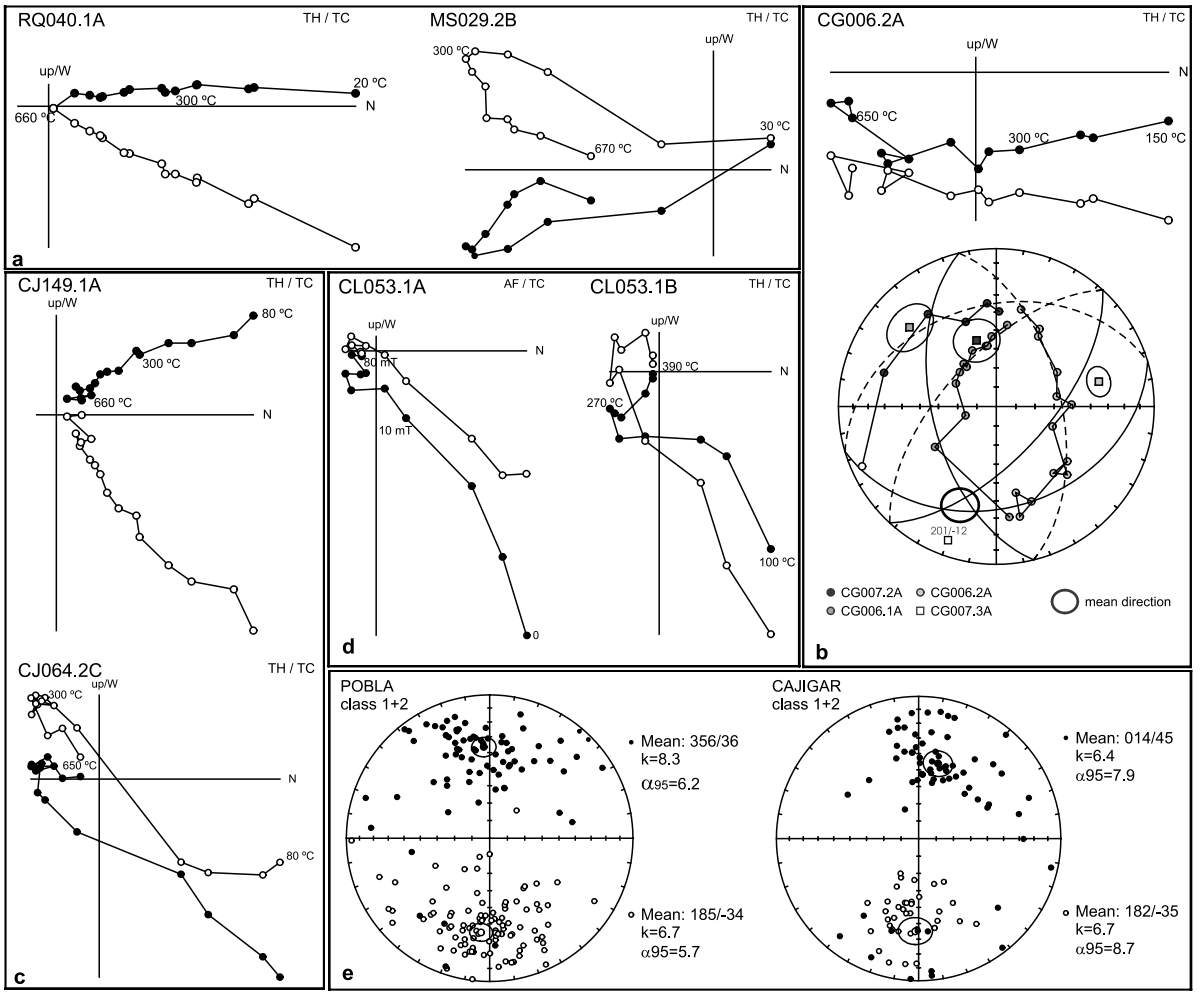

Fig. 2. Demagnetization diagrams of representative samples and mean directions from the La Pobla de Segur Basin and the Sierra de Sis sections. (a) Demagnetization diagrams of samples of Paleozoic-derived sediments in La Pobla de Segur basin, displaying normal and reversed polarities. (b) Demagnetization diagram of a sample with a Cretaceous source area, showing an erratic behavior at high temperature. The diagram below shows the demagnetization circles [27] used to obtain the site mean direction. (c) Demagnetization diagram of samples from the Cornudella and Sis Fms. in the Sierra de Sis section, yielding normal and reversed polarities. (d) Demagnetization diagrams of a lacustrine limestone from the Ermita allogroup in La Pobla de Segur basin, after alternating field demagnetization (specimen 1A) and thermal treatment (specimen 1B) displaying a reverse polarity. (e) Mean directions of the La Pobla de Segur basin and the Sierra de Sis sections. No significant vertical axis rotations are observed.

sent a mainly primary magnetization. Reliability of the magnetostratigraphic sequence is based on the consistency between sites. Thus, single site magnetozones were not taken into account for building the local magnetic stratigraphy (Fig. 3). In particular, the upper part of the Can Gramuntill section yielded erratic results, with both normal and reversed polarities at nearly the same

→

Fig. 3. Local litho- and magnetostratigraphic sections from the Sierra de Sis (Cajigar section) and the La Pobla de Segur basin (Claverol, Can Gramuntill and Rocs de Queralt–Montsor sections) with indication of the charophyte and the vertebrate localities.

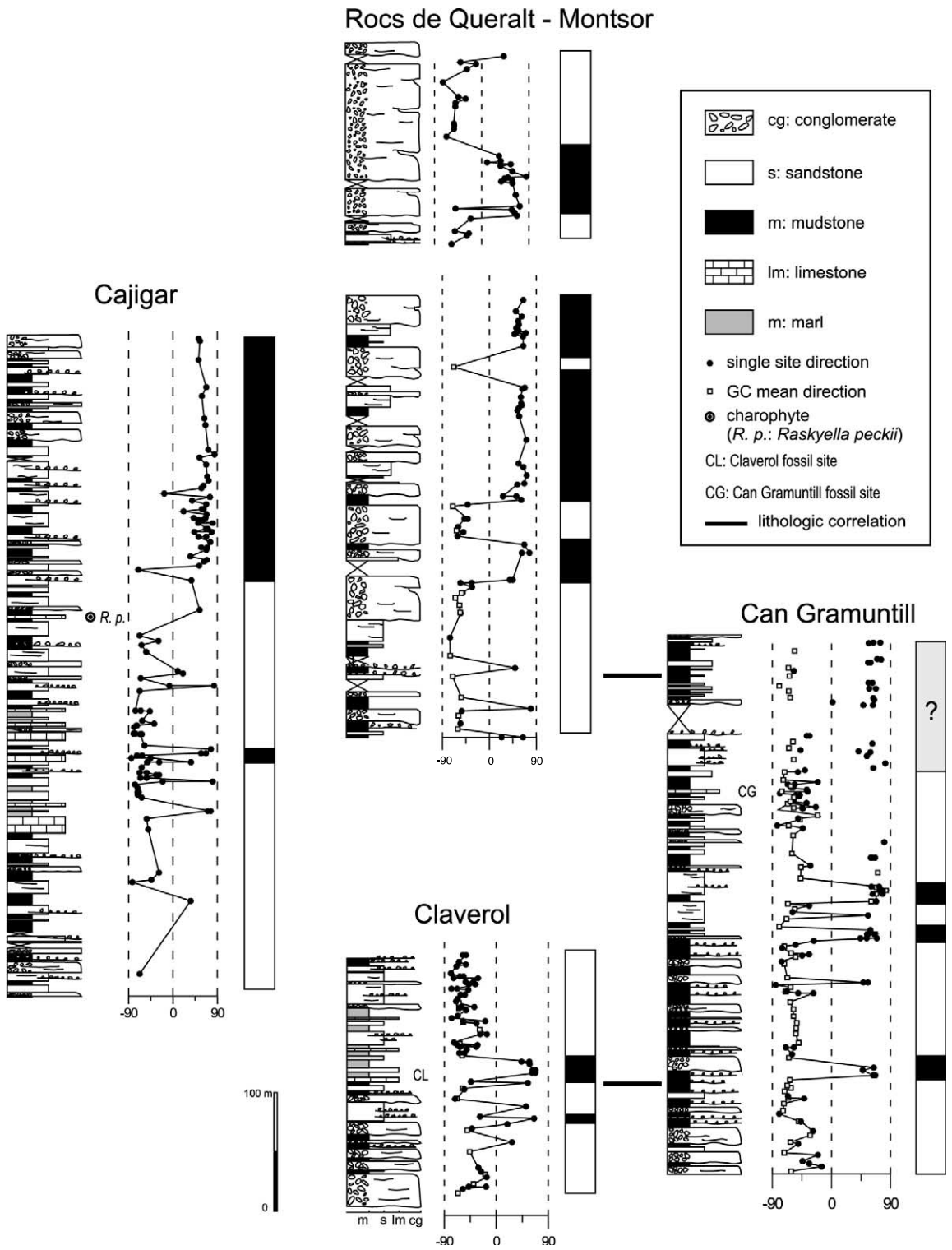
Rocs de Queralt - Montsor
Cajigar
Claverol
Can Gramuntill
R. p.
CL
CG
?
-90
0
90
100 m
0
m s lm cg
cg: conglomerate
s: sandstone
m: mudstone
lm: limestone
m: marl
single site direction
GC mean direction
charophyte
(R. p.: Raskyella peckii)
CL: Claverol fossil site
CG: Can Gramuntill fossil site
lithologic correlation

stratigraphic levels. These inconsistent results in the upper Can Gramuntill section can be overcome because laterally equivalent sediments in the Roc de Queralt section yielded unequivocal reversed polarities. Better results were obtained in the Roc de Queralt section because of the higher proportion of sediments derived from hematite-bearing Paleozoic rocks. We interpret the normal polarity samples scattered along the upper part of the Can Gramuntill section to represent secondary magnetizations. This local remagnetization is possibly associated with the significant environmental change which is recorded at a higher stratigraphic position, marked by the decline of the lacustrine environments and the overall progradation of the alluvial fronts. Such a relative base level drop might have produced selective remagnetization in the then buried sediments to depths of several tens of meters.

3.3. Correlation with the time scale

The magnetostratigraphic correlation of the Sierra de Sis and La Pobla de Segur sections is straightforward on the basis of the long reversed magnetozone R2, which spans the lower part of the two sections (Fig. 4a). This correlation is in agreement with the presumably same age for the lacustrine facies in both the Ermita allogroup (La Pobla de Segur) and Cornudella Fm. (Sierra de Sis).

The local magnetostratigraphic sections can be correlated to the GPTS [29] through consideration of regional stratigraphy and available biochronological information. To date, the only on-site chronological constraints in the Collegats Fm. are the mammal sites of La Pobla de Segur. They have been interpreted as Priabonian in age on the basis of their attribution to the MP17 Mammal Paleogene level [30]. This age contrasts with the Bartonian age attributable to the basal levels of the Sis Fm. based on charophyte assemblages [31] and on their regional stratigraphic relationship with underlying Lutetian marine successions. The two age constraints appear to be contradictory after magnetostratigraphic correlation, since they occur within the same reversed chron R2. From a magnetostratigraphic point of view, a correlation of R2 with the long reversed chron C18r in the early Bartonian is the most likely solution, since the late Bartonian to Priabonian time scale is dominated by long normal geomagnetic chrons. An alternative correlation of R2 with the Priabonian long reversed chron C13r, in line with the mammal age constraints, does not agree with the sequence of magnetic reversals in the upper part of the La Pobla de Segur section (Fig. 4).

In our preferred solution, the N2 to N5 magnetostratigraphic succession, which is characterized by thick normal polarity magnetozones, correlates with the Bartonian to Priabonian C18n to C15n chrons, and the top R6 reversed magnetozone represents part of C13r of the late Priabonian. The proposed correlation does not yield a perfect matching of magnetozones with geomagnetic chron durations. Significant fluctuations in the sedimentation rates are derived (from 0.05 m/kyr to 0.3 m/kyr, Fig. 4b) which are, however, geologically coherent when considered in the tectonic context. A dramatic decrease in the sedimentation rate occurs near the transition from the Ermita to the Pallaresa allogroup. At this point, a break from an overall aggradational architecture to a progradation of massive, amalgamated conglomerates is observed. In the Mediano area, a similar trend is recorded with decreasing sedimentation rates coeval with the progradation of amalgamated conglomerates of the Escanilla Fm. [32]. This is coherent with a context of tectonic uplift, forcing a reduction of the accommodation space and a bypass of sediment towards the west into the Graus-Tremp basin.

3.4. Continental chronostratigraphy of the south-central Pyrenees

The conclusions from the magnetostratigraphy challenge earlier dating of the continental units of La Pobla de Segur basin, which were so far only based on mammal biochronological constraints. The Bartonian to early Priabonian age of the La Pobla de Segur conglomerates enables a new correlation with the western sectors of the south-central Pyrenees, where a robust chronostratigraphy has been built on the basis of marine–continental stratigraphic correlations [10] and magnetostrati-

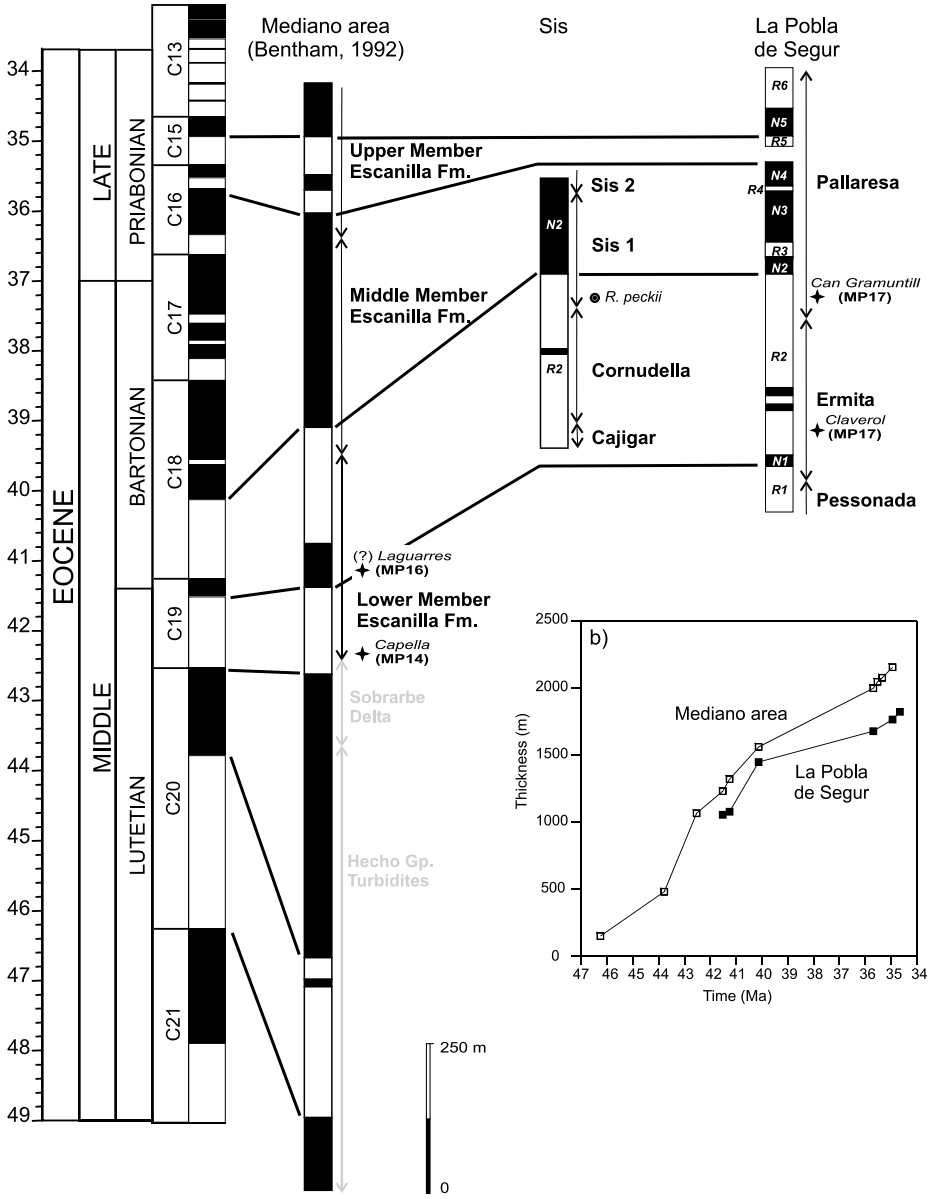

Fig. 4. (a) Correlation of the local magnetostratigraphic sections to the GPTS [29] with indication of the charophyte association and the vertebrate localities with their corresponding MP reference levels. The Mediano area log is a composite section from the Mediano and Eripol magnetostratigraphic sections [32]. (b) Sedimentation rates derived from the proposed correlation for the Mediano area log and the La Pobla de Segur basin section. An important decrease is recorded in both sectors around 40 Ma.

graphic data [32,33] (Fig. 5). The integrated chronostratigraphy in the western region has revealed further disagreements regarding the calibration between the marine and continental biochronological scales as discussed below.

The late Lutetian age of the transitional Capella Fm. is adequately constrained on the basis of the Early Lutetian age of the underlying marine marls of the Perarrua Fm. and the middle to late Lutetian age of marine equivalents (Sobrarbe

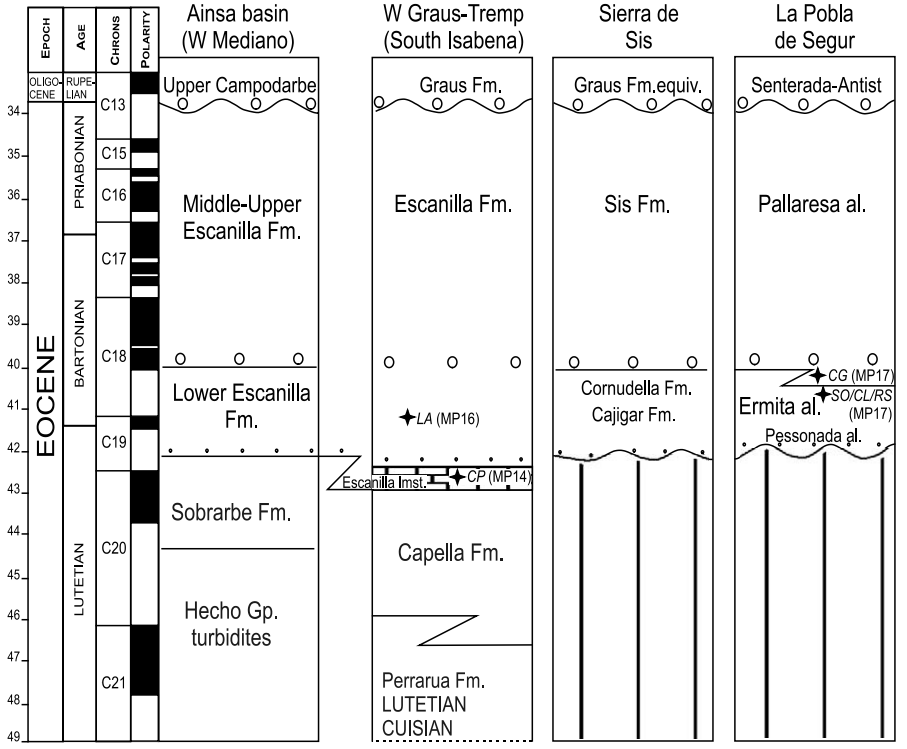

Fig. 5. Chronostratigraphy of the continental sediments of the Ainsa, Graus-Tremp and La Pobla de Segur basins. The fossil localities are indicated as follows: CP: Capella; LA: Laguarres; SO: Sossís; CL: Claverol; CG: Can Gramuntill; RS: Roc de Santa.

Fm.) in the Ainsa Basin [8,17,19]. In the Isábena Valley, the Capella fossil locality, found within the Escanilla limestone, is attributed to the mammal reference level MP14 [34]. MP14 reference faunas were traditionally correlated with Lower Bartonian [35]. This is in conflict with the correlation of the Escanilla limestone to the magnetostratigraphic section of Mediano [32], which places the levels of the Capella fossil locality at the base of chron C19r, in the late Lutetian (Figs. 4 and 5).

The mammal fossil locality of Laguarres, in the coal-bearing lacustrine units of the lower member Escanilla Fm., have yielded mammal assemblages of younger age (MP16) [20]. The correlation of the lower member of the Escanilla Fm. with chrons C19 and C18r in the Mediano area suggests an uppermost Lutetian to lowermost Bartonian age for the Laguarres locality.

4. Implications for the middle–late Eocene European mammal biochronology

The presently accepted calibration of the European continental biochronology correlates the MP14, MP15 and MP16 reference levels with the Bartonian stage, and the MP17 to MP20 reference levels with the Priabonian [1,2,7,36,37]. The magnetostratigraphic data from the southern Pyrenean successions disagree significantly with this chronology and strongly suggest that the MP14 and MP15 reference levels correspond to the late Lutetian, whereas the MP16 and lower MP17 faunas are dated as early Bartonian (Fig. 6).

Although our proposed chronostratigraphy challenges the formerly accepted chronology it is not contradicted by the available biostratigraphic data on the middle–late Eocene in the southern

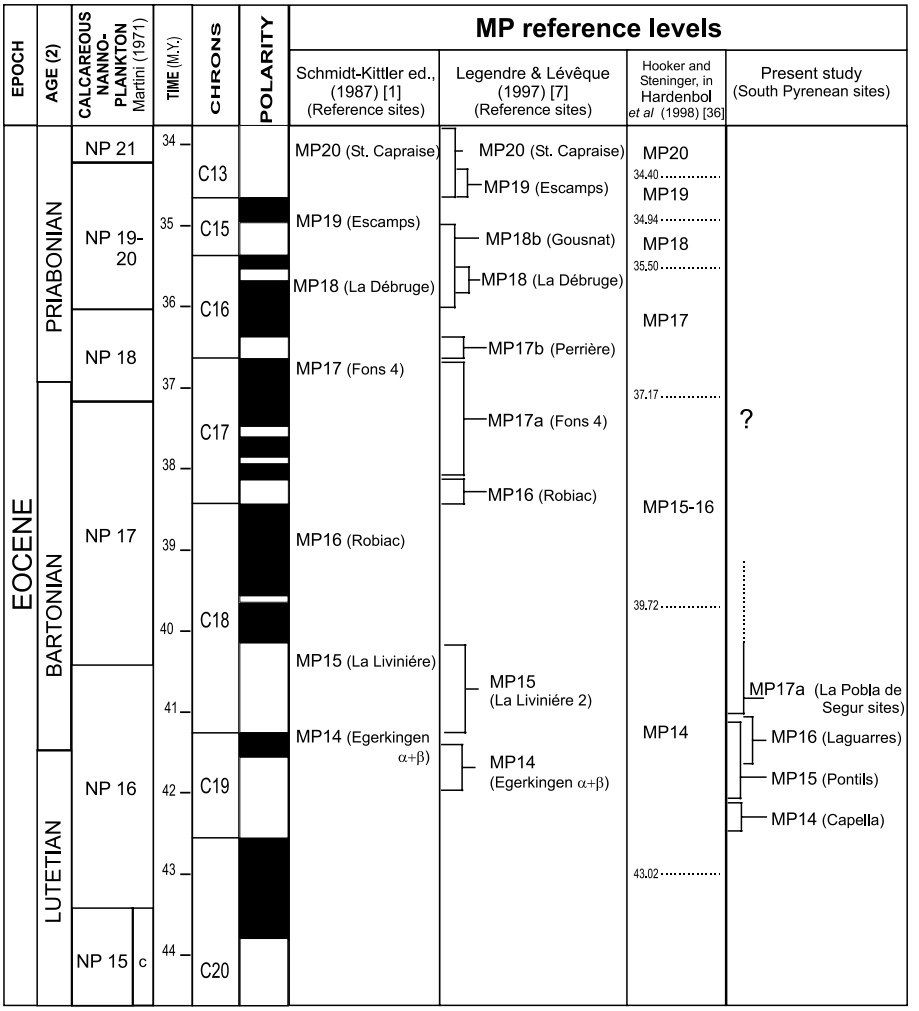

Fig. 6. Correlation of the Middle Eocene MP reference levels to the international reference geochronological scales. Geomagnetic chronology from Cande and Kent [29]. Calcareous nannoplankton zonation from Martini [48] in Berggren et al. [49]

Pyrenees and its foreland basin. In the southeastern margin of the Ebro Basin, the Pontils mammal site (MP15, characterized in this locality by the occurrence of *Pseudoltinomys cosetanus*) had been correlated with the Bartonian [38,39]. Nevertheless, since it was found in a palustrine succession which is overlain by an early Bartonian transgressive marine sequence [40], a late Lutetian age cannot be excluded for this locality. The charophyte assemblages recorded in the Pontils section do not provide further constraints for a Bartonian age since the reported species have an age range from Lutetian to Bartonian [24].

The chronology proposed in this paper is not in conflict with the marine–continental correlations from other western European regions, such as the Paris and Hampshire–London basins. The analysis of these data evidences that some of the discrepancies are within the uncertainties resulting from gaps in the stratigraphic record [5,37,41,42]. The time range of these gaps is difficult to estimate, since the biostratigraphy (mainly based on dinoflagellates and calcareous nannoplankton) is not continuous, and the stratigraphic position of zone boundaries is not always precise [41–46]. Considering these uncertainties, the proposed Lu-

tetian age for the MP14 reference level is certainly not in conflict with biostratigraphic data from the western European basins [36,46] and its correlation with nannoplankton biozone NP-16 in the Paris basin [36,47]. The new proposed chronology should, however, stimulate a re-evaluation of the chronostratigraphy of the reference levels MP11 to MP13, which were thought to represent the complete Lutetian stage [1,2].

With regard to the calibration of the MP15 faunas, no reliable age constraints in western Europe are published supporting a Bartonian age. In the new proposed calibration, the earliest Bartonian correlates with the MP16 reference level. This is in agreement with the early Bartonian age of typical MP16 faunas suggested for the fossil mammal assemblage reported in the Creechbarrow limestone formation in the Hampshire Basin [37,41], although a less precise correlation was later proposed [39].

The correlation of the MP17 faunas of La Pobla de Segur with the early Bartonian represents a major change in the chronology of the European Eocene mammals. In this particular case, increasing the time range of the MP17 faunas from early Bartonian to Priabonian is feasible since no other mammal faunas have been unambiguously correlated with the late Bartonian. Nevertheless, it raises the problem of a significant gap in the fossil mammal record between the MP17a reference level (now early Bartonian) and younger reference levels assigned to the Priabonian. At this point, it is tempting to speculate that this gap could result from inexact chronological attributions of the MP17b to MP19/20 reference levels, since the chronology of these younger reference levels is still not well defined. Therefore, a review of the chronology of MP18 and MP19/20 along the late Bartonian and the Early Priabonian time span cannot be excluded.

5. Conclusions

The new magnetostratigraphic data from the continental sequences of the south-central Pyrenees, together with previous bio- and magnetostratigraphic studies, have led to a new chronostratigraphy of the mammal reference levels MP14 to MP17 with a time scale that substantially changes the traditionally accepted ages. MP14 and MP15 reference levels are now correlated with the late Lutetian. MP16 is constrained to the earliest Bartonian, in the same reversed chron (C18r) as MP17a.

A re-evaluation of the chronological attribution of the reference levels MP11 to MP13 should attribute them to the earlier Lutetian. The considerable gap between MP17a and the younger reference levels could be partially covered after the review of the chronological meaning of the MP17b to MP19/20 mammal assemblages.

The large discrepancies with previous results and the internal uncertainties of the MP level system show that developing regional mammal biostratigraphy, independent of the MP biochronology and supported by robust magnetostratigraphy and radiochronology, would be advisable. Once this biostratigraphic approach is reached the correlation with and among the MP levels could be more completely re-evaluated. Meanwhile, standard chronostratigraphic age attributions based on MP reference levels should be taken with caution and revised in the light of the currently available regional litho-, bio- and magnetostratigraphic information.

Acknowledgements

This paper has been developed in the framework of the projects MARCONI: REN 2001-1734-CO3-03 and CARES: BTE 2001-3650 'Caracterización de Reservorios Sedimentarios' of the MCyT. This research was supported by the Research Group of Geodinàmica i Anàlisi de Conques, 2001 SGR 00074, del Comissionat de Universitats i Recerca de la Generalitat de Catalunya. M.G. was funded by the Ramón y Cajal Program of the MCyT. The authors want to thank Dr. Robert Scholger from the Paleomagnetic Laboratory of the Montanuniversität of Leoben (Austria) and Dr. Hugh Sinclair from the Geology and Geophysics Department of the University of Edinburgh for their hospitality and assistance. The comments and suggestions of Dr. Cor Lan-

gereis and an anonymous reviewer considerably improved the paper content and presentation.*[VC]*

References

[1] N. Schmidt-Kittler, International Symposium on Mammalian Biostratigraphy and Paleocology of the European Paleogene – Mainz, February 18th–21st, in: Münch. Geowiss. Abh. 10 (1987) 312 pp.

[2] BiochroM'97, Synthèses et tableaux de corrélations, in: J.P. Aguilar, S. Legendre, J. Michaux (Eds.), BiochroM'97, Mém. Trav. E.P.H.E. Inst. Montpellier 21 (1997) 769–805.

[3] B. Sigé, S. Legendre, Un outil de la stratigraphie du Tertiaire continental: l'échelle de niveaux-repères de mammifères; spécificité; intérêt des faunes karstiques, in: J.P. Aguilar, S. Legendre, J. Michaux (Eds.), BiochroM'97, Mém. Trav. E.P.H.E. Inst. Montpellier 21 (1997) 47–54.

[4] C. Cavelier, C. Pomerol, Échelle de corrélation stratigraphique du Paléogène, Stratotypes, étages standards, biozones, chimiozones et anomalies magnétiques, Géol. France 3 (1983) 261–262.

[5] J.P. Gély, C. Lorenz, Analyse séquentielle de L'Éocène et de L'Oligocène du Bassin Parisien (France), Rev. Inst. Fr. Pét. 46 (1991) 713–747.

[6] F. Lévêque, Correlating the Eocene–Oligocene mammalian biochronological scale from SW Europe with the marine magnetic anomaly sequence, J. Geol. Soc. London 150 (1993) 661–664.

[7] S. Legendre, F. Lévêque, Étalonnage de l'échelle biochronologique mammalienne du Paléogène d'Europe occidentale: vers une integration à l'échelle globale, in: Biochrom '97, J.P. Aguilar, S. Legendre and J. Michaux, eds. 21, pp. 461–473, Mémoires et Travaux de l'E.P.H.E. Institut de Montpellier, Montpellier, 1997.

[8] H. Schaub, Nummulites et Assilines de la Tethys Paléogéne. Taxonomie, phylogénése et biostratigraphie, Mémoires Suisses Paléont. 104–106 (1981) 1–236.

[9] J. Tosquella, Estudi sedimentològic i biostratigràfic de la Formació Gresos de Roda (Eocè, conca de Tremp-Graus), PhD, Universitat de Barcelona, 1988.

[10] J. Serra-Kiel, J.I. Canudo, J. Dinarés, E. Molina, N. Ortiz, J.O. Pascual, J.M. Samsó, J. Tosquella, Cronoestratigrafía de los sedimentos marinos del Terciario inferior de la Cuenca de Graus-Tremp (Zona Central Surpirenaica), Revista de la Sociedad Geológica de España 7 (1994) 273–297.

[11] P.A. Bentham, D. Burbank, C. Puigdefàbregas, Temporal and spatial controls on the alluvial architecture of an axial drainage system: late Eocene Escanilla Formation, southern Pyrenean foreland basin, Spain, Basin Research 4 (1992) 335–352.

[12] M. Crusafont, Los mamíferos del Luteciense superior de Capella (Huesca) (Nota preliminar), Notas y Comunicaciones del Instituto Geológico y Minero de España 50 (1958) 259–279.

[13] M. Cuevas Gozalo, Sedimentary facies and sequential architecture of tide-influenced alluvial deposits. An example from the Middle Eocene Capella Fm; South-Central Pyrenees; Spain. Geologica Ultraiectana. Utrecht University 61, 1990.

[14] M.L. Casanovas-Cladellas, Estratigrafía y paleontología del yacimiento ludiense de Roc de Santa (Area del Noguera Pallaresa), Paleontologia i Evolució 10 (1975) 1–158.

[15] N. López-Martínez, Los yacimientos de mamíferos del Eoceno de la Pobla de Segur., in: Geología y Paleontología del Eoceno de la Pobla de Segur (Lleida), N. López-Martínez, J. Civis, L. Casanovas and R. Daams, eds., pp. 267, Universitat de Lleida, Lleida, 1998.

[16] E. Mutti, H.P. Luterbacher, J. Ferrer, J. Rosell, Schema estratigrafico e lineamenti di facies del Paleogeno marino della zona centrale sudpirenaica tra Tremp (Catalogna) e Pamplona (Navarra), Mem. Soc. Geol. Italia 11 (1972) 391–416.

[17] A. de Federico, La sedimentación de talud en el sector occidental de la cuenca paleógena de Ainsa, in: Publicaciones de Geología 13, pp. 271, Universitat de Barcelona, Barcelona, 1981.

[18] A. Garrido-Megías, Sobre la estratigrafía de los conglomerados de Campanué (Santa Liestra) y formaciones superiores del Eoceno (extremo occidental de la cuenca Tremp-Graus, Pirineo central, provincia de Huesca), Acta Geológica Hispánica 3 (1968) 39–43.

[19] W.J. Nijman and S.D. Nio, The Eocene Montañana delta (Tremp-Graus Basin, provinces of Lérida and Huesca, southern Pyrenees, N Spain), in: IX Congrés de Sedimentologie, pp. 18, Nice, 1975.

[20] M.T. Antunes, M.L. Casanovas, M.A. Cuesta, L. Checa, J.V. Santafé and J. Agustí, Eocene mammals from Iberian Peninsula, in: J.P. Aguilar, S. Legendre, J. Michaux (Eds.), BiochroM'97, Mém. Trav. E.P.H.E. Inst. Montpellier 21 (1997) 337–352.

[21] A. Reynolds, Tectonically Controlled Fluvial Sedimentation in the South-Pyrenean Foreland Basin, Ph.D. Thesis, University of Liverpool, Liverpool, 1987.

[22] M. Koops, S. van Rossem, Cajigar and Cornudella Formations, in: M.E. Donselaar, C.R. Geel (Eds.), Guide to the Sedimentology of the Tremp-Graus Basin, vol. 33, State University of Utrecht, Utrecht, 1985, pp. 111–121.

[23] S.J. Vincent, Fluvial Paleovalleys in Mountain Belts: An Example from the South Central Pyrenees, Ph.D. Thesis, University of Liverpool, Liverpool, 1993.

[24] C. Martín-Closas, J. Serra-Kiel, P. Busquets, E. Ramos-Guerrero, New correlation between charophyte and larger foraminifera biozones (Middle Eocene, Southeastern Pyrenees), Geobios 32 (1998) 5–18.

[25] P.H.W. Mey, P.J.C. Nagtegaal, K.J. Roberti, J.J.A. Hartevelt, Lithostratigraphic subdivisions of post-Hercynian deposits in the south Central Pyrenees, Spain, Leidse Geol. Meded. 41 (1968) 221–228.

[26] D. Mellere, I conglomerati di Pobla de Segur: Stratigrafia fisica e relazioni tettonica-sedimentazione, Tesi di Dottorato in Scienze della Terra, Universita degli Studi di Padova, Padua, 1992.
[27] P.L. McFadden, M.W. McElhinny, The combined analysis of remagnetization circles and direct observations in paleomagnetism, Earth Planet. Sci. Lett. 87 (1988) 161–342.
[28] P.L. McFadden, M.W. McElhinny, Classification of the reversal test in palaeomagnetism, Geophys. J. Int. 103 (1990) 725–729.
[29] S.C. Cande, D.V. Kent, Revised calibration of the geomagnetic polarity timescale for the Late Cretaceous and Cenozoic, J. Geophys. Res. B Solid Earth Planets 100 (1995) 6093–6095.
[30] U. Checa-Soler, M.L. Casanovas-Cladellas, El Eoceno español: los yacimientos y sus faunas, Paleontol. Evol. 23 (1989–1990) 17–39.
[31] S.J. Vincent, The Sis palaeovalley: a record of proximal fluvial sedimentation and drainage basin development in response to Pyrenean mountain building, Sedimentology 48 (2001) 1235–1276.
[32] P.A. Bentham, The Tectono-Stratigraphic Development of the Western Oblique Ramp of the South-Central Pyrenean Thrust System, Northern Spain, Ph.D. Thesis, University of Southern California, Los Angeles, CA, 1992.
[33] P. Bentham, D.W. Burbank, Chronology of Eocene foreland basin evolution along the western oblique margin of the South-Central Pyrenees, in: P.F. Friend, C.J. Dabrio (Eds.), Tertiary Basins of Spain. The Stratigraphic Record of Crustal Kinematics. World and Regional Geology, vol. 6, Cambridge University Press, Cambridge, 1996, pp. 144–152.
[34] M.C. Cuevas Gozalo, P.L. De Boer, Tide-influenced fluvial deposits; Eocene of the southern Pyrenees, Spain, in: International Symposium on Fluvial Sedimentology Excursion Guidebook, 1989, pp. 215–266.
[35] J.J. Hooker, Mammalian reference levels MP 14–16, in: N. Schmidt-Kittler (Ed.), International Symposium on Mammalian Biostratigraphy and Paleoecology of the European Paleogene, vol. 10, Verlag Friedrich Pfeil, Mainz, 1987, pp. 26–27.
[36] J. Hardenbol, J. Thierry, M.B. Farley, T. Jacquin, P.-C. De Graciansky, P.R. Vail, Mesozoic and Cenozoic sequence stratigraphy of European basins, SEPM Spec. Publ. 60 (1998).
[37] J.J. Hooker, Mammals from the Bartonian (middle/late Eocene) of the Hampshire Basin, southern England, Bull. Br. Mus. Nat. Hist. 39 (1986) 191–478.
[38] P. Anadón, M. Feist, J.L. Hartenberger, C. Muller, J. Villalta-Comella, Un exemple de correlation biostratigraphique entre échelles marines et continentales dans l' Éocène: la coupe de Pontils (Bassin de l' Ebre, Espagne), Bull. Soc. Géol. Fr. XXV (1983) 747–755.
[39] J.J. Hooker, M. Weidmann, The Eocene mammal faunas of Mormont, Switzerland. Systematic revision and resolution of dating problems, Schweiz. Paläontol. Abh. 120 (2000) 143.
[40] J. Serra-Kiel, E. Mató, E. Saula, A. Travé, C. Ferràndez-Cañadell, P. Busquets, J.M. Samsó, J. Tosquella, A. Barnolas, G. Alvárez-Pérez, J. Franqués, J. Romero, An inventory of the marine and transitional Middle/Upper Eocene deposits of the Southeastern Pyrenean foreland basin (NE Spain), Geol. Acta 1 (2003) 201–229.
[41] J.J. Hooker, Britsh mammalian paleocommunities across the Eocene-Oligocene transition and their environmental implications, in: D.R. Prothero, W.A. Berggren (Eds.), Eocene/Oligocene Climatic and Biotic Evolution, Princeton University Press, Princeton, NJ, 1992, pp. 494–515.
[42] J.E. Neal, A summary of Paleogene sequence stratigraphy in northwestern Europe and the North Sea, in: R.W.O.B. Knox, R.M. Corfield, R.E. Dunay (Eds.), Correlation of the Early Paleogene in NW Europe, Geol. Soc. London Spec. Publ. 101 (1996) 15–42.
[43] J.J. Chateauneuf, C. Gruas Cavagnetto, Les zones de Wetzeliellaceae (Dinophyceae) du bassin de Paris. Comparaison et corrélations avec les zones du Paléogène des bassins du Nord-Ouest de l'Europe, Bull. B.R.G.M. Sec. IV 2 (1978) 59–93.
[44] M.-P. Aubry, Northwestern European Paleogene magnetostratigraohy, biostratigraphy, and paleogeography: Calcareous nannofossil evidence, Geology 13 (1985) 198–202.
[45] M.P. Aubry, Paleogene calcareous nannoplankton biostratigraphy of Northwestern Europe, Palaeogeogr. Palaeoclimatol. Palaeoecol. 55 (1986) 267–334.
[46] C. Cavelier, C. Pomerol, Stratigraphy of the Paleogene, Bull. Soc. Géol. Fr. II (1986) 255–265.
[47] W.A. Berggren, D.V. Kent, J.J. Flynn, J.A. Van Couvering, Cenozoic geochronology, Geol. Soc. Am. Bull. 96 (1985) 1407–1418.
[48] E. Martini, Standard Tertiary and Quaternary calcareous nannoplankton zonation, in: Planktonic Conference 2, pp. 739–777, 1971.
[49] W.A. Berggren, D.V. Kent, M.P. Aubry, J. Hardenbol, Geochronology, time scales and global stratigraphic correlation; unified temporal framework for an historical geology, in: W.A. Berggren, D.V. Kent, M.P. Aubry, J. Hardenbol (Eds.), Geochronology, Time Scales and Global Stratigraphic Correlation, SEPM Spec. Publ. 54 (1995) v–vi.

CHAPTER 2.2:

Beamud, E., Muñoz, J.A., Fitzgerald, P.G., Baldwin, S.L., Garcés, M., Cabrera, L., Metcalf, J.R. (2011) Magnetostratigraphy and detrital apatite fission track thermochronology in syntectonic conglomerates: constraints on the exhumation of the South-Central Pyrenees. Basin Research 23, 309-331

Basin Research

Basin Research (2011) 23, 309–331, doi: 10.1111/j.1365-2117.2010.00492.x

Magnetostratigraphy and detrital apatite fission track thermochronology in syntectonic conglomerates: constraints on the exhumation of the South-Central Pyrenees

Elisabet Beamud,*† Josep Anton Muñoz,† Paul G. Fitzgerald,‡ Suzanne L. Baldwin,‡ Miguel Garcés,† Lluis Cabrera† and James R. Metcalf‡

*Laboratori de Paleomagnetisme SCT UB-CSIC, Institut de Ciències de la Terra «Jaume Almera», Barcelona, Spain
†Geomodels Research Institute, Group of Geodynamics and Basin Analysis, Facultat de Geologia Universitat de Barcelona, Barcelona, Spain
‡Department of Earth Sciences, Syracuse University 204 Heroy Geology Laboratory, Syracuse, NY

ABSTRACT

The syntectonic continental conglomerates of the South-Central Pyrenees record the late stages of thin-skinned transport of the South-Pyrenean Central Units and the onset of exhumation of the Pyrenean Axial Zone (AZ) in the core of the orogen. New magnetostratigraphic data of these syntectonic continental conglomerates have established their age as Late Lutetian to Late Oligocene. The data reveal that these materials were deposited during intense periods of tectonic activity of the Pyrenean chain and not during the cessation of the deformation as considered previously. The magnetostratigraphic ages have been combined with new detrital apatite fission track (AFT) thermochronology from AZ-derived granite cobbles within the syntectonic conglomerates. Distribution of the granitic cobbles with different AFT ages and track lengths combined with their depositional ages reveal information on the timing and rate of episodes of exhumation in the orogen. Some AFT ages are considerably older than the AFT ages of the outcropping AZ granitic massifs, indicating erosion from higher crustal levels within the massifs than presently exposed or from completely eroded plutons. Inverse thermal modelling reveals two well-defined periods of rapid cooling in the hinterland at *ca*. 50–40 and *ca*. 30–25 Ma, with another poorly defined cooling episode at *ca*. 70–60 Ma. The lowest stratigraphic samples experienced postburial annealing caused by the deposition of younger syntectonic sediments during progressive burial of the south Pyrenean thrust and fold belt. Moreover, samples from the deeper stratigraphic levels also reveal postorogenic cooling during the Late Miocene as a response to the excavation of the Ebro River towards the Mediterranean Sea. Our data strongly support previous ideas about the burial of the South Pyrenean fold and thrust belt by Late Palaeogene syntectonic conglomerates and their subsequent re-excavation and are consistent with other thermochronological data and thermal modelling from the interior part of the orogen.

INTRODUCTION

Syntectonic sediments shed off an orogen and preserved in the surrounding sedimentary basins yield a long-term, usually continuous, record of the evolving orogenic system. However, syntectonic sediments are normally stored in nondeformed foreland basins adjacent to the fold and thrust belts, and hence usually at great distances away from the interior of the orogen where most thermocronological data constraining exhumation ages are normally obtained (from crystalline basement or preorogenic sequences). Moreover, either the younger foreland basin sediments or those preserved in piggy-back basins are typically continental rather than marine or fossil bearing and therefore supplying few age constraints to the syntectonic sedimentary record.

In the last few decades, systematic magnetostratigraphic studies of synorogenic continental sequences have provided significant time constraints on the evolution of convergent orogenic systems (Burbank *et al*., 1992; Meigs & Burbank, 1997; Jones *et al*., 2004). Simultaneously, thermochronological studies have yielded constraints on the

Correspondence: Elisabet Beamud, Laboratori de Paleomagnetisme SCT UB-CSIC. Institut de Ciències de la Terra «Jaume Almera», C/Solé i Sabarís s/n- 08028 Barcelona, Spain. E-mail: betbeamud@ub.edu

exhumation history of the interior parts of orogens, which are usually interpreted in terms of uplift and exhumation associated with thrust activity (e.g. ter Voorde *et al.*, 2004; Lock & Willett, 2008; Metcalf *et al.*, 2009). However, few studies combine magnetostratigraphy of synorogenic sediments with thermochronological data from pebbles or cobbles of the clastic sequences in a well-constrained tectonosedimentary system with sedimentological and structural data. Integration of these data sets may provide a significant advance in the understanding of the exhumation of orogenic systems and the relationship with syntectonic sedimentation in adjacent basins, which in their turn are fundamental for the understanding of the relationships between surface processes and tectonic forces in orogens. Other approaches to address these issues are mainly through numerical modelling (e.g. Beaumont *et al.*, 2000; Willet *et al.*, 2001; Sinclair *et al.*, 2005).

The excellent state of preservation of the synorogenic materials in the southern Pyrenees, not only in adjacent forelands but also most remarkably on top of the external thrust sheets, and even in relatively interior parts of the chain, makes the Pyrenean orogen a magnificent natural laboratory to attempt such kind of studies in order to unravel the relationships between tectonic and sedimentary processes occurring during mountain building. In this paper, we present for the first time a complete magnetostratigraphic study of the thick succession of syntectonic continental sediments preserved in the innermost piggy-back basin of the southern Pyrenees together with thermochronological data from granitic cobbles sampled through this succession. This study builds on previous work establishing the chronostratigraphic framework for the syntectonic continental sediments of the southern Pyrenees (Bentham & Burbank, 1996; Beamud *et al.*, 2003) and draws on thermochronology studies within the central Pyrenees (Morris *et al.*, 1998; Fitzgerald *et al.*, 1999; Sinclair *et al.*, 2005; Gibson *et al.*, 2007; Metcalf *et al.*, 2009). It has enabled us to relate the exhumation patterns of the interior of the chain with the preserved sedimentary record adjacent to the high relief areas and derive rates of exhumation and sedimentation.

GEOLOGICAL SETTING

The Pyrenees are an asymmetric, doubly vergent orogen formed by the collision between the European and Iberian plates from late Cretaceous to Miocene times (Roest & Srivastava, 1991; Rosenbaum *et al.*, 2002; Muñoz, 2002). The Pyrenean orogen comprises a central duplex structure of south-directed Hercynian basement thrust sheets, the Axial Zone (AZ), which is flanked north and south by oppositely vergent fold and thrust belts and associated foreland basins (Fig. 1). The AZ in the central Pyrenees culminates in an antiformal stack of three upper crustal thrust sheets named from top to bottom, Nogueres, Orri and Rialp (Muñoz, 1992, Fig. 1). To the north, the AZ antiformal stack is bounded by the North Pyrenean Fault (NPF), considered as a Cretaceous major strike slip fault system between the European and the Iberian plates before the onset of the convergence (Choukroune, 1976; Fischer, 1984). Both the AZ and the North Pyrenean zone contain numerous Hercynian granitoid plutons with appropriate minerals suitable for thermochronological analyses (Fig. 1). The AZ formed coeval with thrusting in the southern fold and thrust belt. Rock units within this fold and thrust belt are dominantly a Triassic–Cretaceous succession overlain by syntectonic Upper Cretaceous and Palaeogene sediments. The southern fold and thrust belt consists of three major thrust sheets that developed from Late Cretaceous (Bóixols thrust sheet) to Palaeocene–Early Eocene (Montsec thrust sheet) and Middle Eocene–Oligocene (Serres Marginals thrust sheet) following a forward directed thrust sequence (Fig. 1). Syntectonic sediments accumulated both in the foreland basin and within piggy-back basins preserved on top of all three major thrust sheets. The south-Pyrenean foreland basin (Ebro basin) was initially marine until Middle Eocene, when it was opened towards the Bay of Biscay, followed by a continental stage (Late Eocene–Middle Miocene) once it became an endorheic basin (Pérez-Rivarés *et al.*, 2004; Costa *et al.*, in press). This continental stage resulted from the disconnection of the Atlantic Ocean during the development of the western Pyrenees (Riba *et al.*, 1983). Syntectonic sedimentation in the endorheic Ebro basin raised the base level resulting in the progressive burying of the south Pyrenean fold and thrust belt by continental conglomerates (Coney *et al.*, 1996). Such burial of the thrust wedge enhanced internal deformation. A break-back thrust sequence then developed, as burial by syntectonic conglomerates progressed hindwards, both by reactivation of previously developed thrusts and formation of new thrusts (Vergés & Muñoz, 1990; Muñoz *et al.*, 1997; Muñoz, 2002). Increase of structural relief in the AZ antiformal stack by underthrusting and coeval passive-roof back thrusting between the cover Mesozoic sequence and the basement of the Nogueres thrust sheet along the Triassic evaporites can be considered as a continuation of the internal deformation of the thrust wedge during late burial by syntectonic conglomerates.

As the AZ thrust sheets were exhumed, granitoids enclosed within them were eroded and granitic clasts sub-

Fig. 1. (a) Geological sketch of the South Central Pyrenees highlighting the outcrops of the Upper Palaeogene continental conglomerates and the granitic massifs of the Axial Zone (AZ). The map area corresponding to the AZ modified from Zwart (1979). The position of the magnetostratigraphic logs 'La Pobleta – LP' and 'Montcortés – MC' within the Senterada basin is shown. Position of the cross-section A–A′ in Fig. 2 is also indicated. AFT ages (Ma) of the granitic massifs after (*) Morris *et al.* (1998), (**) Fitzgerald *et al.* (1999), (***) Sinclair *et al.* (2005) and (****) Gibson *et al.* (2007). (b) Simplified stratigraphic logs of the syntectonic conglomerates of Sis, Gurb and La Pobla de Segur-Senterada with indication of the position of the detrital AFT samples. (c) Cross-section for the ECORS seismic profile modified after Muñoz (2002). The square indicates the position of the cross-section of Fig. 2.

sequently included within the Palaeogene synorogenic conglomerates. Accurate dating of the stratigraphic age of the syntectonic conglomerates, combined with apatite fission track (AFT) thermochronology from the granitic cobbles, provides a more complete history of the exhumation in the hinterland of the orogen and the sedimentary response in the piggy-back basins of the South-Central Pyrenees. In comparison with the detrital approach, there have been a number of thermochronological studies in the basement rocks, especially the AZ, exposed in the Pyrenees (Morris *et al.*, 1998; Fitzgerald *et al.*, 1999; Sinclair *et al.*, 2005; Gibson *et al.*, 2007). These studies reveal an overall asymmetric exhumation pattern related to the thrusting, uplift and erosion of the stacked antiformal thrust sheets, with greater and progressively younger exhumation on the southern side of the orogen.

STRATIGRAPHY OF THE SYNTECTONIC CONGLOMERATES

Palaeogene syntectonic conglomerates in the South-Central Pyrenees occur on top of the Montsec and Bóixols thrust sheets, and as explained above, the younger sediments are located progressively northwards, even unconformably overlying the basement rocks of the AZ (Nogueres thrust sheet) (Fig. 1). These syn-tectonic sediments crop out in what is referred to as the Sis, Gurb and La Pobla de Segur/Senterada basins (Mellere, 1993; Vincent, 1993, 2001). The presently disconnected outcrops of these sediments, which gave names to the individual basins, are located along ridges and higher areas between the present rivers and thus were most likely in continuation forming a single basin before the Neogene exhumation and excavation of the present fluvial network (Coney *et al.*, 1996; Fitzgerald *et al.*, 1999). They are mainly composed of alluvial conglomerates with some lacustrine and fluvial deposits. These sediments have been considered previously post-tectonic based on the spectacular unconformity between the less deformed Palaeogene conglomerates above and the folded Mesozoic and Early Palaeogene sediments below (Mey *et al.*, 1968). However, their deposition occurred synchronously to the main tectonic events in the region and they are often folded and thrusted (Rosell & Riba, 1966; Robles, 1982; Mellere, 1992; Vincent, 1993).

The Sis conglomerates are internally divided into the Cajigar, Cornudella, Sis and Collegats formations (Koops & van Rossem, 1985; Vincent, 1993, 2001). Sediments of the Cajigar Fm. are characterized by red silts and conglomerates with a lack in granite clasts and a very low proportion of AZ-derived materials (Vincent, 2001). The overlying Cornudella Fm. is composed of interbedded fluvial and lacustrine sediments, including input of granitic components from the AZ (Vincent, 2001). The upper units of the Sis Formation are composed by stacked red conglomerates internally arranged in four sequences (Sis 1–4, Fig. 1). Granite clasts are regularly found from Sis 1 up to Sis 3 but not in Sis 4 (Vincent, 2001). Overlying an unconformity on top of the succession, the Collegats Fm. (Vincent, 2001) records a marked change in clast provenance with the reintroduction of granitic material and an increase in Palaeozoic and Triassic components.

Further east, La Pobla de Segur conglomerates (Rosell & Riba, 1966; Mellere, 1993) onlap a previously deformed substratum of Mesozoic rocks. They are organized in five allogroups, from base to top: the Pessonada, Ermita, Pallaresa, Senterada and Antist allogroups (Mellere, 1993, Fig. 2). The basal units, the Pessonada and Ermita allogroups, are characterized by monomict conglomerates of local provenance, mainly composed by cobbles of Cretaceous and Jurassic rocks (Mellere, 1992; Barsó & Ramos, 2007). The first occurrence of AZ detritus occurs within the Pallaresa allogroup and extends up through the Senterada and Antist allogroups. The Pallaresa allogroup represents the major alluvial fan complex of the basin and is composed of several interfingering alluvial fan systems, the Montsor, Collegats, Roca del Peso, Roc de Santa, Roca Llania and La Creu systems (Mellere, 1993). The Montsor system is characterized by stacked red polymict conglomerates with a source area within the AZ as shown by the high proportion of Triassic and Palaeozoic clasts; conversely, the Collegats system is composed exclusively of Mesozoic clasts, indicative of a local source area (Mellere, 1993; Barsó, 2007). The Senterada allogroup unconformably overlies both the Pallaresa allogroup in the La Pobla basin and a Palaeozoic and Mesozoic substratum above the Nogueres unit in the Senterada basin (Fig. 2). It is composed of polymict conglomerates organized in three sequences (S1–S3) with a source area located to the N–NE within the Nogueres unit, which is the most internal part of the AZ (Mellere, 1993). Unconformably overlying the Senterada allogroup, both in the La Pobla and the Senterada basins, the Antist allogroup is characterized by massive very coarse alluvial fan conglomerates composed mainly of Palaeozoic clasts from the AZ, with a minor contribution of Triassic clasts (Mellere, 1993; Barsó & Ramos, 2007).

Cropping out between Sis and La Pobla de Segur conglomerates, the upper part of the Gurb conglomerates shows a sequence of units equivalent to the Ermita, Pallaresa (Montsor system) and Senterada allogroups (Fig. 1). Below the Ermita allogroup, the lower part of the Gurb

Fig. 2. (a) Detailed geological map of the La Pobla de Segur and Senterada basins. The position of the cross-section A–A′ and the magnetostratigraphic sections La Pobleta (LP) and Montcortes (MC) within the Senterada basin are shown. The magnetostratigraphic sections of Beamud *et al.* (2003) (Claverol: CL, Carretera Sort: CS, Can Gramutill: CG, Rocs Queralt: RQ and Montsor: MS) within the La Pobla de Segur basin are also located. (b) Cross-section A–A′ across the La Pobla and Senterada basins showing the main structural features of the syntectonic conglomerates. b–b′ corresponds to an enlargement of the central area of cross-section A–A′.

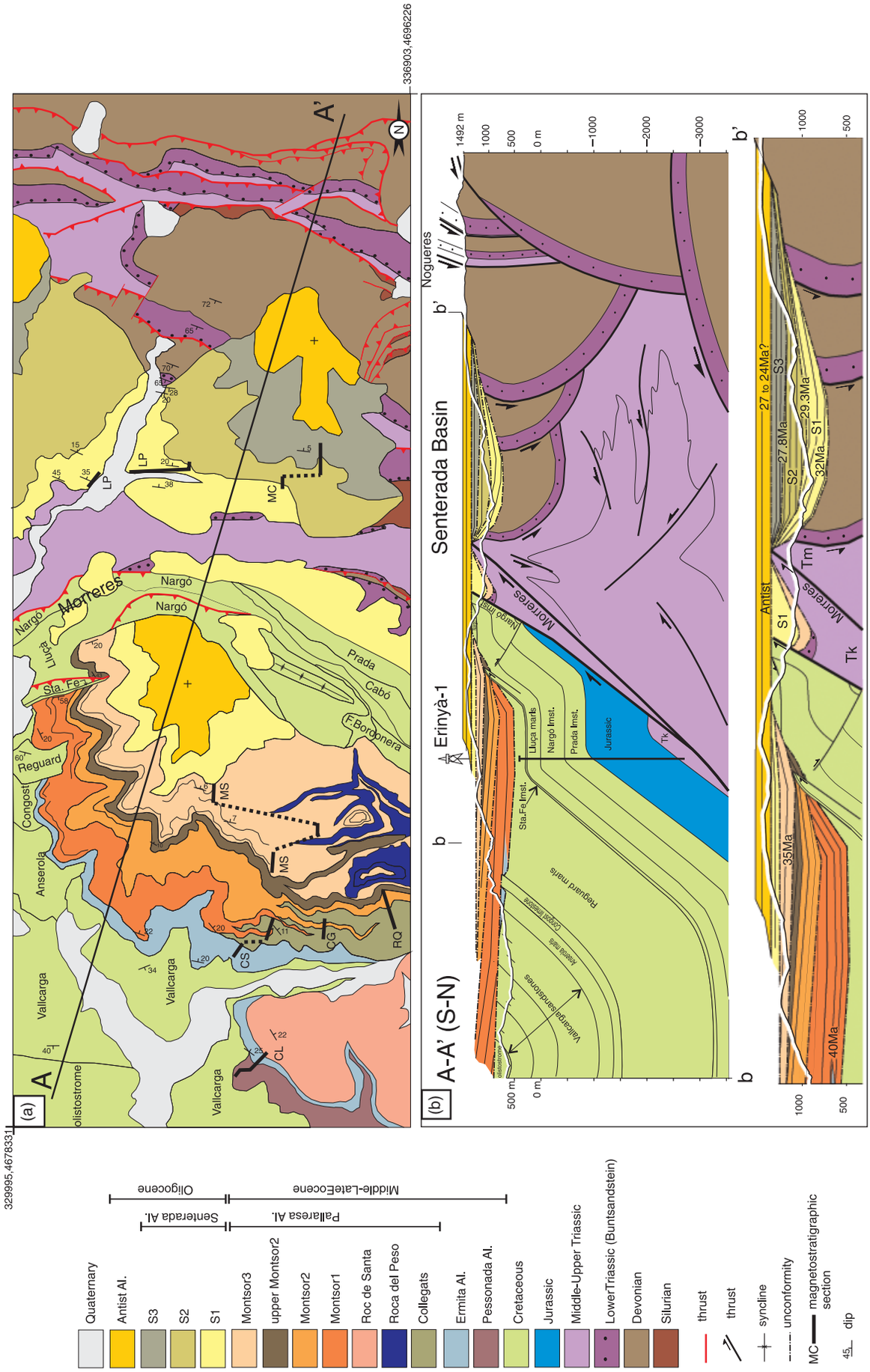

conglomerates consists of the Gurb and Espills formations (Picart *et al.*, 2009). The upper part of the Gurb Formation (Gurb 3 and 4 sequences) is characterized by massive alluvial fan conglomerates with a high proportion of Palaeozoic clasts (Picart *et al.*, 2009), which contrast with the facies and composition of their age-equivalents in the La Pobla de Segur conglomerates (the Pesonada allogroup) composed of Mesozoic clasts (Fig. 1). Palaeozoic clasts are also present in the lower sequences of the Gurb Formation and in the Espills Formation, although in much lower proportions (Picart *et al.*, 2009).

Based on scarce mammal fossils, age constraints on the Sis and La Pobla syntectonic conglomerates were poor but suggested a Late Eocene age for the middle part of the succession (Casanovas, 1975; Antunes *et al.*, 1997; López-Martínez, 1998). However, recent magnetostratigraphic studies have established their age in Middle–Late Eocene (Late Lutetian to Priabonian) (Beamud *et al.*, 2003).

STRUCTURE OF THE CONGLOMERATES

The Sis, La Pobla de Segur and Gurb conglomerates unconformably overlie the deformed Mesozoic to lower Eocene succession of the Bóixols and Montsec thrust sheets (Figs 1 and 2). The basal unconformity in the southern part of the outcrops is mostly horizontal, below flat-lying to northwards tilted panels of conglomeratic beds. In the north, the basal unconformity mainly dips to the south and displays an intricate geometry of palaeovalleys. In these northern areas, strata are flat-lying to southwards tilted with preserved growth geometries (Fig. 2). Thus, beds of conglomerates progressively onlap the unconformity northwards, climbing stratigraphically up-section independent of the geometry of the unconformity. Palaeocurrent indicators within the conglomerates indicate mainly southward flow (Mellere, 1992; Barsó, 2007); thus, northward tilting of the conglomerate units is post-depositional. Growth geometries preserved along the Flamisell and Noguera Pallaresa valleys, north of La Pobla de Segur, between the tilted and subhorizontal beds further north demonstrate that deformation occurred during the sedimentation of the Pallaresa allogroup, probably related with the reactivation of the Bóixols thrust. The beds of the Pallaresa and Senterada allogroups in the La Pobla de Segur and Gurb conglomerates are tilted southwards and folded in the hanging wall of the Morreres backthrust, which is a system of north-directed passive-roof thrusts between the Bóixols and the Nogueres thrust sheets (Figs 1 and 2, Muñoz, 1992). Internal growth sequences and unconformities between the different sequences of these conglomerates show a punctuated activity of the Morreres backthrust system during the sedimentation of these conglomerates (Fig. 2).

The Morreres backthrust partitioned the basin during the sedimentation of the Senterada allogroup. The Senterada basin developed in the footwall of this thrust showing an internal syncline geometry at present. The progressive unconformity in the southern limb demonstrates the activity of the Morreres backthrust during the sedimentation of the Senterada conglomerates. The wedging and tilting of the beds in the northern limb also show that the northern part of the Senterada basin was uplifted during the sedimentation (Fig. 2).

The youngest unit of conglomerates preserved, the Antist allogroup, does not show any tectonic deformation. Beds are subhorizontal and have the same thickness both in the footwall and in the hanging wall of the Morreres backthrust (Fig. 2) demonstrating the cessation of thrusting before deposition of this allogroup (Mellere, 1993).

MAGNETOSTRATIGRAPHY OF THE SENTERADA BASIN

To add temporal constraints to the upper part of the syntectonic conglomerates and the synchronously developed structures, two magnetostratigraphic sections, La Pobleta (LP) and Montcortes (MC), were sampled in the Senterada basin (Figs 1 and 2). Sampling covered no more than the Senterada allogroup as poor-quality exposures hindered the sampling of the Antist allogroup at the very top of the succession. At least two oriented cores per site were obtained with a portable gas-powered drill and a core-orienting fixture. As conglomerates and sandstones are too coarse to yield a primary depositional magnetisation, sampling focused on the interbedded finer grained overbank sediments. Even though the unsuitable coarse sediments dominated most portions of the section, an adequate sampling density of 2–3 m between sites was maintained and 158 sites were sampled through 420 m of the stratigraphic succession.

The palaeomagnetic analysis consisted of stepwise thermal demagnetization of the natural remanent magnetization (NRM) of one to two samples per site. Thermal demagnetization was conducted at intervals of 50–30 °C up to 690 °C. Measurement of the magnetization was performed in superconducting rock magnetometers at the laboratories of the 'Serveis Cientificotècnics UB-CSIC' (Spain) and at the University of Leoben (Austria). Initial NRM ranged from 1.65×10^{-4} to $8.6 \cdot 10^{-3}$ A m^{-1} with mean values around 2.0×10^{-3} A m^{-1}. Zijderveld plots (Fig. 3a) show that the NRM consists of two palaeomagnetic components. The low temperature component, usually removed between 150 and 250 °C, parallels the recent geomagnetic field. The high temperature component, which yields both normal and reversed directions, remains stable up to 600–670 °C, pointing to haematite as the main remanence carrier. The characteristic remanent magnetization (ChRM) directions were calculated by least square analysis after visual inspection of the Zijderveld plots. In most of the samples, the ChRM's were calculated using the origin of coordinates as the vector end points were directed towards the origin at high temperatures and no additional components could be de-

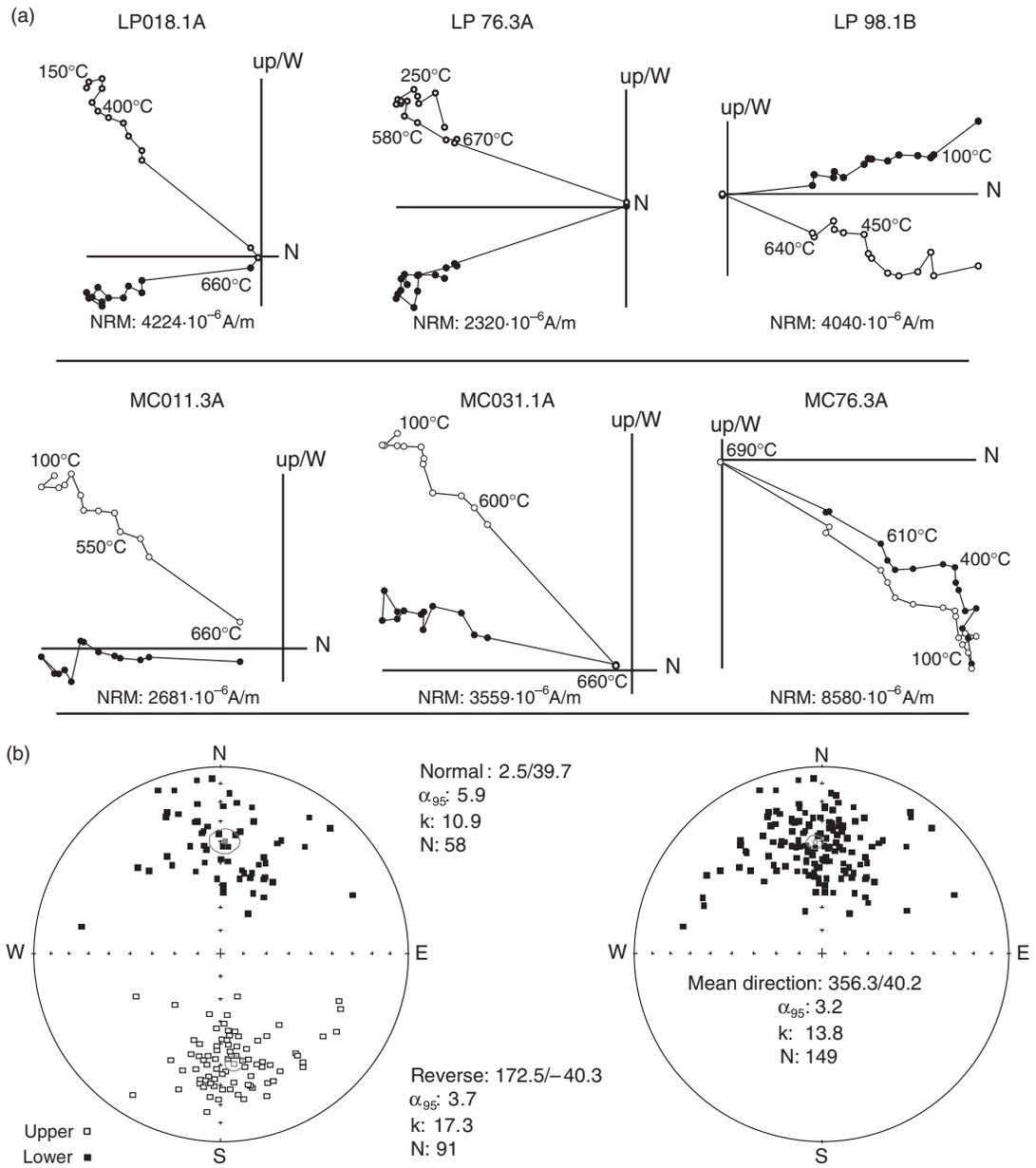

Fig. 3. (a) Demagnetization diagrams of representative samples of La Pobleta (LP) and Montcortes (MC) magnetostratigraphic logs showing normal and reversed polarities. Black and white dots, respectively, indicate horizontal and vertical projection of the vector end points. Diagrams are in tectonic corrected coordinates. (b) Mean direction of the Senterada materials from the LP and MC sections. No vertical axis rotations are observed.

duced. A class B positive reversal test (McFadden & McElhinny, 1990) was obtained (critical angle: 7.1, angle between normal and reversed polarity sets: 7.0, probability of exceeding this angle: 0.055), indicating the successful isolation of the ChRM component. The resulting mean direction revealed no significant vertical axis rotations (Fig. 3b). ChRM directions were used to obtain the latitude of the virtual geomagnetic pole (VGP) at the site level (Fig. 4). Positive and negative latitudes of the VGP were interpreted as normal and reversed polarities, respectively, when building the local magnetic polarity stratigraphy. Single site magnetozones of, particularly, the lower part of the 'LP' section were considered unreliable and were discarded from the composite magnetostratigraphic sequence. The rest of the sequence showed a coherent sequence of normal and reversed polarity magnetozones, each of these defined by at least two consecutive sites (Fig. 4). The resulting magnetic polarity pattern suggests that the directions obtained represent mainly primary magnetization.

Correlation to the geomagnetic polarity time scale

The stratigraphic position of the Senterada allogroup in the La Pobla basin and the reversal pattern obtained enable us to correlate the local magnetostratigraphy with the geomagnetic polarity time scale (GPTS) (Gradstein *et al.*, 2004) (Fig. 5). As the Senterada allogroup crops out

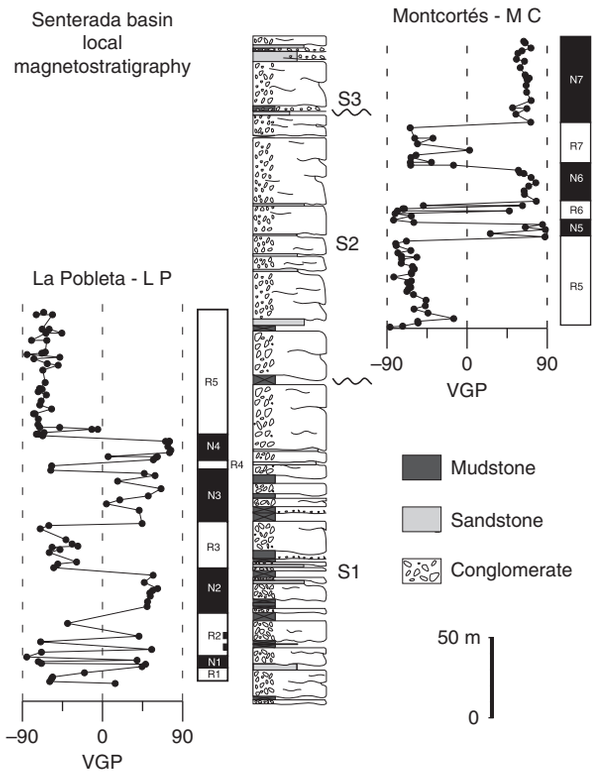

Fig. 4. Palaeolatitude of the VGP and local magnetoestratigraphy for the Senterada basin.

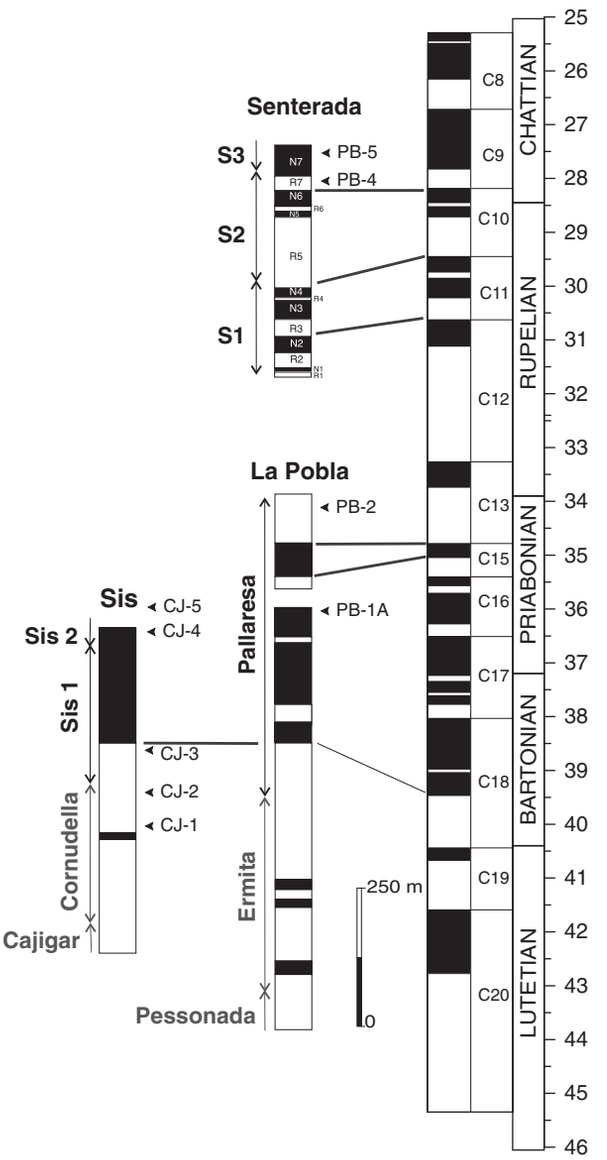

Fig. 5. Correlation of the local magnetostratigraphy to the GPTS (Gradstein *et al.*, 2004) and integration with the previously published data of La Pobla and Sis conglomerates (Beamud *et al.*, 2003). The stratigraphic position of the AFT samples along the magnetostratigraphic sections is shown.

on top of the Pallaresa allogroup (Mellere, 1993) (Fig. 2), deposition of the Senterada conglomerates must necessarily postdate C13r, which is the youngest magnetostratigraphic age for the conglomerates of the Pallaresa allogroup in the La Pobla basin (Beamud *et al.*, 2003). We propose that the first clearly defined magnetozone N2 correlates with the upper part of C12. Paired normal magnetozones N3–N4 and N5–N6 correlate with paired subchrons in C11n and C10n, whereas the long reversed magnetozone R5 matches the long reversed chron C10r. Finally, top magnetozones R7 and N7 are proposed to correlate to chron C9. This correlation yields an Oligocene age for the Senterada allogroup, ranging from Rupelian to Chattian (32–27 Ma).

The correlation with the GPTS allows determination of a mean sedimentation rate of $\sim$0.1 km Myr^{-1} for the Senterada allogroup. This sedimentation rate is similar to that calculated for the top of the La Pobla succession (Beamud *et al.*, 2003). Whereas the age of the overlying Antist allogroup remains unconstrained, a Chattian age appears to be reasonable, assuming the sedimentation rate remains more or less constant at $\sim$0.1 km Myr^{-1}. The overlying 300 m of the Antist allogroup (Mellere, 1993) would thus represent a 3 Myr stratigraphic record, being deposited between 27 and 24 Myr.

Detrital fission track thermochronology

AFT thermochronology is a long established, but ever evolving, technique for determining the thermal histories (less than *ca*. 140 °C) of orogens and sedimentary basins (e.g. Wagner & Reimer, 1972; Naeser *et al.*, 1983; Gleadow & Fitzgerald, 1987; Hurford, 1991; Gallagher *et al.*, 1998). Derived thermal histories can then be used to unravel the exhumation history of orogens, taking into account many variables such as the dynamic geotherm (Grasemann & Mancktelow, 1993; ter Voorde & Bertotti, 1994; Ehlers & Chapman, 1999) and the architecture of the topography (e.g. Ehlers *et al.*, 2001) as well as constraining the regional tectonic history (e.g. Fitzgerald *et al.*, 1995).

Detrital thermochronology involves the single-grain dating of minerals from sediments to constrain the thermal history and exhumation of the source regions, sediment provenance and landscape evolution (e.g. Baldwin *et al.*, 1986; Bernet & Spiegel, 2004; Spiegel *et al.*,

2004; Rahl *et al.*, 2007). Hence, detrital thermochronology relies on techniques such as U–Pb zircon dating, $^{40}Ar/^{39}Ar$ muscovite and biotite dating, zircon fission track dating and (U–Th)/He dating on apatite and zircon, all of which usually permit the precise dating of single grains. AFT analysis is less commonly used for detrital thermochronology because the statistics on the relatively small number of spontaneous tracks present often yield single-grain ages with relatively large errors. It is usually only when AFT thermochronology is undertaken on a number of grains to generate pooled or central ages with lower uncertainties that more precise ages result (e.g. Galbraith, 2005). Thus, AFT thermochronology is typically undertaken on basement or sedimentary rocks where individual grains are likely to share a common thermal history, although individual grains may have differing chemical compositions or different provenance, all of which are usually taken into account during analysis and interpretation. Likewise, AFT detrital thermochronology undertaken on boulders or cobbles, such as from foreland basin deposits, will also generate meaningful counting statistics because the individual grains from each cobble share a common thermal history (e.g. Wagner *et al.*, 1979; Dunkl *et al.*, 1998; Brügel *et al.*, 2003).

Sediment provenance undertaken using detrital thermochronology usually requires > 100 fairly high-resolution single-grain ages (e.g. Brandon *et al.*, 1998). However, use of multiple provenance indicators, for example both fission track thermochronology and *in-situ* Sm-Nd isotopic analyses (Foster & Carter, 2007) will yield a stronger linkage with source regions. The petrography of the pebbles and cobbles may also provide a stronger linkage, especially if there are distinctive lithologies or drainage paths that can be constrained by other means. One of the disadvantages of only using suitable accessory mineral-bearing pebbles and cobbles, typically granitic, for detrital thermochronology is that only the detrital record, the exhumation and transportation of these granitic plutons are being tracked. Typically, for a thorough provenance study, the petrology of all sedimentary components will be included, as it has been for the study of these Pyrenean syn-tectonic conglomerates (Mellere, 1992, 1993; Vincent, 1993, 2001; Barsó, 2007).

An important component to constraining the thermal and exhumational history of orogens using detrital thermochronology is the depositional age of the synorogenic sediments (e.g. Garver *et al.*, 1999). Subtracting the stratigraphic age from the cooling age yields the lag-time (e.g. Garver *et al.*, 1999). As transportation is usually regarded as geologically instantaneous (Brandon & Vance, 1992), it is possible to constrain the timing of exhumation, from the time of closure of the isotopic system to the surface, and assuming a palaeo-geothermal gradient, constrain the exhumation rate (e.g. Garver *et al.*, 1999). Exhumation steady state refers to constant exhumation rates in the source region, which in turn is reflected in uniform lag-times (e.g. Garver *et al.*, 1999). The constructive phase of an orogen is reflected by sediments with decreasing lag-times indicative of increasing exhumation rates, whereas the decay phase of an orogen is reflected by increasing lag-times caused by decreasing exhumation rates (e.g. Brandon & Vance, 1992; Garver *et al.*, 1999; Bernet *et al.*, 2004).

Lower temperature thermochronologic methods are more sensitive to shorter term variations in exhumation rates than higher temperature methods that are more often used for provenance studies (e.g. Bernet & Spiegel, 2004). Methods that incorporate a kinetic parameter used to independently constrain the rate of cooling, such as $^{40}Ar/^{39}Ar$ thermochronology using potassium feldspar multidiffusion domain modelling (McDougall & Harrison, 1999) and AFT thermochronology with confined track-length and apatite compositional measurements (e.g. Ketcham, 2005), will better constrain both the exhumation history of the source region and the post-depositional thermal history of sediments. In addition, geologic constraints on possible T–t paths help constrain thermal models, and in this case the stratigraphic age of each sample provides a robust constraint (minimum age) on when this sample was exhumed to the surface, before transportation and deposition.

We sampled 13 granitic cobbles from the Sis and La Pobla de Segur/Senterada conglomeratic units for detrital AFT analysis (Figs 1b and 5, Table 1). Nine granite cobbles were sampled in the Sis conglomerates from the Cornudella, Sis 1, Sis 2 and Collegats formations. In La Pobla de Segur basin, two granitic samples were obtained from the Pallaresa allogroup, and two from the Senterada allogroup in the Senterada basin.

Depositional ages of the AFT samples

Most of the detrital thermochoronological samples were obtained from the same sections as collected for magnetostratigraphy (Figs 1b and 5), thus most of these samples have well-constrained depositional ages (Table 1). In La Pobla basin, samples from the Pallaresa allogroup PB-1 and PB-2 yield depositional ages of 36 and 34 Ma, respectively. In the Senterada basin, the depositional age of the sample PB-4 was established at 28 Ma and at 27.5 Ma for sample PB-5. In the Sis conglomerates, the depositional ages of samples CJ-1–CJ-3 range around 40 Ma. The overlying samples CJ-4 and CJ-5 have depositional ages around 37 Ma.

Magnetostratigraphic ages could not be obtained for sections where samples PY-71–PY-74 from the Collegats Fm. were collected. There, the outcrop conditions of the Collegats Formation were not good enough for palaeomagnetic purposes. However, we constrained their depositional ages based on the following criteria. The Collegats Fm. has been correlated with the Graus Formation near Graus (Reynolds, 1987; Vincent, 1993, 2001). An age younger than 36.2 Ma has been proposed for the Graus basal unconformity based on magnetostratigraphy (Bentham, 1992; Bentham & Burbank, 1996). The overlying Graus Fm. ranges in age from Late Eocene to Late Oligocene or even up to the Oligocene–Miocene boundary based on micromammal biostratigraphy (Cuevas Gozalo,

Table 1. Fission Track Analytical Results: Pyrenees; Syn-tectonic conglomerates

Sample group	Sample number	Stratigraphic age	UTM coords	Elev. (m)	No. of grains	Standard track density (× 106 cm^{-2})	Fossil track density (× 106 cm^{-2})	Induced track density (× 106 cm^{-2})	χ^2 probability (%)	Dispersion (%)	Central age ± 1σ (Ma)	Mean track length (μm)	SD (μm)	Dpar mean (SD) μm
Serra de Sis Conglomerates														
1	PY-71	Late Oligocene (Chattian), ∼25 Ma	310 176, 4 696 722	1560	28	1.66 (5222)	0.1304 (92)	1.413 (997)	92	< 1	28 ± 3	14.3 ± 0.2 (8)	0.6	2.33 (0.2)
1	PY-72	Late Oligocene (Chattian), ∼25 Ma	308 624, 4 697 279	1480	20	1.68 (5222)	0.1815 (49)	2.033 (549)	97	≪ 1	27 ± 4	14.3 ± 0.3 (22)	1.4	3.66 (0.3)
3	PY-73	Late Eocene (Priabonian), ∼35 Ma	309 221, 4 692 136	1400	25	1.48 (4900)	0.9277 (575)	5.350 (3316)	46	4	46 ± 2	13.9 ± 0.1 (51)	0.9	2.35 (0.2)
3	PY-74	Late Eocene (Priabonian), ∼35 Ma	309 221, 4 692 136	1400	22	1.49 (4900)	0.4968 (295)	2.691 (1598)	23	12	49 ± 4	14.2 ± 0.2 (33)	0.9	2.55 (0.1)
4	CJ-5	Late Eocene (Priabonian), 37 Ma	303 945, 4 687 786	1344	20	1.65 (5392)	0.5345 (296)	2.591 (1435)	74	0	61 ± 4	13.1 ± 0.2 (75)	1.5	2.67 (0.1)
4	CJ-4	Middle Eocene, (Bartonian), 37.5 Ma	304 077, 4 687 971	1302	27	1.63 (5392)	0.3172 (203)	1.58 (1011)	95	0	63 ± 5	12.0 ± 0.4 (27)	1.9	2.61 (0.2)
5	CJ-3	Middle Eocene (Bartonian), 39.7 Ma	303 474, 4 687 090	1260	25	1.32 (4456)	2.157 (1768)	12.15 (9959)	0	16	43 ± 2	12.4 ± 0.1 (100)	1.4	2.94 (0.2)
5	CJ-2	Middle Eocene (Bartonian), 40 Ma	303 348, 4 684 994	1167	25	1.30 (4456)	0.7369 (693)	3.829 (3601)	72	0	45 ± 2	12.8 ± 0.4 (38)	2.2	2.98 (0.4)
5	CJ-1	Middle Eocene (Bartonian), 40.2 Ma	303 095, 4 684 842	1119	13	1.29 (4456)	1.924 (602)	9.267 (2899)	6	10	49 ± 3	12.6 ± 0.2 (49)	1.7	3.14 (0.3)
Senterada Conglomerates														
2	PB-5	Late Oligocene (Chattian), 27.5 Ma	327 978, 4 692 936	1233	15	1.70 (5392)	0.1174 (29)	0.903 (223)	25	23	41 ± 8	13.8 ± 0.3 (1)		3.14 (0.3)
2	PB-4	Late Oligocene (Chattian), 28 Ma	322 021, 4 693 397	1134	25	1.68 (5392)	0.1971 (123)	1.428 (970)	96	0	42 ± 4	14.2 ± 0.2 (14)	0.9	2.95 (0.3)
Pobla de Segur Conglomerates														
3	PB-2	Late Eocene (Priabonian), 34 Ma	337 232, 4 684 514	1136	25	1.67 (5392)	0.3658 (436)	2.61 (1853)	0.5	23	43 ± 3	13.7 ± 0.3 (30)	1.4	3.02 (0.2)
4	PB-1	Middle-Late Eocene, 36 Ma	334 371, 4 682 849	1000	24	1.66 (5392)	1.7112 (350)	8.434 (1725)	64	43	60 ± 4	12.7 ± 0.3 (25)	1.6	2.97 (0.2)

Stratigraphic ages of these samples, as discussed in the text, are largely based on the magnetostratigraphy of these conglomerates (Beamud *et al.*, 2003). Parentheses enclose number of tracks counted (density) or measured (track lengths). Standard and induced track densities were measured on mica external detectors (geometry factor = 0.5), and fossil track densities were measured on internal mineral surfaces. Samples of basement rock were crushed and the apatites separated from them using conventional heavy liquid and magnetic techniques. Apatites were mounted in epoxy resin on glass slides, ground and polished to reveal an internal surface, and then etched for 20 s at room temperature in 5 N HNO_3 to reveal spontaneous fission tracks. Apatite ages were determined using the external detector method and an automated stage. Samples were irradiated at the Oregon State University Nuclear reactor in the slow soaker position B-3 (Thermal column number 5) that has a Cd for Au ratio of 13.6 at the column face. The mounts were counted at a magnification of × 1250 under a dry × 100 objective. Ages were calculated using the zeta calibration method (zeta = 361 ± 10 for dosimeter glass CN5) following the procedures of Hurford & Green (1983) and Green (1985). Analytical errors were calculated using the 'conventional method' (Green, 1981). Track lengths were measured using 'confined' fossil fission tracks using only those that were horizontal (Laslett *et al.*, 1984). Tracks were measured under a × 100 dry objective using a projection tube and a digitizing tablet attached to a microcomputer. Wherever possible, 100 track lengths per sample were measured, the number being less only when insufficient suitable tracks were present in the available apatite. Parentheses indicate number of confined tracks measured.

Table 2. Binomial peak-age fitting for samples containing multiple age populations

Sample	Group	Stratigraphic age (Ma)	*N*	AFT central age (1σ)	Age range (Ma)	P1 ± 1σ (Ma)	P2 ± 1σ (Ma)
PY-74	3	~35	22	49 ± 4	11–93	15 (+13, −7) [10]	52 (+4, −4) [90]
PB-2	3	34	25	43 ± 3	21–132	38 (+3, −3) [74]	64 (+9, −8) [26]
CJ-3	5	39.7	25	43 ± 2	29–64	31 (+2, −2) [19]	46 (+2, −2) [81]
CJ-1	5	40.2	13	49 ± 3	33–73	46 (+9, −8) [72]	60 (+61, −30) [28]

N, number of grains counted; P1 and P2 are fitted binomial peak ages (rounded) quoted at ± 1σ 68%confidence interval). Numbers in the square brackets represent percentage of grains in a given peak.

1990). The stratigraphic position of samples PY-73 and PY-74 near the basal levels of the Collegats Formation just a few metres above the basal unconformity, suggests a depositional age of ~35 Ma. Finally, the uppermost Sis samples PY-72 and PY-71 were obtained from the uppermost levels of the Collegats Formation, which can be correlated to the Antist allogroup in the La Pobla/Senterada basins. The depositional age of this group of samples is extrapolated to 25 Ma.

RESULTS

The detrital AFT ages obtained vary from 63 to 27 Ma (Table 1). AFT age generally increases with the increasing stratigraphic age and depth, as would be expected from progressive erosion of an active orogen (e.g. van der Beek *et al.*, 2006; Rahl *et al.*, 2007). Samples with stratigraphic ages younger than 36 Ma yielded long mean track lengths indicative of rapid cooling and exhumation. Samples with stratigraphic ages older than 36 Ma yielded shorter track lengths distributions suggesting slow cooling and/or longer residence in an AFT partial annealing zone (PAZ) before erosion and deposition, or partial annealing after deposition. Thus, the data appear to follow a relatively straightforward unroofing model of a hinterland with a relatively simple thermal history. Samples buried to depths above an AFT PAZ have not been significantly annealed and retain the hinterland exhumation signal. The timing and integrated rate of exhumation for these samples can be interpreted using a lag-time plot. Note that samples exhumed from within a hinterland PAZ may have partially reset ages and hence may lack geological significance (van der Beek *et al.*, 2006). Following deposition, samples buried deeply will be partially and/or completely reset by annealing, reducing the geological significance of these AFT ages. However, thermal modelling provides information about the degree of annealing and the timing of subsequent (post-depositional) exhumation (e.g. van der Beek *et al.*, 2006), which in this study is very important.

The data fall naturally into five groups depending on their AFT age and stratigraphic position. We introduce the results in a qualitative fashion, before applying inverse thermal modelling using HeFTy (Ketcham, 2005). The overall quality of apatite grains from the granitic cobbles is quite variable, usually good but in some cases very poor (e.g. PY-71) often leading to a lower number of grains counted than desirable (usually 25 grains is preferred) or fewer confined track lengths (100 confined tracks is preferred). Our sampling strategy, with groups of samples collected within close stratigraphic proximity to each other, was designed to negate variable sample quality, and to a large degree this works well as the AFT ages and confined track length distributions are invariably similar among these groups of samples. We also treat all samples and the 'groups' as if they are from the same basin – a reasonable assumption given that the individual basins were probably part of a single larger basin before the Neogene excavation.

To evaluate whether counted grains belong to a single age population (within Poissonian variation), it is standard practice to perform a χ^2 test on the single-grain data (Galbraith, 1981). If the χ^2 probability is $<5\%$, it is likely that the grains counted represent a mixed-age population with real age differences between single grains. The relative error or age dispersion (spread of the individual grain data) is given by the relative standard deviation of the central age. Where the dispersion is low ($< \sim 15\%$), the data are consistent with a single population, and the mean/pooled ages and the central age converge (e.g. Galbraith, 2005). Mixed age-populations are often expected in detrital FT ages where the grains may be from multiple sources (e.g. Brandon, 1992). In the case of granitic cobbles, we do not have this problem as all grains are from the same rock. However, slight (or significant) variations in apatite chemistry between grains in granitic rocks may result in slightly (or significantly) different single-grain ages for grains undergoing the same T–t history (O'Sullivan & Parrish, 1995). Single-grain age variation will be amplified considerably if samples are resident in an AFT PAZ for any length of time. We evaluated all samples for different age populations using binomial peak fitting (e.g. Galbraith & Green, 1990; Brandon, 1992). Four samples had two age populations (Table 2) with the three samples that fail, or very nearly fail χ^2 (CJ-1 and -3, PB-2) as well as PY-74.

Group 1: samples PY-71 and PY-72 (Sis area: Collegats Fm.). The AFT age of these uppermost samples (28 ± 3,

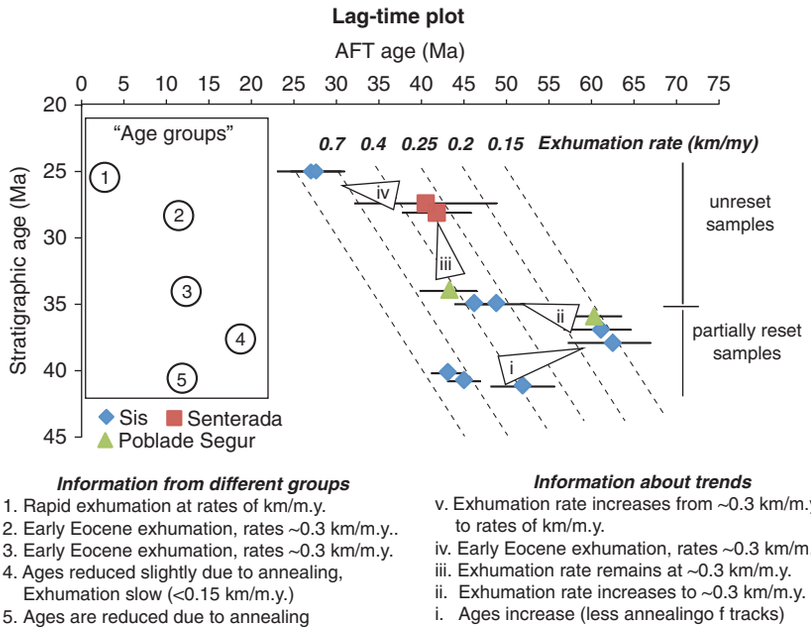

Fig. 6. Lag-time plot (e.g. Garver *et al.*, 1999) for the Sis, La Pobla and Senterada samples.

27 ± 4 Ma) is very close to their stratigraphic age (~25 Ma). Both samples pass the χ^2 test and have low-relative errors with binomial peak fitting indicating that grains from each sample are from one population. The short lag-time, combined with track length constraints (mean track lengths are $>14\,\mu$m with small standard deviations) indicates very rapid exhumation – $>1\,\text{km Myr}^{-1}$ with little or no post-burial annealing.

Group 2: samples PB-4, -5 (Senterada basin: Senterada allogroup). The AFT age (42 ± 4 Ma for PB-4) is much older than the stratigraphic age (*ca.* 28 Ma). Track length constraints (mean length for PB-4 is $>14\,\mu$m with a low standard deviation, there was only one measured track length for PB-5) suggest that the rate of exhumation-related cooling is rapid, with little or no post-burial annealing. However, the relatively long lag-time, ~14 Myr means that there is little control on the exhumation rate, before burial, as samples could take ~14 Myr to be exhumed or be exhumed very rapidly close to the surface where they resided before later erosion, transportation and burial. Both samples pass the χ^2 test, suggesting grains from each sample each form one age population, although PB-5 has a dispersion of 23%. Binomial peak fitting indicates one age population for each sample.

Group 3: samples PY-73 and -74 (Sis area: Collegats Fm.) and PB-2 (La Pobla basin: Pallaresa allogroup). AFT ages are 43 ± 3–49 ± 4 Ma and the stratigraphic age is younger (~35 Ma). The length constraints (mean lengths are long, $\geq 13.7\,\mu$m with low standard deviations) suggest that samples cooled rapidly with little or no significant post-burial annealing, although as for group 2, the relatively long lag-time (~11–14 Myr) means that the rate of pre-depositional exhumation is not well constrained. Of the three samples, two (PY-73 and -74) pass the χ^2 test and have low dispersion suggesting grains from each sample each form one age population. Interestingly binomial peak fitting indicates two age population for PY-74, a dominant peak at ~52 Ma and a minor peak at ~15 Ma. PB-2 fails the χ^2 test and also has a relatively large relative error (23%), with binomial peak fitting indicating two age populations, a dominant peak at ~38 Ma and minor peak at ~64 Ma.

Group 4: samples CJ-4, -5 (Sis area: Sis Fm.) and PB-1 (La Pobla basin: Pallaresa allogroup). AFT ages 61 ± 4–63 ± 5 Ma are significantly older than the stratigraphic age (38–36 Ma). Track-length data with means of 12–13 μm and standard deviations $\geq 1.5\,\mu$m indicate significant annealing. Samples CJ-4 and -5 from Sis both pass the χ^2 test and have low relative errors. The greater number of confined tracks in CJ-5 makes this a better sample to model. Sample PB-1 from the La Pobla de Segur passes the χ^2 test, but has a large relative error (43%), yet binomial peak fitting indicates one age population for PB-1 as well as the other group 4 samples.

Group 5: samples CJ-1, -2, -3 (Sis area: Cornudella and Sis Fms.) AFT ages (43 ± 2–49 ± 3 Ma) are not much older than the stratigraphic age (40.5–39.5 Ma) suggesting relatively rapid exhumation. However, mean track lengths are short, indicating significant annealing. Although CJ-3 has the most measured confined tracks (100), it fails the χ^2 test and also has a relative error of 16%, suggesting the possibility of multiple grain-age populations. Binomial peak fitting indicates two age peaks, a dominant one at ~46 Ma and a minor peak at ~31 Ma. CJ-1 passes the χ^2 test, but barely, and has a low relative error, yet binomial peak fitting indicates two age populations with the dominant peak at ~46 Ma and a very poorly constrained peak at ~60 Ma.

Lag-time plots (AFT age plotted against stratigraphic age, Fig. 6) to determine the rate of exhumation only provide relevant information when the samples have not been annealed, as annealing results in age reduction and hence the lag-time is underestimated and the exhumation rate is overestimated. Thus, lag-time plots to constrain exhumation

rates are only relevant for groups 1–3 where the mean track lengths are long, the AFT ages geologically meaningful and there is little or no post-burial annealing. Whereas AFT ages in group 4 have been annealed (and hence the ages reduced), we can summarize the exhumation history of the hinterland from group 4 up: Exhumation rate was very slow (group 4) with an increasing exhumation rate in the Early Eocene (underway by at least ~49 Ma; group 3). Exhumation rate then remained about the same (group 2) until some time after ~40 Ma the exhumation rate dramatically increases in the hinterland (group 1). Group 5 samples have most likely undergone post-depositional annealing as the AFT age with an increasing stratigraphic age (and hence depth) shows a characteristic abrupt decrease (e.g. van der Beek *et al.*, 2006).

The exhumation rates listed on the top of the lag-time plots were constrained by assuming a closure depth of ~3.7 km. This depth was determined assuming 110 °C cooling (120 °C closure temperature for apatites with these Dpar values minus a mean annual temperature of ~10 °C) divided by a geothermal gradient of 30 °C km^{-1}. The rate was then determined for intervals of 5, 10, 15, 20 and 25 Myr. Note that because of advection of isotherms, exhumation rates $>$ ~0.3 km Myr^{-1} as listed on the graph are an overestimate (Gleadow, 1990). Although these exhumation rates cannot be taken as precise, they do indicate changing patterns over time.

Thermal modelling and data interpretation

In conjunction with the lag-time plots, the binomial peak fitting and qualitative interpretation, thermal modelling (Fig. 7) is used to better constrain the timing of exhumation events in the hinterland, the degree of post-burial annealing and subsequent exhumation of samples back to the surface. Temperature–time paths for individual samples were inverse modelled using *HeFTy* (Ketcham, 2005) and the annealing algorithm of Ketcham *et al.* (2007). The choice of annealing algorithm is important as the samples from deeper stratigraphic levels indicate Late Miocene cooling, following burial and partial annealing of tracks within these samples. Note that some older thermal modelling programs used different annealing algorithms, e.g., those by Laslett *et al.* (1987) and Crowley *et al.* (1991), which produced spurious rapid cooling at low temperatures near the end of the thermal model (typically in Miocene times). This made the interpretation of 'real' late-stage cooling in AFT thermal models somewhat problematic (Laslett & Galbraith, 1996). However, the annealing algorithm of Ketcham *et al.* (1999) (and hence the 2007 algorithm used herein) does not produce this unwarranted late-stage cooling event (e.g. Ketcham *et al.*, 2000) and thus Late Miocene cooling revealed in models, as discussed below, is real.

Age data, length data, Dpar and stratigraphic age all serve as inputs for the modelling (Fig. 7). Dpar varies from 2.3 to 3.7 μm with a mean of 2.9 μm. Relatively high Dpar values such as these indicate that fission tracks in these apatites are more resistant to annealing than in apatites with lower Dpars (e.g. Donelick *et al.*, 1999). The closure temperature for apatites such as these, using Dpar of *ca.* 3 μm and a cooling rate of ~10 °C Myr^{-1}., is ~120 °C with the base of the PAZ *ca.* 140 °C. For comparison, Dpar for apatites from the Maladeta pluton, which is the closest major AZ pluton to these syn-tectonic conglomerates range from 2.5 to 3.6 μm with a mean of 3.0 μm (Metcalf *et al.*, 2009). Our Dpar measurements on Durango apatite and Fish Canyon Tuff age standards, measured using the same etching conditions (5 M HNO_3) were ~2 μm and 2–2.4 μm, respectively. These compare with 1.83 and 2.43 μm reported by Carlson *et al.* (1999) using the etching conditions (5.5 M HNO_3) for which HeFTy is calibrated. The similarity of our Dpar measurements (with one generally shorter and one slightly longer than Carlson *et al.*, 1999) meant that we did not scale our Dpar values for model input.

Each group of samples, based on similar AFT ages and stratigraphic ages, will have similar T–t paths. Although the samples with more confined track lengths have tighter resultant T–t paths (Fig. 7), they are representative of all samples within a group. T–t input constraints for the model are very loose (to allow exploration of as much T–t space as possible), with the starting T–t box constrained above the closure temperature for fission tracks in apatite and at an older age than the oldest AFT age (e.g. Ketcham, 2005), plus a tightly constrained T–t box for the depositional age of the sample.

Group 1: we present the thermal model for PY-72, which of the two samples has the most confined tracks (22). The thermal model supports the simple thermal history of rapid cooling as indicated by long mean lengths and very short lag-times. Rapid cooling was underway at ~30 Ma. The depositional age of ~25 Ma indicates that rapid cooling must have ceased by then, thus rapid cooling (exhumation) in these samples occurred *ca.* 30–25 Ma with little or no post-burial annealing.

Group 2: given that PB-5 only has one measured track length, we do not present an inverse thermal model for this sample. PB-4 only has 14 measured confined tracks, which is really too few to produce well-constrained envelopes of good and acceptable fits. However, of the two samples in this group it is the best one to model, and suggests that rapid cooling (exhumation) is underway from ~50 to ~30 Ma with little or no post-burial annealing.

Group 3: we present the thermal model for PY-73 from Serra de Sis as this has the most confined tracks for this group. The thermal models agree with the qualitative assessment, with the most well-constrained model (PY-73) indicating rapid cooling *ca.* 50–40 Ma, with some possible minor post-burial annealing.

Group 4: we only present the thermal model for CJ-5 because, of the three samples, it has the greatest number of confined tracks, easily passes the χ^2 test and has a very low relative error. The thermal model from this sample is consistent with a period of relatively rapid continuous cooling from *ca.* 70 to 40 Ma. It is possible, but not provable with this data set, that because of the prevalence of a 50–40 Ma cooling event shown in many of the other thermal models

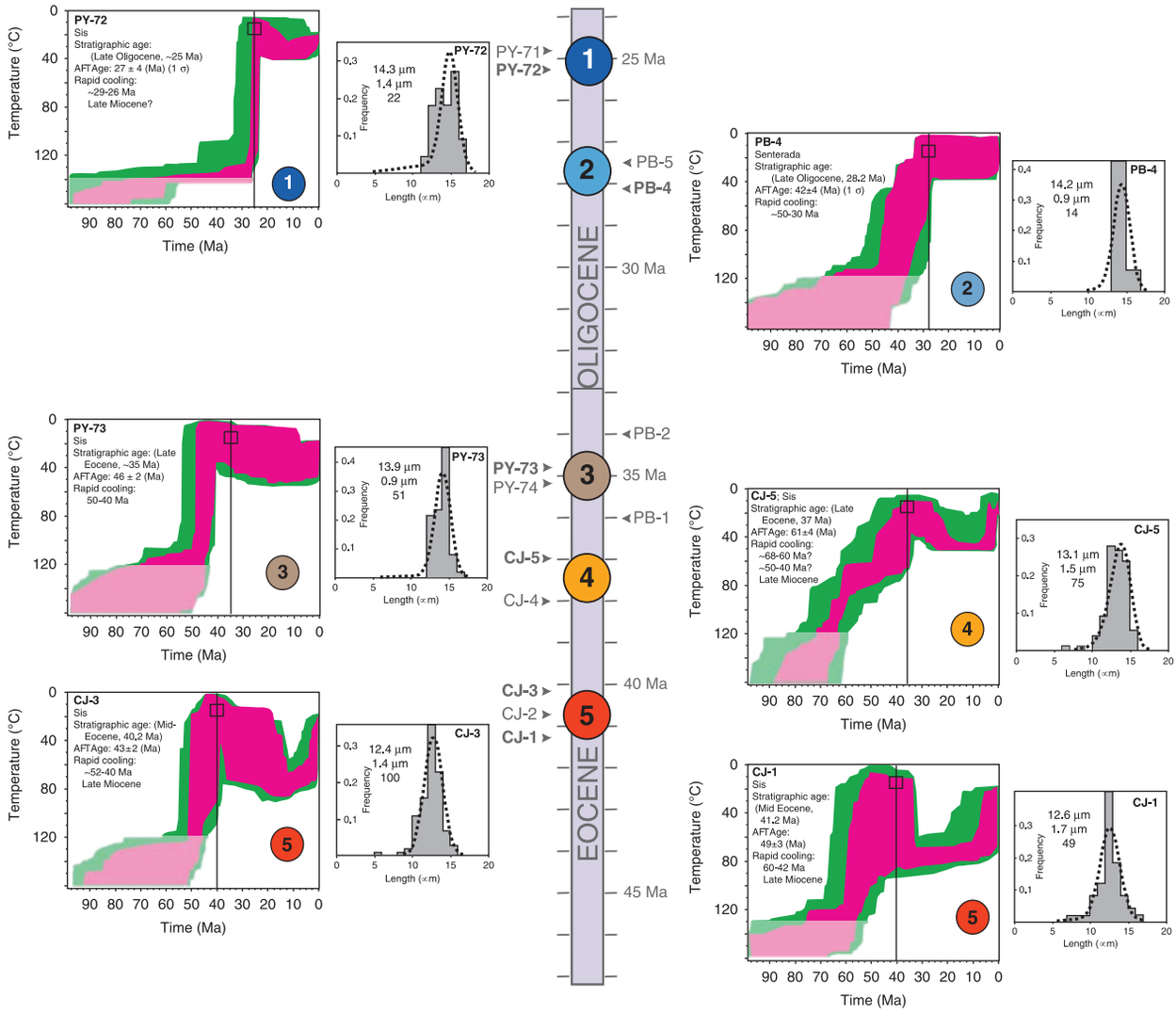

Fig. 7. Samples plotted against stratigraphic position. Temperature–time models of AFT thermochronology data, including stratigraphic constraints for these granitic clasts, were undertaken using HeFTy (*Ketcham*, 2005). Samples are also grouped (1–5 shown in colored circles) according to similar AFT and stratigraphic ages, also shown on the lag-time plot (Fig. 6). For the inverse thermal models, the magenta envelope is a 'good fit' (i.e. the T–t path is supported by the data) and the green envelope an 'acceptable fit' (i.e. the T–t path is not ruled out by the data). Model inputs are multiple T–t boxes with loose constraints designed to offer the opportunity for the model to explore pre-depositional rapid cooling events and post-depositional burial as well as a small T–t box for the stratigraphic (depositional) age of the sample constrained at 10–20 °C to reflect a representative mean palaeo-land surface temperature. Note that the T–t path for each sample must go through the small T–t box for the stratigraphic (depositional) age of the sample. 10 000 paths were run in each model. Modelled track length distributions (dashed line) are compared with measured track length distribution (grey histograms) with measured mean length, standard deviation and number of tracks measured (e.g. 13.1 μm, 1.5 μm, 75 for sample CJ-5) shown for easy reference.

(e.g. groups 2 and 3 that have samples with younger AFT ages) there may be two periods of exhumation-related relatively rapid cooling: an older one at *ca*. 70–60 Ma and the younger event at *ca*. 50–40 Ma. These multiple episodes of pre-depositional cooling, possibly hidden within the time-averaged cooling from 70 to 40 Ma, may not be discernible because each event is not significant enough in the overall thermal history. The thermal model does suggest burial annealing with resultant Late Miocene cooling.

Group 5: we present models for two of the three group 5 samples. Sample CJ-3, which has two age populations but has the most confined tracks of any sample indicates a period of rapid cooling at *ca*. 50–40 Ma, with significant burial annealing and Late Miocene cooling. Sample CJ-1, also with two age populations suggests rapid cooling from *ca*. 60 to 40 Ma. Thermal models for both samples indicate significant post-burial annealing up to temperatures of *ca*. 80 °C.

The information from the thermal models constrains the pre-depositional cooling rates for the different groups (Fig. 7) and the lag-time plots constrain the exhumation rates (Fig. 6). This information can be summarized as follows: group 1 samples were rapidly cooled

($\sim$30 °C Myr^{-1}) due to rapid exhumation, at rates of km Myr^{-1} at $\sim$30 to 25 Ma. Group 2 samples were cooled at rates of 6–10 °C Myr^{-1} due to exhumation at rates $\sim$0.3 km Myr^{-1} from $\sim$50 to 40 Ma. Likewise for group 3 samples, cooling rates are *ca*. 10 °C Myr^{-1} relating to exhumation rates of $\sim$0.25 to 0.4 km Myr^{-1} from $\sim$50 to 40 Ma. For groups 4 and 5 samples, the exhumation rates are not well constrained from the lag-time plot as the samples are partially annealed, and hence these rates are maxima as age reduction (due to annealing) decreases the lag-time and hence increases the apparent exhumation rate. The average cooling rate for group 4 is $\sim$3 °C Myr^{-1} from $\sim$70 to 37 Ma with a maximum time-averaged exhumation rate $<$ $\sim$0.15 km Myr^{-1} However, if there are multiple cooling (exhumation) events recorded in group 4 thermal models at $\sim$70 to 60 ($\sim$5 °C Myr^{-1}) and $\sim$50 to 40 Ma ($\sim$5 °C Myr^{-1}), the exhumation rates for each episode would be obviously higher than the time-averaged rate, likely the same as determined from nonannealed samples (groups 2 and 3) for the $\sim$50 to 40 Ma event at $\sim$0.3 km Myr^{-1}. Group 5 samples have a cooling rate of $\sim$6 to 12 °C Myr^{-1} and a maximum exhumation rate of $\sim$0.5 km Myr^{-1}.

To summarize the data interpretation: AFT central ages generally increase down section, fitting a simple unroofing model of the source region, and then decrease between groups 4 and 5, most likely a result of post-depositional annealing. Overall, we recognize two well-defined periods of rapid cooling at *ca*. 50–40 and 30–25 Ma. The $\sim$50 to 40 Ma event (groups 2, 3, 5 and possibly 4) is associated with cooling rates of $\sim$6 to 10 °C Myr^{-1} and exhumation rates of $\sim$0.2 to 0.3 km Myr^{-1}. The *ca*. 30–25 Ma event (group 1) has cooling rates of $\sim$30 °C Myr^{-1} and exhumation rates in excess of 1 km Myr^{-1}. A poorly defined cooling event (group 4 thermal models) if present, at *ca*. 70–60 Ma likely occurs at rates of $\sim$5 °C Myr^{-1}, with exhumation rates slightly less than the 50–40 Ma event. These cooling events are also supported by binomial peak fitting on samples with multiple age populations (Table 2) defining dominant age populations between 52 and 38 Ma relating to the $\sim$50 to 40 Ma event, minor age populations of $\sim$60 Ma compatible with the possible $\sim$70 to 60 Ma event, and $\sim$31 Ma compatible with the $\sim$30 to 25 Ma event. The data also suggest post-burial partial annealing of fission tracks as samples were heated (buried) into the PAZ. Samples from deeper stratigraphic levels indicate post-orogenic cooling, starting sometime $<$ 10 Ma (Late Miocene).

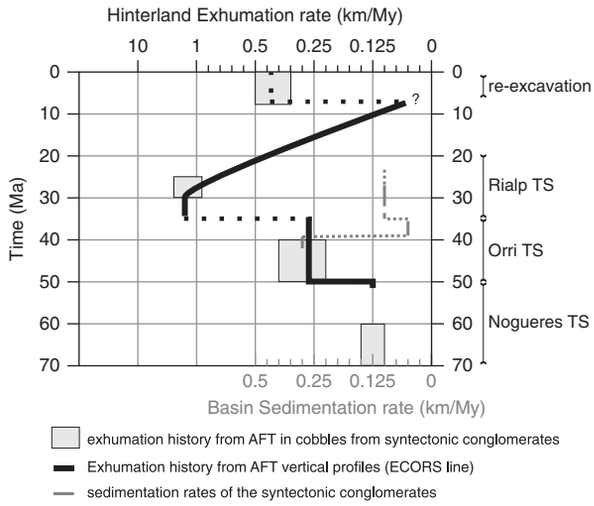

Fig. 8. Evolution of the exhumation rates through time deduced from the AFT of the cobbles in the conglomerates and from the AFT ages from plutons in the hinterland from previous studies (Fitzgerald *et al*., 1999; Metcalf *et al*., 2009). The evolution of the sedimentation rates obtained from the magnetostratigraphy of the syntectonic conglomerates is also plotted (Beamud *et al*., 2003;this study). Timing of thrust sheet movement and re-excavation is represented on the right side of the figure.

DISCUSSION

Comparison of the AFT results with the stratigraphy of the conglomerates

AFT ages ($\sim$63 to 27 Ma) from all sampled cobbles of the syntectonic conglomerates of the Sis, La Pobla and Senterada largely overlap with the timing of exhumation of basement thrust sheets of the central Pyrenean AZ antiformal stack or sheets north of the NPF (Fig. 8) (Morris *et al*., 1998; Fitzgerald *et al*., 1999; Sinclair *et al*., 2005; Gibson *et al*., 2007; Metcalf *et al*., 2009). From these ages and the age of the conglomerates, we can deduce that deposition of Palaeogene conglomerates occurred contemporaneously with the tectonic and erosional exhumation of the AZ. Deformation in the hinterland continued past the deposition of the youngest recorded sediments as demonstrated by the youngest AFT ages of $\sim$20 to 25 Ma from the Barruera massif (Sinclair *et al*., 2005). Therefore, as discussed above, these conglomerates should be considered syntectonic and not post-tectonic or late tectonic as inferred previously.

Following a simple unroofing model for a continuous tectonic exhumation of the inner parts of the orogen and their subsequent erosional denudation, one would expect an inverted stratigraphy of the pebbles in the adjacent syntectonic conglomerates (Colombo, 1994). This is the general trend observed in the stratigraphic record of the Middle Eocene–Late Oligocene conglomerates of the South Central Pyrenees. Thus, Mesozoic limestones are dominant in the pebbles of the lower sequences of the conglomerates (Pessonada and Ermita allogroups in La Pobla conglomerates, Espills and lower Gurb formations in Gurb conglomerates, Cajigar Formation in Sis conglomerates), and Palaeozoic rocks are the dominant lithology for the pebbles in the upper units (Mellere, 1992; Vincent, 2001; Barsó & Ramos, 2007; Picart *et al*., 2009). Despite this general trend, reversals in the 'stratigraphy' of the pebbles are also observed. These reversals are mainly the result of different source areas for vertically stacked units of conglomerates, controlled by the structurally driven growing topography.

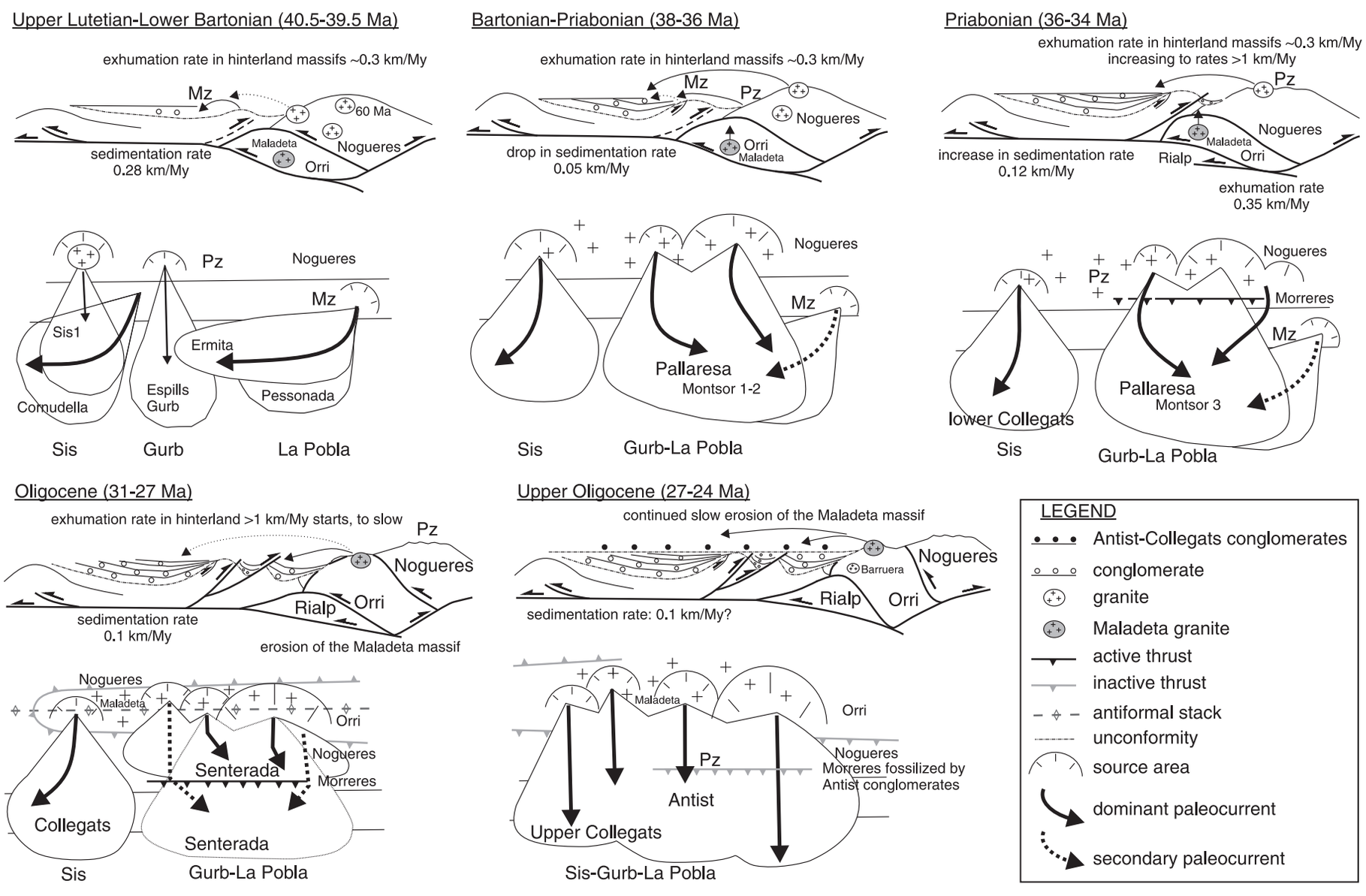

These different source areas are also observed for units in the same stratigraphic position (Fig. 9). Thus, the Pessonada and Ermita conglomerates are made up by mainly Mesozoic and Cenozoic limestones (Mellere, 1992; Barsó & Ramos, 2007), which are laterally equivalent westwards of the Palaeozic sourced Gurb and Cornudella Formations (Vincent, 2001; Picart *et al.*, 2009), respectively. In the Pallaresa allogroup of the La Pobla conglomerates, the Mesozoic limestones-derived conglomerates of the Collegats system pass laterally to the Montsor system with a significant proportion of Palaeozoic basement-derived pebbles (Mellere, 1993). In general, lower units of conglomerates show an increased amount of Palaeozoic pebbles westwards.

Partial annealing of the samples, depth of burial and Late Miocene cooling

The changing track length distributions down section and thermal models indicate that the lower samples experienced progressively greater amounts of post-depositional partial annealing (Fig. 7). We interpret this pattern to result from an increase in temperature due to progressive burial by the younger syntectonic conglomerates. The thermal models suggest that the lowermost samples from the upper levels of the Cornudella Formation (CJ-1, -2) and the lower part of the Sis Formation (CJ-3) have experienced reheating of up to *ca*. 60 °C. Considering a geothermal gradient of 30 °C km^{-1}, which is the gradient calculated by Zeyen & Fernandez (1994) for the present and the gradient estimated from AFT modelling for the Maladeta massif during its Oligocene exhumation (Metcalf *et al.*, 2009), a sedimentary burial by a 2 km thick succession of conglomerates should be expected. Vincent (2001) reported vitrinite reflectance data for coals within the lacustrine levels of the Cornudella Formation that suggested ~2 km burial for this formation, consistent with the AFT models.

At present, the lower part of the Sis conglomerates, as well as the La Pobla ones, are dipping to the north above the flat-lying basal unconformity as explained above. As a result of the tilting and folding of the unconformity and the overlying conglomerates, beds are stacked laterally northwards with a total stratigraphic thickness of 1.4 km for the Sis conglomerates (Vincent, 2001) and 3.5 km for the La Pobla conglomerates (Mellere, 1993). However, the maximum observed vertical stacking thickness for the Sis conglomerates is around 900 m. A problem arises when the geometry and lateral extension of the different sequences of conglomerates are reconstructed above the present topography. Such reconstruction has a significant impact in deciphering the late tectonic to post tectonic configuration of the South-Pyrenean thrust and fold belt. The AFT data and thermal models combined with the existing geological data demonstrate that the Late Oligocene–Early Miocene syntectonic conglomerates extensively covered the south Pyrenean cover thrust sheets while lapping into the southernmost outcrops of the basement of the AZ (Figs 2 and 9). Total thickness and lateral extension of the syntectonic conglomerates should have been great enough to reheat the bottom of the succession (Middle Eocene in age) by ~60 °C, suggesting vertical stacked thicknesses of up to 2 km. Regardless of the intricate geometry of the basal unconformity, resulting in part from synsedimentary folding and thrusting (García-Senz, 2002), the preserved outcrops of conglomerates do not represent isolated preserved palaeovalleys. Instead, they are remnants of a thick sheet of conglomerates connecting the present outcrops of Sis, Gurb and La Pobla, at least during their late stages (Fig. 9), before they were eroded and re-excavated to the present topography and relief by incision of the Ebro fluvial network since Late Neogene times. Cooling during this Late Neogene reexcavation of the conglomerates is also shown by the AFT thermal models of the granitic cobbles, notably the lower samples (Fig. 7). These data support previous ideas suggesting the burial of the South Pyrenean fold and thrust belt by Late Palaeogene syntectonic conglomerates and their subsequent re-excavation (Coney *et al.*, 1996; Muñoz *et al.*, 1997) and are consistent with other thermochronological data and thermal modelling of the interior part of the chain (Fitzgerald *et al.*, 1999; Metcalf *et al.*, 2009).

Periods of rapid cooling in the hinterland

Using the HeFTy inverse models of the granitic cobbles as discussed in the thermal modelling section above (Fig. 7), we have constrained three periods of cooling. Two of these are well constrained and revealed in multiple models. The ~30 to 25 Ma event is evidenced in the uppermost samples (group 1) and in these samples, cooling is very rapid (on the order of 30 °C Myr^{-1}), suggesting rapid exhumation rates of km Myr^{-1}. The ~50 to 40 Ma event is evident (to varying degrees depending on the quality of the data from each cobble) in groups 2–5 and appears less rapid than the younger Oligocene event, on the order of 6–10 °C Myr^{-1}. A possible event at *ca*. 70–60 Ma, which is only delineated in group 4 where the oldest AFTages are recorded, appears to be slower than the other two events, with a cooling rate somewhere on the order of ~5 °C Myr^{-1}, although we stress that this is very approximate.

Fig. 9. Evolution of the Palaeogene piggy-back basins of conglomerates in the Central Pyrenees and their relationships with the structural evolution of the southern Pyrenees as deduced from the magnetostratigraphic and AFTages. Only the main structures and source areas active during the deposition of the syntectonic conglomerates are represented. For each time interval a simplified cross-sectional view and a map representation have been sketched. Sections are based on the ECORS cross-section across the Pallaresa valley (Fig. 2) and on the partially restored cross-sections along the ECORS transect (Muñoz, 2002). Palaeocurrent directions in the map sketches are compiled from Mellere (1992, 1993), Vincent (2001) and Barsó (2007). Sketches not to scale.

Comparison with the thermal/exhumation history of the hinterland (AZ)

The measured AFT central ages of some cobbles as well as their corresponding thermally modelled cooling events go back further in time than the AFT data from the central Pyrenees, from the Hercynian basement of the AZ thrust sheets of the Central Pyrenees and the plutons in the northern Pyrenees (Yelland, 1990; Morris *et al.*, 1998; Fitzgerald *et al.*, 1999; Sinclair *et al.*, 2005; Gibson *et al.*, 2007). This is to be expected because the cobbles in the syn-tectonic conglomerates come from higher structural levels of the plutons, now eroded to deeper structural levels. The poorly delineated oldest cooling/exhumation event at ~70 to 60 Ma is older than any recognized cooling/exhumation event from crystalline basement in the Pyrenees. However, this possible older event is younger than the onset of the Pyrenean convergence and deformation (84 Ma, Garrido-Megías & Ríos Aragues, 1972; Muñoz, 2002; Rosenbaum *et al.*, 2002; McClay *et al.*, 2004), suggesting that it may reflect exhumation of upper parts of the Nogueres thrust sheet (upper unit of the AZ antiformal stack) that have since been completely removed by erosion. It is possible that cobbles were sourced in the northern Pyrenees where the oldest AFT ages have been reported (Lacourt granite: 55 ± 3 Ma, Fitzgerald *et al.*, 1999). However, this scenario seems very unlikely due to the long transport distance required, which contrasts with the proximal character of the conglomeratic sequences and the calculated distances and areal extent of the source areas (Barsó, 2007). Moreover, although it should be expected given the rainfall gradient across the range, it would imply a significant southward migration of the watershed divide. The possible ~70 to 60 Ma cooling/exhumation event correlates well with evidence for thrusting recorded in K-feldspar $^{40}Ar/^{39}Ar$ multi-diffusion domain thermal models (Metcalf *et al.*, 2009) from the footwall of the Nogueres thrust sheet that record thrust-burial (and partial resetting) at about that time, and then cooling/exhumation associated with subsequent erosion following creation of thrust-generated topography. It also correlates with the geological history of the Pyrenees indicating sequential deformation, uplift and exhumation recorded in a temporal series of partially restored cross-sections along the ECORS crustal cross-section (Muñoz, 1992, 2002).

North of the NPF, AFT data from a vertical profile collected in the LaCourt pluton indicate that exhumation there was initiated at *ca.* 50 Ma. Exhumation rates before ~50 Ma were very slow, increasing after this (Fitzgerald *et al.*, 1999). This event is not revealed in AFT data within the AZ as the AFT ages there are younger. However, AFT data in a vertical profile from the Riberot pluton within the Orri thrust sheet record exhumation at a rate ~0.2 km Myr^{-1} from ~43 to ~35 Ma, considered to reflect the continuation of the exhumation episode initiated at ~50 Ma as revealed at LaCourt (Fitzgerald *et al.*, 1999). Within the syn-tectonic conglomerates, the AFT constrained period of exhumation from ~50 to 40 Ma (in some models extending slightly younger) was 0.2–0.3 km Myr^{-1}, which relates well with the AFT data from the AZ. We relate this period of increased exhumation to movement of the Orri thrust sheet and its underthrusting below the Nogueres thrust sheet (Figs 8 and 9).

The age-elevation interpretation of the Maladeta profile in the AZ (Fitzgerald *et al.*, 1999) combined with AFT thermal models on the same samples (Metcalf *et al.*, 2009) indicates slow cooling through the apatite PAZ until ~35 Ma, rapid cooling (~10 °C Myr^{-1}) from ~35 to ~30 Ma, followed by a significant decrease in cooling rates to ~1 °C Myr^{-1} at 25–30 Ma. Within the syn-tectonic conglomerates, the AFT data from cobbles record extremely rapid exhumation rates from ~30 to 25 Ma, which is slightly younger than, but comparable with the hinterland-derived rapid exhumation. Some factors that should be considered when comparing the group 1 data interpretation and models with constraints from the hinterland vertical profiles are: (1) the uncertainties on the two group 1 samples, which constrain this rapid cooling, are large (28 ± 3, 27 ± 4 Ma, ± 1σ); (2) the age of deposition for these group 1 samples is not as well constrained as for other samples, (3) these two samples only reflect their thermal history and not a continuous record of the hinterland, as is better revealed in an AFT vertical profile (AFT age–elevation plot). Therefore, in reality we really can only constrain that rapid cooling at this much faster rate began between groups 2 and 1 samples. Cessation of the rapid cooling in these thermal models does appear to continue longer than in the hinterland vertical profiles, although the larger uncertainties on these AFT ages preclude a definitive conclusion. We have compared our group 1 detrital samples with information from the Maladeta pluton (Fitzgerald *et al.*, 1999; Metcalf *et al.*, 2009). It is logical to assume that these cobbles were eroded from the Maladeta pluton as this pluton lies directly north of these basins. However, we note that the timing of this period of latest Eocene–Early Oligocene rapid cooling in the hinterland gets younger to the west (Fitzgerald *et al.*, 2010; Metcalf *et al.*, 2010).

We relate the dramatic increase in latest Eocene–Early Oligocene exhumation rate (*ca.* 35 Ma as recorded in the hinterland) to movement of the Rialp thrust sheet and the increase in structural relief of the AZ by both underthrusting and internal deformation of the thrust sheets pile (Figs 8 and 9).

Only the youngest AFT central ages around 20–25 Ma from the Barruera massif (Sinclair *et al.*, 2005) have not been found in the granitic cobbles. This is in agreement with the youngest age (27–24 Ma) of the preserved syntectonic conglomerates as deduced from the new magnetostratigraphic data included in this paper. The elevation of the preserved top of depositional surface of the uppermost syntectonic conglomerates is higher than the samples of the Barruera massif that yield the youngest ages, thus these syn-tectonic conglomerates covered the Barruera Massif. These data emphasize the younger deformation ages found in the interior of the orogen with respect to

the thrust ages recorded by the late syntectonic conglomerates in the adjacent foreland basins. However, in the studied transect, younger ages of the lower exposed granitic rocks in the AZ are not related to any out-of-sequence thrusting event as suggested in the Central-Western Pyrenees (Jolivet *et al.*, 2007). Thus, although the Barruera massif, located at the hinge of the AZ antiformal stack cooled through the apatite PAZ at 25–20 Ma, it was most likely not exhumed to the surface until the Late Neogene to recent excavation of the present fluvial system (Fig. 9).

Comparison of exhumation rates with the rate of sedimentation

The magnetostratigraphic and thermochronological ages obtained permit a linkage between the sedimentation rates in the piggy-back basins with the exhumation rates within the hinterland (Fig. 8). The initial sedimentation rates (around 0.3 km Myr^{-1}) are similar to the exhumation rate in the hinterland (0.2–0.3 km Myr^{-1}). During this time, deposited sediments were the Ermita allogroup in the La Pobla area and the Cornudella Fm. in Sis (*ca.* 40 Ma) (Beamud *et al.*, 2003), which are characterized by an aggradational stacking pattern and the development of lacustrine environments indicative of a high accommodation space. Afterwards, a dramatic decrease in sedimentation rate (0.05 km Myr^{-1}) is recorded during the sedimentation of the Pallaresa allogroup (Fig. 8) whereas the exhumation rate in the hinterland remains almost constant. In the Sis area, sediment condensation zones and abandonment surfaces caused by marked changes in sediment flux have been reported at the boundary of Sis 1–Sis 2 members and at the top of the Sis 2 member, pointing to a decrease in the rate of fluvial sedimentation (Vincent, 2001). In both areas, thick conglomeratic packages change to a progradational stacking pattern, suggesting a reduction in the accommodation space. In La Pobla basin, the onset of backthrusting in the Morreres backthrust system is recorded by the geometries and unconformities between the Montsor 1 and Montsor 2 systems around 36 Ma (Figs 2 and 9). Another remarkable change during this stage refers to palaeocurrents, switching from ENE–WSW to a predominantly N–S direction (Mellere, 1992; Barsó, 2007). The exhumation and sedimentation rates increase significantly after 36 Ma (sedimentation rate around 0.1 km Myr^{-1}, exhumation rate in the order of km Myr^{-1}), coinciding with the closing of the Ebro basin due to its disconnection from the Atlantic ocean (Costa *et al.*, in press) and the onset of internal deformation of the orogenic wedge (Muñoz *et al.*, 1997; Muñoz, 2002). Fitzgerald *et al.* (1999) reported a major phase of accelerated exhumation between 35 and ~30 Ma, with rates of 2–4 km Myr^{-1} and total exhumation of about 10 km. It has been recently proposed that the acceleration in the exhumation of the AZ *ca.* 35 Ma could be related to the effect of the high-latitude cooling event recorded at the Eocene–Oligocene boundary (Huyghe *et al.*, 2009). However, both the increase in the exhumation and the sedimentation rates occur before this cooling event. Moreover, recent reconstructions of mean annual temperatures based on whole rock chemical composition and isotopic records of palaeosols sequences of the Eocene–Oligocene boundary within the Ebro basin (Sheldon, 2009) suggest that in this area, located at a medium-low palaeolatitude by this time, no evidences of a major palaeoclimatic change are recognizable.

CONCLUSIONS

New magnetostratigraphic data of the Senterada basin combined with existing data have constrained the age of sedimentation of the several kilometers thick successions of conglomerates preserved in the relatively interior parts of the South Pyrenean fold and thrust belt (La Pobla de Segur/Senterada, Gurb and Sis areas) from 42 to 25 Ma (Late Lutetian to Late Oligocene). The detrital clast AFT ages obtained vary from 63 to 27 Ma. Combined with their stratigraphic ages, samples have been classified in five groups, with AFT ages generally increasing down section except in the most deeply buried samples due to post-depositional partial annealing. Lag-time plots, thermal models and binomial peak-fitting have allowed the definition of three periods of rapid cooling; two well-defined periods *ca.* 50–40 Ma (cooling rates: 6–10 °C Myr^{-1} and exhumation rates around 0.2–0.3 km Myr^{-1}) and *ca.* 30–25 Ma (cooling rates: 30 °C Myr^{-1} and exhumation rates >1 km Myr^{-1}) and a poorly defined event *ca.* 70–60 Ma (cooling rates: around 5 °C Myr^{-1} and exhumation rates around 0.2 km Myr^{-1}).

The magnetostratigraphic and detrital AFT ages obtained overlap most of the AFT thermochronological ages obtained from the basement thrust sheets of the AZ demonstrating that these conglomerates represent the stratigraphic record of the most intense period of exhumation of the basement thrust sheets at the interior of the orogen. Thus, they have to be considered as synorogenic and not post-tectonic (Mey *et al.*, 1968) or late syntectonic (i.e. post-dating the main Pyrenean orogenic phase) as thought previously. Their basal unconformity does not represent the cessation of tectonic activity, as deformation continued in the interior of the chain even after deposition of the younger undeformed conglomerates. This conclusion has to be taken into consideration when interpreting the stratigraphic record of other less-constrained ancient orogens.

Post-depositional annealing experienced by the lowermost samples suggests ~2 km burial by the younger synorogenic conglomerates during progressive burial of the south Pyrenean thrust and fold belt. AFT thermal models of the lower and stratigraphically older samples suggest a rapid exhumation during Late Neogene times (<10 Ma) after burial, and hence partial annealing. This event has been linked to the capture of the Ebro River by the Mediterranean Sea, which occurred between 13.0 and 8.5 Ma (García-Castellanos *et al.*, 2003).

The onset of the Morreres backthrust system at 36 Ma suggests an increase of the structural relief of the antiformal stack by underthrusting of the lower thrust sheet (Rialp) and wedging of the basement thrust sheets into the Triassic evaporites at the bottom of the Bóixols thrust sheet (Fig. 9). Thermochronological data from the basement thrust sheets (Fitzgerald *et al*., 1999; Sinclair *et al*., 2005; Gibson *et al*., 2007; Metcalf *et al*., 2009) and from granitic cobbles of the conglomerates indicate an increase in the exhumation rate within the AZ at about that same time (~35 Ma). Thus, the increase in exhumation rate observed at that time is most likely due to this antiformal stacking, which in turn produced the development of a passive roof backthrust at the top that partitioned the foreland basin.

Most of the conclusions derived from the data presented in this paper emphasize a strong relationship between the structural evolution of the South Pyrenean thrust system, thrusting and exhumation within the interior of the chain and the stratigraphic record in the syntectonic sediments. Thus, tectonic forces are the primary control not only in the observed patterns of exhumation but also in the depositional features of the synorogenic sediments stored in the adjacent basins. The only exhumation event that may have had an external driving mechanism is the Late Neogene re-excavation that was most likely related with re-excavation of the South Pyrenean thrust and fold belt and the overlying syntectonic conglomerates as the Ebro river system drained the previously endorheic Ebro basin into the western Mediterranean.

ACKNOWLEDGEMENTS

This paper is a contribution of the Institut de Recerca Geomodels and the Research Group of Geodynamics and Basin Analysis SGR 2009SGR1198, of the Agencia de Gestio d'Ajuts Universitaris i de Recerca (AGAUR) de la Generalitat de Catalunya. It has been developed in the framework of the projects CGL2007-66431-C02-01 and CGL2007-66431-C02-02/BTE and support from NSF Tectonics grants EAR95-06454 and EAR05-38216. The authors thank the Laboratori de Paleomagnetisme (Serveis Cientificotècnics UB-CSIC). The authors want to thank Dr. R. Scholger from the Paleomagnetic Laboratory of the Montanuniversität of Leoben (Austria) for his hospitality and assistance and D. Barsó and O. Fernández, for field assistance during sampling. Reviewers Massimiliano Zattin, Frederic Mouthereau, Doug Burbank and Editor Peter van der Beek are thanked for their constructive reviews that improved the clarity and completeness of this paper.

REFERENCES

Antunes, M.T., Casanovas, M.L., Cuesta, M.A., Checa, L., Santafé, J.V. & Agustí, J. (1997) Eocene mammals from the Iberian Peninsula. In: *BiochroM'97* (Ed. by J.P. Aguilar, S. Legendre & J. Michaux), *Mem. Trav. E.P.H.E. Inst. Montpellier* **21**, 337–352.

Baldwin, S.L., Harrison, T.M. & Burke, K. (1986) Fission track evidence for the source of Scotland District sediments, Barbados and implications for post-Eocene tectonics of the southern Caribbean. *Tectonics*, **5**(3), 457–468.

Barsó, D. (2007) *Análisis de la procedencia de los conglomerados sinorogénicos de La Pobla de Segur (Lérida) y su relación con la evolución tectónica de los Pirineos centro-meridionales durante el Eoceno medio-Oligoceno*. PhD Thesis, University of Barcelona. 209pp.

Barsó, D. & Ramos, E. (2007) Procedencia de los conglomerados sinorogénicos de La Pobla de Segur, Pirineos centro-meridionales. *Geogaceta*, **41**, 19–22.

Beamud, E., Garcés, M., Cabrera, L., Muñoz, J.A. & Almar, Y. (2003) A new middle to late Eocene continental chronostratigraphy from NE Spain. *Earth Planet. Sci. Lett.*, **216**, 501–514.

Beaumont, C., Muñoz, J.A., Hamilton, J. & Fullsack, P. (2000) Factors controlling the Alpine evolution of the central Pyrenees inferred from a comparison of observations and geodynamical models. *J. Geophys. Res.*, **105**(B4), 8121–8145.

Bentham, P. (1992) The tectono-stratigraphic development of the western oblique ramp of the South-Central Pyrenean thrust system, Northern Spain, PhD Thesis, University of Southern California, 253pp.

Bentham, P. & Burbank, D.W. (1996) Chronology of Eocene foreland basin evolution along the western oblique margin of the South-Central Pyrenees. In: *Tertiary Basins of Spain. The Stratigraphic Record of Crustal Kinematics. World and Regional Geology*, **Vol. 6** (Ed. by P.F. Friend & C.J. Dabrio), pp. 144–152. Cambridge University Press, Cambridge.

Bernet, M., Brandon, M.T., Garver, J.I. & Molitor, B. (2004) Downstream changes of Alpine zircon fission-track ages in the Rhone and Rhine Rivers. *J. Sediment. Res.*, **74**(1), 82–94.

Bernet, M. & Spiegel, C. (2004) Introduction: detrital thermochronology. In: *Detrital Thermochronology – Provenance Analysis, Exhumation, and Landscape Evolution of Mountain Belts* (Ed. by M. Bernet & C. Spiegel), pp. 1–6. Geological Society of America Special Paper, Boulder, CO.

Brandon, M.T. (1992) Decomposition of fission-track grain-age distributions. *Am. J. Sci.*, **292**, 535–564.

Brandon, M.T., Roden-Tice, M.K. & Garver, J.I. (1998) Late Cenozoic exhumation of the Cascadia accretionary wedge in the Olympic Mountains, northwest Washington State. *Geol. Soc. Am. Bull.*, **110**(8), 985–1009.

Brandon, M.T. & Vance, J.A. (1992) Tectonic evolution of the Cenozoic Olympic subduction complex, Washington State, as deduced from fission track ages for detrital zircons. *Am. J. Sci.*, **292**, 565–636.

Brügel, A., Dunkl, I., Frisch, W., Kuhlemann, J. & Balogh, K. (2003) Geochemistry and geochronology of gneiss pebbles from foreland molasse conglomerates: Geodynamic and paleogeographic implications for the Oligo-Miocene evolution of the Eastern Alps. *J. Geol.*, **111**(5), 543–563.

Burbank, D.W., Puigdefabregas, C. & Muñoz, J.A. (1992) The chronology of the Eocene tectonic and stratigraphic development of the eastern Pyrenean foreland basin, Northeast Spain. *Geol. Soc. Am. Bull.*, **104**(9), 1101–1120.

Carlson, W.D., Donelick, R.A. & Ketcham, R.A. (1999) Variability of apatite fission-track annealing kinetics: I. Experimental results. *Am. Mineral.*, **84**, 1213–1223.

Casanovas, M.L. (1975) Estratigrafía y Paleontología del yacimiento ludiense de Roc de Santa (Area del Noguera Pallaresa). *Paleontol. Evol.*, **10**, 1–158.

Choukroune, P. (1976) Structure et évolution tectonique de la zone Nord-Pyrénéenne. Analyse de la déformation dans une portion de chaîne à schistosité subverticale. *Mémoir. Soc. Géol. France*, **127**, 1–116.

Colombo, F. (1994) Normal and reversed unroofing sequences in syntectonic conglomerates as evidence of progressive basinward deformation. *Geology*, **22**(3), 235–238.

Coney, P.J., Muñoz, J., McClay, K.R. & Evenchick, C.A. (1996) Syntectonic burial and post-tectonic exhumation of the southern Pyrenees foreland fold-thrust belt. *J. Geol. Soc. Lond.*, **153**(1), 9–16.

Costa, E., Garcés, M., López-Blanco, M., Beamud, E., Gómez-Paccard, M. & Larrasoaña, J.C. (in press) Closing and continentalization of the South Pyrenean foreland basin (NE Spain): magnetochronological constraints. *Basin Res.*. doi: 10.1111/j.1365-2117.2009.00452.x.

Crowley, K.D., Cameron, M. & Schaefer, R.L. (1991) Experimental studies of annealing of etched fission tracks in fluorapatite. *Geochim. Cosmochim. Acta*, **55**, 1449–1465.

Cuevas Gozalo, M. (1990) Sedimentary facies and sequential architecture of tide-influenced alluvial deposits. An example from the middle Eocene Capella Formation. South-Central Pyrenees, Spain, *Geol. Ultraiectina* **61**, 152pp.

Donelick, R.A., Ketcham, R.A. & Carlson, W.D. (1999) Variability of apatite fission track annealing kinetics II: crystallographic orientation effects. *Am. Mineral.*, **84**, 1224–1234.

Dunkl, I., Graseman, B. & Frisch, W. (1998) Thermal effects of exhumation of a metamorphic core complex on hanging wall syn-rift sediments: an example from the Rechnitz window, eastern Alps. *Tectonophysics*, **297**(1–4), 31–50.

Ehlers, T.A., Armstrong, P.A. & Chapman, D.S. (2001) Normal fault thermal regimes and the interpretation of low-temperature thermochronometers. *Phys. Earth Planet. Interiors*, **126**(3–4), 179–194.

Ehlers, T.A. & Chapman, D.S. (1999) Normal fault thermal regimes: conducive and hydrothermal heat transfer surrounding the Wasatch fault, Utah. *Tectonophysics*, **312**, 217–234.

Fischer, M.W. (1984) Thrust tectonics in the North Pyrenees. *J. Struct. Geol.*, **6**(6), 721–726.

Fitzgerald, P.G., Metcalf, J.R., Baldwin, S.L. & Muñoz, J.A. (2010) Exhumation of the Neouvielle massif in the hanging wall of the Garvarnie thrust, west-central Pyrenees: thermochronologic constraints and comparisons with footwall exhumation. Abstract, *12th International Conference on Thermochronology*, 16–20 August 2010, Glasgow, Scotland.

Fitzgerald, P.G., Munoz, J.A., Coney, P.J. & Baldwin, S.L. (1999) Asymmetric exhumation across the Pyrenean Orogen; implications for the tectonic evolution of a collisional orogen. *Earth Planet. Sci. Lett.*, **173**(3), 157–170.

Fitzgerald, P.G., Sorkhabi, R.B., Redfield, T.F. & Stump, E. (1995) Uplift and denudation of the central Alaska Range: a case study in the use of apatite fission-track thermochronology to determine absolute uplift parameters. *J. Geophys. Res.*, **100**, 20175–20191.

Foster, G.L. & Carter, A. (2007) Insights into the patterns and locations of erosion in the Himalaya – a combined fission-track and in situ Sm–Nd Isotopic Study of Detrital Apatite. *Earth Planet. Sci. Lett.*, **257**, 407–418.

Galbraith, R.F. (1981) On statistical models for fission-track counts. *J. Int. Assoc. Math. Geol.*, **13**(6), 471–478.

Galbraith, R.F. (2005) *Statistics for Fission Track Analysis, Interdisciplinary Statistics Series*. Chapman & Hall/CRC, Boca Raton, FL, 219pp.

Galbraith, R.F. & Green, P.F. (1990) Estimating the component ages in a finite mixture. *Nucl. Tracks Radiat. Measure.*, **17**, 197–206.

Gallagher, K., Brown, R.W. & Johnson, C. (1998) Fission track analysis and its application to geological problems. *Ann. Rev. Earth Planet. Sci. Lett.*, **26**, 519–572.

García-Castellanos, D., Vergés, J., Gaspar-Escribano, J. & Cloetingh, S. (2003) Interplay beteween tectonics, climate and fluvial transport during the Cenozoic evolution of the Ebro Basin (NE Iberia). *J. Geophys. Res.*, **108**, B7, doi:10.1029/2002JB002073.

García-Senz, J. (2002) *Cuencas extensivas del Cretacico Inferior en los Pirineos Centrales, formación y subsecuente inversión*. PhD thesis, University of Barcelona, 310pp.

Garrido-Megías, A. & Ríos Aragues, L.M.A. (1972) Sintesis geologica del Secundario y Terciario entre los rios Cinca y Segre (Pirineo Central de la vertiente sur pirenaica, provincias de Huesca y Lerida). Summary of Mesozoic and Tertiary geology between the Cinca and Segre Rivers, southern slope of the Central Pyrenees, Huesca and Lerida provinces. *Bol. Geol. Minero*, **83**(1), 1–47.

Garver, J.I., Brandon, M.T., Roden, M.M.K. & Kamp, P.J.J. (1999) Exhumation history of orogenic highlands determined by detrital fission track thermochronology. In: *Exhumation Processes, Normal Faulting, Ductile Flow and Erosion* (Ed. by U. Ring, M.T. Brandon, G.S. Lister & S.D. Willet), pp. 283–304. Geological Society Special Publications, London, UK.

Gibson, M., Sinclair, H.D., Lynn, G.J. & Stuart, F.M. (2007) Late- to post-orogenic exhumation of the Central Pyrenees revealed through combined thermochronological data and modelling. *Basin Res.*, **19**(3), 323–334.

Gleadow, A.J.W. (1990) Fission track thermochronology – reconstructing the thermal and tectonic evolution of the crust. In: *Pacific Rim Congress* (pp. 15–21. Gold Coast, Queensland.

Gleadow, A.J.W. & Fitzgerald, P.G. (1987) Uplift history and structure of the Transantarctic Mountains: new evidence from fission track dating of basement apatites in the Dry Valleys area, southern Victoria Land. *Earth Planet. Sci. Lett.*, **82**, 1–14.

Gradstein, F.M., Ogg, J. & Smith, A. (2004) *A Geologic Time Scale 2004*. Cambridge University Press, Cambridge.

Grasemann, B. & Mancktelow, N.S. (1993) Two-dimensional thermal modelling of normal faulting: the simplon fault zone, Central Alps, Switerland. *Tectonophysics*, **225**, 155–165.

Green, P.F. (1981) A new look at statistics in fission-track dating. *Nucl. Tracks Radiat. Measure.*, **5**(1–2), 77–86.

Green, P.F. (1985) Comparison of zeta-calibration base-lines for Fission-Track dating of apatite, zircon and sphene. *Chem. Geol.*, **58**(1–2), 1–22.

Hurford, A.J. (1991) Uplift and cooling pathways derived from fission track analysis and mica dating: a review. *Geol. Rundschau*, **80**(1), 349–368.

Hurford, A.J. & Green, P.F. (1983) The zeta-age calibration of fission-track dating. *Isotope Geosci.*, **1**(4), 285–317.

Huyghe, D., Mouthereau, F., Castelltort, S., Filleaudeau, P.Y. & Emmanuel, L. (2009) Paleogene propagation of the southern Pyrenean thrust wedge revealed by finite strain analysis in frontal thrust sheets: implications for mountain building. *Earth Planet. Sci. Lett.*, **288**, 421–433.

Jolivet, M., Labaume, P., Monie, P., Brunel, M., Arnaud, N. & Campani, M. (2007) Thermochronology constraints for the propagation sequence of the south Pyrenean basement thrust system (France-Spain). *Tectonics*, **26**(5) TC 5007-1-17.

Jones, M.A., Heller, P.L., Roca, E., Garcés, M. & Cabrera, L. (2004) Time lag of syntectonic sedimentation across an al-

luvial basin, theory and examples from the Ebro Basin, Spain. *Basin Res.*, **16**(4), 489–506.

Ketcham, R.A. (2005) Forward and reverse modeling of low-temperature thermochronology data. In: *Low-Temperature Thermochronology: Techniques, Interpretations and Applications* (Ed. by P.W. Reiners & T.A. Ehlers), *Rev. Mineral. Geochem.* **58**(1), 275–314.

Ketcham, R.A., Carter, A., Donelick, R.A., Barbarand, J. & Hurford, A.J. (2007) Improved measurement of fission-track annealing in apatite using c-axis projection. *Am. Mineral.*, **92**(5–6), 789–798.

Ketcham, R.A., Donelick, R.A. & Carlson, W.D. (1999) Variability of apatite fission track annealing kinetics iii: extrapolation to geological time scales. *Am. Mineral.*, **84**, 1235–1255.

Ketcham, R.A., Donelick, R.A. & Donelick, M.B. (2000) Aftsolve: a program for multi-kinetic modeling of apatite fission-track data. *Geol. Mater. Res.*, **2**, 1–32.

Koops, M. & van Rossem, S. (1985) Cajigar and cornudella formations. In: *Guide to the sedimentology of the Tremp-Graus Basin*, **Vol. 33** (Ed. by M.E. Donselaar & C.R. Geel), pp. 111–121. State University of Utrecht, Utrecht.

Laslett, G.M. & Galbraith, R.F. (1996) Statistical modeling of thermal annealing of fission tracks in apatite. *Geochim. Cosmochim. Acta*, **60**, 5117–5131.

Laslett, G.M., Gleadow, A.J.W. & Duddy, I.R. (1984) The relationship between fission-track length and track density in apatite. *Nucl. Tracks Radiat. Measure.*, **9**(1), 29–38.

Laslett, G.M., Green, P.F., Duddy, I.R. & Gleadow, A.J.W. (1987) Thermal modelling of fission tracks in apatite: 2. A quantitative analysis. *Chem. Geol.*, **65**, 1–13.

Lock, J. & Willett, S. (2008) Low-temperature thermochronometric ages in fold-and-thrust belts. *Tectonophysics*, **456**(3–4), 147–162.

López-Martínez, N. (1998) Los yacimientos de mamíferos del Eoceno de La Pobla de Segur. In: *Geología y Paleontología del Eoceno de La Pobla de Segur (Lleida)* (Ed. by N. López-Martínez, J. Civis, M.L. Casanovas & R. Daams) Universitat de Lleida, Lleida, 267pp.

McClay, K., Muñoz, J.A. & Garcia-Senz, J. (2004) Extensional salt tectonics in a contractional orogen; a newly identified tectonic event in the Spanish Pyrenees. *Geology*, **32**(9), 737–740.

McDougall, I. & Harrison, T.M. (1999) Geochronology and thermochronology by the $^{40}Ar/^{39}Ar$ method. *Oxford Monographs on Geology and Geophysics*. Oxford University Press, New York, 269pp.

McFadden, P.L. & McElhinny, M.W. (1990) Classification of the reversal test in paleomagnetism. *Geophys. J. Int.*, **103**, 725–729.

Meigs, A.J. & Burbank, D.W. (1997) Growth of the Pyrenean orogenic wedge. *Tectonics*, **16**(2), 239–258.

Mellere, D. (1992) *I conglomerati di Pobla de Segur: Stratigrafia fisica e relazioni tettonica-sedimentazione*. Tesi di Dottorato in Scienze della Terra, Universita degli Studi di Padova, 203pp.

Mellere, D. (1993) Thrust-generated back-fill stacking of alluvial fan sequences, South Central Pyrenees, Spain (La Pobla de Segur Conglomerates). In: *Tectonic Controls and Signatures in Sedimentary Successions* (Ed. by L. Frostick & R.J. Steel), *Spec. Publ. Int. Assoc. Sediment*. **20**, 67–88.

Metcalf, J.R., Fitzgerald, P.G., Baldwin, S.L. & Muñoz, J.A. (2009) Thermochronology of a convergent orogen: constraints on the timing of thrust faulting and subsequent exhumation of the Maladeta Pluton in the Central Pyrenean Axial Zone. *Earth Planet. Sci. Lett.*, **287**(3–4), 488–503.

Metcalf, J.R., Fitzgerald, P.G., Baldwin, S.L., Muñoz, J.A. & Perry, S.E. (2010) Along-strike variation in the exhumation of the Pyrenean orogen; insights from the Orri thrust sheet in the footwall of the Gavarnie thrust, south-central Pyrenees. Abstract, *12th International Conference on Thermochronology*, 16th–20th August 2010, Glasgow, Scotland

Mey, P.H.W., Nagtegaal, P.J.C., Roberti, K.J. & Hartevelt, J.J.A. (1968) Lithostratigraphic subdivisions of post-Hercynian deposits in the south Central Pyrenees, Spain. *Leidse Geol. Meded.*, **41**, 221–228.

Morris, R., Sinclair, H., Yelland, A., Hovius, N. & Leeder, M. (1998) Exhumation of the Pyrenean orogen; implications for sediment discharge. *Basin Res.*, **10**(1), 69–85.

Muñoz, J.A. (1992) Evolution of a continental collision belt; ECORS-Pyrenees crustal balanced cross-section. In: *Thrust Tectonics* (Ed. by K. McClay), pp. 235–246. Chapman & Hall, London.

Muñoz, J.A. (2002) The Pyrenees alpine tectonics; I, the alpine system north of the Betic Cordillera. In: *The Geology of Spain* (Ed. by W. Gibbons & T. Moreno), p. 649. The Geological Society, London.

Muñoz, J.A., Coney, P.J., McClay, K.R. & Evenchick, C.A. (1997) Syntectonic burial and post-tectonic exhumation of the southern Pyrenees foreland fold-thrust belt; discussion and reply. *J. Geol. Soc. Lond.*, **154**, 361–365.

Naeser, C.W., Bryant, B., Crittenden, M.D. & Sorensen, M.L. (1983) Fission-track ages of apatite inthe Wasatch Mountains, Utah: an uplift study. *Geol. Soc. Am. Mem.*, **157**, 29–36.

O'Sullivan, P.B. & Parrish, R.R. (1995) The importance of apatite composition and single-grain ages when interpreting fission track data from plutonic rocks: a case study from the Coast Ranges, British Columbia. *Earth Planet. Sci. Lett.*, **132**, 213–224.

Pérez-Rivarés, F.J., Garcés, M., Arenas, C. & Pardo, G. (2004) Magnetostratigraphy of the Miocene continental deposits of the Montes de Castejón (central Ebro basin, Spain): geochronological and paleoenvironmental implications. *Geol. Acta*, **2**(3), 221–234.

Picart, J., Carrera, N., Solé, J., Montaner, J., Rivas, G., Muñoz, J.A., Serra, L., Beamud, E., Arbués, P., Mencos, J. & Perea, H. (2009) *Tremp 252-1-2 (65-22) [document cartogràfic]. 1:25000. Sèrie Mapa Geològic de Catalunya 1:25000, Geotreball 1.* Institut Cartogràfic de Catalunya (ICC) Servei Geològic de Catalunya (IGC), Barcelona.

Rahl, J.M., Ehlers, T.A. & van der Pluijm, B.A. (2007) Quantifying transient erosion of orogens with detrital thermochronology from syntectonic basin deposits. *Earth Planet. Sci. Lett.*, **256**, 147–161.

Reynolds, A. (1987) *Tectonically controlled fluvial sedimentation in the South-Pyrenean Foreland Basin*. PhD Thesis, University of Liverpool, Liverpool, 309pp

Riba, O., Reguant, S. & Villena, J. (1983) Ensayo de síntesis estratigráfica y evolutiva de la cuenca terciaria del Ebro. In: *Geología de España. Libro Jubilar* J.M. Ríos, **Vol. II** (Ed. by IGME), pp. 131–159. Instituto Geológico y Minero de España, Madrid.

Robles, S. (1982) Estudio comparativo del sistema aluvial del borde suroccidental de los Catalánides en la transversal de Prat de Comte (Tarragona) y los abanicos aluviales de Pobla

de Segur (PrePirineo de Lérida). *Acta Geol. Hispán.*, **17**(4), 255–269.

Roest, W.R. & Srivastava, S.P. (1991) Kinematics of the plate boundaries between Eurasia, Iberia, and Africa in the North Atlantic from the Late Cretaceous to the present. *Geology*, **19**(6), 613–616.

Rosell, J. & Riba, O. (1966) Nota sobre la disposición sedimentaria de los conglomerados de La Pobla de Segur (provincia de Lérida). *Quinto Congreso Internacional de Estudios Pirenaicos, Jaca (Pamplona)*, 3–16, Instituto de Estudios Pirenaicos CSIC

Rosenbaum, G., Lister, G.S. & Duboz, C. (2002) Relative motions of Africa, Iberia and Europe during Alpine Orogeny. *Tectonophysics*, **359**(1–2), 117–129.

Sheldon, N. (2009) Nonmarine records of climatic change across the Eocene Oligocene transition. In: *The Late Eocene Earth—Hothouse, Icehouse, and Impacts* (Ed. by C. Koeberl & A. Montanari), *Geol. Soc. Am. Spec. Pap.* **452**, 241–248.

Sinclair, H.D., Gibson, M., Naylor, M. & Morris, R.G. (2005) Asymmetric growth of the Pyrenees revealed through measurement and modeling of orogenic fluxes. *Am. J. Sci.*, **305**(5), 369–406.

Spiegel, C., Siebel, W., Kuhlemann, J. & Frisch, W. (2004) Toward a comprehensive provenance analysis: a multi-method approach and its implications for the evolution of the central Alps. In: *Detrital Thermochronology – Provenance Analysis, Exhumation, and Landscape Evolution of Mountain Belts* (Ed. by M. Bernet & C. Spiegel), *Geol. Soc. Am. Spec. Pap.* 37–50.

ter Voorde, M. & Bertotti, G. (1994) Thermal effects of normal faulting during rifted basin formation. 1. A finite difference model. *Tectonophysics*, **240**, 133–144.

ter Voorde, M., de Bruijne, C., Cloetingh, S. & Andriessen, P. (2004) Thermal consequences of thrust faulting: simultaneous versus successive fault activation and exhumation. *Earth Planet. Sci. Lett.*, **223**, 397–415.

van der Beek, P., Robert, X., Mugnier, J.L., Bernet, M., Huyghe, P. & Labrin, E. (2006) Late miocene – recent exhumation of the central Himalaya and recycling in the Foreland Basin assessed by apatite fission-track thermochronology of Siwalik Sediments, Nepal. *Basin Res.*, **18**, 413–434.

Vergés, J. & Muñoz, J.A. (1990) Thrust sequence in the southern central Pyrenees. *Bull. Soc. Geol. France*, **6**(2), 265–271.

Vincent, S.J. (1993) *Fluvial paleovalleys in mountain belts: An example from the south-central Pyrenees*. PhD Thesis, University of Liverpool, Liverpool, 407pp.

Vincent, S.J. (2001) The Sis paleovalley a record of proximal fluvial sedimentation and drainage basin development in response to Pyrenean mountain building. *Sedimentology*, **48**, 1235–1276.

Wagner, G.A., Miller, D.S. & Jäger, E. (1979) Fission track ages on apatite of Bergell rocks from central Alps and Bergell boulders in Oligocene sediments. *Earth Planet. Sci. Lett.*, **102**, 395–412.

Wagner, G.A. & Reimer, G.M. (1972) Fission track tectonics: the tectonic interpretation of fission track apatite ages. *Earth Planet. Sci. Lett.*, **14**, 263–268.

Willet, S.D., Slingerland, R. & Hovius, N. (2001) Uplift, shortening and steady state topography in active mountain belts. *Am. J. Sci.*, **301**, 455–485.

Yelland, A.J. (1990) Fission track thermotectonics in the Pyrenean Orogen. *Nucl. Tracks Radiat. Measure.*, **17**(3), 293–299.

Zeyen, H. & Fernandez, M. (1994) Integrated lithospheric modeling combining thermal, gravity, and local isostasy analysis; application to the NE Spanish geotransect. *J. Geophys. Res.*, **99**(B9), 18,089–18,102.

Zwart, H.J. (1979) The geology of the central Pyrenees. *Leidse Geol. Mededelingen*, **50**, 1–74.

Manuscript received 24 March 2010; In revised form 30 September 2010; Manuscript accepted 4 October 2010.

CHAPTER 2.3:

Muñoz, J.A., Beamud, E., Fernández, O., Arbués, P., Dinarès-Turell, J., Poblet, J. The Ainsa Fold and Thrust Oblique Zone of the Central Pyrenees: kinematics of a curved contractional system from paleomagnetic and structural data. Tectonics (in press)

The Ainsa Fold and Thrust Oblique Zone of the Central Pyrenees: Kinematics of a Curved Contractional System from Paleomagnetic and Structural Data

Josep-Anton Muñoz[1], Elisabet Beamud [1,2], Oscar Fernández[3], Pau Arbués[1], Jaume Dinarès-Turell [4], and Josep Poblet [5]

[1] Integration of structural, stratigraphic and paleomagnetic data from the N-S trending structures of the Ainsa Oblique Zone reveals the kinematics of the major thrust salient in the central Pyrenees. These structures experienced clockwise vertical-axis rotations that vary from 70º in the east (Mediano anticline) to 55º in the west (Boltaña anticline). Clockwise vertical-axis rotations of 60º to 45º occurred from early Lutetian to late Bartonian when the folds and thrusts of the Ainsa Oblique Zone developed. This vertical-axis rotation stage resulted from a difference of about 50 km in the amount of displacement on the Gavarnie thrust, and an accompanying change in structural style at crustal scale from the central to the western Pyrenees, related to the NE-SW trending pinch out of Triassic evaporites at its basal detachment. A second rotation event of at least 10º took place since Priabonian as a result of a greater displacement of the Serres Marginals thrust sheet with respect to the Gavarnie thrust sheet above the Upper Eocene-Oligocene salts. The deduced kinematics demonstrates that the orogenic curvature of the central Pyrenees is a progressive curvature resulting from divergent thrust transport direction. Layer-parallel shortening mesostructures and kilometer-scale folds also developed by a progressive curvature related to divergent shortening directions during vertical-axis rotation. Rotation space problems were solved by along-strike extension which triggered the formation of transverse extensional faults and diapirs at the outer arcs of structural bends.

1. Introduction

[2] Curved fold and thrust belts in map view are common features in orogenic systems [*Macedo and Marshak*, 1999; *Marshak*, 2004]. Their interpretation has concentrated the attention of many researchers in the last decades, mostly after the application of paleomagnetic techniques to unravel vertical-axis rotations and decipher the displacement fields [*Schwartz and Van der Voo*, 1984; *Allerton*, 1998; *Sussman and Weil*, 2004; *Soto et al.*, 2006; *Weil et al.*, 2010].

1 Institut Geomodels, Departament de Geodinàmica i Geofísica, Facultat de Geologia, Universitat de Barcelona, zona universitària de Pedralbes, 08028-Barcelona, Spain.
2 Laboratori de Paleomagnetisme CCiTUB-CSIC, Institut de Ciències de la Terra "Jaume Almera", C/Solé i Sabarís s/n, 08028-Barcelona, Spain.
3 Repsol Exploración – Dirección de Geología, Méndez Álvaro 44, 28045 Madrid, Spain.
4 Istituto Nazionale di Geofisica e Vulcanologia (INGV), Via di Vigna Murata 605, I-00143 Rome, Italy
5 Departamento de Geología, Universidad de Oviedo, C/ Jesús Arias de Velasco s/n, 33005-Oviedo, Spain

Corresponding author: Josep Anton Muñoz -phone number +34 934 021394- and email -jamunoz@ub.edu-.

[3] Curved orogens or fold and thrust systems have been classified into primary, progressive and secondary according to the timing between thrusting and rotation and the presence or absence of vertical-axis rotation [*Weil and Sussman*, 2004; *Weil et al.*, 2010].

[4] Primary arcuate fold and thrust systems formed originally with a curved geometry with no vertical-axis rotation. They normally result from the inversion of a previous irregular fault or basin geometry. At the other end of the spectrum, secondary curved systems or oroclines are formed by the bending of initially linear structures about a vertical-axis [*Marshak*, 2004]. Secondary curves caused by bending are characterized by vertical-axis rotations that post-date the initiation of thrusting with a gradation of rotation directions and magnitudes around the salient and dependent on a second stage of deformation. Secondary curves caused by shearing are characterized by localized vertical-axis rotations adjacent to the shear zones with possible rotations in the adjacent foreland. Vertical-axis rotations occur during or after thrusting depending on the timing of the shear zone development and their magnitude decreases abruptly away from the shear zone. In progressive curved systems structures, the strike of structures

changes progressively during deformation, and can form by divergent thrust transport trajectories or by parallel slip showing an along-strike displacement gradient during thrusting [*Elliot*, 1976]. In such cases rotation and thrusting occur simultaneously [*Weil et al.*, 2010].

[5] The southern Pyrenees show numerous oblique and transversal structures (Figure 1) that have been interpreted as a result of primary, progressive or secondary curves. In order to explain the observed curvature and the oblique structures, practically all the possible models have been proposed: primary curvature inherited from the geometry of Mesozoic basins [*Vergés*, 1993; *Larrasoaña et al.,* 2003], primary oblique structures developed by along-strike mechanical contrasts in the detachment level [*Storti et al*., 2007; *Vidal et al.,* 2009], primary to progressive curvature triggered by thickness differences of the inverted basins with no significant vertical-axis rotations [*Soto et al.*, 2002], progressive curvature formed by lateral gradients of thrust displacement with constant transport direction [*Sussman et al*., 2004], and secondary curvatures due to superimposed folding [*Garrido-Megías*, 1973; *Megías*, 1982], among others.

[6] Each of these models predicts different kinematic histories that can be compared with structural and paleomagnetic data. Distribution and magnitude of vertical-axis rotations are normally determined by paleomagnetic studies, which provide the most robust data to distinguish between the different types of orogenic curvature [*Soto et al*., 2006; *Weil et al.*, 2010]. Nevertheless, due to the common protracted deformation history found in most orogens, caution is needed to accurately interpret paleomagnetic data, and the timing of the magnetization with respect the structural evolution should be considered.

[7] A better understanding of the kinematic evolution and processes that produce fold and thrust curved patterns can be achieved by integrating internal deformation data with paleomagnetic studies [*Hindle and Burkhard*, 1999; *Yonkee and Weil*, 2010a; *Weil et al.*, 2010].

[8] A significant amount of paleomagnetic studies have been published in the Central Pyrenees aiming not only to date the well-preserved synorogenic successions but also to decipher vertical-axis rotations. The combination of magnetostratigraphic [*Bentham and Burbank*, 1996; *Hogan and Burbank*, 1996; *Beamud et al.,* 2003; *Oms et al.*, 2003; *Mochales*, *et al.*, 2012a; *Rodríguez-Pintó et al*., 2012; *Rodríguez-Pintó et al*., 2013] and magnetotectonic studies [*Dinarès-Turell*, 1992; *Pueyo*, 2000; *Pueyo et al.,* 2002, 2003a, 2004; *Mochales et al*., 2012b] has revealed the existence of significant vertical-axis rotations as well as their chronology and relationships with the main structures.

[9] Clockwise vertical-axis rotations have been documented by several paleomagnetic studies in the south western-central Pyrenean area, including not only the study area (Ainsa basin) but also the structures located westward in the Sierras Exteriores (Figure 2) [*Dinarès-Turell*, 1992; *Pueyo*, 2000; *Pueyo et al.,* 2002, 2004; *Fernández-Bellon*, 2004; *Rodríguez-Pintó et al.,* 2013; *Mochales et al*., 2012b; *Oliva-Urcia et al*., 2012a; *Ramón et al.*, 2012]. Such clockwise rotations explain the occurrence of N-S to NW-SE structures that are oblique to the main WNW-ESE Pyrenean trend that characterizes the southern Central Pyrenees. Vertical-axis rotations account for progressive or secondary curvature and have been explained by differential displacement of the South Pyrenean thrust sheets [*Soto et al*., 2006; *Oliva-Urcia and Pueyo*, 2007a].

[10] The oblique structures of the South Central Pyrenees have also been the focus for studies of internal strain [*Holl and Anastasio*, 1995a] and mesostructural analysis [*Holl and Anastasio,* 1995b; *Tavani et al*., 2006, 2012], which together with recent studies on anisotropy of magnetic susceptibility (AMS) [*Oliva-Urcia et al.,* 2009; *Mochales et al*., 2010] add further constraints in the understanding of the kinematic evolution of these structures.

[11] The structures in the Ainsa basin define the most prominent fold and thrust curvature in the Central Pyrenees (Figure 1). It is an excellent location to study kinematics of orogenic curvature because of: i) the quality of exposures, ii) the access to different structural levels due to a late structural tilting, iii) the time constraints yielded by the unique preservation of growth strata, and iv) the available subsurface data (exploration wells and seismic sections).

[12] However, despite the amount of studies done in the area dealing with different disciplines there is not yet a comprehensive model that honors all the available sedimentological, structural and paleomagnetic data. The study presented here builds on previous published works as well as on the work done in the area of the Ainsa basin by the authors in the last two decades on: sedimentology of the different involved sedimentary systems [*Arbués et al*., 2011], 3D structural reconstruction of the entire basin [*Fernández-Bellon*, 2004; *Fernández et al*., 2004, 2012], tectono-sedimentary relationships [*Muñoz et al.,* 1994, 1998; *Poblet et al.,* 1998], mesostructural analysis [*Tavani et al*., 2006, 2012] and paleomagnetic studies [*Dinarès-Turell,* 1992; *Beamud et al.,* 2003; *Fernández-Bellon*, 2004]. By integrating these studies we reduce the limitations of the interpretations based on individual data sets. In this paper we bring new paleomagnetic and structural data and present a new model for the kinematics of the entire Ainsa fold and thrust oblique zone. Our work pretends to

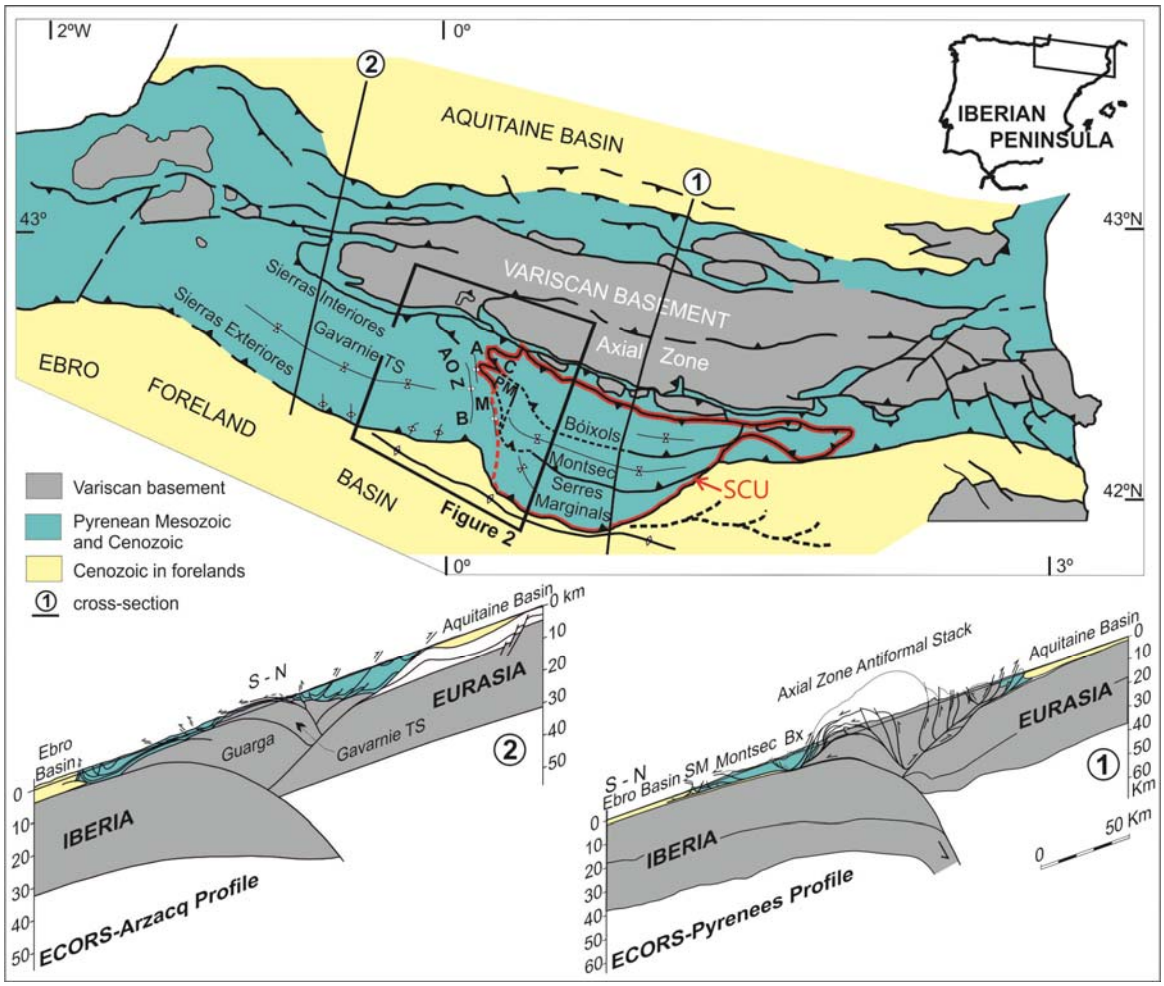

Figure 1. Location of the study area. Structural sketch showing the main structural units of the central Pyrenees and the major anticlines of the Ainsa Oblique Zone at the western boundary of the major thrust salient in the central Pyrenees. Crustal cross-sections at both sides of the Ainsa Oblique Zone illustrate changes of the structural style along strike. ECORS section from *Muñoz* [1992] and the Arzacq section modified from *Teixell* [1998]. AOZ: Ainsa Oblique Zone, A: Añisclo Anticline, B: Boltaña Anticline, M: Mediano Anticline, C: Cotiella, PM: Peña Montañesa, SCU: South Pyrenean Central Unit, Bx: Bóixols, SM: Serres Marginals.

gain insight into a better understanding of the three dimensional kinematic evolution and processes that produce orogenic curvature.

[13] The study area has the additional interest of the interaction between slope to deltaic sedimentary systems and the evolving structural topography from a deep-water to an emergent fold and thrust belt. This extraordinary tectono-sedimentary variety and the outcrop quality make that area a superb natural laboratory. The Ainsa basin is well known among the geological community for the sedimentary models of turbidite systems and their related fluvio-deltaic and carbonate platform systems [*Mutti et al.*, 1988]. However, little is known yet about the kinematic 3D evolution of the structures that developed during the sedimentation of the Ainsa basin infill. This is fundamental for the proper understanding of the facies arrangement and internal architecture of the Ainsa basin slope and deltaic sediments which are a reference among sedimentologists for turbidite facies models and field analogues for exploration and production purposes [*e.g.*, *Falivene et al.*, 2010]. Results of our work add new constraints for the understanding of the sedimentary pathways and sedimentary dispersal of the slope systems of the Ainsa basin.

2. Geological Setting

[14] The Pyrenean orogen formed as the result of the collision between the Iberian and European plates from Late Cretaceous to Miocene times [*Roest and Srivastava*, 1991; *Muñoz*, 2002; *Rosenbaum et al.*, 2002]. It is an asymmetric doubly vergent orogenic wedge that resulted from the subduction of the Iberian lithospheric mantle and lower crust under the European plate, and the thrusting of upper crustal rocks to the north and

south (Figure 1) [*Muñoz*, 1992]. Shortening along the central sector totals approximately 150 km (147 km according to *Muñoz* [1992]; 165 km according to *Beaumont et al.* [2000]) with a transport direction to the south [*Vergés*, 1993; *Rosenbaumet al.*, 2002]. The Pyrenees, with a regional WNW-ESE trend, consist of a central duplex of south-directed Variscan basement thrust sheets (referred to as the Axial Zone) which are flanked to north and south by oppositely vergent fold and thrust belts and associated foreland basins (Figure 1). The southern fold and thrust belt is formed by a set of imbricate thrust sheets of Mesozoic and Tertiary cover rocks that developed from Late Cretaceous to Oligocene times in a piggy-back sequence over the autochthonous rocks of the Ebro foreland basin [*Séguret*, 1972; *Garrido-Megías*, 1973; *Cámara and Klimowitz*, 1985; *Muñoz*, 1992]. Syntectonic Eocene-Oligocene sedimentation and burial of the frontal thrust sheets promoted synchronous thrusting of the south-Pyrenean thrust wedge. As a result, previously developed thrusts were locally reactivated as out-of-sequence thrusts [*Muñoz et al.,* 1997; *Muñoz*, 2002].

[15] Three major cover thrust sheets constitute the southern fold and thrust belt. From north to south (and in order of emplacement) these thrust sheets are (Figures 1 and 2): the Cotiella-Bóixols thrust sheet developed during the Late Cretaceous, the Peña Montañesa-Montsec thrust sheet formed during the Paleocene-late Ypresian and the Sierras Exteriores-Serres Marginals thrust sheet developed during Lutetian-Oligocene times. Southward displacement on the cover thrust sheets is fed by basement thrusts in the Axial Zone [*Séguret,* 1972; *Cámara and Klimowitz*, 1985]. In the case of the Sierras Exteriores-Serres Marginals, displacement is mainly accounted for by the Gavarnie, Bielsa and Guarga basement thrusts that moved mostly diachronously and in succession [*Séguret,* 1972; *Cámara and Klimowitz*, 1985; *Martínez-Peña and Casas-Sainz*, 2003]. The Gavarnie thrust started to develop during early Lutetian times (the age of the onset of folding in its hangingwall, *Séguret* [1972]; *Fernández et al.* [2012]), feeding displacement along the Sierras Exteriores thrust in its leading edge in what *Labaume et al.* [1985] called the Gavarnie Nappe (referred to as the Gavarnie or Gavarnie-Sierras Exteriores thrust sheet in this article). Displacement continued until it was tilted, folded, and passively transported southwards from Late Eocene times by the Guarga and related basement thrusts (Figure 1) in what *Labaume et al.* [1985] called the Gavarnie Detachment Unit (referred to as the Sierras Exteriores thrust in this article). The Late Eocene-Oligocene age of the Guarga thrust is demonstrated by the relationships between the basement cut-off line in its hangingwall and the Guarga synclinorium [*Fernández et al.*, 2012] and the age of the growth strata preserved in its core [*Puigdefàbregas*, 1975; *Fernández-Bellon*, 2004]. Motion on deep post-Gavarnie thrust sheets was responsible for the Late Eocene-Oligocene structures observed in the Jaca basin and Sierras Exteriores [*Labaume et al.,* 1985; *Teixell*, 1996] which have been erroneously used to date motion on the Gavarnie thrust.

[16] The main thrust sheets of the south central Pyrenees described above were considered to form a major structural unit referred to as the South Pyrenean Central Unit [*Séguret,* 1972] (Figure 1). The western boundary of this unit was interpreted to correspond to the N-S trending folds of the Ainsa area studied in this paper. However, there was no consensus among geologists on the location or nature of such boundary. Some authors considered it was located in the Mediano anticline [*Séguret,* 1972] while others placed it further west, along the Boltaña anticline [*Soto et al.,* 2002] (Figure 1). Detailed 3D reconstruction of the area integrating surface and seismic data [*Fernández-Bellon,* 2004*; Fernández et al.,* 2004, 2012] revealed that these folds are part of the Gavarnie-Sierras Exteriores thrust sheet, which represents the westward continuation of the Serres Marginals thrust sheet. The absence of any major lateral structure between the Sierras Exteriores and Serres Marginals thrust sheets means that the South Pyrenean Central Unit as defined by *Séguret* [1972] is not a structural unit; in consequence, referring to the oblique Ainsa folds as its western limit is not applicable.

[17] Nonetheless, a major structural change does occur between the central and the west-central southern Pyrenees. In the central Pyrenees, east of the studied area, the basement thrust sheets form an antiformal stack with a significant structural relief [*Muñoz,* 1992]. Southward, the Mesozoic cover sequence is detached along the Triassic evaporites to form the Bóixols, Montsec and Serres Marginals thrust sheets (Figure 1, section 1). In the Axial Zone, Triassic evaporites also decouple Mesozoic units from the antiformally stacked basement units. On the contrary, in the west-central Pyrenees there are no Triassic evaporites between Upper Cretaceous and Paleozoic rocks along the Axial Zone. As a result, the Mesozoic and Paleogene cover is coupled to the basement and basement thrust sheets are mostly imbricated, instead of piled one on top of the other, constituting an imbricate hinterland dipping duplex [*Cámara and Klimowitz,* 1985; *Labaume et al.,* 1985*; Teixell,* 1996, 1998]. The change in thrusting geometry in turn leads to a more distributed structural relief in the west-central Pyrenees. As basement thrust sheets are located further south in the west-central than in the central Pyrenees, the cover thrust sheets are widely exhumed in the west. Thus, the western lateral

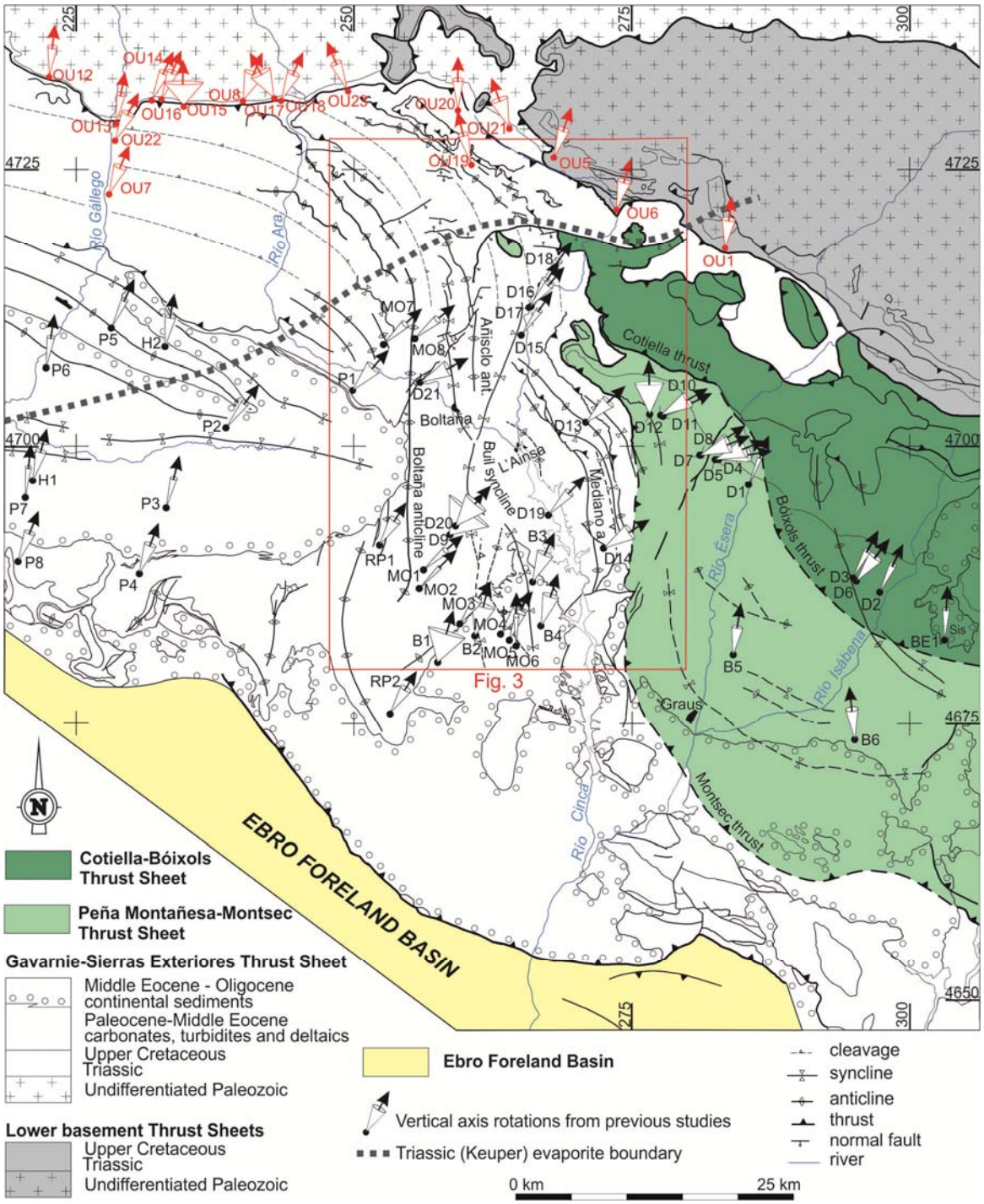

Figure 2. Structural map of the Ainsa Oblique Zone and surrounding areas. Location of the paleomagnetic sites with mean values of rotation from previous studies (B: *Bentham* [1992]; BE: *Beamud et al.* [2003]; D: *Dinarès-Turell* [1992]; H: *Hogan* [1993]; MO: *Mochales et al.* [2012b]; OU: *Oliva-Urcia and Pueyo* [2007]; P: *Pueyo et al.* [2003a]; RP: *Rodríguez-Pintó et al.* [2013]). Cones represent α_{95} values of the paleomagnetic directions. Red sites correspond to remagnetized sites from *Oliva-Urcia* [2004]. See location in Figure 1 and data in Table S1 of supplementary material. Red square indicates the position of the study area represented in Figure 3.

equivalents of the Peña Montañesa-Montsec and Cotiella-Bóixols thrusts have been uplifted and eroded, whereas the lower Gavarnie-Sierras Exteriores thrust sheet occupies a wide area (Figure 1), only disrupted along its northern edge by a minor fold and thrust system (Larra-Monte Perdido, Figure 3) in the footwall of the eroded Peña Montañesa thrust. As a consequence of the changes in thrust geometry and imbrication, the basement thrust sheets along the Axial Zone

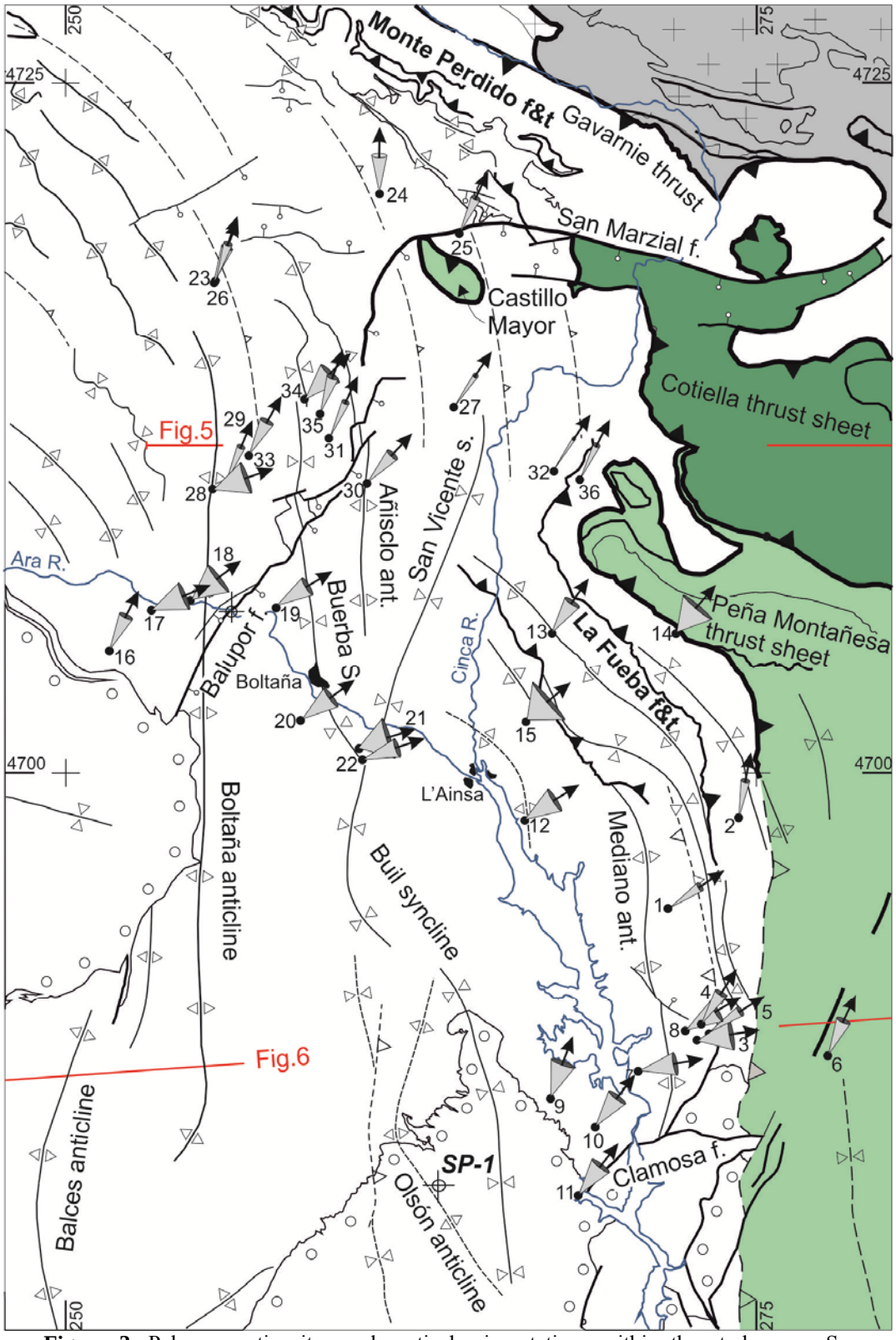

Figure 3. Paleomagnetic sites and vertical-axis rotations within the study area. See location in Figure 2. Cones represent the declination error obtained from $\alpha_{95}/\cos I$. The map legend is the same as in Figure 2. Red lines indicate the location of the cross-sections presented in Figures 5 and 6. f: fault, f&t: fold and thrust system, ant: anticline, s: sincline

plunge westward and the structural relief decreases in the same direction (Figure 1, sections 1 and 2). The change in structural relief is not sharp and occurs across a wide area that coincides with the extent of the N-S trending structures of the studied area. The significance of these changes in the

geometry of the Axial Zone and cover thrust sheets, as well as their structural expression, will be discussed herein.

[18] Major thrusts and related folds and cleavage of the Ainsa basin in the Gavarnie thrust sheet display a regional curvature from WNW trends in the northwestern part to N trends in the central part of the Ainsa basin [*Choukroune and Séguret,* 1973] to define what is referred to in this paper as the Ainsa Oblique Zone (Figures 1 and 2). The transition from this zone to the WNW Pyrenean trends of the Tremp-Graus piggy-back basin and Serres Marginals eastward is concealed by synorogenic sediments and overprinted by salt structures (Figures 2 and 3).

3. Stratigraphy and Structure of the Study Area

[19] The most conspicuous structural feature of the Ainsa basin is a system of kilometer-scale N-S trending folds in the footwall of the Cotiella and Peña Montañesa-Montsec thrust sheets (Figures 1, 2 and 3), referred to as the Sobrarbe fold system [*Fernández-Bellon,* 2004; *Fernández et al.*, 2012]. These folds are detachment to fault-propagation folds, which detached into the Triassic evaporites and deform the Upper Cretaceous-Paleogene stratigraphic succession of the Gavarnie thrust sheet. In addition to the Sobrarbe fold system, the sediments of the Ainsa basin are deformed in its proximal area, adjacent to the Peña Montañesa-Montsec thrust sheet, by a deep-water fold and thrust system which has been named La Fueba thrust system [*Fernández-Bellon,* 2004; *Fernández et al.*, 2012]. All these structures display curvature in map-view over a range of scales.

3.1. Tectonostratigraphic Units

[20] The oldest rocks outcropping north of the study area are Devonian and Carboniferous shales, sandstones and limestones which constitute the Variscan basement of the Gavarnie thrust sheet [*Ríos et al.*, 1982a]. Unconformably above, Triassic sediments are irregularly distributed. Upper Triassic Keuper shales, evaporites and salts are truncated westward below the unconformity at the bottom of the Upper Cretaceous limestones, defining a NNE-SSW trending edge (Figure 2). Such sediment distribution controlled the structural evolution of the area as will be discussed later. In the study area, lower Triassic red beds (Buntsandstein facies) are only observed in the footwall of the Gavarnie thrust sheet, unconformably overlying the post-Variscan granites [*Ríos et al.*, 1982a].

[21] Unconformably above the Triassic reds beds, evaporites and salt, or directly on top of the Variscan basement rocks, the stratigraphic succession of the study area consists of the following main tectonostratigraphic units (Figure 4):

[22] 1) Upper Cretaceous limestones, marls and calcarenites; 2) Paleocene carbonates and clastic sediments; 3) the Lower Eocene *Alveolina* Limestone and a succession of marls and limestones above; 4) Lower Eocene (Cuisian) *Alveolina* and Nummulitid limestones (Santa Marina Fm.) which are the lateral equivalent of the lower part of the Ainsa slope complex (San Vicente Fm. 1); 5) Middle Eocene platform limestones (Guara Fm.) and the lateral equivalent upper part of the Ainsa slope complex (San Vicente Fm. 2); 6) Middle-Upper Eocene deltaic (Sobrarbe Fm.) to continental sediments (Escanilla Fm.); and 7) Oligocene-Miocene continental deposits.

[23] The Upper Cretaceous succession of the Gavarnie thrust sheet consists of two tectonostratigraphic subunits. The lower one is made up by upper Cenomanian-lower Santonian limestones ("Calcaires des Canyons") [*Fournier,* 1905] that represent the post-rift succession on the margin of the Lower Cretaceous rift, which was located to the NE of the studied area. They thin from a few hundreds of meters in the northwest, where they unconformably overlay the basement rocks of the Gavarnie thrust sheet, to few tens of meters in the south, on top of the Triassic evaporites (as evidenced by the borehole Surpirenaica-1 [*Lanaja and Navarro,* 1987] and the outcropping core of the Mediano anticline [*Garrido-Megías,* 1973]). Next to the rift margin they reach a thickness up to 5 km in the Cotiella thrust sheet [*García-Senz*, 2002; *McClay et al.*, 2004]. Above, the younger upper Santonian-Maastrichtian subunit developed in a foreland basin setting during the inversion of the Cotiella-Bóixols thrust sheet [*García-Senz,* 2002]. Thickness of these Upper Cretaceous synorogenic sediments varies from up to 3 km in the Montsec thrust sheet, to 500-700 m in the Gavarnie thrust sheet, or few tens of meters in the most frontal thrusts sheets of the Sierras Exteriores.

[24] Upper Cretaceous rocks are overlain by 100 to 400 m of Paleocene shallow water limestones and dolomites which grade in the SE corner of the studied area (Mediano anticline) into a succession of red beds and fresh water limestones (Garumnian facies). This transition is also observed in the Montsec thrust sheet east of the Esera valley [*Baceta et al.*, 2004; *Robador,* 2008] (Figure 2). The lower Ilerdian is represented in the Ainsa basin area by the *Alveolina* Limestone [*Mey et al.,* 1968]. This formation represents a widespread transgressive episode event in the south Pyrenean foreland basin. Its thickness ranges from 70 to 150 m and coincides with the end of a relatively quiescent period which started in Paleocene times.

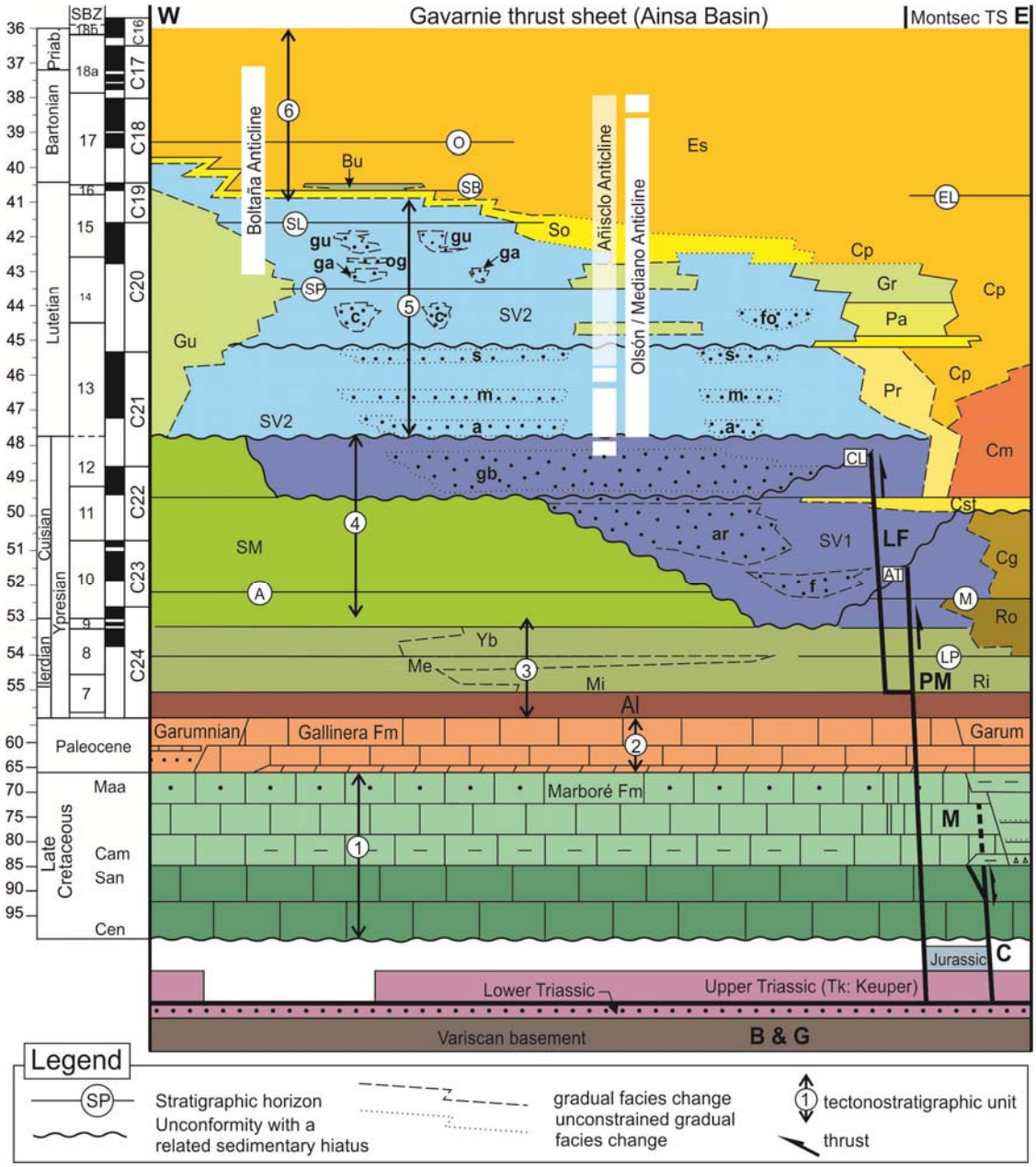

Figure 4. Chronostratigraphic diagram showing the main stratigraphic units of the Gavarnie thrust sheet and surroundings. Lithostratigraphic units: Es, Escanilla; Bu, Buil; So, Sobrarbe; Gu, Guara; Gr, Grustán; Pa, Pano; Cp, Capella; Pr, Perarrúa; Cm, Campanué; Cst, Castissent; SM, Santa Marina, Cg, Castigaleu; Ro, Roda; Yb, Yeba; Ri, Riguala, Me, Metils; Mi, Millaris; Al, Alveolina limestone. SV1-2: San Vicente Formation. Turbidite systems: gu, Guaso; og, O Grao; ga, Gabardilla; c, Coscojuela; fo, Formigales; s, Sieste; m, Morillo; a, Ainsa; gb, Gerbe-Banastón; ar, Arro; f, Fosado. Horizons: O, Olsón; EL, Escanilla limestone; SB, Santa Bárbara; SP, San Pedro; SL, San Lino; M, Morillo limestone; A, Ascaso; LP, La Puebla. Thrust sheets: C, Cotiella; M, Montsec; PM, Peña Montañesa; B & G, Bielsa and Guarga; LF, La Fueba thrust system.Unconformities: AT, L'Atiart; CL, Charo-Lascorz. Litho- and chronostratigraphic information compiled from: *Bentham et al.* [1992], *Bentham and Burbank* [1996], *Barnolas and Gil-Peña* [2001], *López-Blanco et al.* [2003], *Mochales et al.* [2012a], *Rodríguez-Pintó et al.* [2012], *Serra-Kiel et al.* [1994]. Eocene time scale from *Gradstein et al.* [2004]. SBZ biozones calibration to the time scale integrates data from *Costa et al.* [2013] and *Rodriguez-Pintó et al.* [2012].

Above, a succession of marls and limestones completes the lower Eocene series (Millaris, Metils and Yeba Fms.) [*Van Lunsen,* 1970; *Barnolas and Gil-Peña,* 2001; *Mochales et al*., 2012a] (Figure 4).

[25] The Ainsa slope complex is as much as a 4 km thick succession of primarily mudstones with several encased turbidite systems, each one being a few hundreds of meters thick [*Arbués et al.,* 2007]. These sediments, described as the San Vicente Formation [*Van Lunsen,* 1970; *De Federico*, 1981], are the main infill of the well-known Ainsa basin and represent the proximal slope facies of the deeper water siliciclatic complexes in the Jaca basin, located westward (Hecho Group), [*Mutti et al.,* 1972].

[26] The Lower Eocene part of the Ainsa slope complex developed in the footwall of the Peña Montañesa-Monsec thrust sheet in a foredeep setting (Figures 2, 4, 5 and 6). Sedimentation occurred synchronously with the La Fueba deep-water fold and thrust system in the footwall of the Peña Montañesa-Montsec thrust as its hangingwall was displaced southward [*Muñoz et al.,* 1994]. The slope sediments were primarily fed from a fluvio-deltaic complex located in the east, on top of the Montsec thrust sheet (the Montañana Group of the Graus-Tremp piggy-back basin) [*Nijman and Nio,* 1975]. Southward, the turbiditic trough of the Ainsa basin was bounded by a carbonate platform (Santa Marina Fm.) [*Barnolas et al.,* 1991]. This platform retreated in front of the Peña Montañesa-Montsec thrust sheet as the thrust sheet moved southward. Slope sediments onlap the back-stepped margin of the platform and incorporate resedimented carbonates triggered by the tilting of the platform [*Arbués et al.,* 2011].

[27] At Middle Eocene times deformation progressed into the footwall of the Peña Montañesa thrust sheet. As a result, the Gavarnie thrust sheet developed and the floor of the Ainsa basin was deformed by the Sobrarbe fold system (Figures 5 and 6). The Ainsa basin changed from a foredeep to a piggy-back basin and its infill developed a shallowing-upward sequence. The upper parts of the slope complex and its carbonate and deltaic equivalents as well as the fluvio-deltaic complex above (Sobrarbe deltaic system and Escanilla Fm.) [*Dreyer et al.,* 1999] were sedimented during fold growth [*Poblet et al.,* 1998]. Westward, the fluvial red beds of the Escanilla Fm. grade laterally into the deltaic sandstones of the Sobrarbe delta, which in turn are the lateral equivalent of the upper part of the slope sediments of the San Vicente Fm. (Figure 4).

[28] The youngest marine sediments in the studied area correspond with the Buil Nummulitic banks at the bottom of the Escanilla Fm. [*Mateu-Vicens et al.,* 2012]. Above, fluvial sediments of the Escanilla Fm. are Bartonian to Priabonian in age [*Bentham*, 1992; *Bentham et al.,* 1992; *Mochales et al.,* 2012a]. The middle to upper part of the Escanilla Fm. is equivalent to the Campodarbe Group [*Puigdefàbregas,* 1975], which lies unconformably on top of the Middle Eocene limestones on the western limb of the Boltaña anticline (Figure 2).

[29] The Escanilla Fm. and older formations are unconformably overlain by the Oligocene-Miocene continental sediments, which extensively cover the southern part of the studied area [*Puigdefàbregas,* 1975; *Luzón*, 2005] (Figure 3). These sediments consist of conglomerates at the northern margin of the basin passing southwards into sandstones and mudstones. They were deposited synchronously with the frontal thrust structures [*Luzón*, 2005].

3.2. The Sobrarbe fold system

[30] The Sobrarbe fold system consists of four major N-S trending anticlines, which from east to west are: the Mediano, Olsón, Añisclo and Boltaña anticlines. Between them synclines occur, the most prominent of which is the Buil syncline (Figures 2, and 3). These folds have been described by many authors due to the high obliquity of their trends with respect the main E-W to ESE-WNW Pyrenean structural trend [*Séguret,* 1972*; Garrido-Megías,* 1973*; Puigdefàbregas,* 1975*; Mutti et al.,* 1988*; Martínez Peña,* 1991*; Soto and Casas,* 2001*; Soto et al.,* 2002]. *Fernández et al.* [2012] have recently described in detail the 3D geometry of these folds based on the integration of surface and subsurface data, following a fully 3D reconstruction approach [*Fernández et al*., 2004].

[31] The Mediano anticline is a 20 km long detachment fold cored by Triassic evaporites. Its structure and along-strike evolution were described by *Poblet et al.* [1998]. In its southern sector it displays eastward vergence (Figure 6) and a northward plunge of about 10º. It is bound to the south by the faults bounding the Clamosa Triassic salt dome [*Teixell and Barnolas,* 1995]. To the north, the Mediano anticline changes to a NW-SE trend before terminating below the turbidites of the Ainsa basin (Figures 2 and 3). The Mediano anticline has been considered as an oblique structure related to the Montsec thrust [*Farrell et al.,* 1987; *Martínez-Peña,* 1991; *Bentham and Burbank,* 1996] or as a structure belonging to the Montsec thrust sheet [*Soto et al.,* 2002; *Mochales et al.,* 2012b]. However, the Mediano anticline is younger than the Montsec thrust. Growth geometries clearly demonstrate that the Mediano anticline developed during the Middle Eocene, from early Lutetian to Bartonian times [*Poblet et al.,* 1998], whereas the Montsec thrust and its northern continuation into the Atiart thrust are unconformably overlain by late Ypresian sediments [*Soler and Garrido-Megías,* 1970; *Garrido-Megías,* 1973; *Muñoz et al.,* 1994]. Age

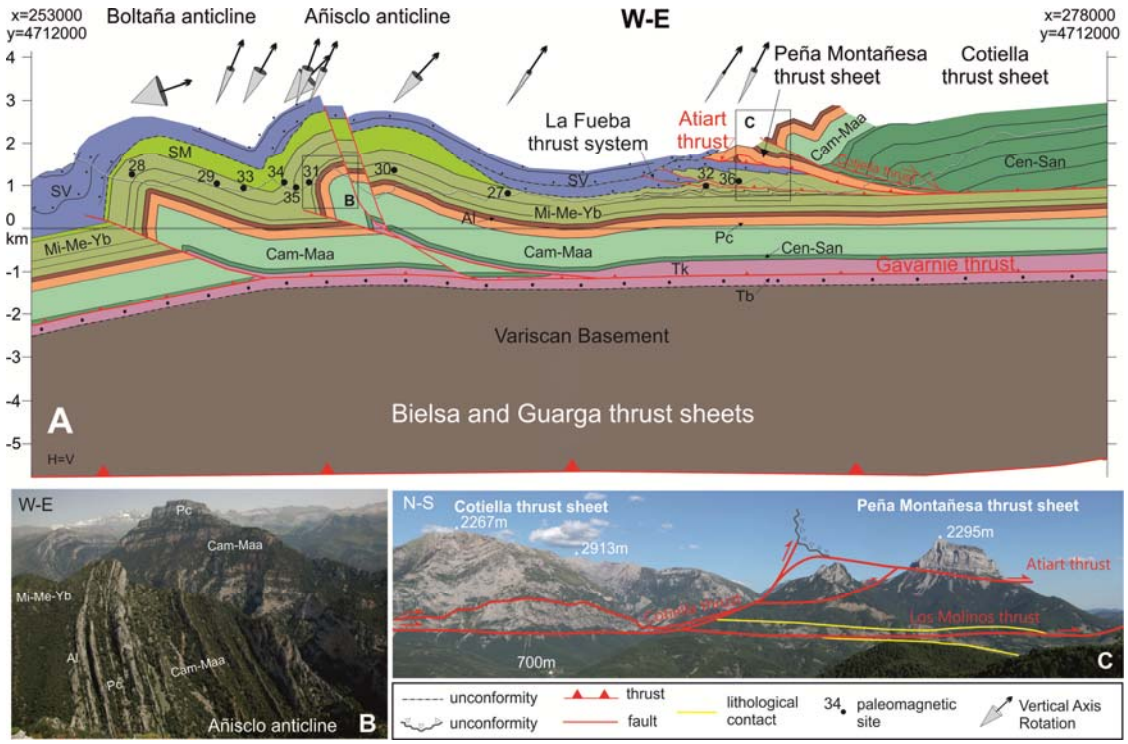

Figure 5. A. Cross-section of the northern part of the Ainsa Oblique Zone, across the Boltaña and Añisclo anticlines in the Gavarnie thrust sheet and the Peña Montañesa and Cotiella thrust sheets. Lithostratigraphic units like in figure 4. B. Photograph of the Añisclo anticline. C. Photograph and structural sketch of the Peña Montañesa and Cotiella thrust sheets.

constraints, surface and subsurface data and stratigraphic differences demonstrate the Mediano anticline is part of the Gavarnie thrust sheet in the footwall of the Peña Montañesa-Montsec thrust sheet [*Fernández-Bellon,* 2004; *Fernández et al.,* 2012], (Figure 6).

[32] West of the Mediano anticline, the Olsón anticline has no evident expression at surface, as it is located below the Buil syncline (Figures 3 and 6). However, it has been imaged by seismic data and drilled by the Surpirenaica-1 well [*Lanaja and Navarro,* 1987]. The Olsón anticline is 10 km long and has an associated westward directed thrust in its central part (Figure 6). Seismic sections show growth geometries of the Middle Eocene slope to deltaic sediments located below the fluvial sediments cropping out in the core of the Buil syncline. Thus, it developed synchronously with the Mediano anticline, although it stopped growing earlier.

[33] The Añisclo anticline is the fold with the deepest level of exhumation in the study area, along with the Mediano anticline, and as a result the Upper Cretaceous limestones crop out in its core (Figure 5). It occupies the same structural position east of the Boltaña anticline as the Olsón anticline. However, careful analysis of seismic profiles along with detailed structural analysis of the Añisclo anticline, reveal that the Olsón anticline dies out to the north, under the Buil syncline, and so does the Añisclo anticline to the south (Figure 3). These folds are not connected as previously suggested by *Soto and Casas* [2001] [*Fernández et al.,* 2012]. The Añisclo anticline is a fault-propagation fold in its central part characterized by a vertical to steeply overturned frontal limb (Figure 5). The fold axis plunges southward at about 10º increasing up to 25º in its southernmost termination where the fold opens progressively and changes to a detachment anticline [*Tavani et al.,* 2006]. This transition coincides with a sharp change of the dip of the forelimb from vertical to moderately dipping to the SW, and with a change of the fold axis trend from N-S to NW-SE (Figure 3). See *Tavani et al.* [2006] for a detailed description of the Añisclo anticline and its related mesostructures. Growth strata are only preserved over the fold's southern termination. There, the oldest evident synfolding sediments are the lower Lutetian turbidites of the Ainsa system [*Arbués et al.,* 2007]. Thus, the Añisclo anticline grew synchronously with the Mediano anticline. However, and based on the 3D reconstruction of distinct surfaces of the Ainsa basin, an initial development of the Añisclo anticline during the sedimentation of the upper part of the Gerbé-Banastón turbidite system (Figure 4) cannot be ruled out [*Fernández et al.,* 2012].

[34] The Boltaña anticline is the most prominent anticline of the Sobrarbe system (Figures 2 and 3).

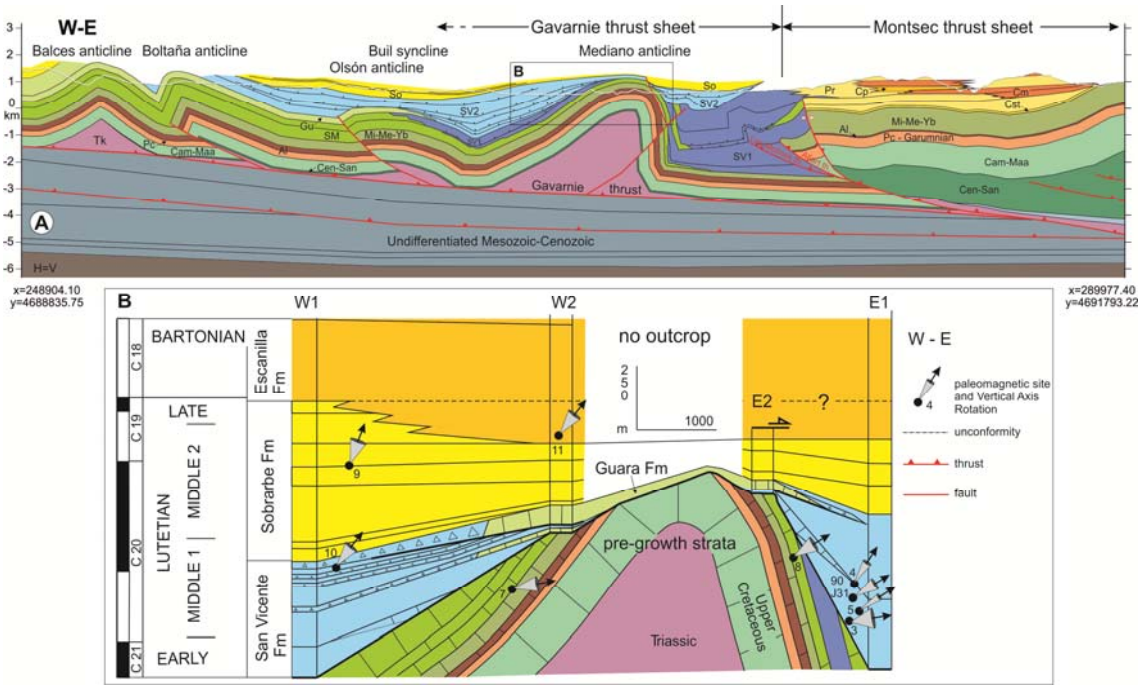

Figure 6. A. Cross-section of the southern part of the Ainsa Oblique Zone. Lithostratigraphic units like in figure 4. B. Enlargement of the Mediano anticline and location of the paleomagnetic sites with respect to the syn-folding growth sequence. W1, W2, E1 and E2 correspond to four stratigraphic columns constructed across the growth sequence, two of them in the west limb and two of them in the east limb of the anticline.

It has been traditionally considered the boundary between the Jaca and Ainsa basins as it marks an outcrop discontinuity of the lower and middle Eocene slope sediments [*Mutti et al.,* 1988]. This fold is related to the propagation of the westward verging Boltaña blind thrust (Figures 5 and 6). The Boltaña anticline is over 25 km long and presents a very constant N-S trend with practically no plunge. However, at its northern termination it changes to a NW-SE trend where the anticline opens and splits into a system of smaller NW-SE trending folds (Figures 2 and 3). These folds are located in the hangingwall of a thrust splay of the Gavarnie thrust that represents the continuation of the Boltaña thrust (Figure 2) [*Fernández et al.*, 2012]. This thrust system is located below the Monte Perdido thrust system and does not branch with it [*Millán et al.,* 2006], contrary to its interpretation as the floor and frontal thrust of the Monte Perdido fold and thrust system [*Séguret*, 1972; *Lacroix et al.,* 2011]. Toward the south, the Boltaña anticline ends south of the study area where it is relayed by the Balces anticline [*Millán,* 1996] (Figures 2 and 3). This anticline shows a prominent curved axial surface, describing an arc of about 45º (southwestwards convex) in map view [*Rodriguez-Pintó et al.*, 2013] (Figure 2).

[35] The age of growth of the Boltaña anticline is constrained by the geometry and sedimentological characteristics of the syntectonic sediments. In the western forelimb of the Boltaña anticline, along the Ara River valley, a thick succession from the lower Eocene slope sediments of the San Vicente Fm. to the upper Eocene continental deposits of the Campodarbe Group shows an apparently continuous growth wedge geometry in map view (Figure 7). Such map pattern was initially considered to reflect the growth of the anticline [*Puigdefábregas,* 1975]. However, detailed mapping of this area reveals an unconformity in the Lutetian slope succession which separates the growth strata from the pre-folding sediments (Figure 7). Below this unconformity, the lower Lutetian beds of turbidites and marls unconformably overlie and onlap the Lower Eocene platform beds of the Santa Marina Fm. The intersection lines between the slope and the platform beds (onlap lines) are subvertical to steeply plunging to the north and are subparallel to the northern edge of the Eocene foreland platform and to the strike of the gravitational collapse surfaces described by *Barnolas and Teixell* [1994] that truncate the underlying platform (Figure 7b). This relationship indicates that sediments below the unconformity were deposited on a northwards tilted carbonate platform (Santa Marina Fm.) and that fanning of beds records the tilting of the foreland platform. On the contrary, above the unconformity, the onlap lines of the middle Lutetian to Bartonian growth strata are moderately dipping to the south (Figure 7b) and subparallel to the fold axis, as can be expected for growth strata.

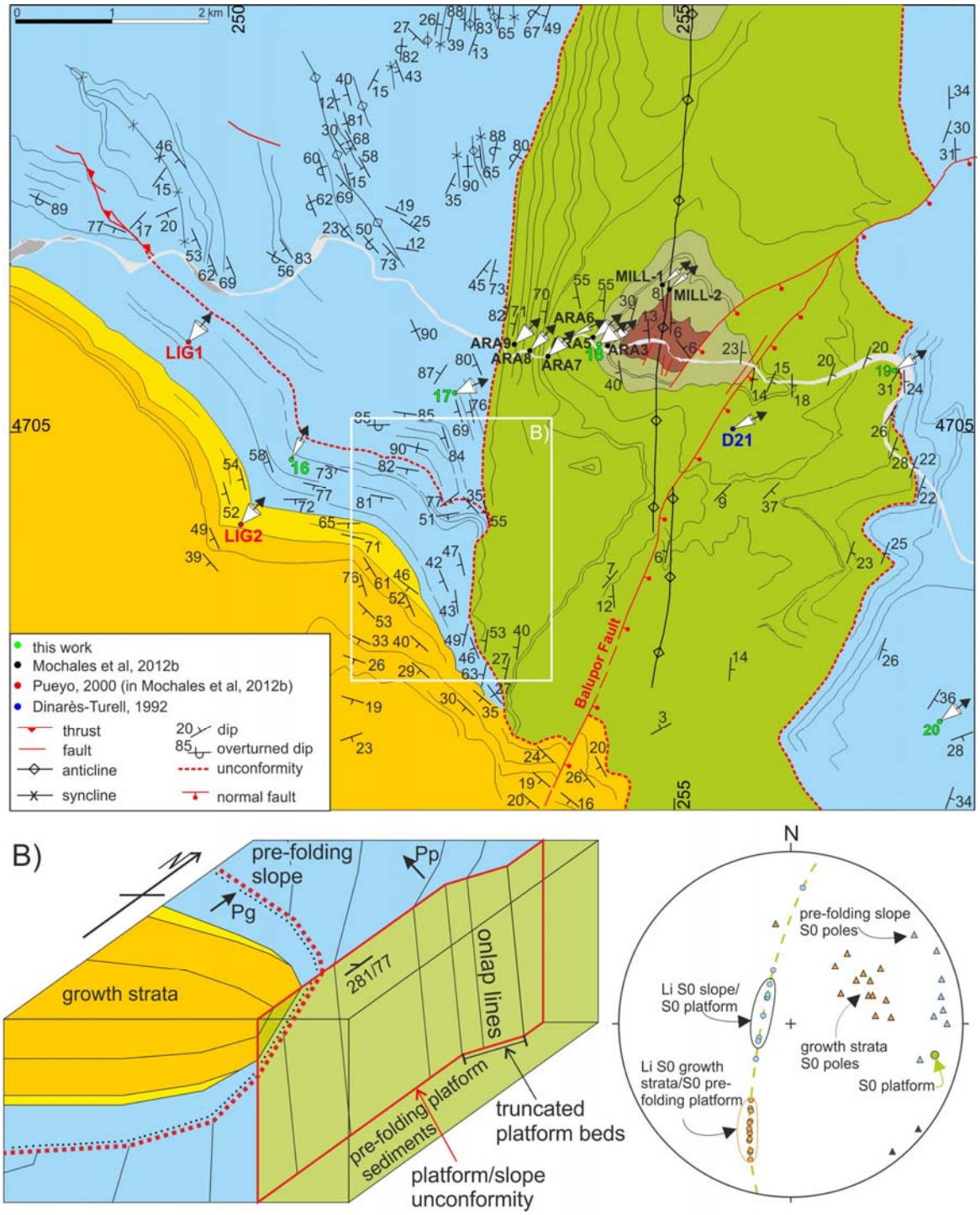

Figure 7. Detailed map of the Boltaña anticline and paleomagnetic data in this area from this and previous studies (see Table S1 in supplementary material). White square indicates the position of the 3D block diagram (B) which shows in detail the unconformity between the pre-folding platform and slope sediments and the growth strata. Pp: paleocurrent directions of the pre-folding slope; Pg: paleocurrent directions of the growth strata. The stereogram represents the poles of bedding of the pre-folding platform and the pre-folding slope sediments, and the poles of bedding of the growth strata. The intersection lineations between the slope and the platform bedding and between the growth strata and the pre-folding platform are also included.

Paloecurrent directions in the pre–unconformity slope sediments on both limbs of the Boltaña anticline are at present directed to the NW (when unfolded) and would be parallel or slightly oblique to the onlap lines, but at a high angle to the axis of the Boltaña anticline. These sedimentological and structural data confirm that lower Lutetian slope sediments deposited before the onset of growth of

the Boltaña anticline. Conversely, paleocurrent directions of the middle Lutetian turbidites at the bottom of the growth sequence are subparallel to the axis of the anticline. In the eastern backlimb of the Boltaña anticline, where the moderate dip of bedding hampers the discrimination of the growth strata, a change of the turbidite paleoflow directions from NW-SE (oblique to and across the fold) during the sedimentation of the upper Ypresian-lower Lutetian turbidite systems of the Ainsa basin (Gerbé-Banastón, Ainsa, Morillo and Sieste), to N-S (parallel to the fold) during deposition of middle Eocene systems (Gabardilla, Guaso), has also been observed [*Arbués et al.,* 2011]. Correlation of the Gabardilla system with the magnetostratigraphic succession of *Mochales et al.* [2012a] yields an age of approximately 42.5 Ma for this system. In conjunction with the above described geometrical features of the growth strata, unconformities, paleocurrent directions and recent magnetostratigraphic data, onset of growth of the Boltaña anticline can be dated as middle Lutetian. This age is also consistent with the middle Lutetian folding event described in the western limb of the Balces anticline, based on the unconformity observed in the Lutetian Guara limestones (Figure 4) [*Millán et al*., 2000; *Barnolas and Gil-Peña,* 2001]. The end of formation of the Boltaña anticline took place before the deposition of the lower part of the Campodarbe Fm. during early Priabonian times [*Puigdefábregas,* 1975*; Montes,* 1992*; Barnolas and Gil-Peña,* 2001]. This age attribution challenges the role of the anticline as a paleogeographical barrier during the deposition of the upper Ypresian to middle Lutetian San Vicente Fm. as previously suggested [*Puigdefábregas,* 1975*; Mutti et al.,* 1985, 1988].

3.3. The La Fueba Thrust System

[36] Thrusts and related folds of the La Fueba thrust system are located east of the Mediano anticline, in the footwall of the Peña Montañesa-Montsec thrust sheet. The La Fueba system, also called Arro system by some authors [*Barnolas et al.,* 1991; *Martínez-Peña,* 1991; *Casas et al*., 2002], consists of a set of NW-SE to N-S trending structures, verging toward the SW and parallel to the main Peña Montañesa-Montsec thrust to which they are connected (Figures 2, 3, 5, 6 and 8) [*Muñoz et al.,* 1994]. The structure of this system has been described by many authors [*Nijman and Nio,* 1975*; Mutti et al.,* 1988*; Barnolas et al.,* 1991*; Martínez-Peña,* 1991; *Travé et al.,* 1997, 1998; *Barnolas and Gil-Peña,* 2001*; Casas et al.,* 2002; *Fernández et al.,* 2012], the most prominent structures being the L'Atiart and Los Molinos thrusts and their related hangingwall anticlines and footwall synclines (Figure 8).

[37] The L'Atiart thrust is the most relevant structure of this system with several kilometers of displacement as it is the oblique ramp connecting the Montsec and Peña Montañesa thrusts [*Soler and Garrido-Megías,* 1970*; Nijman and Nio,* 1975*; Farrell et al.,* 1987; *Fernández et al.,* 2012]. The other thrusts scarcely accumulate 2 km of total displacement [*Barnolas et al.,* 1991].

[38] Thrusts and related folds of the La Fueba system show a change of trend from NW-SE in the north to N-S in the south, similar to that of the Mediano anticline (Figure 8). The same change of trend along the structural bend is also observed in the mesostructures related with the thrusts. Thrusts in the La Fueba system have fault zones that are meter-thick shear zones characterized by strongly foliated sediments and an S-C-C'-type shear fabric [*Travé et al.,* 1997*; Lacroix et al.,* 2011]. In the NW area, where thrusts and folds have a NW-SE trend, shear planes mostly strike parallel to the trend of the main thrusts and most of the striations on the calcite veins located along the shear planes are dip-slip (diagram 1 in Figure 8). As the strike of thrusts changes, the amount of trend or pitch dispersal of shear planes and striations increases and is proportional to the deviation of thrust strike from the regional WNW-ESE trend (compare data of the L'Atiart thrust along the bend from NW to SE; diagrams 1, 2 and 3 of Figure 8): striations indicate almost pure dip-slip motion in NW-SE striking thrusts, but range from dip-slip to strike-slip for N-S trending thrusts, always transporting the hangingwall or eastern block to the SW. Often, more than one generation of striations with different pitch is superimposed in the same shear calcite veins. Chronological criteria between them are rare, but when visible, strike-slip striations (dextral) are younger than the reverse dip-slip ones, as also suggested by *Travé et al.* [1997, 1998]. In general, shear zones and related striations show a more complicated pattern in the portions where thrusts trend N-S, suggesting fault reactivation in addition to rotation. This is particularly evident along the Los Molinos thrust (diagrams 4 and 5 in Figure 8). Moreover, in the structurally shallower parts of the thrusts, conjugate shears and minor thrusts and backthrusts coexist resulting in more complicated diagrams (diagram 5 in Figure 8).

[39] The age of the La Fueba thrust system is constrained by the preserved syntectonic sediments. It developed mostly during the late Ypresian (Cuisian) when deep-water emergent thrusts controlled the transition from the deltaic sediments in the hangingwall to the slope sedimentary systems of the Ainsa basin in the footwall (Figures 4 and 6). Thrusts mostly developed in a piggy-back sequence. Each major thrust has a related major unconformity or truncation surface, which developed by gravitational extensional collapse or successive gravitational failures of the rising hangingwall

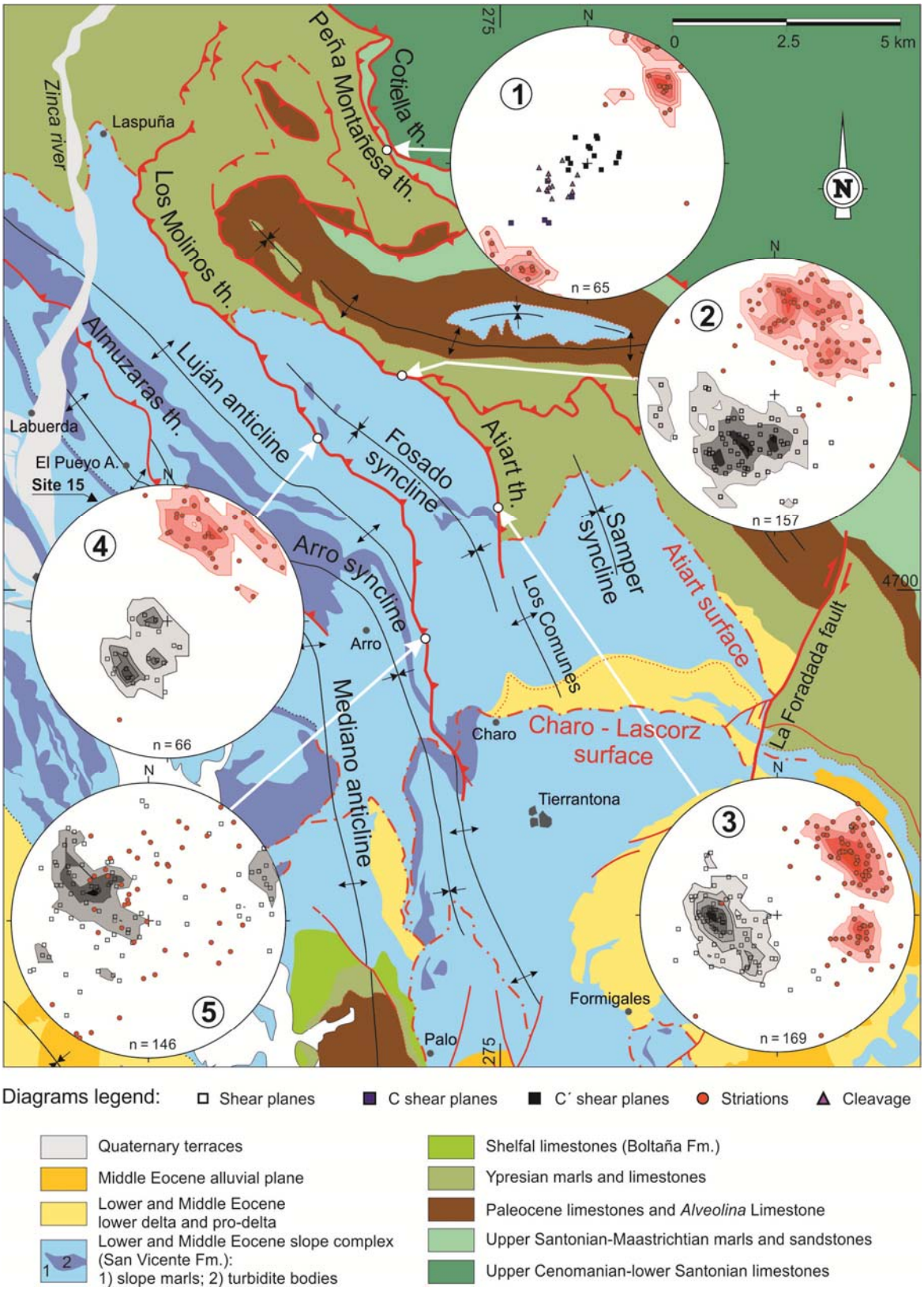

Figure 8. Detailed map and kinematic data of the main thrusts in the La Fueba fold and thrust system.

[*Muñoz et al.*, 1994]. The most significant and preserved pairs of surfaces are the L'Atiart thrust-L'Atiart truncation surface and Los Molinos thrust-Charo-Lascorz truncation surface (Figure 8) [*Soler and Garrido*, 1970; *Mutti et al.*, 1988; *Muñoz et al.*, 1994]. The first one is early-middle

Cuisian in age and the second one is latest Cuisian (Figure 4). Unconformities have also been slightly deformed, either during the displacement on the lower and younger thrusts of the La Fueba system or during subsequent reactivation of the main thrust planes.

[40] Structures of the la Fueba thrust system have the same structural position and probably the same age as (or slightly older than) the Monte Perdido thrust and related folds, which deform the Cretaceous to Paleogene succession of the Gavarnie thrust sheet (Figures 2 and 3). The frontal part of the Monte Perdido fold and thrust system deforms the Cuisian turbidites in the footwall of the La Peña Montañesa thrust sheet at its westernmost outcrop in the Castillo Mayor klippe (Figure 3).

3.4. Mesoscopic Structures: Cleavage, Fracture, Fault and Vein Networks

[41] The Gavarnie thrust sheet in the Ainsa fold and thrust oblique zone displays systematic suites of mesoscopic structures that accommodated internal strain, including spaced cleavage, fracture and vein networks, minor folds, and minor faults [*Holl and Anastasio,* 1995a*; Tavani et al.,* 2006, 2012].

A regional pressure solution cleavage is observed in the Mesozoic-Paleogene sediments at the northern exposures of the Gavarnie thrust sheet of the study area [*Choukroune and Séguret,* 1973]. Cleavage is axial planar to regional and mesoscale folds, and parallels the strike of the fold and thrust structures of the Gavarnie thrust sheet. As a result, attitude of the cleavage planes shows the same map pattern as the above described thrusts and folds, and emphasizes the change of the structural trend from WNW-ESE to N-S at the NW corner of the Ainsa Oblique Zone (Figures 2 and 3). The cleavage intensity decreases southward to form a cleavage front as described by many authors [*Séguret,* 1972*; Choukroune,* 1976*; Holl and Anastasio,* 1995a*; Oliva-Urcia et al.,* 2008]. However, such cleavage front is not a sharp feature, as the occurrence of the cleavage depends also on the mechanical stratigraphy and the structural position with respect to the folds affecting the Gavarnie thrust sheet [*Holl and Anastasio,* 1995a; *Tavani et al.,* 2006]. Cleavage changes from pervasively distributed in the northern areas to more localized in higher structural levels to the south. This transition is obvious in the Boltaña, and Añisclo anticlines. Thus, in the northern part of these folds, where they trend NW-SE, cleavage is pervasive and penetrative all around the fold, regardless of both anticlines being open. Southward, where the folds change their trend to N-S into the oblique zone and they become significantly tighter, cleavage is more localized and mainly restricted to the vertical to overturned forelimb [*Tavani et al.,* 2006]. Such internal strain gradient also occurs in an E-W direction. Thus, in the forelimb of the Añisclo anticline, at the central part, pressure-solution cleavage is closely spaced, and locally, up to 3 different sets of cleavage planes are observed (normal, oblique and parallel to bedding) [*Tavani et al.,* 2006]. In the same transect (Figure 5), the forelimb of the Boltaña anticline only shows a family of spaced layer normal pressure-solution cleavage at high angles to bedding [*Tavani et al.,* 2012]. The Mediano anticline is located southward of the cleavage front as well as is the southern part of the Boltaña anticline [*Holl and Anastasio,* 1995b].

[42] Pressure-solution cleavage is parallel to the fold axis, remaining subperpendicular to bedding in fold limbs and hinge zones, and evenly spaced throughout. Such bedding/cleavage relationships are only overprinted by selective cleavage infilling in the vertical to overturned forelimb of fault-related folds. These angular and spacing relationships indicate that pressure-solution cleavage formed before and at the initial stages of deformation by layer parallel shortening and was subsequently tilted along with bedding during large-scale folding and thrusting. Locally, it continued to develop during fold tightening [*Tavani et al.,* 2006]. Layer parallel shortening directions give the orientation of finite and instantaneous shortening axes. These directions are roughly perpendicular to the structural trend around the Ainsa Oblique Zone and are consistent with the shortening directions inferred from mechanically twinned calcite grains and minor faults [*Holl and Anastasio,* 1995b]. *Holl and Anastasio* [1995a] estimated that the amount of layer parallel shortening increases from < 5%, 2 km forward of the cleavage front, to ~ 30% 7 km hindward of the cleavage front, and then remains constant further hindward.

[43] Fracture and veins show a systematic symmetry with respect to large-scale folds. The most common fracture and vein systems are those parallel (longitudinal) and perpendicular (transversal) to the fold axis. Transversal joints and veins are the predominant fracture system in the Añisclo anticline [*Tavani et al.,* 2006]. In the Boltaña anticline, apart from the transversal joints and veins, the main fracture system corresponds to longitudinal extensional faults. These faults were the result of E-W stretching, parallel to the shortening direction, and developed before and synchronously with folding [*Tavani et al.,* 2012]. Extensional fracture assemblages predominate in the central and southern parts of the Boltaña anticline. In these areas the major mesoscale record of the E-W oriented layer parallel shortening, perpendicular to the fold trend, is provided by AMS data [*Mochales et al.,* 2010] as

the mesostructural pattern only rarely includes contractional structures. Changes of both direction and shape of the AMS ellipsoid record the increasing amount of deformation from the southern parts of the Ainsa Oblique Zone to the northern parts where cleavage is well developed [*Dinarès-Turell and Parés,* 1992; *Parés and Dinarès-Turell,*1993].

In the northern parts of the Boltaña anticline, conjugated strike-slip faults, tilted along with bedding during folding, are part of the contractional assemblage together with pressure-solution cleavage [*Tavani et al.,* 2012]. In the Añisclo anticline tilted strike-slip faults have also been observed [*Tavani et al.,* 2006].

[44] Field observations of mutually cross-cutting relationships between the main pressure-solution cleavage set, strike-slip and extensional faults and joints/veins support the interpretation that they developed coevally.

3.5. Macroscopic Structures: Extensional Faults

[45] The youngest structures observed in the Ainsa Oblique Zone correspond to NE-SW trending extensional faults described as the Balupor-San Marzial fault system by Fernández-Bellon (2004). They have a variable trend from N-S to E-W (Figures 2 and 3). Among them the most prominent one is the San Marzial fault which has a curvilinear map pattern and a throw of about 1 km [*Ríos et al.,* 1982a, b]. It cuts the Cotiella-Peña Montañesa thrust sheets and the Gavarnie thrust sheet below, but it does not displace the Gavarnie thrust (Figure 3). Extensional faults of this system obliquely truncate the Boltaña and Añisclo anticlines and are associated with extensive Triassic outcrops along the NW of the Cotiella thrust sheet. In cross-section they appear as extensional collapse features of the anticlines as they partially reactivate their related thrusts at depth (Figure 5). These extensional faults control along-strike changes in the geometry of the Boltaña and Añisclo anticlines, suggesting some synchronicity with fold growth [*Fernández et al.,* 2012], and are known to be active at least until Priabonian times as they offset sediments of the late Eocene Campodarbe Group (Figure 7).

[46] The extensional faults that define the southern boundary of the Mediano anticline (Clamosa faults), [*Teixell and Barnolas*, 1995] are similar in nature to the Balupor-San Marzial system in that they both are interpreted to be contained entirely within the Gavarnie thrust sheet, they are active at least until the Oligocene (as evidenced by their cutting relationships with sediments of that age), they cross-cut the entirety of a major anticline (the Mediano anticline), and are related to major outcrops of Triassic shales and evaporites (Figure 3). Furthermore, the Balupor-San Marzial and the Clamosa faults are located where the N-S trend of the Ainsa oblique structures swings to a NW-SE trend to the north (Balupor-San Marzial) and to the south (Clamosa). These coincidences are strong indications for a common origin for both systems of extensional faults.

4. Paleomagnetism in the Ainsa Basin

4.1. Previous paleomagnetic studies

[47] Several paleomagnetic studies have revealed important clockwise (CW) vertical-axis rotations in the sediments of the Ainsa Basin [*Dinarès-Turell*, 1992; *Fernández-Bellon*, 2004; *Mochales*, 2011; *Mochales et al*., 2012a, b]. *Dinarès-Turell* [1992] reported significant vertical-axis rotations (up to 60º) in the Ilerdian and Cuisian platform sediments in the Boltaña and Mediano anticlines. This rotation decreases to 40º in the middle Lutetian sediments of the Sobrarbe Fm. *Mochales et al.* [2012b], in a detailed study of the vertical-axis rotations experienced by the Boltaña anticline combined with the magnetostratigraphy of a complete succession of the Ainsa basin [*Mochales et al*., 2012a], reported a CW rotation which decreases from 52º in the Lower Eocene sediments of the core of the anticline to a few degrees in the Upper Eocene sediments in its eastern limb. Upper Lutetian sediments sampled in a magnetostratigraphic study by *Bentham* [1992] in the western limb of the Mediano anticline revealed around 30º of CW rotation. This regional CW rotation pattern is in concurrence with the up to 40º of CW rotation documented by *Pueyo et al.* [1997], *Pueyo* [2000] and *Pueyo et al.* [2002, 2003a] in Bartonian to Chattian materials west of the Ainsa basin, along the south Pyrenean thrust front of the Sierras Exteriores (Figure 2). Data from the magnetostratigraphic studies by *Hogan* [1993] in younger sediments of the Jaca basin and by *Pueyo* [2000], *Oms et al*. [2003] and *Pueyo et al.* [2003b] along the Jaca-Boltaña transect show around 30º of CW rotations. However, vertical-axis rotations measured east of the Ainsa Basin in Eocene sediments of the Tremp-Graus basin are mostly smaller than 20º [*Dinarès-Turell,* 1992*; Dinarès et al.,* 1992*; Beamud et al.,* 2003] (Figure 2). This fact, combined with evidence of counterclockwise (CCW) vertical-axis rotation on the eastern oblique thrust zone of the Montsec unit [*Dinarès-Turell,* 1992*; Dinarès et al.,* 1992, *Sussman et al.,* 2004] led *Dinarès et al.* [1992], *Muñoz* [1992] and *Vergés* [1993] to consider that deformation in the central part of the Montsec thrust occurred by plane strain, validating the restoration of the ECORS-Pyrenees cross-section [*Beaumont et al.,* 2000].

[48] A recent compilation of paleomagnetic data in Permian-Triassic red beds of the central-western Pyrenees has reported no significant vertical-axis

rotation of the sites located in the footwall of the Gavarnie thrust sheet in the study area [*Oliva-Urcia et al.,* 2012b]. The same authors describe a slight CW vertical-axis rotation of 8º-10º for the Upper Cretaceous paleomagnetic component in the Sierras Interiores (Gavarnie thrust sheet west of the study area) and an average CW vertical-axis rotation of 14º for the remagnetized component in the Cretaceous and Paleogene rocks of the Monte Perdido thrust system (Figure 2) [*Oliva-Urcia and Pueyo*, 2007b; *Oliva-Urcia et al.,* 2012b].

[49] Regardless the significant amount of available paleomagnetic data [*López et al.,* 2008] all these paleomagnetic studies have yielded varying interpretations. Some of the inconsistencies between interpretations arise from the irregular density of sampling and the natural scattering of data, but also derive from the lack of integration with structural and stratigraphic data.

4.2. Paleomagnetic sampling and laboratory procedures

[50] Our study has focused on complementing previous paleomagnetic works in the Ainsa basin. Sampling was designed to optimize the distribution of sites in previously non-sampled structures like the Mediano anticline and to delineate rotation patterns along the strike of folds and across their associated growth sediments.

[51] 36 sites were sampled in order to characterize the distribution of vertical-axis rotations within the Ainsa fold and thrust oblique zone (Figure 3). Sampling was carried out by gathering between 8 and 11 cores per site. To average the Earth's magnetic field, cores were sampled along 5 to 10 m of stratigraphic profile. Samples were obtained with a portable gasoline power drill and were oriented *in situ* with a compass mounted on an orienting device with inclinometer. Sampling focused on limestones, marls, marly limestones and fine-grained sandstones from middle Ilerdian to upper Lutetian stratigraphic units. Analyses were carried out in the Paleomagnetic Laboratory of Barcelona (CCiTUB-CSIC). They consisted of stepwise thermal demagnetization with demagnetizers TSD-1 (Schonstedt) and MMTD-80 (Magnetic Measurements) at steps of 20º and 30º up to 500ºC. Stepwise alternating field demagnetization was also conducted with a GSD-5 (Schonstedt) up to 100 mT with no apparent improvement in the quality of the demagnetization trajectories. Subsequent measurement of the Natural Remanent Magnetization (NRM) after each demagnetization step was carried out in superconducting rock magnetometers (SRM755R by 2G Enterprises and GM400 by Cryogenic Consultants). Intensity of initial NRM of samples is in the range $9 \cdot 10^{-5}$ to $3 \cdot 10^{-3}$ A/m. Demagnetization diagrams of representative samples are represented in Figure 9a. In most of the samples a low temperature component is observed, which remains stable up to 250-300º C or 15 mT and which is mainly parallel to the present day magnetic field in geographic (*in situ*) coordinates. This component will not be taken into account for further calculations. The characteristic component of each sample was calculated by best-fit method after visual inspection of the demagnetization diagrams using the Paldir software developed by the Utrecht Paleomagnetic Laboratory. This component is generally well-defined between 300 and 400ºC or 15 and 50 mT, pointing to (titano)magnetite as the main remanence carrier. However, this is most probably not the only magnetic carrier. Rock magnetism analyses in previous studies have revealed the presence of iron-sulphides and high coercivity minerals together with magnetite in the limestones of the Boltaña, Yeba and Metils Fms. and in the *Alveolina* Limestone [*Mochales et al.*, 2012a]. The calculated characteristic components of each site were corrected for bedding dip with two different approaches (Table 1). The directions for sites far from the more prominent folds were corrected by rotating bedding to horizontal along the bedding strike line. On the other hand, directions measured on the Boltaña, Añisclo and Mediano anticlines were restored by taking the fold geometry into account. The dense dip data set recorded in the area, with up to 5000 readings of bedding attitudes, were used to calculate the geometric elements of the main folds or parts of major folds for each site or group of sites. Rotation of the measured magnetic declinations were performed taking into account the fold axis of the best cylindrical fit geometry as well as the best conical fit in some of the folds in order to avoid spurious rotation results [*Pueyo et al.,* 2003a]. Rotations were done using a code written for the Orient program by H. Charlesworth [*Charlesworth et al.,* 1989]. This procedure only yielded significantly different results for the Mediano anticline, for which directions were restored according to the conical geometry of the fold (Table 1).

[52] Mean directions were calculated for each site from the single characteristic components (Figure 9b and Table 1) and then compared with the reference Eocene direction for stable Iberia [*Taberner et al.,* 1999] to obtain a measure of the vertical-axis rotation at each site with its associated uncertainty [*Demarest*, 1983]. The reference direction was recalculated for the Ainsa coordinates with the via pole conversion method [*Noel and Batt*, 1990] getting a direction of 004/52.

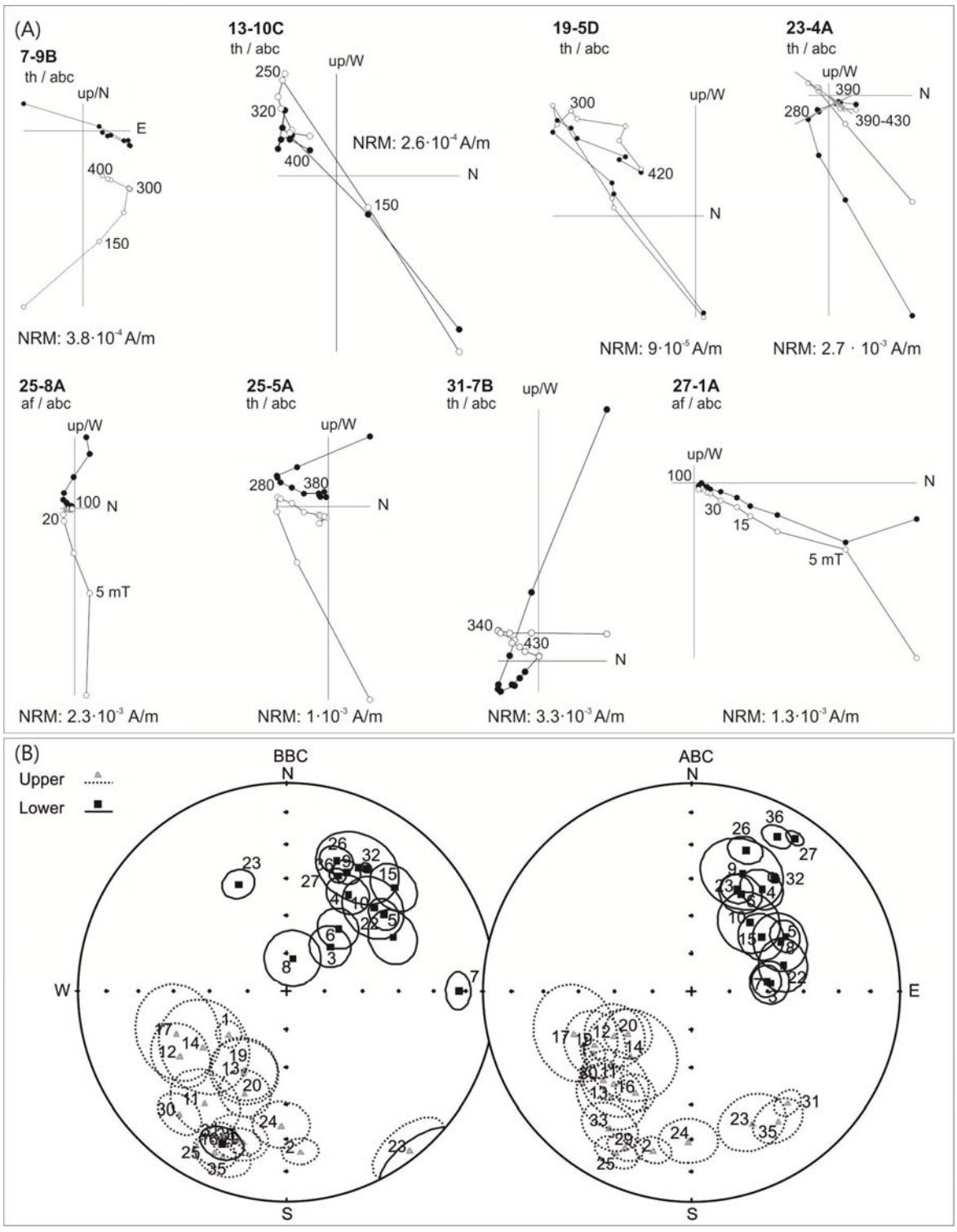

Figure 9. A) Zijderveld demagnetization diagrams of representative samples. Open (solid) symbols represent projection onto the vertical (horizontal) planes. All diagrams are represented after bedding correction (abc). AF: alternating field demagnetization, units are mT, TH: thermal demagnetization, units are ºC. Grey lines in sample 23-4A represent the characteristic components calculated: an intermediate temperature component between 280-390 ºC of reversed polarity and a high temperature component of normal polarity, defined between 390 and 430 ºC. B) Stereographic projection of the mean directions and obtained α_{95} at site level before (BBC) and after (ABC) bedding correction. Projections are on upper (grey color, dashed lines) and lower hemisphere (black color, solid lines).

5. Results of Paleomagnetic Data

5.1. Stability of the magnetization

[53] In order to verify the primary character of magnetization, fold tests [*McFadden*, 1990] and direction/correction tilt tests [*Enkin*, 2003] were performed on the Boltaña (sites 16, 17, 18, 19, 20, 21 and 22), Añisclo (sites 30, 31, 34 and 35) and Mediano anticlines (sites 3, 4, 5, 7, 8, 9 and 10) and on an outcrop-scale anticline in the footwall of the Almuzaras thrust, south of El Pueyo de Araguás (site 15) (Figures 3, 8 and 10). Positive fold and direction/correction tilt tests with a statistical best grouping around 100% of unfolding were obtained in site 15 and in the Boltaña and Mediano anticlines, pointing to a pre-folding origin of the magnetization, as previously documented by numerous studies in the region [*Mochales et al.*, 2012a,b; *Rodríguez-Pinto et al.*, 2012]. Although in these positive fold tests paleomagnetic directions group after bedding correction, some scatter in trends remains. This dispersion obeys both inherent different qualities of the paleomagnetic signal and the syntectonic character of the sediments, with younger materials recording less amount of rotation, as evidenced in the Mediano anticline. In the forelimb of the Añisclo anticline both negative fold and direction/correction tests were obtained with a best-fit at 5% of unfolding and a greater dispersion for tectonic-corrected (100% unfolding) magnetic vectors. Furthermore, tectonic-corrected directions from sites 31 and 35 indicate CCW rotations that would contradict the regional CW rotation pattern. The fold test is not significant for sites 30 and 34 as both sites show very small differences between *in situ* and tectonically corrected directions due to the low dip of bedding. However, the structural position of site 34 within the cleavage domain and the fact that sites 31 and 35 within the same fold yield a negative fold test lead us to interpret site 34 as remagnetized. Unfortunately, there are no arguments to establish the primary or secondary origin of magnetization of site 30. Therefore, sites 31, 34 and 35 (and maybe 30) are assumed to have been remagnetized after bed tilting but prior to the end of the regional rotation, and record a minimum value of rotation in this sector. Their remagnetization is interpreted to be related to their location in the more deformed forelimb of the Añisclo anticline where cleavage is well developed.

[54] In the northern sector of the study area, sites 23, 24, 25 and 26 are placed within a cleavage domain marked by the presence of a penetrative pressure-solution cleavage visible at outcrop scale (Figure 3). As previously said, Triassic, Cretaceous and Eocene rocks within this domain are affected by a generalized reversed polarity remagnetization event [*Oliva-Urcia and Pueyo*, 2007; *Oliva-Urcia et al.*, 2008; *Oliva-Urcia et al.*, 2012a] (red arrows in Figure 2). It should be noted that two components have been identified in site 23 (Figure 9a, Table 1): a "high temperature" component defined between 390 and 430 ºC yielding normal polarity and assumed to represent a primary magnetization, and an "intermediate temperature" component defined between 280 and 390 ºC which always exhibits reversed polarity and which we interpret to be linked to the pressure-solution remagnetization event reported by *Oliva-Urcia et al.* [2008]. Similarly, its neighboring site 26 also exhibits two components, including a reversed polarity intermediate temperature component defined between 250 and 350 ºC, although less well defined than in site 23. It is worth noticing that the NRM intensity of these sites is strikingly high (in the range of $2\text{-}8\cdot10^{-3}$ A/m). Sites 24 and 25 only reveal one characteristic component of reversed polarity, for which primary or secondary origin is difficult to test as no fold test can be performed due to the constant and low dip of bedding. However, the high intensity of the NRM in these sites (in the range of $3\text{-}4\cdot10^{-3}$ A/m), the constantly reversed polarity of the characteristic component, the low inclination of their tectonic corrected ChRMs and their structural position within the cleavage domain make these sites as suspect of being remagnetized during the pressure-solution remagnetization event. Furthermore, they record a remagnetized direction in continuation with the area described by *Oliva-Urcia and Pueyo* [2007] and *Oliva-Urcia et al.* [2008].

[55] Southwards, sites 27, 32 and 36 are also located within the cleavage domain and exhibit high intensity NRM's and anomalously low inclinations. However, these sites yield normal polarity contradicting the observed reversed polarity for the remagnetized component [*Oliva-Urcia et al.,* 2008]. Far from the cleavage domain, in the footwall of the Peña Montañesa thrust sheet, site 2 also shows an anomalously low inclination and an unrotated mean direction, which make it suspicious of being remagnetized.

5.2. Vertical-axis rotations in the Ainsa fold and thrust oblique zone

[56] Restored values of the mean magnetic declinations in the 36 sites studied in this work (Table 1) together with the published paleomagnetic data (Table S1 in supplementary material) display systematic variations around the Ainsa Oblique Zone (Figures 3 and 11). Practically all the samples record a clockwise vertical-axis rotation. Barring remagnetized sites, mean values range from ~ 80 º CW rotation (sites 3 and 7, lower Lutetian materials near the Mediano anticline) to ~ 20 ºCW (primary component of site

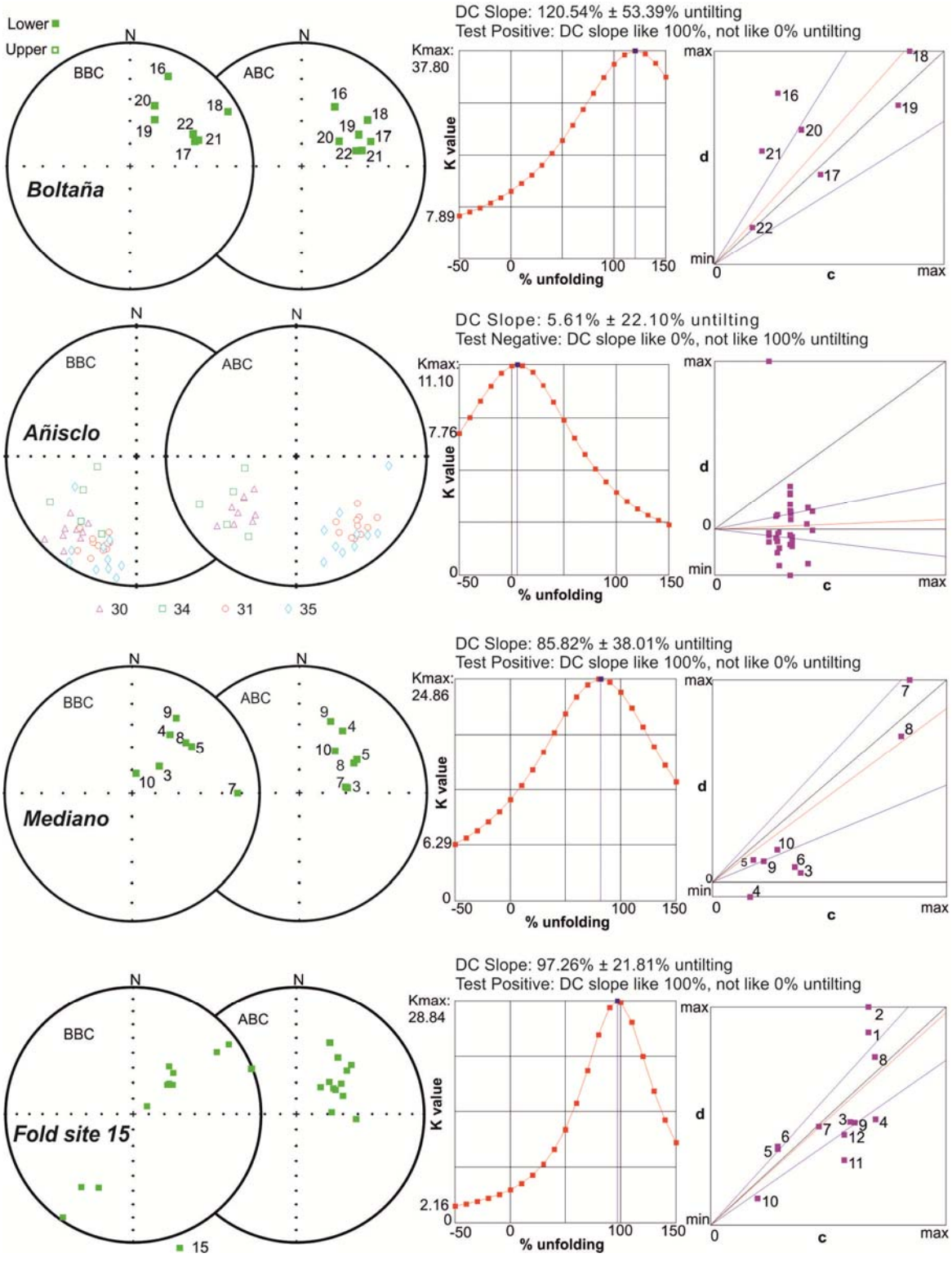

Figure 10. Results of the fold tests [*McFadden*, 1990] and the direction-correction tilt tests [*Enkin*, 2003] performed in the study area. Tests have been done in the Boltaña (sites 16 to 22), Añisclo (sites 30-31 and 34-35) and Mediano (sites 3 to 5 and 7 to 10) anticlines and in site 15, an outcrop scale anticline in the hangingwall of the Almuzaras thrust south of El Pueyo de Araguás. Open (solid) symbols represent projection on the upper (lower) hemisphere.

Table 1 – Geographic, stratigraphic, structural and paleomagnetic information of the studied sites. (1) UTM coordinates, (2) Stratigraphic age, (3) Structure: anticline or syncline name and fold axis trend and plunge (if determined), (4) bedding attitudes for the different sites in dip direction/dip, (5) N: number of samples considered per site, (6) tectonic corrections applied – cyl: cylindrical fold geometry considered, bc: bedding correction, con: conical fold geometry considered, corr3 represents the correction taken into account in this study, (7) Fold Test scale, O: outcrop, S: structure. Declination error calculated as α_{95}/cosI. The net rotation (β) has been obtained after comparison of the mean directions at the site level with the Eocene reference direction for stable Iberia from *Taberner et al.* [1999] relocated to the study area coordinates according to the via pole conversion method. Confidence values for the calculated rotations obtained after *Demarest* [1983].

23, middle Ilerdian (early Ypresian) materials cropping out at the northern edge of the Añisclo anticline) (Table 1). Plotted on a map these values reveal a clear pattern in the magnitude of vertical-axis rotation through space and time (Figure 11).

[57] Sites eastward of the studied area, in the central parts of the Montsec and Bóixols thrust sheets do not record any significant rotation, consistently with paleomagnetic data located further east [*Dinarès-Turell*, 1992; *Beamud et al.*, 2003] (Figure 11). An axial surface of rotation can be defined east of the study area (Figure 11), delineating the boundary between the non-rotated areas of the south central Pyrenees and the areas of the Montsec and Gavarnie thrust sheets that have experienced CW vertical-axis rotation. This axial surface coincides with the eastern edge of the circular bend connecting the N-S trending structures of the Ainsa Oblique Zone and the western edge of the Montsec thrust sheet with the E-W to WNW-ESE structural trend further east (Figure 11). The intersection between this eastern axial surface and the thrust front of Serres Marginals–Sierras Exteriores is characterized by a thrust reentrant (Figure 11).

[58] From the eastern axial surface, the amount of clockwise rotation increases westward toward the central part of the studied area, where structures predominantly trend N-S, both in the hangingwall of the Peña Montañesa-Montsec thrust sheet and in the Ainsa Basin. In this area, data presented in this study (Figure 3) and previous work (Figure 2) reveal rotations between ~ 25º and 80º CW (Figure 11). West of the Ainsa Oblique Zone, where structures trend WNW-ESE, clockwise vertical-axis rotations decrease to an average value of 10º to slightly higher values (Figure 11). According to *Dinarès-Turell* [1992]; *Bentham* [1992] and *Pueyo* [2000] a regional background rotational base value of 15º-20º can be assumed for the Gavarnie-Sierras Exteriores thrust sheet, recorded in the youngest sediments sampled, in the Escanilla and Campodarbe Fms. [*Pueyo*, 2000; *Bentham*, 1992; *Mochales et al.,* 2012b]. Therefore, in the N-S trending structures of the Ainsa Oblique Zone, the differential vertical-axis rotation values recorded by the Eocene sediments with respect to the Gavarnie-Sierras Exteriores regional value are in the order of 10º-70º (Figure 11).

[59] Vertical-axis rotations have been recorded all along the Sierras Exteriores structures [*Oliva-Urcia et al., 2012a; Ramón et al., 2012; Pueyo-Anchuela et al.*, 2012]. Further west, in the western Pyrenees, no significant vertical-axis rotations have been recorded by paleomagnetic data [*Larrasoaña et al*., 2003], defining a western limit for vertical-axis rotation.

[60] CW vertical-axis rotation can be further constrained to the hangingwall of the Gavarnie thrust and the older thrust sheets transported piggy-back in its hangingwall. Paleomagnetic data recorded in the north of the study area as well as westward, along the northern Mesozoic and Paleogene rocks of the Gavarnie thrust sheet (Sierras Interiores) [*Oliva-Urcia and Pueyo*, 2007b; *Oliva-Urcia et al.,* 2012b] indicate that the Triassic red beds in the footwall of the Gavarnie thrust sheet, north of the Cotiella thrust sheet, have not experienced any significant vertical-axis rotation (Figure 2) [*Oliva-Urcia et al.,* 2012b]. This is further confirmed by the absence of any major structural bend or curvature in the lower, younger basement-involved thrust sheets below the Gavarnie thrust north of the Ainsa Oblique Zone (Figure 2).

[61] The amount of CW vertical-axis rotation depends also on the age of the sampled sediments. The highest values of rotation have been recorded by the Lower Eocene sediments and these values generally decrease with age (Figure 11). Mediano anticline is the area where the relationship between age and amount of rotation can be established best (Figures 6 and 12a). If data from the present study are combined with data by *Dinarès-Turell* [1992] and *Bentham* [1992], data cover sediments from Ilerdian to upper Lutetian age over a relatively small area within which there are no major faults, making it reasonable to assume that there are no local factors interfering with regional rotation. It can be observed that rotations between 58º and 80º are recorded in sediments of Ilerdian and Cuisian age, and in one sample of lower Lutetian age (site 3). The magnitude of rotation then decreases progressively through Lutetian times to reach minimum values of rotation during the upper

	Location		Stratigraphy	Structure		Bedding	Magnetic Components														Magnetic Stability and Age			β Net rotation
							In situ (geograph. coord.)				Bed. Corr.													
	(1)		(2)	(3)		(4)	(5)				(6)										(7)			Reference direction 004/53
Site	Long	Lat	Stratigraphic Age	Structure	Trend/plunge	dip dir/dip	N	D&I (bbc)	α95	K	corr1	D(abc)	corr2	D(abc)	corr3	D&I (abc)	α95	K	Dec_err	Fold Test	% unfold	Stability	(Taberner et al, 1999)
1 (MM1)	271670	4695020	Middle Cuisian			003/18	8	233 / -61.7	5.2	113.8					cyl	237.9 / -43.7	5	109	6.92				54+/-10.3
2 HM1)	274350	4698290	Middle Cuisian			090/32	7	174.9 / -24	6.2	94.8	cyl	189.2	bc	199	con	193.4 / -23	6	115	6.52				9 +/-10
3 (FM1)	272800	4690350	Lower Lutetian	Mediano anticline		138/21	7	44.5 / 65.4	12.6	23.8	cyl	84.4	bc	86.7	con	83.6 / 58.8	8	24	15.44	S	85.82	pre	79+/-17.2
4 (FM2)	273030	4690520	Lower Lutetian	Mediano anticline		003/05	7	32.5 / 44	7.8	60.2					cyl	34.6 / 40	8	60	10.44	S	85.82	pre	31+/-12.9
5 (FM3)	273040	4690520	Lower Lutetian	Mediano anticline		185/11	8	51.7 / 40	5.6	97.8	cyl	59.6	bc	53.2	con	59.4 / 46.5	6	98	8.72	S	85.82	pre	55+/-11.6
6 (FM4)	277560	4689660	Lower - Middle Lutetian			355/15	8	39.6 / 57.8	7.8	51.5					cyl	26.9 / 46.2	8	52	11.56				23+/-13.9
7 (YM1)	270700	4689190	Upper Ilerdian	Mediano anticline		278/42	10	89.9 / 18.3	8.9	38.4					cyl	82.2 / 60	6	56	12.00	S	85.82	pre	78+/-14.2
8 (YM2)	272400	4690650	Upper Ilerdian	Mediano anticline		080/34	8	11.1 / 76.8	12	22.4					cyl	60.9 / 49.4	11	29	16.90	S	85.82	pre	57+/-18.5
9 (SM1)	267530	4688130	Middle Lutetian	Mediano anticline		264/12	6	30.1 / 31.5	15.2	20.3	cyl	23.1	bc	18.9	con	23.4 / 38	15	20	19.04	S	85.82	pre	19+/-20.5
10 (PM1)	269100	4687090	Middle Lutetian	Mediano anticline		248/14	7	46.2 / 41.4	9.6	40.7	cyl	39.7	bc	34.1	con	40 / 54.2	12	28	20.51	S	85.82	pre	36+/-21.9
11 (EM1)	268630	4684920	Upper Lutetian	Mediano anticline		186/09	7	216.1 / -34.1	12.6	23.8	cyl	219.9	bc	218.5	con	219.8 / -41.8	13	24	17.44				36+/-19
12 (AP1)	266540	4698290	Middle Cuisian	Mediano anticline		234/15	6	238.6 / -40.1	11.5	34.9	cyl	240.2	bc	238.1	con	239.9 / -55	12	35	20.92				56+/-22.3
13 (AP2)	267580	4705000	Middle Cuisian			061/20	7	207.6 / -53.8	10.7	74.7					cyl	217.2 / -36.4	13	52	16.15				33+/-17.9
14 (OA1)	272090	4705040	Lower - Middle Cuisian			193/11	5	235.8 / -50.2	17.3	20.5					cyl	223.2 / -55	18	19	31.38				39+/-32.3
15 (BA1)	266600	4701670	Upper Cuisian - Lower Lutetian			213/27	12	46 / 28.7	23.4	4.4	cyl	52.8	bc	43.1	con	51.9 / 54.8	9	27	15.61	O	97.26	pre	48+/-17.4
16 (AB)	251535	4704356	Lower Lutetian	Boltaña anticline	185/0	171/82	8	203 / 22	7.5	55.1					cyl	209 / -44	7.3	57.8	10.15	S	120.54	pre	25+/-12.4
17 (JB)	253031	4705874	Lower Lutetian	Boltaña anticline	185/0	258/85	6	249 / -43	16.9	16.6					cyl	250 / -40	17.6	15.4	22.98	S	120.54	pre	66+/-24.7
18 (YB)	254488	4706261	Upper Ilerdian	Boltaña anticline	185/0	269/54	8	241 / 10	22.4	7					cyl	235 / -35	22.2	7.2	27.10	S	120.54	pre	51+/-27.9
19 (BB)	257560	4705951	Upper Cuisian	Boltaña anticline	185/0	121/31	6	208 / -55	10.6	40.8					cyl	241 / -46	12.5	29.8	17.99	S	120.54	pre	57+/-20.2
20 (CB)	258408	4701832	Lower Lutetian	Buil syncline	185/0	159/69	7	202 / -46	9.4	42.3					cyl	236 / -60	9.5	41.6	19.00	S	120.54	pre	52+/-21.4
21 (SB)	260560	4700852	Lower Lutetian	Buil syncline	185/0	222/12	7	069 / 40	22	9.5					cyl	075 / 48	23	9.4	34.37	S	120.54	pre	71+/-35.2
22 (GB)	260682	4700467	Lower Lutetian	Buil syncline	185/0	203/19	9	063 / 42	9.3	31.5					cyl	074 / 52	10	27.3	16.24	S	120.54	pre	70+/-17.9
23 (AN1)	255461	4717875	Middle Ilerdian			095/45	8	336 / 43	6.4	75.1					bc	24 / 45	6	76	8.49				20+/-11.4
23 (AN1)	255461	4717875	Middle Ilerdian			095/45	8	142 / -4	12.5	20.6					bc	155 / -31	12	24	14.00			post	?
24 (AN2)	261380	4720904	Lower Ilerdian	Añisclo anticline	155/06	006/79	4	182 / -36	10	26					bc	181 / -29	10	26	11.43				-3+/-13.7
25 (AN3)	264261	4719592	Lower Ilerdian	Añisclo anticline	155/06	144/05	12	204 / -17	7	37					bc	205 / -16	7	37	7.28				21+/-10.5
26 (AN4)	255359	4717714	Middle Ilerdian			040/05	11	021 / 33	6	60					bc	021 / 28	6	60	6.80				17+/-10.2
27 (BL1)	264043	4713214	Upper Ilerdian	Añisclo anticline	175/10	068/33	10	024 / 39	3	276					bc	034 / 12	3	219	3.07			post?	30+/-8.2
28 (BL2)	255208	4710255	Upper Ilerdian	Boltaña anticline	185/0	274/83	3	057 / 58	24	27					bc	073 / 19	24	27	25.38				69+/-26.5
29 (BL3)	255847	4710475	Upper Ilerdian	Boltaña anticline	185/0	092/17	6	196 / -26	6	132					bc	203 / -20	6	131	6.39				19+/-9.9
30 (BL4)	260898	4710445	Middle Ilerdian	Añisclo anticline	185/20	200/20	9	221 / -23	8	48					bc	225 / -40	8	45	10.44	S	5.61	post?	41+/-12.9
31 (BL5)	259503	4712061	Middle Ilerdian	Añisclo anticline	175/10	081/90	11	204 / -26	5	85					bc	139 / -30	5	73	5.77	S	5.61	post	20+/-9.6 (minimum)
32 (BL6)	267643	4710863	Upper Ilerdian			146/04	11	033 / 30	2	582					bc	036 / 33	2	504	2.38	S		post?	32+/-8
33 (BL7)	256609	4711485	Upper Ilerdian	Boltaña anticline	185/0	110/26	7	198 / -27	10	42					bc	211 / -25	10	42	11.03				27+/-13.4
34 (BL10)	258686	4713538	Upper Ilerdian	Añisclo anticline	175/10	090/10	8	220 / -45	16	14					bc	227 / -38	20	15	25.38	S	5.61	post?	43+/-26.5
35 (BL11)	259195	4712972	Middle Ilerdian	Añisclo anticline	175/10	080/84	11	201 / -16	17	12					bc	146 / -26	9	33	10.01	S	5.61	post	18 (minimum)+/-12.6
36 (BL12)	268580	4710575	Upper Ilerdian			030/20	11	027 / 36	5	104					bc	029 / 16	5	100	5.20			post?	25+/-9.2

Lutetian to Bartonian (15º to 35º) (Figures 3, 6, 11 and 12a).

[62] This pattern of decreasing rotation with age is also observed across the Boltaña anticline along the Ara River. Sites in the pre-folding sequence of Cuisian age (sites 18, 19 and D21, Figures 7 and 12b) and lower Lutetian age (sites 17, 20, 21 and 22, Figures 3, 7 and 12b) present CW rotations ranging from 50 to 70º, whereas younger upper Lutetian sediments located above the unconformity at the bottom of the synfolding package present less rotation, although still significant (site 16 and sites from *Pueyo* [2000]) (Figures 7 and 12b).

Considering the sites of our study and the sites recently published by *Mochales et al.* [2012b], an average CW vertical-axis rotation of ~ 55º can be estimated for the pre-folding sediments in this transect of the Boltaña anticline (Figure 12b). Unpublished data by *Mochales* [2011] in the middle Lutetian-Bartonian growth sediments on the western limb of the Boltaña anticline, in the area of the map in Figure 7, confirm the decrease of the rotation with age in the synfolding sediments, and therefore the synchronicity between folding and vertical-axis rotation. If we plot

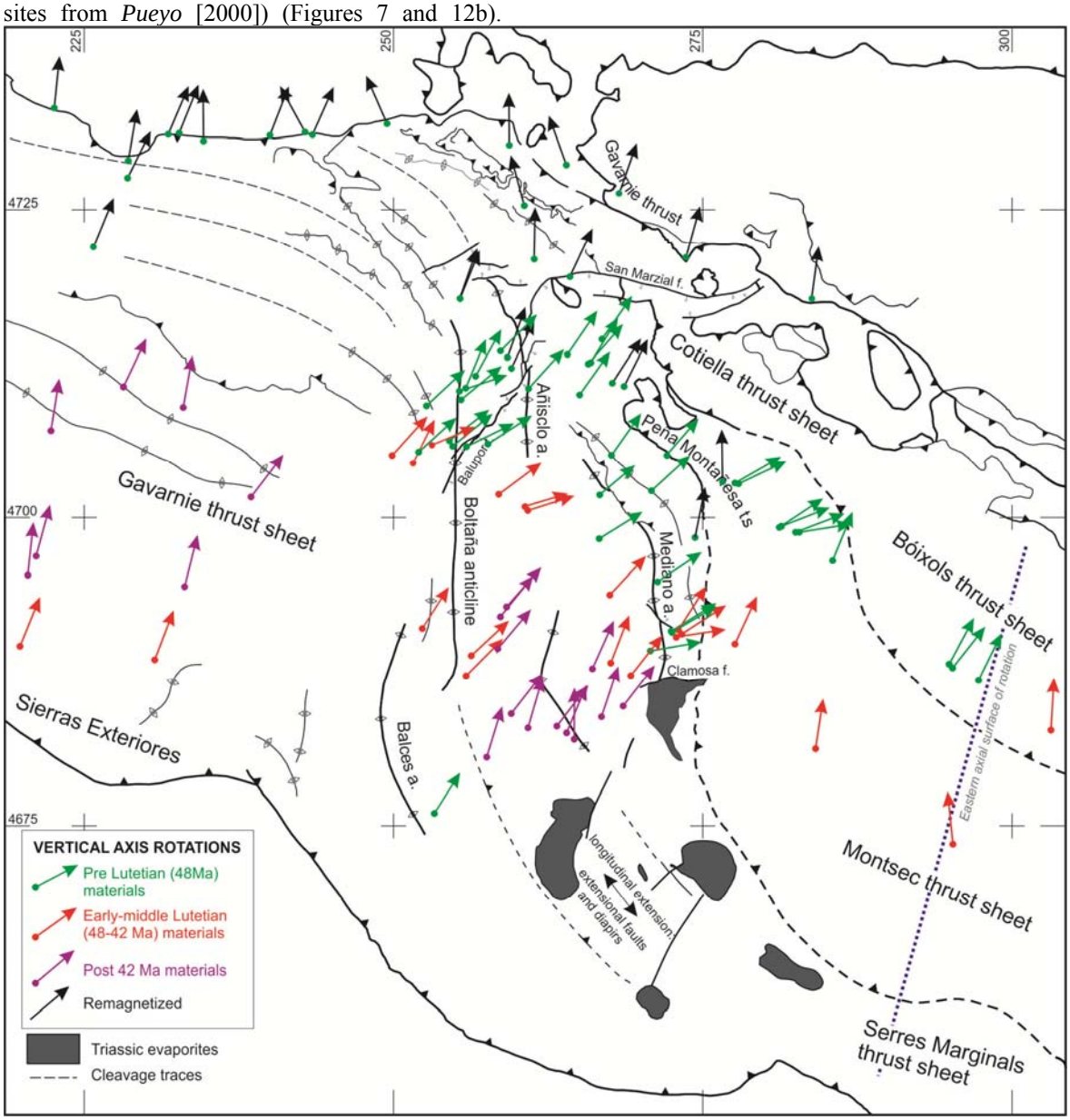

Figure 11. Simplified map and sketch of the vertical-axis rotations within the study area. Vertical-axis rotations are grouped in three categories according to the age of the sampled sediments. Remagnetized sites are distinguished as black arrows. f: fault, a:anticline, t.s.: thrust sheeet

together our data with the data set from *Mochales et al.* [2012b], including data for the southern edge of the Boltaña anticline, a linear fit with an almost constant CW vertical-axis rotation of about 50º is

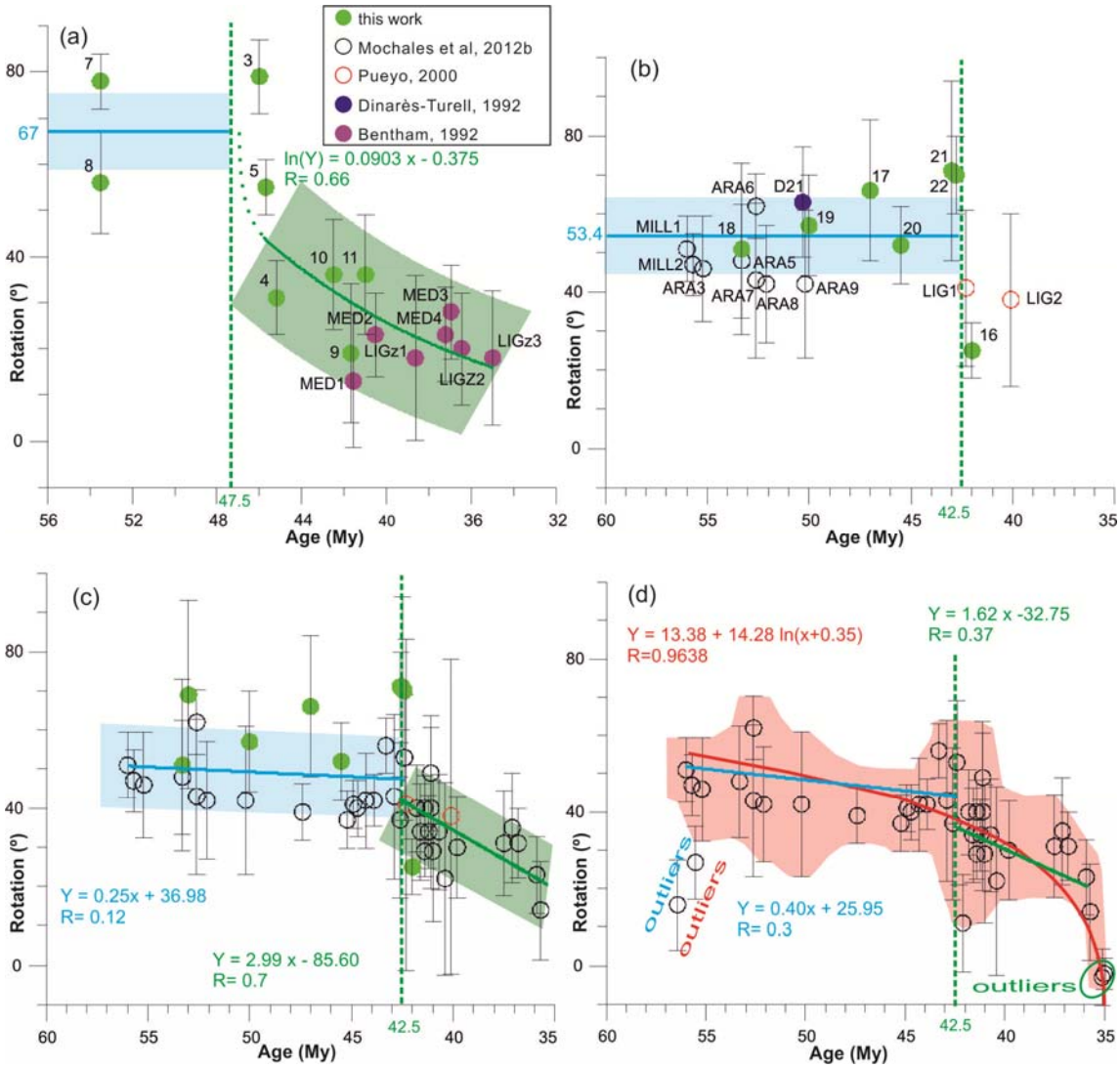

Figure 12. Rotation vs. time plots for the Mediano (a) and the Boltaña anticlines (b to d). (a) Data for the Mediano anticline from this study and from *Bentham* [1992] as cited in *Mochales et al.* [2012b]. Blue line within the amount of rotation represents the mean rotational angle for the data before the growth of the structure at 47.5 Ma. After 47.5 Ma the data follow a decreasing exponential function. (b) Data from this and previous studies along the Ara River transect (sites located in Figure 7). Blue line within the amount of rotation represents the mean rotational angle for the data before the growth of the structure at 42.5 Ma, the light blue band represents a +/- 10º envelope. (c) Data from this work and from previous studies fit by linear regressions before and after 42.5 Ma. Sites marked as outliers in (d) have been removed in this plot, as well as site CAS5 from *Mochales et al.* [2012b]. (d) Data from *Mochales et al.* [2012b] with logarithmic and linear regression adjustments. Red line represents the logarithmic adjustment published in *Mochales et al.* [2012b]. Blue line represents a new linear regression for data before the growth of the anticline at 42.5 Ma. Green line represents the linear regression for data within the growth strata. Sites marked as outliers in the figure have not been included to calculate the regression lines.

obtained for the older sediments cropping out in the core of the Boltaña anticline (Ypresian-lower Lutetian) (Figure 12c). Most significantly, a change in the rotational pattern is observed at about 42.5 Ma: the age of the oldest sediments above the unconformity on the western limb of the Boltaña anticline, and therefore the interpreted onset of fold growth. Younger sediments show a decrease in the amount of vertical-axis rotation with time from middle Lutetian to Priabonian times (Figure 12c, d).

[63] Apart from the regional E-W gradient of the vertical-axis rotation across the N-S trending structures of the Ainsa Oblique Zone, and differences with the age of the sampled sediments, a north-south gradient is observed in map-view

along the N-S trending folds. This gradient stands out very clearly along the Boltaña and Añisclo anticlines (Figures 3 and 11). Highest rotation values are located in the central part of the Boltaña anticline and in the southern termination of the Añisclo anticline (Figure 11). These values decrease progressively northward, regardless of the continuation of the folds northward with a near-constant N-S trend. Such a decrease of the rotation angle is the result of the superposition of two effects. The most evident one is the remagnetization of internally deformed areas near the northern terminations of the Añisclo and Boltaña anticlines, north of the cleavage front [*Oliva-Urcia and Pueyo,* 2007; *Oliva-Urcia et al.,* 2008]. However, a true gradient in the amount of vertical-axis rotation along strike is also observed when taking account the primary component of sites 23 and 26. This rotational gradient can be explained by the lateral propagation of folds during syn-rotational folding, and a related migration of the pin-point of vertical-axis rotation during fold growth and rotation (Figure 13).

[64] The La Fueba fold and thrust structures and the Peña Montañesa thrust sheet show a significant CW vertical-axis rotation with values higher than 35º and up to 80º, with the exception of site 2, which has been probably remagnetized as discussed before, or reveals the effect of local deformation (Figure 11). In the area where thrusts and folds of the La Fueba system trend NW-SE the declination is roughly perpendicular to the thrust trend and parallel to the main and earlier striations along the shear planes (Figures 3, 8 and 11). Further south where thrusts bend to a more N-S trend, the amount of vertical-axis rotation also increases (site 1). Conversely, further north, in the Cinca valley where the structural trend is also N-S, as indicated by the orientation of cleavage, the amount of vertical-axis rotation decreases to values of 30º (sites 27, 32, 36 from this study and D15, D16, D17 and D18 from Dinarès-Turell, 1992). This reveals a rotation gradient in a N-S direction that is similar to what is observed further west in the Añisclo and Boltaña anticlines related to the northward migration of the rotational pin-point (Figure 13).

5.3. Paleomagnetic directions vs. structural trend

[65] A strike test has been performed in order to evaluate changes in the paleomagnetic data with respect to the structural trend (Figure 14 and Table S2 in supplementary material) [*Schwartz and Van der Voo,* 1983; *Eldredge et al.,*1985; *Lowrie and Hirt,* 1986; *Yonkee and Weil*, 2010b]. Application of this test is not straightforward in the study area, regardless the significant amount of available paleomagnetic data and the pronounced change of strike of the Ainsa Oblique Zone structures with respect the regional Pyrenean structural trend (Figure 11). Difficulty of the application of the strike test is due to the syntectonic nature of most of the sampled sediments, the remagnetization of the sites located in the most deformed northern areas and the longitudinal growth of structures during the vertical-axis rotation (Figure 13). Strike tests were designed to be applied in pre-tectonic rocks on long, linear, continuous mountain belts [*Schwartz and Van der Voo,* 1983; *Lowrie and Hirt,* 1986]. In the study area evaluation of the tectonic curvature by the strike test requires a filtering of the sites. Accordingly, we have only used non-remagnetized sites in pre-folding sediments located near the core of the structures. In addition, we have rejected the sites that yield paleomagnetic directions with high dispersion (α_{95}>15º) or anomalous inclination (Table S2).

[66] The structural trend for each plotted site has been calculated from the analysis of bedding (about 5000 dip measurements in the study area) and fold trace data. For the sites located eastwards of the study area the structural trend has been estimated from structural map patterns of the main structures at kilometric-scale areas. In this way, we have reduced to a minimum the dispersion of individual strike values of bedding and averaged out local noise.

[67] The strike test on filtered data of the study area including areas further east (where structures show a regional Pyrenean WNW-ESE trend) yielded a slope of the regression line of 0.46 and a t-test for the significance of the slope of 5.514 (red line in Figure 14). This value is higher than the t for the null hypothesis at 95% of probability (2.045) and therefore the obtained slope is significant. If sites from the Boltaña anticline are removed from the analysis because of its younger age (grey line in Figure 14), the slope of the strike-test for the sites along the older and inner structures of the Gavarnie thrust sheet increases to 0.58 with a t-test value of 5.69. In this case, the slope of the regression line is also significant as the t for the null hypothesis at 95% probability is smaller (2.080) than the obtained t-test value. Finally, if sites suspicious of remagnetization in these inner structures are also removed in the strike test (black line in Figure 14) both the slope and the t-test values increase to 0.649 and 6.927, respectively. This regression is also significant as t is bigger than the t for the null hypothesis at 95% probability (2.093).

[68] All these values indicate that the studied thrust salient is a progressive arc with about 50% secondary curvature related to vertical-axis rotation. For the older structures of the Gavarnie thrust sheet, secondary curvature would represent up to 65%.

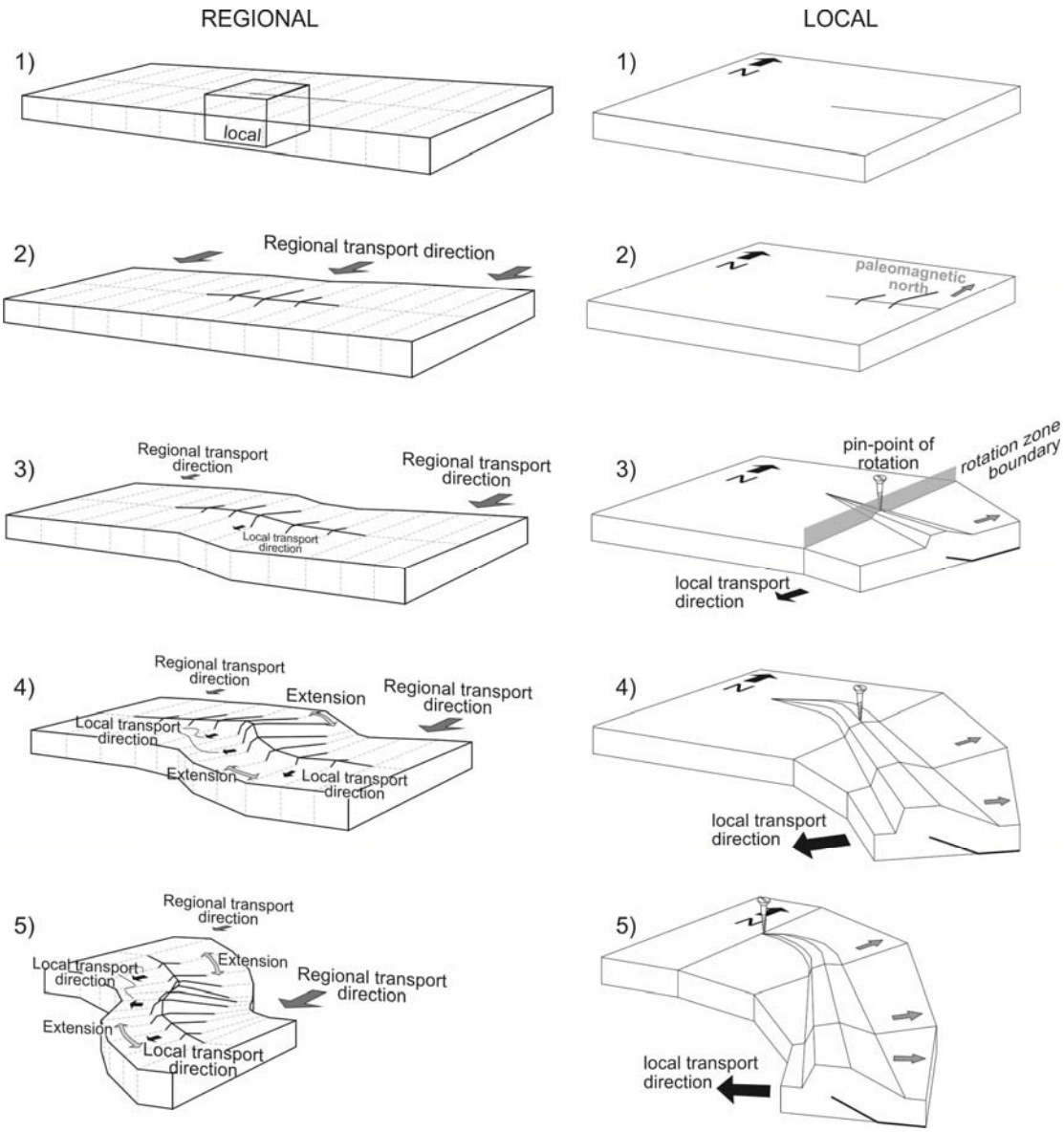

Figure 13. Schematic diagram showing the different stages of the evolution of the main fault-related folds of the Ainsa Oblique Zone and their longitudinal propagation during the CW vertical-axis rotation. The box in stage 1 of the regional evolution marks the area enlarged and shown in the local evolution section (growth of the Boltaña anticline). Note the differences on the amount of vertical-axis rotation along-strike in the fold termination despite the constant strike of the fold. Regional and local transport directions are distinguished. Grey arrows on local evolution section represent paleomagnetic directions.

6. Discussion: structural evolution and kinematics

[69] From all the above described structural features and the paleomagnetic data it follows that there is an obvious relationship between the N-S trend of structures in the Ainsa basin and the CW vertical-axis rotations recorded by the measured paleomagnetic directions. The N-S trend is a consequence of CW rotation of the entire Ainsa Oblique Zone, synchronous to the growth of the folds, indicating that the curvature is progressive in origin. However, determining the precise kinematics and origins of this vertical-axis rotation is not possible without integrating paleomagnetic data with structural, sedimentologic and orogen-scale constraints.

[70] The importance of integrating other types of data when interpreting paleomagnetic data in this area stems from the fact that the magnitude of the vertical-axis rotation is not constant over the Ainsa Oblique Zone regardless the constant strike of the

structures (as indicated by the significant dispersion of data in the strike test plot, Figure 14). The vertical-axis rotation depends on many factors such as the position of sites relative to structures, the age of the sampled sediments, superposition of secondary magnetization during deformation, and local deformation by minor structures, among others. In addition to these different factors, paleomagnetic data may show significant error bars. As a consequence, when interpreting the paleomagnetic data of the area, significant different interpretations may arise with the same data set if the combination of the aforementioned factors is not borne in mind. Most importantly, the integration of the stratigraphic and structural data with the paleomagnetic data in this study has reduced uncertainties of the interpretation of the paleomagnetic data and constrained the proposed structural evolution for the Ainsa Oblique Zone. Analysis of paleomagnetic data and statistical tests or regressions to fit the distribution of data should be conditioned by geological constraints, as previously discussed for the strike test. Otherwise, the conclusions obtained may contradict geological field observations or regional scale constraints, and consequently, have no validity.

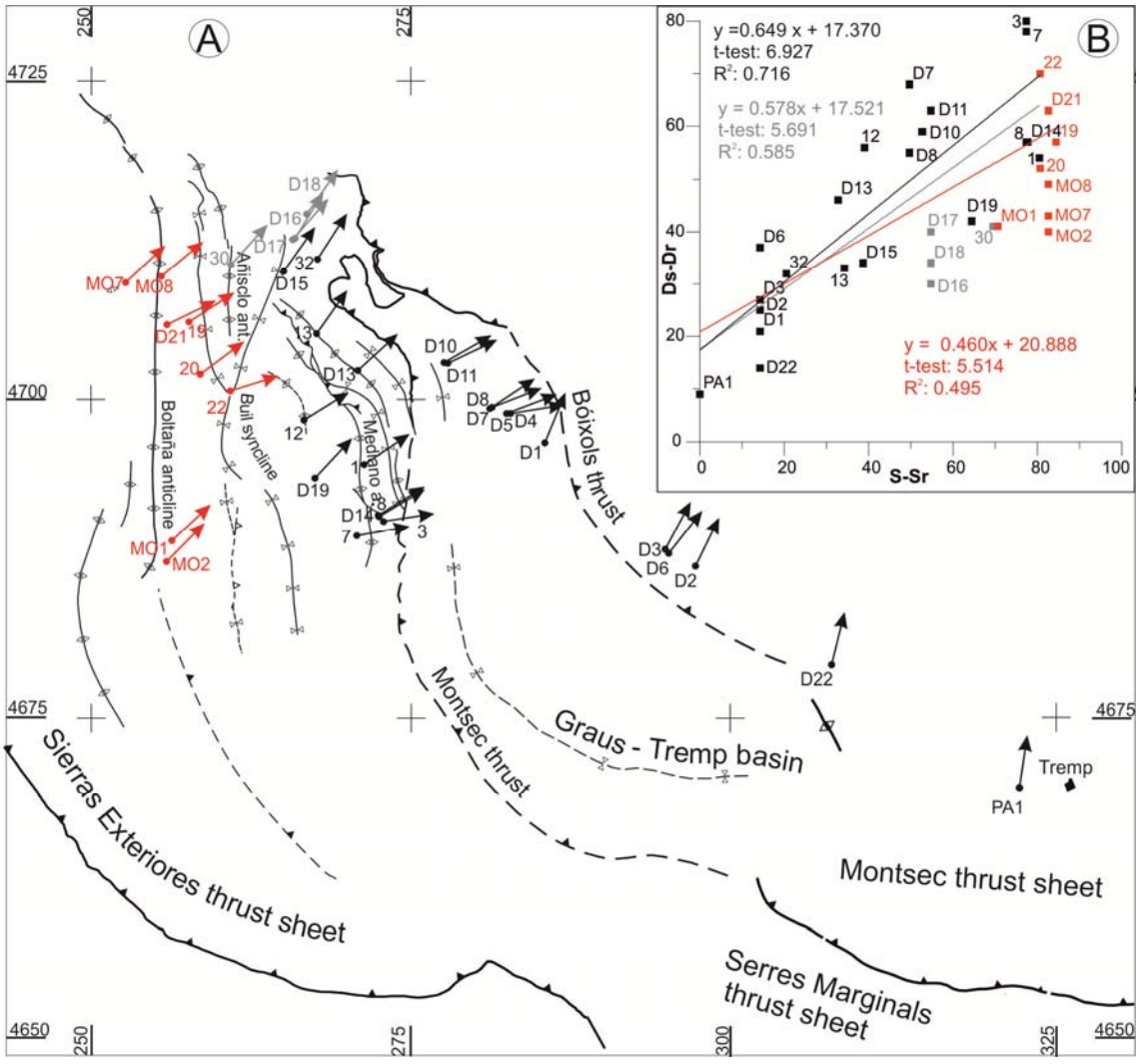

Figure 14. (A) Simplified structural map with location of the paleomagnetic sites used for the strike-test of the study area. Only sites from pre-tectonic units with α_{95} less than 15º have been considered (see supplementary material Table S2 for details). Red dots represent sites from the Boltaña anticline and the grey ones represent sites suspicious of being remagnetized. (B) Strike-test for the Ainsa Oblique Zone. Regression lines and t-test parameters for the significance of the slope of the obtained regression are indicated. Black line represents the regression taking into account only the sites represented in black (without the Boltaña sites and the ones suspicious of being remagnetized). Grey line represents the regression taking into account black and grey sites (without the Boltaña sites). Finally, all the sites (black, grey and red) have been considered to obtain the red regression line.

6.1. Age and magnitude of the vertical-axis rotation

[71] Two distinct CW vertical-axis rotation events can be defined in the study area: the first one during early Lutetian to Priabonian times, and the second one of Priabonian to Oligocene age.

The older vertical-axis rotation event (early Lutetian to Priabonian) is restricted to the Gavarnie thrust sheet and older thrust sheets in its hangingwall that were passively rotated (*e.g.* Montsec, Bóixols). Vertical-axis rotation occurred during the emplacement of the Gavarnie-Sierras Exteriores thrust sheet (Middle to Late Eocene) and the development of the folds and thrusts of the Ainsa Oblique Zone. This synchronicity is documented by the rotation of the Mediano and Boltaña anticlines during growth. Both anticlines record significant CW vertical-axis rotation in their pre-growth strata (50º-70º) and progressively less rotation in their syn-growth strata. In the case of the Mediano anticline, whose growth starts during the early Lutetian [*Poblet et al.*, 1998; *Fernández et al.*, 2012], the decrease in the amount of rotation can be observed from 47.5 Ma (the age of the unconformity marking initial fold growth, *Poblet et al.*, [1998]) onwards (Figure 12a). Syn-folding rotation of the Mediano anticline continued at a decreasing rate at least into the Priabonian (Figure 12a). A similar relationship between folding and vertical-axis rotation is observed for the Boltaña anticline. Growth of this anticline starts at approximately 42.5 Ma (as discussed above). This age threshold corresponds to a change in the magnitude of CW vertical-axis rotation when analyzing data along a single transect across the Boltaña anticline (to reduce the potential impact of lateral gradients in vertical-axis rotation, Figure 12b). This age coincides with the inflection point in the magnitudes of vertical-axis rotation documented by *Mochales et al.* [2012b] at ~ 42 Ma. Vertical-axis rotation during the growth of the Boltaña anticline is interpreted to have been relatively constant in rate, although it might have decreased with time as in the case of the Mediano anticline (Figures 12b, c).

[72] This interpretation counters that by *Mochales et al.* [2012b], who propose the existence of a pre-folding CW rotation of 15º and an acceleration of vertical-axis rotation after 42 Ma (Figure 12d), based on the analysis of averaged data from different locations along the trend of the Boltaña anticline. However, given the significant lateral variations in vertical-axis rotation recorded in the study area, a more conservative approach to analysis is required. As way of illustration, if data from the Boltaña anticline presented in this paper are added to the data by *Mochales et al.* [2012b], the pre-folding rotation is no longer evident due to the greater scatter of data (which is due to the variations in vertical-axis rotation of the anticline along strike and evidenced by a lack of correlation between age and rotation magnitude) (Figure 12c). Furthermore, the acceleration in the rate of vertical-axis rotation documented by these authors is strongly conditioned by two facts. Firstly, their analysis is based on treating data from long before the onset of fold growth (more than 13 Ma prior to onset of fold growth) and data synchronous with fold growth together, without allowing for the possibility of a change in the kinematics of vertical-axis rotation prior to and synchronous with folding. Secondly, they incorporate in their analysis the two youngest samples, dated as 35 Ma, that yield a near zero vertical-axis rotation (compare Figures 12c, d). However, sites sampled nearby by *Bentham* [1992] in sediments of the same age, although less robust than some of the data by *Mochales et al.* [2012b], yield CW vertical-axis rotations of ~ 20º +/- 10º, that are consistent with the existence of a second (Priabonian-Oligocene) regional CW vertical-axis rotational event already solidly documented by multiple authors [*Bentham*, 1992; *Pueyo*, 2000; *Oliva-Urcia and Pueyo*, 2007b; *Oliva-Urcia et al.*, 2012b], and discussed below.

[73] Synchronous with growth and rotation of the Sobrarbe folds, the previously developed La Fueba thrusts to the northeast were reactivated as oblique to dextral strike-slip faults as they were passively rotated as indicated by the spread in and superposition of fault kinematic indicators (Figure 8).

[74] During this first event of rotation, the process of vertical-axis rotation continued to progress westward beyond the Boltaña anticline to the structures of the Sierras Exteriores [*Millán et al.*, 2000]. *Pueyo et al.* [1997] suggested a diachronous end of the vertical-axis rotation along the Sierras Exteriores from early Priabonian (Arguis area) to Late Oligocene at their western edge, overlapping temporally with the second rotation event and making them difficult to distinguish.

[75] At the last stages of this first rotational event (late Lutetian-Bartonian) a secondary magnetic component developed in the most deformed and internal areas affected by penetrative cleavage. The limited amount of rotation affecting this secondary component indicates it is mostly posterior to the main rotation event in the Gavarnie thrust sheet. *Oliva-Urcia and Pueyo* [2007] suggested that the age of the remagnetized secondary component is younger than basement tilting in the hangingwall of the Gavarnie thrust, but synchronous to cleavage development. In addition, these authors attributed the average 14º CW vertical-axis rotation of this secondary component as well as the 8º CW rotation of the

primary component in Upper Cretaceous sediments to a moderate rotation related to a gradient in shortening during the emplacement of the Guarga thrust sheet. The age of cleavage formation and remagnetization is consistent with the late stages of growth and CW vertical-axis rotation of the Añisclo anticline, its related cleavage and remagnetization of the forelimb where cleavage infilling occurred, as will be further discussed in the next subsection.

[76] The second and younger CW vertical-axis rotation event, Priabonian-Oligocene in age, is responsible for the rotation of the remagnetized components. This event is related to the underthrusting of the Guarga basement unit below the northern parts of the Ainsa and Jaca basins (Figures 1 and 15a) and the southward-directed transportation of the previously deformed Mesozoic and Paleogene sediments of the Gavarnie-Sierras Exteriores thrust sheet [*Martínez-Peña and Casas-Sainz*, 2003; *Fernández et al.*, 2012]. It affected a broader area than the previous one, including all the Sierras Exteriores (Figure 12). In this work an average of 10º has been attributed to this rotation event, taking into account not only paleomagnetic data of the internal areas [*Oliva-Urcia and Pueyo*, 2007b; *Oliva-Urcia et al.*, 2012b], but also the CW vertical-axis rotation experienced by the younger sediments in the Sierras Exteriores and the sites located westward of the eastern axial surface of rotation (Figure 11).

[77] This second CW rotation event was enhanced by further southward displacement of the south Pyrenean thrust sheets in its central realm (Bóixols, Montsec and Serres Marginals) on top of the Lower Priabonian-Oligocene (?) salts of the Ebro basin. This is accompanied by a change in the structural configuration from a footwall flat along the Lower Priabonian evaporites under the Serres Marginals thrust sheet in the east [*Teixell and Muñoz*, 2000], to a footwall ramp cutting the equivalent age clastics under the Sierras Exteriores in the west [*Millán et al.,* 2006; *Pueyo et al*., 2004]. The overall result is a change in the structural trend of the Sierras Exteriores and eastern Jaca basin toward a more NW-SE trend (Figures 1 and 2).

[78] Rotation during this second event was synchronous with the CCW vertical-axis rotation of about 20º reported in the NE-SW trending oblique zone at the eastern edge of the central Pyrenees [Sussman et al., 2004].

[79] Once the space/time relationships between the oblique structures of the Gavarnie thrust sheet and the CW vertical-axis rotations have been established, a cause-effect relationship can be assumed between them (as also indicated by the strike test of paleomagnetic data in the pre-folding sediments, Figure 14). It can be interpreted that the onset of the vertical-axis rotation was related to the onset of the contractional deformation in the Gavarnie thrust sheet. This onset was not synchronous and migrated from NE to SW. The oldest structures are the Mediano and Añisclo anticlines that started to develop at early Lutetian times (or even at late Cuisian times) as clearly revealed by the preserved growth sediments [*Poblet et al*., 1998; *Fernández et al.*, 2012]. Onset of folding was coeval with the onset of vertical-axis rotation as demonstrated by paleomagnetic data (Figures 6, 7 and 12). Deformation migrated to the SW to form the Boltaña anticline at middle Lutetian times, as did the onset of vertical-axis rotation (Figures 7 and 12). An average total CW vertical-axis rotation of 45º to 55º occurred during the development of the Boltaña and Mediano anticlines, once we subtract the younger Priabonian-Oligocene post-folding rotation of at least 10º.

6.2. Mesostructures development and remagnetization

[80] Structures related to layer-parallel shortening such as cleavage and fracture systems developed since the earlier stages of folding in the Ainsa Oblique Zone. These mesostructures, together with older structures in the La Fueba and Monte Perdido fold and thrust systems, experienced CW vertical-axis rotation as they developed. They preserved the parallelism relative to fold axes because the local shortening direction remained perpendicular to the fold axes during CW vertical-axis rotation due to divergent slip trajectories (that can be accounted for with a progressive curvature model).

Regional pressure solution cleavage and fracture systems developed during the deformation of the Gavarnie thrust sheet and consequently during the CW vertical-axis rotation that formed the Ainsa Oblique Zone. The development of the pervasive regional cleavage has been interpreted to occur in the Gavarnie thrust sheet at temperatures higher than 190ºC and up to 240ºC, based on illite cristallinity data [*Holl and Anastasio*, 1995] and oxygen isotope and fluid inclusion microthermometry analysis of veins related with the displacement of coeval thrusts [*Lacroix et al.,* 2011]. Such temperature requires a significant burial of the youngest deformed lower Eocene turbidites, which can be estimated for a given geothermal gradient. Calculated paleogeothermal gradients in the area vary from 15ºC/km [*Holl and Anastasio*, 1995b] to 34ºC/km [*Lacroix et al.,* 2011] giving a range of burial at the cleavage front between 12 and 6 km, respectively. Such burial cannot be explained only by sediment burial of the synorogenic sediments. Burial resulted from thrust sheet stacking of the Monte Perdido thrust sheets and, mostly, the Cotiella-Peña Montañesa thrust sheets (with stratigraphy more than 5 km thick)

above. Basement-involved lower and younger thrusts (Bielsa and Guarga thrusts among others, Late Eocene-Miocene in age) were responsible for the subsequent tilting and exhumation of the Cotiella, Peña Montañesa and Gavarnie thrust sheets in the northern part of the studied area, and as a consequence they decreased tectonic burial as they developed (Figure 2). The southern tip of such tilt by basement underthrusting corresponds with the cut-off line of the Paleozoic basement in the hangingwall of the Guarga thrust sheet, which runs parallel to and near the trace of the Guarga synclinorium (Figures 2 and 15a) [*Fernández et al.,* 2012].

[81] Cleavage started to develop in the footwall of the Peña Montañesa and Cotiella thrust sheets at late Ypresian to early Lutetian times when the La Fueba and Monte Perdido fold system formed. Cleavage is pervasive in the Monte Perdido system as it developed under the Peña Montañesa thrust sheet (present outcrops are located northward of the Castillo Mayor klippe, under the now eroded western prolongation of the Peña Montañesa thrust, Figure 2). In the La Fueba system, cleavage is restricted to the areas near the axial surface of the fault-related folds at hectometric to regional scale. Cleavage continued its development during the middle Lutetian to Late Eocene times when the Gavarnie thrust was active and the Sobrarbe fold system developed in its hangingwall.

[82] According to *Tavani et al.* [2006] a regional and delocalized spaced pressure solution cleavage developed in the Upper Cretaceous-Lower Eocene sediments since the early stages of folding by layer-parallel shortening and continued developing during a late localized deformation stage by selective infilling of solution cleavage in the forelimb and in the near foreland. Cleavage in the Añisclo anticline developed about 1-2 km below the synorogenic topographic surface as growth sequences of the turbidites of the Ainsa basin are well preserved (Figure 4). The location and age of these sediments constrain not only the burial depth, but also the timing of fold growth and cleavage development as previously described.

[83] A pervasive remagnetization characterized by a high intensity reverse magnetic component has been observed in the rocks deformed by regional cleavage [*Oliva and Pueyo*, 2007; *Oliva-Urcia et al.,* 2008, 2009, 2012b] and in the samples collected in the northern areas, where pressure solution cleavage is well developed (generally over 20% of shortening). The presumed mechanism for explaining this remagnetization is the liberation and reorientation of the magnetic carrying minerals in the cleavage domains as solution progressed during cleavage intensification [*Evans and Elmore*, 2006; *Oliva-Urcia et al*., 2008; *Elmore et al.,* 2012]. According to *Oliva-Urcia et al*. [2008], remagnetization is post-folding and post-tilting of the basement in the Gavarnie thrust sheet, as suggested by the fold tests and the amount of vertical-axis rotations observed with respect to other non-remagnetized sites. Nevertheless, folding and basement tilting in the hangingwall of the Gavarnie thrust sheet can be perfectly synchronous. Cleavage developed from the earliest stages of folding, and remagnetization must have been synchronous to the development of axial plane cleavage, if we accept the proposed mechanism. Consequently, remagnetization probably occurred at the last stages of folding, once a threshold in the amount of strain was achieved to permit the reorientation of minerals in the cleavage domains. Our data supports this idea as the sites sampled in the forelimb of the northern part of the Añisclo anticline are remagnetized but yet they show a moderate CW vertical-axis rotation (21º-25º). These moderate angles of rotation would record the last stages of rotation of the Añisclo anticline after cleavage developed significantly in the forelimb. Remagnetization might also be a somewhat diachronous event; if it was synchronous with cleavage intensification at the last stages of folding and CW rotation in the Ainsa Oblique Zone it would have occurred as deformation progressed west and south through time.

[84] During the middle Lutetian-early Bartonian time interval, which is the most probable age of cleavage intensification in the Gavarnie thrust sheet, reversal polarities are predominant. This could explain the observed reverse polarity in the remagnetized sampled sites. On the other hand, the moderate values of CW vertical-axis rotation of the normal polarity sites 27, 32 and 36 and the high intensity of the NRM, together with their location in the highly cleavaged area trending N-S east of the Añisclo anticline suggest that they were affected by remagnetization at the last stages of CW vertical-axis rotation. The normal polarity of the magnetization would fit with a remagnetization related with a cleavage that developed progressively during Middle and Late Eocene times in the Gavarnie thrust sheet and the CW vertical-axis rotation at its eastern part. Further work should be conducted in the area to confirm these ideas. Finally, the moderate CW rotation of the remagnetized component in the Sierras Interiores during the second Late Eocene-Oligocene CW vertical-axis rotation event would be also consistent with a Mid- to Late Eocene age for the remagnetization.

6.3. Restoration and structural evolution

[85] The structures of the Ainsa Oblique Zone have been restored in map view, taking into account paleomagnetic data as well as structural and sedimentological data (Figure 15). For simplification the Ainsa Oblique Zone and

surrounding areas have been split into regions with an average CW vertical-axis rotation as recorded by pre-folding strata.

[86] A first step of restoration consisted in the removal of the second and youngest (Priabonian-Oligocene) regional CW rotation of 10º west of the defined eastern axial surface (Figure 15a). Although it may represent a minimum value, a slightly higher value of rotation would not change the paleogeographic reconstructions or the derived conclusions significantly. The displacement gradient along the south-directed Pyrenean thrust required for this rotation is of 22 km. The axis of rotation related to this shortening gradient has been located in the western edge of the Sierras Exteriores as suggested by *Pueyo et al.* [2004] and *Ramón et al.* [2012]. It is located along strike of the frontal thrust 50 km west of the edge of the map in Figure 15a. Once the younger regional Priabonian-Oligocene vertical-axis rotation has been restored, the resultant map shows a systematic variation of the mean magnetic declinations around the curved structural trends of the Ainsa Oblique Zone and western Montsec thrust sheet (Figure 15a). In the map of Figure 15a

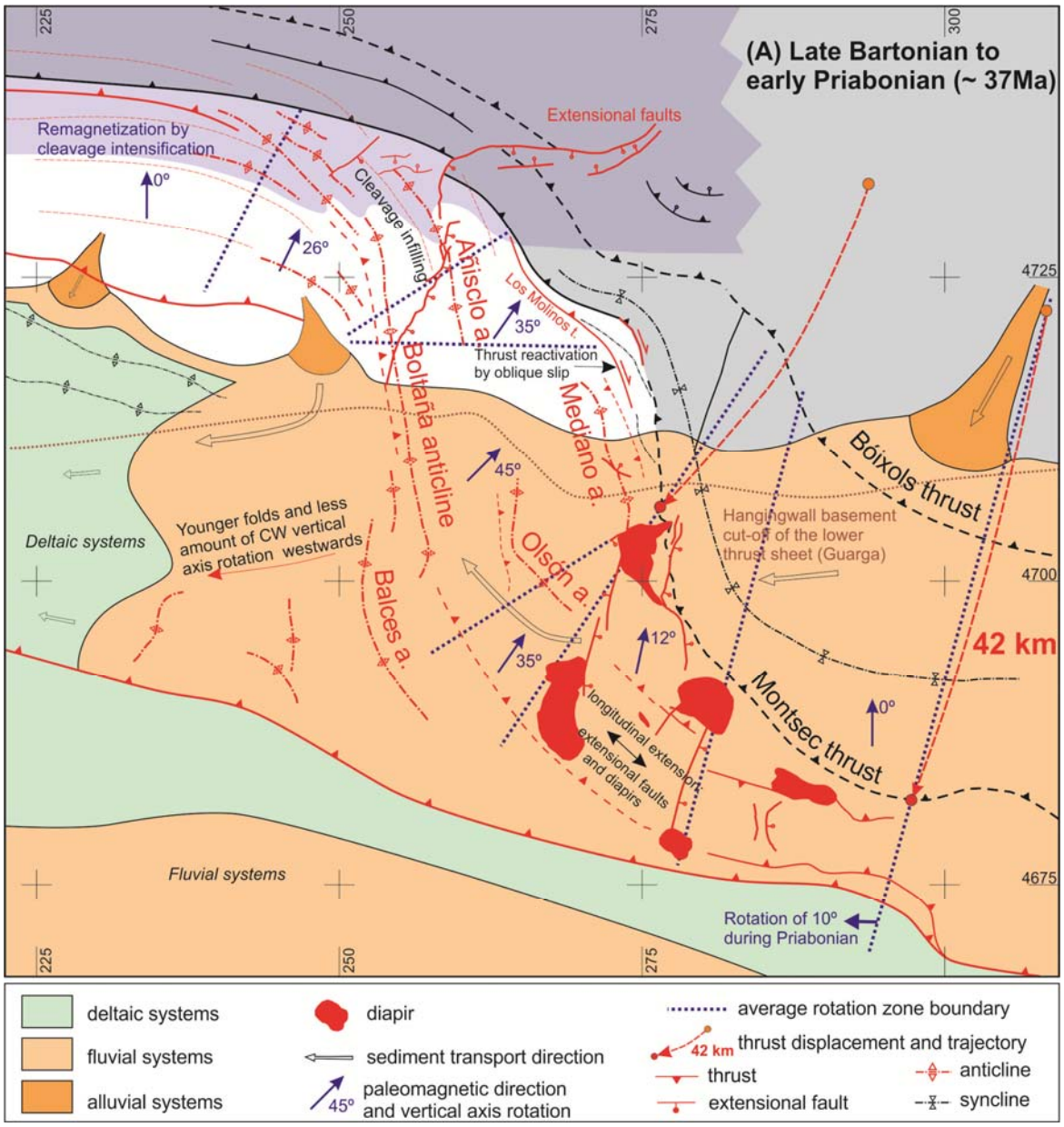

Figure 15. Map reconstructions of the Ainsa Oblique Zone for the Middle to Late Eocene time span. (A) Late Bartonian to early Priabonian (~37 Ma), (B) Middle Lutetian (42 Ma) and (C) Early Lutetian (48 Ma). Colors represent facies and sedimentary systems. Red lines represent the active structures in every stage. Same legend for B and C.

only the amount of vertical-axis rotation that occurred between middle Lutetian (43 Ma) and late Bartonian-early Priabonian (38-37 Ma) has been annotated. This represents the period of time during which all the structures of the Ainsa Oblique Zone were active. In the northern bend, CW vertical-axis rotation increases as structures change their trend from E-W (090-100 azimuth) to N-S (170 azimuth). In the central part of the Ainsa Oblique Zone, where structures trend 170N, rotation was maximum (45º CW) during that period of time. CW vertical-axis rotation then decreases again in the southern bend as structures change towards E-W trends. This rotational pattern, combined with the lack of significant rotation in adjacent areas, indicates that vertical-axis rotations were associated with large-scale thrusting in the salient, as also expressed by the strike plot (Figure 14).

[87] A restored map at middle Lutetian times (42 Ma) illustrates the geometry and position of the main structures of the Gavarnie thrust sheet during the early stages of deformation (Figure 15b). Sobrarbe folds have been restored taking into account the shortening calculated in the E-W cross-sections (Figures 5 and 6) and the 3D restoration based on the 3D structural reconstruction made by *Fernández et al.* [2012].

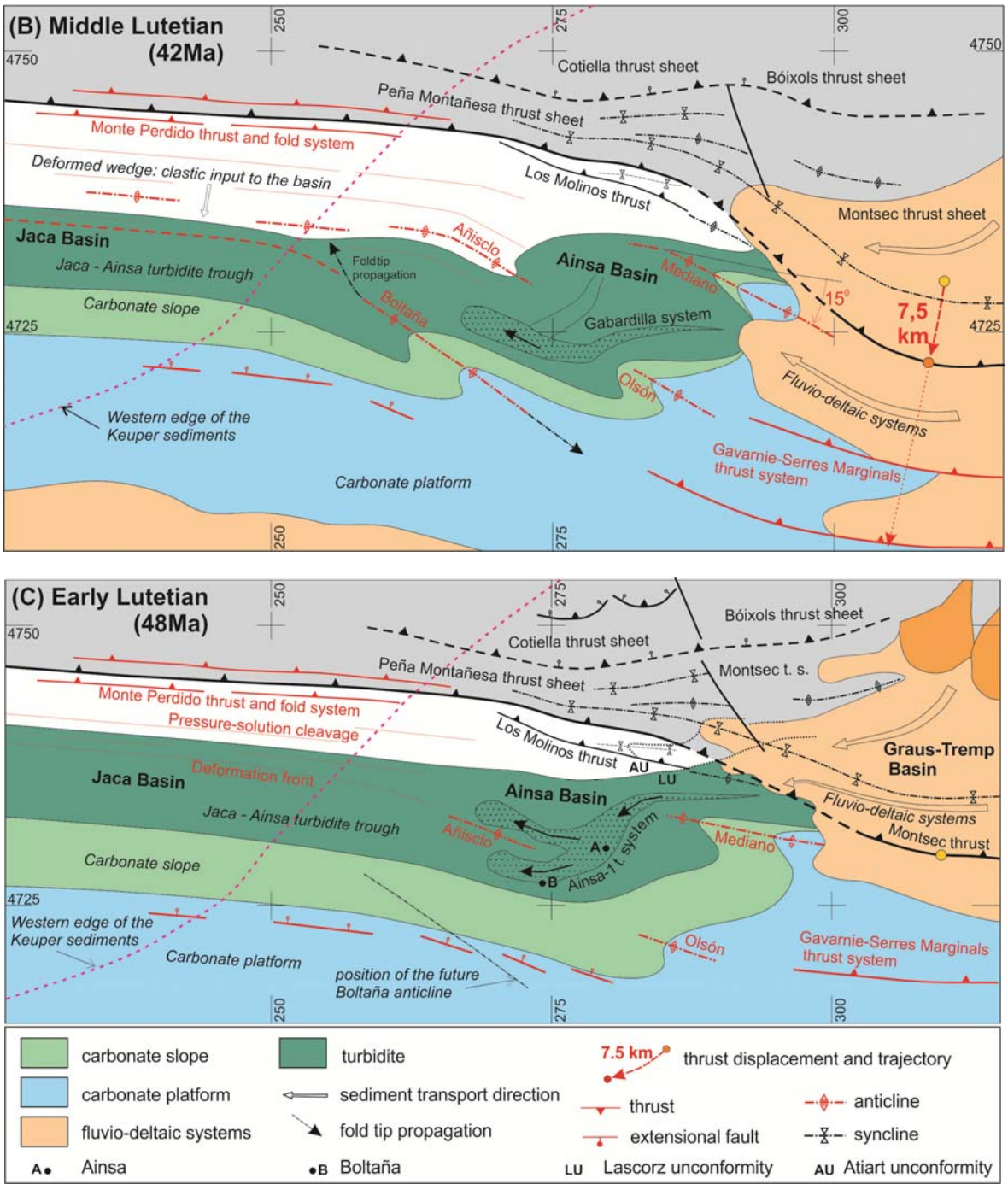

Total displacement of the thrusts related with the Sobrarbe folds totals about 5 km [*Fernández et al*., 2012]. However, total shortening is greater as shortening taken up by folding needs to be added. In the southern section, across the Mediano anticline (Figure 6), a shortening of 7.5 km has been calculated. At middle Lutetian times, the onset of growth of the Boltaña anticline controlled the dispersal of the turbidite systems in the Ainsa basin which were fed from fluvio-deltaic systems in the east. The Boltaña anticline grew as an oblique structure at the thrust front of the Gavarnie thrust sheet. The Boltaña anticline developed parallel to the Mediano anticline which had by then already experienced a CW vertical-axis rotation of about 15º. Forward of the thrust front, the carbonate platform experienced extensional deformation by flexure of the foreland [*Barnolas and Teixell,* 1994; *Tavani et al.*, 2012]. The tip of the Boltaña anticline propagated northwestward into the western termination of the Keuper sediments as deformation progressed during Lutetian and Bartonian times, and CW vertical-axis rotation increased.

[88] The restored map at early Lutetian times depicts the original position of the earliest structures of the Gavarnie thrust sheet once the Peña Montañesa-Montsec thrust sheet was already emplaced (Figure 15c). The Montsec thrust was connected with its western continuation (Peña Montañesa thrust) along a slightly oblique, long ramp, showing a primary curvature. The buried oblique ramp determined the transition between the fluvio-deltaic systems deposited on top of the Graus-Tremp piggy-back basin and the slope systems of the Ainsa basin. The growing Mediano and Añisclo anticlines controlled sedimentation of slope turbidites of the Ainsa basin. Nevertheless, they were connected with their deeper equivalents of the Jaca basin as there were no transversal structural barriers (Figure 15c).

6.4. Origin of curvature and the influence of detachments

[89] Timing and spatial relations of paleomagnetic data with respect to the trend of the structures indicate that curvature developed during thrusting and folding within the Ainsa Oblique Zone, which eliminates models of primary curvatures and secondary oroclines. Moreover, the fact that the Sobrarbe folds constitute a coherent structural unit at the eastern part of the Gavarnie thrust sheet, rules out previous interpretations that consider any of the major folds of the Sobrarbe system (e.g. Mediano or Boltaña anticlines) as related to main oblique ramps [*Cámara and Klimowitz,* 1985; *Mutti et al.,* 1988; *Anastasio and Holl*, 2001; among others].

[90] Layer parallel shortening directions can be derived from axis-parallel pressure solution cleavage (Figures 2 and 3) [*Holl and Anastasio,* 1995a, b; *Tavani et al.,* 2006], fault assemblages, twinned calcite grains and AMS. The maximum shortening direction is subperpendicular to the structural trend around the Ainsa Oblique Zone and westward, defining a radial pattern [*Parés and Dinarès-Turell*, 1993; *Holl and Anastasio,* 1995b; *Tavani et al.,* 2006; *Mochales et al., 2010*]. These observations rule out progressive curved models with parallel thrust slip. Moreover, parallel thrust slip models require a significant distributed longitudinal stretching to account for the observed vertical-axis rotations, whereas the amount of extension parallel to the Añisclo and Boltaña anticlines has been quantified as less as 0.5% [*Tavani et al.,* 2006, 2012]. This leaves only progressive curvature models that combine divergent emplacement and differential shortening [*Yonkee and Weil*, 2010b] as the kinematic model that suitably accounts for the obliquity and curvature of the Ainsa Oblique Zone and the related major thrust salient of the south-central Pyrenees.

[91] Notwithstanding, primary curvature would have had a moderate contribution to the final geometry of the thrust salient (Figures 15c and 16).

[92] Furthermore, a divergent emplacement model with curved slip trajectories and progressive westward migration of deformation explains that with a decreasing amount of vertical-axis rotation westward, the trend of the folds is still parallel, and consequently, the amount of obliquity of the folds increases also westward. The increase of obliquity westward from the Mediano anticline to the Boltaña anticline, and further west toward the N-S folds of the Sierras Exteriores, is illustrated by the strike test (Figure 14). The slope of the regression for the sites located in the inner salient of the Gavarnie thrust sheet (including La Fueba fold and thrust system and the Mediano anticline) increases if the northernmost, possibly remagnetized sites are removed (Figure 14). On the contrary, if the sites along the younger Boltaña anticline are included the slope decreases, demonstrating a higher primary contribution of the curvature toward the external parts of the Gavarnie thrust sheet. Finally, a progressive model of curvature with divergent thrust trajectories explains the observed strain pattern in the Sobrarbe anticlines. Divergent thrust slip requires longitudinal extension at the structural bends (Figures 13 and 15a). The Balupor-San Marzial faults are the result of such extension in the northern bend. They were synchronous with the vertical-axis rotation and folding. The location of these extensional faults was controlled by the western limit of the Keuper evaporites, which in turn also controlled the position of the structural bend. In the southern bend the transverse extensional faults and the salt diapirs (*e.g.* Clamosa) record strike-parallel

extension during vertical-axis rotation (Figure 15). The amount of extension, of approximately 12 km, as estimated by the width of the diapirs, is consistent with the calculated thrust displacement and thrust trajectories (Figure 15a). Diapirs were enhanced in the southern bend by a thicker salt layer, whereas in the northern bend the reduced thickness of Keuper sediments inhibited the development of salt structures. The edge of the Keuper sediments not only controlled the location of the northern bend of the Ainsa Oblique Zone and the extensional faults, but also a change of the structural style from local to regional scale. The high amplitude Añisclo and Boltaña anticlines, cored by Keuper salts, are replaced along the northern bend by a belt of smaller folds and a widespread pressure solution cleavage (Figures 2 and 11).

[93] At a regional scale, the presence of the Triassic detachment level at the bottom of the Mesozoic stratigraphic succession favored the antiformal stack geometry of the basement-involved thrust sheets of the central Pyrenees [*Beaumont et al.*, 2000], and its absence to the west is responsible for the change in geometry of the thrust system to form an imbricate stack (Figure 1).

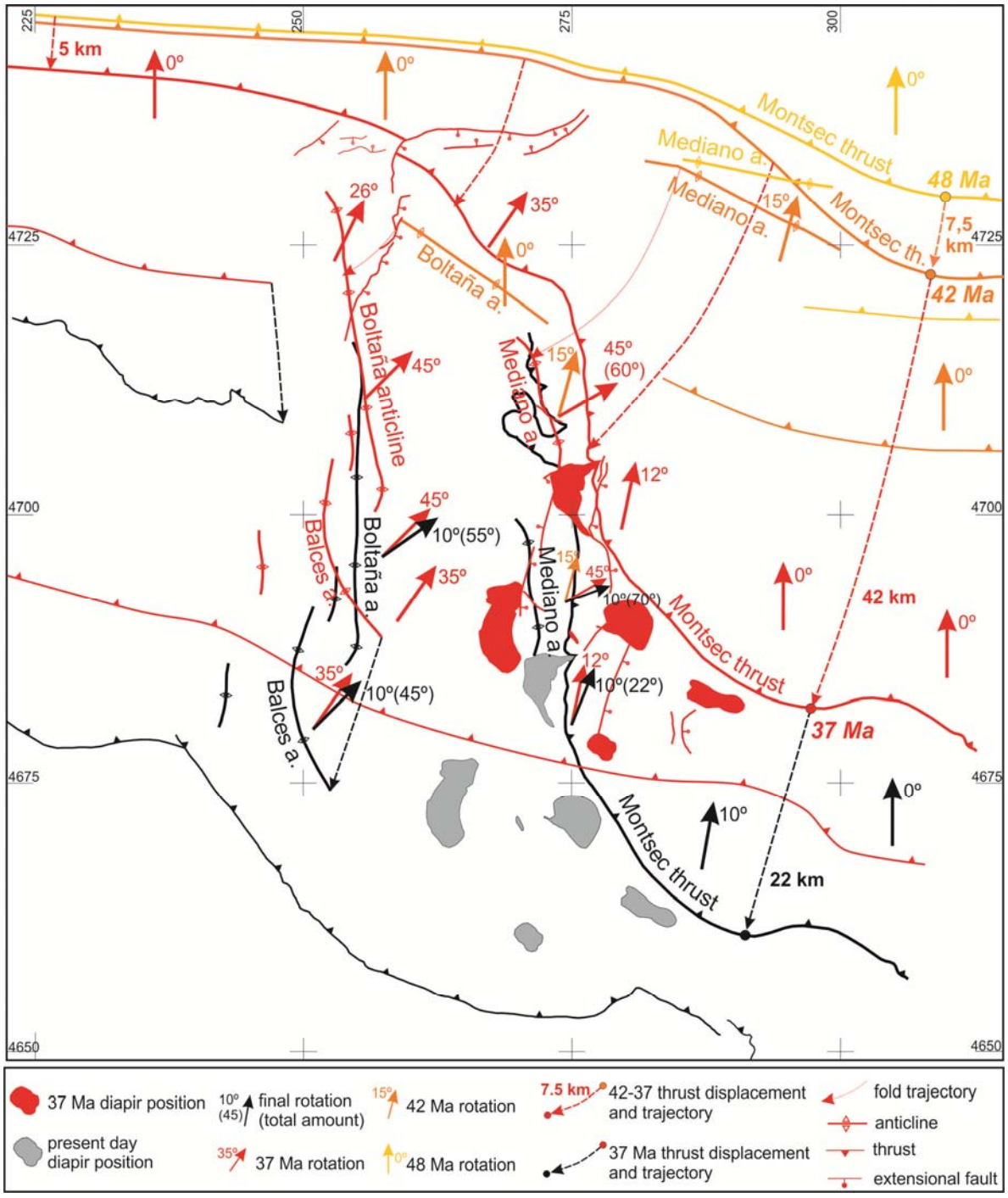

Figure 16. Synthesis of the evolution of the study area during the different stages (48 Ma, 42 Ma, 37 Ma and present day). Structures and arrows depicting CW vertical-axis rotation have been colored for each stage. The Montsec thrust has been depicted as a passive marker as a reference for the rotation of pre-Gavarnie structures during the differential displacement on the Gavarnie thrust (that led to the CW vertical-axis rotation and the formation of the Ainsa Oblique Zone structures).

6.5. Thrust displacement and displacement gradient

[94] A significant thrust displacement gradient is necessary to explain the paleomagnetic and structural data in the Ainsa Oblique Zone. A displacement gradient of 44.5 km has been calculated between 48 Ma and 37 Ma to develop the structures of the Ainsa Oblique Zone and the coeval CW vertical-axis rotation (Figure 16). If we add to this a known minimum displacement of 5 km for the Gavarnie thrust west of the Ainsa Oblique Zone [*Teixell*, 1996] a total minimum thrust displacement of 49.5 km for the Serres Marginals thrust system during the early Lutetian-late Bartonian time span is obtained. This displacement is probably greater as shortening related with the Gavarnie thrust and related folds is also greater. The estimated 44.5 km of differential shortening during this interval (9 Ma) occurred by further southward displacement of the Serres Marginals thrust sheet on top of the Keuper salts with respect to its western equivalent (Gavarnie-Sierras Exteriores thrust sheet) west of the Ainsa Oblique Zone, where the Triassic evaporites are absent. The previously emplaced Montsec-Peña Montañesa and Bóixols-Cotiella thrust sheets were transported piggy-back and bent to form a prominent thrust salient synchronously with the development and CW vertical-axis rotation of the Ainsa Oblique Zone at the eastern part of the Gavarnie thrust sheet (Figures 14, 15 and 16).

[95] During this time there is no record of a symmetric CCW vertical-axis rotation event at the eastern edge of the central Pyrenean thrust salient (the so called South Pyrenean Central Unit, Figure 1). There, the Triassic salts continue eastward at the bottom of the Mesozoic succession and the age of CCW vertical-axis rotation is younger [*Sussman et al.*, 2004] and coeval with the second Late Eocene-Oligocene rotation event. This CCW vertical-axis rotation event post-dates fold growth of the Ainsa Oblique Zone and is related with differential displacement of the sole thrust system on top of the Priabonian-Lower Oligocene salts and their lateral equivalent sediments. These observations, along with the sinchronicity of vertical-axis rotation and post-Montsec fold growth, rule out the interpretations that link the obliquity of the Sobrarbe fold system to the emplacement of the Montsec-Peña Montañesa thrust sheet [*Séguret*, 1972; *Farrell et al.*, 1987; *Bentham et al.*, 1992; *Soto et al.*, 2002; *Mochales et al.*, 2012b].

[96] A minimum differential displacement of 22 km has been estimated to account for the youngest (Priabonian-Oligocene) CW vertical-axis rotation. This displacement and the related gradient were produced by the Priabonian salt basin configuration and its associated lateral strength variations. This rotation resulted into a wider and lower amplitude thrust salient (the rotation pin points were located about 250 km apart, beyond the studied area), and was superimposed on the previous curved folds and thrusts of the Ainsa Oblique Zone (Figure 16).

[97] Taking into consideration both rotational events, a total differential displacement of 66.5 km across the Ainsa Oblique Zone is required to explain the structural, sedimentologic and paleomagnetic data. A possible explanation for this differential displacement gradient is the difference in total shortening along the Pyrenean orogeny, as is expected from the work by *Teixell* [1998] and *Beaumont et al.* [2000], who estimated shortening to be of 80 km west of the Ainsa Oblique Zone and 165 km east of the Ainsa Oblique Zone respectively (Figure 1). The calculated 71.5 km of total displacement on the Serres Marginals thrust sheet is also consistent with the estimated thrust displacements by *Beaumont et al.* [2000] along the ECORS cross-section for the Middle Eocene-Oligocene interval.

[98] If the difference in shortening is related to the underthrusting of basement units, basement stacking in the central Pyrenees could provide the excess mass necessary to compensate the deficit caused by vertical-axis rotation. Alternatively, as the rotation was controlled by the distribution of the detachment horizons in the cover succession (Triassic and Priabonian salts), the displacement gradient could be compensated by an increase of thrust displacement in the Axial Zone and northern Pyrenees west of the Ainsa Oblique Zone.

7. Conclusions

[99] Integration of structural, sedimentological and paleomagnetic data reveals a systematic relationship between the structures of the Ainsa Oblique Zone, their temporal evolution, the strain history and vertical-axis rotation and remagnetization. The kinematic model that best matches all the observed data is that of a curved fold and thrust belt developed by progressive

curvature with a divergent thrust transport direction.

This kinematic evolution resulted from along-strike differential shortening localized by the distribution of the weak evaporite horizons at the bottom of the detached Mesozoic and Paleogene successions during two main rotational events. During the main event, Middle Eocene in age (Lutetian to Priabonian), the fold and thrusts of the Ainsa Oblique Zone, at the eastern part of the Gavarnie thrust sheet, developed synchronously with up to 60º of CW vertical-axis rotation in response to an estimated 44.5 km of differential displacement along the orogen. The second rotation event, Late Eocene-Oligocene in age, added a further 10º of CW vertical-axis rotation associated to a displacement gradient of 22 km. A total differential thrust displacement of 66.5 km across the entire Ainsa Oblique Zone has been estimated to account for the observed structural pattern and the CW vertical-axis rotation of the restored mean magnetic declinations (Figure 16). Folding and vertical-axis rotation in the Ainsa Oblique Zone was also accompanied by the formation of mesostructures (cleavage and fractures). Intense layer-parallel shortening related to cleaveage (over 20%) led to the remagnetization of the internal areas of the Gavarnie thrust sheet during its emplacement and synchronous with the CW vertical-axis rotation of the Sobrarbe folds.

[100] Space problems related to the regional CW vertical-axis rotations were compensated by the formation of the Balupor and San Marzial extensional faults in the northern bend and transverse extensional faults and diapirs in the southern bend where Triassic salts were significantly thicker (Figure 16). In addition, oblique to strike-slip displacements reactivated previously developed thrusts during the CW vertical-axis rotation.

[101] Among the different analyzed factors the most significant mechanism controlling the kinematic evolution of the Ainsa Oblique Zone is the distribution and strength variations of the Triassic sediments at the basal detachment. They not only controlled the location and the structural pattern of the curved structures, but also determined a change in the structural style at a crustal-scale of the Pyrenean thrust system at both sides of the Ainsa Oblique Zone. This study also illustrates the changing synorogenic topography of a foreland basin setting associated with a progressive curved contractional system and the power of the understanding of its kinematics to unravel the dispersal patterns of the sedimentary systems.

[102] Finally, this study emphasizes the importance of integrating sedimentological, structural and paleomagnetic data to understand the kinematics of curved contractional systems. It also highlights that statistical analysis of paleomagnetic data has to be constrained by structural and stratigraphic data in order to avoid conclusions that contradict geological field observations and regional constraints.

[102] Acknowledgements. This work was funded by the project INTECTOSAL (CGL2010-21968-C02-01) and by the "Grup de Recerca de Geodinàmica i Anàlisi de Conques 2009SGR1198" Secretaria d'Universitat i Recerca del Departament d'Economia i Coneixement de la Generalitat de Catalunya. Josep Poblet acknowledges financial support by research projects: "Geociencias en Iberia: estudios integrados de topografía y evolución 4D [TOPO-IBERIA]" (CSD2006-041) and "Desarrollo de fracturas y venas asociadas al plegamiento [FRAVEPLE]" (CGL2011-23628) funded by Spanish Ministries. Thanks to the Paleomagnetic Laboratory of Barcelona (CCiTUB-CSIC) where the paleomagnetic analyses were carried out. Midland Valley is thanked for providing the 2DMove software. We thank Emilio Pueyo, Antonio Casas and an anonymous reviewer for the fruitful and constructive revisions which have significantly improved the original submitted manuscript.

References

Allerton, S. (1998), Geometry and kinematics of vertical-axis rotations in fold and thrust belts, *Tectonophysics, 299*, 15–30.

Anastasio, D.J., and J.E. Holl (2001), Transverse fold evolution in the External Sierras, southern Pyrenees, Spain, *Journal of Structural Geology, 23*, 379-392.

Arbués, P., D. Mellere, O. Falivene, O. Fernández-Bellón, J. A. Muñoz, M. Marzo, and J. M. de Gibert (2007), Context and architecture of the Ainsa-1-quarry channel complex, Spain, in *Atlas of deep-water outcrops*, edited by T. H. Nilsen, R. D. Shew, G. S. Steffens and J. R. J. Studlick, *AAPG Studies in Geology*, 56, CD-ROM, 20 pp.

Arbués, P., M. Butillé, M. López-Blanco, M. Marzo, O. Monleon, J. A. Muñoz, and J. Serra-Kiel (2011), Exploring the relationships between deepwater and shallow-marine deposits in the Aínsa piggy-back basin fill (Eocene, South-Pyrenean Foreland Basin), in *Post-Meeting Field trips Guidebook*, 28th IAS Meeting, Zaragoza, edited by C. Arenas, L. Pomar and F. Colombo, Sociedad Geológica de España, Geo-guias, 8, 199-240.

Baceta, J.I, V. Pujalte, J. Serra-Kiel, A. Robador, and X. Orue-Etxebarria (2004), El Maastrichtiense final- Paleoceno e Ilerdiense inferior de la Cordillera Pirenaica, in *Geología de España*, edited by J.A. Vera, SGE-IGME, 308-313.

Barnolas, A., J.M. Samsó, A. Teixell, J. Tosquella, and M. Zamorano (1991), Evolución sedimentaria entre la Cuenca de Graus-Tremp y la Cuenca de Jaca-Pamplona, in I Congreso del Grupo Español del Terciario, Guide Book 1, edited by F. Colombo, EUMO Gràfic, Vic, Spain, 123 pp.

Barnolas, A., and A.Teixell (1994), Platform sedimentation and collapse in a carbonate-dominated margin of a foreland basin (Jaca Basin, Eocene, southern Pyrenees), *Geology*, *22*, 1107-1110.

Barnolas, A., and I. Gil-Peña (2001), Ejemplos de relleno sedimentario multiepisódico en una cuenca de antepaís fragmentada: La Cuenca Surpirenaica, *Boletín Geológico y Minero, 112 (3)*, 17-38.

Beamud, E., M. Garcés, L. Cabrera, J.A. Muñoz, and Y. Almar (2003), A new middle to late Eocene continental chronostratigraphy from NE Spain, *Earth and Planetary Science Letters, 216*, 501-514.

Beaumont, C., J. A. Muñoz, J. Hamilton, and P. Fullsack, (2000), Factors controlling the Alpine Evolution of the

Central Pyrenees inferred from a comparison of observations and geodynamical models, *Journal of Geophysical Research, 105(B4),* 8121-8145.

Bentham, P. (1992), *The tectono-stratigraphic development of the western oblique ramp of the South-Central Pyrenean thrust system, Northern Spain*, PhD Thesis, University of Southern California. 253 pp.

Bentham, P.A., Burbank, D.W., and Puigdefàbregas, C. (1992), Temporal and spatial controls on the alluvial architecture of an axial drainage system: late Eocene Escanilla Formation, southern Pyrenean foreland basin, Spain. *Basin Research, 4*, 335-352.

Bentham, P.A., and D.W. Burbank (1996), Chronology of Eocene foreland basin evolution along the western oblique margin of the South-Central Pyrenees, in *Tertiary basins of Spain*, edited by P.F. Friend and C.J. Dabrio, Cambridge University Press, 144-152.

Cámara, P., and J. Klimowitz (1985), Interpretación geodinámica de la vertiente centro-occidental surpirenaica (Cuencas de Jaca-Tremp), *Estudios geológicos*, *41*, 391-404.

Casas, A.M., R. Soto, and B. Martínez-Peña (2002), Geometrical relationships between unconformities and subsequent folding: the Arro fold system (southern Pyrenees), *Comptes Rendus Geoscience, 334,*765-772.

Charlesworth, H., D. Cruden, J. Ramsden, and Q. Huang (1989), ORIENT: an interactive Fortran 77 program for processing orientations on a microcomputer, *Computer & Geosciences, 15,* 275-293.

Choukroune, P. (1976), Structure et évolution tectonique de la zone nord-pyrénéene. Analyse de la déformation dans une portion de chaîne à schistosité subverticale, *Mémoires Societé Géologique France, 127,* 116 pp.

Choukroune, P., and M.Séguret (1973), *Carte structurale des Pyrénées, 1/500.000*, Université de Montpellier - ELF Aquitaine.

Costa, E., M. Garcés, M. López-Blanco, J. Serra-Kiel, G. Bernaola, L. Cabrera and E. Beamud (2013), The Bartonian-Priabonian marine record of the eastern South Pyrenean Foreland Basin (NE Spain): A new calibration of the larger foraminifers and calcareous nannofossil biozonation, *Geologica Acta, 11 (2),* 177-193.

De Federico, A. (1981), La sedimentación de talud en el sector occidental de la cuenca paleógena de Aínsa. Publ. de Geología, Univ. de Barcelona, 12. 271 pp.

Demarest, H. H. (1983), Error analysis for the determination of tectonic rotation from paleomagnetic data, *Journal of Gephysical Research*, *88 (B5),* 4321-4328.

Dinarès-Turell, J. (1992), *Paleomagnetisme a les unitats sudpirinenques superiors. Implicacions estructurals*. PhD thesis, Univ. de Barcelona. 462 pp.

Dinarès-Turell, J., and J.M. Parés (1992), The use of AMS to determine the petrofabric in weakly deformed rocks: a case study from the Eocene in the Ainsa Basin (Central Pyrenees), *Geogaceta, 12,* 22-25.

Dinarès, J., E. McClelland, and P. Santanach (1992), Contrasting rotations within thrust sheets and kinematics of thrust tectonics as derived from palaeomagnetic data: an example from the Southern Pyrenees, in *Thrust Tectonics*, edited by K.R. McClay, Chapman & Hall, London, 235-246.

Dreyer, T., J. Corregidor, P. Arbués, and C. Puigdefàbregas (1999), Architecture of the tectonically influenced Sobrarbe deltaic complex in the Ainsa Basin, northern Spain, *Sedimentary Geology, 127,* 127-169.

Eldredge, S., V. Bachtadse, and R. Van der Voo (1985), Paleomagnetism and the oroclines hypothesis, *Tectonophysics, 119*, 153-179, doi: 10.1016/0040-1951(85)90037-X.

Elliot, D. (1976), The motion of thrust sheets, *Journal of Geophysical Research, 81,* 949-963.

Elmore, R.D., A.R. Muxworthy, and M. Aldana (2012), Remagnetization and chemical alteration of sedimentary rocks, in *Remagnetization and chemical alteration of sedimentary rocks*, edited by R.D. Elmore, A.R. Muxworthy, and M. Aldana, 1-21, Geological Society, London, Special Publications, 371.

Enkin, R.J. (2003), The direction–correction tilt test: an all-purpose tilt/fold test for paleomagnetic studies, *Earth and Planetary Science Letters, 212 (1-2),* 151-166.

Evans, S.C., and R.D. Elmore (2006), Fluid control of localized mineral domains in limestone pressure solution structures, *Journal of Structural Geology, 28,* 284-301.

Falivene, O, P. Arbués, J. Ledo, B. Benjumea, J.A. Muñoz, O. Fernández, and S. Martínez (2010), Synthetic seismic models from outcrop-derived reservoir-scale three-dimensional facies models: The Eocene Ainsa turbidite system (southern Pyrenees), *AAPG Bulletin, 94(3)*, 317-343.

Farrell, S.G., Williams, G.D., and Atkinson, C.D. (1987), Constraints on the age of movement of the Montsec and Cotiella Thrusts, south central Pyrenees, Spain, *Journal of the Geological Society of London, 144*, 907-914.

Fernández-Bellon, O. (2004), *Reconstruction of geological structures in 3D. An example from the Southern Pyrenees*. PhD thesis, Universitat de Barcelona. 321 pp.

Fernández, O., J.A. Muñoz, P. Arbués, O. Falivene, and M. Marzo (2004), Three-dimensional reconstruction of geological surfaces: an example of growth strata and turbidite systems from the Ainsa basin (Pyrenees, Spain), *American Association of Petroleum Geologists Bulletin, 88(8)*, 1049–1068.

Fernández, O., J.A. Muñoz, P. Arbués, and O. Falivene (2012), 3-D Structure and evolution of an oblique system of relaying folds: The Ainsa basin (Spanish Pyrenees), *Journal of the Geological Society of London*, *169*, 545-559,doi: 10.1144/0016-76492011-068.

Fournier, E. (1905), Études géologiques sur la partie occidentale de la chaîne des Pyrénées entre la vallée d'Aspe et de celle de la Nive, *Bulletin Societé Géologique France, 4 serie, 5*, 699-725.

García-Senz, J. (2002), *Cuencas extensivas del cretácico inferior en los Pirineos centrales, formación y subsecuente inversión*. Unpublished PhD thesis, Universitat de Barcelona. 310 pp.

Garrido-Megías, A. (1973), *Estudio geológico y relación entre tectónica y sedimentación del Secundario y Terciario de la vertiente meridional pirenaica en su zona central (provincias de Huesca y Lérida).* PhD Thesis, Universidad de Granada. 395 pp.

Gradstein, F.M., J.G. Ogg and A.G. Smith (2004), *A Geologic Time Scale 2004*. Cambridge University Press, Cambridge, 589 pp.

Hindle, H., and M. Burkhard (1999), Strain, displacement and rotation associated with the formation of curvature on fold belts; the example of the Jura arc, *Journal of Structural Geology, 21*, 1089-1101, doi: 10.1016/ S0191-8141(99)00021-8.

Hogan, P.J. (1993), *Geochronologic, tectonic and stratigraphic evolution of the Southwest Pyrenean foreland basin, Northern Spain.* Unpublished PhD Thesis, Univ. of Southern California. 219 pp.

Hogan, P.J., and D.W. Burbank (1996), Evolution of the Jaca piggy-back basin and emergence of the External Sierras, southern Pyrenees, in *Tertiary basins of Spain,* edited by P.F. Friend, and C.J. Dabrio, 153-160, Cambridge University Press.

Holl, J. E., and D. J. Anastasio (1995a), Kinematics around a large-scale oblique ramp, southern Pyrenees, Spain, *Tectonics 16(5*), 1368-1379.

Holl, J. E., and D. J. Anastasio (1995b), Cleavage development within a foreland thrust and fold belt, southern Pyrenees, Spain, *Journal of Structural Geology, 17 (3)*, 357-369.

Labaume, P., M. Séguret, C. Seyve (1985), Evolution of a turbiditic foreland basin and analogy with an accretionary prism: Example of the Eocene South-Pyrenean basin, Tectonics, 4 (7), 661-685.

Lacroix, B., M. Buatier, P. Labaume, A. Travé, M. Dubois, D. Charpentier, S. Ventalon, and D. Convert-Gaubier (2011), Microtectonic and geochemical characterization of thrusting in a foreland basin: Example of the South-Pyrenean orogenic wedge (Spain), *Journal of Structural*

Geology, 33, 1359-1377.

Lanaja, J. M. and Navarro, A. (1987), Contribución de la exploración petrolífera al conocimiento de la geología de España, 465 pp., Instituto Geológico y Minero de España, Madrid. ISBN: 84-7474-398-2 – modificada la cita al text de l'article.

Larrasoaña, J.C., J.M. Parés, H. Millán, J. del Valle, and E.L. Pueyo (2003), Paleomagnetic, structural, and stratigraphic constraints on the traverse fault kinematics during basin inversion: The Pamplona Fault (Pyrenees, north Spain), *Tectonics, 22 (6),* 1071, doi: 10.1029/2002TC001446.

López-Blanco, M., M. Marzo and J.A. Muñoz (2003), Low-amplitude, synsedimentary folding of a deltaic complex: Roda sandstone (lower Eocene), South-Pyrenean Foreland Basin, *Basin Research*, *15 (1)*, 73-95.

López, M.A., C. Oliván, B. Oliva, E.L. Pueyo, and the GeoKin3DPyr working group (2008), Pyrenean Paleomagnetic databases, *Geotemas, 10*, 1219-1222.

Lowrie, W., and A.M. Hirt (1986), Paleomagnetism in arcuate mountain belts, in *The Origin of Arcs, Dev. Geotectonics* 21, pp. 141-158, Elseveier, Amsterdam.

Luzón, A. (2005), Oligocene-Miocene alluvial sedimentation in the northern Ebro Basin, NE Spain: Tectonic control and palaeogeographical evolution, *Sedimentary Geology, 177*, 19-39.

Macedo, J. and S. Marshak (1999), Controls on the geometry of fold-thrust belt salients, *Geological Society of America Bulletin, 111*, 1808-1822.

Marshak, S. (2004), Salients, recesses, arcs, oroclines, and syntaxes - A review of ideas concerning the formation of map-view curves in fold-thrust belts, in *Thrust tectonics and hydrocarbon systems,* edited by K.R. McClay, *AAPG Memoir 82*, 131-156.

Martínez Peña, M.B. (1991), La estructura del límite occidental de la unidad surpirenaica central, PhD thesis, University of Zaragoza, Spain, 380 pp.

Martínez-Peña, M.B., and A.M. Casas-Sainz (2003), Cretaceous-Tertiary tectonic inversion of the Cotiella Basin (Southern Pyrenees, Spain), *International Journal of Earth Sciences (Geologische Rundschau), 92*, 99-113.

Mateu-Vicens, G., L. Pomar, and C. Ferrández (2012), Nummulitic banks in the upper Lutetian "Buil level", Ainsa Basin, South Central Pyrenean Zone: the impact of internal waves, *Sedimentology, 59(2),* 527-552.

McClay, K., J. A. Muñoz, and J. García-Senz (2004), Extensional Salt Tectonics in a Contractional Orogen: a Newly Identified Tectonic Event in the Spanish Pyrenees, *Geology, 32 (9)*, 737-740.

McFadden, P.L. (1990), A new fold test for paleomagnetic studies, Geophysical Journal International, 103 (1), 163-169. DOI: 10.1111/j.1365-246X.1990.tb01761.x

Megías, A. G. (1982), Nueva hipótesis paleogeográfica sobre el Cretácico surpirenaico, *Cuadernos de Geología Ibérica, 8*, 1005-1015.

Mey, P.H.W., P.J.C. Nagtegaal, K.J. Roberti, and J.J.A. Hartevelt (1968), Lithostratigraphic subdivision of post-Hercynian deposits in the south-central Pyrenees, Spain, *Leidse Geologische Mededelingen, 431*, 221-228.

Millán, H. (1996) *Estructura del frente de cabalgamiento surpirenaico en las Sierras Exteriores Aragonesas*. Unpublished PhD thesis, Universidad de Zaragoza. 213 pp.

Millán, H., M. Aurell, and A. Melendez (1994), Synchronous detachment folds and coeval sedimentation in the Prepyrenean External Sierras (Spain), *Sedimentology, 5,* 1001-1024.

Millán, H., E.L. Pueyo, M. Aurell, A. Luzón, B. Oliva, M.B. Martínez-Peña, and J. Pocoví (2000), Actividad tectónica registrada en los depósitos terciarios del frente meridional del Pirineo central, *Revista de la Sociedad Geológica de España, 13,* 279-300.

Millán, H., B. Oliva, and J. Pocoví (2006), La transversal de Gavarnie-Guara. Estructura y edad de los mantos de Gavarnie, Guara-Gèdre y Guarga (Pirineo centro-occidental), *Geogaceta, 40,* 35-37.

Mochales, T. (2011), *Chronostratigraphy, vertical-axis rotations and AMS in the Boltaña anticline (Southern Pyrenees): kinematic implications*. Unpublished PhD thesis, Universidad de Zaragoza. 222 pp.

Mochales, T., E.L. Pueyo, A.M. Casas, A. Barnolas, and B. Oliva-Urcia (2010), Anisotropic magnetic susceptibility record of the kinematics of the Boltaña Anticline (Southern Pyrenees). *Geological Journal, 45*, 562-581, doi: 10.1002/gj.1207.

Mochales, T., A. Barnolas, E.L. Pueyo, J. Serra-Kiel, A.M. Casas, J.M. Samsó, J. Ramajo, and J. Sanjuán (2012a), Chronostratigraphy of the Boltaña anticline and the Ainsa Basin (Southern Pyrenees), Geological Society of American Bulletin, 124 (7-8), 1229-1250. doi:10.1130/B30418.1

Mochales, T., A.M. Casas, E.L. Pueyo, and A. Barnolas (2012b), Rotational velocity for oblique structures (Boltaña anticline, Southern Pyrenees), *Journal of Structural Geology, 35,* 2-16, doi: 10.1016/j.jsg.2011.11.009.

Montes, M.J. (1992), Sistemas deposicionales en el Eoceno medio - Oligoceno del Sinclinorio-Río del Guarga (Cuenca de Jaca, Pirineo Central), in *Simposios, III Congreso Geológico de España y VIII Congreso Latinoamericano de Geología. Tomo 2*, Salamanca, 150-160.

Muñoz, J. A. (1992), Evolution of a continental collision belt: ECORS-Pyrenees crustal balanced section, in *Thrust Tectonics*, edited by K. R. McClay, 235-246, Chapman and Hall, London.

Muñoz, J. A. (2002), The Pyrenees, in *The Geology of Spain*, edited by W. Gibbons and T. Moreno, 370-385, Geological Society of London, London.

Muñoz, J.A., K.R. McClay, and J. Poblet (1994), Synchronous extension and contraction in frontal thrust sheets of the Spanish Pyrenees, *Geology, 22*, 921-924.

Muñoz, J. A., P.J. Coney, K.R. McClay, and C.A. Evenchick (1997), Discussion on syntectonic burial and post-tectonic exhumation of the southern Pyrenees foreland fold-thrust belt, *Journal of the Geological Society, London, 154*, 361-365.

Muñoz, J.A., P.Arbués, and J. Serra-Kiel (1998), The Ainsa Basin and the Sobrarbe oblique platform sequences deposited synchronously with a submarine emergent thrust system, in *Field Trip Guide Book,* edited by A.Meléndez-Hevia and A.R. Soria, 15th IAS Congress, Alicante (Spain), 213–223.

Mutti, E., H. Luterbacher, J. Ferrer, and J. Rosell (1972), Schema stratigrafico e lineamenti di facies di Paleogene marino nella zona central subpirenaica tra Tremp (Catalogna) e Pamplona (Navarra), *Memorie Società Geologica Italiana, 11,* 391-416.

Mutti, E., E. Remacha, M. Sgavetti, J. Rosell, R. Valloni, and M. Zamorano (1985), Stratigraphy and facies characteristics of the Eocene Hecho Group turbidite systems, South-Central Pyrenees. Excursion 12, in *6th European Regional Meeting Excursion Guidebook - IAS*, edited by M.D Milà, and J. Rosell. Institut d'Estudis Ilerdencs, Lleida, 519-576.

Mutti E., M. Séguret, and M. Sgavetti (1988), *Sedimentation and deformation in the Tertiary sequences of the Southern Pyrenees*. AAPG Mediteranean Basins Conference, Nice. Field Trip Guidebook 7, 169 pp.

Nijman, W., and S.D. Nio (1975), The Eocene Motañana delta, in *Sedimentary evolution of the Paleogene South Pyrenean Basin*, edited by J. Rosell and C. Puigdefàbregas, IAS 9th International Congress Nice, B, 56 pp.

Noel, M. and C.M. Batt (1990), A method for correcting geographically separated remanence directions for the purpose of archaeomagnetic dating, *Geophysical Journal International, 70*, 201-204.

Oliva-Urcia, B. (2004), *Geometría y cinemática rotacional en las Sierras Interiores y Zona Axial (sector de Bielsa) a partir del análisis estructural y paleomagnético*. PhD thesis, University of Zaragoza, 290 pp.

Oliva-Urcia, B., and E.L. Pueyo (2007a), Gradient of shortening and vertical-axis rotations in the Southern Pyrenees (Spain), insights from a synthesis of paleomagnetic data. *Revista de la Sociedad Geológica de España, 20 (1-2),* 105-118.

Oliva-Urcia, B., and E. L. Pueyo (2007b), Rotational basement kinematics deduced from remagnetized cover rocks (Internal Sierras, Southwestern Pyrenees), *Tectonics, 26*, TC4014, doi: 10.1029/2006TC001955.

Oliva-Urcia, B., E.L. Pueyo, and J.C. Larrasoaña (2008), Magnetic reorientation induced by pressure solution: A potencial mechanism for orogenic-scale remagnetizations, *Earth and Planetary Science Letters, 265*, 525–534.

Oliva-Urcia, B., C. Larrasoaña, E.L. Pueyo, A. Gil-Imaz, P. Mata, J.M. Parés, and A.M. Schleicher (2009), Complex magnetic subfabrics in a well-developed cleavage domain, Internal Sierras (Pyrenees, Spain), *Journal of Structural Geology, 31(2)*, 163–176.

Oliva-Urcia, B., A. M.Casas, E.L.Pueyo, and A. Pocoví, (2012a), Structural and paleomagnetic evidence for non-rotational kinematics in the western termination of the External Sierras (southwestern central Pyrenees), *Geologica Acta, 10 (2),* 125-144, doi: 10.1344/105.000001704.

Oliva-Urcia, B., E.L. Pueyo, J.C. Larrasoaña, A.M. Casas, T. Román-Berdiel, R. Van der Voo, and R. Scholger (2012b), New and revisited paleomagnetic data from Permian-Triassic red beds: Two kinematic domains in the west-central Pyrenees, Tectonophysics, 522-523, 158-175, doi:10.1016/j.tecto.2011.11.023.

Oms, O., J. Dinarès-Turell, and E. Remacha (2003), Magnetic stratigraphy from deep clastic turbidites: An example from the Eocene Hecho Group (Southern Pyrenees), *Stud. Geophys. Geod. 47*, 275-288.

Parés, J.M., and J. Dinarès-Turell (1993), Magnetic fabric in two sedimentary rock-types from the southern Pyrenees, *J. Geomag. Geoelectr*, *45 (2)*, 193-205.

Pascual, J.O., J.M. Parés, C.G. Langereis, and J.D.A. Zijderveld (1992), Magnetostratigraphy and rock magnetism of the Ilerdian stratotype at Tremp, Spain, *Physics of the Earth and Planetary Interiors, 74,* 139-157.

Poblet, J., J.A. Muñoz, A. Travé, and J. Serra-Kiel (1998), Quantifying the kinematics of detachment folds using three-dimensional geometry: Application to the Mediano anticline (Pyrenees, Spain), *Geological Society of America Bulletin, 110(1),* 111-125.

Pueyo, E. (2000), *Rotaciones paleomagnéticas en sistemas de pliegues y cabalgamientos. Tipos, causas, significado y aplicaciones. (Ejemplos de las Sierras Exteriores y Cuenca de Jaca, Pirineo Aragonés).* PhD thesis, Universidad de Zaragoza. 296pp.

Pueyo, E.L., H. Millán, A. Pocoví, and J.M. Parés (1997), Cinemática rotacional del cabalgamiento basal surpirenaico en las Sierras Exteriores Aragonesas: Datos magnetotectónicos, *Acta Geológica Hispánica, 32 (3-4),* 237-256.

Pueyo, E.L, H. Millán, and A. Pocoví (2002), Rotation velocity of a thrust: a paleomagnetic study in the External Sierras (Southern Pyrenees), *Sedimentary Geology, 146*, 191-208.

Pueyo, E.L., J.M. Parés, H. Millán, and A. Pocoví (2003a), Conical folds and apparent rotations in paleomagnetism (A case studied in the Southern Pyrenees). In: Paleomagnetism applied to tectonics; a tribute to Rob Van der Voo. Edited by: Mac Niocaill, C., T.H. Torsvik, and B. A. van der Pluijm, *Tectonophysics, 362 (1-4)*, 345 - 366.

Pueyo, E.L., A. Pocoví, J.M. Parés, H. Millán, and J.C. Larrasoaña (2003b), Thrust ramp geometry and spurious rotations of paleomagnetic vectors, *Studia Geophysica Geodetica, 47*, 331-357.

Pueyo, E.L, A. Pocoví, H. Millán, and A.J. Sussman (2004), Map-view models for correcting and calculating shortening estimates in rotated thrust fronts using paleomagnetnic data, in *Orogenic Curvature: Integrating Paleomagnetic and Structural Analyses*, edited by A.J. Sussman and A.B. Weil, 55–71, Geological Society of America Special Paper 383.

Pueyo-Anchuela, O., E.L Pueyo, A. Pocoví, and A. Gil-Imaz (2012), Vertical-axis rotations in fold and thrust belts: Comparison of AMS and paleomagnetic data in the Western External Sierras (Southern Pyrenees), *Tectonophysics, 532-535*, 119-133, doi: 10.1016/j.tecto.2012.01.023.

Puigdefàbregas, C. (1975), La sedimentación molásica en la cuenca de Jaca, *Pirineos, 104,* 1-188.

Ramón, M.J., E.L.Pueyo, J.L.Briz, A.Pocoví, and J.C.Ciria (2012), Flexural unfolding in 3D using paleomagnetic vectors, *Journal of Structural Geology, 35*, 28-39, doi: 10.1016/j.jsg.2011.11.015.

Ríos Aragüés, L.M., J.M. Lanaja del Busto, J.M. Ríos Mitchell, and F.J. Marín Blanco (1982a), *Mapa geológico de España 1:50000. Segunda serie. Hoja 179, Bielsa*. IGME.

Ríos Aragüés, L.M. Lanaja del Busto, J.M. and E. Frutos Domingo (1982b), *Mapa geológico de España 1:50000. Segunda serie. Hoja 178, Broto*. IGME.

Robador, A. (2008), El Paleoceno e Ilerdiense inferior del Pirineo occidental: Estratigrafía y sedimentología, Publicaciones del Instituto Geológico y Minero de España, serie Tesis Doctorales, 12. 285 pp. Madrid, Spain. ISBN: 978847840734

Roest, W.R., and S.P. Srivastava (1991), Kinematics of the plate boundaries between Eurasia, Iberia, and Africa in the North Atlantic from the Late Cretaceous to the present, *Geology*, *19*(6), 613-616.

Rodríguez-Pintó, A., E.L. Pueyo, J. Serra-Kiel, J.M. Samsó, A. Barnolas, and A. Pocoví (2012), Lutetian magnetostratigraphic calibration of larger foraminifera zonation (SBZ) in the Southern Pyrenees: The Isuela section, *Palaeogeography, Palaeoclimatology, Palaeoecology, 333-334*, 107-120.

Rodríguez-Pintó, A., E.L.Pueyo, A.Pocoví, M.J.Ramón, and B. Oliva-Urcia (2013), Structural control on overlapped paleomagnetic vectors: A case study in the Balzes anticline (Southern Pyrenees), *Physics of the Earth and Planetary Interiors, 215, 43-57*, doi: 10.1016/j.pepi.2012.10.005

Rosenbaum, G., G.S. Lister, and C. Duboz (2002), Relative motions of Africa, Iberia and Europe during Alpine orogeny, *Tectonophysics, 359*, 117-129.

Schwartz, S.Y., and R. Van der Voo (1983), Paleomagnetic evaluation of the orocline hypothesis in the central and southern Appalachians, *Geophysical Research Letters, 10*, 505-508, doi: 10.1029/GL010i007p00505.

Séguret, M. (1972), Étude tectonique des nappes et séries décollées de la partie centrale du versant sud des Pyrénées – Caractère synsédimentaire, rôle de la compression et de la gravité, Série géologie structurale, 2, Publications de l'Universite des Sciences et Techniques du Languedoc (USTELA), Montpellier, France, 155 pp

Serra-Kiel, J., J.I. Canudo, J. Dinarès, E. Molina, N. Ortiz, J.O. Pascual, J.M. Samsó, and J. Tosquella (1994), Cronoestratigrafía de los sedimentos marinos del Terciario inferior de la Cuenca de Graus-Tremp (Zona Central Surpirenaica), *Revista Sociedad Geológica España, 7,* 273-297.

Soler, M., and A. Garrido Megías (1970), La terminación occidental del manto de Cotiella, *Pirineos, 98*, 5-12.

Soto, R., and A.M. Casas (2001), Geometría y cinemática de las estructuras norte-sur de la Cuenca de Aínsa, *Revista de la Sociedad Geológica de España 16(3-4),* 199-211.

Soto, R., A.M. Casas, F. Storti, and C. Faccenna (2002), Role of lateral thickness variations on the development of oblique structures at the western end of the South Pyrenean Central Unit, *Tectonophysics 350*, 215-235.

Soto, R., A.M. Casas-Sainz, and E.L. Pueyo (2006), Along-strike variation of orogenic wedges associated with vertical-axis rotations, *Journal of Geophysical Research (Solid Earth), 111 (B10)*, B10402- B10423.

Storti, F., R. Soto, F. Rossetti, and A.M. Casas-Sainz (2007), Evolution of experimental thrust wedges accreted from along-strike tapered, silicone-floored multilayers, *Journal of the Geological Society, London, 164*, 73-85.

Sussman, A.J., and Weil (2004), *Orogenic Curvature: Integrating Paleomagnetic and Structural Analyses*, Geological Society of America Special Paper 383, 258 pp.

Sussman, A.J, R.F. Butler, J. Dinarès-Turell, and J. Vergés (2004), Vertical-axis rotation of a foreland fold and implications for orogenic curvature: an example from the

Southern Pyrenees, Spain, *Earth and Planetary Science Letters, 218 (3-4)*, 435-449.

Taberner, C., J. Dinarès-Turell, J. Jiménez, and C. Docherty (1999), Basin infill architecture and evolution from magnetostratigraphic cross-basin correlations in the southeastern Pyrenean foreland basin, *Geological Society of America Bulletin, 11(8),* 1155-1174.

Tavani, S., F. Storti, O. Fernández-Bellon, J.A. Muñoz, and F. Salvini (2006), 3-D deformation pattern analysis and evolution of the Añisclo anticline, southern Pyrenees, *Journal of Structural Geology, 28,* 695–712.

Tavani, S., O. Fernández, and J.A. Muñoz (2012), Stress fluctuation during thrust-related folding. Example form the Boltaña Anticline (Pyrenees, Spain), in *Faulting, Fracturing and Igneous Intrusion in the Earth's Crust*, edited by D.Healy, R.W.H. Butler, Z.K. Shipton and R.H. Sibson, 131-140, Geological Society, London, Special Publications, 367.

Teixell, A. (1996), The Ansó transect of the southern Pyrenees: basement and cover thrust geometries, *Journal of the Geological Society, London, 153*, 301-310.

Teixell, A. (1998), Crustal and orogenic material budget in the west central Pyrenees, *Tectonics, 17(3),* 395-406.

Teixell, A., and A. Barnolas (1995), Significado de la discordancia de Mediano en relación con las estructuras adyacentes (Eoceno, Pirineo Central), *Geogaceta, 18,* 34-37.

Teixell, A., and J.A. Muñoz (2000), Evolución tectono-sedimentaria del Pirineo meridional durante el Terciario: una síntesis basada en la transversal del río Noguera Ribagorçana, *Revista de la Sociedad Geológica de España, 15(2),* 251-264.

Travé, A., P. Labaume, F. Calvet, and A. Soler (1997), Sediment dewatering and pore fluid migration along thrust faults in a foreland basin inferred from isotopic and elemental geochemical analyses (Eocene southern Pyrenees, Spain), *Tectonophysics, 282,* 375-398.

Travé, A., P. Labaume, F. Calvet, A. Soler, J. Tritlla, M. Buatier, J-L. Potdevin, M. Séguret, S. Raynaud, and L. Briqueu (1998), Fluid migration during Eocene thrust emplacement in the south Pyrenean foreland basin (Spain): an integrated structural, mineralogical and geochemical approach, in *Cenozoic Foreland Basins of Western Europe*, edited by A. Mascle, C. Puigdefàbregas and M. Fernández, 163-188, Geological Society Special Publications 134.

Van Lunsen, H. (1970), Geology of the Ara-Cinca region, Spanish Pyrenees, *Bulletin Societé Géologique France, VI(2)*, 265-271.

Vergés, J. (1993), *Estudi tectònic del vessant sud del Pirineu oriental i central. Evolució cinemàtica 3D*. PhD thesis, Universitat de Barcelona, 203 pp.

Vidal, O., H. A. Koyi, and J.A. Muñoz (2009), Formation of orogen-perpendicular thrusts due to mechanical contrasts in the basal décollement in the Central External Sierras (Southern Pyrenees, Spain), *Journal of Structural Geology, 31*, 523-539.

Weil, A.B., and A. Sussman (2004), Classifying curved orogens based on the timing relationships between structural development and vertical-axis rotations, in *Orogenic Curvature: Integrating Paleomagnetic and Structural Analyses*, edited by A.J.Sussman, and A.B. Weil, 1–17, Geological Society of America Special Paper 383.

Weil, A.B., A. Yonkee, and A. Sussman (2010), Reconstructing the kinematic evolution of curved mountain belts: A paleomagnetic study of Triassic red beds from the Wyoming salient, Sevier thrust belt, U.S.A., *Geological Society of America Bulletin, 122,* 3-23, doi: 10.1130/B26483.1.

Yonkee, A., and A.B. Weil (2010a), Reconstructing the kinematic evolution of curved mountain belts: Internal strain patterns in the Wyoming salient, Sevier thrust belt, U.S.A. *Geological Society of America Bulletin, 122 (1/2),* 24-49, doi: 10.1130/B26484.1.

Yonkee, A., and A.B. Weil (2010a), Reconstructing the kinematic evolution of curved mountain belts: Internal strain patterns in the Wyoming salient, Sevier thrust belt, U.S.A. Geological Society of America Bulletin, 122 (1-2), 24-49, doi: 10.1130/B26484.1.

TABLE S1

Bentham (1992)

label	site	polar.	chron	age	geo coords		bedding		BBC				ABC				β
					lat (N)	long	dd	dip	Dg	Ig	α95	k	Ds	Is	α95	k	
B1	Alz	N	/	Lut-Bart	/	/	/	/	352	41	30	7	2	48	25	7.7	19
		R	/		/	/	/	/	208	-14	35	5.4	218	-24	32	8.3	
B2	Erp	N	/	Bart-Priab	/	/	/	/	20	49	7	12.7	34	54	8	11.6	18
		R	/		/	/	/	/	192	2	22	5	184	-20	21	6	
B3	Med	N	/	Lut-Bart	/	/	/	/	29	41	7	13.2	22	53	6	14.4	26
		R	/		/	/	/	/	211	-9	16	6.5	212	-25	15	8.9	
B4	Lig	N	/	Bart-Priab	/	/	/	/	8	45	14	5	12	51	12	9.1	20
		R	/		/	/	/	/	200	-20	14	7.1	209	-24	15	7.5	
B5	Es	N	/	Lutetian	/	/	/	/	/	/	/	/	12	49	16.8	5.8	11
		R	/		/	/	/	/	/	/	/	/	199	-35	15.8	6.4	
B6	Las	N	/	Lut-Bart	/	/	/	/	/	/	/	/	5	52	16.5	12.2	-2
		R	/		/	/	/	/	/	/	/	/	184	-45	17.3	9.8	

Dinarès-Turell (1992), Dinarès-Turell et al (1992)

label	site	polar.	chron	age	UTM			bedding		BBC				ABC				β
					zone	X	Y	dd	dip	Dg	Ig	α95	k	Ds	Is	α95	k	
D1	89J36	R	/	Ypresian	31	285500	4696500	30	53	207	2	4.4	98	205	-51	4.2	107.4	21
D2	89J38	N	/	Ypresian	31	297300	4686800	43	9	32	50	8.3	40	29	59	6.8	58.1	25
D3	90J11	N	/	Ypresian	31	294900	4688100	225	16	34	29	7	44	31	45	6.1	56.3	27
D4	90J13	N	/	Ypresian	31	282800	4698800			71	-19	16	11	84	59	13.1	16.5	80
D5	90J14	N	/	Ypresian	31	282500	4698800	203	34	49	33	18	13	72	61	16.5	14.3	68
D6	90J19	R	/	Ypresian	31	295200	4687800	104	23	197	-50	9.7	23	221	-44	13.8	12	37
D7	90J22	R	/	Ypresian	31	281100	4699200	156	38	223	-33	18	16	252	-39	15.8	18.9	68
D8	90J23	R	/	Ypresian	31	281200	4699200			236	38	8.9	28	239	-59	8.5	26.9	55
D9	90J25	N	/	Lutetian	31	258700	4692000	245	7	45	42	38.8	6.6	42	42	38.8	6.6	38
D10	90J27	R	/	Ypresian	31	277600	4702800	162	15	231	-37	15	36	243	-41	15.4	36.4	59
D11	90J28	R	/	Ypresian	31	277800	4702700	230	82	242	29	4.7	376	247	-51	4.1	500.2	63
D12	90J29	R	/	Ypresian	31	276600	4702900	220	35	206	-40	25	10	182	-72	25.1	10.2	-4
D13	90J30	R	/	Mid Cuisian	31	270800	4702200	199	17	227	-12	15	21	230	-27	13.2	26.7	46
D14	90J31	N	/	Cuisian	31	272400	4690800	87	31	19	72	15	28	61	49	14.6	28.5	57
D15	90J32	N	/	Up Ilerdian	31	265000	4710000	107	17	30	28	5.9	243	38	23	5.9	243.9	34
D16	90J33	N	/	Up Ilerdian	31	265900	4712600	141	8	25	36	9.7	168	34	33	9.7	162.7	30

D17	90J34	N	/	Up Ilerdian	31	265700	4712500	141	8	41	30	8.6	206	44	38	8.6	205.6	40
D18	90J35		/	Ypresian	31	266800	4714500	161	10	216	-13	6.7	186	218	-19	6.8	400.6	34
D19	90J36	N	/	Mid Lutetian	31	268000	4694000	233	17	48	38	8.8	76.3	46	55	9.3	69	42
D20	90J38	R	/	Lutetian	31	259100	4692800	81	40	161	-66	23	121	224	-48	23	120.4	40
D21	90J39	R	/	Ypresian	31	255900	4705800	107	15	233	-57	14.1	19.2	247	-47	14.1	19.3	63
D22	90J12	N	/	Ypresian	31	285200	4696200	243	23	31	33	8.9	142	18	51	7.3	15	14

Pascual et al (1992)

label	site	polar.	chron	age	UTM zone 31		bedding		BBC				ABC				β
					X	Y	dd	dip	Dg	Ig	α95	k	Ds	Is	α95	k	
PA1	Tremp	N+R		Ilerdian	322000	4669200	/	/	/	/	/	/	13	46	4	10	9

Hogan (1993)

label	site	polar.	chron	age	geo coords		bedding		BBC				ABC				β
					lat (N)	long	dd	dip	Dg	Ig	α95	k	Ds	Is	α95	k	
H1	Mn	N		Bart-Priab	/	/	/	/	9	45	12.2	5.4	6	21	12.2	5.4	12
		R			/	/	/	/	204	-41	6.8	6.8	200	-22	6.4	7.6	
H2	Yb	N		Bart-Priab	/	/	/	/	318	77	8.9	6.1	11	38	9	6	29
		R			/	/	/	/	43	-68	/	/	228	-45	31.3	3.1	

Pueyo (2000)

label	sector	site	polar.	age	UTM zone 30		bedding		BBC				ABC				β
					X	Y	dd	dip	Dg	Ig	α95	k	Ds	Is	α95	k	
P1	JAN	96	R+N	Lutetian	743257	4707555	236	68	223	29	22	5	222	-38	/	/	38
		97	R	Lutetian	743900	4705643	244	54	227	18	20	6	225	-34	/	/	
P2	Gug (N)	124	N	Priabonian	732940	4703735	209	85	41	-44	9	17	40	39	/	/	33
		125	R	Rupelian	732543	4702270	200	42	197	24	33	30	197	-18	/	/	
		126	N	Rupelian	731870	4699610	197	9	33	34	11	22	35	43	/	/	
P3	Gug (S)	127	N+R	Priabonian	727000	4692102	167	12	191	-26	7	22	194	-37	/	/	10
		128	N+R	Rupelian	726803	4695000	352	10	198	-57	17	10	193	-48	/	/	
P4	Gua	48	R	Bartonian	718612	4688160	340	28	234	-73	8	24	188	-54	/	/	17
		49	R	Bartonian	716960	4687580	350	31	245	-59	16	8	212	-42	/	/	
		51	R	Bartonian	720960	4688480	337	44	273	-51	16	20	216	-49	/	/	
		53	N	Bartonian	725649	4687162	328	27	60	66	11	18	13	55	/	/	
		54	N	Bartonian	726150	4687530	320	65	97	63	15	10	344	42	/	/	
		55	N	Bartonian	724067	4688980	9	20	17	55	13	13	14	35	/	/	

		56	N+R	Priabonian	735752	4689703	339	22	46	33	18	11	35	22	/	/	
		57	N	Bartonian	735485	4690154	351	31	45	37	11	20	33	15	/	/	
		58	R	Priabonian	733057	4690152	352	30	227	-53	13	23	207	-31	/	/	
		59	N	Priabonian	730448	4689900	355	25	10	64	17	8	3	39	/	/	
		60	N	Bartonian	730915	4688770	354	34	75	69	14	13	25	48	/	/	
P5	Bas	88	N	Priabonian	716854	4708632	211	77ov	20	-49	7	57	19	53	/	/	15
		91	R	Upper Lutetian	731223	4704250	212	75	217	26	25	8	219	-49	/	/	
		92	N+R	Upper Lutetian	727989	4705471	25	55	281	81	25	11	14	37	/	/	
		93	R	Lower Bartonian	720528	4707963	23	66ov	203	76	24	3	203	-38	/	/	
		94	N	Lower Bartonian	717850	4709330	40	77ov	30	-59	9	29	33	43	/	/	
		95	N+R	Lower Bartonian	720420	4714200	159	25	181	-27	16	20	190	-50	/	/	
P6	Mon (N)	88	N	Priabonian	716854	4708632	31	77ov	20	-49	7	57	19	53	/	/	5
		123	N	Priabonian	711377	4706077	19	48	325	74	6	73	4	32	/	/	
P7	Mon (S)	119	R	Priabonian	714710	4691626	350	25	167	-56	7	30	167	-31	/	/	2
		120	R	Rupelian	715391	4694106	4	25	190	-62	12	12	186	-37	/	/	
		121	R	Rupelian	714726	4696459	4	14	205	-55	7	18	199	-42	/	/	
P8	Agl	37	N	Bartonian	712345	4688300	292	60	61	30	11	19	9	46	/	/	18
		38	N	Bartonian	711997	4688350	317	37	56	50	5	68	16	42	/	/	
		39	R	Bartonian	716000	4688590	10	32	266	-84	5	70	201	-56	/	/	
		45	N	Bartonian	715640	4687720	354	23	76	75	5	110	26	61	/	/	

Beamud et al (2003)

label	site	polar.	chron	age	geo coords		bedding		BBC				ABC				β
					lat (N)	long	dd	dip	Dg	Ig	α95	k	Ds	Is	α95	k	
BE1	Sis	N+R	C18R+C18N	Bartonian	42.31º	0.61º E	/	/	3.8	48.7	5.1	20.7	7	39.4	5.2	19.3	3

Oliva-Urcia (2004), Oliva-Urcia & Pueyo (2007), Oliva-Urcia et al (2008)

label	site	polar.	chron	age	geo coords		bedding		BBC				ABC				β
					lat (N)	long	dd	dip	Dg	Ig	α95	k	Ds	Is	α95	k	
OU19	AÑI8	R	/	Maastrichtian	42º38'54"	0º4'5" E	194	18	168	-16	10	/	164	-34	/	/	/
OU18	OTA6	R	/	Cenom-Santonian	42º41'43"	0º7'41"W	28	68ov	207	-34	13	19	32	-33	/	/	/
OU15	TEN2	R	/	Maastrichtian	42º40'43"	0º14'6"W	180	57	175	-24	41	7	151	-80	/	/	/
OU14	ASN3	R	/	Cenom-Santonian	42º41'16"	0º15'23"W	186	45	207	-32	10	23	256	-71	/	/	/
OU21	PIN1	R	/	Cenom-Santonian	42º40'27"	0º6'36"E	224	36	163	-19	17	6	148	-33	/	/	/
OU23	TOU4	R	/	Maastrichtian	42º42'10"	0º1'43"W	350	89ov	160	-41	11	84	0	-39	/	/	/
OU13	ELE1	R	/	Cenom-Santonian	42º40'7"	0º19'14"W	178	59	193	-40	8	56	309	-74	/	/	/

OU20	MAR2	R	/	Maastrichtian	42º41'16''	0º2'41''E	214	17	178	-42	10	25	165	-55	/	/	/
OU8	ARA8	R	/	Maastrichtian	42º42'20''	0º31'36''W	200	25	205	-48	19	18	227	-76	/	/	/
OU16	TEN3	R	/	Cenom-Santonian	42º41'16''	0º14'54''W	164	65	225	-53	10	47	302	-37	/	/	/
OU12	PIE3	R	/	Cenom-Santonian	42º42'23''	0º23'51''W	177	45	189	-57	9	30	330	-76	/	/	/
OU22	ELE5	R	/	Eocene (Hecho Gp)	42º39'29''	0º19'14''W	194	84	209	-40	13	16	352	-53	/	/	/
OU17	OTA2	R	/	Cenom-Santonian	42º41'24''	0º8'48''W	172	44	155	-39	21	10	105	-75	/	/	/
OU7	ELE7	R	/	Eocene (Hecho Gp)	42º37'58''	0º19'36''W	63	20	205	24	15	15	208	-8	/	/	/
OU1	(1) TRI-2	R	/	Triassic red beds	42º35'6''	0º19'56''W	205	85	190	-16	14	17	77	-72	/	/	/
OU2	(6)TRI-7	R	/	Triassic red beds	42'36'37''	0º14'48''W	210	20	198	-22	14	22	195	-44	/	/	/
OU5	(5)TRI-6	R	/	Triassic red beds	42'38'24''	0º12'58''W	212	45	191	-34	8	36	149	-71	/	/	/

Mochales et al (2012a,b)

label	site	polar.	chron	unit	UTM			bedding		BBC				ABC				β
					zone	X	Y	dd	dip	Dg	Ig	α95	k	Ds	Is	α95	k	
MO1	CAS1	R	C20R	La Patra Mb	31	256294	4691407	80	23	218	-73	7.1	59.5	240	-52	7	61.3	56
	CAS2	R	C20R	La Patra Mb	31	256321	4691421	82	26	210	-60	20.4	7.3	227	-45	21	7	43
	CAS3	N+R	C20N	La Patra Mb	31	256494	4691358	95	27	3	63	22	12.3	41	53	19.8	14.8	37
	CAS4	N+R	C20N	La Patra Mb	31	256746	4691181	86	20	45	60	18.9	6.8	57	50	16.1	9	53
	CAS5	N+R	C20N	La Patra Mb	31	257491	4691559	94	22	340	56	13.8	19.5	15	58	12.7	22.7	11
	CAS6	N+R	C20N	La Patra Mb	31	257975	4691523	87	24	18	59	10.9	20.4	44	46	11.1	19.8	40
	CAS7	R	C19R	Sobrarbe Fm	31	258412	4691197	84	21	207	-56	8.1	40.9	224	-41	8.3	38.4	40
	CAS8	R	C19R	Sobrarbe Fm	31	258754	4691296	82	22	205	-55	20.5	55.8	224	-41	20.6	55.4	40
									MO1:	20	62	8	48	45	49	7	63	41
MO2	COS1	R+N	C21R	Paules Mb	31	255470	4690014	88	18	197	-67	7	43.6	223	-58	7.1	41.9	39
	COS2	R+N	C20R	Paules Mb	31	256062	4690160	80	27	184	-63	6.5	45.4	221	-48	7.3	36.1	37
	COS3	R	C20R	Paules Mb	31	256184	4690146	80	25	199	-63	5.4	59.7	225	-46	6.2	45.6	41
	COS4	R	C20R	Paules Mb	31	256266	4689306	89	20	203	-64	4.3	124	224	-50	7.2	45.7	40
	COS5	R	C20R	Paules Mb	31	256376	4689286	89	27	199	-67	12	17	226	-50	12.2	16.6	42
	COS6	R	C20R	Paules Mb	31	256562	4689281	86	26	188	-69	7.7	35.7	226	-55	6.5	50.3	42
									MO2:	195	-66	3	415	224	-51	4	303	40
MO3	MON1	R+N	C20N	Sobrarbe Fm	31	260535	4686825	98	23	195	-52	12	21.7	218	-41	12.3	20.7	34
	MON2	R+N	C19R	Sobrarbe Fm	31	260888	4686646	100	22	180	-59	7.5	46.8	213	-55	6.4	64	29
	MON3	R	C19R	Sobrarbe Fm	31	261090	4686522	100	23	193	-51	9.5	26.7	218	-45	9.3	27.5	34
	MON4	N+R	C19R	Sobrarbe Fm	31	261307	4686392	113	17	16	49	19	7.4	33	49	18	8.2	29
	OLS1	R	C19R	Sobrarbe Fm	31	260618	4685394	124	25	215	-36	16	12.7	233	-32	14.8	14.6	49
	OLS2	R+N	C19R	Escanilla Fm	31	260898	4685156	126	21	215	-32	13.4	20.5	218	-24	14.7	17.4	34

	OLS3	R+N	C18R	Escanilla Fm	31	261182	4684942	135	16	208	-16	24.4	6.1	206	-21	24.4	6.1	22
	OLS4	R+N	C18R	Escanilla Fm	31	261394	4684706	91	16	29	36	13.2	16	214	-41	12.8	17	30
									MO3:	22	43	13	22	37	38	11	31	33
MO4	ESC3	N	C17N.2n	Escanilla Fm	31	262072	4683329	170	10	31	27	13.4	9.7	35	34	13.4	9.7	31
	ESC2	N	C17N.1n	Escanilla Fm	31	262256	4683133	158	13	27	45	14	14.2	39	52	14	14.2	35
	ESC1	N	C16N.2n	Escanilla Fm	31	262320	4682955	155	15	18	50	8.9	30	35	60	8.9	30	31
									MO4:	26	41	20	38	36	49	21	37	32
MO5	ESC4	N	C16N.2n	Escanilla Fm	31	262532	4682604	185	10	26	17	9.7	25.5	27	26	9.7	25.5	23
	ESC5	R	C16N.1r	Escanilla Fm	31	262605	4682420	175	16	195	21	12.5	28.5	198	-36	12.5	28.5	14
									MO5:	20	3	153	5	23	31	82	28	19
MO6	ESC6	R	C15	Escanilla Fm	31	262776	4682247	175	16	180	-31	7.3	49.3	181	-47	7.3	49.3	-3
	ESC7	N+R	C15N	Escanilla Fm	31	262872	4682316	173	3	1	44	4.1	111	2	47	4.1	110.6	-2
									MO6:	0	38	29	78	2	47	1.5	28244	-2
MO7	ARA1	R	C24R	Alveolina lmst	31	254791	4706181	273	29	225	-35	12.7	17.1	200	-50	11.7	20	16
	ARA2	R	C24R	Metils Fm	31	254554	4706253	273	29	226	-29	10.4	15.5	209	-53	9.5	16.1	25
	ARA3	R	C24R	Yeba Fm	31	254464	4706224	272	50	249	-9	10.7	21.1	230	-52	13.6	13.4	46
	ARA4	N+R	C24R	Yeba Fm	31	254394	4706252	279	54	243	3	24.4	5.4	39	32	28	4.9	35
	ARA5	R	C24N.1r	Lw Boltaña Mb	31	254216	4706317	274	63	37	-7	13.7	12.1	52	46	14.6	10.7	48
	ARA7	R+N	trC24n.1N/C23r	Lw Boltaña Mb	31	253975	4706280	274	64	245	2	24.7	6.8	227	-52	19.8	10	43
	ARA6	R	C23R	Lw Boltaña Mb	31	253910	4706069	278	72	252	22	8.3	25.7	246	-43	8.2	26.2	62
	ARA8	R	C23R	Up Boltaña Mb	31	253750	4706135	276	68	249	13	13.7	40.4	226	-50	15	33.6	42
	ARA9	R	C22R	Up Boltaña Mb	31	253519	4706413	277	82	229	33	35.9	19.3	226	-35	18.9	65.4	42
									MO7:	60	0	36	3	47	46	8	46	43
MO8	MILL1	R	C24R	Millaris Fm	31	255245	4706873	283	6	240	-50	8.2	26.4	235	-54	8.4	24.9	51
	MILL2	R	C24R	Millaris Fm	31	255192	4706943	280	6	236	-37	7.9	28.3	231	-43	8	27.9	47
									MO8:	268	-43	29	74	233	-49	25	103	49

Rodríguez-Pinto et al (2013)

label	site	polar.	chron	age	UTM			bedding		BBC				ABC				β
					zone	X	Y	dd	dip	Dg	Ig	α95	k	Ds	Is	α95	k	
RP1	SS01	R	/	Lutetian	30	748105	4691307	97	40	170	-50	12	33	216	-5	11	33	32
	SS02	R	/	Lutetian	30	747957	4691454	102	81	146	-33	8	104	235	-41	9	86	51
	SS03	R	/	Lutetian	30	747978	4688942	103	51	192	-63	6	58	249	-34	7	54	65
	SS04	R	/	Lutetian	30	747387	4688669	95	43	208	-73	5	114	253	-38	5	97	69
	SS05	R	/	Lutetian	30	747160	4688582	89	36	227	-61	10	14	247	-31	10	14	63
	SS06	R	/	Lutetian	30	746484	4687200	82	41	207	-59	6	35	234	-27	6	35	50

RP2	SI	N	/	Cuisian-Lw Lut	/	/	/	/	/	5	61	8	7	21	42	9	6	17
	SI	R	/	Cuisian-Lw Lut	/	/	/	/	/	184	-46	4	17	191	-23	5	17	7

TABLE S2

Figure 14 sites

label	site	author	age	structure	UTM coordinates zone 31		Ds	Dr	Ds-Dr	S	source	Sr	S-Sr
PA1	Tremp	Pascual	Ilerdian		~ 322000	~ 4669200	13	4	9	97.3	map	97.3	0
D1	89J36	Dinarès-Turell	Ypresian		285500	4696500	205	4	21	111.5	map + stereo	97.3	14.2
D2	89J38	Dinarès-Turell	Ypresian		297300	4686800	29	4	25	111.5	map + stereo	97.3	14.2
D3	90J11	Dinarès-Turell	Ypresian		294900	4688100	31	4	27	111.5	map + stereo	97.3	14.2
D6	90J19	Dinarès-Turell	Ypresian		295200	4687800	221	4	37	111.5	map + stereo	97.3	14.2
90J12	90J12	Dinarès-Turell	Ypresian		285200	4696200	18	4	14	111.5	map	97.3	14.2
32	BL6	this work	up Ilerdian		267643	4710863	36	4	32	117.8	stereo	97.3	20.5
D13	90J30	Dinarès-Turell	Mid Cuisian		270800	4702200	230	4	46	130	map	97.3	32.7
13	AP2	this work	mid Cuisian		267580	4705000	217	4	33	131.6	stereo	97.3	34.3
D15	90J32	Dinarès-Turell	Up Ilerdian		265000	4710000	38	4	34	136	stereo	97.3	38.7
12	AP1	this work	mid Cuisian		266540	4698290	240	4	56	136.3	stereo	97.3	39
D7	90J22	Dinarès-Turell	Ypresian		281100	4699200	252	4	68	147	map	97.3	49.7
D8	90J23	Dinarès-Turell	Ypresian		281200	4699200	239	4	55	147	map	97.3	49.7
D10	90J27	Dinarès-Turell	Ypresian		277600	4702800	243	4	59	150	map	97.3	52.7
D11	90J28	Dinarès-Turell	Ypresian		277800	4702700	247	4	63	152	map	97.3	54.7
D19	90J36	Dinarès-Turell	Mid Lutetian		268000	4694000	46	4	42	161.7	stereo	97.3	64.4
3	FM1	this work	low Lutetian	Mediano	272800	4690350	84	4	80	174.7	stereo	97.3	77.4
7	YM1	this work	up Ilerdian	Mediano	270700	4689190	82	4	78	174.7	stereo	97.3	77.4
8	YM2	this work	up Ilerdian	Mediano	272400	4690650	61	4	57	174.7	stereo	97.3	77.4
D14	90J31	Dinarès-Turell	Cuisian	Mediano	272400	4690800	61	4	57	175	stereo	97.3	77.7
1	MM1	this work	mid Cuisian	Mediano	271670	4695020	238	4	54	177.8	stereo	97.3	80.5
20	CB	this work	low Lutetian	Boltaña	258408	4701832	56	4	52	177.9	stereo	97.3	80.6
22	GB	this work	low Lutetian	Boltaña	260682	4700467	74	4	70	177.9	stereo	97.3	80.6
D21	90J39	Dinarès-Turell	Ypresian	Boltaña	255900	4705800	247	4	63	180	stereo	97.3	82.7
MO7	ARA sites	Mochales	Ypresian	Boltaña	~ 254200	~ 4706200	47	4	43	180	stereo	97.3	82.7
MO8	MILL sites	Mochales	Ypresian	Boltaña	~ 255200	~ 4706900	233	4	49	180	stereo	97.3	82.7
MO2	COS sites	Mochales	Lutetian	Boltaña	~ 255000	~ 4690000	224	4	40	180	map	97.3	82.7
19	BB	this work	up Cuisian	Boltaña	257560	4705951	61	4	57	181.8	stereo	97.3	84.5
MO1	CAS sites	Mochales	Lutetian	Boltaña	~ 257000	~ 4691300	45	4	41	168	stereo	97.3	70.7
D16	90J33	Dinarès-Turell	Up Ilerdian		265900	4712600	34	4	30	152	map + stereo	97.3	54.7
D17	90J34	Dinarès-Turell	Up Ilerdian		265700	4712500	44	4	40	152	map + stereo	97.3	54.7
D18	90J35	Dinarès-Turell	Ypresian		266800	4714500	218	4	34	152	map	97.3	54.7
30	BL4	this work	mid Ilerdian	Añisclo	260898	4710445	225	4	41	166.9	stereo	97.3	69.6

CHAPTER 3- SYNTHESIS and DISCUSSION

3.1.- Chronostratigraphy of the Tertiary syntectonic materials

3.2.- Biochronological implications

3.3.- Kinematics, exhumation and tectonosedimentary evolution of the South-Central Pyrenees

3.1.- CHRONOSTRATIGRAPHY OF THE TERTIARY SYNTECTONIC MATERIALS

One of the main contributions of this PhD thesis is the continuous absolute dating of the syntectonic conglomerates of La Pobla de Segur, Senterada and Sis (Chapter 2.1 and 2.2). Correlation of the local magnetostratigraphies to the GPTS (Gradstein et al., 2004) has established the age of their deposition from Lutetian up to Chattian (from chron 19r up to chron 9n) (Figure 5 in chapter 2.2). Integration of these results with previous magnetostratigraphic works within the Ainsa Basin (*Bentham et al.*, 1992; *Mochales et al.*, 2012; *Rodriguez-Pinto et al.*, 2012) has allowed the establishment of a new chronostratigraphy for the Eocene-Oligocene materials of the South-Central Pyrenees (Figure 3.1). The chronostratigraphic panel spans from the Tertiary materials that crop out near the Ara river within the Gavarnie-Sierras Exteriores thrust sheet, through the ones cropping out between the Ésera and Isábena rivers within the Montsec thrust sheet, to the syntectonic materials flanked by the Isábena and the Noguera Pallaresa rivers within the Bóixols thrust sheet.

Figure 3.1- Eocene Chronostratigraphy of the South-Central Pyrenees, from the Ainsa basin to the La Pobla de Segur. Lithostratigraphic units: Mr, Merli reef; Is/Be: Iscles-Berganuy reefs; Bu, Buil; So, Sobrarbe; Cp, Capella; Pr, Perarrúa; Cst, Castissent; Al, Alveolina limestone. SV1-2: diferent units making the San Vicente Formation. Turbidite systems: gu, Guaso; og, O Grao; ga, Gabardilla; c, Coscojuela; fo, Formigales; s, Sieste; m, Morillo; a, Ainsa; gb, Gerbe-Banastón; ar, Arro; f, Fosado. Horizons: O, Olsón; EL, Escanilla limestone; SB, Santa Bárbara; SP, San Pedro; SL, San Lino; M, Morillo limestone; A, Ascaso; LP, La Puebla; Lu, Santa Llucia. Thrust sheets: C, Cotiella; Bo, Bóixols; M, Montsec; PM, Peña Montañesa; B & G, Bielsa and Guarga; LF, La Fueba thrust system. Litho and chronostratigraphic information compiled from: *Barnolas & Gil-Peña* (2001), *Bentham et al.* (1992), *Bentham & Burbank* (1996), *López-Blanco et al.* (2003), *Mochales et al.* (2012), *Rodríguez-Pintó et al.* (2012), *Serra-Kiel et al.* (1994). Time scale from *Gradstein et al.* (2004). SBZ biozones calibration to the GPTS integrates data from Costa et al. (2013) and Rodríguez-Pintó et al. (2012)

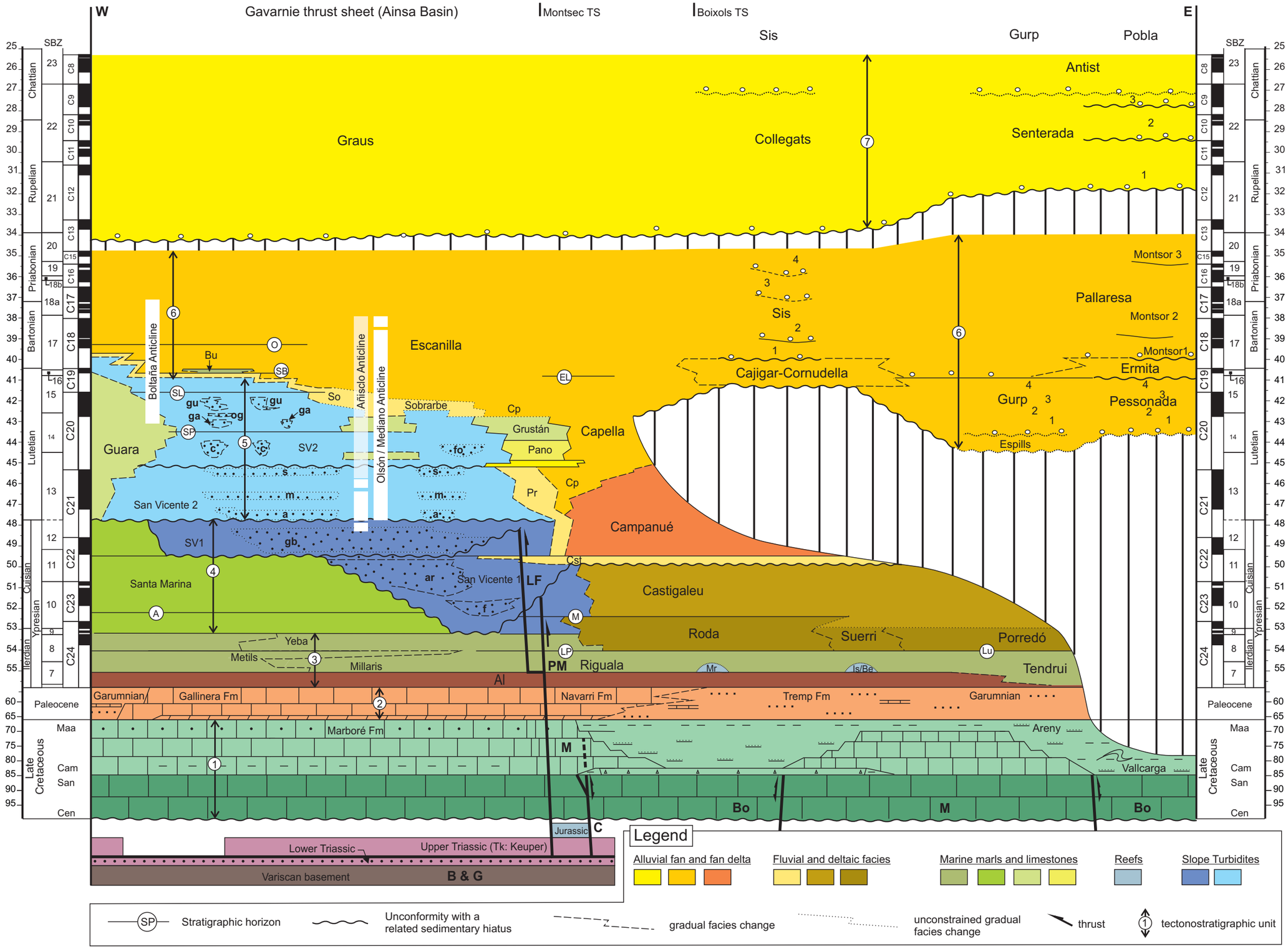
W
Gavarnie thrust sheet (Ainsa Basin)
Montsec TS
Boixols TS
E
Sis
Gurp
Pobla
SBZ
Chattian
Rupelian
Priabonian
Bartonian
Lutetian
Cuisian
Ypresian
Ilerdian
Paleocene
Late Cretaceous
Maa
Cam
San
Cen
Graus
Collegats
Antist
Senterada
Montsor 3
Pallaresa
Montsor 2
Montsor1
Ermita
Pessonada
Espills
Escanilla
Cajigar-Cornudella
Gurp
Sis
Boltaña Anticline
Añisclo Anticline
Mediano Anticline
Olsón / Mediano
Guara
SV2
San Vicente 2
SV1
Santa Marina
San Vicente 1
LF
Capella
Grustán
Pano
Sobrarbe
Cp
Pr
Campanué
Csl
Castigaleu
Roda
Suerri
Porredó
Tendrui
Riguala
PM
Al
Yeba
Metils
Millaris
Garumnian
Gallinera Fm
Navarri Fm
Tremp Fm
Marboré Fm
Areny
Vallcarga
M
Bo
Jurassic
C
Lower Triassic
Upper Triassic (Tk: Keuper)
Variscan basement
B & G
Legend
Alluvial fan and fan delta
Fluvial and deltaic facies
Marine marls and limestones
Reefs
Slope Turbidites
Stratigraphic horizon
Unconformity with a related sedimentary hiatus
gradual facies change
unconstrained gradual facies change
thrust
tectonostratigraphic unit

Pessonada 4, the youngest unit of the Pessonada allogroup, is the lowermost unit with magnetostratigraphic age control within the La Pobla Basin, correlated to chron C19r (Lutetian). Unfortunately, the lower units (Pessonada 1 to 3) didn't yield satisfactory results due to a weak paleomagnetic signal. Therefore, the age of the lowest 600 m of syntectonic conglomerates within La Pobla basin remains unconstrained. However, assuming a similar sedimentation rate than the obtained for the upper levels (0.3 m/ky) (chapter 2.1 and 2.2), the base of the unit could extend about 2 My down into the Lutetian. The Gurp Fm. in the Gurp conglomeratic succession is proposed to correlate with the Pessonada units of La Pobla basin due to its stratigraphic position below the Ermita allogroup, its similarity of facies and its arrangement in 4 sequences like the Pessonada allogroup (*Picart et al.*, 2009). The lowermost unit, the Espills Fm. could be either equivalent or slightly older than the Pessonada Fm. The dominantly lacustrine units of the Ermita allogroup would have their equivalents in the lacustrine units of the Cornudella Fm. at Sis, being deposited during the uppermost Lutetian and Bartonian (C18r). To the west, these materials correlate with the fluvial Escanilla Fm. and the deltaic Sobrarbe Fm. (*Bentham et al.*, 1992; *Mochales et al.*, 2012). On top of the Escanilla limestone, the Escanilla Fm. is proposed to correlate with the upper part of Cajigar-Cornudella Fm.-Ermita allogroup and the Sis Fm. and the Pallaresa allogroup to the east. Within the Ainsa Basin, the youngest units of the Escanilla Fm. are correlated to chron C15n (Priabonian) (*Bentham et al.*, 1992). To the east, the Pallaresa allogroup in the La Pobla basin yields a slightly younger age (C13r). The Sis Fm. conglomerates have been precisely dated by magnetostratigraphy up to the base of Sis 2 Mb. and they would be lateral equivalents to the Montsor 1 and 2 members of the Pallaresa allogroup in La Pobla basin. Unconformably above the Pallaresa allogroup, the Senterada allogroup spans from C12r up to C9n (Rupelian to Chattian). A gap of 2 Ma exists between the uppermost levels of the Pallaresa allogroup and the Senterada allogroup. Although unconstrained, the time gap of this unconformity is supposed to decrease towards the west, where the base of the Graus conglomerates has been dated as younger than C15n (*Bentham*, 1992; *Bentham & Burbank*, 1996). The Graus conglomerates range in age from Late Eocene to Late Oligocene or even to the Oligocene-Miocene boundary based on micromammal biostratigraphy (*Cuevas Gozalo*, 1989). The age of the Antist conglomerates is not precise as their outcrop conditions didn't allow magnetostratigraphic dating. However, a deposition between 27 and 24 Ma (Chattian up to the Oligocene-Miocene boundary) is plausible assuming the sedimentation rate obtained for the underlying Senterada allogroup keeps constant. In the Isábena valley, the Collegats Fm. has been correlated with the Graus conglomerates near Graus (*Reynolds*, 1987; *Vincent*, 1993,

2001). Therefore, deposited on top of a pronounced unconformity, the Graus and Collegats Fms. would be the western lateral equivalents of the Senterada and Antist allogroups.

3.2.- BIOCHRONOLOGICAL IMPLICATIONS

Chapter 2.1 presents a new calibration of the Eocene MP14 to MP17 reference levels based on the magnetostratigraphy of La Pobla de Segur and Sis conglomerates and its integration with the South-Central Pyrenees Eocene chronostratigraphic framework (Figure 6 in Chapter 2.1).

In this section, an updated calibration is presented (Figure 3.2). The main changes include a correlation to the newer GPTS (*Gradstein et al.*, 2004) and the integration of the results of a new magnetostratigraphic section from the SE margin of the Ebro basin (the Pontils section; *Beamud et al.*, 2012). This section includes the Pontils fossil site, assigned to the MP15 reference level *(Anadón et al*., 1983). The results of the Pontils magnetostratigraphy are presented as Supplementary material (see Supplementary material 2).

It can be observed in Figure 3.2 that calibration of both the marine biozones (calcareous nannoplankton: NP, and larger foraminifera shallow benthic zones: SBZ) and the mammal reference levels (MPs) have not reached estability and new proposals of calibration are common (*Barberà et al.*, 2001; *Costa et al.*, 2011; *Costa et al.*, 2013, *Rodríguez-Pintó et al.*, 2012). Changes in calibration of the marine biozones may have also implications for the chronology of the continental reference levels, as marine-continental stratigraphic relationships are frequently used to calibrate the continental units.

The proposed calibration of the Eocene MP reference levels MP14 to MP17 with the GPTS (*Gradstein et al.*, 2004) based on the Southern Pyrenees and Ebro basin fossil sites is summarized in Figure 3.2, where it is compared to previous proposals (*Schmidt-Kittler*, 1987; *Legendre & Leveque*, 1997; *Hooker & Steninger*, 1998). In the light of these results, MP14 and MP15 are correlated to the Lutetian, specifically, the Pontils fossil locality (MP15) is constrained to chron C19n. MP17a is correlated to the lower Bartonian, within C18r. It can be observed that a reduced time span is left for MP16 in this calibration.

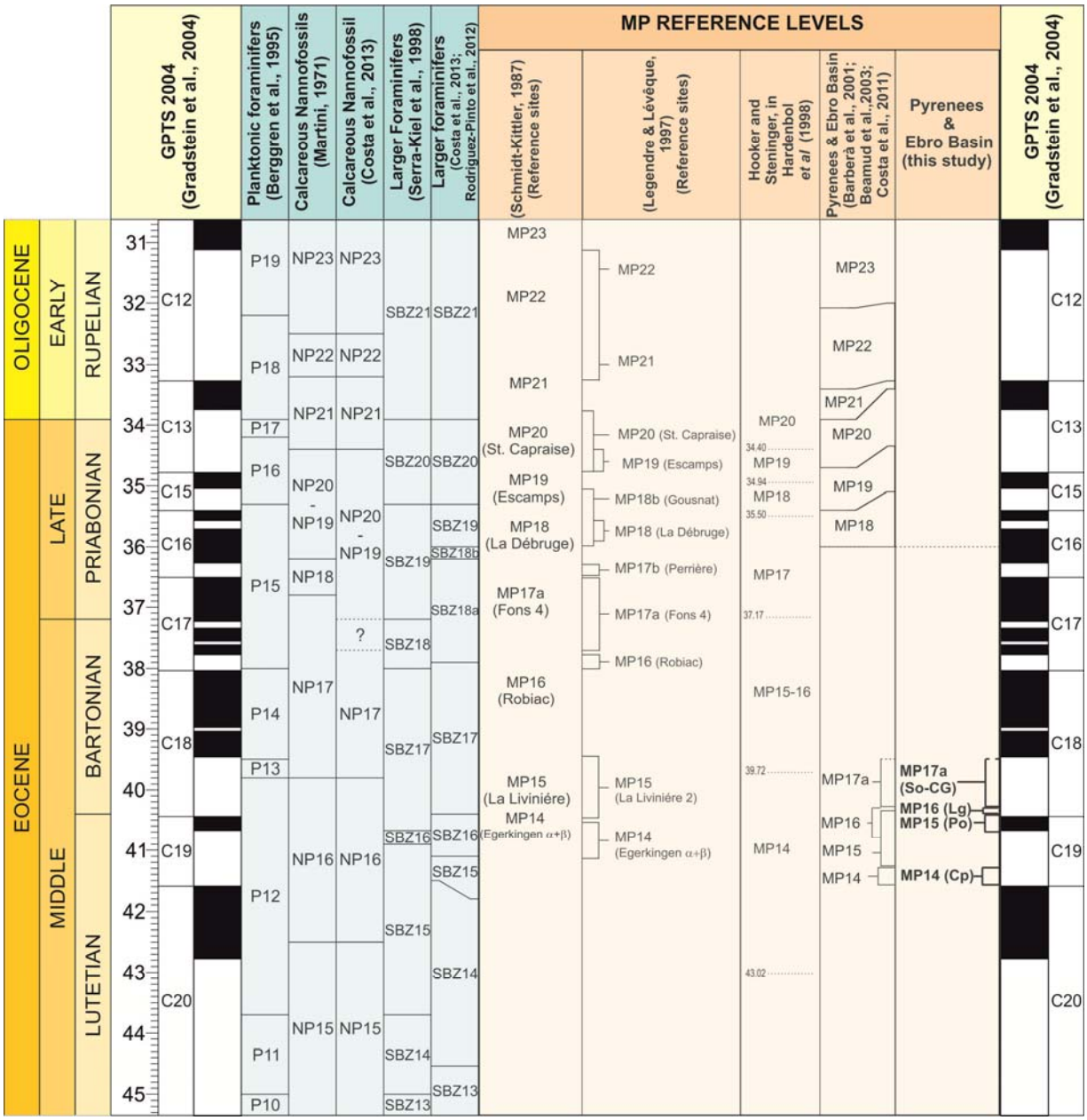

Figure 3.2.- Correlation of the south Pyrenean and Ebro Basin Eocene fossil sites and their assigned MP reference levels to the GPTS (*Gradstein et al.*, 2004) and comparison with previous calibrations. So-CG: Sossís-Can Gramuntill, Lg: Laguarres, Po: Pontils and Cp: Capella fossil sites.

3.3.- KINEMATICS, EXHUMATION AND TECTONOSEDIMENTARY EVOLUTION OF THE SOUTH-CENTRAL PYRENEES

The kinematic and tectonosedimentary evolution of the South Central Pyrenees and the coeval exhumation history of the Axial Zone can be constrained significantly from the integration of the thermochronologic and paleomagnetic (magnetostratigraphy and magnetotectonics) results.

The magnetotectonic study (chapter 2.3) allows the quantification of vertical axis rotations caused by differential transport during thrust sheet emplacement. These data can be integrated with the vast paleomagnetic dataset available in this region (Figure 3.3; tables S1) in order to assess the age and areal distribution of vertical axis rotations within the southern Pyrenean fold and thrust belt. The South-Central Pyrenees can be divided in three sectors according to the amount of vertical axis rotations recorded; a central sector, defined between the Isábena and the Segre rivers, with no significant vertical axis rotations (*Bentham*, 1992; *Dinarès-Turell*, 1992; *Pascual et al.*, 1993; *Beamud et al.*, 2003, 2011); an eastern sector beyond the Segre river with ~ 20° counterclockwise vertical axis rotations, associated to the reactivation of the Montsec thrust sheet and the progression of the Serres Marginals thrust sheet during Late Eocene-Oligocene times (*Dinarès-Turell*, 1992; *Sussman et al.*, 2004); and a western sector beyond the Isábena-Ésera rivers to the west, with significant clockwise vertical axis rotations varying from 10° to 80° mainly concentrated within the Ainsa Oblique Zone (*Dinarès-Turell*, 1992; *Bentham*, 1992; *Fernández-Bellon*, 2004; *Mochales et al.*, 2012a; *Rodríguez-Pintó et al.*, 2013; *Muñoz et al.*, in press). The boundary between the non-rotated areas of the South-Central Pyrenees and the areas of the Montsec and Gavarnie thrust-sheets that have experienced clockwise vertical axis rotations defines a NNE-SSW axial surface along the Esera Valley. Additionally, a N-S trend in the amount of vertical axis rotations is also observed in the western sector, with maximum values to the south, near the Mediano anticline, and minimum values to the north.

Figure 3.3- Geological map and main structural units of the South-Central Pyrenees, with indication of the vertical axis rotations derived from this (red arrows) and previous works (grey arrows). See Table S3.3 in this section for details on the compilation from previous authors and Table 1 in chapter 2.3 for details of the sites from this work.

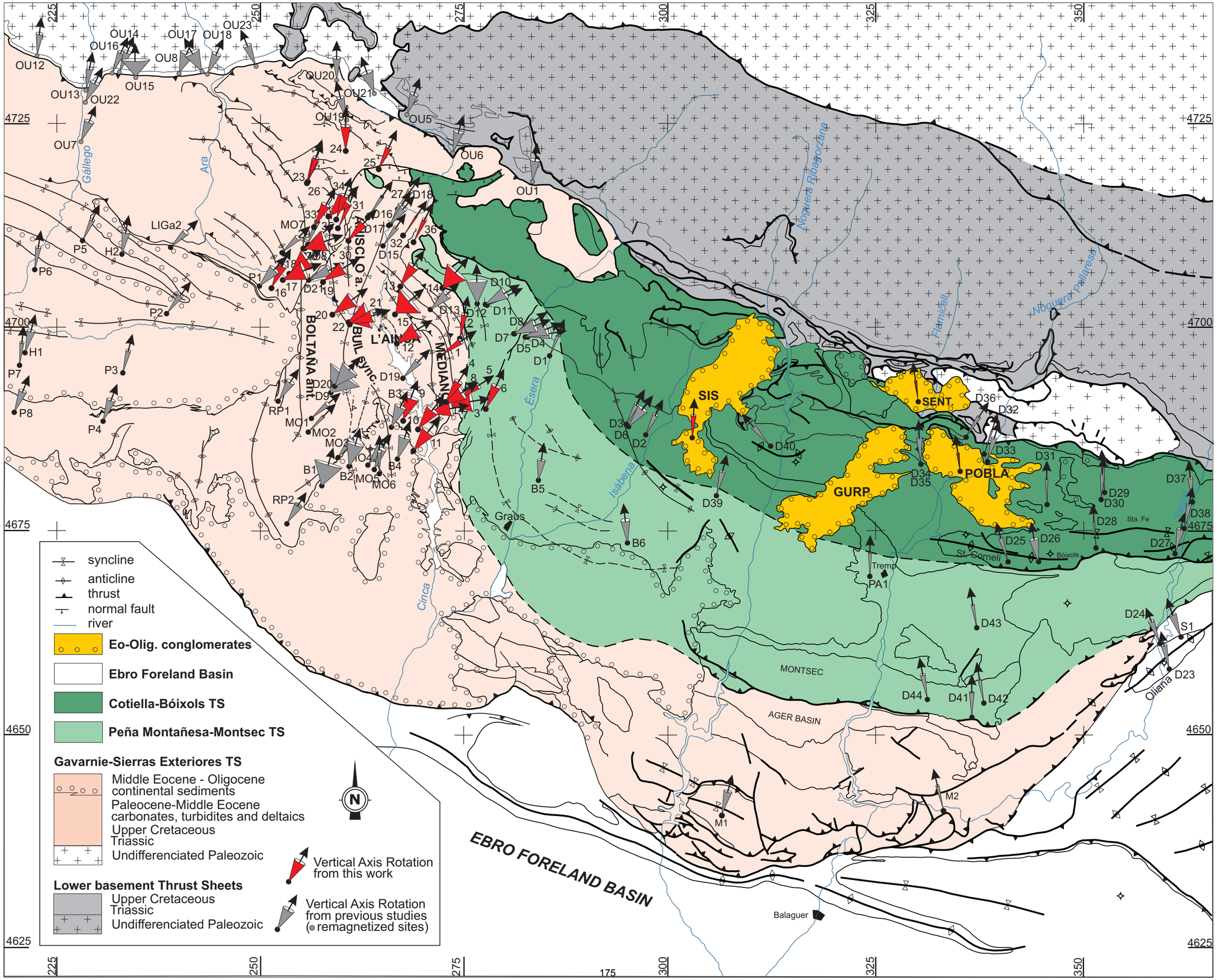
OU12
OU13
OU14
OU16
OU15
OU22
OU8
OU17
OU18
OU23
OU20
OU21
OU19
OU5
OU6
OU1
OU7
Gállego
Ara
LIGa2
P5
H2
P6
P2
P1
H1
P7
P3
P8
P4
RP1
RP2
MO1
MO2
MO3
MO4
MO5
MO6
MO7
B1
B2
B4
B5
B6
ISCLO a.
BOLTAÑA ant.
BUIL sync.
L'AINET
MEDIANO
D1
D2
D3
D4
D5
D6
D7
D8
D9
D10
D11
D12
D13
D15
D16
D17
D18
D19
D20
Ésera
Isábena
Graus
Cinca
SIS
GURP
SENT.
POBLA
D25
D26
D27
D28
D29
D30
D31
D32
D33
D34
D35
D36
D37
D38
D39
D40
D41
D42
D43
D44
Noguera Ribagorzana
Flamicell
Noguera Pallaresa
Sta. Fe
St. Corneli
Bóixols
Tremp
PA1
MONTSEC
AGER BASIN
EBRO FORELAND BASIN
M1
M2
S1
D23
D24
Oliana
Balaguer
syncline
anticline
thrust
normal fault
river
Eo-Olig. conglomerates
Ebro Foreland Basin
Cotiella-Bóixols TS
Peña Montañesa-Montsec TS
Gavarnie-Sierras Exteriores TS
Middle Eocene - Oligocene continental sediments
Paleocene-Middle Eocene carbonates, turbidites and deltaics
Upper Cretaceous
Triassic
Undifferenciated Paleozoic
Lower basement Thrust Sheets
Upper Cretaceous
Triassic
Undifferenciated Paleozoic
Vertical Axis Rotation from this work
Vertical Axis Rotation from previous studies (remagnetized sites)
N
225
250
275
300
325
350
175
4725
4700
4675
4650
4625

The chronostratigraphic panel presented in section 3.1, yields the temporal and spatial framework to analyse the variations in vertical axis rotations in time and space (Figure 3.4). In the western sector, it can be observed a decrease in the amount of vertical axis rotation with time. It is particularly noticeable in the Mediano anticline, where Ypresian to lower Lutetian materials record about 80° of CW vertical axis rotation (sites 3, 7 and 8), progressively decreasing upwards during Lutetian times to 55° (site 5) and 30° (site 4). This pattern is also observed along the Boltaña anticline, although the vertical axis rotations are younger compared to the Mediano anticline, with maximum values around 55°. This is explained because the Boltaña anticline formed later than the Mediano anticline; the onset of growth of the Mediano anticline is set around 48 Ma, whereas the Boltaña anticline started to grow around 42.5 Ma, as deformation progressed from east to west within the Gavarnie thrust sheet. The age of the main rotation event within the Gavarnie thrust sheet is constrained to Lutetitan to Bartonian times, when all the structures of the Ainsa Oblique Zone were active. The synchronicity between structures and rotations reveals that the origin of the curvature of the Ainsa Oblique Zone obeys to a model of progressive arc formed by divergent thrust transport. Further east, within the Bóixols thrust sheet, ~30° clockwise vertical axis rotations are recorded in the Ypresian materials cropping out around the Isábena valley (*Dinarès-Turell*, 1992; figures 3.3 and 3.4, table S1). The overlying Upper Lutetian to Bartonian materials of Sis don't record any significant vertical axis rotation, which constrains the age of this rotation to Cuisian-Early to Middle Lutetian times in this sector.

Figure 3.4- Chronostratigraphy of the South-Central Pyrenees, from the Ainsa basin to La Pobla de Segur with indication of vertical axis rotations from this and previous studies (*Bentham*, 1992; *Dinarès-Turell*, 1992; *Pueyo*, 2000; *Mochales et al,*. 2012a; *Pascual et al.*, 1993). On the right, the evolution of exhumation rates with time on the Axial Zone derived from vertical profiles (*Fitzgerald et al.*, 1999) and from this work (section 2.3: *Beamud et al., 2011*) are indicated. See figure caption of Figure 3.1 for description of the lithostratigraphic units.

The thermochronologic results (chapter 2.2) combined with the ages of the syntectonic materials (chapter 2.1, 2.2 and 3.1) allow to link the events occurring in the Axial Zone and the coeval deposition within the adjacent sedimentary basins (Figure 3.4). The magnetostratigraphic and detrital fission tracks ages obtained largely overlap with the thermochronological ages yielded by the basement thrust sheets of the central Pyrenean antiformal stack or thrust sheets north of the North Pyrenean Fault (*Fitzgerald et al*., 1999; *Sinclair et al.*, 2005). Therefore, the Paleogene materials of the South-Central Pyrenees were deposited during the most intense periods of exhumation within the core of the orogen. Only the youngest thermochronological ages of 20-25 Ma recorded in the Barruera massif (*Sinclair et al.*, 2005) are not found in the syntectonic conglomerates, in agreement with the ages deduced for the youngest materials (Upper Oligocene to Lower Miocene for the Antist allogroup). The elevation of the preserved top depositional surface of these conglomerates, suggests these conglomerates covered the Barruera massif. Most of the syntectonic materials of Sis, Gurp and La Pobla were sedimented during the movement of the Orri thrust sheet which promoted erosion of the Nogueres thrust sheet, piggy-back transported above. Since Priabonian times (~ 35 Ma), the onset of activity within the Rialp thrust sheet augmented the structural relief of the Axial Zone with enhanced exhumation rates from ~ 0.3 km/My to several km/My.

All these results can be integrated to deduce the tectonosedimentary evolution for the South-Central Pyrenees during Eocene-Oligocene times. It is summarized in 4 main stages in Figures 3.5 to 3.8: Middle Lutetian (~42 Ma), Bartonian to Early Priabonian (~37 Ma), Late Priabonian (~34 Ma) and Oligocene (31 to 27 Ma), respectively.

At Early Lutetian times (~ 48 Ma) deformation progressed forward from the Peña Montañesa-Montsec thrust sheet into the foreland to develop the Gavarnie-Serres Marginales thrust sheet. This caused the change of the Ainsa basin from a foredeep to a piggy-back basin. Sedimentation occurred simultaneously to the deformation of the basin floor by the Sobrarbe fold system (Figure 3.1). Sedimentation rates were low during this period, around 0.03 km/My for the Guara limestones (*Rodríguez-Pintó et al.*, 2012) and 0.07 km/My during the turbiditic sedimentation of the San Vicente Fm. (*Mochales et al.*, 2012b). Mediano, Olson and Añisclo anticlines started to grow with an ENE-WSW orientation. At this time the emergent frontal thrust system of the Gavarnie thrust sheet was located in the Monte Perdido fold and thrust belt, which connected to the La Fueba thrust system by a slightly oblique ramp, drawing a primary arc (Figure 15c, section 2.3). Further east, La Pobla de Segur area was an uplifted region with no deposition (Figure 3.1). To the north, the Axial Zone was uplifted at ~ 0.3

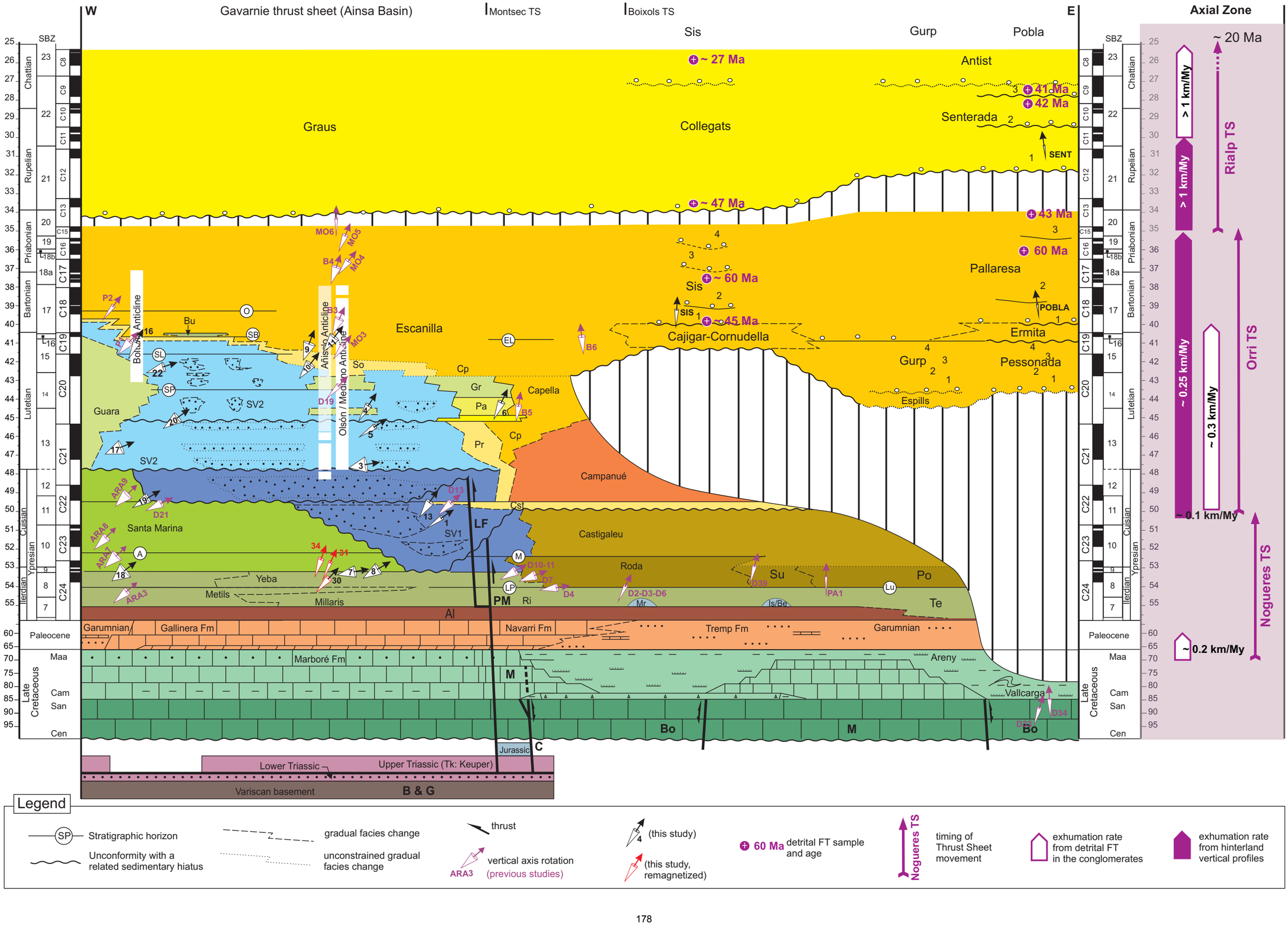
W
Gavarnie thrust sheet (Ainsa Basin)
Montsec TS
Boixols TS
E
Axial Zone
Sis
Gurp
Pobla
~ 27 Ma
Antist
41 Ma
42 Ma
Graus
Collegats
Senterada
SENT
~ 47 Ma
43 Ma
60 Ma
Pallaresa
~ 60 Ma
Sis
POBLA
~ 45 Ma
SIS
Cajigar-Cornudella
Ermita
Gurp
Pessonada
Espills
MO6
MO5
B4
MO4
P2
Bohoa Anticline
Bu
O
SB
B3
Añisclo Anticline
MO3
Escanilla
EL
B6
SL
SP
SV2
Guara
Olsón / Medano Anticline
So
Cp
Gr
Capella
Pa
B5
Pr
Cp
Campanué
Cst
D19
D13
ARA9
D21
Santa Marina
LF
SV1
Castigaleu
ARA8
ARA7
A
ARA3
Yeba
Metils
Millaris
M
LP
PM
Ri
D10-11
D7
D4
Roda
D2-D3-D6
Mr
Is/Be
Su
D39
PA1
Lu
Po
Te
Al
Garumnian
Gallinera Fm
Navarri Fm
Tremp Fm
Garumnian
Marboré Fm
Areny
Vallcarga
D34
Bo
M
Jurassic
C
Lower Triassic
Upper Triassic (Tk: Keuper)
Variscan basement
B & G
SBZ
Chattian
Rupelian
Priabonian
Bartonian
Lutetian
Cuisian
Ypresian
Ilerdian
Paleocene
Late Cretaceous
Maa
Cam
San
Cen
C8
C9
C10
C11
C12
C13
C15
C16
C17
C18
C19
C20
C21
C22
C23
C24
~ 20 Ma
> 1 km/My
Rialp TS
> 1 km/My
~ 0.25 km/My
~ 0.3 km/My
Orri TS
~ 0.1 km/My
Nogueres TS
~ 0.2 km/My
Legend
Stratigraphic horizon
Unconformity with a related sedimentary hiatus
gradual facies change
unconstrained gradual facies change
thrust
vertical axis rotation (previous studies)
(this study)
(this study, remagnetized)
60 Ma detrital FT sample and age
Nogueres TS
timing of Thrust Sheet movement
exhumation rate from detrital FT in the conglomerates
exhumation rate from hinterland vertical profiles

km/My with erosion located within the Nogueres thrust sheet caused by the underthrusting of the Orri thrust sheet.

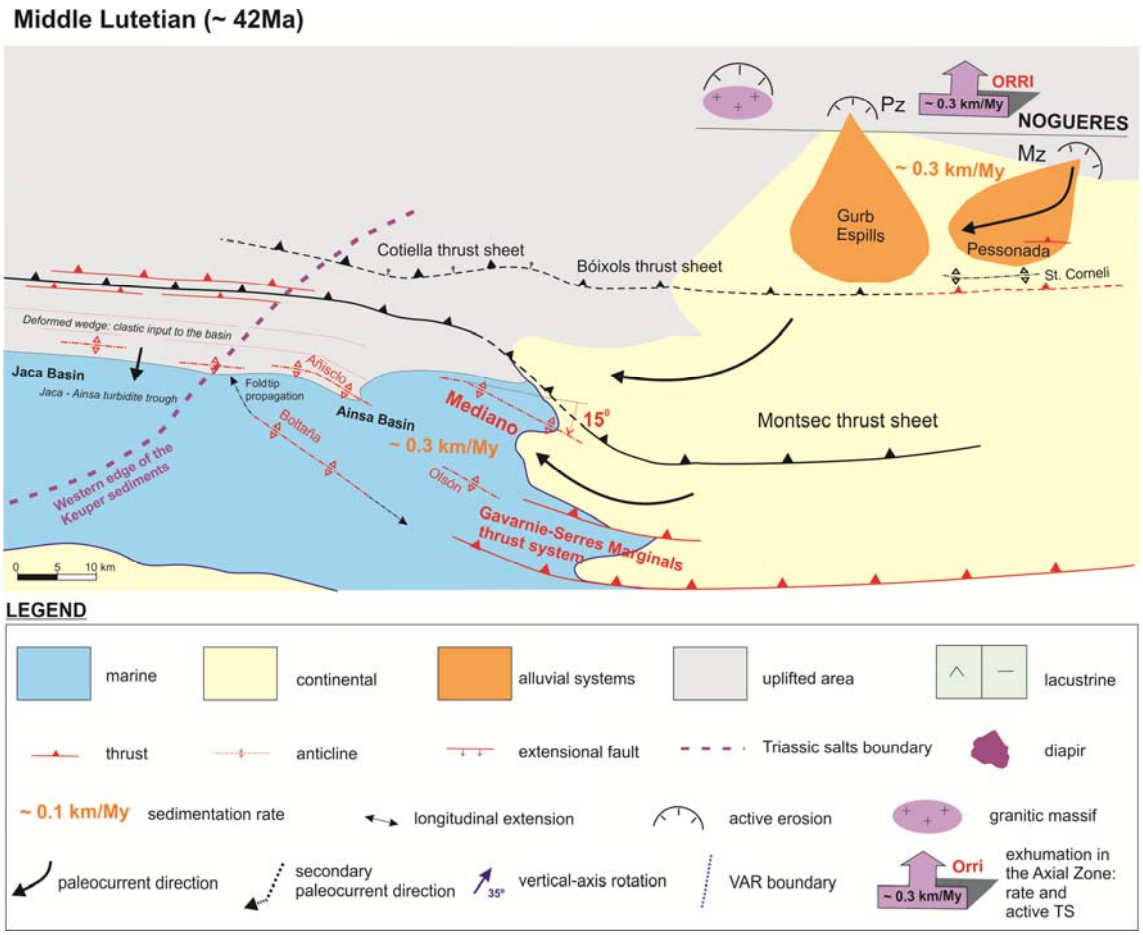

Figure 3.5- Tectonosedimentary evolution of the South-Central Pyrenees for Middle Lutetian times. Red lines indicate active structures. Sedimentation rates in the Ainsa basin from *Mochales et al.* (2012b).

During Middle Lutetian times (~ 42 Ma), the Boltaña anticline started to grow as an oblique structure to the Gavarnie frontal thrust and parallel to the Mediano anticline, which by then was already rotated 15° clockwise due to the propagation of the deformation in the Gavarnie thrust sheet. Sedimentation rates within the Ainsa basin rise to values close to 0.3 km/My (*Mochales et al.*, 2012). In La Pobla de Segur and Gurp area the generation of accommodation space in front of the Axial Zone antiformal stack allows the deposition of the Espills and Gurp Fms. and the Pessonada allogroup. The Bóixols thrust was reactivated synchronously with thrust activity at the thrust front. A break-back thrust sequence developed in its hanginwall during the sedimentation of the Pessonada allogroup as demonstrated by progressive unconformities (*Mellere*, 1992). To the north, exhumation in the Axial Zone continued stable around 0.3 km/My with erosion localized within the Nogueres thrust sheet, promoted by underthrusting of the Orri thrust sheet. Nevertheless, the main source area of

the alluvial fans was located within the nearby Mesozoic materials (*Mellere*, 1992; *Barsó*, 2007).

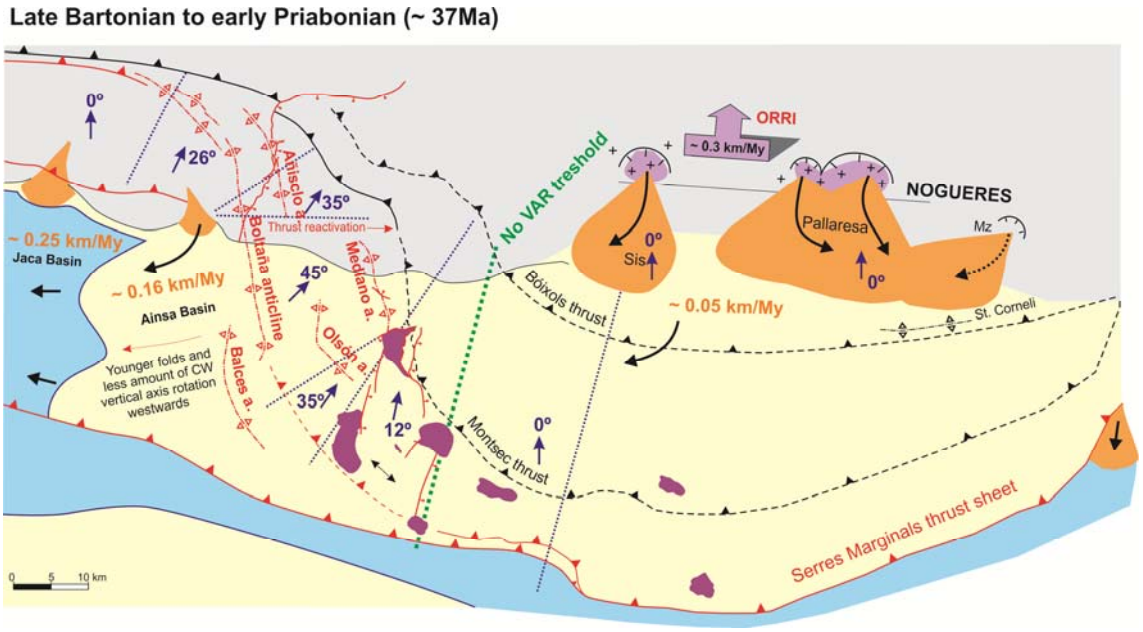

Figure 3.6- Tectonosedimentary evolution of the South-Central Pyrenees for Late Bartonian to early Priabonian times. Same legend as in Figure 3.5. Sedimentation rates in the Jaca basin from *Hogan & Burbank* (1996) reinterpreted by *Costa et al.* (2010) and, in the Ainsa basin from *Bentham* (1992) and *Mochales et al.* (2012b).

Between Bartonian and Priabonian times (until ~ 37 Ma) all the structures of the Ainsa region were active, with clockwise vertical axis rotations up to 45° synchronous to the movement of the thrust sheets and the fold growth. This synchronicity points to a model of progressive arc due to divergent thrust emplacement to explain the origin of the curvature in the Ainsa Oblique Zone. This model requires longitudinal extension, which in this area is achieved by a system of transverse to highly oblique extensional faults. Longitudinal extension was also accommodated by diapirs in the areas where Triassic salt thickness was significant. Conversely to the general rotation of the Ainsa oblique zone, the materials in Sis and La Pobla regions don't record vertical axis rotations during this period. Therefore, a no-rotation threshold line can be delineated coinciding with the eastern edge of the circular trend connecting the N-S structures of the Ainsa Oblique Zone with the western limit of the Montsec thrust with an E-W trend to the east. A generalized dramatic reduction in sedimentation rates in the South Pyrenean basins occurs during this time. Values as low as 0.05 km/My and 0.16 km/My are recorded in La Pobla and Ainsa regions respectively (*Beamud et al.*, 2003, 2011; *Mochales et al.*, 2012; *Bentham*, 1992). To the west, in the Jaca basin, sedimentation rates are around 0.25 km/My (*Hogan & Burbank*, 1996 reinterprteted by *Costa et al.*, 2010). These values reveal a gradient in sedimentation rates, increasing from east to west. This gradient

would be caused by a reduction in accommodation space eastward, which would be related to the progression of the deformation to the SW.

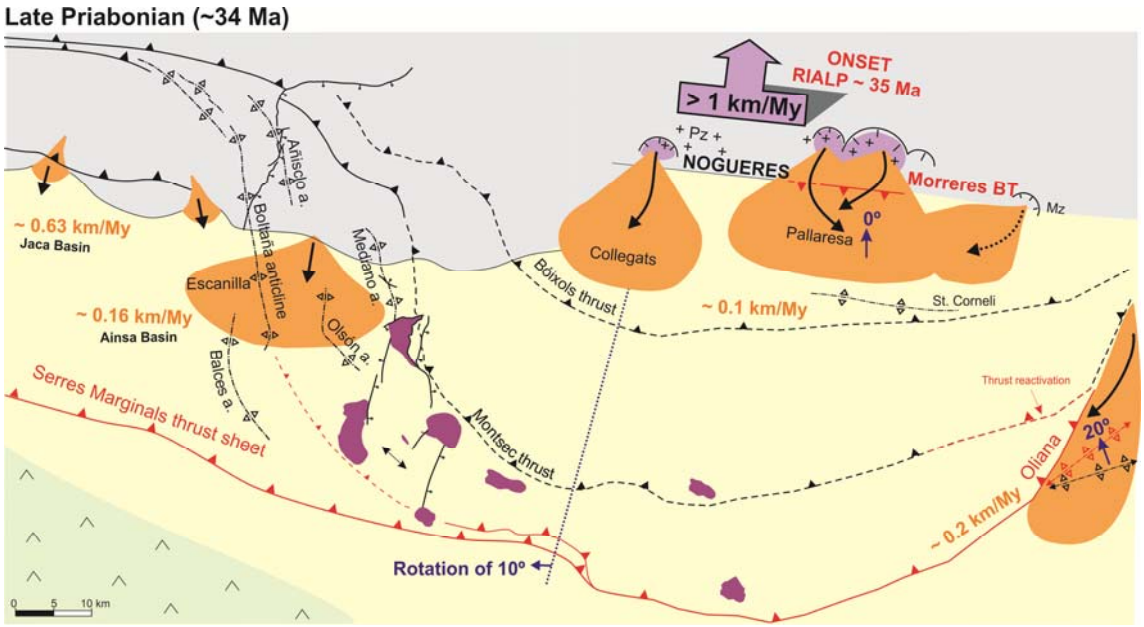

Figure 3.7- Tectonosedimentary evolution of the South-Central Pyrenees for Late Priabonian times. Same legend as in Figure 3.5. Sedimentation rates in the Jaca basin from *Hogan & Burbank* (1996) reinterpreted by *Costa et al.* (2010) and, in the Ainsa basin from *Bentham* (1992). Data from the Oliana anticline from Sussman et al., (2004), *Vergés* (1993), *Burbank et al.* (1992) and *Burbank & Vergés* (1994).

Disconnection from the Atlantic Ocean at 36 Ma (*Costa et al.*, 2010) controled the sedimentation of the southpyrenean basins during Priabonian times. A trough in which most of the materials were preserved was created while ceasing the by-pass of sediments to the west. This produced a general increase in sedimentation rates. In the Jaca basin sedimentation rates increase from 0.25 km/My to 0.63 km/My (*Hogan & Burbank*, 1996 reinterpreted by *Costa et al.*, 2010). In La Pobla region, sedimentation rates rise to 0.1 km/My, with a general change in paleocurrent directions from mostly E-W to N-S directions. Basin closure and related back filling also induced a migration of the deformation to inner parts of the chain, revealed by the activity of the Morreres backthrust and a huge increase in exhumation rate within the Axial Zone. Exhumation rates higher than 1 km/My are recorded due to the onset of displacement of the Rialp thrust sheet. No vertical axis rotations are recorded in La Pobla area during this time. To the east, a counterclockwise rotation of about 20° took place in the Oliana anticline linked to the reactivation of the Montsec thrust sheet and the movement along Serres Marginals thrust sheet on top of the foreland (*Sussman et al.*, 2004). The translation of the Serres Marginals thrust sheet on top of the upper Eocene salts during this period added a clockwise rotation of about 10° to the previously formed thrust salient in the Ainsa Oblique zone.

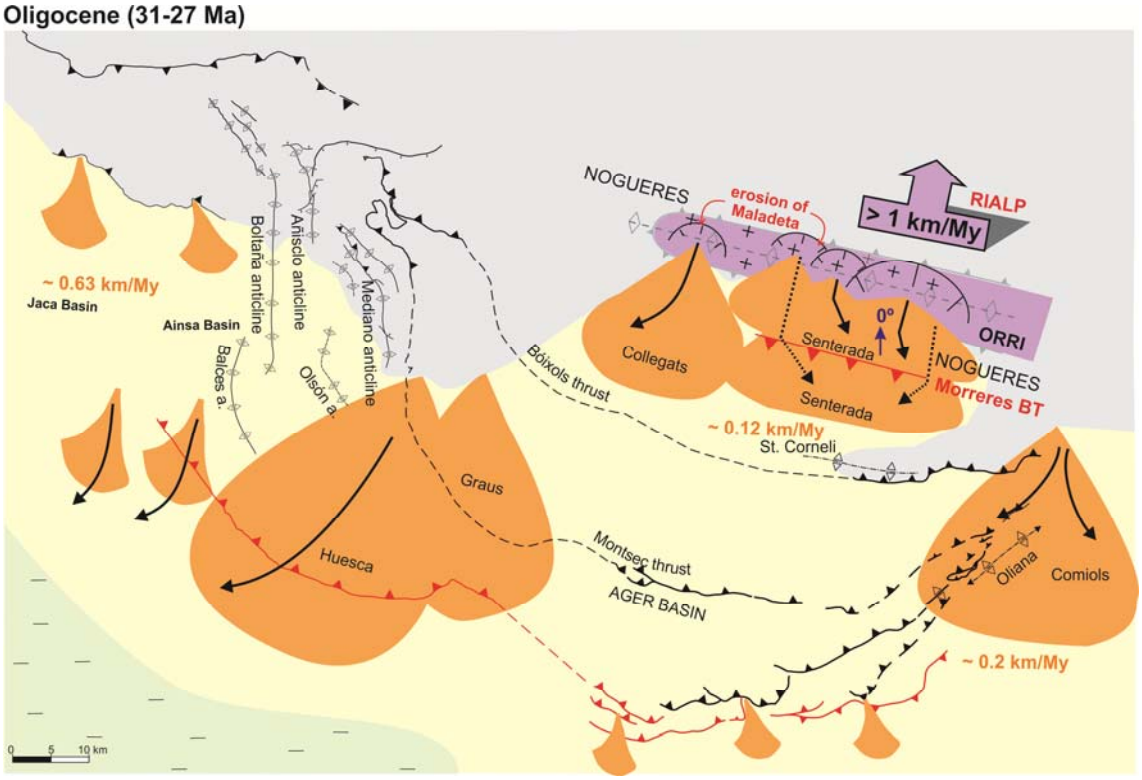

Figure 3.8 - Tectonosedimentary evolution of the South-Central Pyrenees for Oligocene times. Same legend as in Figure 3.5. Data from the Oliana-Comiols area from *Vergés* (1993) and *Burbank et al.* (1992). Alluvial systems in the western sector, from *Luzón et al.* (2005). Sedimentation rates for the Jaca basin from *Hogan & Burbank* (1996) reinterpreted by *Costa et al.* (2010)

The Oligocene (~ 31-27 Ma) is characterized by a generalized alluvial sedimentation in the South Pyrenean basins with sedimentation rates similar to the previous stage. In La Pobla region, the main depositional area moves northwards into the Senterada subbasin, created on the footwall of the Morreres backthrust, above the Nogueres thrust sheet. Source area is located immediately to the north within the Axial Zone, with the erosion of the Orri thrust sheet caused by the underthrusting of the Rialp thrust sheet below. Exhumation in the Axial Zone is high (> 1 km/My) and causes the erosion of the Maladeta granitic massif. No vertical axis rotations are recorded by the Senterada allogroup during this time. The generalized alluvial sedimentation during Oligocene times fossilized the tectonic structures and covered the deformation front with thickness up to 2 km, as deduced from the partial annealing experienced by the lowermost stratigraphic samples in the Sis region (section 2.2). Recent thermochronological models (*Fillon et al.*, 2013) confirm the Oligocene-Miocene overfilling of the Ebro Basin, with 1.6 km of sediment aggradation in its northern edge. Data from *Fillon et al.*, (2013) also suggest that the Ager Basin, located on the footwall of the Montsec thrust (Figure 3.8) was covered by about 2.6 km of conglomerates, either by an extension of the Huesca fan to the east or the Oliana fan to the west (Figure 3.8).

The thermal models presented in section 2.3 indicate postorogenic cooling during the Late Miocene. The driving mechanism of this exhumation event would be the erosion and re-excavation of the materials that buried the South Pyrenean fold and thrust belt caused by the capture of the Ebro River to the Mediterranean Sea from the last 10 Ma. Models from *Fillon & van der Beek* (2012) predict a decrease of maximum elevation of the conglomerates and incision of the valleys in the southern Pyrenees from 9 Ma to present. Thus, these authors propose that the opening of the Ebro basin occurred at latest during the Tortonian, well before previously suggested Messinian times, and that late Neogene/Quaternary climate change had little effect on the post-orogenic erosional history of the Southern Pyrenees.

TABLE S3.3 - detailed information for sites of Figure 3.3

Bentham (1992)

label	site	polar.	chron	age	geo coords		bedding		BTC				ATC				β
					lat (N)	long	dd	dip	Dg	Ig	α95	k	Ds	Is	α95	k	
B1	Alz	N	/	Lut-Bart	/	/	/	/	352	41	30	7	2	48	25	7.7	19
		R	/		/	/	/	/	208	-14	35	5.4	218	-24	32	8.3	
B2	Erp	N	/	Bart-Priab	/	/	/	/	20	49	7	12.7	34	54	8	11.6	18
		R	/		/	/	/	/	192	2	22	5	184	-20	21	6	
B3	Med	N	/	Lut-Bart	/	/	/	/	29	41	7	13.2	22	53	6	14.4	26
		R	/		/	/	/	/	211	-9	16	6.5	212	-25	15	8.9	
B4	Lig	N	/	Bart-Priab	/	/	/	/	8	45	14	5	12	51	12	9.1	20
		R	/		/	/	/	/	200	-20	14	7.1	209	-24	15	7.5	
B5	Es	N	/	Lutetian	/	/	/	/	/	/	/	/	12	49	16.8	5.8	11
		R	/		/	/	/	/	/	/	/	/	199	-35	15.8	6.4	
B6	Las	N	/	Lut-Bart	/	/	/	/	/	/	/	/	5	52	16.5	12.2	-2

Dinarès (1992)

label	site	polar.	chron	age	UTM			bedding		BTC				ATC				β
					zone	X	Y	dd	dip	Dg	Ig	α95	k	Ds	Is	α95	k	
D1	89J36	R	/	Ypresian	31	285500	4696500	30	53	207	2	4.4	98	205	-51	/	/	21
D2	89J38	N	/	Ypresian	31	297300	4686800	43	9	32	50	8.3	40	29	59	/	/	25
D3	90J11	N	/	Ypresian	31	294900	4688100	225	16	34	29	7	44	31	45	/	/	27
D4	90J13	N	/	Ypresian	31	282800	4698800			71	-19	16	11	84	59	/	/	80
D5	90J14	N	/	Ypresian	31	282500	4698800	203	34	49	33	18	13	72	61	/	/	68
D6	90J19	R	/	Ypresian	31	295200	4687800	104	23	197	-50	9.7	23	221	-44	/	/	37
D7	90J22	R	/	Ypresian	31	281100	4699200	156	38	223	-33	18	16	252	-39	/	/	68
D8	90J23	R	/	Ypresian	31	281200	4699200			236	38	8.9	28	239	-59	/	/	55
D9	90J25	N	/	Lutetian	31	258700	4692000	245	7	45	42	38.8	6.6	42	42	38.8	6.6	38
D10	90J27	R	/	Ypresian	31	277600	4702800	162	15	231	-37	15	36	243	-41	/	/	59
D11	90J28	R	/	Ypresian	31	277800	4702700	230	82	242	29	4.7	376	247	-51	/	/	63
D12	90J29	R	/	Ypresian	31	276600	4702900	220	35	206	-40	25	10	182	-72	/	/	-4
D13	90J30	R	/	Mid Cuisian	31	270800	4702200	199	17	227	-12	15	21	230	-27	/	/	46
D14	90J31	N	/	Cuisian	31	272400	4690800	87	31	19	72	15	28	61	49	/	/	57
D15	90J32	N	/	Up Ilerdian	31	265000	4710000	107	17	30	28	5.9	243	38	23	/	/	34
D16	90J33	N	/	Up Ilerdian	31	265900	4712600	141	8	25	36	9.7	168	34	33	/	/	30

D17	90J34	N	/	Up Ilerdian	31	265700	4712500	141	8	41	30	8.6	206	44	38	/	/	40
D18	90J35		/	Ypresian	31	266800	4714500	161	10	216	-13	6.7	186	218	-19	/	/	34
D19	90J36	N	/	Mid Lutetian	31	268000	4694000	233	17	48	38	8.8	76.3	46	55	9.3	69	42
D20	90J38	R	/	Lutetian	31	259100	4692800	81	40	161	-66	23	121	224	-48	23	120.4	40
D21	90J39	R	/	Ypresian	31	255900	4705800	107	15	233	-57	14.1	19.2	247	-47	14.1	19.3	63
D22	90J12	N	/	Ypresian	31	285200	4696200	243	23	31	33	8.9	142	18	51	7.3	15	14
D23	89J15	N	/	Bartonian	31	361800	4658800	134	42	344	-4	8.6	61	350	32	7.2	106	-14
D24	89J23	N	/	Eocene	31	359300	4660900	332	47	3	73	5	124	342	28	6.8	67	-22
D25	JDT24 H	N	/	Lower K	31	342600	4669900	152	81	332	-24	5.5	106	332	57	5.5	106	-17
D26	JDT27 H	N	/	Lower K	31	346000	4670100	166	38	341	15	10.7	6	338	53	10.7	6	-11
D27	JDT30 H	N	/	Lower K	31	361100	4371200	128	38	6	-54	9.5	27	2	52	8.7	32.1	13
D28	JDT36 H	N	/	Lower K	31	350800	4672200	353	39	313	78	2.1	261	343	41	2.3	220	-5
D29	JDT38 H	N	/	Lower K	31	353600	4676100	192	44	359	20	3.7	130	345	62	3.6	136	-4
D30	JDT39 H	N	/	Lower K	31	353600	4675800	187	30	357	24	3.9	80	352	53	5.1	47	3
D31	JDT40 H	N	/	Lower K	31	346000	4679000	202	36	3	27	3.2	207	348	59	3.2	200	-1
D32	JDT41	N	/	Lower K	31	338200	4683700	224	38	21	19	2.6	233	7	52	2	390	18
D33	JDT42	N	/	Upper K	31	337900	4682800	198	18	13	22	6.8	99	12	40	6.7	101.2	17
D34	JDT43	N	/	Upper K	31	330300	4683400	206	69	11	-2	6.4	58.1	352	63	6.8	51.8	-3
D35	JDT44	N	/	Upper K	31	330200	4684500	212	44	13	25	2.8	194	349	64	2.7	196.2	-6
D36	89J14	N	/	Lower K	31	335500	4686200			347	-73	5.1	143	22	42	5	145.1	33
D37	89J7	N	/	Lower K	31	362600	4676200	203	53	2	9	6.4	58.3	344	56	6	65.2	-5
D38	89J10	N	/	Upper K	31	362000	4673800	291	17	36	60	7.2	52.7	6	60	6	73.8	11
D39	89J12	N	/	Ypresian	31	307400	4682200	230	22	27	31	7.6	147	18	51	7.3	161.1	14
D40	89J40	N	/	Lower K	31	313800	4688900	174	64	325	-5	6.3	148	308	48	6.3	150.5	-41
D41	JDT23	N	/	Jurassic	31	336800	4652100	27	22	319	60	9.5	30.6	344	47	8.1	41.5	2
D41	JDT48	N	/	Jurassic	31	336800	4652300	37	26	310	56	6.3	90	342	47	6.4	90	0
D42	JDT49	N	/	Lower K	31	337500	4652900	5	12	331	56	3.8	109	339	45	3.6	126.2	-10
D43	JDT58	N	/	Upper K	31	341600	4663300	260	16	10	57	3.3	159	345	59	3.8	117	-10
D44	JDT60	N	/	Lower K	31	331900	4652900	27	7	329	61	7.9	43.6	338	57	6.1	72.5	-11

Pascual et al (1992)

label	site	polar.	chron	age	UTM zone 31		bedding		BTC				ATC				β
					X	Y	dd	dip	Dg	Ig	α95	k	Ds	Is	α95	k	
PA1	Tremp	N+R		Ilerdian	322000	4669200	/	/	/	/	/	/	13	46	4	10	9

Hogan (1993)

label	site	polar.	chron	age	geo coords		bedding		BTC				ATC				β
					lat (N)	long	dd	dip	Dg	Ig	α95	k	Ds	Is	α95	k	
H1	Mn	N		Bart-Priab	/	/	/	/	9	45	12.2	5.4	6	21	12.2	5.4	12
		R			/	/	/	/	204	-41	6.8	6.8	200	-22	6.4	7.6	
H2	Yb	N		Bart-Priab	/	/	/	/	318	77	8.9	6.1	11	38	9	6	29
		R			/	/	/	/	43	-68	/	/	228	-45	31.3	3.1	

Meigs et al (1996); Meigs & Burbank (1997)

label	site	polar.	chron	age	UTM zone 31		bedding		BTC				ATC				β
					X	Y	dd	dip	Dg	Ig	α95	k	Ds	Is	α95	k	
M1	Baldellou	N		Eocene-Oligocene	296869	4644003	296	76	59	14	9.3	7.9	18.4	35.2	9.2	8.1	11
	Baldellou	R		Eocene-Oligocene	296869	4644003	28	33	178.5	-77.7	7.4	7.6	200	-47	6.5	9.5	
								M1:	49	48	180	2.7	19	41	26.1	93.4	
M2	Artesa S.	N+R			337254	4640236	349	33	358	60	6	3	354.2	27.1	4.2	5.2	-14

Pueyo (2000)

label	sector	site	polar.	age	UTM zone 30		bedding		BTC				ATC				β
					X	Y	dd	dip	Dg	Ig	α95	k	Ds	Is	α95	k	
P1	JAN	96	R+N	Lutetian	743257	4707555	236	68	223	29	22	5	222	-38	/	/	38
		97	R	Lutetian	743900	4705643	244	54	227	18	20	6	225	-34	/	/	
P2	Gug (N)	124	N	Priabonian	732940	4703735	209	85	41	-44	9	17	40	39	/	/	33
		125	R	Rupelian	732543	4702270	200	42	197	24	33	30	197	-18	/	/	
		126	N	Rupelian	731870	4699610	197	9	33	34	11	22	35	43	/	/	
P3	Gug (S)	127	N+R	Priabonian	727000	4692102	167	12	191	-26	7	22	194	-37	/	/	10
		128	N+R	Rupelian	726803	4695000	352	10	198	-57	17	10	193	-48	/	/	
P4	Gua	48	R	Bartonian	718612	4688160	340	28	234	-73	8	24	188	-54	/	/	17
		49	R	Bartonian	716960	4687580	350	31	245	-59	16	8	212	-42	/	/	
		51	R	Bartonian	720960	4688480	337	44	273	-51	16	20	216	-49	/	/	
		53	N	Bartonian	725649	4687162	328	27	60	66	11	18	13	55	/	/	
		54	N	Bartonian	726150	4687530	320	65	97	63	15	10	344	42	/	/	
		55	N	Bartonian	724067	4688980	9	20	17	55	13	13	14	35	/	/	
		56	N+R	Priabonian	735752	4689703	339	22	46	33	18	11	35	22	/	/	
		57	N	Bartonian	735485	4690154	351	31	45	37	11	20	33	15	/	/	
		58	R	Priabonian	733057	4690152	352	30	227	-53	13	23	207	-31	/	/	
		59	N	Priabonian	730448	4689900	355	25	10	64	17	8	3	39	/	/	
		60	N	Bartonian	730915	4688770	354	34	75	69	14	13	25	48	/	/	

P5	Bas	88	N	Priabonian	716854	4708632	211	77ov	20	-49	7	57	19	53	/	/	15
		91	R	Upper Lutetian	731223	4704250	212	75	217	26	25	8	219	-49	/	/	
		92	N+R	Upper Lutetian	727989	4705471	25	55	281	81	25	11	14	37	/	/	
		93	R	Lower Bartonian	720528	4707963	23	66ov	203	76	24	3	203	-38	/	/	
		94	N	Lower Bartonian	717850	4709330	40	77ov	30	-59	9	29	33	43	/	/	
		95	N+R	Lower Bartonian	720420	4714200	159	25	181	-27	16	20	190	-50	/	/	
P6	Mon (N)	88	N	Priabonian	716854	4708632	31	77ov	20	-49	7	57	19	53	/	/	5
		123	N	Priabonian	711377	4706077	19	48	325	74	6	73	4	32	/	/	
P7	Mon (S)	119	R	Priabonian	714710	4691626	350	25	167	-56	7	30	167	-31	/	/	2
		120	R	Rupelian	715391	4694106	4	25	190	-62	12	12	186	-37	/	/	
		121	R	Rupelian	714726	4696459	4	14	205	-55	7	18	199	-42	/	/	
P8	Agl	37	N	Bartonian	712345	4688300	292	60	61	30	11	19	9	46	/	/	18
		38	N	Bartonian	711997	4688350	317	37	56	50	5	68	16	42	/	/	
		39	R	Bartonian	716000	4688590	10	32	266	-84	5	70	201	-56	/	/	
		45	N	Bartonian	715640	4687720	354	23	76	75	5	110	26	61	/	/	

Beamud et al (2003), Beamud et al (2011)

label	site	polar.	chron	age	geo coords		bedding		BTC				ATC				β
					lat (N)	long €	dd	dip	Dg	Ig	α95	k	Ds	Is	α95	k	
SIS	Sis	N	C18N	Bartonian	42.3114	0.6157	/	/	3	52	6.6	21.8	4	41	6.9	20.1	3
		R	C18R	Bartonian	42.3114	0.6157	/	/	185	-45	8.2	18.7	191	-38	8.3	18.4	
								BE1:	3.8	48.7	5.1	20.7	7	39.4	5.2	19.3	
POBLA	Pobla	N	C18n-C15n	Bartonian-Priabonian	42.2668	0.9828	/	/	349	48	5	14.9	355	34	5.3	14.9	-7
		R	C19r-C13	Bartonian-Priabonian	42.2668	0.9828	/	/	176	-52	9	9.8	181	-37	9	9.8	
								BE2:	351	50	4.7	12.5	357	35	4.7	12.5	
SENT	Senterada	N	C12n-C9n	Oligocene	42.3412	0.9661	/	/	5	58	5.4	13.1	2	40	5.9	10.9	-8
		R	C12r-C9r	Oligocene	42.3412	0.9661	/	/	169	-56	3.8	16.3	172	-40	3.7	17.3	
								BE3:	355	57	3.1	14.4	356	40	3.2	13.8	

Sussman et al (2004)

label	site	polar.	chron	age	UTM zone 31		bedding		BTC				ATC				β
					X	Y	dd	dip	Dg	Ig	α95	k	Ds	Is	α95	k	
S1	mean	N+R		Upper Eocene-Oligoc.			/	/					348	47	9	/	-20

Oliva-Urcia (2004), Oliva-Urcia & Pueyo (2007), Oliva-Urcia et al (2008)

label	site	polar.	chron	age	geo coords	bedding	BTC	ATC	β

label	site	polar.	chron	age	lat (N)	long	dd	dip	Dg	Ig	α95	k	Ds	Is	α95	k	β
OU19	AÑI8	R	/	Maastrichtian	42º38'54"	0º4'5'' E	194	18	168	-16	10	/	164	-34	/	/	/
OU18	OTA6	R	/	Cenom-Santonian	42º41'43"	0º7'41''W	28	68ov	207	-34	13	19	32	-33	/	/	/
OU15	TEN2	R	/	Maastrichtian	42º40'43"	0º14'6"W	180	57	175	-24	41	7	151	-80	/	/	/
OU14	ASN3	R	/	Cenom-Santonian	42º41'16"	0º15'23''W	186	45	207	-32	10	23	256	-71	/	/	/
OU21	PIN1	R	/	Cenom-Santonian	42º40'27"	0º6'36''E	224	36	163	-19	17	6	148	-33	/	/	/
OU23	TOU4	R	/	Maastrichtian	42º42'10"	0º1'43"W	350	89ov	160	-41	11	84	0	-39	/	/	/
OU13	ELE1	R	/	Cenom-Santonian	42º40'7''	0º19'14''W	178	59	193	-40	8	56	309	-74	/	/	/
OU20	MAR2	R	/	Maastrichtian	42º41'16"	0º2'41''E	214	17	178	-42	10	25	165	-55	/	/	/
OU8	ARA8	R	/	Maastrichtian	42º42'20"	0º31'36''W	200	25	205	-48	19	18	227	-76	/	/	/
OU16	TEN3	R	/	Cenom-Santonian	42º41'16"	0º14'54''W	164	65	225	-53	10	47	302	-37	/	/	/
OU12	PIE3	R	/	Cenom-Santonian	42º42'23"	0º23'51''W	177	45	189	-57	9	30	330	-76	/	/	/
OU22	ELE5	R	/	Eocene (Hecho Gp)	42º39'29"	0º19'14''W	194	84	209	-40	13	16	352	-53	/	/	/
OU17	OTA2	R	/	Cenom-Santonian	42º41'24"	0º8'48"W	172	44	155	-39	21	10	105	-75	/	/	/
OU7	ELE7	R	/	Eocene (Hecho Gp)	42º37'58"	0º19'36"W	63	20	205	24	15	15	208	-8	/	/	/
OU1	(1) TRI-2	R	/	Triassic red beds	42º35'6''	0º19'56''W	205	85	190	-16	14	17	77	-72	/	/	/
OU2	(6)TRI-7	R	/	Triassic red beds	42'36'37''	0º14'48''W	210	20	198	-22	14	22	195	-44	/	/	/

Mochales et al (2012a,b)

label	site	polar.	chron	unit	UTM			bedding		BTC				ATC				β
					zone	X	Y	dd	dip	Dg	Ig	α95	k	Ds	Is	α95	k	
MO1	CAS1	R	C20R	La Patra Mb	31	256294	4691407	80	23	218	-73	7.1	59.5	240	-52	7	61.3	56
	CAS2	R	C20R	La Patra Mb	31	256321	4691421	82	26	210	-60	20.4	7.3	227	-45	21	7	43
	CAS3	N+R	C20N	La Patra Mb	31	256494	4691358	95	27	3	63	22	12.3	41	53	19.8	14.8	37
	CAS4	N+R	C20N	La Patra Mb	31	256746	4691181	86	20	45	60	18.9	6.8	57	50	16.1	9	53
	CAS5	N+R	C20N	La Patra Mb	31	257491	4691559	94	22	340	56	13.8	19.5	15	58	12.7	22.7	11
	CAS6	N+R	C20N	La Patra Mb	31	257975	4691523	87	24	18	59	10.9	20.4	44	46	11.1	19.8	40
	CAS7	R	C19R	Sobrarbe Fm	31	258412	4691197	84	21	207	-56	8.1	40.9	224	-41	8.3	38.4	40
	CAS8	R	C19R	Sobrarbe Fm	31	258754	4691296	82	22	205	-55	20.5	55.8	224	-41	20.6	55.4	40
									MO1:	20	62	8	48	45	49	7	63	41
MO2	COS1	R+N	C21R	Paules Mb	31	255470	4690014	88	18	197	-67	7	43.6	223	-58	7.1	41.9	39
	COS2	R+N	C20R	Paules Mb	31	256062	4690160	80	27	184	-63	6.5	45.4	221	-48	7.3	36.1	37
	COS3	R	C20R	Paules Mb	31	256184	4690146	80	25	199	-63	5.4	59.7	225	-46	6.2	45.6	41
	COS4	R	C20R	Paules Mb	31	256266	4689306	89	20	203	-64	4.3	124	224	-50	7.2	45.7	40
	COS5	R	C20R	Paules Mb	31	256376	4689286	89	27	199	-67	12	17	226	-50	12.2	16.6	42
	COS6	R	C20R	Paules Mb	31	256562	4689281	86	26	188	-69	7.7	35.7	226	-55	6.5	50.3	42

									MO2:	195	-66	3	415	224	-51	4	303	40
MO3	MON1	R+N	C20N	Sobrarbe Fm	31	260535	4686825	98	23	195	-52	12	21.7	218	-41	12.3	20.7	34
	MON2	R+N	C19R	Sobrarbe Fm	31	260888	4686646	100	22	180	-59	7.5	46.8	213	-55	6.4	64	29
	MON3	R	C19R	Sobrarbe Fm	31	261090	4686522	100	23	193	-51	9.5	26.7	218	-45	9.3	27.5	34
	MON4	N+R	C19R	Sobrarbe Fm	31	261307	4686392	113	17	16	49	19	7.4	33	49	18	8.2	29
	OLS1	R	C19R	Sobrarbe Fm	31	260618	4685394	124	25	215	-36	16	12.7	233	-32	14.8	14.6	49
	OLS2	R+N	C19R	Escanilla Fm	31	260898	4685156	126	21	215	-32	13.4	20.5	218	-24	14.7	17.4	34
	OLS3	R+N	C18R	Escanilla Fm	31	261182	4684942	135	16	208	-16	24.4	6.1	206	-21	24.4	6.1	22
	OLS4	R+N	C18R	Escanilla Fm	31	261394	4684706	91	16	29	36	13.2	16	214	-41	12.8	17	30
									MO3:	22	43	13	22	37	38	11	31	33
MO4	ESC3	N	C17N.2n	Escanilla Fm	31	262072	4683329	170	10	31	27	13.4	9.7	35	34	13.4	9.7	31
	ESC2	N	C17N.1n	Escanilla Fm	31	262256	4683133	158	13	27	45	14	14.2	39	52	14	14.2	35
	ESC1	N	C16N.2n	Escanilla Fm	31	262320	4682955	155	15	18	50	8.9	30	35	60	8.9	30	31
									MO4:	26	41	20	38	36	49	21	37	32
MO5	ESC4	N	C16N.2n	Escanilla Fm	31	262532	4682604	185	10	26	17	9.7	25.5	27	26	9.7	25.5	23
	ESC5	R	C16N.1r	Escanilla Fm	31	262605	4682420	175	16	195	21	12.5	28.5	198	-36	12.5	28.5	14
									MO5:	20	3	153	5	23	31	82	28	19
MO6	ESC6	R	C15	Escanilla Fm	31	262776	4682247	175	16	180	-31	7.3	49.3	181	-47	7.3	49.3	-3
	ESC7	N+R	C15N	Escanilla Fm	31	262872	4682316	173	3	1	44	4.1	111	2	47	4.1	110.6	-2
									MO6:	0	38	29	78	2	47	1.5	28244	-2
MO7	ARA1	R	C24R	Alveolina lmst	31	254791	4706181	273	29	225	-35	12.7	17.1	200	-50	11.7	20	16
	ARA2	R	C24R	Metils Fm	31	254554	4706253	273	29	226	-29	10.4	15.5	209	-53	9.5	16.1	25
	ARA3	R	C24R	Yeba Fm	31	254464	4706224	272	50	249	-9	10.7	21.1	230	-52	13.6	13.4	46
	ARA4	N+R	C24R	Yeba Fm	31	254394	4706252	279	54	243	3	24.4	5.4	39	32	28	4.9	35
	ARA5	R	C24N.1r	Lw Boltaña Mb	31	254216	4706317	274	63	37	-7	13.7	12.1	52	46	14.6	10.7	48
	ARA7	R+N	trC24n.1N/C23r	Lw Boltaña Mb	31	253975	4706280	274	64	245	2	24.7	6.8	227	-52	19.8	10	43
	ARA6	R	C23R	Lw Boltaña Mb	31	253910	4706069	278	72	252	22	8.3	25.7	246	-43	8.2	26.2	62
	ARA8	R	C23R	Up Boltaña Mb	31	253750	4706135	276	68	249	13	13.7	40.4	226	-50	15	33.6	42
	ARA9	R	C22R	Up Boltaña Mb	31	253519	4706413	277	82	229	33	35.9	19.3	226	-35	18.9	65.4	42
									MO7:	60	0	36	3	47	46	8	46	43
MO8	MILL1	R	C24R	Millaris Fm	31	255245	4706873	283	6	240	-50	8.2	26.4	235	-54	8.4	24.9	51
	MILL2	R	C24R	Millaris Fm	31	255192	4706943	280	6	236	-37	7.9	28.3	231	-43	8	27.9	47
									MO8:	268	-43	29	74	233	-49	25	103	49

Rodríguez-Pinto (2013)

label	site	polar.	chron	age	UTM			bedding		BTC				ATC				β
					zone	X	Y	dd	dip	Dg	Ig	α95	k	Ds	Is	α95	k	
RP1	SS01	R	/	Lutetian	30	748105	4691307	97	40	170	-50	12	33	216	-5	11	33	32
	SS02	R	/	Lutetian	30	747957	4691454	102	81	146	-33	8	104	235	-41	9	86	51
	SS03	R	/	Lutetian	30	747978	4688942	103	51	192	-63	6	58	249	-34	7	54	65
	SS04	R	/	Lutetian	30	747387	4688669	95	43	208	-73	5	114	253	-38	5	97	69
	SS05	R	/	Lutetian	30	747160	4688582	89	36	227	-61	10	14	247	-31	10	14	63
	SS06	R	/	Lutetian	30	746484	4687200	82	41	207	-59	6	35	234	-27	6	35	50
RP2	SI	N	/	Cuisian-Lw Lut	/	/	/	/	/	5	61	8	7	21	42	9	6	17
	SI	R	/	Cuisian-Lw Lut	/	/	/	/	/	184	-46	4	17	191	-23	5	17	7

REFERENCES

Barberà, X., Cabrera, L., Marzo, M., Parés, J. M., & Agustí, J. (2001). A complete terrestrial Oligocene magnetostratigraphy from the Eastern Ebro Basin, Spain. *Earth and Planetary Science Letters*, *187*(1-2), 1–16.

Barnolas, A., & Gil-Peña, I. (2001). Ejemplos de relleno sedimentario multiepisódico en una cuenca de antepaís fragmentada: La Cuenca Surpirenaica. *Boletín Geológico y Minero*, *112*(3), 17–38.

Barsó, D. (2007). *Análisis de la procedencia de los conglomerados sinorogénicos de La Pobla de Segur (Lérida) y su relación con la evolución tectónica de los Pirineos centro-meridionales durante el Eoceno medio-Oligoceno*. PhD Thesis. Universitat de Barcelona. 209 pp.

Beamud, E., Garcés, M., Cabrera, L., Muñoz, J.A., & Almar, Y. (2003). A new middle to late Eocene continental chronostratigraphy from NE Spain. *Earth and Planetary Science Letters*, *216*(4), 501–514.

Beamud, E., Muñoz, J. A., Fitzgerald, P. G., Baldwin, S. L., Garcés, M., Cabrera, L., & Metcalf, J. R. (2011). Magnetostratigraphy and detrital apatite fission track thermochronology in syntectonic conglomerates: constraints on the exhumation of the South-Central Pyrenees. *Basin Research*, *23*(3), 309–331.

Beamud, E., Costa, E., Garcés, M., Marín, M. A., Cabrera, L., Roca, E., & Gómez-Paccard, M. (2012). An integrated Eocene chronostratigraphy for the central sector of the SE margin of the Ebro Basin. *VIII Congreso Geológico de España - Geotemas 13* (p. 350). Oviedo.

Bentham, P. (1992). *The tectono-stratigraphic development of the western oblique ramp of the South-Central Pyrenean thrust system, Northern Spain*. PhD Thesis. University of Southern California. 253 pp.

Bentham, P. A., Burbank, D. W., & Puigdefàbregas, C. (1992). Temporal and spatial controls on the alluvial architecture of an axial drainage system: late Eocene Escanilla Formation, southern Pyrenean foreland basin, Spain. *Basin Research*, *4*, 335–352.

Bentham, P. A., & Burbank, D. W. (1996). Chronology of Eocene foreland basin evolution along the western oblique margin of the South-Central Pyrenees. In P. F. Friend & C. J. Dabrio (Eds.), *Tertiary basins of Spain* (pp. 144–152). Cambridge University Press.

Berggren, W. A., Kent, D. V., Aubry, M. P., & Hardenbol, J. (1995). Geochronology, time scales and global stratigraphic correlation; unified temporal framework for an historical geology. In B. W.A., D. V. Kent, M. P. Aubry, & J. Hardenbol (Eds.), *Geochronology, Time Scales and Global Stratigraphic Correlation* (pp. v–vi). SEPM Special Publication 54.

Burbank, D. W., Puigdefàbregas, C., & Muñoz, J. A. (1992). The chronology of the Eocene tectonic and stratigraphic development of the eastern Pyrenean foreland basin, northeast Spain. *Geological Society Of America Bulletin*, *104*, 1101–1120.

Burbank, D. W., & Vergés, J. (1994). Reconstruction of topography and related depositional systems during active thrusting. *Journal of Geophysical Research*, *99*(B10), 20281–20297.

Costa, E., Garcés, M., López-Blanco, M., Beamud, E., Gómez-Paccard, M., & Larrasoaña, J. C. (2010). Closing and continentalization of the South Pyrenean foreland basin (NE Spain): magneto-

chronological constraints. *Basin Research*, *22*(6), 904–917.

Costa, E., Garcés, M., Sáez, A., Cabrera, L., & López-Blanco, M. (2011). The age of the "Grande Coupure" mammal turnover: New constraints from the Eocene–Oligocene record of the Eastern Ebro Basin (NE Spain). *Palaeogeography, Palaeoclimatology, Palaeoecology*, *301*(1-4), 97–107.

Costa, E., Garcés, M., López-Blanco, M., Serra-Kiel, J., Bernaola, G., Cabrera, L., & Beamud, E. (2013). The Bartonian-Priabonian marine record of the eastern South Pyrenean Foreland Basin (NE Spain): A new calibration of the larger foraminifers and calcareous nannofossil biozonation. *Geologica Acta*, *11*(2), 177–193.

Cuesta, M. A., Checa Soler, L., & Casanovas-Cladellas, M. L. (2006). Artiodáctilos del yacimiento de Sossís (Eoceno Superior, Cuenca Prepirenaica, Península Ibérica). *Revista Española de Paleontología*, *21*(2), 123–144.

Cuesta Ruiz-Colmenares, M., Checa Soler, L., & Casanovas-Cladellas, M. L. (2006). Artiodáctilos del yacimiento de Sossís (Eoceno superior, Cuenca Prepirenaica, Península Ibérica). *Revista Española de Paleontología*, *21*(2), 123–144. Gradstein, F. M., Ogg, J. G., & Smith, A. A. (2004). *A Geologic Time Scale 2004* (p. 589). Cambridge: Cambridge University Press.

Cuevas-Gozalo, M. (1989). *Sedimentary facies and sequential architecture of tide-influenced alluvial deposits. An example from the Middle Eocene Capella Fm; South-Central Pyrenees; Spain*. *Geologica Ultraiectina* Vol. 61, 152 pp.

Dinarès-Turell, J. (1992). *Paleomagnetisme a les unitats sudpirinenques superiors. implicacions estructurals*. PhD Thesis. Universitat de Barcelona. 462 pp.

Fernández-Bellon, O. (2004). *Reconstruction of geological structures in 3D. An example from the Southern Pyrenees*. PhD Thesis. Universitat de Barcelona. 321 pp.

Fillon, C., & van der Beek, P. (2012). Post-orogenic evolution of the southern Pyrenees: constraints from inverse thermo-kinematic modelling of low-temperature thermochronology data. *Basin Research*, 24, 418-436.

Fillon, C., Gautheron, C. & van der Beek, P. (2013). Oligocene-Miocene burial and exhumation of the Southern Pyrenean foreland quantified by low-temperature thermochronology. *Journal of the Geological Society, London*, 170, 67-77.

Fitzgerald, P. G., Muñoz, J. A., Coney, P. J., & Baldwin, S. L. (1999). Asymmetric exhumation accross the Pyrenean orogen: implications for the tectonic evolution of a collisional orogen. *Earth and Planetary Science Letters*, *173*(3), 157–170.

Gradstein, F. M., Ogg, J. G., & Smith, A. A. (2004). *A Geologic Time Scale 2004* (p. 589). Cambridge: Cambridge University Press.

Hardenbol, J., Thierry, J., Farley, M. B., Jacquin, T., De Graciansky, P. C., & Vail, P. R. (1998). *Mesozoic and Cenozoic sequence stratigraphy of European basins*. SEPM Special Publication 60.

Hogan, P. J. (1993). *Geochronologic, tectonic and stratigraphic evolution of the Southwest Pyrenean foreland basin, Northern Spain*. PhD Thesis. University of Southern California. 219 pp.

Hogan, P. J., & Burbank, D. W. (1996). Evolution of the Jaca piggy-back basin and emergence of the External Sierras, southern Pyrenees. In P. F. Friend & C. J. Dabrio (Eds.), *Tertiary basins of Spain* (pp. 153–160). Cambridge University Press.

Legendre, S., & Lévêque, F. (1997). Étalonnage de l'échelle biochronologique mammalienne du Paléogène d'Europe occidentale: vers une integration à l'échelle globale. In J. P. Aguilar, S. Legendre, & J. Michaux (Eds.), *BiochroM'97. Memoire Trav. E.P.H.E* (pp. 461–473). Montpellier: Inst. Montpellier 21.

López-Blanco, M., Marzo, M., & Muñoz, J. A. (2003). Low-amplitude, syn-sedimentary folding of a deltaic complex: Roda sandstone (lower Eocene), South-Pyrenean Foreland Basin. *Basin Research*, *15*(1), 73–95.

Luzón, A. (2005). Oligocene-Miocene alluvial sedimentation in the northern Ebro Basin, NE Spain: Tectonic control and paleogeographical evolution. *Sedimentary geology*, *177*, 19–39.

Martini, E. (1971). Standard Tertiary and Quaternary calcareous nannoplankton zonation. *Planktonic Conference 2* (pp. 739–777).

Meigs, A. J. (1995). *Thrust faults, thrust sheets and thrust belts: New insights from the Spanish Pyrenees*. PhD Thesis. University of Southern California. 275 pp.

Meigs, A. J., & Burbank, D. W. (1997). Growth of the South Pyrenean orogenic wedge. *Tectonics*, *16*(2), 239–258.

Meigs, A. J., Vergés, J., & Burbank, D. W. (1996). Ten-million-year history of a thrust sheet. *Geological Society Of America Bulletin*, *108*(12), 1608–1625.

Mellere, D. (1992). *I conglomerati di Pobla de Segur: Stratigrafia fisica e relazioni tettonica-sedimentazione*. PhD Thesis. Universita degli studi di Padova. 203 pp.

Mochales, Tania, Casas, A. M., Pueyo, E. L., & Barnolas, A. (2012a). Rotational velocity for oblique structures (Boltaña anticline, Southern Pyrenees). *Journal of Structural Geology*, *35*, 2–16.

Mochales, T., Barnolas, A., Pueyo, E. L., Casas, A. M., Serra-Kiel, J., Samsó, J. M., & Ramajo, J. (2012b). Chronostratigraphy of the Boltaña anticline and the Ainsa Basin (Southern Pyrenees). *Geological Society of American Bulletin*, *124*(7-8), 1229–1250.

Muñoz, J. A., Beamud, E., Fernández, O., Arbués, P., Dinarès-Turell, J., & Poblet, J. (submitted). The Ainsa fold and thrust Oblique Zone of the Central Pyrenees: kinematics of a curved contractional system from paleomagnetic and structural data. *Tectonics*.

Oliva-Urcia, B. (2004). *Geometría y cinemática rotacional en las Sierras Interiores y Zona Axial (sector de Bielsa) a partir del análisis estructural y paleomagnético*. PhD Thesis. Universidad de Zaragoza. 290 pp.

Oliva-Urcia, B., & Pueyo, E. L. (2007). Rotational basement kinematics deduced from remagnetized cover rocks (Internal Sierras, Southwestern Pyrenees). *Tectonics*, *26*, TC4014.

Oliva-Urcia, B., Pueyo, E. L., & Larrasoana, J. C. (2008). Magnetic reorientation induced by pressure solution: A potencial mechanism for orogenic-scale remagnetizations. *Earth and Planetary Science Letters*, *265*, 525–534.

Pascual, J. O., Parés, J. M., Langereis, C. G., & Zijderveld, J. D. A. (1992). Magnetostratigraphy and rock magnetism of the Ilerdian stratotype at Tremp, Spain. *Physics of the Earth and Planetary Interiors*, *74*, 139–157.

Picart, J., Carrera, N., Solé, J., Montaner, J., Rivas, G., Muñoz, J. A., Serra, L., et al. (2009). Tremp 252-1-2 (65-22) [document cartogràfic]. 1:25000. Sèrie Mapa Geològic de Catalunya 1:25000,

Geotreball 1. Institut Cartogràfic de Catalunya (ICC) Servei Geològic de Catalunya (IGC).

Pueyo, E. (2000). *Rotaciones paleomagnéticas en sistemas de pliegues y cabalgamientos. Tipos, causas, significado y aplicaciones. (Ejemplos de las Sierras Exteriores y Cuenca de Jaca, Pirineo Aragonés)*. PhD Thesis. Universidad de Zaragoza. 296 pp.

Reynolds, A. (1987). *Tectonically controlled fluvial sedimentation in the South-Pyrenean Foreland Basin*. PhD Thesis. University of Liverpool. 309 pp.

Rodríguez-Pintó, A., Pueyo, E. L., Serra-Kiel, J., Samsó, J. M., Barnolas, A., & Pocoví, A. (2012). Lutetian magnetostratigraphic calibration of larger foraminifera zonation (SBZ) in the Southern Pyrenees: The Isuela section. *Palaeogeography, Palaeoclimatology, Palaeoecology*, *333-334*, 107–120.

Rodríguez-Pintó, A., Pueyo, E. L., Pocoví, A., Ramón, M. J., & Oliva-Urcia, B. (2013). Structural control on overlapped paleomagnetic vectors: A case study in the Balzes anticline (Southern Pyrenees). *Physics of the Earth and Planetary Interiors*, *215*, 43–57.

Schmidt-Kittler, N. (1987). International Symposium on Mammalian Biostratigraphy and Paleoecology of the European Paleogene - Mainz February 18th-21st. *Münch. Geowiss. Abh. 10* (p. 312).

Serra-Kiel, J., Hottinger, L., Caus, E., Drobne, K., Fernández-Cañadell, C., Jauhri, A. K., Less, G., et al. (1998). Larger foraminiferal biostratigraphy of teh Tethyan Paleocene and Eocene. *Bulletin de la Societè Geologique de France*, *169*(2), 281–299.

Sinclair, H. D., Gibson, M., Naylor, M., & Morris, R. G. (2005). Asymmetric growth of the Pyrenees revealed through measurement and modeling of orogenic fluxes. *American Journal of Science*, *305*(5), 369–406.

Sussman, A. J., Butler, R. F., Dinarès-Turell, J., & Vergés, J. (2004). Vertical-axis rotation of a foreland fold and implications for orogenic curvature: an example from the Southern Pyrenees, Spain. *Earth and Planetary Science Letters*, *218*(3-4), 435–449.

Vergés, J. (1993). *Estudi tectònic del vessant sud del Pirineu oriental i central. Evolució cinemàtica 3D*. PhD Thesis. Universitat de Barcelona. 203 pp.

Vincent, S. (1993). *Fluvial Paleovalleys in Mountain Belts: An Example from the South Central Pyrenees*. PhD Thesis. University of Liverpool. 407 pp.

Vincent, S. J. (2001). The Sis palaeovalley: a record of proximal fluvial sedimentation and drainage basin development in response to Pyrenean mountain building. *Sedimentology*, *48*, 1235–1276.

CHAPTER 4- CONCLUSIONS

4. CONCLUSIONS

The results presented in this Thesis are derived from the integration of magnetostratigraphic, magnetotectonic and thermochronological data, together with structural and sedimentological information from the south-central Pyrenees. The integration of these datasets permits quantification and unraveling the timing of differential crustal movements during orogen evolution, including thrusting events, uplift and exhumation, subsidence or vertical axis rotations. This is important to establish coherent kinematic models and to understand the relationships between surface processes and tectonic forces.

The new magnetostratigraphic ages presented challenge previous dating of the synorogenic continental units preserved in the inner parts of the South Pyrenean fold and thrust belt and enable a precise chronostratigraphic framework for the Eocene-Oligocene syntectonic materials of the South-Central Pyrenees and the recorded tectonic and sedimentological events. In addition, this new chronostratigraphy substantially changes the traditionally accepted ages of the European reference levels MP14 to MP17. The South Pyrenean and Ebro basin fossil localities representing from MP14 to MP17 reference levels would be significantly older than previously considered. MP14 and MP15 are correlated to Lutetian whereas MP16 and MP17 would be Bartonian in age. These results reveal that chronostratigraphic age attributions based on MP reference levels should be taken with caution and revised in the light of all the available regional litho-, bio- and magnetostratigraphic information.

This new chronology establishes the deposition of the synorogenic materials of La Pobla/Senterada and Sis between Lutetian and Oligocene times. Therefore, these materials were deposited in piggy-back basins coinciding with the most intense periods of exhumation in the core of the orogen related to underthrusting and growth of the Axial Zone antiformal stack. Three main periods of exhumation linked to the movement on the Nogueres, Orri and Rialp thrust-sheets have been deduced from detrital thermochronology combined with in-situ thermochronology of the source region. Since sediment supply was granted by the uplifting Pyrenees, accommodation space must have exerted a significant control in changes in the sedimentation rates within the piggy-back and foreland basins. From Lutetian to early Bartonian times sedimentation rates in the piggy-back basins were similar to the exhumation rates in the inner zones caused by the underthrusting of the Orri thrust sheet. Sedimentation in the adjacent basins was characterized by aggradational stacking patterns and development

of lacustrine environments indicative of high accommodation space in the South Pyrenean basins during this period. A dramatic decrease in sedimentation rates took place in the South Pyrenean basins during Bartonian times, whereas the exhumation rates remained almost constant. Progradational stacking patterns, sediment condensation zones and abandonment surfaces in the syntectonic conglomerates point to a reduction in accommodation space during this time. The reduction in accommodation space was more pronounced in the eastern sector, in La Pobla area, than to the west, in the Ainsa and Jaca areas, as a consequence of the migration of the deformation to the SW. The studied materials also reveal a strong interplay between base level changes in the Ebro foreland basin and the tectonosedimentary evolution of the south-central Pyrenees. Sedimentation rates recovered after the closure of the Ebro basin during Priabonian times, as most of the material was preserved due to the ceasing of the by-pass of sediments to the west. The closure of the south Pyrenean Ebro foreland basin and the related backfilling favored a migration of the deformation to inner parts of the chain and a dramatic increase in exhumation rate in the Axial Zone due to the onset of underthrusting of the Rialp thrust sheet. Base level drop by the posterior capture of the Ebro River by the Mediterranean Sea during Miocene times induced re-excavation of the piggy-back/foreland basins and forced post-orogenic exhumation within the Axial Zone.

Deposition of these materials also coincides with gradients of thrust displacement of the thrust sheets that account for the oblique structures and thrust salients in the South Central Pyrenees. The precise ages of the sedimentary successions of the south-central Pyrenees constrain the 60° to 45° clockwise vertical axis rotations on its western tip to Lutetian to Bartonian times when the structures of the Ainsa Oblique Zone developed. This rotation resulted from about 50 km of differential displacement on the Gavarnie thrust sheet caused by the distribution of the Triassic evaporites at its basal detachment. The synchronicity between thrusting and vertical-axis rotations points to a model of progressive arc due to divergent thrust emplacement to explain the origin of the curvature in the Ainsa Oblique Zone. Transverse extensional faults and diapirs formed at the outer arcs in response to rotation space problems. Translation of the Serres Marginals thrust sheet on top of the foreland since Priabonian times added a secondary rotation of about 10° in the western sector and produced anticlockwise rotations at its eastern part. Therefore, the accurate dating of these materials reveals a diachrony in the formation of both ends of the thrust salient of the south-central Pyrenees.

The results exposed in this Thesis highlight a strong relationship between the structural evolution of the South Pyrenean thrust system, thrusting and exhumation in the

Axial Zone and the stratigraphic record of the synorogenic materials. Tectonic forces controlled not only the observed patterns of exhumation but also the evolution of the synorogenic topography of the piggy-back and foreland basins and the depositional features of the synorogenic sediments.

SUPPLEMENTARY MATERIAL 1

Magnetostratigraphic sections and Paleomagnetic directions

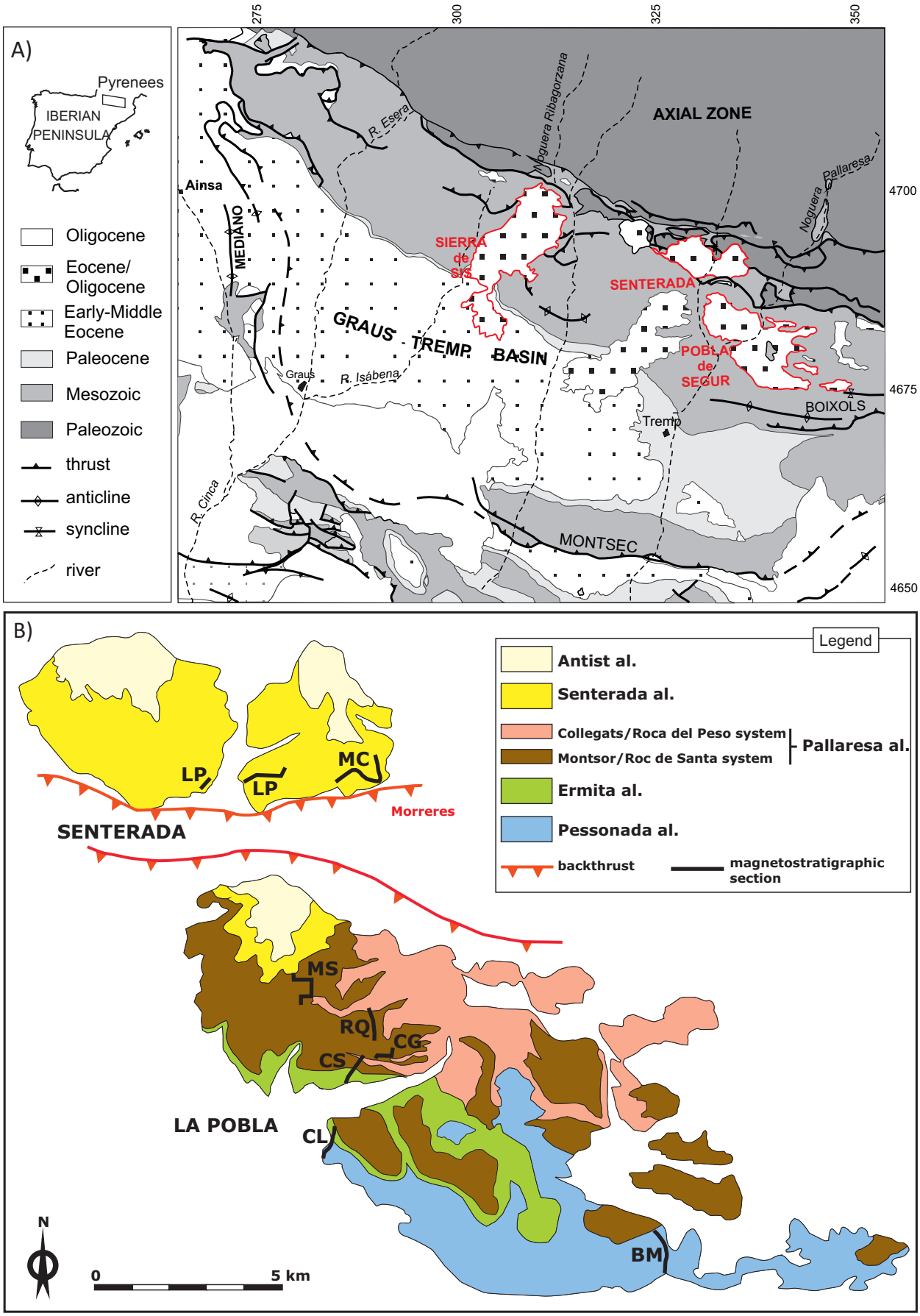

Figure S1.1- A) Simplified geological map of the South-Central Pyrenees. Modified from *Beamud et al.*(2003). La Pobla de Segur, Senterada and Sis conglomeratic bodies are highlighted in red. **B)**Stratigraphy of the La Pobla de Segur and Senterada basins and location of the magnetostratigraphic sections. (Modified from Mellere, 1992)

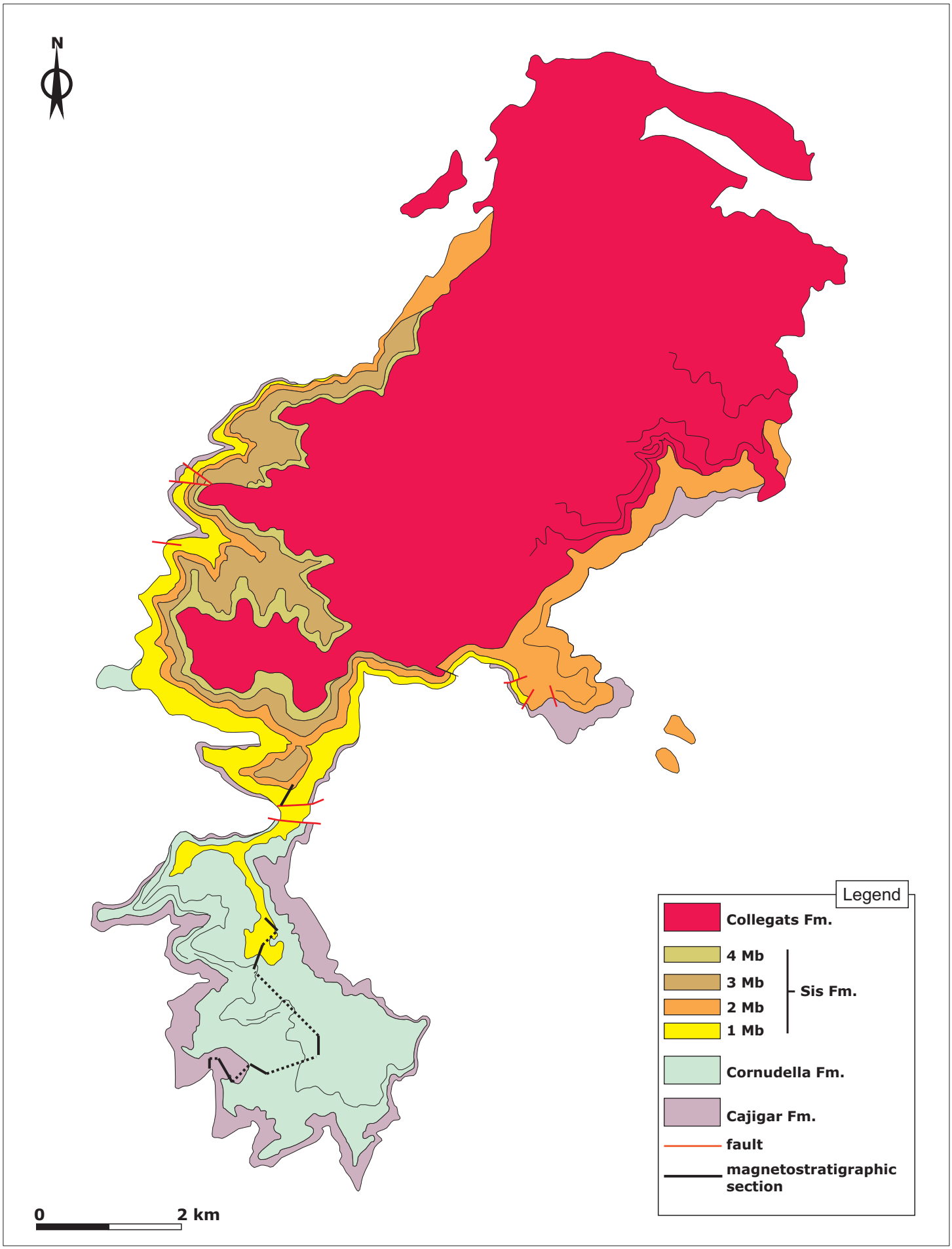

Figure S1.2- Location of the magnetostratigraphic section CJ in Sis. (Modified from Vincent, 1993)

BM: Barranc de Boumort. Base: 42.210637 N, 1.094326 E, 1136 m. Top: 42.220737 N, 1.087469 E, 1538 m

sample	level (m)	Dg	Ig	Dt	It	latp	Int. (E-6 A/m)	error	Quality	Trange	comments
BM002.2A	14.8	180.00	-70.51	181.61	-60.54	-88.57	30.17	1.767655	2	4	340-370
BM004.2A	18.9	354.90	45.72	356.31	35.85	67.35	89.21	2.288981	2	3	290-330
BM005.1A	22	137.76	-35.47	142.18	-28.38	-47.7	41.86	9.036659	2	3	350-390
BM015.2A	52.4	149.25	-39.95	153.27	-31.62	-56.03	37.53	6.577087	2	2	440-480
BM020.1A	72.2	192.07	-57.79	190.61	-47.85	-74.11	80.84	8.048362	2	3	400-440
BM021.1B	73.8	390.20	27.96	388.41	18.84	48.98	60.18	6.541924	2	2	440-520
BM022.1A	74.4	336.33	33.52	339.88	15.06	51.08	67.18	1.517382	2	2	400-520
BM023.1A	79	352.74	44.34	354.52	24.50	60.16	47.21	8.259667	2	3	310-370
BM025.2A	89	375.82	67.07	369.47	47.45	74.28	111.06	2.639849	2	3	290-390
BM026.3A	94	398.47	31.74	393.43	15.28	44.64	134.71	3.273737	2	2	250-370
BM027.3A	109.7	395.65	40.12	389.18	22.97	50.47	103.05	4.347187	2	3	300-390
BM029.4A	110.7	190.71	-59.29	189.47	-49.33	-75.71	27.03	9.731164	2	3	340-370
BM031.1A	112.7	99.86	-60.39	116.32	-58.09	-42.62	29.41	9.726328	2	3	250-310
BM039.1A	142	422.41	53.84	412.65	47.72	45.85	25.96	5.208444	2	3	340-400
BM040.2A	143.5	210.92	-28.37	209.05	-19.31	-48.85	38.68	10.90142	2	3	410-430
BM042.3A	146.5	316.63	54.96	325.35	47.74	59.04	63.39	7.86713	2	2	350-470
BM050.2A	163	409.46	32.48	405.73	25.11	41.01	71.80	6.593795	2	3	370-410
BM051.3A	166	176.06	-24.11	176.59	-14.23	-54.8	24.21	6.707126	2	3	350-390
BM052.3A	168.5	270.11	-54.40	256.86	-52.39	-30.5	35.62	4.563838	2	3	280-310
BM066.2A	202	140.18	-83.00	166.55	-74.25	-69.98	29.03	17.99626	2	3	280-370
BM072.3A	215.5	187.58	-57.83	187.05	-47.84	-75.45	47.62	8.058631	2	2	460-520
BM073.1C	219.3	391.47	28.12	389.58	19.09	48.47	61.44	16.26812	2	2	370-520
BM083.1B	242.5	379.54	40.31	377.85	30.59	59.99	71.25	4.650788	2	3	250-350
BM084.1B	247	356.35	70.95	359.18	61.02	89.35	16.47	9.130763	2	3	390-430
BM088.2B	261.5	155.65	-62.88	162.74	-53.86	-74.37	47.47	4.708771	2	3	370-390
BM090.2B	272.3	124.40	-31.81	129.16	-26.53	-38.04	39.75	8.442868	2	3	400-430
BM105.2A	324.2	214.50	-37.70	211.42	-28.85	-51.93	49.12	7.099459	2	3	300-350
BM113.1A	358	239.10	-23.15	236.18	-17.07	-30.6	23.49	24.34154	2	3	340-380
BM117.2A	372	248.41	-48.71	239.47	-43.53	-38.91	51.81	5.040387	2	3	400-420
BM118.2C	373.5	106.88	-87.82	173.39	-79.34	-62.72	77.03	4.313734	2	3	360-400
BM120.1A	378	192.23	-68.83	190.05	-58.88	-81.97	8.88	1.145602	2	3	300-320

sample	level (m)	Dg	Ig	Dt	It	latp	Int. (E-6 A/m)	error	Quality	Trange	comments
BM123.1A	404.8	140.57	-18.78	142.43	-11.52	-40.65	73.22	3.744224	2	3	370-390
BM124.1A	405.5	161.02	-27.18	162.66	-17.98	-53.58	54.03	11.09594	2	3	340-360
BM128.1A	423.5	98.78	-80.11	141.76	-75.52	-59.84	51.99	5.095785	2	3	400-440
BM131.2A	440.8	227.63	-51.77	220.63	-43.99	-52.95	123.54	7.018575	2	2	280-320
BM132.1A	441.8	160.35	-37.88	162.96	-28.69	-59.29	56.96	9.078018	2	3	460-490
BM141.2B	469.7	192.08	-46.08	191.07	-36.15	-65.88	110.42	4.855765	2	3	250-320
BM142.3A	477.7	219.94	-56.45	213.17	-47.91	-60.18	282.80	3.810293	2	3	400-440
BM146.2A	486.2	204.01	-42.85	201.61	-33.32	-59.71	121.03	4.390915	2	3	280-300
BM150.2A	496	232.06	-21.40	229.73	-14.43	-34.06	99.67	10.20495	2	3	340-400
BM151.2A	499	246.23	-32.69	241.27	-27.49	-30.9	45.08	1.726393	2	3	330-350
BM152.1A	501	315.70	41.06	321.30	34.16	49.72	73.26	2.76199	2	3	300-350
BM153.2B	503.5	345.51	34.76	347.36	25.28	58.99	51.40	6.46594	2	3	400-440
BM157.2A	522.5	190.22	-63.59	188.91	-53.62	-79.28	46.66	4.971328	2	3	460-490
BM160.1A	530	211.93	-41.15	208.74	-32.10	-55.1	54.68	5.766647	2	3	380-400
BM166.2A	548.5	200.55	-42.97	198.57	-33.29	-61.17	240.61	2.869274	2	3	420-440
BM171.1B	561.5	173.76	-33.43	174.78	-23.60	-59.68	45.10	8.478666	2	3	340-380
BM181.2A	593	300.25	36.74	306.29	31.99	38.21	97.69	8.23197	2	3	300-380
BM006.1A	24.5	146.63	59.78	132.37	66.86	10.82	43.22	7.794354	3	3	360-380
BM007.1A	25.7	360.48	38.42	360.98	28.45	62.84	55.38	7.830201	3	4	200-340
BM009.1A	32.2	224.17	25.49	227.86	33.05	-15.29	46.86	2.721521	3	3	340-370
BM010.2A	37.7	130.54	-19.02	132.85	-13.03	-35.24	46.05	6.612007	3	4	300-320
BM011.1B	41.7	150.03	38.63	144.38	46.55	-12.57	51.85	10.28481	3	3	400-440
BM012.2A	44.3	354.66	-41.89	352.56	-51.70	15.05	58.26	10.56372	3	2	480-560
BM013.3A	47.7	176.10	18.09	175.41	27.96	-32.68	25.60	8.799747	3	2	480-520
BM017.3A	60	425.98	-10.64	428.02	-15.34	10.53	32.62	9.200908	3	3	300-370
BM018.1B	65.3	137.74	15.75	135.15	22.38	-22.2	39.41	6.838693	3	3	310-370
BM024.3A	84	223.20	40.15	239.75	53.09	3.6	80.89	5.243369	3	2	480-560
BM028.3A	110.2	114.80	38.32	106.79	41.05	4.18	41.02	8.299275	3	3	360-380
BM030.1A	111.9	133.90	58.08	118.57	63.32	12.94	105.66	2.187529	3	3	300-370
BM032.1A	122.2	122.55	23.47	118.20	27.77	-9.6	70.58	3.268065	3	2	370-480
BM034.2A	126.2	269.80	-17.44	266.79	-16.27	-7.95	56.58	6.698856	3	3	370-440
BM035.3A	129	275.65	-8.83	274.10	-8.81	0.04	58.04	2.592037	3	2	480-520

sample	level (m)	Dg	Ig	Dt	It	latp	Int. (E-6 A/m)	error	Quality	Trange	comments
BM037.2A	136.4	251.38	50.86	263.81	53.88	18.34	38.00	4.073187	3	3	370-410
BM038.1A	138.2	301.68	76.50	327.53	69.95	65.71	33.82	9.145619	3	4	250-310
BM041.2A	145.5	323.59	-62.61	306.39	-69.11	-15.59	29.32	9.148373	3	3	330-350
BM045.2A	150.3	138.98	22.73	135.34	29.45	-18.87	31.42	14.40821	3	3	390-410
BM046.2B	153	377.27	64.51	374.10	54.68	76.94	55.18	6.433483	3	4	200-310
BM047.3A	155.7	201.49	-0.92	201.68	8.67	-39.36	46.64	4.343391	3	3	340-400
BM048.2A	157.5	179.21	24.39	178.61	34.33	-28.83	26.77	2.557066	3	3	310-340
BM049.3A	161.5	115.07	8.75	113.33	12.05	-12.7	23.10	10.53841	3	4	250-280
BM053.1A	169.7	214.35	69.39	236.01	77.17	26.18	94.20	5.443289	3	3	340-370
BM055.1A	175	161.28	61.95	150.06	70.71	10.6	37.49	2.515887	3	4	250-280
BM056.2A	177.5	135.00	2.80	134.19	9.18	-27.37	59.19	4.450544	3	3	280-370
BM061.2A	192.5	324.41	13.26	325.48	5.59	39.91	54.07	3.327632	3	4	350-370
BM062.2A	193	358.10	54.81	359.39	44.86	74.15	65.69	2.527602	3	3	280-340
BM064.2A	197	214.06	6.96	215.05	15.66	-30.41	67.63	2.541193	3	3	360-400
BM065.3A	198.2	205.25	58.75	213.50	67.89	7.66	30.17	10.18993	3	4	340-360
BM067.2A	205	212.23	56.47	221.71	64.99	6.63	99.17	3.068353	3	3	430-470
BM074.2B	221.4	230.92	41.18	238.41	47.67	-0.9	99.92	4.917972	3	2	490-520
BM077.3A	228.7	206.59	47.00	211.76	56.13	-5.87	17.60	32.60399	3	3	330-350
BM078.1A	229.5	180.84	25.51	180.39	35.48	-28.09	26.00	8.912411	3	3	390-430
BM080.2B	235.3	336.33	34.95	339.04	26.06	56.18	65.59	6.408285	3	3	370-460
BM085.1A	254	363.85	61.10	364.11	51.10	78.99	61.90	5.908163	3	2	400-460
BM086.2B	256	384.07	34.91	382.25	25.40	55.24	61.81	7.434356	3	2	330-460
BM092.2A	280.5	184.02	-50.05	184.18	-40.05	-70.19	33.90	4.952567	3	3	370-390
BM094.1B	288	133.50	-48.78	141.03	-42.03	-53.2	25.33	15.50651	3	3	300-370
BM095.2B	289.5	98.90	-56.32	113.18	-54.39	-38.6	24.81	6.685843	3	3	350-400
BM097.2A	296.7	267.73	-23.46	263.60	-21.84	-12.3	31.67	7.735476	3	3	300-370
BM098.3A	298.5	196.64	26.43	197.94	36.20	-25.44	21.96	4.149203	3	3	300-370
BM101.2A	317	215.99	10.81	217.41	19.33	-27.54	16.95	16.09597	3	3	370-430
BM102.1A	319.4	210.37	-15.80	209.53	-6.73	-43.01	30.26	10.67853	3	3	330-370
BM104.2A	323.2	225.92	-33.55	222.32	-25.78	-43.6	52.22	10.40912	3	3	330-350
BM106.1A	328	201.25	7.05	201.85	16.64	-35.42	69.29	5.540358	3	3	350-390
BM107.3A	329.5	251.49	1.40	252.03	5.36	-11.33	28.06	10.42274	3	3	400-430

sample	level (m)	Dg	Ig	Dt	It	latp	Int. (E-6 A/m)	error	Quality	Trange	comments
BM109.2A	342.5	254.11	3.60	254.99	7.10	-8.59	18.57	11.56795	3	3	350-370
BM110.2A	347	190.96	-3.25	190.99	6.69	-43.27	36.62	6.972611	3	3	420-440
BM114.1A	365.5	275.15	-29.24	269.59	-28.78	-10.57	43.24	5.979609	3	3	400-440
BM115.2A	367.5	170.50	1.57	170.22	11.25	-41.2	83.21	4.264711	3	3	320-340
BM127.1B	412.3	199.21	8.81	199.82	18.49	-35.12	71.96	11.98234	3	3	420-440
BM130.1A	433.5	205.03	-30.54	203.44	-21.09	-52.54	43.10	8.008471	3	3	420-440
BM135.2A	448	443.68	-68.62	109.31	-68.35	-42.78	336.34	3.866705	3	3	400-440
BM137.2C	453.2	199.01	17.60	200.05	27.28	-30.31	81.66	11.20816	3	2	420-440
BM138.1A	456	120.45	-67.01	137.67	-61.33	-59.06	32.94	3.058589	3	3	490-520
BM144.1A	483.3	185.46	-59.82	185.35	-49.82	-77.57	28.63	9.297735	3	4	380-440
BM148.2A	492.7	269.12	-78.17	231.94	-73.79	-54.2	153.08	2.49977	3	2	340-420
BM149.2A	495	105.33	-25.86	109.85	-23.68	-22.92	81.34	3.883801	3	3	300-430
BM155.3A	513	282.08	-14.37	279.43	-15.38	1.63	91.23	8.155678	3	2	360-420
BM161.2B	534	448.33	-59.56	105.33	-59.24	-35.63	59.19	6.43572	3	2	320-340
BM164.1A	541	239.71	-4.83	239.44	0.98	-21.74	218.06	2.918341	3	3	400-430
BM174.2A	569.5	189.52	12.87	189.78	22.84	-35.07	54.16	13.60893	3	3	380-440
BM176.1B	576.7	215.10	28.04	218.43	36.55	-18.02	40.22	7.598855	3	3	420-440
BM179.2A	589.7	307.95	-72.06	274.94	-75.02	-34.29	84.40	3.930074	3	3	380-440
BM180.1A	591	390.90	66.33	383.82	57.06	71.24	104.04	8.0443	3	3	420-440
BM182.2A	594.5	95.91	-8.98	97.46	-8.68	-8.46	34.85	3.281703	3	3	320-440
BM008.1A	27.8	187.77	-27.82	187.57	-17.83	-56.17	38.65	44.04355	4	2	* 440-560
BM058.2A	184.7	219.92	-42.03	215.70	-33.61	-51.47	30.84	25.65184	4	3	* 200-400

CL: Claverol. Base: 42.245585 N, 0.985105 E, 709 m. Top: 42.249736 N, 0.991451 E, 781 m

sample	level (m)	Dg	Ig	Dt	It	latp	Int (E-6 A/m)	error	Quality	Trange	comment
Gcmean N=5	17.5	182.7	-64.4	191.2	-37.2	-66.51	11.4	29.1			
CL005.2A	21	159	-44	170	-22	-57.91	107	22	2	2	550-600
CL006.1A	22.7	261	-29	252	-13	-17.71	395	1	2	3	450-500
CL006.3A	22.7	133	-36	147	-22	-47.84	435	4	2	3	350-500
Gcmean N=6	25.1	245.7	-52.2	230.8	-29.5	-39.27	3	49.2			
CL011.1A	30.5	282	-41	263	-32	-16.66	67	25	2	2	600-630
GCmean5	32.75	300.5	-49.8	268.4	-46.4	-19.34	6.4	36.4			
CL012.2A	35	257	-39	244	-21	-26.44	112	3	2	3	400-500
CL013.1A	38	127	-13	131	-5	-30.94	393	5	2	3	350-580
Gcmean N=5	50.75	254.7	-64.4	229.2	-42.6	-46.07	16.5	28.1			
CL021.2A	58.5	438	41	424	23	27.19	69	8	2	3	350-550
GCmean7	68.1	253	-70	227	-48.3	-50.29	12.8	19.9			
CL024.3A	69.5	326	-72	252	-69	-42.3	94	13	2	2	550-630
CL025.1A	73	249	36	268	51	19.37	1048	3	2	2	200-400
CL027.1B	77.5	396	78	390	54	65.4	233	4	2	3	400-500
CL028.1A	79	117	-14	123	-12	-28.14	62	9	2	1	630-650
CL031.3A	87	366	32	369	9	51.39	35	9	2	3	450-610
CL034.1B	93.2	180	-68	192	-45	-71.45	85	1	2	3	400-450
Gcmean N=4	93.5	192.7	-68.7	199.1	-45	-67.84	18.8	29.5			
CL039.2A	101	275	-79	227	-60	-55.28	64	9	2	3	550-580
Gcmean N=3	101.7	252	-78.7	221.1	-57.2	-58.53	204.8	14.3			
CL042.1A	106	387	52	386	28	54.62	217	6	2	3	250-550
CL043.2A	107	150	-19	154	-5	-43.91	66	5	2	2	550-640
CL046.1A	114	393	80	388	56	67.73	79	7	2	4	200-450
CL046.1B	114	438	83	398	61	62.08	27	9	2	4	400-999
CL046.2A	114	384	65	385	41	62.01	61	10	2	3	370-490
CL047.1A	116	362	63	372	40	68.05	335	1	2	3	390-410
CL047.2A	116	375	60	379	36	62.51	166	4	2	3	350-550
CL049.3A	121	381	55	383	31	57.75	76	9	2	3	310-370
CL050.1A	123	410	50	403	27	43.66	129	5	2	3	390-470
CL050.3A	123	377	51	380	27	57.1	115	11	2	1	350-640

sample	level (m)	Dg	Ig	Dt	It	latp	Int (E-6 A/m)	error	Quality	Trange	comment
Gcmean N=5	128	105.7	-66.6	139.2	-58	-59.05	32.7	15.4			
CL053.1B	130	442	-69	130	-66	-54.96	22	24	2	3	350-390
CL053.2B	130	446	-75	144	-68	-64.1	16	10	2	4	250-300
CL054.3A	133	198	-31	196	-12	-51.09	22	8	2	4	250-300
Gcmean N=4	134	201.9	-34.3	199.8	-15.9	-51.61	13.4	27.6			
CL055.1A	135	174	-46	177	-28	-62.47	23	20	2	3	330-430
CL055.4A	135	226	-20	223	-5	-34.74	35	1	2	3	400-450
CL056.1A	136.5	138	-64	157	-49	-67.78	49	12	2	4	300-450
CL056.2A	136.5	444	-50	107	-51	-32.52	29	13	2	3	350-410
Gcmean N=5	137.5	128.7	-62.7	149.9	-49.6	-63.21	19.2	19.2			
CL057.1B	138.5	149	-66	165	-50	-73.38	32	10	2	3	390-450
CL059.1B	145	248	-30	241	-19	-27.88	128	5	2	3	390-430
CL059.3B	145	93	-24	101	-24	-16.5	115	4	2	3	350-550
Gcmean N=3	148.75	121	-18	125.3	-9.6	-28.85	52.5	28.5			
CL063.3A	153.7	244	-37	235	-25	-34.47	38	8	2	4	290-350
Gcmean N=6	154.65	225.1	-57.9	213	-41.6	-57.14	4.1	39.4			
CL064.2A	155.5	124	-57	144	-46	-57.23	64	19	2	3	350-500
CL064.3A	155.5	251	-16	247	-7	-19.25	35	6	2	4	330-350
CL065.3A	158	169	-68	177	-49	-77.37	50	6	2	4	310-390
CL066.3A	160	264	-80	212	-67	-66.78	40	4	2	3	400-580
CL068.1A	164.5	221	-49	213	-32	-52.45	75	14	2	3	410-430
Gcmean N=5	165.75	155.8	-54.5	164.7	-37.5	-65.11	7.1	32.6			
CL069.1A	167	139	-55	153	-40	-60.24	111	8	2	3	450-500
CL069.4B	167	110	-42	124	-36	-38.21	68	10	2	3	450-490
Gcmean N=4	170.15	173.7	-50.5	177.1	-31.8	-64.8	100.9	12.5			
CL071.3A	171.5	177	-57	180	-39	-69.74	42	12	2	4	300-450
CL072.5A	173.5	193	-57	191	-38	-67.1	113	4	2	3	450-500
CL073.3A	176.7	151	-52	161	-35	-61.94	213	2	2	3	370-450
CL073.4A	176.7	156	-37	161	-21	-54.45	131	8	2	3	250-540
CL074.1A	180.5	276	-69	237	-61	-48.58	81	6	2	3	470-490
CL075.1A	181.5	197	-73	192	-54	-77.83	304	4	2	3	350-500
CL075.2A	181.5	164	-56	171	-38	-67.72	450	3	2	3	430-470

sample	level (m)	Dg	Ig	Dt	It	latp	Int (E-6 A/m)	error	Quality	Trange	comment
CL076.1A	185	126	-27	132	-17	-36.22	555	1	2	3	390-470
CL076.2A	185	159	-24	161	-7	-47.67	602	4	2	3	500-580
CL077.1A	187	146	-40	154	-25	-53.15	161	9	2	3	350-500
CL077.2A	187	214	-19	212	-2	-39.71	401	4	2	3	450-490
CL078.2A	190	98	-41	114	-38	-31.67	68	4	2	3	430-470
CL078.4A	190	142	-70	162	-54	-73.95	108	5	2	3	300-500
CL079.2A	191.5	188	-38	188	-19	-56.72	391	1	2	3	430-450
CL079.4A	191.5	170	-48	174	-30	-63.3	99	1	2	3	540-580
CL080.3A	194	184	-70	185	-51	-78.67	496	2	2	3	540-580
CL082.3B	199.5	176	-56	180	-38	-69.04	538	1	2	3	450-500
CL083.2A	201	147	-40	154	-24	-52.67	726	2	2	3	450-540
CL084.4A	203	152	-55	162	-39	-64.77	336	3	2	3	240-370
CL086.2A	208.5	191	-31	191	-12	-52.48	98	8	2	3	500-580
CL086.3A	208.5	233	-62	216	-47	-57.71	116	9	2	3	430-470

CS: Carretera Sort. Base: 42.261762 N, 0.985335 E, 578 m. Top: 42.268049 N, 0.985701 E, 823 m

sample	level (m)	Dg	Ig	Dt	It	latp	Int (E-6 A/m)	error	Quality	Trange	comment
N=4	2	138.1	-52.8	152.7	-43.3	-61.65					
CS003.3A	6	259	-21	255	-12	-15.16	58	3	2	3	440-500
CS004.2A	8.5	127	-18	131	-13	-34	58	5	2	3	450-500
CS005.2A	10.5	277	-71	244	-62	-44.21	18	12	2	4	300-400
CS006.3A	15.7	261	-34	254	-25	-20.57	124	8	2	4	380-440
N=3	17.5	179.2	-58	185.1	-42.7	-71.97					
CS008.2A	25	132	-41	143	-34	-50.79	88	6	2	3	550-600
N=4	26.5	159.3	-44.7	166.9	-31.8	-62.54					
N=6	32.5	237.2	-29.5	233.3	-16.4	-32.36					
CS012.2B	36	247	-32	241	-20	-28.25	240	7	2	1	600-650
CS014.2B	44	149	-22	153	-12	-46.59	37	14	2	2	500-550
N=5	44.25	229.8	-54.7	222.1	-40.2	-50.13					
CS016.1A	50.5	148	-68	169	-56	-79.75	120	7	2	3	520-560
N=5	53	153.1	-60.8	167.7	-48.4	-73.72					
N=4	59	167.5	-57.3	176.6	-43	-72.47					
CS023.2A	63.5	224	-34	221	-19	-41.63	62	10	2	3	380-440
N=6	64	184.6	-50.6	188.1	-35	-65.99					
CS024.1A	65.5	144	-56	158	-45	-66.11	95	6	2	3	500-550
N=5	69.5	160.4	-56.5	171.2	-43.1	-71.31					
N=3	72.5	151.5	-46.4	161.1	-34.7	-61.82					
N=4	74.5	157.6	-52	167.6	-39.2	-67.37					
N=5	79	171.5	-44	176.7	-29.6	-63.41					
CS032.1B	83	344	50	352	36	66.67	234	6	2	3	550-610
CS032.2A	83	348	44	354	30	63.3	245	4	2	3	300-550
CS033.1A	87.5	318	32	325	24	47.53	227	7	2	3	400-550
CS034.1A	89.5	351	46	357	31	64.29	102	3	2	3	300-450
N=5	98	170.4	-46.4	176.3	-32.1	-64.91					
CS036.1A	101	155	-42	163	-30	-60.02	91	5	2	3	470-550
CS038.1B	106.7	177	-54	183	-39	-69.59	94	2	2	3	470-530
CS038.2B	106.7	156	-38	162	-26	-57.44	61	9	2	3	400-460
N=4	110.5	222.1	-48.2	217.5	-33.2	-50.08					

sample	level (m)	Dg	Ig	Dt	It	latp	Int (E-6 A/m)	error	Quality	Trange	comment
N=4	118.2	169.5	-28.3	172.6	-14.3	-54.36					
N=5	123	161.8	-29.4	165.8	-16.4	-53.84					
N=3	127.3	112.2	-56.1	134	-52.4	-52.88					
N=5	133	186.1	-36.5	188.1	-20.9	-57.72					
N=5	139	198.8	-43.6	199	-27.6	-57.87					
N=5	145	121.5	-62	145.9	-55.4	-62.98					
CS056.1A	152.5	255	-38	246	-28	-27.62	43	14	2	3	480-520
CS056.2B	152.5	132	-41	143	-34	-50.79	83	5	3	3	450-550
N=6	153.75	194.6	-62.1	196.4	-46.2	-70.1					
CS057.2A	154	166	-51	174	-37	-67.76	32	9	2	2	400-600
N=3	157.5	252.3	-80.9	218.9	-67.3	-62.32					
CS059.1B	159.4	173	-76	187	-61	-84.81	55	6	2	3	500-550
CS060.1B	161.5	365	31	366	16	55.45	229	5	2	3	420-580
CS060.2A	161.5	322	30	328	21	47.98	177	6	2	2	400-610
CS060.3A	161.5	420	59	408	46	48.5	157	6	2	3	350-500
N=4	165.6	169.5	-50	176.3	-35.7	-67.25					
N=4	177.25	170.7	-56.6	178.7	-42.1	-71.98					
CS065.2A	179.3	179	-63	186	-48	-75.89	52	5	2	3	300-450
N=6	183.25	132.2	-46.8	145.3	-39	-54.71					
CS067.3B	184.3	120	-41	133	-36	-44.74	46	12	2	3	440-500
CS068.2B	185.3	92	-47	110	-50	-34.18	9	16	2	3	440-500
N=6	186.25	118.8	-61.8	143.9	-55.8	-61.67					
CS070.1A	190.7	190	-68	194	-52	-75.3	34	7	2	3	380-480
N=5	192.1	181.9	-58.6	187.2	-43.1	-71.78					
CS071.1A	193.5	197	-36	197	-20	-54.72	69	10	2	3	520-580
CS079.2B	196.6	446	-42	102	-47	-26.97	32	17	2	3	500-580
CS072.1A	198.9	356	52	362	38	68.97	101	10	2	3	350-550
CS072.1B	198.9	343	28	347	15	53.48	153	8	2	3	350-590
CS072.2A	198.9	432	60	416	49	43.95	129	4	2	3	440-520
N=7	202.4	363.2	50.6	367	35.2	66.37					
CS073.1B	202.4	384	40	383	24	54.17	89	4	2	4	440-480
CS073.2A	202.4	350	47	356	33	65.45	105	3	2	3	400-520

sample	level (m)	Dg	Ig	Dt	It	latp	Int (E-6 A/m)	error	Quality	Trange	comment
CS073.2B	202.4	384	43	383	27	55.68	70	4	2	3	470-550
CS074.2B	205.9	314	52	329	43	59.2	145	5	2	1	480-650
N=4	208.75	177.6	-67.8	186.4	-52.5	-79.5					
N=5	215.25	138.5	-60.4	157	-50.4	-68.56					
CS080.1A	218.3	266	69	310	70	55.48	84	5	2	3	440-590
CS081.1A	221	136	-51	150	-42	-59.36	41	2	2	2	600-630
N=5	223.75	129.1	-50.1	144.3	-42.8	-55.88					
CS083.2B	226.5	109	-35	120	-33	-34.03	60	6	2	3	440-530
N=3	228	170.1	-48.7	176.5	-34.4	-66.41					
N=2	230	375.4	45.9	376.3	30	60.31					
CS085.2B	230	374	58	375	42	68.08	49	4	2	3	440-550
N=3	236.3	376.5	60.2	377.5	44.2	68.23					
CS087.1A	236.3	365	69	371	53	77.71	146	4	2	2	400-600
CS087.2B	236.3	388	57	385	42	62.56	225	5	2	3	400-590
N=3	239.5	342.8	68.8	357.8	54.8	82.82					
CS089.1A	239.5	298	81	353	71	76.09	99	5	2	2	480-630
CS089.1B	239.5	355	58	362	44	73.39	82	9	2	3	440-550
CS089.2A	239.5	342	64	355	50	77.81	210	4	2	3	400-550
N=3	242.15	351.2	52	358	37.4	68.55					
CS091.1B	242.6	379	49	379	33	60.81	134	4	2	3	470-570
CS091.2A	242.6	336	59	349	46	72.59	169	6	2	3	400-550
N=4	249.75	198.1	-20.7	198.2	-4.7	-46.86					
N=4	254.35	340	55.6	350.6	42.3	70.54					
N=5	259.05	223.4	-42.7	219.3	-27.8	-46.47					
CS099.2A	260.3	239	-32	235	-19	-32.16	122	4	2	3	400-490
CS102.1A	267	219	83	365	81	59.78	79	7	2	3	350-530
CS102.1B	267	335	45	343	33	61.71	107	8	2	3	310-520
CS102.2A	267	354	48	359	34	66.32	37	6	2	3	400-560
N=7	270.6	192.3	-44.1	193.8	-28.2	-60.23					
CS109.2A	280.3	319	72	347	61	80.37	115	12	3	3	310-460
N=7	285.85	176.7	-35.6	179.8	-20.7	-58.4					
CS114.1A	292	186	-8	186	7	-43.86	79	1	2	4	350-400

sample	level (m)	Dg	Ig	Dt	It	latp	Int (E-6 A/m)	error	Quality	Trange	comment
N=4	294.15	166.3	-47.4	173.3	-33.5	-65.34					
CS115.1A	294.2	138	-77	172	-65	-82.63	76	15	2	3	550-580
N=4	299.25	149.7	-25	154	-14.2	-48.07					
CS118.2A	300.2	152	-28	157	-17	-50.78	56	2	2	3	350-450
CS119.1B	301.8	256	-19	252	-10	-16.67	78	6	2	4	350-400
N=4	302.9	256.6	-29.1	250.7	-19.6	-21.02					
CS122.2A	307.5	170	-68	182	-53	-81.12	36	7	2	4	370-430
N=5	312.75	163.4	-49.8	171.4	-36.2	-66.64					
CS126.2A	314.7	125	-51	142	-44	-54.83	141	6	2	3	400-490

CG: Can Gramuntill. Base: 42.268043 N, 1.005201 E, 669 m. Top: 42.269327 N, 1.007057 E, 705 m

sample	level (m)	Dg	Ig	Dt	It	latp	Int (E-6 A/m)	error	Quality	Trange	comment
CG001.1A	308.5	294	-72	248	-66	-43.38	210	2	2	2	540-600
CG01.100C	308.5	209	-24	208	-7	-43.87	158	19	2	1	670-690
N=7	309.25	206.2	-49.9	204.2	-32	-57.63					
CG02.100A	309.5	153	-17	156	-4	-44.33	99	8	2	1	610-640
CG003.2A	310	257	-34	249	-24	-23.89	32	7	2	3	350-450
CG004.3A	313.4	139	-55	156	-44	-64.3	13	20	2	3	540-570
CG04.200A	313.4	127	-25	134	-18	-37.96	128	5	2	2	550-580
N=7	314.7	159.6	-46.2	167.8	-31.2	-62.49					
CG005.2B	316	170	-36	174	-20	-57.59	476	4	2	3	250-400
N=4	318.25	194.4	-41.7	195.1	-23.8	-57.38					
CG007.3A	319	202	-30	201	-12	-49.27	26	6	2	3	540-570
CG008.2A	320	176	-29	178	-13	-54.24	206	2	2	3	400-540
CG08.100A	320	157	-23	160	-9	-48.24	221	5	2	4	250-450
CG009.2B	321.5	160	-67	175	-51	-78.67	11	12	2	4	350-400
N=6	323	165.9	-63	177.4	-46.8	-75.58					
CG10.100A	323	252	-49	239	-37	-36.42	158	6	2	3	350-450
CG11.300A	324.5	121	-29	130	-24	-37.61	23	3	2	3	450-500
CG012.1A	326.5	181	-44	185	-27	-61.66	321	0	2	2	570-630
CG12.200A	326.5	191	-42	193	-24	-58.18	411	6	2	1	610-690
N=7	327.75	195.9	-51.4	196.4	-33.4	-62.2					
CG13.300A	329	230	-64	204	-48	-66.56	144	2	2	4	300-350
CG13.300A	329	208	-66	218	-47	-56.27	144	14	2	3	300-500
CG14.200A	331	103	-20	109	-20	-20.94	51	10	2	2	580-610
N=5	332.85	180.3	-62.4	186.5	-45	-73.39					
N=9	339.5	179.3	-59.2	185.3	-41.9	-71.34					
CG019.1A	339.5	194	-29	194	-11	-51.21	234	1	2	1	630-650
CG020.3B	341	265	-62	242	-51	-40.47	40	3	2	3	540-570
CG022.1A	343	364	49	368	31	63.52	57	8	2	2	600-630
CG24.200A	347	351	71	363	54	81.89	548	3	2	3	200-580
N=3	350.15	180.1	-36.8	182.8	-19.5	-57.65					
CG029.2A	353	320	42	330	31	53.81	59	1	2	3	350-450

sample	level (m)	Dg	Ig	Dt	It	latp	Int (E-6 A/m)	error	Quality	Trange	comment
CG032.3B	356.3	390	56	387	38	59.17	38	16	2	3	450-540
CG033.1A	357	423	50	412	36	41.13	82	3	2	3	450-500
CG34.100A	358	134	-36	143	-26	-47.17	111	4	2	3	450-550
N=5	359.75	165.1	-48.9	172.7	-33.1	-64.97					
CG037.2A	363.5	376	51	376	33	62.14	111	5	2	5	250-350
N=6	365	205.3	-51.2	203.6	-33.3	-58.64					
CG041.1A	370	220	-23	219	-6	-37.54	25597	2	1	2	350-630
CG41.200A	370	197	5	197	23	-33.52	10500	2	1	1	300-670
CG042.1B	396	361	41	364	29	62.97	1105	2	2	2	400-600
CG42.100B	396	372	16	372	4	48.29	686	3	1	1	500-670
CG043.1A	398.5	104	25	99	23	1.52	422	7	2	2	500-630
CG044.2A	400.5	384	56	383	44	64.92	123	4	2	3	400-550
CG045.3A	402	371	45	372	33	63.63	188	2	2	4	350-450
N=3	402.5	173	-41.2	180.3	-28.8	-63.07					
N=6	407.85	191.1	-47.8	192.7	-35.9	-65.16					
CG052.3A	410	347	31	350	21	57.37	152	5	2	2	300-630
CG52.100A	410	352	47	357	36	67.52	176	8	2	2	350-640
N=4	412.25	189.1	-69.7	192.9	-57.8	-79.46					
CG055.2A	415	366	29	368	18	56.19	145	5	2	3	350-550
CG55.100A	415	373	44	374	32	62.34	111	4	2	3	400-550
N=6	420.75	196	-48.7	196.7	-36.7	-64.01					
CG060.1A	425	191	-34	192	-22	-57.4	224	5	2	2	550-600
N=7	427.5	170.5	-44.1	175	-33.4	-65.57					
CG064.1A	432	355	27	357	16	55.76	421	2	2	2	550-630
CG64.200A	432	363	35	365	23	59.37	446	4	2	1	400-610
CG065.2A	434.5	359	58	364	47	75.53	196	5	2	3	200-450
CG66.200A	435	350	50	356	39	69.47	129	3	2	3	350-500
N=6	441.85	229.2	-62.9	221.2	-52.1	-56.3					
CG071.1A	448.5	346	30	349	20	56.6	130	4	2	3	500-600
CG072.2A	449	356	56	361	45	74.24	350	2	2	3	300-550
CG72.200A	449	368	44	370	32	63.63	263	5	2	2	350-610

RQ: Rocs de Queralt. Base: 42.268416 N, 1.022150 E, 625 m. Top: 42.275545 N, 1.010412 E, 944 m

sample	level (m)	Dg	Ig	Dt	It	latp	Int (E-6 A/m)	error	Quality	Trange	comments
RQ001.1B	0	93	45	439	41	23.43	56	7	2	3	350-600
RQ01.300A	0	370	48	370	33	64.24	189	5	2	3	250-550
N=5	7.3	213.8	-54.8	207.2	-41	-60.64	10	31.3			
RQ05.100C	12	192	-32	192	-18	-55.29	82	9	2	2	550-580
N=3	18.5	188.4	-38	188.7	-23.6	-59.08	13.4	59			
RQ09.200A	22.5	175	-25	176	-11	-53.08	43	9	2	3	450-550
RQ010.1A	24.5	382	75	376	60	77.97	143	9	2	3	250-520
RQ10.200A	24.5	368	68	368	53	79.24	148	5	2	3	400-550
N=4	34	198.7	-33.2	197.8	-18.8	-53.82	8.5	45.2			
N=4	52	168.6	-55.4	173.5	-40.8	-70.29	236.5	11.5			
RQ17.100B	59	406	15	405	3	32.71	116	4	2	2	580-610
N=4	69.5	157.3	-63.2	167.3	-50.5	-75.01	13.3	50.5			
RQ25.300A	85	153	-65	166	-52	-75.3	67	13	1	2	450-580
RQ29.100B	105.5	148	-41	154	-29	-55.12	84	3	2	2	550-580
N=3	106.25	158.9	-36.1	162.6	-22.6	-55.91	45.2	30.8			
N=4	112.5	190.3	-35.3	190	-20.7	-57.21	26.7	34.9			
N=5	119	186.1	-48.1	186.7	-33.3	-65.22	87.1	12			
RQ036.1A	123	224	-48	217	-35	-51.25	53	15	2	3	520-560
N=3	123	211.6	-41.1	208.1	-27.2	-53.07	35	35.2			
RQ37.200B	128	232	-22	229	-11	-33.23	119	7	2	4	300-450
RQ038.2A	131.5	162	-33	165	-20	-55.42	181189	7	2	3	400-560
RQ38.200B	131.5	178	11	177	26	-33.93	276000	2	1	1	300-690
RQ039.1B	134	321	17	323	7	39.11	8680	1	1	1	350-560
RQ39.100C	134	328	21	331	10	44.71	6890	1	1	1	500-690
RQ040.1A	157	347	43	351	29	62.1	1092	3	1	1	300-660
RQ40.200B	157	353	62	358	48	76.65	991	5	2	1	450-670
RQ41.300A	164	373	53	372	38	66.75	167	5	2	2	400-580
RQ042.1B	171	382	-84	180	-81	-59.88	3265	2	2	2	300-600
RQ42.100A	171	317	-85	208	-78	-61.03	3140	3	1	1	250-640
RQ045.2A	174.5	149	-31	153	-19	-49.79	1365	2	2	1	250-600-?
N=5	176	189	-44.8	189.3	-30	-62.61	11.9	24.6			

sample	level (m)	Dg	Ig	Dt	It	latp	Int (E-6 A/m)	error	Quality	Trange	comments
RQ046.1A	179	193	-40	193	-25	-58.72	322	6	2	1	400-640
RQ46.100B	179	212	-53	207	-39	-59.7	269	5	1	3	350-500
RQ047.2B	186	187	-15	187	-1	-47.73	16720	2	1	2	400-600
RQ47.200A	186	199	-9	199	6	-41.53	7380	4	1	1	500-670
N=3	196.5	242.9	-84.3	202.5	-71.3	-70.12	5.5	102.9			
RQ051.2A	198	265	-61	243	-55	-41.63	87	7	2	3	480-560
RQ052.1A	202	330	49	338	37	61.53	1222	2	1	1	250-660
RQ52.400A	202	333	47	340	34	60.89	1240	7	2	1	250-690
RQ053.3A	205	374	27	374	12	51.7	152	5	1	1	350-640
RQ53.100A	205	421	18	418	8	25.99	322	6	2	1	350-640
RQ055.1B	215	393	44	388	28	53.52	323	6	1	1	600-660
RQ056.2A	216	344	53	350	37	66.77	376	4	2	1	450-640
RQ057.1A	223	379	64	375	47	71.38	734	3	1	1	300-640
RQ058.3A	230	367	50	367	33	64.97	752	2	1	1	350-600
RQ059.3A	233	345	35	348	19	55.81	414	2	1	1	350-640-?
RQ060.3A	253	362	58	364	41	70.9	1084	2	1	1	300-660-?
RQ061.3A	273	323	48	332	35	57.01	575	4	2	1	200-600-?
RQ062.2A	278	332	37	337	23	53.68	557	5	1	2	200-600-?
RQ063.1B	280	340	38	344	22	56.12	1329	3	1	2	450-600-?
RQ064.2A	282.5	344	46	349	30	62.16	1920	3	1	1	300-640
RQ065.2A	284	340	45	345	30	60.82	1214	3	1	1	300-600-?
RQ066.4A	289.5	356	40	358	24	60.2	1123	2	2	2	300-560-?
RQ068.2A	296.5	348	46	352	30	62.92	831	3	1	1	300-640-?
RQ069.3B	297.5	345	54	351	38	67.72	1483	2	1	1	250-560-?
N=3	315	165.6	-54.4	171.5	-38.4	-68.13	60.5	18.8			
RQ73.300A	333	331	54	341	40	64.86	1100	3	1	1	300-670
RQ74.200A	341	356	48	359	31	64.41	3500	1	1	1	450-690
RQ75.200B	343	330	23	334	14	47.98	5160	2	1	1	550-690
RQ76.100A	344	337	54	347	43	69.65	2970	2	1	1	300-690
RQ77.200A	346	339	33	343	22	55.75	2440	1	1	1	450-690
RQ78.100B	348	342	25	344	13	51.58	1820	2	1	1	350-670-?
RQ79.300A	351	338	34	343	23	56.27	2070	2	1	1	450-690

sample	level (m)	Dg	Ig	Dt	It	latp	Int (E-6 A/m)	error	Quality	Trange	comments
RQ80.200B	354	332	35	338	25	55.15	3460	1	1	1	450-690
RQ81.100B	358	333	45	341	35	61.94	3970	2	2	1	640-690
RQ83.200B	362.5	337	24	340	14	50.62	1830	3	1	1	500-670
RQ84.300B	372	386	60	385	46	64.79	1690	3	1	1	300-670

MS: Montsor. Base: 42.278558 N, 0.991347 E, 1045 m. Top: 42.291541 N, 0.978072 E, 1229 m

sample	level (m)	Dg	Ig	Dt	It	latp	int (E-6 A/m)	error	Quality	Trange	comments
MS001.300A	0	188	-31	189	-21	-57.6	325	8	2	1	610-670-?
MS002.100A	7	250	-35	245	-28	-28.36	183	15	2	1	610-670
MS003.200A	9	207	23	208	33	-24.41	110	2	2	1	610-640-670
MS004.300A	11	149	-30	152	-23	-51.13	279	6	2	1	610-640-?
MS006.200C	21.5	220	19	222	28	-20.99	1320	4	2	1	580-670-?
MS007.100B	24	379	53	378	43	67.21	1290	8	1	1	450-690
MS008.200A	26.5	366	39	367	29	62.52	1220	3	1	1	500-640-?
MS009.100A	29	392	48	390	38	57.3	738	3	1	2	400-610-640
MS010.100A	30	142	-34	146	-28	-49.95	366	6	1	1	580-640-?
MS011.200A	32	369	55	370	45	72.27	1670	4	1	1	500-670
MS013.100A	41.5	352	42	355	32	64.69	1690	3	1	1	550-690
MS015.200A	51.5	336	37	340	30	58.7	555	3	2	3	550-580-?
MS016.100A	53	321	10	322	4	37.3	511	3	2	1	610-640-?
MS017.100A	54.5	309	56	321	51	57.42	811	8	2	2	500-610-670
MS018.100A	55.7	397	26	396	17	43.88	1120	4	1	2	500-610-670
MS019.100B	56.4	306	48	315	44	49.78	233	1	2	1	640-670-?
MS020.100A	57	362	72	367	62	84.78	1390	3	2	2	400-550-?
MS021.100A	61.5	314	54	324	48	58.2	759	6	2	1	580-670-?
MS027.100B	66	401	12	400	3	35.73	4500	4	1	1	450-670
MS023.100B	67.5	377	31	377	21	55.23	867	9	2	1	550-610-?
MS024.200B	69	252	39	260	44	10.19	624	6	2	1	610-670
MS025.200A	70	410	27	407	18	37.29	1360	5	1	1	500-670
MS026.200B	74.5	440	52	430	47	32.75	716	1	1	2	450-550-?
MS028.100A	91	191	-48	191	-38	-67.1	974	2	1	1	550-640-?
MS029.200B	97.5	167	-21	169	-13	-52.98	1120	4	1	1	450-670-690
MS031.100B	100	151	-30	155	-23	-52.7	993	1	1	1	610-670-?
MS032.100B	102	168	-22	170	-13	-53.2	3260	2	1	1	580-670-690
MS033.200A	116.5	204	-27	204	-17	-50.32	1990	1	1	2	350-580-
MS034.200B	119.5	131	-43	139	-38	-49.89	788	5	1	1	580-670-?
MS035.100B	123	237	-23	235	-15	-30.65	1150	2	1	1	610-690-?
MS036.200B	124.5	155	-12	156	-4	-44.33	982	2	1	1	640-690-?

sample	level (m)	Dg	Ig	Dt	It	latp	int (E-6 A/m)	error	Quality	Trange	comments
MS037.100B	137	180	-55	183	-45	-74.07	1350	2	1	1	350-550-?
MS039.100A	148	118	-18	121	-16	-28.2	535	6	1	1	640-670-690
MS040.200A	152.5	396	-59	404	-68	-10.9	1250	5	1	1	610-670-690
MS041.200B	154	113	-45	123	-43	-40.5	4760	4	1	1	450-640-670
MS042.100A	159	411	39	408	31	41.88	845	4	1	1	610-640-670
MS005.100A	20	157	46	149	54	-8.09	360	7	3	1	670-690-?
MS014.100B	50	129	51	117	54	6.02	629	3	3	1	610-640-?
MS014.100B	50	384	30	383	20	52.22	679	8	4	3	* 300-580
MS015.200A	51.5	389	56	389	56	66.99	592	6	4	3	* 300-580
MS019.100B	56.4	363	41	365	32	64.69	632	6	4	3	* 250-550
MS019.100B	56.4	431	17	429	11	19.2	289	5	4	1	* 580-670-?
MS024.200B	69	380	49	379	39	64.26	799	8	4	2	* 400-610
MS030.100B	99	390	19	389	10	44.71	346	9	4	3	* 300-550
MS038.200A	146	411	-13	413	-21	18.08	462	8	4	1	* 450-670

LP: La Pobleta. Base: 42.337836 N, 0.950954 E, 768 m. Top: 42.341472 N, 0.986550 E, 1001 m

sample	level (m)	Dg	Ig	Dt	It	latp	Int (E-6 A/m)	error	Quality	Trange	comments
LP50.100A	11	316	-17	310	-33	14.14	1470	2	2	1	640-670-?
LP51.200A	12.2	151	-54	156	-35	-59.33	1330	2	2	1	640-670-?
LP52.200A	14	225	-52	210	-38	-57.3	682	6	2	1	610-690
LP53.300A	15	440	-75	132	-65	-56.07	848	5	2	1	640-690
LP54.200A	17.7	234	03	236	11	-20.28	201	5	2	1	610-670-?
LP55.300A	21.5	398	28	393	14	44.33	558	8	1	1	500-640-?
LP57.200B	23	384	39	381	10	48.33	481	6	2	1	500-610
LP58.300A	23.5	418	-73	151	-67	-68.7	3200	3	1	1	500-690-?
LP59.100A	24.7	151	-72	172	-44	-72.21	1550	5	1	1	610-670-?
LP60.100B	25.5	410	36	401	12	38.77	657	2	1	1	610-640-670
LP61.100A	27.5	426	-83	174	-63	-85.14	3380	1	1	1	580-670-?
LP62.300B	30.5	129	-68	168	-41	-68.71	1320	3	1	1	670-690
LP63.300A	32.2	357	50	363	15	55.23	1530	2	1	1	300-610-?
LP64.200B	37	173	-75	187	-40	-69.61	3550	1	1	1	580-640-?
LP65.100A	40.5	347	21	348	-11	40.92	584	4	2	3	250-550
LP66.100A	48.5	105	-42	129	-30	-39.34	1600	10	1	1	580-690
LP68.100A	59	337	46	344	10	50.12	5910	4	1	1	500-670-?
LP69.100A	62	348	44	352	07	50.56	2730	4	1	1	450-640-?
LP70.300A	65.5	322	56	338	22	53.65	1360	5	1	1	500-610-670
LP71.200A	67.5	325	55	339	20	53.12	1980	2	1	1	640-690
LP72.400A	69	329	58	343	23	56.27	4510	3	1	1	500-640-690
LP73.300A	70.2	339	66	350	29	61.85	1990	0	1	1	640-670-690
LP74.100A	74	280	55	316	36	46.88	959	13	1	1	610-670
LP75.100A	78.5	382	58	372	21	56.86	587	4	1	1	610-670
LP76.300A	83.2	149	-56	162	-21	-54.85	2740	1	1	1	550-670-690
LP77.100A	85.5	111	-58	143	-33	-50.32	1340	6	1	1	580-670-690
LP78.100C	86.8	449	-39	115	-30	-29.14	665	3	1	1	640-670
LP79.200A	92.7	153	-63	167	-27	-59.83	879	2	1	1	640-690
LP80.200A	94.5	120	-52	144	-26	-47.8	1410	2	1	1	610-690
LP81.300A	96	100	-65	146	-42	-56.66	775	2	2	1	670-690-?
LP82.100A	96.7	445	-38	112	-32	-27.72	1000	4	1	1	450-670

sample	level (m)	Dg	Ig	Dt	It	latp	Int (E-6 A/m)	error	Quality	Trange	comments
LP83.300A	98	100	-41	124	-26	-34.14	866	2	1	1	610-670-?
LP84.100A	100.7	218	-35	210	-03	-41.14	656	2	2	1	670-690-?
LP85.100B	107.5	162	-77	175	-40	-70.02	539	6	2	1	670-690-?
LP86.100A	109.5	154	-64	167	-28	-60.39	1470	2	1	1	580-640-690
LP87.100B	110.8	290	51	317	29	44.51	310	5	2	1	400-550
LP88.200A	119	383	30	380	-06	41.2	1380	4	1	1	550-610-?
LP89.300A	123	256	12	267	19	4.36	533	10	2	1	610-670-?
LP90.200A	125.5	339	-06	332	-41	19.31	1600	7	1	1	640-690
LP91.200A	128	275	60	319	41	51.28	715	2	1	2	300-550
LP92.100A	132.5	336	71	351	35	65.77	1250	2	1	1	610-670-?
LP93.400A	137.2	262	26	281	25	16.87	1290	3	1	1	610-690-?
LP94.200A	140.7	290	67	331	40	58.97	1130	1	1	1	610-670-?
LP95.300A	142	331	42	339	07	46.92	983	6	1	1	400-670
LP96.300A	144	164	-59	171	-22	-58.14	1900	3	1	1	450-690
LP97.200A	146.7	141	-61	160	-27	-57.1	1840	3	1	1	350-640-670
LP98.100B	150.5	344	57	351	20	57.06	1840	5	1	1	500-640-670
LP99.200B	152	388	64	374	28	60.05	2030	6	1	1	500-640-?
LP01.300A	152.5	328	53	331	45	61.59	1880	6	1	1	100-640
LP001.2A	152.5	278	03	278	01	6.25	338	6	2	1	600-660-680
LP002.1A	155	379	59	374	52	75.3	1205	4	1	1	450-660-?
LP003.3A	156.5	362	56	360	48	76.74	2028	2	1	1	200-600-?
LP004.1A	158.7	341	60	343	52	73.44	2976	4	1	1	150-630-?
LP005.2A	162	387	59	381	52	70.8	45213	3	1	3	150-550
LP005.2A	162	350	57	350	49	75.23	1597	11	1	1	550-660
LP05.300A	162	382	60	376	53	74.69	57500	2	1	1	100-690
LP006.3A	165.5	154	-56	157	-48	-67.21	1017	4	1	1	550-630-?
LP007.1B	166.5	175	-54	174	-46	-74.29	934	4	1	1	600-630-?
LP07.200B	166.5	151	-77	158	-70	-71.39	1370	5	1	1	300-690
LP008.2B	167.5	185	-40	183	-33	-65.55	2555	3	1	1	400-660
LP009.2B	169.5	285	-42	278	-45	-12.06	620	7	1	1	550-680
LP09.200C	169.5	285	-31	280	-34	-5.36	442	24	2	1	610-670
LP010.3A	170.7	418	-83	119	-82	-48.15	373	13	2	1	450-660-

sample	level (m)	Dg	Ig	Dt	It	latp	Int (E-6 A/m)	error	Quality	Trange	comments
LP10.200A	170.7	156	-61	158	-53	-70.65	842	5	2	1	640-690
LP011.3B	172.5	185	-51	183	-43	-72.52	2935	3	1	1	450-680
LP012.1A	176	191	-52	188	-44	-72.21	521	3	2	1	630-680
LP013.1B	179.2	184	-57	182	-49	-77.5	5433	3	1	1	300-680-?
LP13.200A	179.2	184	-55	182	-47	-75.81	5100	2	1	1	300-690
LP014.3A	182.2	249	-73	227	-70	-57.24	870	4	2	1	450-550-?
LP015.2B	184.7	194	-50	191	-43	-70.46	984	1	1	1	630-660-680
LP016.2A	187.2	183	-46	182	-38	-68.97	1155	3	1	1	630-660-680
LP017.2A	191	160	-45	161	-37	-63.09	2986	5	1	1	450-660-?
LP019.2A	193	183	-53	176	-43	-72.39	2262	3	1	1	450-630-?
LP018.1A	194.5	170	-53	166	-41	-67.89	4000	2	1	1	350-680
LP020.3A	195	170	-58	165	-46	-70.71	2378	3	1	1	450-630-?
LP021.1B	198.7	193	-41	187	-32	-64.35	993	5	1	1	350-660-?
LP022.2B	206.5	183	-45	178	-35	-66.93	1496	2	2	1	400-630-?
LP023.3A	209.5	142	-44	143	-32	-49.86	1540	4	1	1	150-660
LP024.3A	210.5	162	-48	160	-36	-62.01	2729	4	1	1	200-680
LP025.2A	213.5	176	-64	168	-53	-77.14	3981	3	1	1	200-680
LP026.1A	214.5	142	-40	143	-28	-48.05	916	3	1	1	600-680-?
LP027.3A	216.2	197	-66	183	-57	-84.76	3689	3	1	1	250-680
LP028.2A	217	184	-48	178	-37	-68.28	2992	3	1	1	350-680
LP029.2A	217.7	189	-41	184	-31	-64.19	6988	3	1	1	400-660
LP031.2A	225	192	-38	187	-29	-62.52	1063	3	1	1	200-630
LP31.100B	225	179	-64	176	-52	-79.81	2330	5	1	1	200-690
LP032.2A	229.5	165	-48	162	-37	-63.58	225	7	2	1	550-600-?
LP32.300A	229.5	215	-25	212	-16	-45.76	378	2	2	1	610-670
LP33.300A	232	186	-36	184	-24	-60.05	8710	2	1	1	350-640
LP033.1A	232	175	-49	171	-38	-67.72	4056	6	2	1	250-600
LP034.2A	241	159	-39	158	-27	-56.17	1939	8	1	1	200-660
LP034.3A	241	176	-59	170	-48	-74.48	2629	4	1	1	350-660
LP035.1A	242.5	200	-45	192	-37	-66.11	1856	3	1	1	200-550
LP56.100A	22.5	359	-28	362	-47	19.48	741	3	3	1	400-550-?
LP67.100B	57.5	324	58	343	29	59.47	1420	11	3	2	400-550-?

sample	level (m)	Dg	Ig	Dt	It	latp	Int (E-6 A/m)	error	Quality	Trange	comments
LP030.2A	223	371	-22	375	-30	29.98	471	1	3	1	350-500-?
LP67.100B	57.5	347	60	357	27	61.87	960	21	4	3	* 350-550
LP84.100A	100.7	180	-21	180	17	-39.01	826	1	4	3	* 500-580
LP001.2A	152.5	323	41	325	34	52.11	672	8	4	3	* 300-600
LP012.1A	176	339	36	340	28	57.63	320	9	4	2	* 400-600

MC: Montcortes. Base: 42.337900 N, 0.994597 E, 988 m. Top: 42.342164 N, 1.007128 E, 1151 m

sample	level (m)	Dg	Ig	Dt	It	Int (E-6 A/m)	latp	err	Q	T	comments
MC001.1A	0.7	372	-80	177	-59	2401	-87	2	1	1	500-630-?
MC002.1A	1.3	216	-83	187	-44	1736	-73	2	1	1	400-630-?
MC003.1A	3.3	124	-61	153	-30	1835	-55	2	1	1	400-630-?
MC004.2A	4.3	188	-56	185	-16	1883	-56	2	1	1	400-660-?
MC005.2A	6	287	-27	264	-30	246	-15	5	2	1	600-660-?
MC006.2A	9.5	225	-44	212	-12	423	-44	4	1	1	350-630-?
MC007.2A	12	181	-63	181	-23	1378	-60	2	1	1	400-550-?
MC008.3A	14	149	-44	158	-08	118	-47	11	3	5	150-250
MC009.2A	17.5	156	-40	162	-03	421	-46	4	2	1	350-550-?
MC010.1A	21	165	-40	173	-25	2374	-60	4	1	1	250-630-?
MC011.3A	23	167	-53	179	-36	2367	-68	3	1	2	350-660
MC014.1A	24.5	176	-51	185	-34	623	-66	5	1	1	550-630-?
MC015.3B	25.5	182	-50	189	-31	2440	-63	4	1	1	100-660-?
MC012.2B	26	181	-50	189	-32	1619	-64	3	1	1	100-600
MC016.3A	28.5	161	-45	168	-38	1124	-67	4	1	1	100-660-?
MC017.3A	29.5	176	-36	179	-28	638	-63	5	1	1	550-630-?
MC018.2A	32	180	-72	190	-63	3878	-82	2	1	1	350-660-?
MC019.2A	34	172	-36	176	-28	2353	-62	3	1	1	350-660-
MC020.2A	34.8	196	-45	198	-35	4062	-62	2	1	1	400-660-?
MC021.1B	37	150	-40	156	-35	2251	-59	3	1	1	100-630-?
MC022.2A	38.5	163	-36	168	-29	469	-61	4	1	1	100-600-?
MC023.3A	40.5	177	-54	183	-45	906	-74	5	2	1	250-660-?
MC024.1A	43	167	-53	174	-45	2531	-74	2	1	1	100-630-?
MC025.1A	44.3	129	-52	141	-49	5097	-56	3	1	1	100-660-?
MC026.2B	45	188	-58	193	-49	2094	-74	3	1	1	100-600-?
MC027.1A	47	167	-58	175	-50	4494	-78	2	1	1	100-660-?
MC028.2A	48.5	141	-52	151	-48	3523	-63	3	1	1	100-660-?
MC029.1A	51.5	159	-62	170	-55	1357	-80	4	1	2	100-660
MC030.2A	52.8	170	-60	178	-52	1571	-80	2	1	2	500-660
MC031.1A	54.3	193	-53	196	-43	2886	-68	3	1	2	500-660
MC032.3A	57	348	72	362	63	1181	87	3	1	1	100-630-?

sample	level (m)	Dg	Ig	Dt	It	Int (E-6 A/m)	latp	err	Q	T	comments
MC033.2A	59	429	32	426	24	893	26	7	1	2	150-600-?
MC035.3A	61.5	351	68	362	60	3110	88	3	1	1	200-660-?
MC036.1A	63	347	42	352	34	579	65	3	1	1	500-630-?
MC037.1A	64.7	352	60	357	57	1415	85	3	1	1	150-550-?
MC038.3A	66	204	-41	205	-37	800	-60	4	1	1	450-600-?
MC039.1B	67.5	169	-58	174	-56	3504	-83	4	1	1	200-600-?
MC040.3A	70	157	-40	159	-38	622	-63	5	1	1	350-500-?
MC041.1A	71.5	170	-57	174	-54	683	-81	2	1	1	300-600-?
MC042.2A	73.2	398	32	398	28	413	47	8	1	1	150-500-?
MC42.400A	73.2	193	-65	196	-62	361	-78	4	2	1	550-670-?
MC043.1B	74.5	187	-46	189	-42	1085	-70	4	1	1	250-550-?
MC43.300B	74.5	195	-54	197	-50	1250	-72	3	1	1	350-690-?
MC044.2B	76.5	397	63	397	59	767	62	3	1	1	150-500-?
MC44.300A	76.5	210	-25	210	-21	245	-49	10	2	1	640-670
MC045.2A	79.2	371	59	374	56	1238	78	4	1	1	150-600-?
MC046.3A	83.5	352	35	354	32	1980	65	3	1	1	100-450-?
MC047.3A	85.7	389	55	390	51	2055	64	2	1	1	100-600-?
MC048.2A	88.7	386	64	388	60	1487	69	3	1	1	100-600-?
MC049.2A	90.7	361	52	364	49	5407	77	4	1	1	200-600-?
MC050.3A	94	379	58	381	54	2728	72	3	1	1	250-600-?
MC051.3A	96.5	383	47	384	43	1721	64	3	1	1	100-550-?
MC052.2A	97	359	52	361	22	2974	59	4	1	1	200-600-?
MC053.3A	98.5	366	50	366	20	2847	58	3	1	1	150-600-?
MC054.2B	101.7	256	-16	251	-04	1709	-15	6	2	1	600-640-?
MC54.300A	101.7	185	-60	186	-30	1170	-63	2	2	1	610-670-?
MC55.200A	103.5	181	-60	183	-30	1230	-64	7	1	1	300-580-?
MC055.1B	103.5	137	-30	144	-08	211	-40	7	2	1	450-600-?
MC056.1B	106.5	150	-60	166	-33	1154	-63	5	1	1	500-640-?
MC057.3A	108	204	-54	197	-25	957	-57	4	1	1	200-600-?
MC58.400A	111	248	16	260	28	799	3	7	2	1	550-610-640
MC059.1B	115	182	-46	183	-16	1156	-56	5	2	1	250-600-?
MC060.2A	118.5	281	-56	243	-48	1292	-38	3	1	1	250-640-?

sample	level (m)	Dg	Ig	Dt	It	Int (E-6 A/m)	latp	err	Q	T	comments
MC60.200B	118.5	291	-72	222	-60	981	-59	4	1	1	500-690
MC061.1A	125	166	-60	174	-31	623	-64	8	1	1	400-640-?
MC062.3A	128.5	333	71	352	43	1136	71	10	1	1	150-640-?
MC064.3A	133.5	108	67	315	79	1195	55	6	2	1	100-640-?
MC065.3A	137	093	63	345	76	913	67	7	2	1	100-640-?
MC066.1A	137.5	362	21	357	07	3031	51	6	1	1	100-600-?
MC067.2A	142	385	51	361	42	2123	72	5	1	1	350-640-?
MC068.3A	147.2	387	43	367	36	2656	67	6	1	1	250-640-?
MC069.1A	151.5	365	56	344	40	1902	66	6	1	1	250-640-?
MC070.2A	154.7	379	47	359	36	1990	68	4	1	1	100-640-?
MC071.2A	156	373	54	351	41	1902	70	11	1	1	400-640-?
MC072.2A	156.5	389	59	383	47	1932	67	7	1	1	100-640-?
MC73.300A	158	422	78	394	69	2110	65	3	1	1	100-670
MC74.200A	162.5	406	60	396	51	2730	60	3	1	1	100-670-?
MC75.200A	166.5	399	62	390	52	2610	64	3	1	1	100-670-?
MC76.300A	167.8	392	43	388	32	6650	55	3	1	1	400-690
MC77.300A	171.5	391	45	387	34	3440	57	5	1	1	100-690
MC78.100A	173	347	41	349	29	2660	62	7	1	1	100-690
MC79.100A	174.8	364	54	364	42	4470	72	3	1	1	100-640
MC80.100A	178	370	46	369	34	2470	65	4	1	1	100-670
MC81.300A	179	393	56	386	45	5030	64	2	1	1	100-690
MC034.2A	60	386	64	387	54	1228	68	9	4	1	* 300-660
MC44.300A	76.5	397	39	397	35	448	51	11	4	3	* 100-550
MC054.2B	101.7	372	32	371	02	1354	48	25	4	3	* 20-550
MC63.300B	131	401	67	338	55	274	72	13	4	3	* 150-500
MC063.1A	131	398	61	347	51	295	75	17	4	1	* 200-640

CJ: Cajigar. Base: 42.273772 N, 0.603743 E, 1124 m. Top: 42.314870 N, 0.615712 E, 1420 m

sample	level (m)	comp level (m)	Dg	Ig	Dt	It	Int (E-6 A/m)	latp	err	Q	T
CJ005.1A	19	19	145.7916	-65.79913	149.6	-61.2	-67.63	271.4368	4.3196	2	1
CJ018.4A	80.5	80.5	68.03454	51.48316	424.1	44.3	35.84	234.6322	8.1746	2	9
CJ025.1A	96.5	96.5	172.1564	-72.215	186.0	-66.1	-82.55	137.6825	3.9269	1	3
CJ026.1A	98.5	98.5	174.9521	1.360583	174.5	07.0	-43.92	153.5485	6.7134	2	3
CJ028.1A	104.5	104.5	177.7387	28.92252	174.3	34.7	-28.38	67.07249	3.547	2	9
CJ041.2C	141	141	141.512	-30.17441	145.9	-28.3	-50.03	187.0276	4.8141	2	9
CJ044.3A	150	150	215.7482	-51.36165	218.5	-41.7	-53.38	58.74094	3.5438	2	9
CJ046.2A	156.5	156.5	373.9498	61.73019	382.7	53.4	70.37	172.5165	4.1521	1	9
CJ046.1A	156.5	156.5	360.3674	58.25813	370.7	51.3	76.62	148.8774	11.167	2	1
CJ050.2A	168	168	198.8768	-51.81515	204.4	-43.2	-63.6	244.7726	4.3748	2	9
CJ051.2A	170.5	170.5	188.009	-56.19082	196.3	-48.5	-71.65	550.5572	1.3431	1	9
CJ052.1A	172.5	172.5	190.9954	-75.97395	207.5	-67.5	-69.52	89.87089	7.0352	2	4
CJ052.2A	172.5	172.5	188.6698	-73.77383	204.4	-65.5	-72.02	121.7222	6.6152	2	9
CJ053.2A	176	176	193.2072	-68.04448	204.4	-59.6	-71.66	197.5478	3.5926	2	9
CJ054.2A	179	179	179.9765	-58.84518	190.6	-52.0	-77.19	197.6928	4.5416	2	9
CJ055.1A	181.5	181.5	216.9938	24.17429	215.5	33.8	-20.94	587.0077	3.7992	1	1
CJ055.3A	181.5	181.5	350.5279	58.14688	362.5	52.4	80.75	1484.896	3.2683	1	1
CJ055.3A	181.5	181.5	351.4356	58.78677	363.5	52.9	80.49	1128.675	2.9977	1	1
CJ056.1A	184.5	184.5	204.5223	-36.61875	207.3	-27.6	-53.72	94.53461	5.3841	2	2
CJ056.2B	184.5	184.5	162.6569	-40.41379	169.9	-36.3	-66.28	56.93414	6.8583	2	0
CJ056.2B	184.5	184.5	162.6569	-40.41379	169.9	-36.3	-66.28	56.93414	6.8584	2	2
CJ057.2A	187	187	185.2524	28.82064	180.5	35.4	-28.14	228.5421	4.116	1	1
CJ057.1A	187	187	143.1628	3.569616	142.5	03.7	-34.38	127.7881	3.4551	2	1
CJ058.1A	189	189	184.0577	-19.11787	186.1	-12.3	-53.52	118.0713	2.6824	1	1
CJ058.2B	189	189	174.3696	-42.23224	181.0	-36.4	-67.92	647.9305	3.7222	1	1
CJ059.3B	193.5	193.5	140.9054	-48.31026	152.0	-47.5	-63.59	397.2139	4.3308	1	2
CJ060.1A	198	198	197.2535	-25.59422	199.4	-17.3	-52.46	365.5891	3.2782	1	1
CJ060.2A	198	198	191.7468	-19.11616	193.5	-11.4	-51.54	429.7755	2.3929	1	1
CJ062.2C	198	198	199.4691	24.57783	196.4	32.9	-27.9	403.4827	3.4854	1	1
CJ062.1A	198	198	399.7342	14.96559	400.1	05.2	36.57	97.14331	9.6007	2	1
CJ063.1A	201.5	201.5	174.6781	-1.749535	174.5	03.6	-45.62	212.7848	1.3505	1	1

sample	level (m)	comp level (m)	Dg	Ig	Dt	It	Int (E-6 A/m)	latp	err	Q	T
CJ063.2B	201.5	201.5	164.9602	-61.41116	179.4	-56.3	-84.54	182.4029	3.4691	1	2
CJ064.2A	203.5	203.5	193.4196	-43.82354	198.3	-35.7	-62.68	801.2203	2.4814	1	1
CJ064.2C	203.5	203.5	183.6967	-55.03327	192.4	-47.8	-73.25	393.4589	7.5879	1	1
CJ065.2A	205.5	205.5	340.2648	26.61887	344.6	23.1	56.91	352.2565	8.7555	1	1
CJ065.1A	205.5	205.5	374.1076	53.01505	380.6	44.8	66.84	430.1765	6.2684	2	1
CJ066.1A	209	209	362.8157	62.02425	374.1	54.7	76.95	209.0732	6.9061	1	1
CJ067.1B	212	212	146.2487	-36.66294	153.5	-35.3	-58.06	41.20241	15.238	2	1
CJ068.1B	221.5	221.5	190.9363	-49.17401	197.2	-41.3	-66.57	201.9214	2.8522	1	3
CJ068.1A	221.5	221.5	195.6133	-47.28424	200.8	-39.0	-63.31	259.0646	5.4608	2	9
CJ069.1A	222	222	174.5658	-59.41897	186.4	-53.2	-80.09	301.397	2.8829	1	2
CJ069.1C	222	222	181.8169	-59.01259	192.1	-51.9	-76.32	505.5023	2.2139	1	2
CJ070.1A	227.5	227.5	175.1003	-58.05235	186.3	-51.8	-78.94	60.93855	9.9265	2	9
CJ071.1A	229	229	180.9498	-52.58455	189.4	-45.7	-73	664.8004	4.3243	1	3
CJ071.1C	229	229	177.4988	-52.54033	186.4	-46.1	-74.27	758.42	6.2732	1	3
CJ077.2A	230.5	230.5	202.4227	2.318863	201.8	11.0	-38.2	100.7453	1.8197	2	2
CJ072.1A	233	233	191.2528	-41.7223	196.1	-33.9	-62.62	283.2099	1.2225	2	4
CJ079.3A	241	241	182.9918	-5.419611	183.3	01.2	-47	37.36454	11.954	2	2
CJ075.1A	241.5	241.5	199.7654	-57.84973	206.3	-49.1	-65.6	474.5906	2.2042	1	3
CJ075.2A	241.5	241.5	141.3732	-64.13882	161.2	-62.5	-76.21	309.1907	3.2476	1	3
CJ084.1A	258	258	174.5712	-41.72583	181.1	-35.9	-67.58	75.10023	6.2127	2	1
CJ086.1A	262.5	262.5	338.3456	61.16652	353.7	57.1	83.34	74.71767	14.963	2	9
CJ086.2A	262.5	262.5	103.4691	11.56036	102.3	05.2	-7.29	117.9443	6.6542	2	2
CJ087.2A	269	269	179.0504	-39.95044	184.8	-33.5	-65.67	1004.263	3.7147	1	1
CJ088.1B	273	273	439.0767	37.23705	436.3	28.2	20.09	336.3466	3.1781	2	9
CJ089.2A	275	275	94.09312	34.72056	090.2	27.1	9.46	56.7919	3.7351	2	2
CJ094.2A	291	291	180.3438	-20.99563	181.0	-13.2	-54.38	294.6266	4.1825	1	1
CJ096.1A	297	297	191.9776	-41.54948	192.3	-33.6	-63.89	183.0564	8.316	2	1
CJ101.2A	0.5	300.5	217.8468	2.01E-02	218.9	12.9	-29.69	74.91586	9.5489	2	2
CJ102.1A	5	305	161.6234	-55.66433	167.1	-40.4	-67.96	74.45232	9.1162	2	9
CJ107.1A	26.5	326.5	364.9749	25.93321	364.1	12.2	53.69	219.3884	2.4037	1	1
CJ107.2A	26.5	326.5	357.064	26.70791	356.8	12.7	54.02	133.3999	9.3442	2	1
CJ118.3A	51.5	351.5	416.5157	32.68112	411.9	26.8	37.39	90.02136	6.7264	2	1

sample	level (m)	comp level (m)	Dg	Ig	Dt	It	Int (E-6 A/m)	latp	err	Q	T
CJ120.1A	60.5	360.5	160.4602	-55.31455	164.2	-45.8	-70.16	94.00955	10.03	2	9
CJ121.2A	64	364	417.3727	58.94487	405.8	52.7	53.17	142.2981	4.7422	2	1
CJ122.2A	67.5	367.5	390.0626	51.63415	385.1	42.8	62.94	66.74726	12.738	2	1
CJ123.1A	69	369	310.9707	79.70959	334.8	71.6	68.6	191.1978	6.9308	2	9
CJ124.1B	72	372	436.1512	49.26096	425.8	46.0	35.36	72.27865	11.835	2	1
CJ126.2B	77.5	377.5	349.049	47.82796	350.7	38.0	67.63	149.2217	4.0348	2	1
CJ127.2B	79.5	379.5	400.81	51.23398	394.2	43.3	57.17	98.09202	3.4133	2	9
CJ127.3A	79.5	379.5	355.2516	49.21355	356.0	39.2	69.61	61.36693	3.1322	2	9
CJ128.3A	84	384	372.0659	59.06247	369.5	49.2	75.6	109.2211	9.1301	2	9
CJ129.1A	88.5	388.5	414.4107	54.80375	404.8	48.3	51.91	273.1951	4.7775	2	9
CJ129.2B	88.5	388.5	387.4182	56.50869	382.1	47.4	67.45	250.267	1.8166	2	9
CJ130.1A	92.5	392.5	378.656	66.49669	373.5	56.9	78.6	165.5312	5.1182	2	9
CJ130.2A	92.5	392.5	427.4484	53.46684	416.5	48.7	43.45	106.8107	5.9047	2	1
CJ131.1A	95	395	372.921	47.58772	371.0	37.8	66.97	265.5963	4.6541	1	9
CJ131.2A	95	395	380.7628	56.7811	376.6	47.3	70.7	418.1612	3.7124	1	1
CJ132.1A	100	400	399.7557	40.19056	395.3	32.2	51.07	134.5927	1.9032	2	9
CJ132.2B	100	400	364.8888	62.62882	363.7	52.7	80.52	105.8207	3.6593	2	1
CJ133.1B	102.5	402.5	377.4827	22.01437	376.6	12.5	51.14	232.7466	3.0858	1	9
CJ133.2B	102.5	402.5	367.6776	35.61425	366.9	25.7	60.62	385.7352	5.0619	1	1
CJ134.1A	104.5	404.5	409.3871	33.72368	405.1	26.9	42.19	70.98324	8.9652	2	9
CJ134.2A	104.5	404.5	394.3899	59.50105	387.0	50.9	66.06	129.3415	6.0591	2	9
CJ135.1A	107.5	407.5	384.2369	55.21992	379.7	45.9	68.04	170.9014	8.1207	1	1
CJ136.1A	110	410	433.1945	21.70524	429.7	18.5	21.35	679.7832	5.2972	2	9
CJ137.3A	112	412	357.9146	37.60691	358.1	27.6	62.3	167.9615	8.8133	1	9
CJ137.2A	112	412	377.5783	36.24379	375.8	26.7	58.69	312.2263	11.908	2	9
CJ138.1A	116	416	376.2628	49.86386	373.7	40.2	67.5	235.2826	4.6445	1	1
CJ139.1B	119	419	293.4003	45.64072	301.8	41.0	38.74	201.8342	7.0719	2	9
CJ140.2A	122	422	361.2299	55.92601	361.0	45.9	74.97	133.6662	4.6146	1	9
CJ141.1B	125	425	134.2555	20.08751	131.1	26.9	-17.81	89.50636	6.0374	2	9
CJ142.1A	129.5	429.5	348.3843	31.68803	349.4	21.9	57.71	195.8899	1.5907	2	9
CJ143.1A	131.5	431.5	403.8304	58.08409	391.0	47.8	61.66	124.2646	3.9879	2	9
CJ144.2B	136	436	362.9919	56.35246	360.7	42.5	72.31	195.9791	5.4465	1	9

sample	level (m)	comp level (m)	Dg	Ig	Dt	It	Int (E-6 A/m)	latp	err	Q	T
CJ145.1A	139.5	439.5	355.9875	53.15063	355.5	39.2	69.54	88.76057	10.552	2	9
CJ148.2A	149.5	449.5	341.4316	54.88034	344.4	41.1	67.23	112.8381	5.4569	1	9
CJ149.1A	155.5	455.5	308.7323	56.02742	319.7	45.2	53.75	112.033	2.3564	1	9
CJ150.1A	158	458	361.7164	70.17185	358.7	56.2	84.37	89.98086	7.8614	1	9
CJ151.1B	162	462	375.3366	57.45557	369.8	44.2	71.76	500.8658	2.7517	1	9
CJ155.1A	183	483	364.2714	47.32239	362.3	33.5	65.93	91.75948	6.7761	2	9
CJ156.1A	188.5	488.5	345.3105	47.22123	346.9	33.4	63.49	189.1682	1.4108	1	9
CJ159.1C	207.5	507.5	352.4637	36.28799	352.7	22.3	58.64	69.42686	5.363	2	9
CJ161.2A	215	515	359.4587	49.85864	358.3	35.9	67.55	151.9946	4.911	2	9
CJ166.1A	238	538	371.1823	23.9119	369.9	10.5	51.96	589.8507	2.3942	2	9
CJ167.2A	254	554	349.4715	30.07638	349.9	16.1	54.77	979.3558	1.0345	1	9
CJ170.1B	256	556	375.1637	25.48675	373.5	12.3	51.99	230.7024	4.4811	1	1
CJ001.1A	6	6	110.4509	-16.59011	111.6	-14.0	-20.7	143.4395	5.0777	3	4
CJ004.3A	16	16	434.1848	13.4677	433.0	12.9	16.94	337.3732	3.7679	3	1
CJ005.2B	19	19	163.8638	-20.19533	164.0	-15.2	-52.66	296.9201	7.1078	3	9
CJ006.2B	23.5	23.5	238.9996	-32.70724	236.1	-30.8	-35.99	304.627	6.3486	3	9
CJ008.1A	33	33	181.1857	-75.94948	178.3	-71.0	-76.81	74.83396	11.25	3	9
CJ011.3A	56	56	190.3475	-10.15163	190.9	-03.6	-48.34	207.8073	4.4278	3	9
CJ015.2A	64.5	64.5	225.0929	-47.80711	224.5	-39.8	-48.23	58.15557	14.988	3	9
CJ021.2A	90.5	90.5	133.4199	-29.63946	137.9	-28.8	-45.04	34.37859	8.8956	3	9
CJ023.1A	92.5	92.5	157.6894	-13.8611	159.2	-10.0	-48.41	273.7439	2.0178	3	9
CJ024.1A	95	95	313.0143	49.45047	322.1	48.4	57.01	361.1617	2.9291	3	1
CJ027.1A	102	102	178.64	15.65108	176.8	21.6	-36.42	115.9438	6.4049	3	9
CJ030.1A	109	109	347.8442	60.65707	357.3	55.2	83.11	186.6118	2.1941	3	1
CJ030.2A	109	109	196.3277	-36.05953	198.3	-28.7	-58.76	83.32239	10.154	3	9
CJ032.2A	115.5	115.5	168.0855	-13.31028	169.3	-08.3	-50.7	51.34697	12.706	3	9
CJ033.2A	119.5	119.5	149.7061	-11.34758	151.0	-08.6	-44.09	251.406	1.3342	3	9
CJ034.1A	123	123	365.6151	50.28428	370.2	43.5	71.11	405.6404	2.0028	3	1
CJ035.2A	126	126	217.7043	-56.02453	218.1	-48.0	-56.68	234.1239	1.7506	3	9
CJ036.2A	130	130	201.7337	-10.18375	202.0	-02.6	-44.5	197.9843	9.6768	3	9
CJ038.1B	136	136	111.5816	-27.40273	115.8	-29.7	-29.61	208.258	0.9175	3	9
CJ041.1A	141	141	167.3563	-12.73109	168.5	-07.8	-50.27	49.50249	11.051	3	9

sample	level (m)	comp level (m)	Dg	Ig	Dt	It	Int (E-6 A/m)	latp	err	Q	T
CJ042.2A	143.5	143.5	157.9818	-32.39579	163.6	-29.2	-59.82	47.7638	13.431	3	9
CJ042.3A	143.5	143.5	262.8017	-24.39861	261.0	-15.7	-12.02	82.24693	5.0754	3	9
CJ047.1A	159.5	159.5	167.8359	-27.04844	171.9	-22.4	-58.54	41.24801	12.045	3	3
CJ047.2B	159.5	159.5	165.5759	-55.62687	177.3	-50.7	-78.91	44.9888	9.0215	3	9
CJ048.1A	162	162	189.0864	18.52691	186.2	25.7	-33.88	144.5559	2.9909	3	9
CJ048.2B	162	162	241.2632	-13.28277	241.0	-03.4	-22.23	209.6494	8.3153	3	9
CJ049.1A	165	165	186.1299	-59.89642	195.9	-52.3	-74.33	130.0664	2.2301	3	9
CJ049.2A	165	165	213.2463	-50.41948	216.3	-40.9	-54.53	144.558	14.9	3	9
CJ050.1A	168	168	133.442	-29.89876	139.3	-30.9	-46.9	43.26555	27.459	3	2
CJ059.2A	193.5	193.5	246.6886	-8.429424	246.5	01.2	-16.73	208.0056	2.9813	3	9
CJ066.3A	209	209	277.9753	-34.86151	273.8	-27.6	-7.05	118.0156	8.6994	3	4
CJ070.2A	227.5	227.5	233.917	-6.713117	233.9	03.3	-24.6	92.03818	11.217	3	3
CJ077.3A	230.5	230.5	185.3782	8.077997	183.9	14.9	-39.99	78.16061	10.946	3	1
CJ072.2B	233	233	212.9182	-58.07432	216.9	-48.5	-57.79	155.3847	2.0261	3	9
CJ073.2B	236	236	215.8368	-23.73507	216.8	-14.1	-42.18	36.44397	5.9913	3	3
CJ074.2A	238.5	238.5	193.0018	-64.37265	202.8	-56.1	-71.58	140.6388	2.0278	3	9
CJ079.2A	241	241	128.4145	21.94753	124.8	19.3	-17.44	97.26675	6.4799	3	2
CJ076.1B	244	244	155.6441	-56.06715	168.8	-52.6	-77.31	10.06673	13.258	3	3
CJ080.1B	245	245	103.6968	-21.17101	107.3	-27.1	-22.33	33.79134	11.572	3	9
CJ080.2B	245	245	168.7858	22.02966	164.7	26.2	-32.14	76.27991	5.48	3	9
CJ082.1A	250	250	221.0097	-11.23029	221.2	-01.4	-34.38	89.97534	11.371	3	9
CJ083.1A	255	255	297.8206	61.45399	316.7	64.0	59.05	66.3675	6.8818	3	9
CJ083.1B	255	255	244.1742	48.1107	247.3	57.8	11.24	85.10371	12.976	3	1
CJ084.2B	258	258	188.6404	-68.32925	201.2	-60.3	-74.19	54.75965	7.6701	3	9
CJ085.1A	260	260	92.21805	-68.42226	116.1	-74.7	-48.3	110.4396	4.1199	3	1
CJ085.2A	260	260	169.5854	6.715161	168.2	11.2	-40.86	84.22099	7.0689	3	9
CJ088.2A	273	273	250.7558	-65.47681	245.8	-55.9	-40.07	42.87054	13.195	3	9
CJ090.1A	277	277	179.0802	-23.6743	182.0	-17.4	-56.56	44.466	15.579	3	9
CJ090.3A	277	277	93.26012	37.33072	449.1	29.6	11.25	45.13121	3.5905	3	9
CJ091.1A	280	280	102.3821	-19.39092	105.7	-25.6	-20.57	47.59755	6.5275	3	9
CJ092.1A	285.5	285.5	203.7061	-56.55706	202.3	-48.6	-68.01	44.65179	7.6851	3	3
CJ092.2A	285.5	285.5	217.1709	-36.52265	215.3	-29.1	-49.64	87.12379	9.8234	3	9

sample	level (m)	comp level (m)	Dg	Ig	Dt	It	Int (E-6 A/m)	latp	err	Q	T
CJ093.2A	288	288	213.921	-25.93049	212.9	-18.3	-46.26	41.32746	5.9182	3	9
CJ101.1B	0.5	300.5	176.2588	-26.59744	176.8	-10.7	-52.99	48.41025	3.5575	3	9
CJ097.1A	302	302	180.3074	-24.95511	181.1	-17.2	-56.48	33.51557	2.6331	3	9
CJ098.2A	305	305	167.0763	-20.78196	168.2	-13.7	-53.14	75.6099	4.9192	3	9
CJ102.2A	5	305	148.0162	-68.5693	161.6	-54.2	-73.78	50.1063	4.4637	3	9
CJ103.1B	9.5	309.5	269.987	-35.4186	259.1	-33.3	-20.05	76.22916	11.45	3	9
CJ103.2A	9.5	309.5	417.48418	-57.79098	444.6	-63.7	-25.45	103.6319	4.8128	3	9
CJ104.2A	13	313	367.6487	40.82978	366.7	24.9	60.19	49.03797	9.4038	3	9
CJ105.1B	18	318	220.2981	-0.362999	221.3	12.1	-28.74	79.6379	18.792	3	9
CJ105.3A	18	318	35.4818	-86.50513	173.5	-76.8	-67.13	50.56888	4.4791	3	9
CJ106.2B	21	321	391.07869	57.0404	383.0	42.5	64.06	58.72789	1.1423	3	9
CJ109.1A	34.5	334.5	123.344	-29.65079	128.2	-20.3	-34.9	50.60273	2.3085	3	9
CJ109.2B	34.5	334.5	188.5508	-40.69678	186.4	-27.1	-61.51	44.97415	13.287	3	9
CJ110.2B	37	337	186.9276	17.93944	188.5	31.5	-30.15	45.97448	8.0004	3	9
CJ111.2A	40	340	130.0807	-28.3113	134.1	-17.9	-37.98	104.1671	8.6887	3	9
CJ115.1A	41	341	206.0722	15.41372	207.7	24.3	-29.38	29.67033	9.5029	3	9
CJ112.1A	44	344	189.8237	-23.52366	188.7	-10.0	-51.94	66.91185	10.851	3	9
CJ117.2A	49	349	328.7771	70.87812	338.9	61.9	74.52	156.332	8.0694	3	9
CJ117.3B	49	349	366.0142	44.58572	365.2	34.6	66.32	53.24985	14.627	3	9
CJ113.1A	49.5	349.5	181.4015	-39.88837	180.3	-26.0	-61.4	46.1678	13.908	3	9
CJ113.2A	49.5	349.5	185.238	-22.63576	184.5	-08.9	-51.97	84.14471	8.4872	3	9
CJ118.1A	51.5	351.5	351.5733	9.867232	351.7	00.0	47.04	107.2447	3.7629	3	9
CJ119.2A	55	355	256.2358	6.713558	257.6	09.0	-6.04	137.7257	5.9447	3	9
CJ120.3A	60.5	360.5	418.2018	46.52611	410.4	40.7	44.35	143.5761	6.6978	3	9
CJ121.1A	64	364	353.7686	81.24915	357.1	71.3	76.27	117.5813	10.495	3	9
CJ122.1A	67.5	367.5	102.7464	58.37996	446.2	59.2	28.04	58.29524	7.6611	3	9
CJ126.1A	77.5	377.5	399.4447	48.16059	393.6	40.1	55.99	116.9429	3.4674	3	9
CJ128.2A	84	384	400.586	45.537	395.1	37.6	53.76	57.66711	5.5184	3	9
CJ135.2A	107.5	407.5	270.675	-3.879311	270.0	-03.9	-1.31	109.4651	2.1803	3	9
CJ136.2A	110	410	338.5706	-4.426061	338.0	-13.7	36.82	620.473	1.0517	3	1
CJ146.1A	143	443	251.8756	-23.86932	246.4	-20.3	-24.43	95.38795	4.3581	3	9
CJ153.1A	169	469	119.5891	25.39176	113.0	32.9	-3.89	27.18296	8.2721	3	9

sample	level (m)	comp level (m)	Dg	Ig	Dt	It	Int (E-6 A/m)	latp	err	Q	T
CJ154.1B	175	475	337.0125	-25.25246	334.3	-38.5	21.75	85.14694	5.9771	3	9
CJ158.1A	205	505	426.8137	35.73086	418.3	30.6	34.3	161.3259	8.0597	3	9
CJ160.1A	213	513	366.4763	-7.950666	367.3	-21.6	36.08	40.41253	13.982	3	9
CJ165.1B	233	533	395.4534	-22.30957	400.5	-32.4	19.42	165.4772	5.8616	3	9
CJ001.2A	6	6	165.0347	42.65199	164.6	47.6	-17.59	254.3041	3.9438	4	9
CJ002.1A	9.5	9.5	143.7295	30.16455	142.3	34.6	-19.5	124.8768	18.489	4	9
CJ003.2B	13	13	332.3422	2.004118	332.3	-02.8	39.66	333.7136	3.7889	4	1
CJ006.1A	23.5	23.5	366.8205	16.93229	366.4	12.1	53.38	267.3718	4.7264	4	1
CJ009.1B	36	36	286.7234	-30.40524	284.0	-32.5	-1.94	144.679	7.8762	4	9
CJ010.2B	47	47	137.8235	29.99861	133.2	29.9	-17.5	442.5857	1.4717	4	9
CJ011.1A	56	56	109.8488	17.78379	107.8	14.1	-8.08	87.30197	11.852	4	9
CJ017.2A	74	74	304.6458	39.51732	311.3	39.8	45.19	228.5924	12.292	4	9
CJ021.3A	90.5	90.5	190.8896	21.64399	189.0	28.6	-31.86	76.11046	12.24	4	9
CJ022.2A	89	89	271.1985	25.44693	274.6	30.3	14.22	67.02186	12.197	4	9
CJ023.2A	92.5	92.5	102.4942	15.89374	100.7	12.1	-3.72	262.8004	13.264	4	9
CJ024.2A	95	95	108.7536	11.84967	107.4	08.9	-9.67	153.0686	2.2025	4	9
CJ025.3A	96.5	96.5	294.0505	-78.8742	264.5	-74.6	-38.59	78.93681	6.4341	4	9
CJ029.1B	104.5	104.5	207.7468	61.63499	203.4	69.4	7.47	554.3508	5.1928	4	9
CJ034.2B	123	123	137.6013	-26.77402	141.5	-25.4	-45.94	88.16291	17.314	4	9
CJ035.1A	126	126	331.1766	-44.24959	323.4	-46.6	12.14	286.8516	3.048	4	9
CJ037.2A	132	132	386.3997	58.69884	388.8	50.9	64.78	209.7189	5.5928	4	9
CJ038.2A	136	136	274.8801	-29.5454	271.6	-24.8	-7.55	204.5721	3.8318	4	9
CJ039.1B	138	138	338.9195	-38.8595	332.7	-42.4	18.56	56.64766	6.7327	4	9
CJ039.2A	138	138	333.6245	76.84182	357.3	72.1	75.06	159.7441	6.5936	4	9
CJ040.1A	138.5	138.5	191.8426	-55.04216	196.2	-47.8	-71.25	14.12973	10.568	4	9
CJ043.2B	146.5	146.5	319.421	37.58921	327.1	37.4	55.12	87.70359	7.5024	4	9
CJ045.1B	153	153	412.2423	-56.09598	412.3	-66.1	-11.75	18.68614	22.95	4	9
CJ053.1A	176	176	412.0203	-55.76202	412.0	-65.8	-11.31	175.876	2.7655	4	4
CJ054.1A	179	179	267.4666	-69.45035	256.6	-60.8	-35.2	102.8983	5.2672	4	9
CJ067.2A	212	212	127.3427	12.35654	125.5	09.7	-21.75	44.78228	17.533	4	4
CJ073.1A	236	236	268.954	44.62656	276.3	52.2	25.65	44.509	20.524	4	4
CJ081.1B	247	247	307.2808	-44.76642	298.4	-41.5	2.83	57.73239	8.6388	4	9

sample	level (m)	comp level (m)	Dg	Ig	Dt	It	Int (E-6 A/m)	latp	err	Q	T
CJ082.2B	250	250	266.9773	-45.40099	262.2	-37.0	-19.34	32.65143	1.2103	4	9
CJ091.2A	280	280	129.4793	17.35494	126.7	14.9	-20.45	80.65089	9.0911	4	9
CJ095.1A	293.5	293.5	274.2997	54.21713	285.5	54.9	33.45	73.9903	9.3529	4	9
CJ106.1A	21	321	359.1169	46.49955	359.7	30.5	64.11	38.76324	20.418	4	9
CJ108.3A	32.5	332.5	172.5387	-3.282098	172.5	10.7	-41.82	88.48871	6.1445	4	9
CJ110.1A	37	337	250.9896	47.23815	266.5	48.5	16.97	60.22742	7.3374	4	9
CJ114.2A	37.5	337.5	186.9857	6.927959	187.8	20.6	-36.57	53.45876	14.645	4	9
CJ115.2B	41	341	195.4615	73.54363	216.4	82.7	30.28	104.26	10.723	4	9
CJ116.1A	43	343	130.3173	16.89774	127.5	23.2	-17.41	56.79316	9.8308	4	9
CJ116.2A	43	343	447.27761	58.76589	431.6	56.9	36.5	77.88789	7.8979	4	9
CJ119.1B	55	355	127.2302	17.20815	124.2	23.1	-15.44	73.0849	9.3841	4	9
CJ125.2A	74.5	374.5	425.7356	23.85003	422.2	19.4	27.16	95.57052	5.4933	4	9
CJ163.1A	224.5	524.5	221.4607	50.82534	238.0	58.8	7.25	46.45227	8.6585	4	9

SUPPLEMENTARY MATERIAL 2

Magnetostratigraphy of the Pontils section (SE Ebro Basin)

An integrated Eocene chronostratigraphy for the central sector of the SE margin of the Ebro Basin.

Cronoestratigrafía integrada del Eoceno del sector central del margen SE de la Cuenca del Ebro.

E. Beamud[1,2], E. Costa[2], M. Garcés[2], M.A. Marín[2], L. Cabrera[2], E. Roca[2] y M. Gómez-Paccard[3]

1 Laboratorio de Paleomagnetismo (CCiT UB-CSIC). Institut de la Ciències de la Terra "Jaume Almera", Solé i Sabarís, s/n, 08028 Barcelona, Spain. betbeamud@ub.edu
2. Grup de Geodinámica i Anàlisi de Conques, Institut Geomodels, Facultat de Geologia Universitat de Barcelona, C/Martí i Franqués s/n, 08028 Barcelona, Spain elicosta@ub.edu, mgarces@ub.edu, Miquel-Angel.MARIN@beicip.com, lluis.cabrera@ub.edu, eduardroca@ub.edu
3. Institut de Ciències de la Terra "Jaume Almera", Solé i Sabarís, s/n, 08028 Barcelona, Spain. mgomezpaccard@ictja.csic.es

Abstract: The Paleogene sedimentary record in the Pontils area (SE sector of the Ebro Basin) consists of a ~ 2000-m-thick sequence formed by the Mediona Fm, the Orpí Fm, the Pontils Gp, the Santa Maria Gp and the Sant Miquel de Montclar Conglomerates. The age of these materials is loosely constrained based on stratigraphic relationships with marine sediments and punctual mammal fossils and charophyte assemblages within the continental materials. In order to precise their chronology, a magnetostratigraphic section up to 1500-m-thick in the Pontils-Sant Miquel de Montclar area has been studied and correlated to the Global Polarity Time Scale. From this correlation the age of the Pontils Gp is established in Lutetian to middle Bartonian, the Collbàs Fm would be middle Bartonian and the overlying Sant Miquel Conglomerates would range from Bartonian to Priabonian. This new chronology has been integrated with recent magneto- and biostratigraphic studies in more northeasterly sectors of the SE margin of the Ebro Basin (Igualada and Montserrat areas). This new and continuous chronological framework is essential to unravel and quantify the rates of change in the Ebro Basin-Catalan Coastal Ranges system.

Key words: Magnetostratigraphy, Eocene, Ebro Basin.

Resumen: *El registro sedimentario paleógeno de la zona de Pontils (sector SE de la Cuenca del Ebro) consiste en una secuencia de unos 2000 m de potencia formada por la Fm. Mediona, la Fm. Orpí, el Gp. Pontils, el Gp. Santa Maria y los Conglomerados de Sant Miquel de Montclar. La edad de estos materiales es poco precisa en base a relaciones estratigráficas con materiales marinos y datos puntuales de asociaciones de carófitas y mamíferos fósiles en los materiales continentales. Con el objetivo de precisar esta cronología, se ha estudiado una sección magnetoestratigráfica de unos 1500 m de potencia que se ha correlacionado con la Escala de Tiempo de Polaridad Geomagnética. A partir de esta correlación, la edad del Gp. Pontils se establece en Luteciense-Bartoniense medio, la Fm. Collbàs tendría una edad Bartoniense y los conglomerados de Sant Miquel de Montclar abarcarían el Bartoniense-Priaboniense. Esta nueva cronología se ha integrado con estudios magneto- y bioestratigráficos recientes en sectores situados más al NE en el mismo margen de la cuenca (áreas de Igualada y Montserrat). Este nuevo marco cronológico continuo es esencial para descifrar y cuantificar las tasas de evolución del sistema formado por la Cuenca del Ebro y las Cadenas Costeras Catalanas.*

Palabras clave: *Magnetoestratigrafía, Eoceno, Cuenca del Ebro.*

INTRODUCTION

The South Pyrenean Foreland Basin (NE Spain, Figure 1) has an exceptional sedimentary record with up to 5000 meters of marine and continental sediments ranging in age from Upper Cretaceous to Middle Miocene. Moreover, the present level of erosion of the basin infill and its surrounding mountain ranges is at an optimal stage for studying tectonostratigraphic relationships on surface, making this region a natural laboratory for the study of collision belts and their adjacent foreland systems.

Recent bio- and magnetostratigraphic studies within the central sector of the SE margin of the Ebro Basin (Igualada and Montserrat areas; Costa et al., in press; Gómez-Paccard et al., in press) have provided a precise chronology of the Eocene-Oligocene infilling of this basin margin. Nevertheless, time constraints still lack in more southwesterly positions (Pontils/Sant Miquel de Montclar area).

In this contribution we present the integration of a new magnetostratigraphy based chronology in the Pontils area with the established Igualada-Montserrat chronostratigraphy. This will provide a continuous chronological framework for the central part of the SE margin of the Ebro Basin which will allow constraining

the margin evolution and calculating rates of change of this geodynamic system.

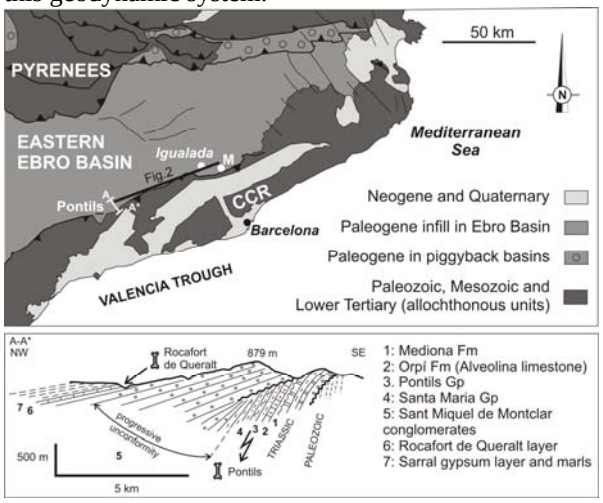

FIGURE 1. *Geological map of the eastern Ebro Basin. The position of the cross section A-A* and the lithostratigraphic sketch (Figure 2) are shown. M indicates the Montserrat area, CCR: Catalan Coastal Ranges. Cross section A-A* redrawn from Anadón et al (1987)*

GEOLOGICAL SETTING AND STRATIGRAPHY

The Ebro Basin is a triangular shaped foreland basin bounded by three Alpine thrust-and-fold belts, the Pyrenees to the N and the Catalan Coastal Ranges and the Iberian Chain to the SE and SW respectively. These margins were tectonically active during most of the sedimentary basin infilling (latest Cretaceous to Middle Miocene in age).

The Ebro Basin was filled by marine and continental sediments until the Priabonian (Costa et al., 2010), when it was disconnected from the Atlantic Ocean. Following the basin closure, steady and continuous continental sedimentation took place from Late Eocene to the late Middle Miocene (Barberà et al., 2001). During this endorheic stage, alluvial and fluvial sedimentation predominated in the basin margins, whereas in the inner parts fluvial and lacustrine systems were set up.

Our study area is located in the SE margin of the Ebro Basin where the Paleocene to Eocene basin infill records the coeval development of the adjoining Catalan Coastal Ranges contractional structures. Specifically, it is located in the NW limb of a frontal anticline that formed at the tip of a major basement thrust. Growth strata geometries and angular unconformities preserved in the Ebro Basin sedimentary record denote that this fold and its related thrust were formed during the sedimentation of the Sant Miquel de Montclar Conglomerates and after the sedimentation of the underlying continental to shallow marine deposits.

The Paleogene sedimentary record in the Pontils area consists of a ~ 2000-m-thick sequence divided into five lithostratigraphic units (Figure 2). From base to top these units are the Mediona Fm, the Orpí Fm, the Pontils Gp, the Santa Maria Gp and the Sant Miquel de Montclar Conglomerates.

The Mediona Fm (Anadón, 1978) directly overlies the thin Mesozoic cover and consists of an up to 50-m-thick unit of red mudstones with interbedded sandstones and calcareous paleosoils. It was deposited before the Ilerdian marine transgression recorded by the up to 100-m-thick limestones of the Orpí Fm (Ferrer, 1971), informally known as Alveolina limestone.

The Pontils Gp (Ferrer, 1971; Anadón 1978) directly overlies the Orpí Fm and mainly consists of fine-grained terrigenous rocks with minor carbonates and evaporites deposited in continental and transitional environments with a variable thickness from 100 to 800 meters. The Pontils Gp can be subdivided into 7 formations, represented in Figure 2. The uppermost levels of the Pontils Gp contain the classical mammal fossil site of Pontils, attributed to the MP15 mammal Paleogene reference level (Anadón et al., 1983).

Overlying the continental Pontils Gp it crops out the marine Santa Maria Gp (Ferrer, 1971). This unit, 400 to 1000 meters thick, was deposited during the Bartonian transgression and can be divided into three main formations; the Collbàs Fm (limestones and marls with subordinated sandstones and fine conglomerates), the marls of the Igualada Fm, and the coralline limestone unit of the Tossa Fm. Recent bio-magnetostratigraphic studies in the Igualada area have attributed a Bartonian age to the Collbàs Fm and a Priabonian age to the Igualada and Tossa formations (Costa et al., in press).

Finally, the alluvial Sant Miquel de Montclar Conglomerates consist of more than 500 meters of massive conglomerates with interbedded red sandstones and mudstone lenses. Basinwards, the Sant Miquel de Montclar Conglomerates grade to the distal alluvial and fluvial facies of the Artés Fm (Ferrer, 1971). The mammal site of Rocafort de Queralt, assigned to the MP19-20 reference level, has been reported within the lowermost levels of the Artés Fm in the study area (Barberà et al., 2001).

In the northeasterly position of Montserrat only four Paleogene lithostratigraphic units crop out. The lowermost unit, the Mediona Fm, is overlain by the El Cairat Fm (Triassic-derived breccias with an Ypressian estimated age; Anadón 1978). Both on top and interfingering the uppermost levels of the El Cairat Fm, the red sandstones, mudstones and conglomerates of the La Salut Fm crop out (Anadón, 1978). The topmost unit in the Montserrat area is the informal Montserrat Conglomerates, which grade basinwards into distal alluvial sandstones and mudstones and finally into the marine Santa Maria Gp. Recent magnetostratigraphic studies have attributed a Lutetian age to the La Salut Fm and an upper Lutetian to lower Priabonian ages to the Montserrat Conglomerates (Gómez-Paccard et al., in press).

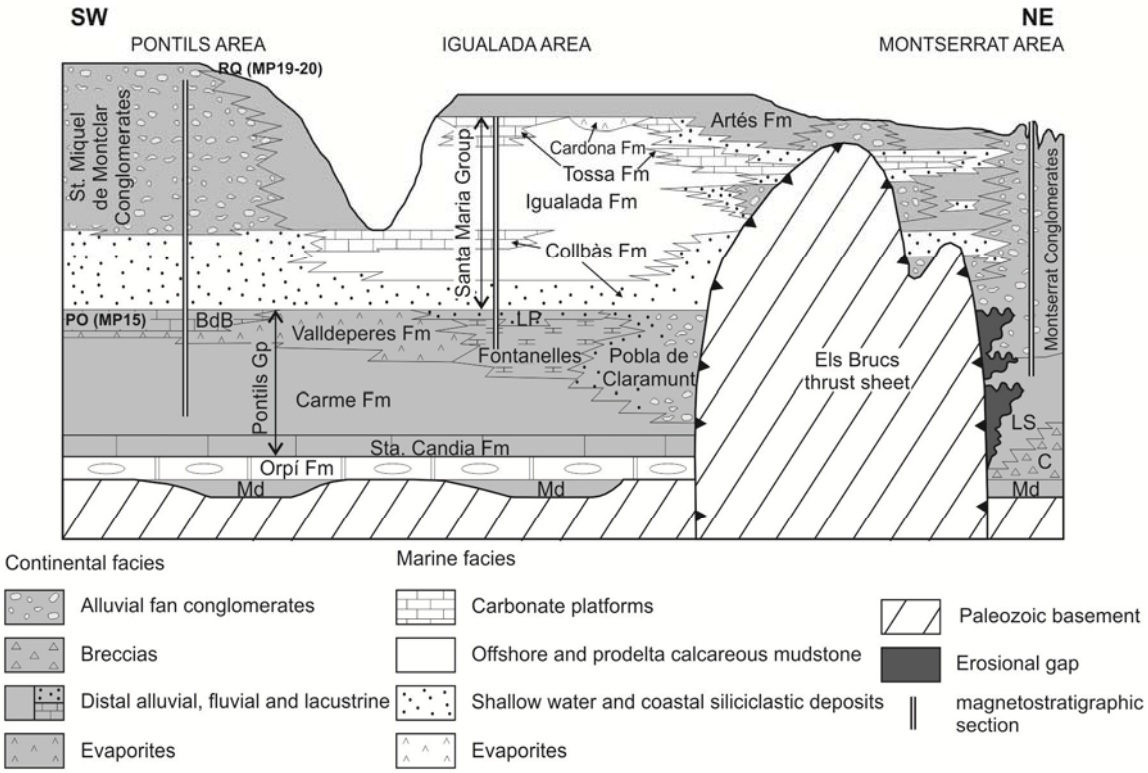

FIGURE 2. *Lithostratigraphic sketch of the Central Sector of the SE margin of the Ebro Basin. The position of the magnetostratigraphic sections is shown. PO indicates the Pontils fossil locality in the Bosc d'en Borràs Fm, (BdB in this figure), RQ indicates the Rocafort de Queralt fossil locality, LP indicates La Portella Fm, Md indicates the Mediona Fm, C indicates the Cairat Fm and LS indicates the La Salut Fm. Redrawn from Anadón et al. (1979) and Costa et al. (in press).*

METHODOLOGY AND RESULTS

238 sites were drilled along ~ 1450 m of sedimentary succession in the Pontils section, comprising the Carme, Valldeperes and Bosc de'n Borras formations (Pontils Gp), the Collbàs Fm (Santa Maria Gp), and the Sant Miquel de Montclar Conglomerates (Figures 2 and 3). At least 2 samples per site were obtained with both an electrical and a gasoline power drills with diamond core bits cooled with water. Samples were oriented *in situ* with a magnetic compass coupled to an orienting device. Laboratory treatment consisted in stepwise thermal demagnetization of, at least, 1 sample per site and subsequent measurement of the Natural Remanent Magnetization (NRM). Samples were heated in a MMTD-80 thermal demagnetizer up to 680 ºC and the NRM was measured in a superconducting rock magnetometer 2G Enterprises in the Paleomagnetic Laboratory of Barcelona (CCiT UB and CSIC).

Characteristic components of the NRM were obtained after visual inspection of the Zijderveld diagrams (Figure 3). The local magnetostratigraphy was determined by calculating the virtual geomagnetic pole paleolatitude per site; positive and negative paleolatitudes were interpreted as normal and reversed polarities respectively.

The obtained local magnetostratigraphy has later been correlated to the Global Polarity Time Scale (GPTS) (Gradstein et al., 2004). From this correlation it can be stated that in this area the sedimentation of the Pontils Gp would extend from Lutetian to middle Bartonian, the Collbas Fm would be middle Bartonian in age and the overlying Sant Miquel Conglomerates would range from Bartonian to Priabonian.

Sedimentary trends have been calculated from this new chronology, ranging from 8 to 24 cm/kyr in the studied section.

CONCLUSIONS

Within the study area new time constraints have been assigned to the Eocene materials of the Pontils Gp, Collbàs Fm and Sant Miquel de Montclar Conglomerates. This allows dating as Bartonian to Priabonian the growth of the NE-trending flexure (Carme-Cabra Anticline) that constitutes the contractional front of the adjoining parts of the Catalan Costal Ranges thrust-and-fold belt. Moreover, the age of the Pontils fossil site (attributed to MP15) has been constrained to the upper part of C19 (late Lutetian). The obtained chronology allows a precise correlation with time-equivalent materials in more northeasterly positions within the Ebro Basin (Igualada and Montserrat areas) yielding an integrated

chronostratigraphic framework for the Eocene record of the SE margin of the Ebro Basin.

ACKNOWNLEDGEMENTS

This work is a contribution of the Geomodels Research Institute and the GGAC Group 2009 SGR 1198 of the *Secretaria d'Universitats i Recerca del Departament d'Economia i Coneixement de la Generalitat de Catalunya*. It was funded by the project COFORSED CGL2010-17479

REFERENCES

Anadón, P. (1978): El Paleógeno continental anterior a la transgresión Biarritziense (Eoceno medio) entre los ríos Gaià y Ripoll (provincia de Tarragona y Barcelona). *Estudios Geológicos*, 34: 341-440.

Anadón, P., Colombo, F., Esteban, M., Marzo, M., Robles, S., Santanach, P. y Solé-Sugrañes, L. (1979): Evolución tectonoestratigráfica de los Catalánides. *Acta Geologica Hispanica*, 14: 242-270.

Anadón, P., Feist, M., Hartenberger, J.L., Muller, C. y Villalta-Comella, J. (1983): Un exemple de correlation biostratigraphique entre échelles marines et continentales dans l' Éocène: la coupe de Pontils (Bassin de l' Ebre, Espagne), *Bulletin de la Société Géologique de la France*, XXV(5): 747-755

Anadón, P., Vianey-Liaud, M., Cabrera, L. y Hartenberger, J.L., (1987): Gisements à vertébrés du paléogène de la zone orientale du bassin de l'Ebre et leur apport à la stratigraphie. *Paleontologia i Evolució*, 21: 117-131.

Barberà, X., Cabrera, L., Marzo, M., Parés, J.M. y Agustí, J. (2001): A complete terrestrial Oligocene magnetostratigraphy from the Ebro Basin, Spain. *Earth and Planetary Science Letters*, 187(1-2): 1-16.

Costa, E., Garcés, M., López-Blanco, M., Beamud, E., Gómez-Paccard, M., Larrasoaña, J.C. (2010): Closing and continentalization of the South Pyrenean foreland Basin (NE Spain): Magnetochronological constraints. *Basin Research*, 22(6): 904-917.

Costa, E., Garcés, M., López-Blanco, M., Serra-Kiel, J., Bernaola, G., Cabrera, L. y Beamud, E. (in press): The Bartonian- Priabonian marine record of the eastern South Pyrenean Foreland Basin (NE Spain): A new calibration of the larger foraminifers and calcareous nannofossil biozonation. *Geologica Acta.*

Ferrer, J. (1971): El Paleoceno y Eoceno del borde suroriental de la Depresión del Ebro (Cataluña). *Mémoires suisses de Paléontologie*, 90: 1-70.

Gómez-Paccard, M., López-Blanco, M, Costa, E., Garcés, M., Beamud, E. y Larrasoaña, J.C. (in press): Tectonic and climatic controls on the sequential arrangement of an alluvial fan/fan-delta complex (Montserrat, Eocene, Ebro basin, NE Spain) *Basin Research.*

Gradstein, F.M., Ogg, J.G., Smith, A.G. (2004): *A Geologic Time Scale* 2004. Cambridge University Press, Cambridge, 589 p.

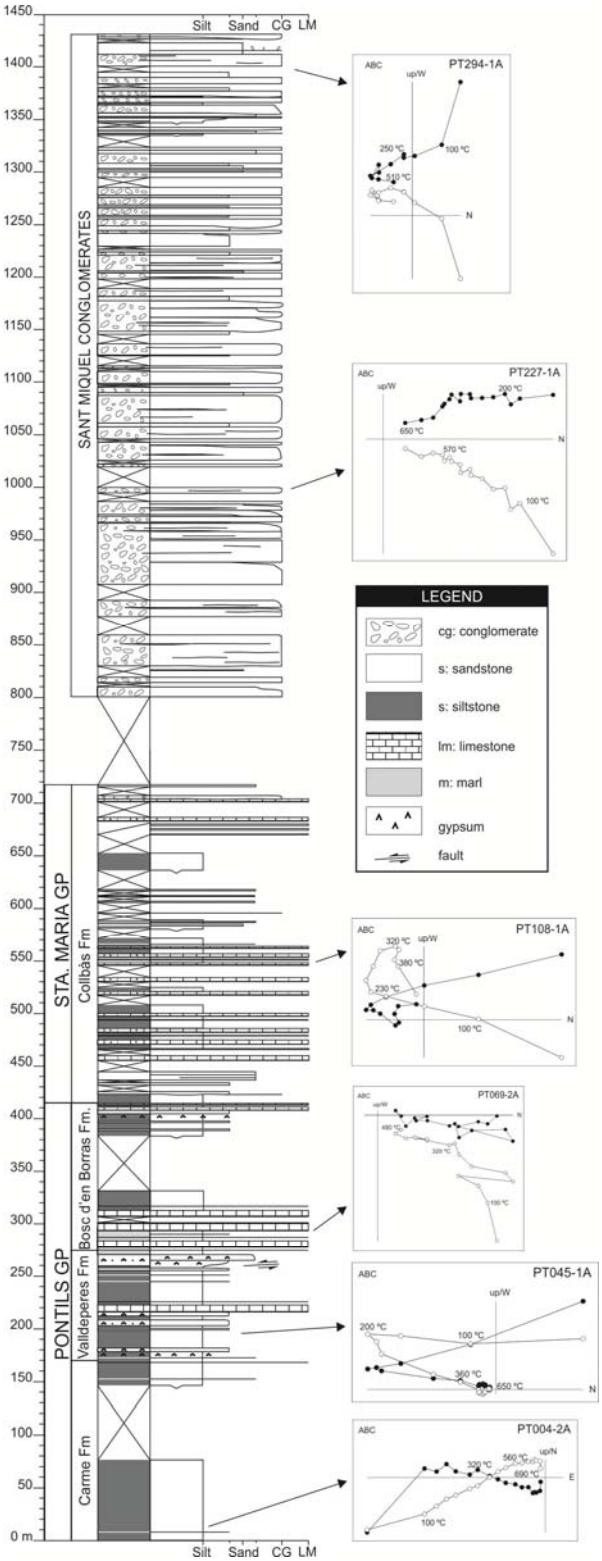

FIGURE 3. *Stratigraphic section and demagnetization diagrams of selected samples for the different formations.*

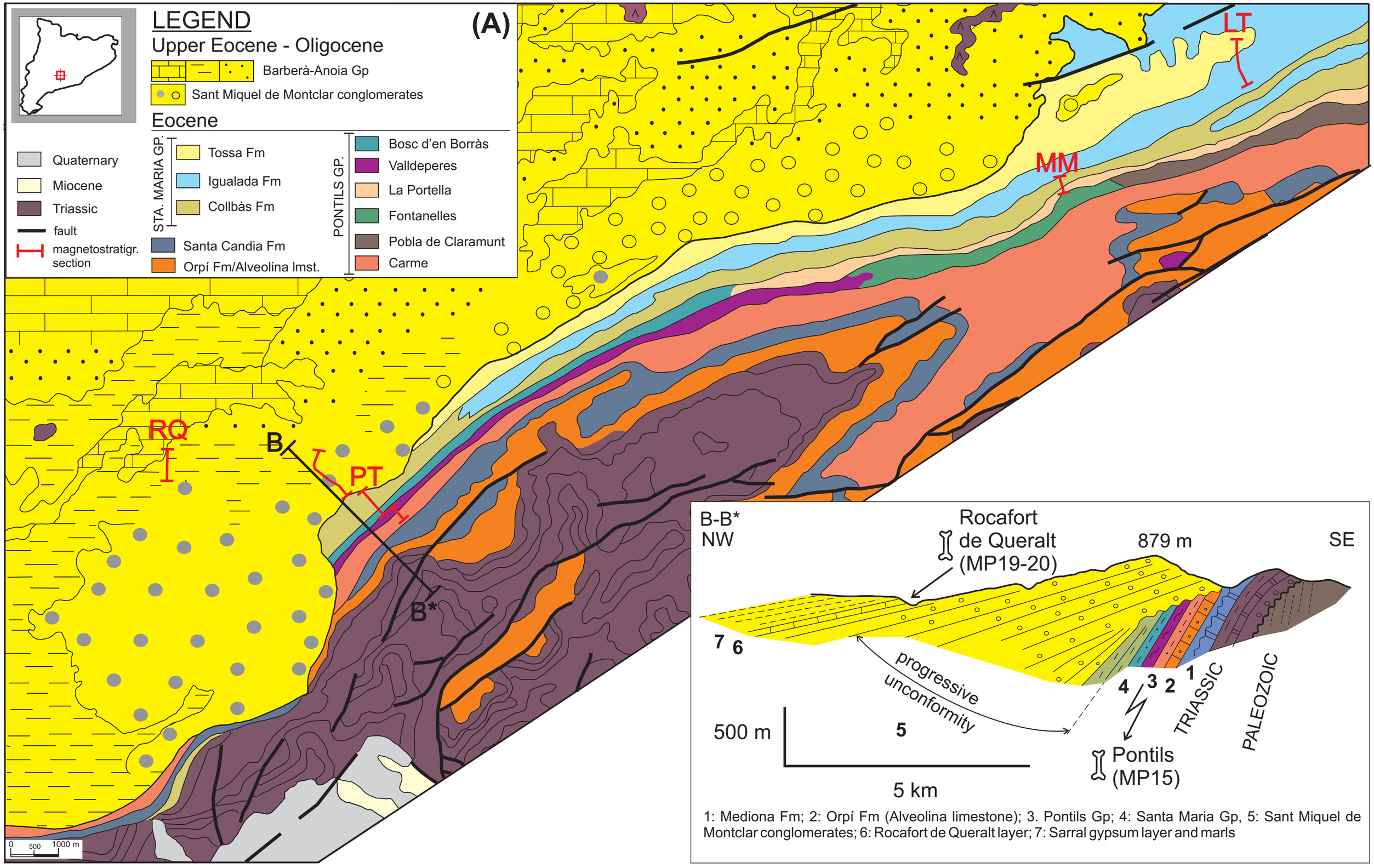

Figure S2.1- A) Geological map of the central sector of the SE margin of the Ebro Basin (Modified from the ICC 1:250000 map). Red lines represent magnetostratigraphic sections; **LT:** La Tossa, **MM:** Santa Maria de Miralles (*Costa et al.*, in press); **RQ**: Rocafort-Vinaixa (*Barberà et al.*, 2001) and **PT:** Pontils.
B-B*) Cross-section through the study area (modified from *Anadón et al.*, 1987). Location of mammal fossil sites **PT** (Pontils, **MP15**) and **RQ** (Rocafort de Queralt, **MP19-20**) is indicated.

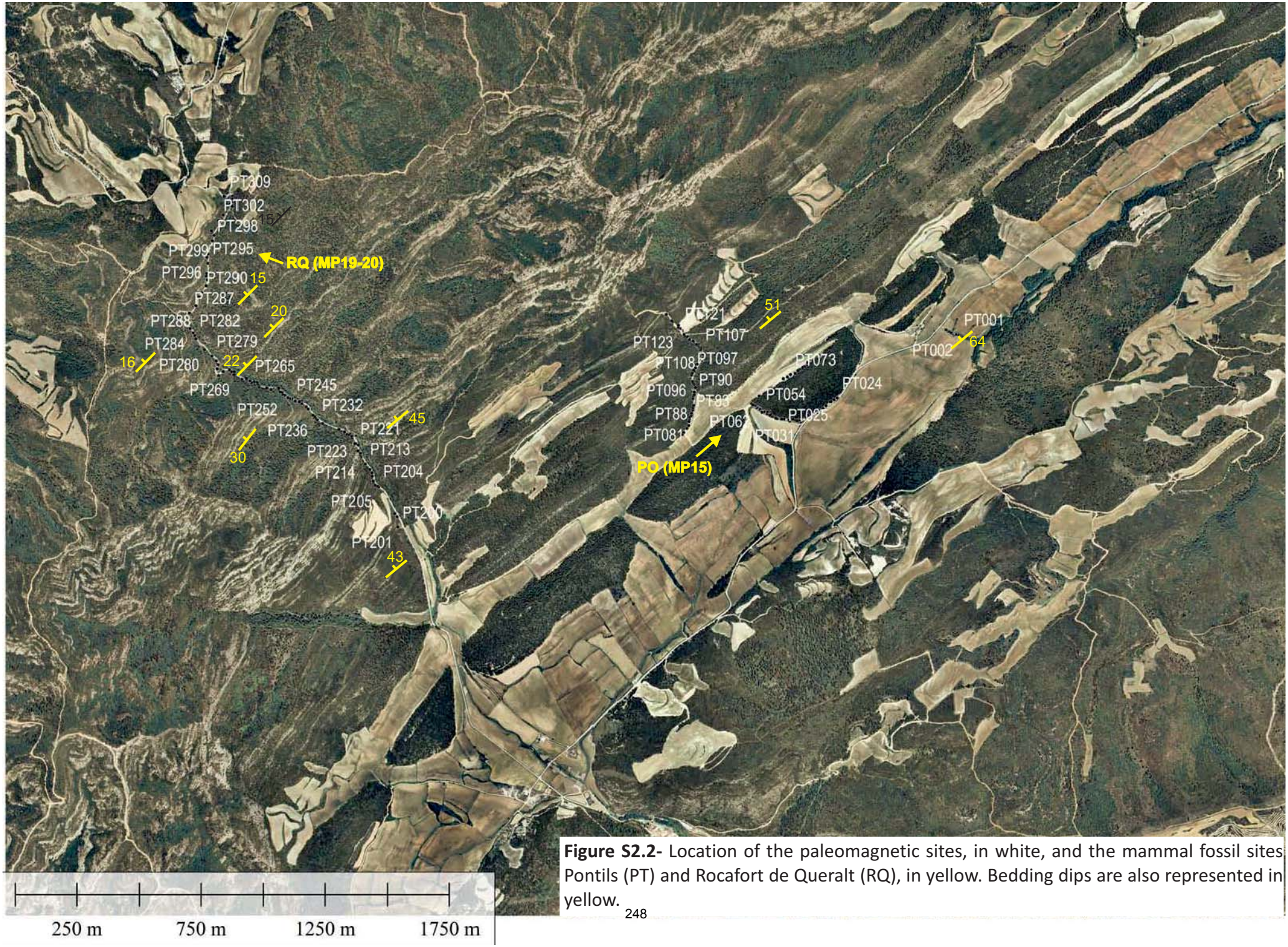

Figure S2.2- Location of the paleomagnetic sites, in white, and the mammal fossil sites Pontils (PT) and Rocafort de Queralt (RQ), in yellow. Bedding dips are also represented in yellow.

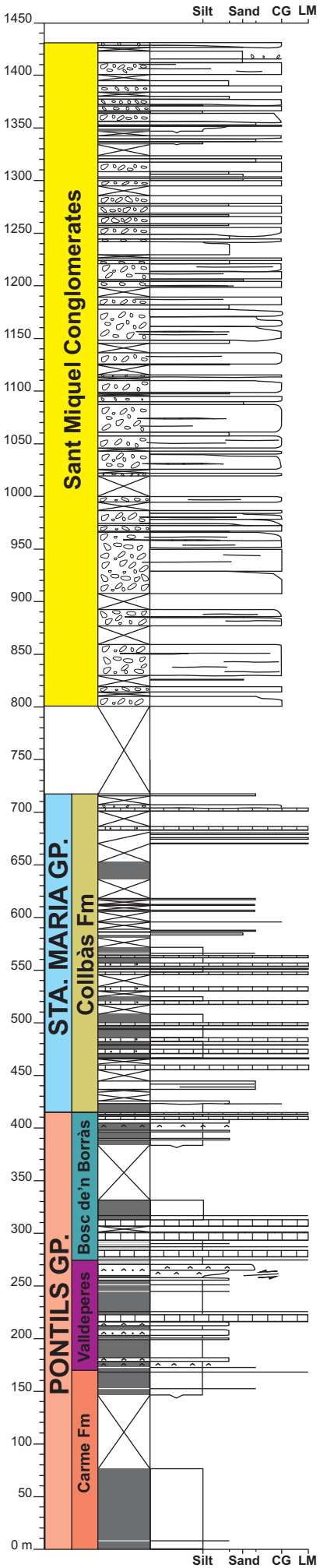

SANT MIQUEL CONGLOMERATES

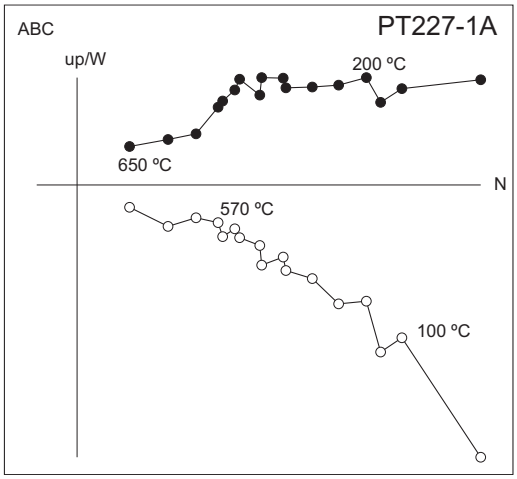

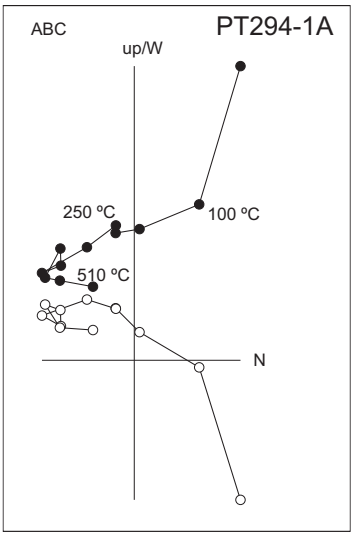

FM. COLLBÀS

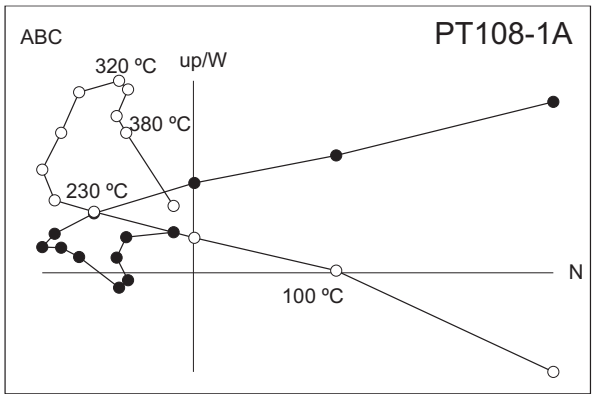

FM. VALLDEPERES

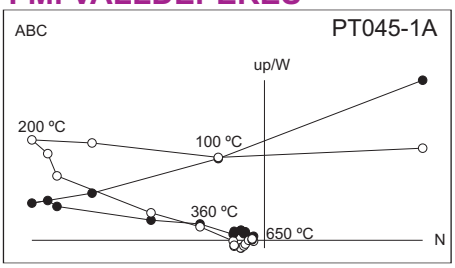

FM. BOSC D'EN BORRAS

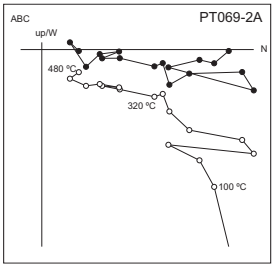

FM. CARME

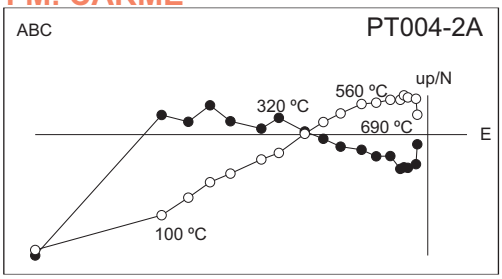

Figure S2.3- Stratigraphic log for the Pontils section and demagnetization diagrams of selected samples from the different formations.Black (white) dots represent projection of the demagnetization vector end-point into the horizontal (vertical) plane.Thermal demagnetization in all cases, temperatures are shown in the diagrams.ABC: after bedding correction

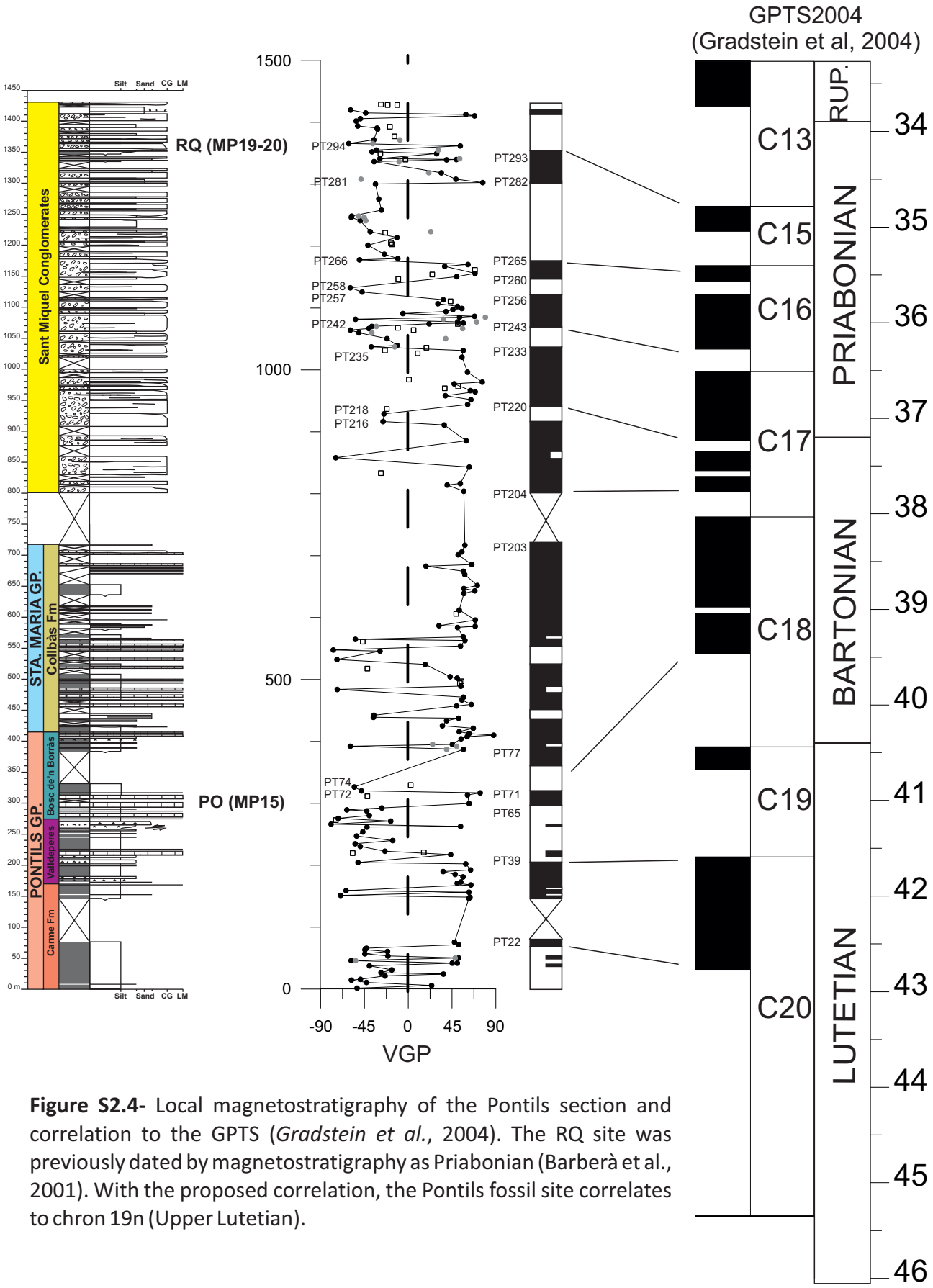

Figure S2.4- Local magnetostratigraphy of the Pontils section and correlation to the GPTS (*Gradstein et al.*, 2004). The RQ site was previously dated by magnetostratigraphy as Priabonian (Barberà et al., 2001). With the proposed correlation, the Pontils fossil site correlates to chron 19n (Upper Lutetian).